R-10-48

Bedrock K_d data and uncertainty assessment for application in SR-Site geosphere transport calculations

James Crawford, Kemakta Konsult AB

December 2010

Svensk Kärnbränslehantering AB
Swedish Nuclear Fuel
and Waste Management Co

Box 250, SE-101 24 Stockholm
Phone +46 8 459 84 00

ISSN 1402-3091
SKB R-10-48

Bedrock K_d data and uncertainty assessment for application in SR-Site geosphere transport calculations

James Crawford, Kemakta Konsult AB

December 2010

Summary

The safety assessment SR-Site is undertaken to assess the safety of a potential geologic repository for spent nuclear fuel at the Forsmark and Laxemar sites. The present report is one of several reports that form the data input to SR-Site and contains a compilation of recommended K_d data (i.e. linear partitioning coefficients) for safety assessment modelling of geosphere radionuclide transport. The data are derived for rock types and groundwater compositions distinctive of the site investigation areas at Forsmark and Laxemar.

Data have been derived for all elements and redox states considered of importance for far-field dose estimates as described in /SKB 2010d/. The K_d data are given in the form of lognormal distributions characterised by a mean (μ) and standard deviation (σ). Upper and lower limits for the uncertainty range of the recommended data are defined by the 2.5% and 97.5% percentiles of the empirical data sets. The best estimate K_d value for use in deterministic calculations is given as the median of the K_d distribution.

Sammanfattning

Säkerhetsanalysen SR-Site genomförs för att bedöma den långsiktiga säkerheten av ett geologiskt slutförvar för använt kärnbränsle vid Forsmark. Denna rapport är en del i en serie som levererar specifika data till säkerhetsredovisningen SR-Site och innehåller en sammanställning av rekommenderade K_d data (linjära fördelningskoefficienter) för modellering av radionuklidtransport i geosfären. De framtagna data är representativa för bergarter och grundvattensammansättningar typiska för platsundersökningsområdena vid Forsmark och Laxemar.

Data har framtagits för alla grundämnen och redoxtillstånd som anses vara viktiga för dosberäkningar i fjärrområdet och som beskrivs i /SKB 2010d/. Fördelningskoefficienterna anges i form av lognormalfördelade osäkerhetsintervall som karakteriseras av ett medelvärde (μ) och standardavvikelse (σ). Övre och undre gränser för osäkerhetsintervallen har definierats som 2.5 % respektive 97.5 % percentilerna av de empiriska dataseten. Det centrala värdet för deterministiska modelleringsändamål anges som medianvärdet av K_d-fördelningen.

Contents

1 Introduction

This report contains a compilation of sorption partitioning (K_d) data recommended for use in the SR-Site safety assessment for the purpose of making radionuclide transport calculations in the geosphere. The K_d data are given as a central best estimate and an uncertainty range. These are intended to be used in deterministic and probabilistic simulations of radionuclide transport in the far-field of the repository environment. The data specifically concern adsorptive retention processes on granitic rocks native to the Forsmark and Laxemar sites. The data contained herein represent a mix of site specific data obtained during the site investigations at Forsmark and Laxemar and data obtained from literature sources.

1.1 Background

SKB, the Swedish Nuclear Fuel and Waste Management Co. is currently preparing a licence application to locate, build and operate a deep repository for spent nuclear fuel. The safety assessment SR-Site forms an integral part of this licence application. In the safety assessment, geosphere transport calculations are made to assess levels of radiological risk associated with different scenarios of repository evolution. Matrix diffusion coupled with sorption is the main retardation mechanism considered in the geosphere transport calculations.

1.2 Scope and objectives

The term *sorption* is a very broad concept that describes a number of processes by which dissolved solutes are sorbed (adsorbed or absorbed) on, or in another substance, e.g. /IUPAC 1997/, which can also be taken to include processes such as surface precipitation and solid solution formation. In the context of radionuclide transport and the sense in which the term is used in this report, *sorption* is used strictly to refer to adsorptive interaction with mineral surfaces by way of electrostatic and covalent chemical bonding and specifically excludes other related processes.

The Swedish concept for disposal of high-level nuclear waste involves isolation of the waste at depth in crystalline bedrock. For this reason, the focus of the present report is sorption processes that may influence the transport of radionuclides within fractured granitic rock-types. In this definition we loosely include the entire family of intrusive (plutonic) igneous rocks common in Sweden. For the purposes of SR-Site, K_d data are derived for sorption on site specific rock types native to the Forsmark and Laxemar area. For the Forsmark site, the metagranite rock type (Granite to granodiorite, metamorphic, medium-grained, SKB rock code 101057) is of principal interest on account of its predominance in the central area of the proposed repository volume /SKB 2010b/. For the Laxemar site, the principal rock type is considered to be a quartz monzodiorite (Granite to quartz monzodiorite, generally porphyritic, SKB rock code 501044) /Crawford and Sidborn 2009/. In this report these rocks are referred to as the *reference rock types* for each respective site.

This report constitutes an update to the K_d data compilation used in the previous SKB safety assessment, SR-Can /SKB 2006/ concerning storage of spent nuclear fuel in a deep geological repository environment. The K_d values given for various radionuclides are used as input parameters to the safety assessment codes FARF31 /Elert et al. 2004/ and MARFA /Painter and Mancillas 2009/ that calculate far-field radionuclide release rates. The representation of sorption phenomena using a K_d approach implies a number of assumptions that are not always fully defensible if the aim is to accurately represent the dynamics of radionuclide transport. In this report, recommendations are provided that are cautiously chosen with regard to the particular transport scenarios being modelled to avoid underestimation of radiological risks. The use of these K_d values in safety assessment codes therefore does not provide a true representation of the transport mechanisms as they might actually occur.

2 Sorption processes in bedrock

Migrating radionuclides are frequently in the form of aqueous ionic species and will tend to sorb on mineral surfaces that possess a net charge of opposite sign. Such interactions are well described in the scientific literature /e.g. Stumm and Morgan 1996/ and the most important mechanisms for this interaction are considered to be ion-exchange and surface complexation. Ion exchange involves a purely electrostatic adsorption process whereas surface complexation typically involves covalent bonding to chemically reactive surface groups on mineral surfaces. The description of surface complexation, however, is complicated by the fact that one frequently speaks of *inner sphere* and *outer sphere* surface complexes. While inner sphere surface complexes involve covalent bonds to surface reactive groups, outer sphere complexation is more electrostatic in nature and is essentially identical to ion exchange (this distinction is discussed in more detail in Section 2.2.2).

Sorption can take place directly on the outer surfaces of flow-bearing fractures, or on grain boundary surfaces and microfractures within the rock matrix where the porewater is effectively stagnant. Sorption can also take place on other materials, such as secondary clay minerals in fracture surface coatings. Generally, sorption processes result in the retardation of radionuclide transport along a flowpath, although when radionuclides sorb on mobile solid materials such as colloids, the effectiveness of the retardation may decrease (there are even some indications of possible migration enhancement in field-scale tracer experiments performed at the Grimsel Test Site /Kurosawa et al. 2006/).

When dissolved radionuclides are sorbed on naturally occurring mobile colloidal solids, the resulting particles are commonly referred to as *pseudo-colloids*. Pseudo-colloid formation involving bentonite colloids is the subject of a separate data report in the SR-Site project /Wold 2009/ and is considered in the safety assessment calculations described in the Radionuclide transport report /SKB 2010d/. Certain radionuclides that are strongly hydrolysed in water and have low solubilities may spontaneously form hydroxide microprecipitates or polymeric forms that are referred to as *eigencolloids* (i.e. pure phase colloids). Redox sensitive solutes with large differences in solubility between oxidised and reduced forms are particularly inclined to form eigencolloids when redox conditions change significantly over short distances such as might occur at a redox front. These processes are not considered relevant for the SR-Site safety assessment and are therefore not modelled in the radionuclide transport calculations. This is predicated partly on the basis that sharp redox fronts are not expected in the repository environment and partly due to the expected ultrafiltration of eigencolloids in the intact bentonite backfill. Further reasoning in support of this assessment can be found in /SKB 2010c/.

There are other processes apart from sorption, such as precipitation and co-precipitation (solid solution formation), which can give rise to additional retardation effects for transported radionuclides. Owing to the difficulties in adequately quantifying and modelling these processes, however, they are not usually considered to contribute significantly to retardation in safety assessments. In reality, however, it is very likely that they exert a very strong retardation effect on migrating radionuclides.

The following sections give a brief overview of the different processes and parameters that influence sorption properties as well as how sorption is modelled. In Section 2.2.2, the simplified modelling approach used in safety assessment is presented and the various advantages and limitations of the approach are discussed. This chapter is not intended to give a textbook description on all relevant aspects of sorption processes and modelling thereof. The main focus is to highlight the central ideas that are currently used to gain insights into the fundamental physics and chemical mechanisms of sorption for the purpose of predicting radionuclide migration in fractured rocks. Processes that are of interest for the SR-Site safety assessment are specifically emphasised, while other processes that are of considered of less relevance are not dealt with in detail.

2.1 Processes and parameters influencing sorption properties

2.1.1 Mineral surfaces and their reactive chemistry

Being a surface mediated process, sorption of radionuclides on rock is sensitive to both the available surface area of sorbing constituent minerals as well as their geochemical properties. Most minerals have a net overall negative charge associated with surfaces at the mineral-water interface at normal groundwater pH levels. This charge is described as having a *permanent* component that is pH-invariant and a *variable* component that varies with the pH of the aqueous phase.

The variable component of the surface charge generally arises due to protonation-deprotonation reactions at the mineral surface, where oxide and hydroxide groups are in contact with water. These are examples of surface complexation reactions. For aluminosilicate clay minerals the charge develops partly due to the above, but also due to the permanent charge at the mineral surface. Permanent charge arises due to so-called *isomorphic substitutions* in the crystal structure itself where one element is substituted for another of similar ionic radius (usually not more than about ±15%) during mineral formation without alteration of the overall crystal structure. Generally, Al^{3+} is substituted for Si^{4+} in tetrahedrally coordinated crystal structures and Mg^{2+}, Fe^{2+}, or Fe^{3+} replacing Al^{3+} in octahedrally coordinated structures thereby giving rise to a net structural negative charge (see Section 2.1.2). Permanent surface charge, however, can also appear by way of imperfections or defects in the lattice structure of crystals although this is usually a minor contributor.

For many oxide, hydroxide, and aluminosilicate minerals the protonation and deprotonation of surface oxide and hydroxyl groups gives rise to charged surface *functional groups* that are responsible for much of the pH-dependent surface charge behaviour of these minerals in environmental systems. These reactions buffer solution pH depending on the numbers and types of surface groups present. It is also possible for charged surface groups to bind aqueous ionic species in various ways (e.g. monodentate- and bidentate complexes, etc.). The chemically reactive functional groups on mineral surfaces are frequently referred to as *sorption sites* or *binding sites* for surface complexation.

Isomorphic substitutions are particularly important in the case of aluminosilicate minerals possessing a *phyllosilicate,* or sheet crystal structure (i.e. clay and mica minerals) owing to their large internal surface area in the form of interlayer planes. This is the main source of surface charge in these minerals since the interlayer planes generally have low chemical reactivity. At disruptions and broken edges of these minerals, however, there are so-called *frayed edge sites* (FES) which can participate in surface complexation reactions and give rise to a pH dependent charge.

When considering the ability of mineral surfaces to influence solution chemistry, it is customary to refer to the cation exchange capacity, or CEC of the mineral. The CEC is the quantity of cations that a mineral can accommodate on its negatively charged surface. It is usually expressed in terms of charge equivalents per unit mass (most frequently in the units *cmol/kg* or the equivalent measure *meq/100 g*). A charge equivalent is equal to one mole of ionic charge, or 6.02×10^{23} ion-exchange sites. The CEC, being measure of negative charge, is therefore comprised of a variable and permanent charge component as outlined above. Although one might seek to differentiate surface complexation binding sites in mechanistic modelling, it should be noted that the CEC implicitly includes the negatively charged surface complexation binding sites in the operative definition of an *ion-exchange site*.

As outlined above, the speciation of reactive surface groups changes with pH owing to protonation-deprotonation reactions. At low pH values, there may be a net positive surface charge owing to a predominance of positively charged groups. At high pH, the opposite may be true and the surface has a net negative charge owing to a predominance of negatively charged surface species. At some pH, the mineral surface may change from a net positive to a net negative surface charge owing to the balance of charge arising due to adsorption of H^+ or OH^-, the permanent charge component, and that of adsorbed electrolyte ions. This is referred to as the point of zero charge, PZC (or pH_{PZC}). To a good approximation, the PZC is roughly inferred from the pH at which electrophoretic mobility of a mineral particle vanishes, the so-called *isoelectric point*, or IEP /Sposito 1998/. To distinguish between the contributions of H^+/OH^- adsorption and the additional effect of permanent charge and adsorbed electrolyte ions, the term *point of zero net proton charge*, PZNPC (or pH_{PZNPC}) is also frequently used. This is also the pH at which a mineral tends to buffer pH in a pure water solution. Although beyond the scope of this report, this short discussion should make the reader aware that the definition of pH_{PZC} is subject to various complicating factors giving rise to a number of different operational and theoretical definitions in the literature.

Generally speaking, the pH_{PZNPC} of silica and aluminosilicate minerals tends to be below pH 4. For aluminium and iron oxides or hydroxides, on the other hand, the pH_{PZNPC} is above pH 7. It should also be noted that the pH_{PZNPC} does not imply that there are no charged surface species existing at this pH, but rather that there are equal amounts of positive and negatively charged surface groups giving rise to a net zero overall charge. For this reason, igneous rocks are classified as being *acidic* or *basic* depending upon their relative silica contents and the surface reactive behaviour that this implies. Felsic rocks such as granite and granodiorite are termed acidic owing to their high silica contents, while Mafic and Ultramafic rocks are basic owing to their low relative silica contents. Under normal groundwater conditions, rocks that are termed acidic have a poor pH-buffering capacity when undergoing dissolution, whereas basic rocks are relatively better at pH buffering.

The surface chemistry of calcite is more complex than the abovementioned minerals on account of the fact that H^+ and OH^- do not influence the surface charging behaviour in the same fashion and the concept of a well-defined pH_{PZNPC} or pH_{PZC} therefore appears to lack physical meaning /Stipp 1999/. Although pH does play a role in the charging behaviour of calcite surfaces it is widely regarded that this occurs primarily by way of altering the speciation of the carbonate ion in solution and the charge determining ions are actually Ca^{2+} and CO_3^{2-} /Madsen 2006/. Although the pH_{PZNPC} does not strictly exist for calcite, its isoelectric point (and related ξ-potential) occurs when the activity of free Ca^{2+} and CO_3^{2-} are equal /Stipp et al. 1998, Madsen 2006/. In the case of calcite it is therefore more appropriate to discuss surface charging behaviour in terms of the pCa_{PZC} or $pCO_{3\ PZC}$. Although sorptive interaction with calcite may be an important mechanism for retention of radionuclides in fracture coatings and a possible confounding factor in sorption experiments where co-precipitation might occur, it is of less relevance for matrix retention processes since calcite is not thought to exist in significant quantities in the rock matrix. Treatment of sorption processes involving calcite is beyond the scope of this report although scoping calculations are made in the SR-Site Radionculide transport report /SKB 2010d/ to quantify the possible impact of calcite solid solutions on radionuclide transport retardation.

The fact that certain minerals such as ferric oxyhydroxides and hematite have isoelectric points close to groundwater pH is of considerable significance especially for radionuclides in oxyanion form since these are most likely to form surface complexes with positively charged surface groups. If the pH is below the pH_{PZNPC} this implies the possibility of increased sorption of oxyanions on these minerals. If, on the other hand, the pH is above the pH_{PZNPC} then the sorption of oxyanions will be much reduced owing to the predominance of negatively charged surface groups. The opposite behaviour can, of course, be expected for radionuclides in cationic form. Most aluminosilicate minerals, however, are predominantly negatively charged for all reasonable groundwater pH levels.

2.1.2 Microstructural properties of rocks and minerals that influence sorptivity

A factor of some importance when considering the reactive properties of rock is the extent to which the constituent minerals have been altered, weathered, or otherwise physically disrupted compared to pristine crystal structures. This is particularly important at the edges of individual crystal grains and at locations that have been disrupted by weathering and grain attrition processes. At these sites there may be reactive surface groups that differ in abundance and reactivity as compared to pristine crystal surfaces. When rock is crushed in order to perform laboratory measurements, new mineral surfaces are created. Different minerals also have different failure modes and the distribution of surface area and sorption sites amongst constituent minerals in the crushed material may not necessarily be representative of undisturbed rock in situ. It is therefore useful to consider the properties of the constituent minerals and how these can be expected to contribute to the overall sorptive properties of the rock when attempting to relate measurements made on rocks in different states of disaggregation and possibly from different sites with different geochemical properties.

The surface area of framework silicate minerals may consist of external crystal surfaces as well as intracrystalline microfractures forming internal surfaces. Generally, however, there is little difference between the internal and external surfaces in terms of their chemical reactivity. Even though they comprise the overwhelming bulk of mineral phases in granitic rocks, most commonly occurring framework silicate minerals tend to be neglected when considering sorption processes owing to their low reactivity when compared to the phyllosilicate minerals. In terrestrial environments, their sorption properties tend to be overwhelmed by the presence of phyllosilicate minerals and ferric and

aluminium oxyhydroxides. Additionally, their surface charge and sorption capacity arises largely due to ionisable surface groups, as isomorphic substitution effects are mostly absent, or at least not a regular and predictable feature of their structure.

Phyllosilicate minerals are layered, consisting of continuous sheets of tetrahedrally coordinated silica (SiO_2) interspersed with sheets of octahedral, gibbsite- ($Al(OH)_3$) or brucite-like ($Mg(OH)_2$) crystal structures. Although these minerals have a relatively complicated configuration, their basic structure can be readily explained in terms of Pauling coordination polyhedra /Pauling 1929/. The specific details of this is not important for the present discussion although it is crucial to note that the tetrahedral (T) and octahedral (O) sheets in clay minerals are stacked in layers that may be separated by water molecules or exchangeable cations that balance the permanent charge in the crystal lattice. These minerals are further categorised according to whether they have two-layer (TO), or three-layer (TOT) repeating structures. The simplest TO clay mineral is kaolinite, consisting of alternating layers of tetrahedral silica and octahedral gibbsite. Kaolinite has no exchangeable cations or water molecules in the interlayer space and is therefore relatively chemically inert compared with many other clay minerals. The distance between the basal plane of the silica T-sheet and the next layer is 7Å including interlayer spacing. The silica-gibbsite TO layers are held together strongly by hydrogen bonds which results in kaolinite being a non-expanding clay.

The TOT clays consist of a gibbsite- or brucite O-layer sandwiched between two silica T-layers. The mineral muscovite, although considered as a primary accessory mineral in granitic rock, can also form by later alteration of orthoclase or plagioclase feldspar. It is considered to be a mica mineral along with biotite, although it shares many similarities with the illite family of clay minerals. In micas, about one in four of the Si^{4+} ions are isomorphically substituted with Al^{3+} in the silica T-layers. This results in a deficiency of positive charge in the sheets that is permanent in the crystal structure and not influenced by solution pH. To balance the excess negative charge, K^+ ions are held in the interlayer by strong electrostatic forces. The basal plane spacing of the micas is on the order of 10Å and the small K^+ ions are difficult to exchange with larger, usually hydrated, ions owing to the narrow spacing between the layers. The narrow spacing and the presence of tightly held cations excludes the penetration of water molecules in the interlayer, and these minerals are therefore non-expanding.

Illite balances excess negative charge by an interlayer of K^+ ions and, like muscovite, has a basal plane spacing of 10Å. Illite, however, is often rather poorly defined owing to its propensity to form mixed-layer clays with smectite minerals. Other cations such as Ca^{2+} or Mg^{2+} can also sometimes substitute for K^+ in the interlayer. The smectites (see Figure 2-1) frequently have isomorphic substitutions of Mg^{2+} or Fe^{2+} in place of Al^{3+} in the gibbsite/brucite O-layers and Al^{3+} or Fe^{3+} instead of Si^{4+} in the silica T-layers. The smectites are swelling clays, the best example of which is Na-montmorillonite, otherwise known as bentonite. Water molecules and exchangeable cations are present in the interlayer spacing, which varies between 12–18 Å depending upon the solution composition and the identity of the interlayer cations (Na^+ ions allow greater expansion than either Ca^{2+} or Mg^{2+}).

The chlorite group of clay minerals are similar to the micas although instead of an interlayer of K^+ ions, the interlayer contains a brucite-like, structure that contains Mg^{2+}, Al^{3+}, or Fe^{3+} coordinated with OH^- groups. A significant difference between the O-layers in chlorite and the brucite-like interlayer structure is that the interlayer structure is only electrostatically bonded to the adjacent layers, whereas there is covalent bonding between the O and T-structures in the TOT layers. The basal plane spacing of chlorites is roughly 14Å. The chlorites are frequently formed as alteration products of biotite. The substitution of Mg^{2+} with Al^{3+} in the brucite-like interlayers of chlorite gives a positive structural charge that counterbalances most of the permanent charge of the T-layers. The CEC of chlorite therefore is significantly less than biotite on account of both the pre-existing charge counterbalance as well as the interlayer structure blocking access for the exchange of cations /Sparks 2003/.

The external surface area of phyllosilicate minerals is in the form of sheet edges as well as the externally exposed basal planes. The basal planes of sheet silicates that are externally exposed may be composed of silica or, in the case of kaolinite, gibbsite layers. The internal surface area is comprised of the interlayers of stacked sheets containing exchangeable cations. Disruptions in the form of microfractures and partially delaminated sheets also occur in these minerals although the surface area contribution of these features is usually insignificant in comparison with the interlayer surface area.

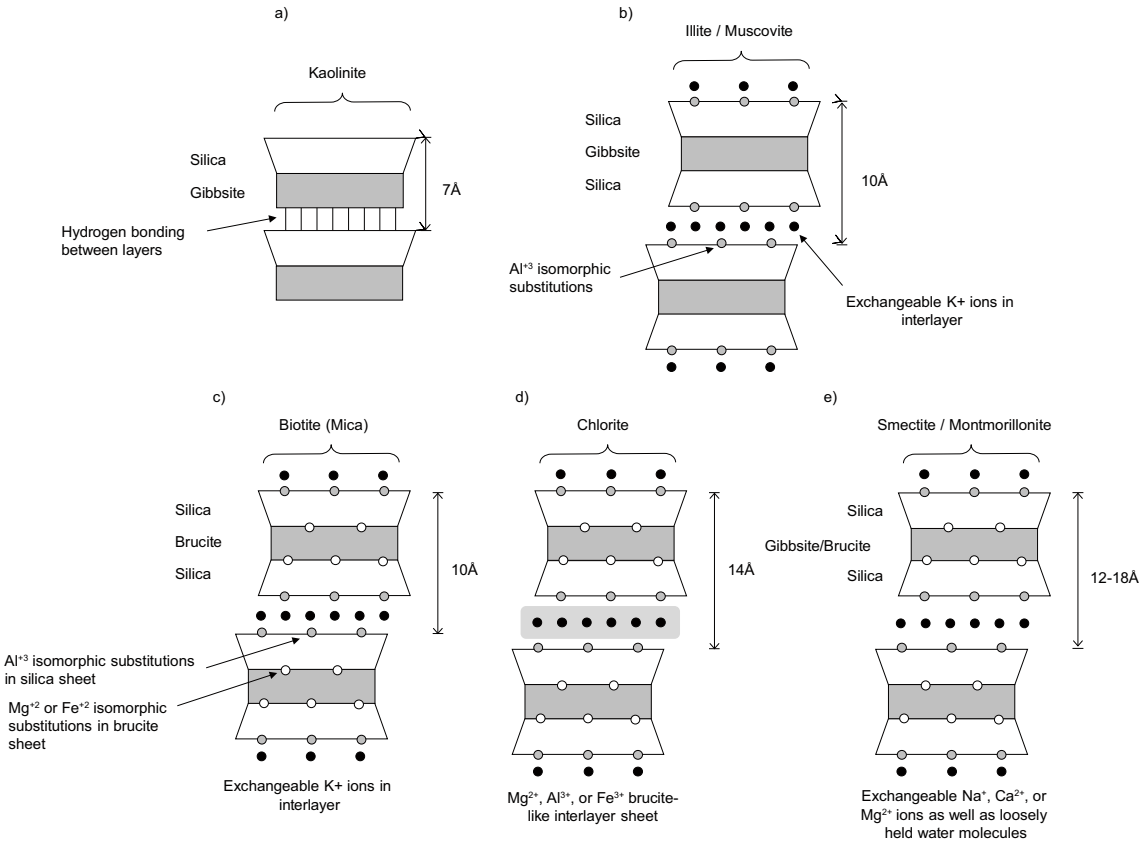

Figure 2-1. *Structure of kaolinite (a), illite/muscovite (b), biotite (c), and minerals belonging to the chlorite (d), and smectite (e) families. All minerals except kaolinite exhibit isomorphic substitutions that result in a charge imbalance that is offset by ions in the interlayer space. Interlayer cations in chlorite are difficult to exchange owing to the brucite-like structure of the interlayer space. Smectites (e) expand and contract upon hydration or dehydration of the interlayer space while the other minerals are non-expanding.*

Silica basal planes (termed *siloxane* surfaces, featuring a repetitive Si-O-Si structure) generally do not contribute significantly to the pH-variable charge component as the bridging bonds are hydrophobic. There is, however, permanent charge at these surfaces arising from isomorphic substitution that will contribute towards the overall CEC of the mineral. At the edges of silica sheets, there may be *silanol* functional groups (Si-OH) that are ionisable. Basal gibbsite planes containing Al-substituted siloxane groups (Al-O-Al) are comparatively more reactive than their true siloxane counterparts and readily contribute to the CEC. The corresponding *aluminol* sites (A-OH) at sheet edges, however, have slightly different reactivity to basal plane Al-substituted siloxane groups and therefore have measurably different reactivity. Analogous functional groups (Mg-OH) and reactive characteristics exist for brucite-like sheet edges. Most Phyllosilicate minerals only have siloxane basal plane outer surfaces as the gibbsite/brucite layers are sequestered between silica sheets. This means that ionisable surface groups essentially only exist at sheet edges in these minerals. In spite of this, the basal plane surfaces do have an ion exchange capacity owing to the permanent charge arising due to isomorphic substitution as well as crystal lattice imperfections.

Although perfectly smooth silica basal planes are characterised by an apparent absence of ionisable surface groups, the sheet structures frequently contain cracks /Brandt et al. 2003/, dislocation cores and stacking faults /Noe and Veblen 1999/, as well as other structural defects that can promote surface reactivity. It is therefore possible for basal planes to have ionisable surface groups at lattice defects, although to a lesser extent than those present at sheet edges owing to their sparse distribution. Broken siloxane bonds at crack defects, for example, form silanol groups when hydrated and thus function in a similar fashion to sheet edge silanol groups. The crack defects are locations where weathering can occur and in strongly weathered clay minerals there is significant pitting and *terrace* etching of the basal planes as they are chemically eroded.

As discussed previously, the internal layers of clay minerals also can participate in ion exchange reactions, thus contributing to the reactivity of these minerals. It should be remembered, however, that the internal surface area of some minerals can be accessed more- or less readily by different cations and the measured CEC is not necessarily a measure of the reactive capacity of the mineral. Cations with very small hydrated radii such as Cs^+, for example, may be able to exchange readily with interlayer K^+ ions in biotite and chlorite whereas larger hydrated cations and aqueous complexes may not be able to access the interlayer regions effectively. Small, hydrated cations can also effectively outcompete cations with larger hydration spheres for edge sites owing to steric effects /Poinssot et al. 1999/.

There is a large body of evidence to suggest that Cs^+ undergoes very strong and selective ion exchange with interlayer K^+ ions in a variety of clay minerals, but most particularly biotite. Although biotite is a minor accessory of granitic rocks, it is of great relevance for retention properties on account of its relatively strong sorptivity for many radionuclides. The CEC of Kaolinite exhibits a strong pH dependence owing to the numerous aluminol sites at externally exposed gibbsite basal planes as well as aluminol and silanol groups at sheet edges. In the case of illites, smectites, and other TOT clay minerals, however, aluminol and silanol groups only exist at the sheet edges and the ion exchange capacity of the basal planes arises entirely due to permanent charge. As permanent charge comprises a larger proportion of the total ion exchange capacity, the CEC of TOT clay minerals is consequently much less sensitive to pH than tectosilicates, oxide, and hydroxide minerals (the CEC of carbonate minerals such as calcite is difficult to place in the context of pH for the reasons outlined previously in Section 2.1.1).

As far as sorption reactivity is concerned, edge sites are thought to be more reactive than basal plane sites. Edge sites are numerically fewer than basal plane sites and it is customary to refer to them generally as *high affinity/low capacity* sites while basal plane sites are referred to as *low affinity/high capacity* sites. It should be noted that this nomenclature is also used to describe different reactive sites on oxide surfaces, which are invoked to explain Langmuir-like behaviour at low surface coverage (more on this later in Section 2.2.2). The relative importance of reactive edge sites increases with decreasing mineral grain size, as they comprise a higher proportion of the overall grain surface area. For clay minerals such as kaolinite that have essentially no accessible internal surface area, the presence of aluminol groups at sheet edges and on external basal planes is very important and their measured CEC varies strongly as a function of particle size. For illites and mica minerals, on the other hand, there is some particle size dependence although the high ion-exchange capacity of the internal layers reduces its overall importance. Cation exchange capacity within the internal layers of clay minerals, however, is not easily accessed and can lead to slow diffusive uptake kinetics. Crushing and grinding of clay minerals may also increase the number of reactive sites on external basal plane surfaces by way of forming new surface cracks.

The framework silicate minerals also contain a variety of lattice imperfections that influence their sorption reactivity. At crystal surfaces these imperfections can include steps, kinks, isolated growth unit outcrops, edge vacancies, surface vacancies, and screw dislocations. These defects arise during crystal growth and are thus an integral feature of mineral structure imprinted already during magmatic differentiation of the rock mineral phases. Crushing and grinding of framework silicate minerals can also create reactive silanol and aluminol groups on external surfaces where chemical bonds are broken. New reactive surfaces can even be created internally as micro fractures or fissures within individual mineral grains. Framework silicates tend to fracture along regular surfaces related to weaknesses in the crystal structure called cleavage planes. Cleavage planes generally coincide with crystal unit cell boundaries, although they are influenced by imperfections and heterogeneities in the crystal lattice.

Tectonic forces and variations of mineral phase density during formation can exert stresses on crystal grains that can lead to the formation of internal micro fractures. Quartz, for example undergoes a volume change upon cooling from 600°C (4–5%) that is significantly larger than other common silicate minerals (1–2%) it may be associated with in granite /Seo et al. 2002/. These stresses in combination with variations in crystal strain due to the presence of dislocations can allow individual crystal grains to develop significant internal microfracturing already during their formation stage. In addition to stress microfracturing within individual mineral grains, the volume change of various mineral phases upon cooling can lead to the formation of grain boundary porosity. Depending upon the degree to which this porosity is interconnected, *deuteric*- (i.e. fluids present already during formation) and *hydrothermal fluids* can access the internal surfaces of the granitic matrix and lead to alteration of the mineral phases.

During weathering of granite, biotite is typically altered to chlorite. This can also be accompanied by the formation of ferric oxide microprecipitates within the rock matrix owing to dissolution of Fe^{2+} ions from the crystal lattice. Feldspars and other tectosilicates undergo alteration or weathering to give muscovite and the other clay minerals (illite, smectite, and mixed layer clays). Clay minerals are generally absent from intact granite, although can form by the more intense weathering processes occurring adjacent to fracture surfaces, particularly where hydrothermal alteration has occurred.

2.1.3 Quantification of sorptive surface area and cation exchange capacity

Surface areas of geological materials are typically measured using the BET method /Brunauer et al. 1938/ which uses nitrogen or argon gas as a probe molecule to gravimetrically assess the mass of a monolayer of adsorbed gas molecules. Although a good proxy for assessing relative sorptive surface areas of pure mineral phases, the correlation between BET surface area and sorptive surface area is less good for mineral mixtures such as granitic rocks owing to the differing sorption site densities of the constituent minerals and their reactivity. It is the relative surface areas of these minerals in contact with the pore water rather than the relative mass or volumetric abundances of the minerals in the rock that determines the overall macroscopic sorptivity for a given total surface area in contact with the porewater. In this report and the other reports comprising SR-Site, the term porewater is used strictly to refer to the water existing in the connected microporosity of the rock. This is a different definition to that typically used in the hydrogeological literature where it usually refers to the water in flow bearing fractures.

Although the BET technique is the most widely used method for surface area measurement, it is less suited to clay minerals owing to the inaccessibility of the interlayer surfaces to the neutral gas probe molecules. There are related techniques that can be used to estimate the interlayer surface area of hydratable and expandable clays (e.g. smectite) although in general they still cannot access the interlayer regions of non-expandable clay minerals such as biotite and illite.

The surface area of tectosilicate minerals is strongly related to particle size and it is not uncommon for smaller crushed rock size fractions (≤ 0.1 mm) to have surface areas 10–100 times greater than particles of mm size and above. Phyllosilicate minerals in granitic rock are usually finely divided and have greater surface areas than the tectosilicates. Typical specific surface areas of phyllosilicate minerals range from 1–10 m^2/g for biotite and chlorite /Malmström et al. 1996, Zazzi 2009/, 65–100 m^2/g for illite, and can be as much as 600–800 m^2/g in the case of smectites such as Na-montmorillonite /Langmuir 1997/. In largely intact granitic rock, however, biotite and chlorite are the most important of the phyllosilicate minerals.

There are a number of methods available for determining the CEC of minerals and mineral mixtures. There are also different meanings and interpretations that can be attached to the measurement results of these methods depending upon discrepancies between conceptual and operational definitions of the CEC. The ion exchange capacity can be operationally defined as the quantity of ions that can be desorbed from a mineral under a given set of experimental conditions (i.e. pH, ionic strength, speciation, solid-liquid ratio, etc.). For cation exchange, this is a measure of a negative surface charge of the material. Depending upon the experimental conditions that have been chosen for the measurement, this operational definition does not always coincide with strict definitions of ion exchange that are used in thermodynamic modelling.

The measurement of CEC usually involves the displacement of *native*, readily exchangeable cations by a *standard* cation whose adsorption can be quantified analytically /Stumm and Morgan 1996/. Many of the older methods use pH buffered contact solutions which may be inappropriate if the pH of the natural system differs from the pH at which the measurement solution is buffered. Today it is generally accepted that the pH at which the measurement is carried out should not differ markedly from the natural pH where sorption is likely to occur in the system in question. Being a sorption process there is also the problem of correct interpretation of experimental results in the light of relevant thermodynamic and kinetic processes (principally diffusion kinetics).

A method that is frequently used in soil science owing to its reproducibility and precision is the $BaCl_2$ compulsive exchange method (ISO 13536). Although accurate, it is a tedious method that requires multiple steps and wet chemical procedures. This method was used in the Forsmark and Laxemar site investigations although was ultimately found to be unsuitable for granitic rock samples

owing to their generally low CEC. A simpler, one step method that allows the simultaneous direct measurement of both the CEC and exchangeable cations is based upon the silver-thiourea ion complex (AgTU). After equilibration, the loss of Ag from solution is measured by means of atomic absorption spectrophotometry (AAS) that also allows the simultaneous measurement of leached cations. For comparative purposes an estimate of CEC can also be made based upon the sum of cation equivalents released during the exchange process.

Another frequently used method is based upon isotope dilution where the solid phase is firstly conditioned by replacement of exchangeable cations with a given index cation (typically Na^+ or Ca^{2+}) and then equilibrated with an electrolyte solution of the same cation ($NaClO_4$ or $Ca(NO_3)_2$) that has been labelled with a radiotracer (^{22}Na or ^{45}Ca) /Baeyens and Bradbury 2004/. The method has the advantage that, being a radiotracer method, it has a high level of sensitivity. A related technique uses rapid tritium exchange and is essentially a quantitative measure of the numbers of hydrated functional groups at the mineral surface.

Cation exchange capacities of common granitic minerals are to some extent dependent on particle size, although more so for tectosilicates since internal surface areas are typically small relative to external surface areas of crushed particles. The CEC of tectosilicates is not particularly interesting since it tends to be dominated by variable charge sites and therefore depends on the pH at which it is measured. The CEC of quartz and K-feldspar, however, has been estimated by /Akiba et al. 1989/ to be roughly in the range 0.1–0.3 cmol/kg for pH in the interval of 6–9. Using isotope dilution techniques /Allard et al. 1983/ reports CEC ranges of 1–2 cmol/kg for biotite, 5 cmol/kg for chlorite and 70–80 cmol/kg for smectites in the pH interval from 5–9.

2.1.4 Aqueous phase chemistry and physicochemical conditions

The chemical composition of groundwater and the reactions between aqueous solutes is of great importance for understanding sorption processes. This influences not only the distribution of radionuclides amongst various aqueous *species*, but also the *ionic strength*. Both of these features have consequences for the distribution of radionuclides between the aqueous and immobile or colloidal solid phases.

It is important to note that both sorption and solubility equilibria (i.e. precipitation/dissolution) may govern the *free concentration* of a solute in a groundwater system by removing or adding it to the aqueous phase. Here, we use the term *solute* to denote any dissolved chemical constituent and the term can therefore refer to the radionuclides themselves or any other substance that one would normally encounter in dissolved form in groundwater. The free concentration of a solute, however, makes up a variable part of the total dissolved concentration of a substance. The distribution of a solute amongst various *species* is termed the *speciation* of the solution.

Influence of speciation

When one or more dissolved species react to form a compound where the individual constituents are held together by chemical bonds rather than by electrostatic forces, the product is termed a *complex*. When discussing the complexation reaction of a specific solute, the dissolved specie with which it reacts is commonly referred to as a *ligand*. Surface complexation is analogous to aqueous phase complexation with the exception that one of the ligands takes the form of a reactive functional group on a mineral surface in the case of surface complexation. The formation of aqueous complexes may greatly affect the distribution of a radionuclide between the aqueous and solid phases both directly and indirectly.

Indirect effects of speciation where the formation of an aqueous complex decreases the sorption and precipitation tendency are commonly important under repository conditions. In many respects, indirect effects of speciation can be likened to a competition between mobile (aqueous) and immobile (surface) ligands to form complexes with a solute. Other indirect effects may occur where other groundwater solutes compete with radionuclides to form complexes with dissolved ligands. This is also analogous to competition amongst groundwater solutes for surface complexation binding sites, which is an example of a direct competitive effect. Direct effects of speciation where an aqueous complex has a greater tendency to sorb than the free solute are also known to occur.

There are a number of different ligands present in groundwater that may influence the speciation of radionuclides. Chief among these are hydroxyl ions (involved in *hydrolysis*), carbonate, and to a lesser extent chloride. Depending on redox conditions, the presence of sulphate or sulphide may also play a role in radionuclide speciation. The role of redox is discussed later as a separate item owing to its overwhelming influence on the mobility of certain radionuclides. In near-surface environments nitrate, small organic acids, *fulvic* and *humic* substances, and bacterial *siderophores* may be important. These ligands, however, are not considered relevant for sorption processes at repository depth and are not considered for the geosphere transport processes in SR-Site (for more information see the SR-Site Geosphere process report /SKB 2010c/).

Two key variables which govern a large portion of radionuclide speciation are the pH and carbonate concentration (or equivalent *partial pressure* of carbon dioxide, pCO_2). These are considered to be of primary relevance for many radionuclides, particularly those that sorb by way of a surface complexation mechanism. To illustrate the complicated interplay between radionuclide speciation, pH, and carbonate it is instructive to consider americium as an example on account of its relatively simple chemistry and insensitivity to redox conditions. The principal hydrolysis reactions involving Am(III) are thought to be:

$$Am^{3+} + H_2O \rightleftharpoons AmOH^{2+} H^+ \quad (2\text{-}1)$$

$$Am^{3+} + 2H_2O \rightleftharpoons Am(OH)_2^+ + 2H^+ \quad (2\text{-}2)$$

$$Am^{3+} + 3H_2O \rightleftharpoons Am(OH)_3 + 3H^+ \quad (2\text{-}3)$$

The relative equilibrium concentrations of Am(III) species can be readily calculated with the aid of a suitable simulation tool such as PHREEQC for a given total concentration of Am(III) dissolved in water containing very little dissolved carbonate (10^{-6} M). The results of this calculation are shown in Figure 2-2 as a function of pH.

If the water contains significant amounts of dissolved carbonate, this can also act as a ligand to bind free Am^{3+} among various dissolved carbonate complexes. The principal carbonate complexes that can be formed by Am(III) according to the SKB thermodynamic database (henceforth, the SKB-TDB /Duro et al. 2006/) are:

$$Am^{3+} + HCO_3^- \rightleftharpoons AmHCO_3^{2+} \quad (2\text{-}4)$$

$$Am^{3+} + HCO_3^- \rightleftharpoons AmCO_3^+ + H^+ \quad (2\text{-}5)$$

$$Am^{3+} + 2HCO_3^- \rightleftharpoons Am(CO_3)_2^- + 2H^+ \quad (2\text{-}6)$$

$$Am^{3+} + 3HCO_3^- \rightleftharpoons Am(CO_3)_3^{3-} + 3H^+ \quad (2\text{-}7)$$

Figure 2-3 shows the effect of a larger fixed total amount of dissolved carbonate (i.e. all free and complexed forms taken together) on the speciation of Am(III). As can be seen from the figure, increasing amounts of dissolved carbonate have an increasing dominance on the speciation of Am(III) at circumneutral pH levels or higher. The binding of Am(III) in carbonate complexes is a form of indirect competitive effect which can potentially reduce the magnitude of sorption if the carbonate concentration is sufficiently high.

Influence of ionic strength

The ionic strength of groundwater exerts a number of direct and indirect effects on sorption depending on the solute concerned and its sorption characteristics. The most obvious ionic strength effect on the partitioning of radionuclides between the solid and aqueous phase involves direct competition of main groundwater components (e.g. Ca^{2+}, Mg^{2+}, Na^+, K^+, etc.) for ion exchange and surface complexation sites. This effect is especially important for ion exchange at permanently charged surface sites. The indirect influence of ionic strength on homogeneous chemical equilibria is well known and can be modelled through the use of activity coefficients in equilibrium mass action equations (see e.g. /Stumm and Morgan 1996/). The activity coefficient is related to the ionic strength I, which is defined as:

$$I = \frac{1}{2}\sum_{i=1}^{n} c_i z_i^2 \quad (2\text{-}8)$$

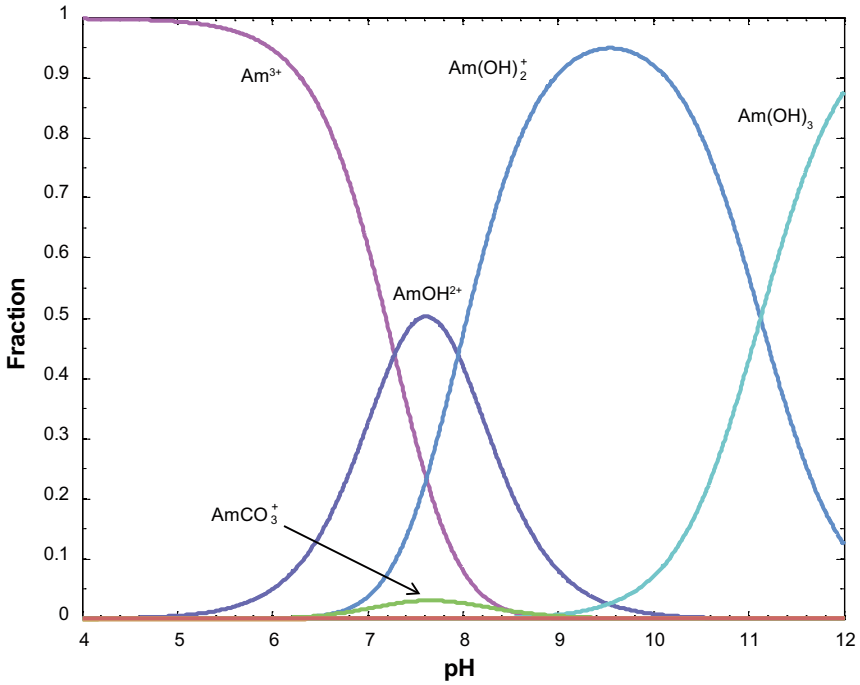

Figure 2-2. *Relative concentration of Am species at equilibrium as a function of pH for a fixed total concentration (10^{-12} M) of dissolved Am(III) and a fixed total concentration (10^{-6} M) of dissolved carbonate. Calculated with the aid of PHREEQC and the SKB thermodynamic database /Duro et al. 2006/.*

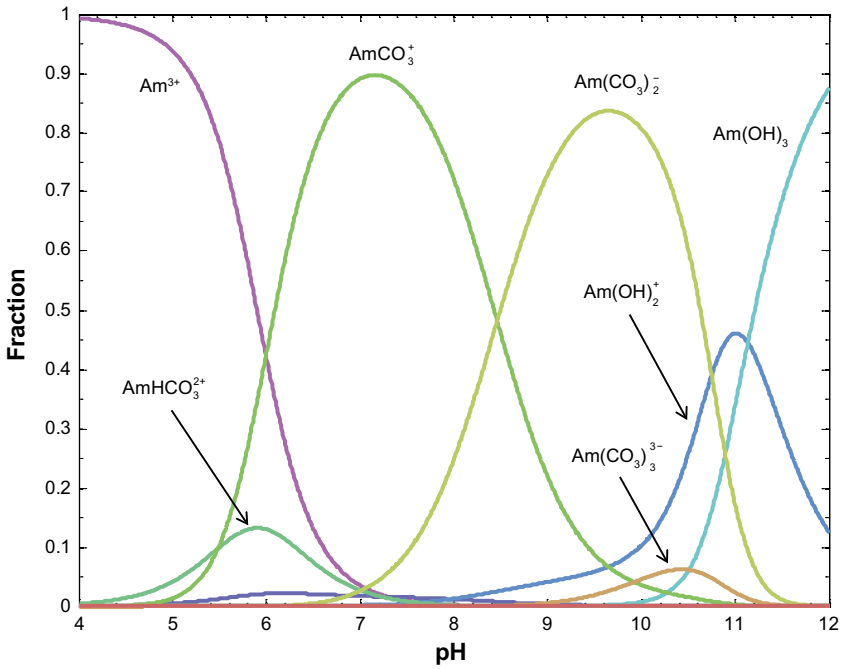

Figure 2-3. *Relative concentration of Am species at equilibrium as a function of pH for a fixed total concentration (10^{-12} M) of dissolved Am(III) and a fixed total concentration (10^{-3} M) of dissolved carbonate. Calculated with the aid of PHREEQC and the SKB thermodynamic database assuming a temperature of 25°C /Duro et al. 2006/.*

Where c_i is the molar concentration and z_i is the charge of ionic species i. The relation between ionic strength and species activity is established through various empirical and theoretical treatments (e.g. the Debye-Hückel and Davies equations, as well as ion association, and specific ion interaction approaches). For a detailed description of these see, e.g. /Grenthe et al. 1997/. Additional ionic strength dependencies are related to surface charge and electrostatic effects in the case of sorption reactions. These are discussed further in Section 2.2.2.

Influence of solubility

The partitioning of radionuclides between the aqueous and solid phases exhibits strongly divergent physical characteristics when the governing processes are precipitation and dissolution rather than surface complexation or ion exchange equilibria. Dissolution and precipitation reactions are, for example, frequently slower than sorption reactions and also may be kinetically hindered even if thermodynamically feasible. In addition, the free radionuclide concentration is independent of the amount or concentration of available solid phase when precipitation/dissolution mechanisms are active. Thus, dissolution and precipitation reactions establish an upper limit on the radionuclide concentration, above which it is physically meaningless to address retention using a K_d-based approach. Having said this, however, it should be noted that dissolution and precipitation do not occur to the exclusion of sorption reactions. Downstream of regions where solubility equilibrium determines the dissolved concentration of a radionuclide, for example, sorption processes would still be expected to govern the transport retardation.

In a broader perspective, this means that while solubility equilibria may govern the concentration of a radionuclide at its source and thus the release rate from a compromised storage canister, the far-field transport retardation is typically mediated by ion-exchange or surface complexation processes. Solubility can also determine the concentration of solutes that compete for sorption binding sites as well as the natural background concentrations of naturally occurring isotopes of a given element. Both of these features are of central importance for establishing relevant conditions for the estimation of conditional K_d values for use in safety assessment calculations.

Under repository conditions, a number of different solid phases, including oxides, hydroxides, carbonates, sulphates, and sulphides have been suggested to control radionuclide solubility. In natural groundwater systems, however, radionuclide concentrations are commonly observed to be lower than that predicted from the solubility of pure mineral phases (e.g. /Bruno et al. 1995, Curti 1999/). This is a phenomenon that has been attributed to the formation of co-precipitates (solid solutions), with lower solubility than the pure phases. While sorption and solubility equilibria are customarily modelled as distinctively separate processes, it has been suggested that they are part of a mechanistic continuum, where ions are incorporated at the solid surface.

Figure 2-4 illustrates the concept of a mechanistic continuum of processes spanning the sorption of a solute merging with surface precipitation and finally pure phase precipitation after a monolayer coverage of the surface has been achieved (e.g. /Zhu 2002/). There are also experimental indications that incipient surface precipitation might even occur prior to full monolayer coverage owing to the formation of polymeric surface complexes of the solute concerned /Katz and Hayes 1995/. The surface gradually accumulates the trace element, thereby forming a solid-solution like phase.

Similar solid solutions can also form through co-precipitation, where the trace element isomorphically substitutes for the host metal during precipitation. In both cases, a surface layer is formed containing the trace metal, which has thermodynamically different properties to the pure solid phase. Co-precipitation of trace metal ions with calcite, barite, and ferric-oxyhydroxides have been most frequently suggested in the scientific literature and the theoretical basis under which these processes are modelled is relatively well-described thermodynamically. Formation of solid solutions can even occur if the host phase is nominally in equilibrium owing to the dynamic nature of such processes where forward (precipitation) and reverse (dissolution) reaction rates are exactly balanced. For a detailed account of these processes see, for example, the state of the art review by the NEA /Bruno et al. 2007/. More recently, co-precipitation phenomena have been suggested as solubility limiting phases in the spent fuel storage canisters and therefore of central importance for estimating near-field release rates. The co-precipitation of radium with barite ($BaSO_4$) is of particular relevance in this respect owing to its potential contribution to far-field dose rates /Grandia et al. 2008/.

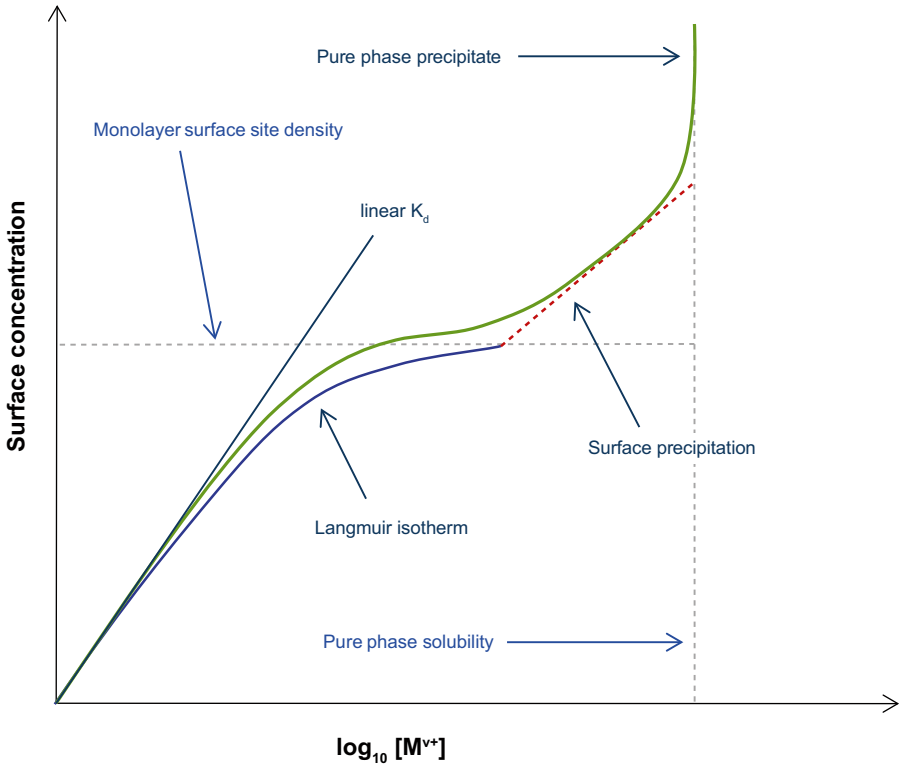

Figure 2-4. *Illustration of the continuum of surface reactive phenomena (green curve) extending from linear sorption (K_d) through, monolayer site saturation (Langmuir isotherm), surface precipitation and finally pure phase precipitation (based on /Zhu 2002/).*

Influence of redox conditions

The redox conditions (as defined by the *redox potential*, Eh) in the groundwater exert a strong influence on radionuclide speciation by way of controlling the predominant valence of radionuclide species present. For some radionuclides (e.g. U, Np, Tc, Pu), redox speciation places an important control on chemical behaviour and thereby also their sorptive properties. This is particularly true for elements that switch between cationic (usually sorbing) and anionic (usually non-sorbing) forms upon changing redox state. Technetium which changes between a cationic +IV and an oxyanion +VII state falls into this category. Other important controls occur where one of the redox states is more readily solubilised or less prone to sorb than the other. Uranium in its oxidised +VI form, for example, is much more soluble than the reduced +IV form, a property that leads to *roll-front* formation in naturally occurring uranium mineralisations which are frequently invoked as natural analogues of repositories for spent nuclear fuel (e.g. /Miller et al. 2000).

The redox state of deep granitic groundwater is largely determined by the presence of redox controlling pairs such as Fe^{3+}/Fe^{2+} and SO_4^{2-}/HS^- and is also related to pH and dissolved carbonate concentration. The Eh of groundwater is extremely difficult to measure accurately and equally difficult to predict on account of slow reaction kinetics involving the redox pairs themselves as well as reactions at measurement electrodes which might involve multiple co-existing redox pairs in disequilibrium (giving rise to so-called *mixed potentials*).

For the purposes of SR-Site it is not altogether clear which of the above mentioned redox couples actually should be controlling groundwater Eh under repository conditions. For this reason, both cases are considered as separate case studies in the groundwater hydrogeochemical simulations used to forecast the evolution of groundwater chemistry in the repository environment /Salas et al. 2010/. For the Fe^{3+}/Fe^{2+} redox pair, equilibrium with $Fe(OH)_3$ is assumed to control the Fe^{3+} concentration using equilibrium constants consistent with the calibration model derived by /Grenthe et al. 1992/. For the SO_4^{2-}/HS^- redox pair, on the other hand, equilibrium with amorphous Fe(II)-monosulphide, $FeS_{(am)}$ is presumed to control the availability of HS^-.

In the previous data compilation /Crawford et al. 2006/ redox conditions were considered to be either strongly reducing or mildly oxidising where a specified reference Eh (–250±100 mV) constituted a broad cut-off between the two. Recommended K_d values were then given for both situations for each radionuclide deemed to be sensitive to redox conditions. In most cases, the reducing form of these radionuclides was presumed to be predominant at repository depth while the oxidising form was typically considered only relevant for the surface environment. This choice was made based on consideration of the most likely range of redox potentials at repository depth and wasn't modelled on a detailed level for individual radionuclides.

In the current compilation, hydrochemical simulation data calculated by /Salas et al. 2010/ (stored in SKB's TRAC system) enabled the detailed examination of redox behaviour for individual elements. The choice of predominant redox state under repository conditions was evaluated by simulation using PHREEQC /Parkhurst and Appelo 1999/ in conjunction with the SKB-TDB /Duro et al. 2006/ at different times during the repository groundwater evolution. This evaluation technique was also extended to the treatment of sorption data where it was deemed necessary to ascertain the most likely redox state present in order to correctly classify the reported data. This is complicated, however, by the fact that for certain elements (principally, Pu) multiple redox states can co-exist simultaneously at equilibrium in nearly equimolar quantities. The situation becomes particularly challenging when one considers that any difference in sorptivity between co-existing redox states might lead to the depletion of the more strongly sorbing state and a consequent readjustment of the redox species distribution in the groundwater under equilibrium conditions. The possibility therefore exists for the relative predominance of redox species to be shifted in the presence of a solid phase relative to that which would be observed in an aqueous phase where sorptive surfaces are absent. These issues are discussed in greater detail in the Appendices to this report where redox speciation is examined on a case by case basis.

It is interesting to note that the prediction of strongly reducing conditions does not necessarily give rise to the most favourable scenario with regard to radionuclide retention. In the case of uranium, for example, strongly reducing conditions would imply both a low solubility of the tetravalent state and strong retention by sorption. The essentially immobile ^{234}U, however, represents a concentrated secondary source of ^{226}Ra which is of considerable significance for calculations of far-field dose rates. If, on the other hand, the groundwater chemistry was to favour the existence of the more soluble and less strongly sorbing hexavalent state, uranium would be mobilised to a greater degree and might not constitute an equally concentrated source of radium daughters. Although the same amount of activity is produced by radioactive decay processes in both situations, the greater dilution of the source in the latter case might give rise to lower far-field dose rates in certain scenarios of repository evolution. This, however, also depends on whether the mobilised uranium is widely disseminated in the geosphere or re-accumulated elsewhere in the system upon encountering altered redox conditions. Owing to this uncertainty, calculations are made in SR-Site for both redox cases in order to account for either possibility.

Although not a direct effect of redox, it should be noted that under certain conditions the retention of radionuclides may be reduced by the presence of strong complexing agents called *siderophores* which are excreted by bacteria. Bacterial siderophores are strong complexing agents released by certain bacteria, usually under oxidising conditions (i.e. when Fe(III) availability is low) by those bacteria that use the Fe(II/III) redox couple as an electron source. These complexing agents can also bind certain radionuclides very strongly, resulting in reduced sorption on geological materials.

Bacteria capable of excreting siderophores have been cultivated from deep groundwater samples obtained at the Äspö Hard Rock Laboratory (HRL) /Johnsson et al. 2006/. It is not currently known whether there is a non-negligible background concentration of these complexing agents within the groundwater from repository depth at the Forsmark or Laxemar sites owing to the difficulty of directly identifying these by routine chemical analysis. Investigations at the Äspö HRL, on the other hand, have confirmed that these substances are not present in the reducing groundwaters typically found at repository depth /Essén et al. 2007/. Given that reducing conditions are expected to prevail at repository depth, however, it is not thought that siderophores should be present in sufficient concentrations to detrimentally impact radionuclide sorption and they are therefore neglected in the data recommendations made for SR-Site.

Influence of temperature

As a general rule, solutes that have exothermic sorption reactions can, on theoretical grounds, be expected to exhibit reduced sorptivity at higher temperatures whereas solutes with endothermic reactions can be expected to have increased sorptivity. Temperature can also have an indirect impact on sorption by altering the species distribution of the solutes in groundwater. By altering the thermodynamic conditions for solution speciation reactions, competitive effects are therefore subtly altered. This direct effect of temperature on reaction equilibrium constants is formalised in the Van't Hoff Equation (e.g. /Langmuir 1997/) which can be used to estimate the effect of temperature:

$$\log \frac{K_1}{K_2} = \frac{\Delta H_r^0}{R}\left(\frac{1}{T_2} - \frac{1}{T_1}\right) \tag{2-9}$$

Where K_i is the reaction equilibrium constant at temperature T_i, parameter R is the universal gas constant, and ΔH_r^0 is the standard enthalpy of the reaction. This expression, however, can only be used if ΔH_r^0 is known and is approximately constant over the temperature interval of interest. In cases where the reaction enthalpy is not constant it is sometimes possible to recast the equilibrium reaction in a so-called *isocoulombic* form where there are identical numbers and types of charge on both sides of the equilibrium reaction equation. Having identical numbers of charge on both sides of the reaction formula allows much of the temperature dependency of the interaction to mutually self-cancel. This is due to the strong temperature dependency of the dielectric constant of water coupled with the fact that the electrostatic interactions between ionic species and water tend to have the strongest influence on the enthalpy of the reaction /Puigdomenech et al. 1999/. An alternative approach used in, for example, PHREEQC is based on the application of an empirical equation of the form:

$$\log K_{eq} = A + BT + \frac{C}{T} + D\log T + \frac{E}{T^2} \tag{2-10}$$

Where parameters A–E are empirical parameters derived by curve fitting actual temperature dependency data, and K_{eq} is the reaction equilibrium constant at temperature T. It is difficult to make robust predictions in groundwater systems where there are many interacting chemical reactions since reaction enthalpy data do not always exist for the full suite of chemical reactions. Extrapolation to temperatures other than the standard temperature of 25°C is therefore fraught with the possibility of error due to internal data inconsistency. This is particularly the case when sorption processes are involved, since reaction enthalpy data for sorption reactions involving relevant minerals generally do not exist at the present time.

It has been noted by /Cronstrand 2005/ that sorption implies a decrease in translational freedom and thus a negative change in entropy, ΔS associated with the process. Since a thermodynamic process at constant temperature and pressure will only occur spontaneously if the change in Gibbs free energy, ΔG is less than zero, this implies exothermicity (i.e. by way of the relation defining the change in Gibbs free energy, $\Delta G = \Delta H – T\Delta S$). Given that temperature conditions in the geosphere are generally expected to be somewhat less than 25°C, one would therefore expect sorptivity to be slightly higher than that established in typical laboratory investigations. This reasoning might only be appropriate for surface complexation reactions, however, since ion-exchange involves displacement of another cation which complicates the interpretation of entropy change. Even in the case of surface complexation, however, one must also consider the entropy change of other processes that must occur for sorption to take place (e.g. deprotonation of surface sites). On the other hand, theoretical analyses for monovalent ions by /Sahai 2000/ using *ab-initio* modelling techniques suggest that cation surface complexation should increase modestly with temperature for most oxides, whereas anion surface complexation is predicted to decrease. Whatever the case may be, the effect of temperature is expected to be small relative to the overall uncertainty of the sorption data and therefore is neglected in SR-Site.

Influence of in situ stress

Although not strictly a chemical effect, in situ stresses have an influence on the sorptivity of rock by reducing access of solutes to the pore system. Increasing stress conditions can compress the available microporous space and pinch off diffusive pathways thereby restricting access to sorption sites. It is therefore possible that the available sorptive surface area under in situ stress conditions might be less than that estimated on the basis of laboratory measurements of BET surface area on intact core samples.

Pore compression does relate to groundwater composition, however, by way of the anion exclusion effect of the electrical double layer (EDL) associated with mineral surfaces in the restricted microporous spaces. The thickness of the EDL is related to the ionic strength of the porewater; the lower the ionic strength, the greater the double layer thickness and vice versa. At sufficiently low ionic strength, contacting or overlapping EDL from adjacent surfaces of micropores may significantly restrict the access of anionic radionuclides to the rock matrix. Anionic solutes, however, tend to have very low sorptivity on account of their preference for positively charged binding sites which are not prevalent at normal groundwater pH levels (ferric oxyhydroxides excluded). In practice this means that their sorptivity is dominated by the free storage capacity of the matrix porewater itself (i.e. the matrix porosity). The effect of this, however, is unclear since it is not currently known by how much the storage capacity decreases on account of pore compression coupled with anion exclusion. Although the effect of anion exclusion is considered in the selection of rock matrix effective diffusivities, the effect on matrix storage capacity is thought to be small relative to other uncertainties and is therefore neglected in SR-Site.

2.2 Overview of sorption modelling approaches

2.2.1 Isotherm based methods

The simplest isotherm based method for modelling sorption is the linear distribution coefficient, or K_d approach. The K_d value (typically given in units of m^3/kg) is simply the ratio of immobilised and dissolved solute that is specific for a particular solid phase composition, water chemistry, and solute concentration. It is an empirical representation of a system that is only strictly applicable under those exact conditions under which it is measured and is not explicitly dependent upon any specific sorption mechanism or speciation considerations. The sorption isotherm is simply defined in terms of the sorbed concentration, S (mol/kg) and aqueous phase concentration, C (mol/m^3) as:

$$S = K_d C \tag{2-11}$$

Although not a physically accurate modelling approach, it is the most widely used owing to the ease with which analytical or numerical solutions can be obtained for transport problems. An intrinsically appealing feature of the linear approach is that it can be very easily related to a retardation effect for solute transport. The retardation effect is a measure of the extent to which the travelling velocity of a solute plume (i.e. a concentration front) is retarded by sorptive interactions relative to the velocity of water. The retardation effect is usually formalised in terms of a retardation factor which is typically defined as:

$$R_f = 1 + \frac{f_e}{\theta_f} \rho_b \frac{\partial S}{\partial C} \tag{2-12}$$

Here, f_e is the fraction of solid material in the medium that can be assumed to be equilibrated with the flowing water, θ_f is the flow porosity of the system, and ρ_b is the bulk density of the solid material. The *sorption intensity*, $\partial S/\partial C$ for the linear isotherm is, of course, equal to the K_d value. In a porous medium, the retardation factor, R_f for a solute undergoing linear equilibrium sorption can therefore be defined as /Neretnieks and Rasmuson 1984/:

$$R_f = 1 + \frac{f_e}{\theta_f} K_d \rho_b \tag{2-13}$$

There are a number of slight variations on this formula depending upon how the variables are defined, but they all have the same physical interpretation as described above. In a discretely fractured system, for example, where the flowing water can equilibrate with the rock matrix to a depth δ_c (δ_t being the transport aperture of the fracture), the average retardation factor for a flowpath, R_f can be written as:

$$R_f = 1 + \frac{2\delta_c}{\delta_t} K_d \rho_b \tag{2-14}$$

The penetration depth, δ_c can be estimated from diffusion theory if the apparent diffusivity of the rock matrix is known and the contact time during which the solute interacts with the rock. Since it is the effective penetration depth associated with solute retardation that is of interest rather than the absolute penetration depth, the appropriate contact time needed to calculate δ_c is not the absolute time, but rather the transport time associated with solute migration /Crawford 2006/.

Other isotherm approaches attempt to capture some of the non-linear behaviour of sorption processes. Here it is important to distinguish between non-linearities that arise due to evolving physicochemical conditions and that arising due to physical properties of the substrate itself. The latter, *classic* non-linearity arises due to the physical limitation implied by the existence of only a finite number of sorption binding sites. In the very simplest case, where there is only a single type of binding site, sorption typically proceeds until the binding sites become fully occupied after which no additional monolayer sorption can take place. This is the basis of the Langmuir isotherm /Langmuir 1918/ which, although originally developed to explain physisorption of gas molecules, is mathematically equivalent to ionic sorption processes of interest in environmental systems. The Langmuir isotherm is frequently given in terms of the fractional occupancy of sorption sites, Γ:

$$\Gamma = \frac{S}{S_{\max}} = \frac{K_L C}{1 + K_L C} \tag{2-15}$$

Where S_{max} is the maximum amount of solute that can be sorbed and K_L is a constant. Even for this most simple of non-linear sorption modelling approaches, difficulties become immediately apparent when a retardation factor is calculated. For a solute that exhibits Langmuirian behaviour, the non-linearity arises because the sorption intensity ($\partial S/\partial C$) varies as a function of aqueous phase concentration:

$$\frac{\partial S}{dC} = \frac{S_{\max} K_L}{\left(1 + K_L C\right)^2} \tag{2-16}$$

The practical consequence of this is that the retardation effect varies depending on which part of the reaction front one considers and the range over which the solute concentration varies. Taking cesium (Cs) as an example, one can surmise that it is not only important to consider the concentration of radioactive ^{135}Cs being transported away from the repository, but also the natural background concentration of non-radioactive ^{133}Cs in the groundwater. If the concentration of ^{135}Cs in the solute plume exceeds the natural background level, then the non-linearity may affect the shape and velocity of the plume. If the concentration of radioactive ^{135}Cs is less than the natural background then the natural background sets the relevant level at which sorptivity should be assessed for transport modelling of the radioisotope.

When one considers the additional effect of non-equilibrium matrix diffusion, the problem becomes even more complex since the solute concentration, and consequently the sorptivity, varies with depth in the rock matrix. Although this can be modelled in numerical transport models with relative ease, the fact that it is not possible to find a closed analytical solution to the migration problem makes the use of the non-linear sorption isotherm less useful for safety assessment in complex hydrogeological settings.

Many solutes start to exhibit non-linearity with regard to solute loading already at concentrations far lower than what would be considered the maximum occupancy. This is generally because different types of sorption sites exist which become successively saturated at different aqueous phase concentration levels. In the case of clays such as illite, for example, it is well known that frayed edge sites (FES) exist with a strong affinity for solutes such as Cs^+ although with a low total sorption capacity (~1% of total CEC). On the other hand, spectroscopic measurements suggest the existence of at least two different sorption sites /Kim and Kirkpatrick 1997/ based upon the interpreted coordination environment of sorbed Cs. As noted by /Baeyens and Bradbury 2004/ this implies at least three different site types in total given that the FES binding sites are too few to be directly identified by spectroscopic methods. The sorption binding sites on pristine surfaces of non-phyllosilicate minerals may also fall into different groups depending on their crystallographic properties and surface reactivity and there is no particular reason as to why only one particular class of binding site should exist. Indeed for rough mineral surfaces, it is likely that there is a range of different binding sites with differing chemical reactive characteristics owing to the local geometry of the surface and the coordination environment of surface reactive groups.

While it is feasible to define multiple surface sites using separate Langmuir isotherms an alternative is to use the Freundlich isotherm. While it could be argued that the Freundlich isotherm sacrifices physical realism (since it does not automatically predict an upper limit to sorptive capacity), it is much simpler than the multi site Langmuir and is often used to model the sorption of solutes that exhibit non-linearities over broad concentration ranges. On the other hand, the fact that there may be many different sorption binding sites with differing sorptive properties means that it might not be possible to realistically parameterise a multisite Langmuir model that satisfactorily captures the non-linearity of sorption over a sufficiently wide range of concentrations. In this respect the Freundlich isotherm could also be considered a more accurate representation of the sorption process itself while being possibly based on

a less rigorous, physical representation. It should be noted, however, that the Freundlich isotherm can actually be derived from first principles using statistical mechanical or kinetic arguments in the same fashion that is possible for the Langmuir isotherm /Appel 1973, Skopp 2009/. In the theoretical derivation, the Freundlich isotherm then represents sorptive behaviour of a surface featuring a multitude of site types with lognormally distributed Langmuir constants. The Freundlich isotherm is defined as:

$$S = K_F C^n \tag{2-17}$$

The sorption intensity ($\partial S/\partial C$) for this isotherm also exhibits a non-linear dependency on aqueous phase concentration:

$$\frac{\partial S}{dC} = K_F n C^{n-1} \tag{2-18}$$

Examples of each of these sorption isotherms are plotted in Figure 2-5 using model parameters taken from /Tsai et al. 2009/ for Cs(I) sorption on crushed granite in contact with deionised water. As can be seen from the plots, each of the isotherms may be useful for modelling purposes in different concentration ranges depending on how experimental data are fitted. Also important to note is the divergence of the different models in different concentration ranges. A K_d value estimated for sorption with a background Cs(I) concentration of 10^{-5} M, for example, would underestimate sorption at much lower concentrations although overestimate sorption at higher concentrations relative to the Freundlich isotherm as illustrated in Figure 2-5. Both the linear K_d and Freundlich isotherm approaches, however, fail to predict saturation at high surface loadings which the Langmuir isotherm does.

Both the Langmuir and Freundlich isotherms as illustrated in Figure 2-5 belong to a class of isotherm described as being *convex*. In the engineering literature they are frequently referred to as *favourable isotherms* since they facilitate more efficient design of separation systems based on adsorption. This is generally true for isotherms where higher aqueous concentrations of solute are associated with reduced sorption relative to that at lower solute concentrations (i.e. the curve of $\partial S/\partial C$ vs. C has a decreasing slope). In a practical sense what this means is that the low concentration leading edge of a solute plume is more strongly retarded than the high concentration regions near the centre of the plume. The fact that different parts of the sorption front move at different speeds, results in a sharpening of the leading edge of the sorption front and a simultaneous broadening of the trailing edge (unrelated to diffusive tailing).

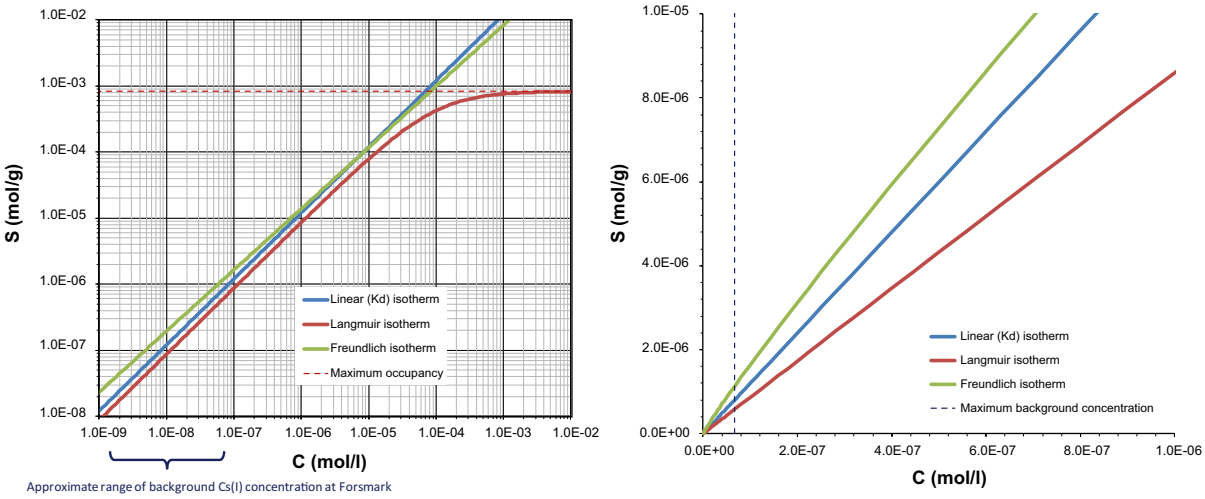

Figure 2-5. *Examples of isotherms commonly used to model Cs(I) on granite shown on log-log axes (left) and linear axes (right). Also shown is the approximate background concentration range of Cs in groundwater at the Forsmark site. Model parameters are taken from /Tsai et al. 2009/ and are for Cs(I) sorption on crushed granite in contact with deionised water.*

Although it is theoretically possible for solutes to exhibit *concave* behaviour (so-called *unfavourable isotherms*) whereby higher aqueous concentrations of solute are associated with greater sorption relative to that at lower solute concentrations, these are not typical of sorption processes relevant for radionuclide transport modelling and do not need to be considered further. It should also be made clear that when concave behaviour is discussed in this sense, we mean purely with regard to the intrinsic non-linearity for the sorbing solute itself. When multicomponent effects are brought into the mix, however, unfavourable behaviour can arise. This is particularly the case for specific classes of ion-exchange reaction where groundwater of one composition displaces groundwater of another composition in an aquifer system.

What is important to realise in the case of the Langmuir and Freundlich isotherms is that it is always possible, in principle, to find a concentration somewhere between the minimum and maximum expected aqueous concentrations where a K_d can be estimated to give the average retardation of the sorption front (however one chooses to define this). The average retardation effect, while useful for risk estimates, does not reproduce details of the leading and trailing edges accurately although in many situations this is a minor issue, particularly with regard to the trailing edge of a solute plume. It is relatively easy to demonstrate this numerically in transport calculations, although it is also a direct consequence of Rolle's theorem for a continuously differentiable function as outlined by /Holzbecher 2000/. As discussed later in Section 2.3.2, this is one of the main justifications for using the linear K_d approach.

There are, of course, many other types of isotherm model that are variations on the basic Langmuir and Freundlich concept. Among these the Tóth, Redlich-Peterson, Dubinin-Radushkevich, hybrid Langmuir-Freundlich, and Frumkin isotherms are noteworthy for their usefulness in modelling aqueous phase sorption processes. A full account of these is beyond the scope of the present document although a very detailed overview is given by /Kinniburgh 1986/. It is interesting to note that the BET method /Brunauer et al. 1938/ used to estimate mineral surface area is also based upon a sorption isotherm model, although being applicable to condensable gas molecules, it also considers multiple layers of adsorbed gas molecules – something that is not strictly applicable to aqueous phase sorption processes of the type discussed here (although it could, in principle, be used to describe surface precipitation).

A particular problem with regard to the simpler sorption isotherm models is that they cannot capture other kinds of non-linearity that might arise, for example, due to changing concentrations of groundwater constituents that compete for the same sorption sites. The simplest isotherm model that can capture competitive behaviour is the multicomponent Langmuir isotherm which is defined for each sorbing solute, *i* as:

$$\Gamma_i = \frac{S_i}{S_{\max}} = \frac{K_{L_i} C_i}{1 + \sum_1^n K_{L_i} C_i} \qquad (2\text{-}19)$$

As can be readily appreciated, the sorption intensity ($\partial S/\partial C$) varies not only as a function of aqueous phase concentration for the migrating radionuclide, but also the concentration of solutes that compete for binding sites. The retardation effect therefore not only has an intrinsic non-linearity related to the concentration of the solute concerned but also a non-linearity related to the spatial and temporal variability of other groundwater constituents. These additional non-linearities can, however, be neglected if sorption experiments are carried out using synthetic or actual groundwater samples that approximate the chemistry of the groundwater under application conditions if it is additionally assumed that the actual groundwater composition is relatively static over the timeframes considered. Over a glacial cycle, this is rarely the case although one still can use simpler sorption modelling approaches in risk assessment calculations if one assumes a pessimistic scenario for groundwater composition as a calculation basis.

There are other multicomponent models, although these have been less adopted in modelling of environmental systems on account of the fact that they are sufficiently complex that mechanistic modelling approaches are often preferable. Some of these models, however, are useful for substrates such as humic substances that are difficult to cast in a mechanistic framework. Examples of some of these approaches are given by /Černík et al. 1996, Rusch et al. 1997, Alkhamis and Wurster 2002, Wu et al. 2002/. It is noted, however, as these models become increasingly sophisticated the boundary between the models regarded as semi-empirical isotherm based methods and the so-called mechanistic models, becomes increasingly blurred. Mechanistic models of sorption are discussed in the next section.

2.2.2 Mechanistic models of sorption

Although some of the sorption isotherm-based approaches described in the previous section can be shown to be thermodynamically rigorous in certain limiting situations, they are generally considered to be semi-empirical in nature. The modelling approaches that are discussed in this section are referred to as mechanistic in that they are more firmly rooted in principles of thermodynamic modelling for chemical reactive processes. In a similar fashion to the semi-empirical approaches, however, it should always be remembered that such models are only as good as the fundamental assumptions underlying their formulation and the quality of the data used to constrain their parameters. It is frequently difficult to extract meaningful parameters for these models without detailed multidimensional datasets and spectroscopic confirmation of sorption mechanisms and they therefore must be deployed with care if subsequently used to inform safety assessment calculations.

Ion exchange models

In the literature it is not always clearly stated what the difference is between ion-exchange and surface complexation models. Generally, however, ion-exchange approaches are used to model purely electrostatic sorptive interactions in association with permanently charged sites. The distinction becomes blurred, however, since sorption of essentially electrostatic nature is also responsible for outer-sphere surface complexation in association with variably charged surface sites. The distinction becomes even more blurred when one considers that the concept of inner-sphere and outer-sphere surface complexation is borrowed from solution chemistry where it refers to the coordination of ionic solutes with polarised groups of water molecules in the hydration sphere of the ion. In some cases, solutes such as Cs^+ effectively lose their hydration sphere when undergoing electrostatic sorption and, for all practical purposes, may be considered de-facto inner-sphere complexes with regard to their coordination environment. Occasionally ion-exchange is used to model processes that may be more accurately described in terms of (outer-sphere) surface complexation mechanisms, and vice versa. It is often unclear in the literature why a particular modelling approach has been adopted and, although frequently justified by observation of an apparent sensitivity of sorption to ionic strength effects, it is rarely defended in a rigorous fashion by way of spectroscopic evidence.

Ion exchange is cast in a mass action formulation of chemical equilibrium which is analogous to that used for other types of chemical reactions. There are a number of different formulations of ion-exchange equilibrium, although they are all characterised by the mass action approach with conditional equilibrium constants called *exchange* or *selectivity coefficients*. They are convenient to work with as their formulation is similar to that used for speciation and dissolution-precipitation equilibria. The main differences between the different formulations of ion exchange equilibria concern differences in the way sorbed component activities are handled. Chemical equilibrium is defined in terms of chemical potentials cast in the framework of the Gibbs-Duhem relation and it is therefore necessary to adopt certain assumptions about the standard states of sorbed components in order to calculate thermodynamically consistent activities and equilibrium constants. For example, in precipitation-dissolution equilibria, the activity of solid phase is always equal to unity (i.e. the reaction is the same regardless of how much or how little solid is present). For ion exchange, however, the concentration or fraction of sorbed substance does influence the equilibrium. Different approaches such as the Gaines-Thomas, Gapon, Vaneslow, and Rothmund-Kornfeld conventions have been developed to account for this.

The Gaines-Thomas convention defines sorbed phase activities based on the equivalent charge fraction (i.e. fraction of the CEC) occupied by sorbed solute. The Vaneslow convention uses mole fractions of exchangeable ions instead of equivalent charge fractions. The Gapon convention, on the other hand, is defined in terms of mole fractions of exchange sites. The Rothmund-Kornfeld approach is essentially a modification of the Vaneslow convention although with an additional semi-empirical exponent for the aqueous phase ions in the mass action formula. Each of these are useful in different situations since the full range of sorptive behaviour over large ranges of surface loading is difficult to model accurately using the mass action approach even though it might be a mechanistically sound description of ion-exchange sorption.

Ion-exchange reactions are usually defined in terms of the sorption of a solute with concurrent displacement of a reference ion. Although other reference ions can be used, Ca^{2+} is typically chosen as the reference in cation exchange since it is frequently the most abundant sorbed cation in environmental systems. If a cation displaces another cation with the same charge (e.g. ion-exchange

of Sr^{2+} and Ca^{2+}) the reaction is termed *homovalent*. If an ion displaces another of unlike charge (e.g. ion-exchange of Na^{+} and Ca^{2+}), the exchange reaction is termed *heterovalent*. Homovalent ion-exchange reactions generally have selectivity coefficients that are approximately constant over wide ranges of surface loading. Heterovalent ion-exchange reactions, however, do not always exhibit constant selectivity coefficients and they must be considered as conditional constants dependent on the particular range of conditions being modelled.

The sorption reaction for Cs(I), for example, is typically written as:

$$2Cs^{+} + CaX_2 \Leftrightarrow Ca^{2+} + 2CsX \tag{2-20}$$

Using the Gaines-Thomas convention, the ion-exchange equilibrium relation is defined as:

$$K_{GT} \cdot \left(\frac{\gamma^2_{Cs^+}}{\gamma_{Ca^{2+}}} \right) = \frac{[E_{Cs}]^2 [Ca^{2+}]}{[E_{Ca}][Cs^{+}]^2} \tag{2-21}$$

Where, E_i is the equivalent fraction of occupied sorption sites for component i and γ_i is the activity coefficient of the aqueous phase component. The selectivity coefficient is K_{GT} to signify that the equilibrium is defined in terms of the Gaines-Thomas convention. Although the K_d value is not dependent on any particular sorption mechanism, it is still possible to define a K_d that operationally describes the ratio of sorbed and dissolved solute in terms of ion-exchange equilibrium equations. For the particular reaction given in Equation 2-20, assuming only trace concentrations of Cs^{+} sorbed on the mineral surface (i.e. $E_{Ca} \approx 1$), and neglecting aqueous phase speciation (and activity coefficients), the K_d for Cs(I) sorption could be given approximately as:

$$K_d = \frac{[E_{Cs}]CEC}{[Cs^{+}]} \approx CEC \sqrt{\frac{K_{GT}}{[Ca^{2+}]}} \tag{2-22}$$

From inspection of the form of Equation 2-22, it should be clear that K_d as it is defined here is conditional on the particular concentration of Ca^{2+} in the groundwater and therefore the K_d can be shown to vary with groundwater ionic strength as reflected by the aqueous Ca^{2+} concentration (also noting that sensitivity of sorption to ionic strength is a hallmark of ion-exchange).

Although this very simple treatment illustrates very simple competitive behaviour in a binary system, the neglect of competition from other cations in the groundwater seriously limits the applicability of Equation 2-22. For more complex groundwater systems, a range of competing ion-exchange reactions need to be considered to calculate the sorbed phase partitioning (or an abstracted conditional K_d value) for a given groundwater composition. A full account of competitive ion-exchange equilibria, however, is beyond the scope of this document and the reader is directed to texts such as e.g./ Appelo and Postma 2005/ or the review article by /Haworth 1990/ for more detailed explanations.

Surface complexation models

In the last thirty years or so, surface complexation models or SCM's have become increasingly popular modelling tools for predicting the transport of solutes in environmental systems. These approaches attempt to model sorption in a similar fashion to aqueous phase complexation reactions while simultaneously accounting for electrostatic interactions with surface functional groups of variable charge. These models are more flexible than ion exchange models as they consider the influence that pH has upon surface charge. In addition, surface complexation models can also model adsorption of trace solutes against the net surface charge of the sorbent /Langmuir 1997/, noting that the net charge simply reflects the overall distribution of positive and negatively charged sites.

When formulating a surface complexation model, it is necessary to define chemical reactions describing the protonation-deprotonation behaviour of surface reactive groups as well as the binding reaction for the sorbing solute under consideration. Sorption models are typically described as being 1-pK or 2-pK depending on how their pH dependent surface charge characteristics are modelled. The pK terminology derives from the corresponding usage for the dissociation of acid molecules in water and is equal to the negative logarithm of the acid dissociation constant ($-\log_{10}K_a$). The most common approach described in the literature is based on the 2-pK formalism since it is conceptually thought to most accurately mirror the true reaction mechanism. As pointed out by /Borkovec 1997/, however, this is actually an erroneous

assumption even though the 1-pK and 2-pK models can be shown to be mathematically equivalent in many situations. This does not necessarily mean that the 1-pK approach is more correct since both may be considered to be approximations of a more complex reality. In the 2-pK approach, the proton mediated ionisation reaction of a surface site is conceptualised to consist of two sequential steps:

$$>SOH^{+}_{2} \Leftrightarrow >SOH + H^{+} \qquad pK_{a1} \qquad (2\text{-}23)$$

$$>SOH \Leftrightarrow >SO^{-} + H^{+} \qquad pK_{a2} \qquad (2\text{-}24)$$

In the 1-pK approach, on the other hand, only one reaction is used:

$$>SOH^{+\frac{1}{2}}_{2} \Leftrightarrow >SOH^{-\frac{1}{2}} + H^{+} \qquad pK_{a} \qquad (2\text{-}25)$$

The reason why the reaction mechanism implied by reaction Equation 2-23 and 2.24 might not be a strictly correct physical interpretation is because when two protons bind to a single oxygen atom, the difference between successive pK values is sufficiently large ($\Delta pK > 10$) that only one reaction step can be reasonably observed within the normally accessible pH range /Hiemstra et al. 1989b/. Instead of envisaging only a single ionisable surface group, the correct physical interpretation of the 2-pK model is based on consideration of a pair of adjacent ionisable groups coordinating a single metal ion. This alternative conceptual picture can then more readily explain the smaller difference between successive pK values ($\Delta pK \sim 2–4$) estimated from 2-pK model fitting to experimental titration data /Borkovec 1997/.

The particular form of the 1-pK reaction can be explained through consideration of the bond valence principle as described by /Hiemstra et al. 1989b, 1996, Venema et al. 1998/. Since (hydr) oxides of trivalent metals such as Al^{3+} and Fe^{3+} are frequently found in octahedral coordination to six oxygen atoms, the Pauling bond valence principle /Pauling 1929/ states that each oxygen atom must neutralise one sixth of the charge of the metal atom. For a trivalent metal atom this gives a bond valence of +½ for a binding site with the oxygen atom coordinating a single metal centre. The fractional charge associated with the bond implies that the hydroxyl group cannot be neutral thus giving rise to the canonical fractional charges in Equation 2-25. Since an additional protonation step is unlikely in the normal pH range, only one pK_a value is required to describe the surface protonation behaviour /Rosenqvist 2002/. Although fractional charges cannot physically exist as such, it should be remembered that this is merely a formal statement of the charge balance for a site and is essentially a mathematical convenience /Hiemstra et al. 1989b/.

In the case of gibbsite ($Al(OH)_3$), both singly-coordinated *aluminol* surface groups (AlOH), and doubly coordinated (Al_2OH) surface groups exist, although with differing distributions on different crystal faces. Generally, the doubly coordinated groups are neutral at normal groundwater pH and are resistant to both protonation and deprotonation reactions. Similar properties can be found for ferric oxides and oxyhydroxides on account of their analogous coordination structure. For silica surfaces, there are *silanol* groups (SiOH) where an oxygen atom coordinates with a single Si atom, and *siloxane* groups (Si_2OH) where an oxygen atom coordinates with two Si atoms. The doubly coordinated siloxane groups have a sufficiently high pK_a value that are very difficult to protonate and may be considered for all practical purposes inert under normal groundwater conditions. Since the central Si atom (+4 charge) is tetrahedrally coordinated with four oxygen atoms in silanol groups, this gives a bond valence of +1 and thus a formally neutral surface hydroxyl group. Silanol groups can deprotonate readily, although are difficult to protonate at normal groundwater pH. This means that the surface charging properties of quartz is largely determined by the deprotonation of the singly coordinated silanol groups /van Hal et al. 1996/.

As this discussion suggests, the situation differs for oxygen atoms in different coordination environments with metal atoms of different valence (i.e. charges other than ±½ are possible in the 1-pK framework) and also predicts that different faces of mineral crystals, on theoretical grounds, can be shown to have different reactive properties. This realisation is the central theme around which the MUSIC /Hiemstra et al. 1989a, b/ and more recent CD-MUSIC /Hiemstra and Van Riemsdijk 1996/ modelling approaches are organised. The fundamental difference between these is that the MUSIC model essentially only describes protonation-deprotonation reactions and surface charge development, whereas the CD-MUSIC model expands the description to include surface complexation reactions of other solutes. In the MUSIC framework, intrinsic pK_a values are estimated theoretically based on explicit consideration of the coordination environment of surface groups.

Although the 2-pK approach is most widely used, there are obvious advantages to the 1-pK approach since it requires one less fitting parameter to model the pH dependent charging behaviour of mineral surfaces. In principle, the proton binding constant in the 1-pK model can be estimated theoretically although this assumes a pristine surface which is rarely the case for real minerals. One typically performs rapid pH titrations of a mineral surface in contact solutions of different ionic strength to distinguish the surface charge characteristics from electrostatic effects. Proton binding constants for the 2-pK reactions are customarily derived by non-linear least squares fitting or, in earlier works, by graphical methods. The 1-pK model is simpler in that the pK_a for the reaction is numerically equal to the negative value of the pH at the pristine point of zero net proton charge (pH_{PZNPC}), although this is not always easy to assess since it is not necessarily the same as the point of net zero charge (pH_{PZC}) as noted in Section 2.1.1. In the 2-pK version, the arithmetic average of the pK_{1a} and pK_{2a} constants is equal to the pH_{PZNPC}. For all practical purposes both models perform identically well. There are, of course, many additional issues that need to be carefully considered when performing surface titrations, particularly biasing effects related to electrode kinetics, mineral dissolution, and diffusive disequilibrium.

Having established the pH dependent charge characteristics of the substrate, it is necessary to perform sorption experiments for range of different contact water compositions that probe the parameter space of the postulated reaction mechanism. Typically in the literature the focus is upon measurement of the pH sorption edge for a solute given that pH has a very strong influence on sorption. A typical template for a metal cation sorption reaction is written in the 2-pK formalism as:

$$>SO^- + M^{v+} \Leftrightarrow >SOM^{v-1} \qquad K_M \qquad (2\text{-}26)$$

In the 1-pK formalism, one might write for an equivalent monodentate reaction:

$$>SOH^{-½} + M^{v+} \Leftrightarrow >SOHM^{v-½} \qquad K_M \qquad (2\text{-}27)$$

Although the parsimony of 1-pK approach is compelling with regard to the description of protonation-deprotonation reactions of surface groups, the less intuitive form of the metal binding reaction may partly explain the enduring popularity of the 2-pK based modelling approaches. A further complication with 1-pK modelling of solute surface complexation (at least for CD-MUSIC) is that the theoretical framework implies several possibilities for the *denticity* of the reaction both with regard to the binding of the sorbing solute itself as well as whether the multi-dentate reactive groups are coordinated to *geminal* (same) or *vicinal* (adjacent) metal centres. Resolution of these issues typically involves synthesis of detailed information derived from crystallography and X-ray spectroscopic measurements of coordination environments of surface sorbed species. This does not seek to claim that multi-dentate surface complexes are not feasible in the other modelling approaches, but the possibility is frequently disregarded in modelling and a simple mono-dentate reaction template is typically assumed. Multi-dentate surface complexation reactions are also problematic since there is no theoretical basis currently available for prediction of surface species activity coefficients (see, e.g. the preface commentary in /Lützenkirchen 2006/). For the monodentate case this is avoided since activity coefficient terms mutually self cancel in the numerator and denominator of the mass action equation. Some investigators ignore this by assuming activity coefficients of unity (e.g. /Appelo and Postma 1999/) while others introduce a surface activity correction term as an additional fitting parameter (e.g. /Dyer et al. 2004/).

Usually a simple electrolyte background solution is used in sorption experiments, typically $NaClO_4$ of some specified ionic strength, to avoid the confounding effect of additional side reactions and competitive sorption with other groundwater constituents. The implicit assumption is that if the postulated reaction mechanism is correct, then additional complexity in the form of additional aqueous phase reactions and competing sorption reactions can be added later in forward modelling without invalidating the model. As noted previously, this constitutes an extrapolation outside of the range of model calibration and should only be done with great care unless reaction mechanisms can be properly validated with spectroscopic measurement data.

A more cautious approach, of course, is to carry out sorption experiments where all groundwater variables of relevance are varied throughout their expected range of variability. At the very least this would involve pH and carbonate as master variables with a groundwater of approximately the same composition as that expected under application conditions (including minor solutes that compete for sorption sites). Even this, however is a large undertaking as a considerable number of independent measurements need to be made to obtain statistically assured data even with an optimised experimental design.

Handling of electrostatic effects

The different SCM's are very similar, differing largely in the way in which electrostatic interaction is handled. Electroneutrality in the solution is always maintained by a loose cloud of electrolyte counter ions adjacent but delocalised to the mineral surface. This is referred to as the *electric double layer* or *diffuse double layer* and exactly counterbalances the net surface charge of the mineral. The physical mineral surface including functional groups and adsorbed ions is referred to as the *Stern* layer and its charge is equal to the sum of permanent charge, net proton charge due to binding of protons or hydroxyl ions, as well as the charge due to inner-sphere and outer-sphere surface complexes. Inner sphere complexes are those formed by direct covalent bonding between a non-hydrated ion and a surface functional group. Outer sphere complexes are those, for example, involving hydrated ions where the ion itself is not directly bound to the surface ligand, but rather by proxy via its associated water molecules. Ions sorbed as inner-sphere complexes are said to belong to the *inner Helmholtz plane* (or *o*-plane), while outer sphere complexes are said to belong to the *outer Helmholtz plane* (or *β*-plane), which is also the boundary of closest approach for ions in the diffuse layer. The outer boundary of the ions in the diffuse layer where the ionic composition is approximately the same as the bulk is referred to as the *d*-plane.

Based on the fundamental principal of electroneutrality, the balance of different surface charge contributions and that of the diffuse layer must sum to zero (e.g. /Stumm and Morgan 1996/):

$$\sigma_P = \sigma_F + \sigma_H + \sigma_{IS} + \sigma_{OS} \quad (2\text{-}28)$$

$$\sigma_P + \sigma_d = 0 \quad (2\text{-}29)$$

Here, σ_F is the permanent charge (see Section 2.1.1), σ_H is the net proton charge, σ_{IS} is the charge of inner sphere surface complexed species, σ_{OS} is the charge of outer sphere surface complexed species. The total net surface charge, σ_p is balanced by the charge associated with the swarm of counter-ions comprising the diffuse layer, σ_d.

In most modelling approaches, however, it is not strictly important to distinguish between the first three terms in Equation 2-28 and one typically defines the charge balance in terms of the net charge of the *o*-plane ($\sigma_F + \sigma_H + \sigma_{IS}$), *β*-plane ($\sigma_{OS}$), and *d*-plane ($\sigma_d$):

$$\sigma_0 + \sigma_\beta + \sigma_d = 0 \quad (2\text{-}30)$$

Since mineral surfaces with significant numbers of surface reactive groups tend to have small permanent charge contributions, σ_F is typically neglected. For basal and interlayer planes of phyllosilicate minerals, however, the opposite is true and this is one of the reasons why ion-exchange is frequently modelled as a separate phenomenon to surface complexation.

The distribution of electrical potential between the surface and the solution represents an energy barrier that influences surface complexation by way of the work that must be done in moving ions across the potential gradient between the charged surface and the bulk solution. As there is no direct way of determining the activity of ions at the mineral surface it must be related to the activity in the bulk solution by taking into consideration the electrostatic work incurred in moving charges to and from the bulk solution and surface. This electrostatic effect is corrected for using the Boltzmann distribution in accordance with the Guoy-Chapman theory of the diffuse double layer.

Since the Gibbs free energy of a surface complexation reaction is made up of a chemical reaction term and a Coulombic contribution, the apparent equilibrium constant for an inner sphere surface complexation, or protonation reaction can be given in the form /Appelo and Postma 2005/:

$$\log_{10} K^{IS}_{\text{app}} = \log_{10} K^{IS}_{\text{int}} + \frac{z F \psi_0}{RT \ln 10} \quad (2\text{-}31)$$

Here, z is the charge number of the surface species, F is Faraday's constant, R is the universal gas constant, and T is the absolute temperature. The variable ψ_0 is the surface potential. Since the surface potential cannot be measured directly, it is necessary to estimate the surface charge, σ and then calculate the potential using a physical model that relates charge and surface potential. The Coulombic contribution (second expression on the right in Equation 2-31) can be considered an electrostatic correction term to the standard mass action expression that one would construct for a surface com-

plexation reaction at equilibrium. It should be noted that although the intrinsic constant K_{int} does not change with solution ionic strength, the apparent equilibrium constant, K_{app} is influenced by ionic strength (and therefore only a *conditional constant*). When deriving protonation/deprotonation and solute binding constants for a variably charged surface it is therefore important to be able to separate the chemical and Coulombic contributions.

In general, all SCM's use the same electrostatic correction factor as defined by Equation 2-31. The main difference between the various SCM's, however, depends mainly upon how the spatial distribution of covalently bonded and electrostatically bonded counter ions is conceptualised. The implicit assumptions in these have consequences for how electrical potential is calculated and the range of phenomena that can be modelled. The different main types of surface complexation models that are discussed in the literature fall into the types illustrated in Figure 2-6.

The simplest model that can be conceptualised, however, neglects electrostatic charge entirely and simply models the surface complexation reactions using conditional equilibrium constants that are not corrected for electrostatic effects. This is referred to as a non-electrostatic model (NEM). Since the thickness of the electrical double layer and consequently, the work required moving charges from the bulk solution to the interface is dependent on ionic strength, one implication of the NEM is that ionic strength effects cannot be modelled and the model is only strictly valid for an approximately fixed groundwater ionic strength.

Constant Capacitance Model (CCM)

In the constant capacitance model (CCM) /Schindler et al. 1976/, it is assumed that both specifically adsorbed ions as well as electrostatically bound counter ions are held tightly in a single layer at a distance exactly adjacent to the surface and no distinction is made between the *o*- and *β*-planes and the diffuse layer. The surface potential, ψ_0 is calculated by assuming that it is balanced by a layer of counter-ions in a physical analogue to a parallel plate capacitor. In this physical model, the variation of electrical potential with distance is linearly related to the surface charge by way of the capacitance of this layer which is treated as a fitting parameter:

$$\sigma_p\ (C/m^2) = C\psi_0 \qquad (2\text{-}32)$$

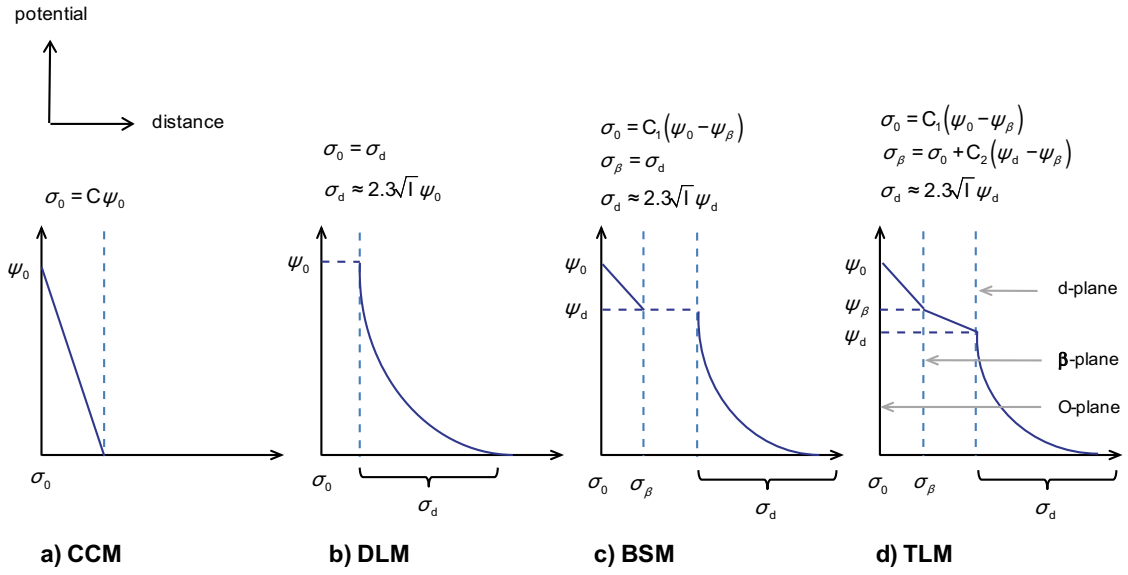

Figure 2-6. *Illustration of different types of surface complexation models differing mainly in the conceptualisation of surface charge. Models shown are a) constant capacitance model (CCM), b) double layer model (DLM), c) basic Stern model (BSM), and d) triple layer model (TLM).*

Since the model is abstracted to a single layer, only inner sphere surface complexes can be modelled with this approach. The model was originally developed for low surface potential and high ionic strength situations where the diffuse layer is sufficiently collapsed that the bulk composition of the aqueous phase and the diffuse layer are roughly the same /Lützenkirchen 1999/. Model parameters are therefore conditional in nature and cannot be extrapolated far outside the range of ionic strength calibration. Although simple, its usefulness stems from the fact that being conditional with regard to ionic strength, it is not necessary to characterise electrolyte binding constants as is necessary for the BSM and TLM approaches.

Diffuse Double Layer Model (DLM)

In the widely used diffuse double layer model (DLM), no distinction is made between the *o*- and *β*-planes, although electrostatically held ions are consigned to the diffuse layer /Stumm et al. 1976/. Similarly to the CCM, only inner sphere surface complexes can be modelled using this approach and therefore the full range of competitive effects between weakly and strongly binding ions cannot be modelled. In this model it is furthermore assumed that there is no potential difference between the surface and the boundary of the *β*-plane and that the electrostatically held ions are dispersed normally to the surface according to a Boltzmann distribution. This gives an exponential decrease in potential with distance from the *β*-plane to the diffuse layer boundary. The DLM is versatile since it is applicable over a wider range of ionic strengths than the CCM approach.

In the DLM, the surface charge is related to the potential by way of a theoretical expression derived from Guoy-Chapman theory (although it is noted that this has also been criticised for not being a physically realistic representation /Fawcett 2006/). For a *symmetric* electrolyte where all major cations and anions are of the same valence, the relation between surface charge and surface potential is given by:

$$\sigma_P\ (\mathrm{C/m^2}) = \sqrt{(8\varepsilon\varepsilon_0 RT)\,I}\,\sinh\left(\frac{F\psi_0}{2RT}\right) \approx 2.3\sqrt{I}\,\psi_0 \qquad (25^\circ\mathrm{C}) \qquad (2\text{-}33)$$

One reason for the popularity of the DLM is that the conditional capacitance of the model is fixed by theory rather than being treated as a fitting parameter and that the square root dependence on ionic strength allows extrapolation to a wider range (i.e. low to mid-range) of ionic strengths than can be considered using the CCM.

A variation of the DLM, known as the basic Stern model (BSM) /Bowden et al. 1977/, differs in that a capacitance is assumed over the interval between the surface and the *o*-plane, with a constant potential assumed between the *o*- and *β*-planes. This model allows for the formation of outer sphere complexes which makes it more similar in many respects to the TLM approach. The basic Stern model, however, requires additional adjustable parameters as discussed below for the TLM.

Triple Layer Model (TLM)

In the triple layer model (TLM), a distinction is made between the *o*- and *β*-planes and, as previously, a Boltzmann distribution describes charge delocalisation in the diffuse layer /Davis et al. 1978, Davis and Leckie 1978, Righetto et al. 1995/. In this model, however, the capacitance between the surface and the *o*-plane, and between the *o*- and *β*-planes are considered together with the distribution of charge in the diffuse double layer. The abstraction to three layers allows for the modelling of outer sphere surface complexes which includes binding of ions belonging to the background electrolyte. Since outer-sphere surface complexes are delocalised from the surface, the electrostatic correction term in Equation 2-31 needs to be adjusted to take this into account:

$$\log_{10} K^{\mathrm{OS}}_{\mathrm{app}} = \log_{10} K^{\mathrm{OS}}_{\mathrm{int}} + \frac{z\,F\left(\psi_0 - \psi_\beta\right)}{RT\ln 10} \qquad (2\text{-}34)$$

The abstraction to three layers, however, implies additional adjustable parameters in the form of the layer capacitances and electrolyte ion binding constants that need to be fitted to experimental data. The additional complexity of the TLM means that it is able to simulate competitive behaviour between weakly sorbing (outer sphere) and strongly sorbing (inner sphere) surface complexes and is workable over a much wider range of ionic strengths than the DLM. For systems where the expected

aqueous phase can change from non-saline to strongly saline conditions over time, this modelling approach is arguably the most versatile. The increased versatility comes, however, at the expense of increased model complexity with additional adjustable parameters.

A variation on the concept of the triple layer model, which accounts for different types of surface site is the charge distribution, multisite complexation (CD-MUSIC) model /Hiemstra and Van Riemsdijk 1996/. This modelling approach is different in that the binding constants can be, at least in principle, determined by theoretical consideration of the coordination environment of surface reactive groups. In practice there are additional uncertainties in the formulation of typical surface complexation problems that necessitate fitting of model parameters to experimentally measured sorption isotherm data. Unlike the other modelling approaches, however, CD-MUSIC does appear to provide a theoretical framework within which molecular level information can be combined with macroscopic measurement data in an internally consistent mechanistic description. Although very promising, a lack of data for minerals of interest in environmental systems, the need for detailed consideration of crystallographic and spectroscopic information, and the wide popularity of the simpler DLM has meant that uptake of this modelling approach has been slow.

Practical considerations related to SCM modelling approaches

The various surface complexation models described above are useful in different situations depending on the range of behaviours that one intends to model. The CCM model for instance is not much better than the NEM model since it is restricted to the ionic strength corresponding to that of the contact solutions used for laboratory experiments from which binding constants are derived. The DLM model is more versatile in that it is relatively simple and applicable to wider range of groundwater compositions although mostly restricted to relatively low ionic strengths. The main disadvantage with these approaches is that competition between inner and outer-sphere surface complexation reactions cannot be handled. For solutes where mixed inner and outer sphere sorption may be important, these modelling approaches are not always satisfactory. It should also be noted that the chemical kinetics of certain sorption reactions is known to be related to the interplay between inner and outer sphere surface complexation mechanisms /Hachiya et al. 1984, Hayes and Leckie 1987, Wehrli et al. 1990/. In order to model inner and outer sphere equilibrium competition and indeed, chemical kinetics of sorption, one must turn to one of the TLM based modelling approaches.

One of the greatest weaknesses associated with surface complexation models, particularly the various forms of the triple layer model, is the number of adjustable parameters that need to be fitted to macroscopic experimental data. Surface complexation models are very sensitive to certain parameters and it is frequently not possible to obtain an optimised set of reaction constants and capacitances that uniquely describe the system being modelled. It is also difficult to properly separate intrinsic and electrostatic effects given that only a very approximate correction is possible in the Guoy-Chapman derived framework. Parameters derived for a particular model (e.g. DLM, TLM, etc) are not transferrable between different modelling approaches and generally the raw data must be reinterpreted to provide model specific parameters.

Validation of these models also typically requires some kind of spectroscopic supporting evidence to show that the reaction mechanisms are reasonable given that one can obtain very convincing fits to data using reactions that are plausible although entirely fictive. As a means of interpolating data sets this is not necessarily a large deficiency since quantitatively accurate results are obtainable even if mechanistic attributes are uncertain. In the absence of very detailed supporting data, however, these models are best not used to make predictions of sorption outside of their range of calibration since their intrinsic non-linear nature can result in strongly deviating and physically non-meaningful results.

As pointed out by /Kulik 2006/, even these very sophisticated modelling approaches can only strictly simulate Langmuir isotherm behaviour with the added possibility of changing populations of surface reactive sites due to evolving bulk solution chemistry. More complex, non-ideal behaviour involving site heterogeneities, lateral interactions, and surface precipitation cannot be modelled in a mechanistically correct manner using these techniques even though there are some semi-mechanistic extensions to the basic models (e.g. /Farley et al. 1985/) that have been proposed to model a wider continuum of processes.

In one of the earliest and most widely known implementations of the DLM /Dzombak and Morel 1990/, it was found that the non-linear appearance of the sorption isotherm for cation adsorption on ferric oxyhydroxides required the definition of two different classes of surface group referred to as *strong* and *weak* sites, respectively. The particular form of the sorption isotherm also requires the strong sites to be few in number whereas the weak binding sites are more numerous. Although mechanistically reasonable and an overall successful modelling technique, there is little spectroscopic support for the particular assumptions inherent in this scheme and it is essentially a semi-empirical approach to modelling sorption heterogeneity. Although approaches such as the CD-MUSIC model attempt to place certain classes of heterogeneity on more mechanistically anchored footing, there are still large gaps in understanding and the availability of data that hamper the deployment of such models in predicting sorption in even simple systems and much less, complex mineral assemblages such as granite.

In spite of this, the ability to model Langmuirian behaviour with dynamic populations of binding sites is a great achievement and must be acknowledged as vastly superior to the assumption of a constant K_d at least in terms of its mechanistic explanatory ability even if not as useful for risk assessment calculations. To illustrate the relation between a simple SCM and the Langmuir isotherm it is useful to consider a simplified example. Here, we shall consider a DLM formulation (actually NEM, as electrostatics are neglected) since this is arguably the most practical for illustrative purposes. Assuming a 1-pK model for pH dependent surface charge and neglecting aqueous phase activities, the mass action equilibrium equations can be given as:

$$K_a = \frac{\left\{>\mathrm{SOH}^{-½}\right\}\left[\mathrm{H}^+\right]}{\left\{>\mathrm{SOH}_2^{+½}\right\}} \cdot \exp\left(-\frac{F\psi_0}{RT}\right) \tag{2-35}$$

$$K_M = \frac{\left\{>\mathrm{SOHM}^{v-½}\right\}}{\left\{>\mathrm{SOH}^{-½}\right\}\left[\mathrm{M}^{v+}\right]} \cdot \exp\left(-\frac{vF\psi_0}{RT}\right) \tag{2-36}$$

Although there are different conventions for defining the activity of the surface species, for the purposes of this discussion we can define them in terms of mole fractions of surface sites. There has been much discussion in recent years concerning appropriate standard reference states for sorbed surface species since the density of charged sites per unit surface area used in the electrostatic correction term is very sensitive to the estimated surface area of the mineral surface. A full discussion concerning this is beyond the scope of this report although a detailed overview of some of the most important issues is documented in /Sverjensky 2003/.

The mole fraction of different surface species must sum to unity, and thus in our particular example:

$$1 = \left\{>\mathrm{SOH}_2^{+½}\right\} + \left\{>\mathrm{SOHM}^{v-½}\right\} + \left\{>\mathrm{SOH}^{-½}\right\} \tag{2-37}$$

If the electrostatic correction terms are neglected, Equation 2-35–2.37 can be combined to give:

$$\left\{>\mathrm{SOHM}^{v-½}\right\} = \frac{\left[\mathrm{M}^{v+}\right]K_aK_M}{\left[\mathrm{H}^+\right] + K_aK_M\left[\mathrm{M}^{v+}\right] + K_a} \tag{2-38}$$

It is easy to see that Equation 2-38 is analogous to that for a Langmuir isotherm:

$$\left\{>\mathrm{SOM}^{v-½}\right\} = \Gamma_s = \frac{\left[\mathrm{M}^{v+}\right]K_L}{1 + \left[\mathrm{M}^{v+}\right]K_L} \tag{2-39}$$

Where, the Langmuir constant is defined as:

$$K_L = \frac{K_aK_M}{K_a + \left[\mathrm{H}^+\right]} \tag{2-40}$$

As can be seen from the definition of the conditional Langmuir constant in Equation 2-40, the simplified NEM surface complexation model not only captures the intrinsic non-linearity of the sorption reaction (i.e. with regard to solute concentration), but also the non-linearity related to the changing population of charged binding sites at different pH levels. Provided the free concentration of the cation M^{v+} is approximately the same as the total concentration, a conditionally constant K_d value could then be defined as:

$$K_d \approx n_s \cdot \frac{K_a K_M}{\left[\mathrm{H}^+\right] + K_a K_M \left[\mathrm{M}^{v+}\right] + K_a} \qquad (2\text{-}41)$$

Where n_s (mol/kg) is the total concentration of binding sites including all speciated forms given in Equation 2-37. If, as is typically the case, the free concentration of M^{v+} represents only a small fraction of the total concentration, then an additional speciation correction term is needed to account for this. In general, this would give additional indirect dependencies for K_d on pH, pCO_2, and possibly other groundwater compositional parameters as discussed previously in Section 2.1.4.

A full account of the different SCM modelling approaches, including their applications to more complex environmental sorbents is beyond the scope of this document and this section should be seen as more of an overview of mechanisms and their abstraction in various modelling approaches. There are a large number of detailed reviews in the open literature /Haworth 1990, Goldberg et al. 2007/ and accounts in various textbooks, e.g. /Stumm and Morgan 1996, Appelo and Postma 2005, Lützenkirchen 2006/ which may serve as a basis for further reading although these are too numerous to give more than a brief listing here. The interested reader is encouraged, however, to revisit some of the original references documented in these sources since this is frequently where many of the underlying assumptions are discussed in greatest detail. The deployment of SCM modelling techniques in more complex environmental systems of interest in nuclear waste management is also documented in the Phase I and II OECD-NEA reports on sorption modelling /NEA 2001b, 2005/ and in e.g. /Davis et al. 1998, Jenne 1998/. At the time of writing of this report, Phase III of the OECD-NEA sorption modelling project is still underway and will result in a guidance document covering many of the unresolved issues highlighted in the Phase II report for this rapidly evolving field.

2.3 Safety assessment modelling

2.3.1 Overview of modelling approach

In the safety assessment framework that underpins the site descriptive models prepared for Forsmark and Laxemar, solute transport is conceptualised to occur by advective flow along a migration path where retention is caused by matrix diffusion and equilibrium sorption on rock matrix microsurfaces /Berglund and Selroos 2003/. For modelling purposes these processes are usually assumed to be reversible and linear (thereby implying a *Fickian* formulation of matrix diffusion). This approach is also used in the SR-Site safety assessment.

In SR-Site, diffusive transport of solute within the rock matrix is characterised by an effective diffusivity, D_e that can vary spatially depending upon the local microstructural properties of the rock. The effective diffusivity of specific solutes in the rock depends on the geometric structure and connectivity of the rock matrix porosity which is conceptualised to consist of both microfractures and grain boundary porosity. The handling of effective diffusivity and data used in SR-Site is discussed in the Data report /SKB 2010b/. In a similar fashion, the sorptive properties of the rock are modelled based on the assumption of a constant linear partitioning coefficient, K_d which also can vary spatially depending on the local mineralogy of the rock and porewater chemistry. The residence time distribution of a solute subject to advective transport and retardation by matrix diffusion and linear sorption is a function of the master variables D_e, K_d and the flow-wetted surface to flow ratio which is also referred to as the *F-factor* or *hydrodynamic transport resistance* /SKB 2010b/. In SR-Site, the diffusive mass transfer to the rock matrix is furthermore assumed to be one-dimensional and perpendicular to the advective flowpath along which the radionuclide is transported. The consequences of this assumption are explored further in /Crawford 2008/ where it is shown that the assumption is cautious within a safety assessment framework and may actually underestimate solute uptake to the rock matrix.

For a spatially variable although temporally constant D_e and K_d, the residence time distribution of a transported radionuclide undergoing first-order decay is described by the Laplace space equation:

$$\tilde{c}_f = \frac{1}{s+\lambda} \exp\left(-t_w \sqrt{s+\lambda}\right) \cdot \exp\left(\int_0^L \psi_m(x) \frac{dF(x)}{dx} dx\right) \qquad (2\text{-}42)$$

Where, s is the Laplace space variable, λ is the radionuclide decay constant, t_w is the advective travel time, $F(x)$ is the F-factor along an advective transport flowpath of length L, and ψ is a function describing the spatially variable retention properties of the rock matrix. Implicit in this mathematical formulation is the assumption of homogeneous (i.e. spatially invariant) matrix retention properties perpendicular to the advective flowpath as outlined above, although the material properties of the rock matrix are allowed to vary along the length of the transport path. For a homogeneous rock matrix of limited extent, δ_m the function ψ is given by:

$$\psi_m = \sqrt{D_e\left(\theta_m + K_d\rho_s\right)\left(s+\lambda\right)}\tanh\left(\delta_m\sqrt{\frac{\left(\theta_m + K_d\rho_s\right)\left(s+\lambda\right)}{D_e}}\right) \qquad (2\text{-}43)$$

Here, θ_m is the rock matrix storage porosity and ρ_s is the true solid rock density (i.e. crystallographic density, excluding porosity). The sum of the parameter group, $K_d\rho_s$ and the porosity, θ_m is the specific volumetric storage capacity of the rock matrix, denoted K. It should be noted that the assumption of a limited matrix depth does not necessarily relate to any physical limitation of connected matrix porosity, but is a modelling convenience arising out of the desire to avoid *double counting* matrix retention where the possibility exists for separate advective flowpaths in close proximity. In SR-Site, the matrix depth is deemed to be equal to half the average separation distance between flow bearing fractures although the physically connected matrix porosity is thought to be unlimited. Further discussion and justification of this can be found in /SKB 2010b/. In the case of a rock matrix of unlimited depth, Equation 2-43 reduces to:

$$\psi_m = \sqrt{D_e\left(\theta_m + K_d\rho_s\right)\left(s+\lambda\right)} = \sqrt{D_e K\left(s+\lambda\right)} = N_{MPG}\sqrt{s+\lambda} \qquad (2\text{-}44)$$

The square root of the effective diffusivity and volumetric storage capacity product is often referred to as the *material properties group* or N_{MPG}. For the simplified case of an unlimited rock matrix and homogeneous rock matrix properties along a flowpath, the residence time distribution for a constant concentration source term is then given by:

$$\frac{C}{C_0} = erfc\left(\frac{F}{2}\cdot\sqrt{\frac{D_e\left(\theta_m + K_d\rho_s\right)}{t-t_w}}\right) = erfc\left(\frac{F}{2}\cdot\frac{N_{MPG}}{\sqrt{t-t_w}}\right) \qquad (2\text{-}45)$$

Although the general principals are similar, it should be noted that in codes used for safety assessment, the algorithmic implementation of the solution to the reactive transport problem may differ slightly to the formulation given above since consideration also must be given to actinide decay chains.

Under the influence of tectonic forces in combination with weathering processes and previous cycles of hydrothermal alteration, it is generally expected that there is variability in material properties of the rock matrix perpendicular to the advective flowpath and extending some distance into the rock from flow-bearing fracture surfaces. Generally, there is a greater intensity of microfracturing and porosity near the fracture surface which is often accompanied by changes in mineralogy. This typically results in enhanced retention properties of the altered rock relative to the unaltered rock further away from the fracture surfaces. In SR-Site, such depth dependent variations in sorptive and diffusive properties are neglected by appealing to arguments of caution. The sorptive and diffusive properties of the rock are therefore assumed to be determined by the properties of the intact and unaltered rock matrix.

In certain situations it may be appropriate to model the additional sorptive retention of radionuclides on a fracture surface coating possessing dissimilar material properties to the rock matrix itself. Since diffusive equilibrium can usually be assumed for fracture coatings over the timescales typical of safety assessment conditions this is usually assumed to be an equilibrium retardation process characterised by a retardation factor R_f. In this case, the retarded advective travel time $R_f t_w$ would be used in place of t_w in Equation 2-42 or 2-45. In SR-Site this additional retention mechanism is also neglected given that fracture coatings are thought to exhibit enhanced retention properties relative to the rock matrix proper and owing to the difficulty in demonstrating the existence of a contiguous fracture coating of specified thickness and sorptivity along the advective flowpaths through the geosphere. Further justification of this assumption may be found in the SR-Site Radionuclide transport report /SKB 2010d/.

2.3.2 Justification for the assumption of a linear sorption process

The use of a Fickian model for solute diffusion in combination with a linear model of sorption are modelling simplifications of what is in reality a complex, coupled reactive transport process. Generally, such simplifications are justified on the basis that the transported radionuclides are considered to be extremely dilute, trace components within the groundwater. There is a broad scientific consensus, however, that provided appropriate parameter values are selected for the prevailing conditions the use of these modelling simplifications is adequate for the goals of safety assessment /McKinley and Scholtis 1993, NEA 2001a, Alexander et al. 2003/.

As outlined in Section 2.1, the sorption of any particular radionuclide is strongly dependent on mineralogy, the accessible sorptive surface area, and groundwater composition which here is taken to include the concentration of the radionuclide itself. The mineralogy and the accessible sorptive surface area of the rock may, for all practical purposes, be assumed to be temporally invariant over the timescale of safety assessment although there may be significant spatial variation within the rock both perpendicular to the surfaces of flow-bearing fractures as well as along advective transport paths. As previously mentioned in Section 2.3.1, only the material property variability along the length of an advective flowpath is considered in SR-Site and variation perpendicular to the fracture surfaces is neglected.

There are a number of reasons why a constant partitioning coefficient is attractive to use in safety assessment modelling. The conditionally constant K_d approach describes solute partitioning as a linear process. Linear systems are convenient to work with, as it is frequently possible to obtain closed-form analytical solutions for the coupled transport and sorption problem. Spatial variations in material properties along a transport path can usually be handled by convolution of residence time distribution functions for individual hydrogeologic and material units. Similar techniques can be used when using particle tracking methods or Laplace space formulated approaches to achieve the same end. Additionally, the influence of different scenarios of near-field release may be easily calculated by convolution of the near-field release boundary condition with the far-field residence time distribution obtained by simulating the breakthrough characteristics of an instantaneous pulse release. This is not possible to do with a non-linear formulation of sorption chemistry.

Although not sufficiently good reason on its own, the hydrological setting of safety assessment studies is frequently sufficiently complex that it is very difficult to simultaneously integrate a highly sophisticated treatment of sorption chemistry and hydrogeological processes. Perhaps more importantly, the inherent non-linearity of mechanistically based chemistry sub-modules makes it exceedingly difficult to distinguish between real non-linear phenomena and spurious numerical artefacts in fully-coupled reactive transport codes. Coupled models using a simplified linear approach to sorption chemistry are thus more transparent and results are more easily understood than approaches involving highly non-linear models of sorption. The number of spatial discretisations and the size of time steps required to obtain a meaningful solution is significantly constrained by considerations of stability and numerical dispersion that can give rise to non-physical phenomena if not handled properly. For sorbing substances, many pore volumes of water must be transported through the system to give even a small spatial redistribution of the sorbed substance. For simulations intending to simulate the chemical evolution of a rock volume over timescales of up to 100 ka and more, this also leads to the requirement of an excessive number of simulation time steps which reduces the realistically achievable number of stochastic realisations when making probabilistic calculations.

The use of more sophisticated models of sorption chemistry does not automatically mean more accurate results, since this is dependent on the robustness of the additional model parameters and their applicability to the system being modelled. If the model parameters are poorly constrained by experimental data, are derived for very different conditions of chemistry and mineralogy, or if the data have been incorrectly interpreted then any additional features derived from a more complex model may not necessarily represent physically meaningful behaviour. Moreover, there is a tendency to automatically believe the legitimacy of the results of more complex models over simpler modelling approaches purely for the reason that they possibly represent a more mechanistically correct description of sorption.

Although there have been considerable advances in recent years in the use of thermodynamic sorption models describing sorption processes on complex, heterogeneous substrates (see e.g. /NEA 2005/), there are still sufficiently large uncertainties and gaps in the availability of data for relevant materials and radionuclides that precludes their direct use in safety assessment studies for fractured

crystalline rock. Even in the more limited role of guiding the selection of conditional K_d values for safety assessment, large uncertainties reduce the applicability of thermodynamic sorption models for the most safety critical radionuclides.

As outlined previously in /Crawford et al. 2006/, a powerful argument for the use of the constant K_d approach in safety assessment is that a large amount of the uncertainty relating to the magnitude of sorption is concentrated into a single variable, the applicability of which can be (at least partially) assessed independently of its implementation in a transport simulation code. Moreover, the retardation implied by the magnitude of the K_d value for the particular radionuclide of concern has a powerful significance, as it is possible to attach a precise physical interpretation to its meaning. This is not always possible to achieve with non-linear, mechanistic approaches, as their physical interpretation (i.e. in terms of intrinsic binding constants, etc.) is often unclear with respect to solute retardation.

Since the aim of safety assessment is to assess radiological risks associated with different scenarios of repository evolution, it is not always necessary or desirable to attempt to simulate sorption processes *exactly* as they would occur in nature. This is largely due to the significantly increased likelihood of introducing serious errors when attempting to model processes with this precision when such features cannot be realistically validated in the system under consideration. Many of the features of the more sophisticated sorption models, however, can be reasonably anticipated and K_d values selected which over-predict radiological consequences in a cautious fashion.

Great care must be exercised nevertheless since what might seem a pessimistic estimate of the retention strength and capacity will possibly underestimate the load of radionuclides available upon remobilisation resulting from changes in chemical or physicochemical conditions. If an excessively low K_d value (although pessimistically estimated for retention) is used, for example, the actual amount of radionuclide that is remobilised may be subsequently underestimated owing to that it may have diffused to a greater depth in the rock matrix than if a larger K_d value were to have been selected. Changes in groundwater chemistry may additionally result in anion-exclusion, solute *lock-in* (reduced out-diffusion of an anionic radionuclide due to anion exclusion effects), or increased impact of surface diffusion for radionuclides that sorb by ion-exchange or outer-sphere surface complexation. In such situations, the peak load and the timing of the release of radionuclides may be erroneously predicted with possibly negative consequences for safety assessment risk metrics.

Generally, the non-linear processes of interest fall into four distinct categories:

- Intrinsic non-linearity relating to the concentration of the radionuclide itself giving rise to Langmuir-like behaviour in the sorption isotherm,
- Non-linearity relating to temporal changes in groundwater chemistry resulting in altered sorptivity of the transported radionuclide (i.e. due to direct and indirect competitive effects, etc.),
- Non-linearity arising due to the concentration of the transported radionuclide locally influencing the groundwater chemistry itself and thereby its own sorptivity,
- Influences of temporal changes in groundwater chemistry on coupled transport properties, principally surface diffusion and anion-exclusion.

In each of the first two categories outlined above, it is generally not necessary to use a complex model of sorption since a constant K_d value can always be selected which is cautious with regard to the radionuclide concentration (determined by the source term or the background concentration of a naturally occurring isotope) and prevailing groundwater composition (established by independent hydrogeochemical modelling). Provided the K_d value is equal to or lower than that expected for the maximum possible radionuclide concentration and most unfavourable groundwater composition possible, the transport of radionuclide will be pessimistically overpredicted.

The third category of non-linearity is more difficult to predict a priori since it depends on a more complicated feedback mechanism by way of the mutual interaction of the radionuclide with other groundwater constituents. For most radionuclides, however, the transported concentration is usually vanishingly small relative to the concentration of other groundwater constituents that govern the groundwater chemistry and this non-linearity can usually be neglected. A possible exception to this is in the case of redox sensitive radionuclides such as uranium where the concentration in the immediate proximity of the source is sufficiently high that it may promote more strongly reducing conditions and thereby self-limit its own

migration due the significantly lower solubility of the reduced form. This, however, can be taken into consideration already in the formulation of the source term and does not strictly need to be considered downstream along a transport path.

Although the fourth category of non-linearity is associated with coupled transport properties rather than sorptivity per se, it is of great relevance to the current discussion since it has a direct impact on the validity of the assumption of caution underlying the choice of K_d value to be used in safety assessment modelling. This generally must be handled on a case by case basis. For the scenarios of repository evolution considered in SR-Site, however, it is thought that the selection of K_d values for the most unfavourable groundwater compositions anticipated is the most cautious choice /SKB 2010c/.

2.4 Parameter variability and uncertainty

2.4.1 Conceptual uncertainty concerning the K_d modelling approach

The conditionally constant K_d approach, being the simplest representation of sorption, is subject to a great many limitations and there are a number of caveats imposed on its usage. As discussed previously in Section 2.3.2, there are several reasons why the K_d approach is favoured over the more sophisticated semi-empirical and mechanistic models that might be available. Generally speaking, the K_d value is simply a statement of the expected equilibrium ratio of sorbed and dissolved solute for a given set of conditions and is not necessarily related to considerations of any specific sorption mechanism or retention process. The use of a constant K_d value in safety assessment modelling, however, implies a retention process with particular characteristics that is combined with a model of advective and diffusive mass transfer to give a quantitative measure of solute transport retardation. For this reason it is very important that the magnitude of the K_d value selected to represent the retardation process correctly captures the physics of the postulated retention mechanism.

The conceptual uncertainty related to the use of a constant K_d, however, also extends to the interpretation of laboratory data used to establish its magnitude. This is a significantly more difficult type of uncertainty to handle owing to that if processes giving rise to retention in laboratory investigations are incorrectly identified as sorption, this can invalidate the subsequent modelling of transport retardation. Although such reaction mechanisms are frequently favourable as additional retardation processes over and above that provided by purely sorptive interactions, the danger of these confounding processes is that they scale differently with regard to the physics of sorptive retardation modelled in safety assessment transport calculations. Great care is generally taken in laboratory investigations to avoid situations where confounding factors might skew the interpretation of sorptive retention. This is generally achieved by using extremely low trace concentrations of radionuclides and designing experiments to avoid situations where abrupt changes in solution chemistry might occur. Such processes, however, are very difficult to control for and in most cases there is still some residual uncertainty concerning the true nature of the retention process as it is quantified. With regard to the forward modelling of sorption, the use of a conditionally constant K_d value is usually contingent upon the following conditions being fulfilled.

- The modelled process is a true equilibrium sorption process.
- The water chemistry, mineralogy, and physical state of the in situ rock are identical to those used in partitioning coefficient data acquisition and do not vary in time and space (as noted previously, certain classes of spatial variation are allowed as long they are quantified by way of flowpath averaging or some equivalent approach).
- The radionuclide concentration range encountered along the transport path must not invalidate the fundamental assumption of intrinsic sorption linearity.

Ordinarily it is not possible to fully satisfy these criteria in safety assessment and expert judgement needs to be exercised in the selection of K_d ranges that cover uncertainties arising due to the criteria not being fully met. The following paragraphs give a brief overview of how this is handled in SR-Site.

Assumption of equilibrium sorption

For solutes where retention is primarily governed by ion-exchange or surface complexation, sorption is generally reversible in a thermodynamic sense although reaction kinetic and diffusive disequilibrium effects are frequently mistaken as evidence of irreversibility. Exceptions to this do occur although typically only when the radionuclide is incorporated into the mineral structure in some way that inhibits subsequent desorption. Notwithstanding this, however, any difference in the chemical kinetics of sorption and desorption might need to be considered if the timescales of these processes are sufficiently large relative to the characteristic times associated with advective and diffusive transport. In most cases of relevance for safety assessment, the intrinsic reaction rates are fast and chemical kinetics can be safely neglected without introducing significant errors (formation of solid solutions being a possible exception).

Assumption of constant and identical material properties

In general, it is highly unlikely that groundwater chemistry, mineralogy, and the physical state of the rock are the same as those under which K_d data are acquired. For this reason it is necessary to introduce correction factors of various kinds to account for these differences. A large part of the subsequent chapters of this report is devoted to the extrapolation of laboratory derived data to K_d values that are considered appropriate for modelled safety assessment conditions. The procedures used to achieve this are described in Chapter 5.

Although the use of a constant K_d value is contingent upon constant material properties, it is possible to handle spatial variability by assigning a conditional K_d value that represents the average sorptive properties of the rock encountered along a flowpath. This can be shown to be robust for certain classes of material property variability and is discussed further in Section 2.4.2. Temporal variability and associated uncertainties, however, result in non-linearities that are difficult to account for in a simple fashion. Various issues related to this and how it is handled in SR-Site are discussed in Section 2.4.3.

Assumption of sorption isotherm linearity

The sorption isotherms for most radionuclides of interest in safety assessment exhibit some kind of intrinsic non-linearity. These are mostly described as having a *convex isotherm* whereby higher aqueous concentrations of solute are associated with reduced sorption relative to that at lower solute concentrations. These are frequently described as being *Langmuirian* in character, where there is a fixed upper limit to the monolayer surface loading of solute that can be achieved by sorptive interactions. Where there are different types and abundances of sorption binding sites, these non-linearities can appear at relatively low concentrations and be related to the successive saturation of different binding sites at different concentrations. This gives rise to perceptible non-linearity over a broad range of concentrations without actually reaching an upper limit until very high concentrations are reached. For a radionuclide pulse release scenario, the convex form of the isotherm generally gives rise to a sharpening of the sorption front leading edge and a broadening of the trailing edge.

It is always possible, however, to identify an intermediate concentration between that of the source and the natural background level that will define an appropriate K_d value that gives a cautious estimate of the sorption front velocity and, consequently, the rate of radionuclide transport (all other things being equal). Since the source concentrations of most sorbing radionuclides are expected to be very low, the relevant concentration level is, in most cases, the background concentration of isotopes for those radionuclides that have naturally occurring counterparts in the groundwater. For radionuclides that do not have naturally occurring isotopes, the source concentration will define the most pessimistic K_d value for a convex isotherm. Although source concentrations are not specifically estimated for use in defining K_d values for radionuclide transport in SR-Site, the recommended K_d values are generally based on sorption data obtained at relevant background concentration levels or at concentrations equal to or higher than what would be reasonably expected in the repository environment.

2.4.2 Spatial variability and uncertainty

It has been previously shown /SKB 2004/ that the material properties of the rock as represented by the N_{MPG} (Equation 2-44) can be integrated along a flowpath in a simple fashion to calculate a flowpath average. This considerably simplifies calculations involving material properties which exhibit

spatial variability along a flowpath. To the extent that material properties are assumed to be constant along the direction of matrix diffusion, although variable along the length of a flowpath, this can also be shown to hold for the case of a rock matrix of limited extent.

Spatial variability can be handled in a number of different ways: by calculating a flowpath average K_d value, by convolution of residence time distributions for different segments of a transport path considered separately, or by explicit consideration of spatially resolved material properties in particle tracking methods. These different approaches, however, can be shown to give theoretically identical results and the choice is one of merely algorithmic convenience. Uncertainty in spatial variability of material properties is handled in SR-Site by stochastic simulations where a range of values representing an interval of the uncertainty distribution of K_d is randomly sampled and used in probabilistic simulations. As an addition to probabilistic simulations, deterministic calculations are performed using a central *best estimate* value of K_d.

For sorbing solutes, K_d is usually considerably larger than the porewater storage term, θ_m/ρ_s and the latter can therefore generally be neglected. If the spatially variable D_e and K_d can be reasonably assumed to be independent lognormal variables, the product of the flowpath mean D_e and K_d can be shown to be equal to the mean of the spatially resolved product of D_e and K_d. This would suggest that the appropriate flowpath average measure of K_d is then the arithmetic mean of the distribution describing spatial variability.

On the basis of this analysis, the arithmetic mean would therefore be recommended for use in deterministic calculations if the probability distribution for K_d can be shown to be dominated by spatial variability. In the data compilation prepared for SR-Site, however, uncertainty is by far the dominant feature of the empirically derived data sets and it is therefore not possible to defend the use of a simple arithmetic mean K_d as a flowpath average for modelling purposes. For this reason, the median of the uncertainty distribution is selected as the most appropriate best estimate K_d value for use in deterministic calculations. For a lognormally distributed variable, the median is numerically less than the arithmetic mean and therefore can be defended as a more cautious choice for the best estimate value.

2.4.3 Temporal variability and uncertainty

Temporal variability is difficult to handle in a conditionally constant K_d framework owing to non-linearity introduced in the solute mass balance as a result of changing sorptivity. Geological weathering processes are sufficiently slow under normal repository conditions that any changes in rock mineralogy can be neglected over the timescale of the safety assessment. Changes in sorptivity resulting from variable groundwater chemistry, however, do occur over time and can have a significant impact on radionuclide migration rates. Groundwater chemistry can be expected to show considerable variation both spatially and temporally in the repository environment. During a glacial cycle these changes are driven by different processes; infiltration of meteoric water in combination with land uplift during the (*interglacial*) temperate period and alternating short duration pulses of dilute, glacial melt water and upconing of deep saline groundwater during glacial advance and retreat. During the phase in which the ice sheet is stable over the repository, the flow of water may be very slow or stagnant.

As a general rule, the temperate period is characterised by a slow freshening of the groundwater surrounding the repository over many thousands of years under the influence of infiltrating meteoric water. During this period, the groundwater evolves towards lower pH levels and higher carbonate concentrations. This is also likely to result in a steady increase in the redox potential over time. The intruding meteoric water displaces saline water in the fracture system and mixes by diffusive exchange with stagnant water in the rock matrix. Changes in groundwater salinity are slow and follow a similar pattern to the residence time distribution function for non-sorbing solutes as predicted by Equation 2-45 (since they are subject to the same delay mechanisms as transported radionuclides). Since many of the components characterising the freshness of groundwater are practically non-sorbing, this implies that the freshening groundwater composition will catch up to and overtake the sorption fronts of many migrating radionuclides given sufficient time.

Depending on the F-factor associated with the recharge/discharge flow path passing through the repository, it may take many hundreds of years up to some tens of thousands of years for the mixing front to reach repository depth. At the time when it does reach the repository, the effective width of the mixing front (say, the distance spanning the 10% and 90% mixing fractions) will then be as much as twice the recharge path length to the surface (for further details refer to Appendix A in

/Crawford and Sidborn 2009/). This implies a very slow change in groundwater chemistry which, for ion-exchanging radionuclides might be expected to lead to steadily increasing sorptivity. In the case of non redox-sensitive radionuclides that form surface complexes, the changing groundwater composition may lead to increased or decreased sorptivity depending on the changing pH and carbonate levels and the sorption reaction characteristics of the radionuclide concerned. For redox sensitive radionuclides, the increasing carbonate content of the groundwater may lead to an increasing redox potential (Eh) and thus reduced sorptivity.

In the phase of the glacial cycle during which the ice sheet is stable over the repository, the flow of water may be very slow or stagnant owing to the approximately constant hydraulic head under the ice sheet. At this time, permafrost may also extend to a significant depth in the rock and hinder the flow of water. The freezing of water in the fracture system may result in the rejection of salt and formation of cryogenic brines around the repository volume, although this is not certain. During this phase, sorptivity may be increased or decreased depending on the properties of individual radionuclides and the actual groundwater composition. Owing to the low flow conditions, reducing conditions are likely to prevail possibly resulting in a lower mobility of redox sensitive radionuclides. The low flow conditions in the repository volume during this phase, however, means that this is of only minor importance for safety assessment purposes and can be neglected.

During glacial retreat, alternating pulses of dilute glacial melt water and deep saline groundwater may intrude into the repository volume. These pulses, however, are expected to be relatively short in duration (a few hundred years) and accompanied by significantly increased flowrates giving a large dilution effect. The relative impact of these intermittent periods of high flow and altered chemistry depends on the form of the radionuclide source term although their limited duration also restricts the amount of already mobilised radionuclide that can diffuse back into the fracture system from the rock matrix. The overall effect is expected to be negligible although can be bounded in safety assessment by estimating the overall dose contribution during these periods under the assumption of weakened or zero sorption. The fact that the glacial ice front at this time is close to the repository and that the site might possibly be submerged below sea level also needs to be considered here since this has a large bearing on the landscape dose factors and the relative levels of radiological risk at such times.

As is discussed in later sections, it is not currently possible to make robust quantitative predictions of whether the sorption of surface complexing radionuclides should increase or decrease in response to altered groundwater composition. This is largely due to the absence of reliable surface complexation models for the sorption of these solutes on granitic rock types. For radionuclides that sorb predominantly by ion-exchange and are thus sensitive to groundwater salinity, modelling can be used to approximately assess relative changes in sorptivity at different times since a rudimentary model of ion-exchange on granite does exist. This is discussed further in Chapter 5.

It was not considered feasible in SR-Site to track detailed spatial and temporal changes in groundwater chemistry along radionuclide migration pathlines associated with specific source locations (i.e. individual canister deposition positions). Even if this was accomplished, the current lack of reliable mechanistic models of radionuclide sorption would limit the value of such information. For this reason it is only strictly possible to consider relative variations between different time periods for the full groundwater composition distribution in the repository volume when making judgements on the influence of spatial and temporal variability or uncertainty in groundwater chemistry. It is also noted that it is very difficult to separate notions of variability and uncertainty when considering groundwater chemistry given that; 1) changes can occur relatively rapidly on the timescale of sorbing radionuclide transport, and 2) groundwater chemistry profiles are established on the basis of hydrogeological simulations that also harbour a number of assumptions and uncertainties.

Acknowledging this restriction, spatial variability and uncertainty of groundwater chemical composition is considered to be a sub-component of overall K_d data uncertainty. Calculations made for the elements where it is possible to approximately estimate the influence of groundwater composition (specifically Cs, Sr, Ra, and possibly Ni) indicate that the impact of variable/uncertain groundwater composition is, in any case, relatively minor in comparison to the overall empirical data uncertainty and therefore does not need to be considered in detail. For these solutes, K_d uncertainty distributions are given for the most *unfavourable* hydrochemical conditions expected during repository groundwater evolution. Although not a strictly correct manner of handling the non-linear effects of evolving groundwater composition, for the purposes of SR-Site this is considered to be the most cautious approach to handling such uncertainties.

For surface complexing solutes it is generally not possible at the present time to relate quantitative or even qualitative changes in sorptivity in a robust fashion between different contact solution compositions used in sorption experiments. The reason for this is explained more fully in Chapter 5 although relates to insufficient tracking and documentation of contact solution chemistry during the course of the sorption experiments that have been used to derive the recommended K_d data. For this reason, it is assumed that the aggregate set of K_d values obtained for different contact solution compositions also spans the range of uncertainty that might arise due to variable or uncertain groundwater composition in the repository environment (and any temporal changes). In practice this means pooling data obtained for different contact solution compositions. For solutes where K_d data are available for a number of different groundwater end-members, this is not an unreasonable assumption. For solutes where data are only available for one or two different groundwater compositions the assumption is likely to be less good. This is discussed on a case by case basis in the appendices to this report.

3 Description of prioritised radionuclides

3.1 Radionuclides of importance for SR-Site

The radionuclides that are considered of importance for SR-Site fall into three different categories of relative importance depending on how they appear in the safety assessment calculations. For nuclides listed as *important*, accurate sorption data are required since they are expected to be released from damaged canisters and will migrate through the geosphere with flowing groundwater. For nuclides listed as being of *minor importance*, accurate sorption data is of less significance on account of their very short half-lives. These nuclides do, however, contribute significantly to calculated dose rates in the case of, for example, a repository intrusion scenario and therefore cannot be entirely neglected. Nuclides listed as *inventory only*, are not important for geosphere transport calculations although they are used to establish inventories of daughter nuclides generated by decay processes. The full list of radionuclides and their classifications are given in Table 3-1 and are taken from the Radionuclide transport report /SKB 2010d/.

Table 3-1. List of radionuclides considered of significance for SR-Site safety assessment calculations /SKB 2010d/.

Important		**Minor importance**		**Inventory only**	
Nuclide	Half-life (y)	Nuclide	Half-life (y)	Nuclide	Half-life (y)
Fission and activation products:					
C-14	5.73×10^{3}	Ag-108m	4.18×10^{2}		
Cl-36	3.01×10^{5}	Cd-113m	1.41×10^{1}		
Cs-135	2.30×10^{6}	Eu-152	1.35×10^{1}		
Cs-137	3.01×10^{1}	H-3	1.23×10^{1}		
I-129	1.57×10^{7}	Ho-166m	1.20×10^{3}		
Nb-94	2.03×10^{4}	Mo-93	4.00×10^{3}		
Ni-59	7.60×10^{4}	Nb-93m	1.61×10^{1}		
Se-79	1.13×10^{6}	Ni-63	1.00×10^{2}		
Sn-126	1.00×10^{5}	Sm-151	9.00×10^{1}		
Pd-107	6.50×10^{6}	Sn-121m	5.50×10^{1}		
Sr-90	2.87×10^{1}				
Tc-99	2.11×10^{5}				
Zr-93	1.53×10^{6}				
Actinides:					
4n decay chain (thorium series)					
Pu-240	6.56×10^{3}	Cm-244	1.81×10^{1}		
Th-232	1.41×10^{10}				
U-236	2.34×10^{7}				
4n+1 (neptunium series)					
Cm-245	8.50×10^{3}	Pu-241	1.44×10^{1}	U-237	1.85×10^{-2}
Am-241	4.32×10^{2}			Pa-233	7.38×10^{-2}
Np-237	2.14×10^{6}				
U-233	1.59×10^{5}				
Th-229	7.34×10^{3}				
4n+2 (radium series)					
Cm-246	4.73×10^{3}	Am-242m	1.41×10^{2}	Am-242	1.83×10^{-3}
Pb-210	2.23×10^{1}	Pu-238	8.77×10^{1}	Cm-242	4.46×10^{-1}
Pu-242	3.73×10^{5}			Np-238	5.80×10^{-3}
Ra-226	1.60×10^{3}			Th-234	6.60×10^{-2}
Th-230	7.54×10^{4}			Pa-234m	2.22×10^{-6}
U-238	4.47×10^{9}				
U-234	2.46×10^{5}				

Important		Minor importance		Inventory only	
Nuclide	Half-life (y)	Nuclide	Half-life (y)	Nuclide	Half-life (y)
4n+3 (actinium series)					
Am-243	7.37×10^{3}	Cm-243	2.91×10^{1}	Np-239	6.45×10^{-3}
Pu-239	2.41×10^{4}				
U-235	7.04×10^{8}				
Pa-231	3.28×10^{4}				
Ac-227	2.18×10^{1}				

3.2 Data sources and correlations

Table 3-2 summarises the different elements and redox states that are considered of relevance for safety assessment calculations in SR-Site. The table also itemises the predominant aqueous species expected for the average groundwater composition projected during repository evolution. In cases where several species are predicted to be present in nearly equimolar concentrations, multiple species have been given in estimated order of relative importance. The table furthermore indicates which sorption mechanism is expected to be controlling radionuclide retention as well as the data source or geochemical analogy invoked where appropriate. Two broad correlation groups are also defined which essentially indicate whether the K_d values appears to exhibit a predominant sensitivity to ionic strength (ion-exchange and outer-sphere surface complexes) or pH and carbonate concentration (mostly inner-sphere surface complexes). Solutes belonging to the same correlation group are expected to be influenced in a similar fashion by uncertain or changing groundwater composition; a feature which is important to consider in stochastic risk calculations. It is acknowledged that this is only a very approximate treatment of correlation given that radionuclides, particularly those featuring possibly mixed sorption mechanisms, may be influenced by ionic strength as well as pH and carbonate to varying degrees and it is very difficult to introduce rigid demarcations between related groups of elements.

In this compilation, K_d data are obtained from a mixture of sources including the Forsmark and Laxemar site investigations and literature data. Correlations in sorptivity are assumed in the assignment of K_d ranges for elements where no data are available (so-called *geochemical analogies*). The use of *analogue* solutes in place of actual data is based on geochemical similarity and consideration of specific reaction mechanisms. It should be noted that certain geochemical analogies indicated in Table 3-2 may be considered of dubious standing although are necessary owing to a lack of data. This appears to be unavoidable at the present time, although generally affects elements that are not of central importance for the safety case involving migration in the geosphere (e.g. Ag and Cd).

The correlation groups given in Table 3-2 are recommended to assist in the stochastic selection of K_d values for use in transport calculations. It is expected, for example, that K_d values for ion exchanging solutes will be mutually correlated with ionic strength. Similarly, for cations that sorb by way of an inner sphere surface complexation mechanism, any shift in hydrochemical conditions should give rise to similar impacts on sorption (although not necessarily in equal proportionality) for all solutes that have an analogous reaction chemistry. An exception is made for redox sensitive solutes since the transition from reducing to oxidising forms occurs at different Eh threshold levels for different elements. Uranium, for example, could possibly be present in oxidised form while plutonium, neptunium, and technetium might still remain in reduced form at the redox potentials projected during the SR-Site temperate period. Correlations between these elements should therefore be handled on a case by case basis.

Table 3-2. List of data sources and geochemical analogies used for specific elements considered in the prioritised list of radionuclides for SR-Site. The identity of most likely dominant aqueous species and presumed sorption binding mechanism (class) is also given where appropriate. For certain solutes it is not possible to say which sorption mechanism is dominant and these are thus labelled as having a "mixed" mechanism. Two correlation groups are also defined for stochastic simulations – these are; (1) K_d predominantly correlated with ionic strength; (2) K_d predominantly correlated with pH and carbonate concentration. A further distinction is made between groups labelled (2a) and (2b) on account of the exceptionally strong analogy between the trivalent actinides and lanthanides although both groups are expected to be influenced in a similar fashion by pH and/or carbonate concentration to varying degrees. Substances labelled with (–) are assumed to not exhibit any correlations on account of their low sorptivity.

Element	Corr. Group	Redox State	Dominant species	Class	Status
Alkali and alkaline earth metals					
Cs	1	+1	Cs^+	IX	site specific data
Ra	1	+2	Ra^{2+}	IX	site specific data
Sr	1	+2	Sr^{2+}	IX	site specific data
Actinides					
Eu	2a	+3	$EuCO_3^+$	IS	site specific data
Ho	2a	+3	$HoCO_3^+$	IS	Am(III)/Eu(III) analogy
Sm	2a	+3	$SmCO_3^+$	IS	Am(III)/Eu(III) analogy
Lanthanides					
Ac	2a	+3	$AcCO_3^+$	IS	Am(III)/Eu(III) analogy
Am	2a	+3	$AmCO_3^+$	IS	site specific data
Cm	2a	+3	$CmCO_3^+$	IS	Am(III)/Eu(III) analogy
Np	2b	+4	$Np(OH)_4$	IS	Pu(IV) analogy
	2b	+5	NpO_2^+, $NpO_2CO_3^-$	IS	site specific data
Pa	2b	+4	$Pa(OH)_4$	IS	literature data
	2b	+5	$PaO_2(OH)$	IS	literature data
Pu	2a	+3	$PuOH^{2+}$, Pu^{3+}	IS	Am(III)/Eu(III) analogy
	2b	+4	$Pu(OH)_4$	IS	literature data
	2b	+5	PuO_2^+	IS	literature data
	2b	+6	$PuO_2(CO_3)_2^{2-}$, PuO_2CO_3	IS	literature data
Th	2b	+4	$Th(OH)_3CO_3^-$	IS	Pu(IV) analogy
U	2b	+4	$U(OH)_4$	IS	with Pu(IV) analogy
	2b	+6	$UO_2(CO_3)_3^{4-}$, $UO_2(CO_3)_2^{2-}$	IS	site specific data
Transition elements					
Ni	1	+2	Ni^{2+}, $NiCl^+$	Mixed	site specific data
Zr	2b	+4	$Zr(OH)_5^-$	IS	literature data
Ag	1	+1	$AgCl_2^-$, $AgCl_4^{3-}$, $AgCl_3^{2-}$	Mixed	Cs(I) analogy
Cd	1	+2	$CdCl^+$, Cd^{2+}, $CdCl_2$	Mixed	Ni(II) analogy
Pb	2b	+2	$PbCO_3$, $PbCl^+$, $PbOH^+$, Pb^{2+}	IS	literature data
Pd	2b	+2	$Pd(OH)_2$	IS	literature data
Mo	–	+6	MoO_4^{2-}	–	assumed non–sorbing
Nb	2b	+5	NbO_3^-, $Nb(OH)_5$	IS	literature data
Tc	2b	+4	TcO(OH)2	IS	Pu(IV) analogy
	–	+7	TcO_4^-	–	assumed non–sorbing
Other					
C	–	+4	HCO_3^-	–	assumed non–sorbing
	–	–4	CH_4 (or organic acids)	–	assumed non–sorbing
Cl	–	–1	Cl^-	–	assumed non–sorbing
I	–	–1	I^-	–	assumed non–sorbing
Se	–	–2	HSe^-	IS	literature data
	–	+4	$HSeO_3^-$, SeO_3^{2-}	IS	literature data
	–	+6	SeO_4^{2-}	IS	literature data
Sn	2b	+4	$Sn(OH)_2$	IS	literature data

Notes: IX (denotes sorption by ion-exchange)
IS (denotes sorption by inner sphere surface complexation)
Mixed (denotes sorption by a possibly mixed mechanism)

3.2.1 Overview of geochemical analogies and periodic trends

With regard to the use of analogue elements for radionuclides where no data are available, consideration must be given to the individual thermodynamic properties of the solutes concerned. For radionuclides that sorb by an ion-exchange mechanism, sorptive strength is correlated with hydrated ionic radius thereby giving rise to the so-called *lyotropic* series where sorptivity of isovalent cations follows the approximate order:

$Ra^{2+} > Ba^{2+} > Sr^{2+} > Ca^{2+} > Mg^{2+}$

$Ag^{+} > Cs^{+} > K^{+} > Na^{+} > Li^{+} > H^{+}$

The lyotropic series is considered to be more or less universally applicable for many different mineral surfaces although there are some deviations for certain clay minerals that have poorly hydrated interlayers. The mechanistic explanation for the lyotropic series is typically framed in terms of the force of electrostatic attraction between the surface and the cation and the limitation imposed by how closely hydrated cations of various sizes can approach the surface. This is essentially Coulombs' law of electrostatic attraction where the force between two charges can be shown to be proportional to the inverse square distance of separation. Cations with large hydration spheres are therefore only held weakly relative to cations with small hydration spheres.

Although a physically appealing description, this explanation breaks down when one considers that cations do not always retain their hydration sphere during sorption. This is particularly the case for sorption of cations on clay interlayer surfaces where loss of the hydration sphere is often required for sorption to occur. In fact, loss of the hydration sphere sometimes gives rise to the formation of effectively inner sphere surface complexes even though the cations may be sorbed by nominally electrostatic interactions. A modified explanation was put forward by /Eisenman 1962/ which extends the description by recognising that ion-exchange is partly electrostatic in nature (as outlined above), but also involves a change in free energy associated with modification of the hydration sphere surrounding the cation as it approaches a surface. Various enhancements in the description of ion-exchange have been proposed by a number of researchers. A concept that has gained increasing popularity is based on the *HSAB* concept of hard and soft acids and bases (see, e.g /Xu and Harsh 1990/ and references therein) which specifically allows for inner-sphere sorption processes. In a revised mechanistic description proposed by /Teppen and Miller 2006/, cation-exchange is described as a two-phase partitioning phenomena whereby the cation with the lower hydration energy is thermodynamically preferred as a surface sorbed species while the more strongly hydrated cation is preferred in the aqueous phase.

Although specific details of these different conceptual models are of interest for mechanistic modelling, they are less edifying for the purposes of the present discussion where the focus is upon identifying the most appropriate geochemical analogues for the sorption of specific radionuclides. What this description should therefore convey to the reader is the fact that there is currently no unifying theory that provides an all encompassing description of ion-exchange phenomena in a satisfactory fashion and there is much overlap with concepts of surface complexation which are typically cast in a completely different conceptual framework.

When discussing hydration properties of ions it is customary to speak in terms of the ratio of the square of the charge number and the ion radius, $\zeta = Z^2 / r$ (this is also referred to as the *electrostatic index*). The free energy of hydration and consequently the logarithm of the equilibrium constant for the first hydrolysis reaction is known to be approximately proportional to the electrostatic index although an empirical correction is required for strongly electronegative elements. Generally the lyotropic series is ordered in terms of increasing electrostatic index. To establish a qualitative order of relative sorptivities on geological materials it is important to also consider concentration effects via the mass action equations describing the ion-exchange equilibria in groundwater which sometimes can have counterintuitive effects on sorption isotherms. It also should be recognised that certain cations (particularly for the divalent transition element cations, Pb^{2+}, Cd^{2+}, Ni^{2+}) can, in principle, also form covalently bonded inner sphere surface complexes which makes ranking these solutes in order of ion-exchange sorptivity speculative if the possibility of multiple binding mechanisms is not considered.

It has been known for some time that intrinsic constants for surface complexation reactions can be related to analogous reactions occurring in the aqueous phase by way of so-called *linear free energy relations*, or *LFER* (see e.g. /Langmuir 1997/ and references therein). An interesting consequence of this analogy is that sorptivity is predicted to increase with hydration energy for a sorbing cation. This is the opposite of the correlation described for ion-exchange reactions as outlined above. The aqueous phase and analogue surface complexation reactions are:

$$M^{z+} + nH_2O \rightleftharpoons M(OH)_n^{z-n} + nH^+ \qquad (n = 1, 2) \qquad (3\text{-}1)$$

$$M^{z+} + >OH + nH_2O \rightleftharpoons >OM(OH)_n^{z-1} + nH^+ \qquad (n = 1, 2) \qquad (3\text{-}2)$$

These are typically presented in graphical form where the logarithm of the intrinsic sorption constant is plotted against the logarithm of the corresponding aqueous hydrolysis reaction. The technique has been used by /Bradbury and Baeyens 2005b/ to model sorption of a number of divalent transition metals and trivalent actinides on montmorillonite (bentonite) and more recently for illite /Bradbury and Baeyens 2009b/.

In spite of the apparent success of this technique, the relation between the hydrolysis reaction of a given cation and its corresponding inner-sphere surface complexation reaction is contingent on the reaction being a simple monomolecular binding reaction with a protonated or deprotonated surface hydroxyl group as outlined in Equation 3-2. The theoretical relationship does not give any additional information on whether the postulated surface complexation mechanism is the most likely to occur. This must usually be confirmed by independent spectroscopic evidence which, for most minerals comprising granitic rock, is sparse or non-existent. This is of great significance for radionuclides that are postulated to form ternary surface complexes with carbonate such as U(VI) and Np(V).

At this time it is not clear whether it is possible to derive thermodynamic correlations between aqueous hydroxy-carbonato complexation reactions and proposed ternary surface complexation reactions involving carbonate owing to the somewhat different stoichiometry of the aqueous phase and postulated sorption reactions (e.g. U(VI) and Np(V)). Also, in most cases there do not appear to be relevant aqueous phase reactions recognised in the thermodynamic databases that could be used as analogies in the same fashion. The aqueous phase reaction of Th(IV) to form the hydroxo-carbonate species, $Th(CO_3)_3(OH)_2^{4-}$ appears to be the only exception, although to the best knowledge of the author the analogous bidentate surface complexation reaction has never been proposed in the literature.

Even though this might be the case, as a general guiding principle, it still appears to be justified to judge the goodness of geochemical analogies by consideration of the broad similarity of their various aqueous phase reactions which would necessarily also include reaction constants for carbonate- and hydroxy-carbonato complex formation. This is not only due to the possibility of ternary surface complex formation, but also because of the strong competitive influence that aqueous phase complexation with carbonate ligands has upon surface complexation. Very different equilibrium constants for the aqueous phase complexation reactions would then imply different competitive effects of carbonate for the radionuclides being compared.

The correlation between the electrostatic index, ζ and the first hydrolysis constant, β_1^0 is shown in Figure 3-1. Interestingly, many of the geochemical analogies of interest for this report can be understood at least qualitatively by examination of this figure. Generally what is found is that isovalent solutes tend to be grouped in sequences that reflect broad similarities in their intrinsic sorptive properties. Solutes that sorb by way of an ion-exchange mechanism, for example, are clustered at the far left-hand lower corner of the figure in order of the lyotropic series. The trivalent actinides and lanthanides are very closely clustered near the centre of the figure indicating the existence of a very good geochemical analogy between these solutes with regard to simple surface complexes of the hydroxo-type as given in Equation 3-2. The tetravalent actinides are less clustered, although similarities in their intrinsic binding constants can also be inferred by way of the LFER principle.

Some deviations from known sorption properties can be seen in Figure 3-1 with regard to the transition metals. Generally, the sorptivity of the divalent transition metals are expected to follow the so-called *Irving-Willams* series (see, e.g. /Langmuir 1997/):

$$Cu^{2+} > Zn^{2+} > Ni^{2+} > Co^{2+} > Fe^{2+} > Mn^{2+}$$

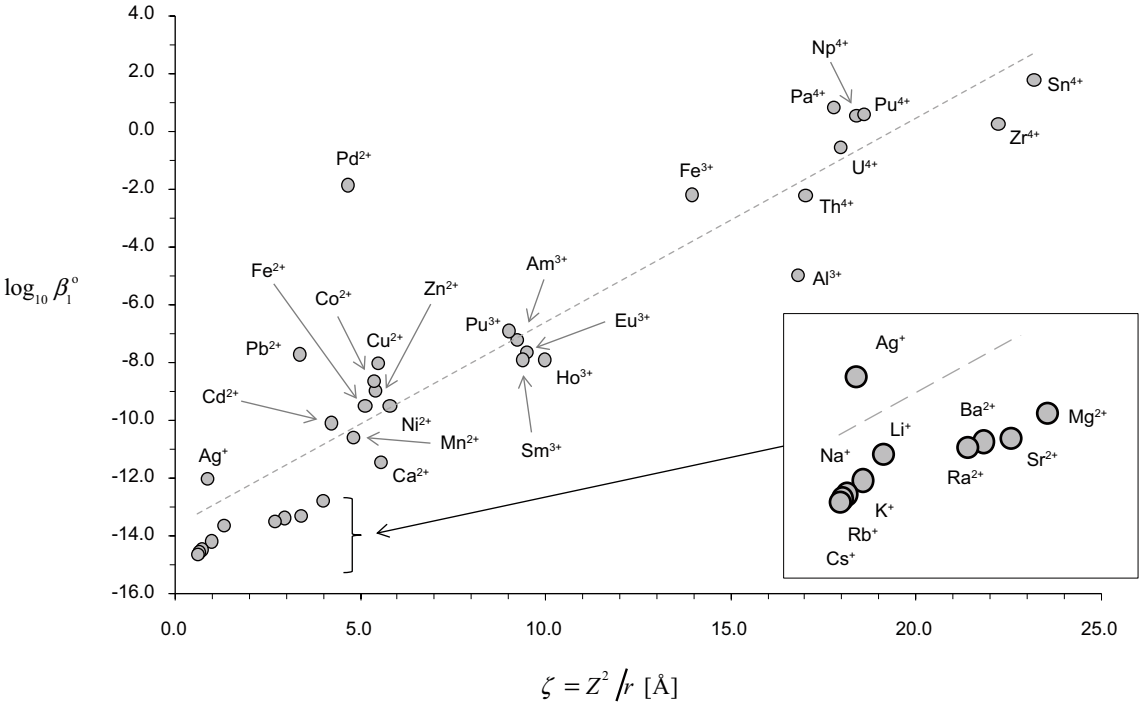

Figure 3-1. *Cross plot showing the correlation between ionic index (ζ) and first hydrolysis constant of various cations (given as log_{10} units). Approximate geochemical analogies between isovalent states can be inferred from the proximity of different species in the figure.*

Although these solutes are closely clustered in the lower left-hand side of the figure indicating approximately analogue behaviour, the relative order of hydrolysis constants does not strictly follow the Irving-Williams sequence which is suggestive of more complex behaviour than can be captured by this simple tableau. Since some of these solutes (e.g. Ni^{2+}) appear to also exhibit ionic strength dependencies, this could be indicative of a mixed mechanism of sorption or at least approximately equal importance of inner- and outer-sphere complexation. Interesting deviations can also be seen for Ag^+ and more particularly for Pd^{2+} which don't seem to fall into line with the systematic behaviour of other solutes in their class.

It is also interesting to note that the relative location of markers for specific solutes (i.e. ordering of hydrolysis constants) shown in Figure 3-1 may differ slightly from other similar plots in the literature (e.g. /Hummel et al. 2002/) depending on different literature data sources used to obtain the hydrolysis constants. Hydrolysis constants in Figure 3-1 are taken from the SKB thermodynamic database /Duro et al. 2006/ where available. For other solutes, the NAGRA database /Hummel et al. 2002/ has been used preferentially and for solutes not represented in either, the MINTEQ database as distributed with the PHREEQC program has been used. Data for Co^{2+} was taken from /Bolzan and Arvía 1962/. Reaction constants for the very weakly hydrolysed solutes Rb^+ and Cs^+ are not usually considered important in thermodynamic modelling so these do not occur in any of the abovementioned databases. For these two solutes, Latimer's equation /Latimer 1926/ has been used to provide an estimate for purely comparative purposes. The trivalent actinides, Ac^{3+} and Cm^{3+} are notable by their absence in all abovementioned thermodynamic databases and therefore have not been included in the analysis.

As mentioned previously, the comparison of electrostatic index and first hydration constant is only a partial representation of the reactive complexity exhibited by these solutes and consideration must also be given to other classes of reactions if accurate geochemical analogies are to be ascertained. For the radionuclides that can exist in trivalent and tetravalent forms, reactions involving carbonate have been pointed out as being particularly relevant. The reactions involving carbonate are difficult to frame in a simple graphic representation, however, owing to the variety of possible reaction stoichiometries and clearly different predominance of various carbonate complexed species at equilibrium.

The trivalent actinides and lanthanides have nearly identical equilibrium constants for hydrolysis and carbonate complexation indicating similar sorptivity and impact of carbonate speciation in groundwater. For the tetravalent actinides, equilibrium constants for hydrolysis and carbonate complexation are broadly similar although there are some differences for higher order hydroxy-carbonato complexes since not all the elements have the same diversity of *recognised* carbonate complexation reactions. Of the tetravalent actinides, Th(IV) has the lowest stability constant(s) for hydrolysis indicating that it should exhibit the weakest sorption and highest solubility. On the basis of their known hydrolysis constants, Sn(IV) and Zr(IV) are predicted to have sorptivities at least as high as the tetravalent actinides. Tc(IV) is different to the other tetravalent species since the naked cationic form is not generally considered to exist in groundwater, although there are several recognised hydrolysis and carbonate reactions listed in the thermodynamic databases involving the basis specie, $TcO(OH)_2$. Tc(IV) is thought, however, to behave in a broadly similar fashion to the other tetravalent elements.

3.2.2 Particular geochemical analogues used in this compilation

Table 3-4 lists the geochemical analogues used for the purposes of assigning data in SR-Site. Cs(I) and Ni(II) are used as geochemical analogues for the sorption of Ag(I) and Cd(II), respectively. Both Ag(I) and Cd(II), however, can form chloride complexes in strongly saline groundwater that might compromise the validity of the assumed analogies given that the speciation of Cs(I) and Ni(II) is not dominated by chloride complexation to the same degree. Also, Ag^+ is a B-type cation /Ahrland et al. 1958/ which arguably makes it more closely related to Hg^+ or Cu^+ than Cs^+. The choice of Cs(I) as an analogue for Ag(I) here is necessitated by an absence of data for the other possible geochemical analogues and appears to be unavoidable. The same analogy was invoked previously by /Carbol and Engkvist 1997/ since it was deemed likely to cautiously underestimate the sorptivity of Ag(I). This previous judgement is accepted in the current compilation as being a reasonable working assumption. Both Ag(I) and Cd(II), however, are less important for radionuclide transport calculations due to the very short half-lives of their relevant radioisotopes so this is not considered to be a major deficiency.

Table 3-3. Summary of relative reactive properties of different redox states of significant elements. For ion-exchange, sorptivity is thought to be inversely related to hydrolysis constant. For surface complexation, binding strength can be posited to be proportionally related to the hydrolysis constant (assuming analogous behaviour for reactions with surface hydroxyl groups). Carbonate complexation constants can signify both extent of competitive binding in the aqueous phase and the possibility for ternary surface complex formation (Np(V) and U(VI).

Oxidation state	Relative order of reaction constants	Reaction class
I (Alkali)	Li > Na > K > Rb > Cs	Hydrolysis
II (Alkaline earth)	Mg > Ca > Sr > Ba > Ra	Hydrolysis
II (Transition)	Pd >> Pb >Ni > Cd	Hydrolysis
III	Ho > Eu > Sm > Am > Pu	Hydrolysis
	Eu > Ho ≈ Am > Sm > Pu	Carbonate complexation
IV	Sn > Pa > Pu >Np >U > Th	Hydrolysis
	Pu > Np > U > Th	Carbonate complexation
V	Np ≈ Pu	Hydrolysis
	Pu > Np	Carbonate complexation
VI	U > Pu	Hydrolysis
	U > Pu	Carbonate complexation

Note: Although Li, Na, K, Rb, Mg, Ca, Ba are not radionuclides in spent fuel, as groundwater constituents they are nonetheless important for understanding competitive ion-exchange in groundwater.

Table 3-4. Summary of geochemical analogues used for assigning K_d data in SR-Site (this data compilation). Analogues of questionable validity are labelled with an asterisk (*).

Analogue species	Representing
Cs(I)	Ag(I)*
Am(III)/Eu(III)	Ho(III), Sm(III), Pu(III), Ac(III), Cm(III)
Ni(II)	Cd(II)*
Pu(IV)	Np(IV), U(IV), Th(IV), Zr(IV)*, Sn(IV)*, Tc(IV)*
Non-sorbing	Cl(-I), I(-I), C(IV,-IV), Tc(VII), Mo(VI)

Other geochemical analogues not listed in Table 3-4 have been used in an indirect fashion in this compilation. In the model of ion-exchange which is used to predict changes in Ra(II) sorptivity in response to groundwater salinity, for example, a geochemical analogy is assumed to exist with Ba(II) when assigning selectivity coefficients for the ion-exchange reaction of Ra^{2+}. Other analogies are invoked in specific cases when assessing the reasonableness of K_d values established on the basis of sparse literature data. The sorption of Pb(II) on granite, for example, is only reported in a single reference and the analogue solute, Ni(II) is therefore used to assess whether the proposed K_d data are appropriate. On the basis of this comparison, a case could be made for the use of K_d data for Ni(II) in place of that recommended for Pb(II) sorption as a possible sensitivity analysis. This is likely to be very pessimistic, however, given the much higher first hydrolysis constant for Pb^{2+} which indicates stronger inner sphere surface complexation for Pb(II).

Most radionuclides that are predominantly speciated as anions or oxyanions are assumed to be non-sorbing. Selenium, Se(-II,IV,VI) is an exception owing to the availability of sorption data that indicates weak, although non-negligible sorption. Since sorption of anions should only occur on positively charged sites, only minerals featuring point of zero charge near groundwater pH are likely to sorb Se species. For granitic rocks, only microprecipitates of hematite in the rock matrix porosity are likely to fall into this category (e.g. /Jan et al. 2007, 2008/). Carbonate is not expected to sorb significantly in the rock matrix owing to its much higher concentration in groundwater. Elevated carbonate concentrations, however, may be important for limiting the sorption of Se by direct competition for binding sites on hematite.

3.2.3 Overview of available site specific data

During the Forsmark and Laxemar site investigations, sorption was quantified on crushed bore core samples of different representative rock types taken from each respective site. Sorption measurements were made for Cs, Sr, Am/Eu, Ra, Ni, U, and Np which were chosen to represent a broad spectrum of sorbing properties reflecting both ion-exchange and surface complexation binding mechanisms. Measurements, in some cases, were made using Eu instead of Am although the data for both elements are subsequently pooled under the assumption of geochemical analogy between the two elements.

The sorption measurements were made using a variety of contact groundwater compositions described as being *Fresh*, *Marine*, *Saline*, and *Brine* in character. An additional groundwater type of brackish non-marine character was defined for the Laxemar site and is referred to in this report as *Type V*. Compositions of the different groundwater types are given in Table 3-5. It should be noted that the groundwater type described as Saline was defined with slightly different composition for the Forsmark and Laxemar sites. These are specified as *Saline (Fm)* and *Saline (Lx)*, respectively.

Although there were roughly 950 data points each for Cs, Sr, and Am/Eu sorption at the Forsmark site, these were based on crushed rock samples from eight different borehole sections featuring three distinct rock types. Sorption data for Ni, Ra, Np(V), and U(VI) (roughly 200 data points each) were based on crushed rock samples from two borehole sections representing a single rock type. Similarly, there were 1,038 data points each for Cs, Sr, and Am/Eu sorption for Laxemar site-specific rock types. These were based on crushed rock samples from five different borehole sections featuring four distinct rock types. Sorption data for Ni, Ra, Np(V), and U(VI) (roughly 100 data points each) were based on crushed rock samples from one borehole section representing a single rock type.

Table 3-5. Groundwater compositions used in sorption studies for Forsmark and Laxemar site investigations. The compositions (mg/l) are based on groundwater sampled in specific intervals of the indicated boreholes and are deemed to be approximately representative of the main groundwater classes characteristic of each site.

Name	Type I	Type II	Type IIIa	Type IIIb	Type IV	Type V
Type	Fresh	Marine	Saline (Fm)	Saline (Lx)	Brine	Brackish
Borehole	HSH02	KFM02A	KFM03	KSH01A	KLX02	KLX04
Interval	0–200m	509–516m	639–646m	558–565m	1383–1392m	510–515m
Li^+	0.016	0.051	0.028	0.58	4.85	0.0152
Na^+	127	2 120	1 690	3 230	7450	691
K^+	2.16	33.3	14.2	12.4	32.6	3.19
Rb^+	(0-0252)[A]	0.0628	0.0393	0.0424	0.178	0.0424
Cs^+	(1.17×10^{-3})[A]	1.79×10^{-3}	7.09×10^{-4}	1.37×10^{-3}	0.0186	1.37×10^{-3}
NH_4^+	(0-0947)[A]	0.04	0.204	0.04	0.56	0.0319
Mg^{2+}	1.43	232	52.7	44.7	1.2	6.9
Ca^{2+}	5.21	934	1 470	2 190	14 800	234
Sr^{2+}	0.0695	7.95	16.9	32.2	253	4.67
Ba^{2+}	(1-29)[A]	0.188	0.0907	0.188	0.024	0.188
Fe^{2+}	(0-364)[C]	1.20	0.233	0.686	3.45	0.09
Mn^{2+}	0.02	2.12	0.318	0.46	1.11	0.109
F^-	3.03	0.9	0.204	0.967	(1-6)[D]	2.7
Cl^-	21.5	5 150	5 190	8 800	36 800	1 480
Br^-	(0-2)[B]	22	38.9	71	509	13.4
SO_4^{2-}	8.56	510	195	221	1 210	104
Si(tot)	6.56	5.2	6.28	4.7	2.6	6.63
HCO_3^-	252	124	21.9	12	42	51.4
S^{2-}	(0-01)[B]	0.05	0.0295	0.05	0.05	$6.0\ 10^{-3}$
pH	8.58	7.1	7.55	7.45	6.8	7.83

A) No measurements available, data imported from borehole KSH01.

B) Based on detection limit.

C) Based on the Fe-tot measurement.

D) No measurements available, data imported from borehole KLX02.

Although the large number of data points gives the impression that there is a very good statistical basis for parameterisation of site specific materials, it should also be remembered that the total number of data points includes replicates as well as different contact times and particle size fractions of the same crushed core samples.

3.2.4 Overview of literature data

Most literature data examined are based on crushed samples taken from single borehole sections at a particular site. These generally take the form of replicate samples for a single particle size and contact time (occasionally different spike concentrations of the element being studied). The range of experimental conditions represented in these data sets is typically less than for the site specific data sets described in Section 3.2.3 and the ranges of apparent variability are consequently narrower. For obvious reasons, however, this doesn't necessarily imply a lower level of uncertainty and it is important to take into consideration the possibility that bounds of uncertainty may be underestimated and thus incautious for the purposes of safety assessment calculations unless handled properly.

The literature references used for specific elements in this data compilation are summarised in Table 3-6. Since some of the literature sources have been used in a supporting role (either in addition to site-specific data, or purely for comparative purposes) how the data have actually been used is also specified.

Table 3-6. Summary of data sources for elements or redox states where site specific data are unavailable. Literature sources are divided into three categories (A), (B), or (C) depending on their usage in this compilation (see description of categories in table footnotes).

Element (redox state)	Reference	Usage
Pb(II)	/Papelis 2001/	(A)
Np(IV)	/Huitti et al. 1996/	(C)
Np(V)	/Huitti et al. 1996/	(B)
Ni(II)	/Kulmala and Hakanen 1993/	(C)
Nb(V)	/Kulmala and Hakanen 1993/	(A)
Pd(II)	/Tachi et al. 1999/	(A)
Pu(IV,V,VI)	/Huitti et al. 1996, Kulmala et al. 1998/	(A)
Pa(V)	/Huitti et al. 1996, Kulmala et al. 1996/	(A)
Ra(II)	/Kulmala and Hakanen 1995, Huitti et al. 1996/	(C)
Se(-II,IV,VI)	/Ticknor et al. 1996, Papelis 2001/	(A)
Tc(IV)	/Huitti et al. 1996/	(C)
Sn(IV)	/Ticknor et al. 1996/	(A)
U(VI)	/Huitti et al. 1996/	(B)
U(IV)	/Huitti et al. 1996/	(C)
Zr(IV)	/Huitti et al. 1996/	(A)

Notes: (A) literature data used as a primary basis for K_d recommendation
(B) used together with site investigation data to provide K_d recommendation
(C) supporting data for comparative purposes only (not used in K_d recommendation)

In this data compilation, estimates of K_d uncertainty for the typically small literature data sets have been augmented by a resampling approach. The underlying uncertainties associated with the individual data points are therefore included when estimating the overall uncertainty of the recommended K_d range. This gives an expanded uncertainty range over that which would be otherwise obtained by only considering the variance of the central estimates themselves as is customary in statistical analysis. For data where the individual measurements have high statistical precision relative to the variance of the set, this makes very little difference to the estimated uncertainty distribution. For data where the precision of individual measurements is low, this is important feature of the overall data uncertainty that cannot be neglected.

For the literature data sources, the uncertainty of the transfer factors used to extrapolate to site-specific conditions (see Section 5.1.1) were also formally propagated in the estimation of the K_d data uncertainty for individual data points. The overall uncertainty of the extrapolated data is then assumed to be a convex combination of the underlying uncertainty distributions comprising the set. This is particularly important for data sets comprised mainly of replicate measurements for a single rock sample, contact time, particle size, and groundwater composition since the variance of the measurement data is not likely to be truly representative of the actual data uncertainty.

Full propagation of measurement and transfer factor uncertainty was not performed for the site investigation data since these data sets were typically much larger and represent a greater diversity of experimental conditions (particle sizes, groundwater compositions, contact times, etc.) than that typical of the literature data. Another reason is that the transfer factors for site specific materials were considered more accurate than those calculated for literature data since the materials have been characterised using largely identical methods. Consequently, the uncertainty of the extrapolation is a smaller component of the overall data uncertainty and could be reasonably neglected for the site investigation data. An argument could be still be made, however, for the propagation of transfer factor uncertainties in the case of the site investigation data, although the recompense for doing this was considered outweighed by the possibility of risk dilution in probabilistic calculations and thus not merited. A detailed account of the handling of uncertainties for the data obtained from literature sources can be found in Appendix C.

4 Conditions for which data are supplied

4.1 Physical state of the bedrock

Recommended K_d data are supplied for unaltered matrix rock typical of the Forsmark and Laxemar site investigation areas. For Forsmark the reference rock type has been chosen as granite to granodiorite, metamorphic, medium-grained (SKB rock code 101057). For the Laxemar site, the Ävrö granite rock type has been chosen (SKB rock code 501044). These are selected as the reference rock types on account of the fact that they are dominant within the candidate rock volume at each site and also because the overwhelming majority of the sorption data are for these particular rock types making them an obvious choice for transport model parameterisation. Although it is theoretically possible to calculate flow-path averaged data for rock volumes containing more than one rock type, this was deemed inappropriate for the purposes of SR-Site since insufficient material property data are available for the different rock types in order for this to be done in a dependable manner.

The data are numerically corrected to more accurately represent the properties of the intact rock through the use of transfer factors which take into account total surface area and cation exchange capacity (CEC) of the materials. The surface area of intact rock has been assessed by characterisation of monolithic samples judged to be relatively undisturbed. It is assumed that the BET surface area of the monolithic samples of the site specific rocks are sufficiently representative that they can be used as a proxy for the rock matrix under in situ stress conditions.

Layers of hydrothermal alteration or weathering extending away from fracture surfaces into the rock matrix are expected to be associated with enhanced retention properties relative to the unaltered rock. This is due partly to the increased effective diffusivity near fracture surfaces on account of greater intensity of microfracturing, and partly due to increased sorptivity. Increased sorptivity of altered rock types is related to both the greater sorptive surface area associated with the altered rock as well as the formation of secondary minerals (e.g. hematite microprecipitates) that may have greater sorptivity than the original mineral phases. Since sorptivity of altered rocks does not always scale proportionally with total surface area as quantified by the BET method it was not deemed feasible to quantitatively account for the increased retention in the vicinity of fracture surfaces in a defensible manner for SR-Site safety assessment calculations. At the same time, it is also noted that this is one of the main conceptual uncertainties associated with the use of surface area correction factors for the extrapolation of generic sorption data to site-specific materials.

Although different samples of nominally similar rock types typically exhibit sorptive properties that appear to scale reasonably well with BET surface area, the different mineralogy of dissimilar rock types introduces considerable uncertainty when handling generic data. In most cases examined in this compilation, however, it appears that scaling generic sorption data with regard to BET surface area results in correction factors that may be too large and thus tend to give cautiously low extrapolated K_d values.

Additional retardation of radionuclide transport in fracture coatings has not been quantified. This is partly due to the difficulty in showing that data for a limited number of borehole intercepts with flow-bearing fractures can be extrapolated to the entire migration path and also due to the problem of estimating the additional retention in a defensible fashion based on limited statistical data for mineral abundances in fracture coatings and their sorptive properties. The additional retention may include sorption on clay minerals (e.g. chlorite, illite, smectite, etc.) and possible co-precipitation processes involving fracture minerals such as calcite and barite.

The main purpose of this compilation is to supply data for the unaltered rock matrix which is deemed to provide the bulk of the transport retardation at safety assessment timescales. Transport scenarios incorporating processes not related to sorption on the unaltered rock matrix are beyond the scope of this report and are the subject of other data reports (e.g. colloid transport) or are handled in the higher level reports of SR-Site. The neglection of retardation processes in fracture coatings and alteration layers adjacent to fracture surfaces is deemed cautious with regard to the transport scenarios to be modelled in SR-Site. It is noted, however, that certain hydrochemical scenarios may arise where it may be important to consider remobilisation of radionuclides associated with fracture filling minerals. This possibility is dealt with specifically in the SR-Site Radionuclide transport report /SKB 2010d/.

4.2 Hydrogeochemistry under application conditions

4.2.1 Overview of a glacial cycle

Simulations documented in /Salas et al. 2010/ are used to establish hydrochemical profiles of major groundwater constituents during the different time domains considered in SR-Site. In this compilation, much of the focus has been on the temperate period extending from the contemporary groundwater situation to that predicted to prevail at 9,000 y. As discussed previously in Section 2.4.3, the slow land uplift continuing since the previous Weichselian glaciation in combination with infiltration of meteoric water is expected to result in a gradual freshening of the groundwater hydrochemistry surrounding the repository. At some point in the future it is expected that glacial conditions will be restored in Scandinavia. Although many of the specific details are subject to uncertainty, it is possible to paint a broad picture of the sequence of events as they are expected to unfold during the glacial cycle. To a large extent this is informed by understanding of previous cycles of glaciation and interpretation of the imprint they have left on both the geology and hydrochemistry of the Forsmark and Laxemar sites.

The glacial cycle is divided up into a number of periods referred to as *temperate*, *peri-glacial*, *glacial*, and *submerged*. The term peri-glacial is used to describe the cold climate period prior to ice-front advance where processes related to freezing of water may significantly affect the hydrogeology and hydrochemistry of the site. The submerged period refers to the time domain after ice-front retreat where the isostatic load of the ice sheet has depressed the crust sufficiently that the site is inundated with marine water and consequently below sea level. Figure 4-1 illustrates the reference glacial cycle of 120 ka duration which is used as a basis for the geosphere transport assessment /SKB 2010d/. Although the evolution of groundwater hydrogeology and hydrochemistry is a continuous process, it is useful to consider certain representative timeframes during the glacial cycle to gain an appreciation of how groundwater hydrogeology and hydrochemistry are affected. The resulting *snapshots* of hydrogeological and hydrochemical conditions then can be used to inform the discussion of likely impacts on radionuclide transport.

There are a number of different hydrogeological and hydrochemical changes that occur during the glacial cycle that are important to consider. The first sequence of events during the temperate domain has already been discussed. An example of the expected evolution of groundwater composition (salinity) is shown in Figure 4-2. During the ice-front advance, the large hydraulic gradient near the advancing front of the ice margin results in dilute glacial meltwater being forced to great depth in the rock before exiting downstream of the advancing front although still short of the repository location. The meltwater comes in part from water under the ice itself held in a liquid state by isostatic pressure and partly from water draining from the surface of the ice through *moulins* near the ice margin (see Figure 4-3).

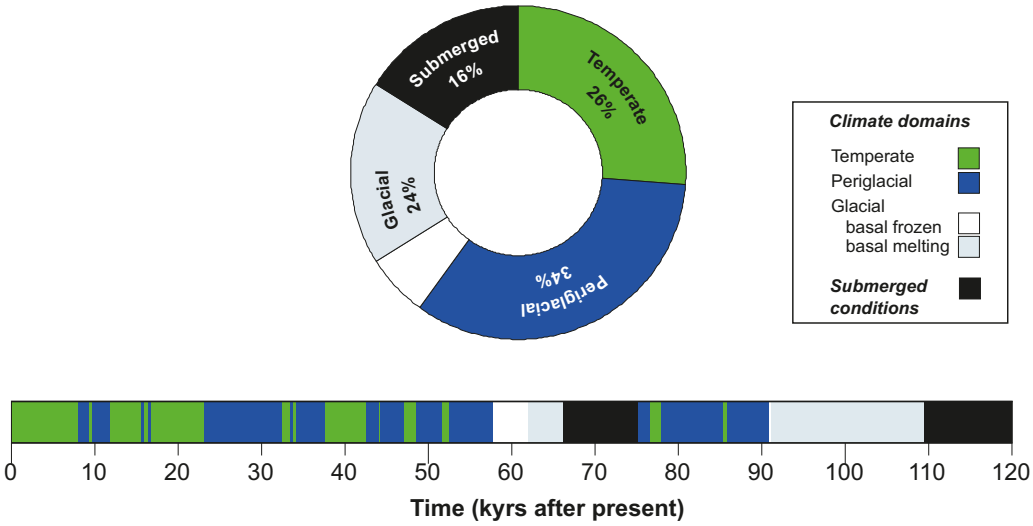

Figure 4-1. *Simplified illustration of a glacial cycle showing timing and duration of climate domains and submerged conditions at Forsmark in the SR-Site reference glacial cycle (120 ka). The bar below the pie chart shows the development of climate-related conditions for the reference glacial cycle as a time series of climate domains and submerged periods. Figure taken from /SKB 2010a/.*

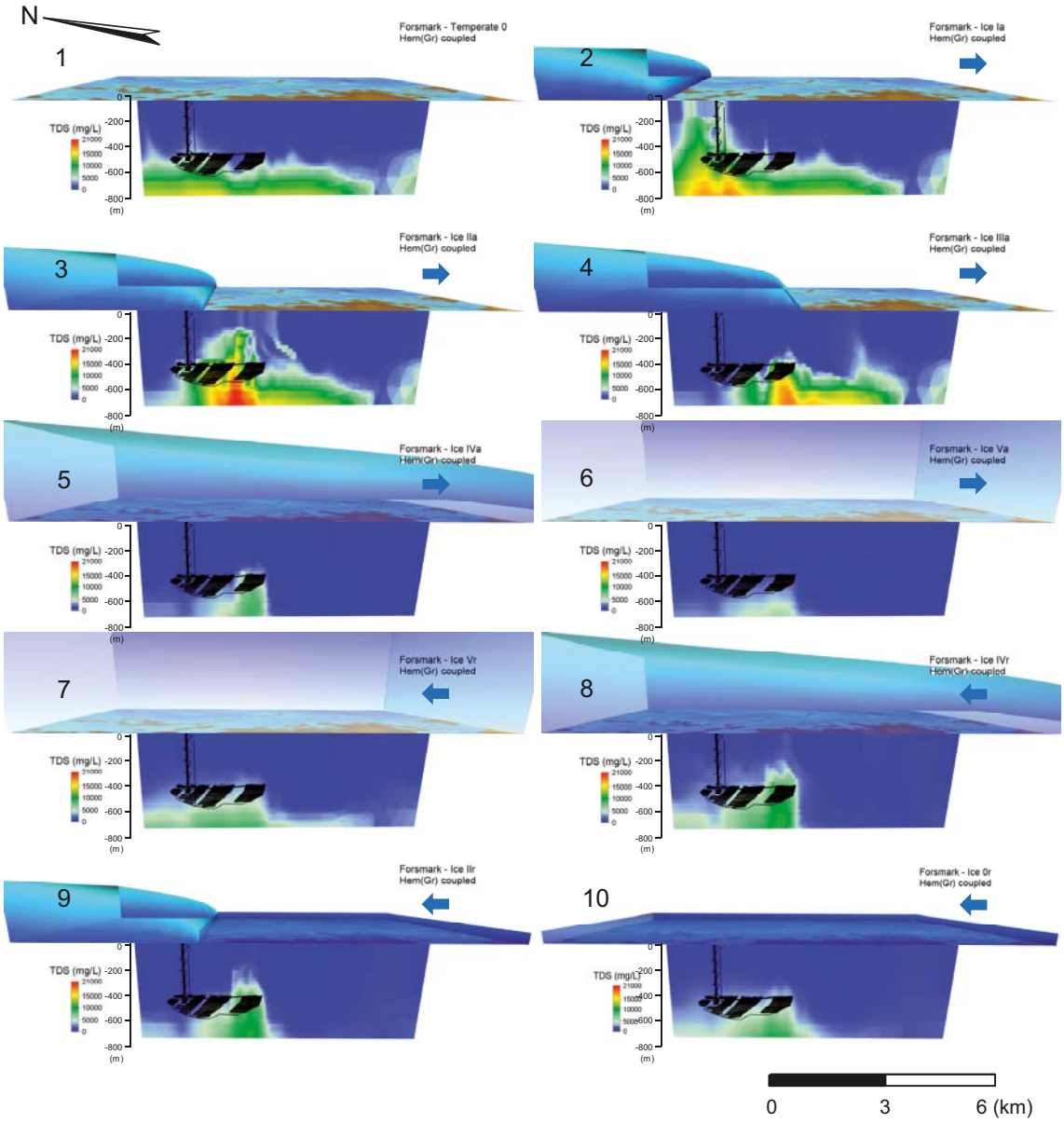

Figure 4-2. *Illustration of the evolution of groundwater salinity (vertical slices showing total dissolved solids, TDS mg/l) throughout a glacial cycle showing different snapshots of expected conditions at different times. The figure shows salinity profiles during ice sheet advance (1 to 6), and ice sheet retreat (7 to 10). When the ice sheet retreats the area is covered by a 100 m deep glacial meltwater lake. Figure taken from /Salas et al. 2010/.*

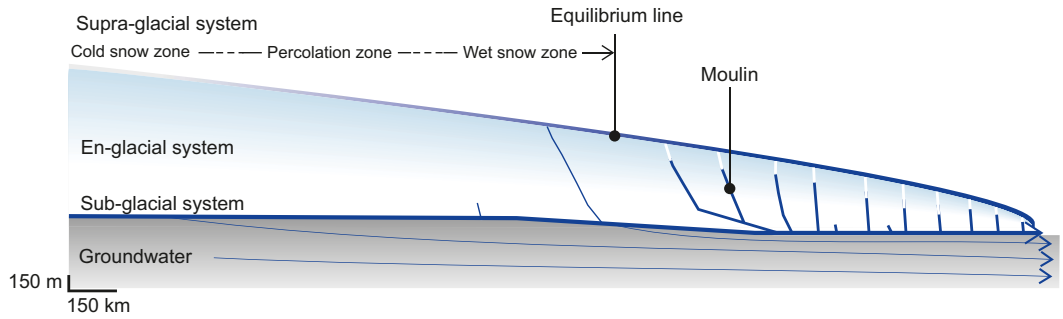

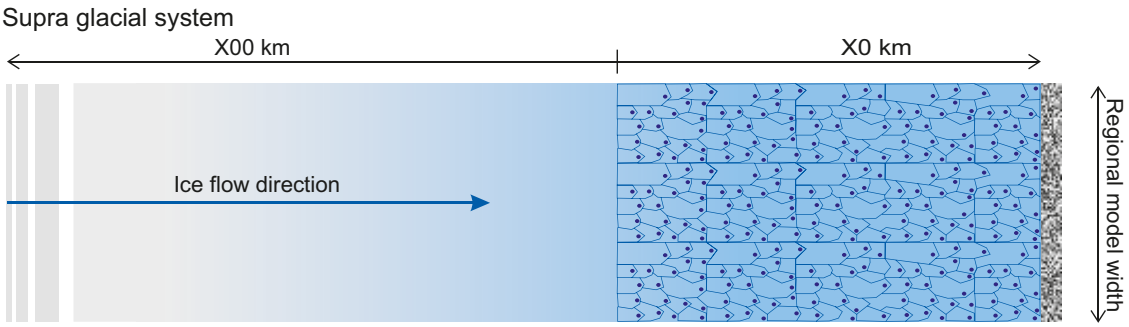

In the ablation area, downstream of the equilibrium line, a system of catchment areas is assumed. Each catchment area is assumed to be connected to the en- and sub-glacial systems through which surface melt water is assumed to reach the bed.

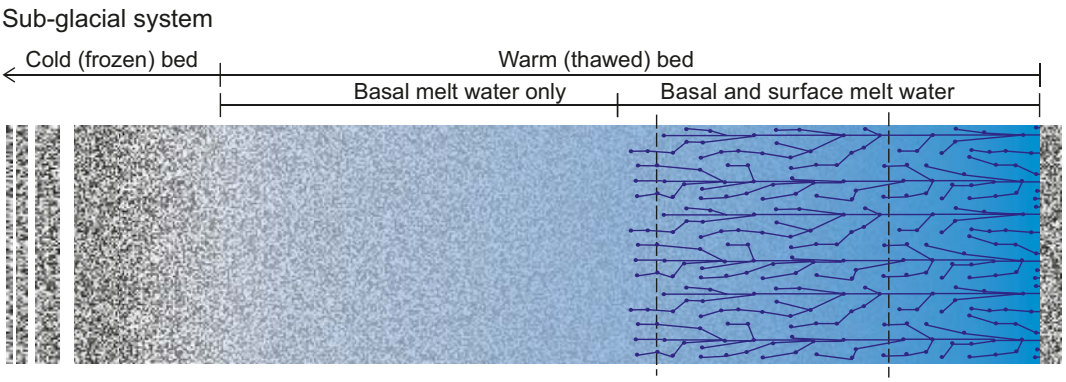

In the area of basal melting, where the water supply is from basal melting only, a slow system is assumed. In the ablation area, downstream the equilibrium line, where both basal and surface melt water are assumed to reach the bed, a fast system with channels or tunnels is assumed.

Figure 4-3. *Schematic illustration of an ice front showing meltwater in the subglacial system and drainage of surface water through moulins near the ice front margin. Figure taken from /SKB 2010a/.*

The disturbance in hydrogeological conditions displaces the existing saline water in the fracture system forcing it downwards and forwards. This results in *saline upconing* of deep brine groundwater to shallower depths in the repository vicinity. As the ice margin approaches and passes over the repository, the flows are partly reversed and meltwater begins to penetrate the repository environment. Since the hydraulic connectivity of the fracture system and conductivity of the rock is very heterogeneous, some recharge flowpaths experience very large and rapid changes in groundwater chemistry, whereas others are hardly affected. Generally it is the flowpaths characterised by high Darcy fluxes and low F-factors that experience the greatest changes.

After the ice margin has passed, the flow gradually decreases until at some point nearly stagnant conditions are achieved owing to the extremely low hydraulic gradients under the main part of the ice sheet and the influence of permafrost which reduces inflows to the groundwater system. The large mass of ice on top of the land mass simultaneously pushes down on the crust which has an influence

on hydraulic conductivity of the rock. During this phase of the repository evolution which may last up to about 10–20 ka /SKB 2010d/, flows are much reduced relative to the temperate phase and flowpaths are longer to the discharge locations downstream of the ice front. Salt stored in the rock matrix begins to diffuse back out into the diluted fracture water and slowly restores salinity in the fracture system.

As the ice front begins to retreat, a similar sequence of processes is set in motion although in reverse. In this case, the newly re-established saline groundwater in the fracture system may be rapidly flushed out by the forced intrusion of meltwater in the vicinity of the ice front. After the retreating ice front passes over the repository location, another episode of saline upconing might also occur. After the ice front has retreated even further, the saline conditions typical of the temperate period becomes slowly re-established. At this time, the isostatic load of the ice will result in the repository site being submerged below sea level.

The uplift of the crust due to glacial rebound will slowly change the shoreline location and topographic elevation of the land relative to the sea. The slowly changing topographical conditions and shoreline results in the repository eventually becoming an inland location. The slowly evolving hydrogeological situation then results in a gradual freshening of groundwater in the repository environment due to infiltrating meteoric water and a return to temperate conditions. Such glacial cycles can be expected to reoccur with a predetermined periodicity and changing intensity with time as described in the SR-Site Climate report /SKB 2010a/. During the full glacial cycle, there may also be transients (i.e. *stadial* and *interstadial* periods) as well as shorter glacial and interglacial periods.

4.2.2 Issues of importance for assignment of conditional K_d values

Although the description of a glacial cycle given in Section 4.2.1 gives a broad overview of the main events characterising the evolution of the groundwater system, this does not by itself fully inform the discussion of the particular impacts on radionuclide retention and migration processes. The main feature of importance for assignment of reliable conditional K_d values is, of course, the hydrochemical profile of groundwater in the repository environment. In spite of this, it is also important to consider flow rates and the F-factor during the different phases of repository evolution. This is important since it is not only the groundwater composition that determines transport of radionuclides, but also the flow rate, F-factor, and the duration of different hydrogeological-hydrochemical phases during which migration of radionuclides may occur.

It is also highly relevant to not only consider average changes in groundwater chemistry throughout the repository volume as a whole, but also how these are resolved in space and time. Owing to the heterogeneous nature of the fracture network, certain recharge flowpaths that transect the repository are associated with greater flowrates and lower F-factors than other flowpaths. In the context of groundwater chemistry evolution, it is not only the F-factor characterising the discharge flowpath between a canister position and the surface that is of significance, but also the recharge flowpath leading from the surface to the particular canister position. In certain respects, the F-factor of the recharge flowpath can be more important since it has a direct bearing on the rate of change of groundwater chemistry at the radionuclide source location. This has a strong influence on the magnitude of the conditional K_d value that is appropriate for describing radionuclide transport downstream along a migration path from the canister position.

Generally, the fast flowpaths featuring elevated flow and relatively low F-factors can be expected to exhibit greater fluctuations in chemical composition. When the regional hydraulic gradient increases in response to ice front advance or retreat, these flowpaths undergo larger relative changes with regard to flow and F-factor than flowpaths that experience more subdued changes. Some flowpaths may become more active during glacial advance and retreat owing to the changing hydraulic boundary conditions, effects of isostatic loading, and permafrost while others may become less active. Flow trajectories may also change slowly or quickly on the timescale of solute transport, which might leave more slowly migrating radionuclides effectively trapped in low flow regions while transporting other nuclides along freshly activated, although previously less active flowpaths. It is difficult to predict a priori how changes in groundwater chemistry will propagate along a flowpath relative to the transport of the nuclides, although one would expect the groundwater composition to approximately follow the same trends observed at the canister release locations although time-shifted forward by virtue of being downstream of the release location.

It is expected that solute plumes of sorbing nuclides will migrate more slowly than the groundwater mixing fronts which, to a large extent, are dominated by the transport of effectively non-sorbing components. Even if many of the major groundwater constituents do participate in ion-exchange reactions, their high concentrations and low sorptivity means that they can be considered effectively non-sorbing for the purposes of the safety assessment calculations. The situation is additionally complicated by chemical reactions involving minerals (e.g. calcite, ferric oxyhydroxides, and amorphous ferrous monosulphide) which buffer groundwater pH, carbonate concentration, and redox potentials. These chemical processes are considered in the hydrogeochemical calculations made by /Salas et al. 2010/ although they are not correlated to individual migration paths in the subsequent modelling described in the SR-Site Radionuclide transport report /SKB 2010d/.

The relatively rapid progression of mixing fronts along certain flowpaths means that many of the migrating nuclides may experience multiple cycles of groundwater mixing fronts catching up and overtaking them. In some cases this might be expected to give rise to strongly non-linear effects in their migration properties. Since it is not currently feasible to simulate geosphere transport involving non-linear sorption processes in a straight-forward manner in SR-Site, pessimistic scenarios for groundwater composition are chosen in order to cautiously overestimate radiological risks. Implicit in this treatment of sorption is the acknowledgement that predicted residence time distributions of radionuclides are largely fictive since they may not accurately represent the migration process as it actually occurs.

It is not currently possible to quantitatively relate changes in sorptivity with evolving groundwater chemistry for many of the safety relevant nuclides. This is primarily due to a lack of detailed, multi-dimensional data sets of unambiguous sorption data for relevant geological materials. An exception is made in the case of redox sensitive solutes where the aqueous phase chemistry is sufficiently well-understood to predict which redox state should be predominant. Generally, the redox sensitive solutes are expected to exhibit reduced mobility under strongly reducing conditions and increased mobility under mildly reducing or oxidising conditions. For a small number of elements that sorb by means of ion-exchange, it is possible to make approximate estimates of the impact of changing groundwater chemistry using a thermodynamic modelling approach. This principally involves assessing the impact of changing ionic strength on ion-exchange sorptivity. How these changes in sorptivity are quantified is discussed in more detail in Section 5.1.1.

In cases where it is not possible to quantitatively estimate the impact of changing groundwater composition, it is necessary to combine sorption data representing a wide range of contact water compositions. In this manner, uncertainty arising due to the diversity of hydrochemical conditions during the different time domains is approximately accounted for. In cases where it is possible to make quantitative predictions of altered sorptivity, it is important to consider the entire glacial cycle to ascertain which groundwater conditions should be deemed most representative for safety assessment calculations involving radionuclide transport. Although very brief periods of high salinity and flowrate are expected during ice margin advance and retreat (see Figure 4-2), these are thought to be sufficiently short-lived that they can be neglected. This must also be considered in the context of *landscape dose factors* (LDF's) for the particular time domain under consideration which may alter its relative importance for radiological risk.

The challenge is then to identify the most unfavourable (although still representative) conditions expected for nuclide transport and assume this as a pessimistic scenario for assignment of conditionally constant K_d values. Since the statistics of groundwater composition are not representative of individual migration paths, this represents a large epistemic uncertainty which gives rise to large ranges of uncertainty for the recommended K_d values. The handling of this uncertainty is discussed in more detail in Chapter 5.

5 Quantification of data and uncertainties

Since sorption partitioning data are obtained by laboratory experiments involving crushed and sieved rock samples in contact with synthetic groundwater, corrections typically need to be made to extrapolate the data to site-specific, in situ conditions. This may include; corrections for the state of disaggregation of the laboratory samples relative to the in situ rock, corrections for differences in mineralogy, and corrections for deviations in the in situ groundwater composition. Section 5.1 gives a detailed overview of the approach used to transfer data derived from laboratory investigations to in situ conditions. Section 5.2 contains a brief summary of element specific features and processes and presents the recommended data.

5.1 Procedures for extrapolation of data and quantification of uncertainty

Owing to large uncertainties concerning the interpretation of time dependencies in the laboratory data, no attempt has been made to model or filter the data with regard to sorption contact time. The slow diffusive redistribution of solute from the contacting solution and external surfaces to the internal surfaces of crushed rock particles implies a sorptivity that increases slowly with time. Since the modelling of diffusive disequilibrium tends to give inflated and uncertain upper limits for the K_d value, the neglection of this process is thought to be a relatively cautious assumption. Other uncertainties relating to chemical weathering or compositional drift during the course of experiments is captured by not excluding data for the largest particle sizes and shortest contact times to give a cautiously bounded lower limit to the K_d uncertainty distribution. This discussion concerns mostly the site specific data sets where detailed data for different particle size fractions and contact times are available. For literature data, however, the sampled experimental parameter space is frequently sparser (e.g. data typically consists of a single size fraction and contact time) and potentially associated with greater levels of uncertainty.

The corrections applied to the data take the form of; 1) a mechanical damage transfer factor to account for the differences in sorptive surface area between crushed and in situ rock, and; 2) a CEC (cation exchange capacity) transfer factor to account for mineralogical differences between the rock used in experiments and the site specific rock. The mechanical damage transfer factor is based on the ratio of measured BET surface areas of the intact rock relative to the crushed samples used in experiments. The CEC transfer factor is based on CEC measurements wherever possible, although in some cases Fe-content or estimated biotite mineral fractions have been used as proxy indictors of CEC. In cases where multiple size fractions have been used in laboratory investigations, an additional surface area normalising transfer factor is used to provide a common reference basis for calculations.

As outlined previously, the objective of this report is generally not to provide a description of sorptive chemistry that captures radionuclide retention processes exactly as they would occur in the geosphere. Instead the primary function of the work undertaken is to make recommendations of K_d values that are cautiously chosen with regard to the particular transport scenarios modelled to avoid underestimation of radiological risks in the SR-Site safety assessment.

5.1.1 Overview of transfer factor approach for sorption property correction

In this K_d data compilation, a number of *transfer factors* (using the terminology of /Bradbury and Baeyens 1998/) are used to account for various biases in the underlying measurement data derived from laboratory experiments. The approach is broadly similar to that discussed previously in /Crawford et al. 2006/ although with some minor modifications. The transfer factors employed in this work are:

f_A A surface area normalisation transfer factor which accounts for the difference in sorptive surface area amongst different size fractions used in laboratory investigations. It is defined as the ratio of the sorptive surface area of a reference size fraction of crushed rock relative to the actual size fraction used in the experiment. This allows data obtained for different size fractions to be converted into a mutually compatible form that can then be pooled before extrapolation to in situ conditions.

f_m A mechanical damage transfer factor which accounts for differences between the sorptive surface area of the reference size fraction of crushed rock and undisturbed rock in situ.

f_{cec} A transfer factor which accounts for differences between the cation exchange capacity (CEC) of the site specific rock type and that used in laboratory experiments.

f_{chem} A transfer factor which accounts for differences between the groundwater chemistry under application conditions in situ and that used in laboratory investigations.

Since the first three transfer factors f_A, f_m, and f_{cec} are defined as ratios of variables that have either normal or log-normally distributed uncertainty ranges, the transfer factors themselves also have log-normally distributed uncertainty ranges. Since the apparent R_d values are also defined as ratios of activity (or concentration), they too are expected to be associated with log-normally distributed uncertainties. The first three transfer factors are multiplicative (additive in logarithmic space) and are applied in the following fashion:

$$R_d^{\wp} = R_d \cdot f_A \qquad (5\text{-}1)$$

$$K_d^{\wp} = R_d^{\wp} \cdot f_m \cdot f_{cec} \qquad (5\text{-}2)$$

Although the chemistry transfer factor is defined as a ratio, there is no particular reason for this to be log-normally distributed since it contains elements of both uncertainty and spatial variability (typically non-random). In the cases where f_{chem} can be estimated, the uncertainty range for the conditional K_d value corresponding to a particular groundwater hydrochemical profile is obtained by convolution of the individual probability density functions describing $K_d^{\wp}$ and f_{chem}.

$$K_d = K_d^{\wp} \otimes f_{chem} \qquad (5\text{-}3)$$

The different forms of the R_d and K_d partitioning coefficients used in Equations 5-1 to 5-3 have the following specific meanings:

R_d is the apparent sorption partitioning coefficient (i.e. raw data estimate) derived from laboratory measurements for a particular crushed particle size fraction.

$R_d^{\wp}$ is a surface area normalised sorption partitioning coefficient for a specific crushed rock reference size fraction.

$K_d^{\wp}$ is the recommended, site-specific sorption partitioning coefficient for sorption on intact rock in situ. It is applicable for the actual groundwater composition used in the laboratory investigation.

K_d is the recommended, site-specific sorption partitioning coefficient for sorption on intact rock in situ. The K_d value is corrected for application groundwater compositions differing from the reference groundwater composition used in the laboratory investigation.

Although individual $K_d^{\wp}$ values calculated using Equation 5-2 are formally associated with log-normally distributed uncertainties, the ensemble distribution of pooled $K_d^{\wp}$ values is not always log-normally distributed. This depends entirely on the heterogeneity of the underlying data sets that are pooled together and their applicability for the site specific conditions. In most cases, however, the pooled distributions of $K_d^{\wp}$ values are sufficiently well-behaved that a simple log-normal uncertainty distribution can be assumed in describing the aggregate data set.

Implicit in the use of these transfer factors is the assumption that diffusive disequilibrium can be neglected when using sorption data derived from laboratory investigations. Generally the neglection of diffusion gives pessimistic predictions of K_d values since sorptivity should always be underestimated. There is a noteworthy time dependency with a trend towards larger R_d values at increasing contact times in the sorption data reported in the site investigations. The origin of this time dependency is unclear as it does not always appear to be fully compatible with simple models of diffusive uptake. Slow weathering processes, for example, can also contribute to the slow change in sorptivity over time. It may also be the case that there are other processes which introduce additional biases related to contact solution composition that cannot be properly accounted for at this time (e.g. changes in headspace pCO_2, chemical kinetics, etc.).

The pragmatic approach has therefore been to treat data from all particle size fractions and contact times with equal dignity thereby consolidating these additional epistemic uncertainties together as part of an overall envelope of data uncertainty. In most cases the between-sample variability appears to be sufficiently large that the overall temporal trend is weak when considering the aggregate data set and differences in sorptive surface area appears to be the dominant factor.

Calculation of the surface area normalisation transfer factor, f_A

In the laboratory investigations connected with the site descriptive modelling for Forsmark /Byegård et al. 2008/ and Laxemar /Selnert et al. 2009/, sorption measurements were performed on a number of different size fractions of crushed rock obtained from bore core samples. BET surface area measurements were also performed on crushed rock although using size fractions that sometimes differed from those used in sorption experiments as indicated in Table 5-1.

Precise particle size measurements were not made on the sieve size fractions used in the laboratory investigations. Instead, the mean particle size is estimated using the model described by /André et al. 2008a/ where a uniform distribution of particle sizes spanning the upper (d_2) and lower (d_1) sieve size is assumed:

$$d_m = \frac{3}{4}\left(\frac{d_2^4 - d_1^4}{d_2^3 - d_1^3}\right) \qquad (5\text{-}4)$$

Sorption, being a surface mediated process, is strongly coupled to the surface area of different minerals present in a geological matrix. The quantification of how sorptivity varies with surface area is therefore a particularly important aspect of data transfer from laboratory measurements to safety assessment conditions. If sorption data derived from a number of particle sizes or different sources are to be used to recommend K_d ranges for safety assessment, it is first necessary to transform the data into a form that allows the data to be pooled in a consistent fashion. Since the BET surface area measurements documented in the site investigations were not always available for the same particle sizes as those used in sorption measurements, there is also a necessity to extrapolate the sorption data to some reference particle size where surface area measurements are available.

Table 5-1. Summary of measurements performed on crushed rock size fractions in the Forsmark /Byegård et al. 2008/ and Laxemar /Selnert et al. 2009/ site investigations. The (mean) particle size is estimated using Equation 5-4.

Sieve size (mm)	Particle size (mm)	Sorption meas.	BET meas.
0.063–0.125	0.101	Yes	Yes
0.25–0.5	0.402	Yes	No
1.0–2.0	1.607	Yes	No
2.0–4.0	3.214	No	Yes

The specific surface area of crushed rock is equal to a contribution from external particle surfaces and the surface area of the internal porosity of the particles. The contribution from the internal porosity is customarily assumed to be statistically invariant over different size fractions as is the average surface roughness and sphericity of irregular particles comprising the crushed rock samples. Under these assumptions, the specific surface area of different particle size fractions can be given using the equation:

$$A_s\left(\mathrm{m}^2/\mathrm{g}\right) = A_{\mathrm{ext}} + A_{\mathrm{int}} = \frac{6\lambda}{\rho_b d_m} + A_{\mathrm{int}} \qquad (5\text{-}5)$$

If specific surface area measurements of different particle size fractions are available, the surface roughness/sphericity parameter, λ and specific internal surface area, A_{int} can be obtained from the slope and intercept of the linear regression line best describing the measurement data plotted against the inverse of average particle size, $1/\mathrm{d_m}$. The site specific BET measurement data described in /Byegård et al. 2008/ and /Selnert et al. 2009/ were performed on duplicate samples of the 0.063–0.125 mm and 2–4 mm size fraction. Owing to the low number of replicates and the use of only two size fractions, this results in a considerable uncertainty in both the slope and intercept of the regression line for the data, particularly if the underlying assumptions of the simplified regression model are not properly fulfilled.

The approach adopted in this compilation is to firstly introduce a transfer factor, f_A that allows the sorption data obtained for different crushed rock size fractions to be scaled to a convenient reference particle size. Since the largest particle size fraction is theoretically most similar to undisturbed in situ rock, the 2–4 mm particle size was chosen as the appropriate reference size for this calculation. Assuming that the sorptivity of different crushed rock fractions of the same rock type scales linearly with BET surface area, Equation 5-5 can be used to define the surface area transfer factor, f_A as:

$$f_A = \left(\frac{6\lambda}{\rho_b d_{ref}} + A_{\mathrm{int}}\right) \Bigg/ \left(\frac{6\lambda}{\rho_b d_m} + A_{\mathrm{int}}\right) \qquad (5\text{-}6)$$

Where d_{ref} is the reference particle size and d_m is the average particle size according to the particle size distribution model (e.g. Equation 5-4). In order to circumvent problems relating to extrapolation from small sample numbers and provide cautious transfer factors for surface area effects related to particle size, there are two important limiting cases to consider:

1. External surface area of crushed particles is the dominant contributor to total sorptive surface area ($f_A \approx d_m / d_{ref}$).
2. Internal surface area of crushed particles is the dominant contributor to total sorptive surface area ($f_A \approx 1$).

In the first case, it is not necessary to know the surface area of the internal porosity since the external surface area of the crushed rock particles is assumed to be dominant. Furthermore, if the surface roughness/sphericity can be assumed to be approximately constant over different size fractions, it is not necessary to know its value exactly since it occurs in both the numerator and denominator of Equation 5-6 and mutually cancels. In the second case, if the internal surface area is very large then there should be no measurable difference between the properties of small and large particles since the specific surface area is approximately the same in both cases (implying no surface area correction is necessary). According to the simplified model of surface area partitioning, the correction factor f_A therefore is constrained to always lie between the ratio of characteristic particle sizes (d_m/d_{ref}) and unity.

In reality, particles always have a geometric external surface area that must be equal to or greater than that of a sphere of equivalent volume (since a sphere is the minimal surface that can enclose a volume in three-dimensional space). In many studies documented in the literature (e.g. /White and Brantley 2003/), the external surface area of particles can be shown to be significantly greater than that of a sphere of equivalent volume, hence the use of a surface roughness/sphericity factor to modify the size of the external surface area. In /André et al. 2009/, for example, λ is found to vary between about 6–13 based upon linear regression of data using Equation 5-5. The value of λ is highly variable and depends on how the rock is crushed and can vary significantly between different samples and rock types depending on their material properties. The impact of the different assumptions contained in the limiting cases (1) and (2) outlined above is illustrated in Figure 5-1 where raw site investigation data (R_d) for Am sorption using saline groundwater is extrapolated to the reference size fraction (3.214 mm) using Equation 5-1.

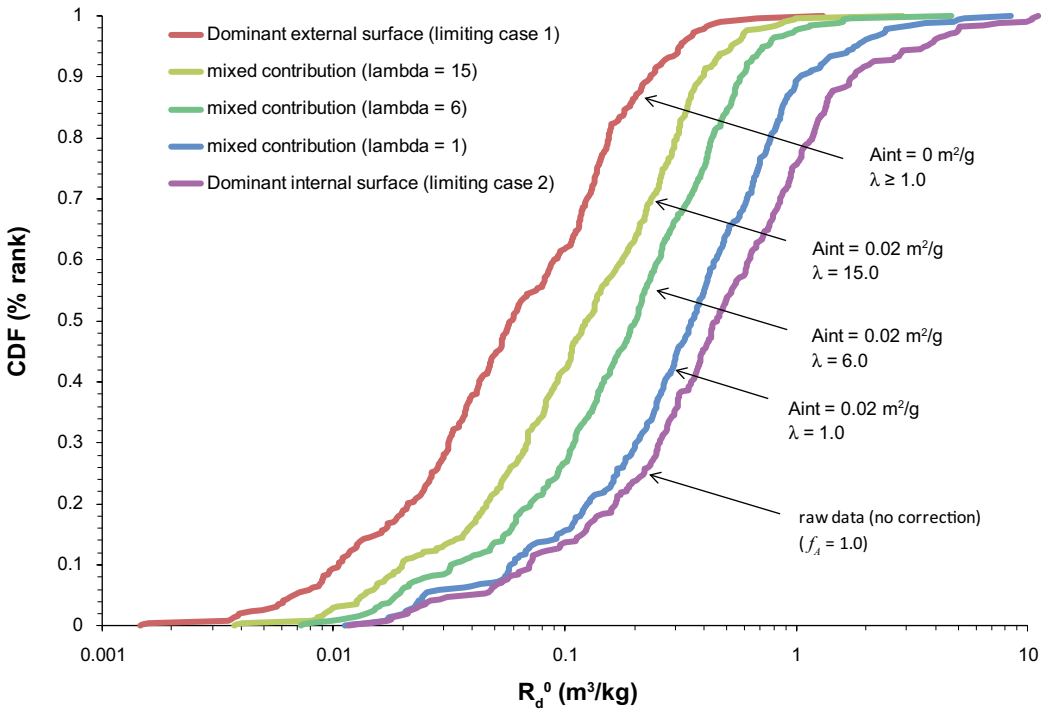

Figure 5-1. *Surface-area corrected, R_d^0 (m^3/kg) values assuming different cases of surface area distribution according to Equation 5.6. Cases labelled (1) and (2) are limiting and all other variants are constrained to lie between these cases. Data are for an ensemble data set of Am(III) sorption measurements on different particle size fractions of crushed rock in contact with saline water /Byegård et al. 2008/ and are presented as a cumulative distribution function (CDF).*

For the purposes of safety assessment, the most defensible choice is to assume that the external particle surfaces dominate the measured BET surface area of crushed rock samples as this will tend to overpredict the correction required and give smaller R_d^0 values as can be readily appreciated from Figure 5-1. As can be seen from Table 5-2, the smallest size fractions are associated with the largest corrections. For the 0.063–0.125 mm fraction, for example, the correction implies a reduction of the measured R_d value by factor of 32, whereas for the largest size fraction used in sorption measurements (1–2 mm) the correction implies a reduction by only a factor of 2. Since the smallest size fractions also can be safely assumed to have the greatest surface area contribution from freshly created external surfaces, the assumption appears to be cautious.

It should be noted that in this report, the use of the surface area transfer factor f_A is limited to the site investigation data from Forsmark and Laxemar where data is available for different crushed size fractions. The use of the f_A transfer factor allows the data set to be pooled in a straight-forward fashion before extrapolation to in situ conditions. For literature data where only a single size fraction is used, f_A has not been calculated since the actual size fraction used in experiments can be adopted directly as the reference size.

Table 5-2. Surface area normalisation transfer factors, f_A for different size fractions of crushed rock used in Forsmark and Laxemar site investigatons.

Sieve size (mm)	Particle size (mm)	f_A	$1/f_A$
0.063–0.125	0.101	0.0313	32
0.25–0.5	0.402	0.125	8
1.0–2.0	1.607	0.5	2
2.0–4.0	3.214	1	1

Calculation of the mechanical damage transfer factor, f_m

This transfer factor accounts for differences in sorptive surface area between the reference size fraction of crushed rock used in laboratory investigations and that of undisturbed rock in situ. Although linear regression of BET surface area data can be used to estimate the internal surface area of crushed rock particles, mechanical damage arising from the crushing process induces additional microfracturing which supplements the pre-existing surface area of the internal porosity. The bias introduced by using the estimated internal surface area of the rock as a proxy for the sorptive surface area under in situ conditions can then result in the recommendation of non-cautious K_d data ranges for safety assessment.

To avoid this, it is necessary to measure the sorptive surface area of the rock under as close to in situ conditions as possible. Generally this is not possible to fully achieve owing to stress release and drilling induced mechanical damage incurred when extracting bore core samples. If the rock samples are of a sufficiently large and monolithic form, however, the error introduced is likely to be small. The BET surface areas of intact rock core samples from the Forsmark and Laxemar site investigation areas have been measured by /André et al. 2009/. The internal surface area of the 400–500 g monoliths was found to be 0.018±0.005 m^2/g (3 replicates) for the Forsmark rock and 0.025±0.028 m^2/g (6 replicates) for the Laxemar rock. The larger standard error of the Laxemar measurements is thought to be due to the greater number of samples used. Since the BET surface area measurements of the crushed rock samples used in the site investigations were also based on small numbers of replicates, 2σ errors were propagated in the Gaussian error analysis as is standard laboratory practice for such small sample sizes. Once again assuming that the sorptivity of different crushed rock fractions scales in an approximately linear fashion with BET surface area, the mechanical damage transfer factor, f_m is defined as:

$$f_m = \frac{A_0}{A_{ref}} \qquad (5\text{-}7)$$

Where A_0 (m^2/g) is the measured BET surface area of the core sample and A_{ref} (m^2/g) is the corresponding surface area of the reference size fraction of the crushed rock used in the sorption characterisation. In this report it is assumed that the uncertainty distribution for both the numerator and denominator of Equation 5-7 is lognormally distributed. This gives slightly more pessimistic mechanical transfer factors than if normal uncertainties were to be assumed. This choice is considered to be motivated in the current data compilation for reasons of caution given the very low sample numbers upon which the calculations are based. It can also be motivated on account of the fact that the frequently high relative errors associated with the measurement data would otherwise suggest the existence of physically non-meaningful, negative surface areas. The choice of a lognormal form for the uncertainty distribution is therefore a logical choice to avoid such situations. In either case, the ratio of normally-distributed or lognormally-distributed variables gives a lognormally distributed transfer factor as a result. Using the Forsmark core sample results allows data for both investigation sites (and literature data) to be scaled to Forsmark site specific conditions. The results for Forsmark are given in Table 5-3.

Calculation of the cation exchange capacity (CEC) transfer factor, f_{cec}

In the Forsmark and Laxemar site investigations, cation exchange capacities of crushed rock samples were measured for site specific rock types. These data are also reported in /Byegård et al. 2008/ and /Selnert et al. 2009/. The gravimetric measurement technique was based on the ISO 13536 standard which uses a 1 M $BaCl_2$ solution to displace ion-exchanged cations followed by a step in which the exchanged Ba^{2+} ions are in turn displaced by Mg^{2+} (0.02 m $MgSO_4$ solution) and then precipitated as insoluble $BaSO_4$ (barite). The CEC data for rocks sampled from both investigation areas are given in Table 5-4.

As can be seen from Table 5-4, the CEC measurements for site specific rock materials are subject to large uncertainties. Generally, only a small part of the Mg^{2+} is absorbed in the Ba^{2+} displacement step which renders it difficult to verify a concentration decrease from a blank solution. This is compounded by the relatively large uncertainty in Mg^{2+} concentrations (~5%) which means that in most cases statistically verifiable CEC estimates cannot be made.

Table 5-3. Mechanical damage transfer factor, f_m scaled to Forsmark specific conditions. The f_m values are calculated using Equation 5-7 assuming an available matrix porosity surface area of 0.018±0.005 m²/g. The error estimates for f_m are derived for 2σ errors using Gaussian error propagation. It is noted that the large error estimates for f_m (in some cases are equal to or larger than the central estimate) are simply a measure of the statistical dispersion of the transfer factor uncertainty distribution on an arithmetic scale and should not be taken to imply the existence of negative arithmetic transfer factors.

Borehole	Sample depth	A_{ref}	f_m	$\log_{10} f_m$
KFM01A	103 m	0.024±0.022	0.74±1.39	0.14±0.56
KFM01A	487 m	0.047±0.004	0.38±0.56	–0.46±0.22
KFM01A	908 m	0.030±0.001	0.60±0.31	–0.27±0.21
KFM02A	552 m	0.041±0.010	0.44±0.32	–0.35±0.30
KFM03A	536 m	0.013±0.003	1.38±0.91	0.13±0.27
KFM06A	440 m	0.035±0.005	0.52±0.30	–0.32±0.24
KFM07A	387 m	0.032±0.008	0.56±0.41	–0.25±0.30
KLX02	217 m	0.061±0.006	0.29±0.16	–0.57±0.23
KLX02	753 m	0.042±0.010	0.43±0.29	–0.38±0.28
KLX02A	509 m	0.029±0.006	0.62±0.40	–0.23±0.27
KLX02A	682 m	0.037±0.007	0.48±0.31	–0.34±0.26
KLX02A	936 m	0.096±0.004	0.19±0.10	–0.77±0.21
KLX03A	522 m	0.035±0.0004	0.51±0.26	–0.34±0.21
KLX04A	489 m	0.042±0.002	0.43±0.22	–0.41±0.21
KLX04A	718 m	0.029±0.021	0.61±0.93	–0.02±0.50
KLX05	482 m	0.094±0.007	0.19±0.10	–0.76±0.22
KSH01A	981 m	0.051±0.009	0.35±0.22	–0.48±0.25

Table 5-4. Cation exchange capacities (cmol/kg) measured for Forsmark and Laxemar rock types. The measurements are for single samples (no replicates) with 1σ error estimates based on 5% uncertainty in Mg^{2+} quantification. In cases where no statistically verifiable CEC could be measured a value specified as less than the detection limit is given.

Borehole	Sample depth	Rock type	Size fraction (mm)	CEC (cmol/kg)
KFM01A	103 m	101057	0.063–0.125	0.9±0.7
			1–2	< 1
KFM01A	487 m	101057	0.063–0.125	0.7±0.6
			1–2	< 1.2
KFM01A	908 m	101057	0.063–0.125	< 0.6
			1–2	< 0.9
KFM02A	552 m	101051	0.063–0.125	2.6±2.0
			1–2	< 1.2
KLX02	217 m	501056	0.063–0.125	< 2.5
			1–2	< 1.0
KLX03A	522 m	501046	0.063–0.125	2.1±1.4
			1–2	0.9±0.7
KLX02A	682 m	501031	0.063–0.125	2.3±1.4
			1–2	1.0±0.6
KLX04A	489 m	501036	0.063–0.125	2.2±0.9
			1–2	1.0±0.7
KLX05	482 m	501036	0.063–0.125	2.3±1.8

This presents a problem for comparison between site specific rock types and literature data since it is not possible to calculate robust CEC transfer factors scaled to the site specific materials. In granitic rocks the CEC is generally dominated by the so-called *dark minerals* consisting of biotite, hornblende, and to a lesser extent chlorite. The Fe content of the rock is also very closely related to the biotite and hornblende concentrations. If the biotite contents of the rock materials reported in the literature data are known then approximate transfer factors can be estimated on the basis of the relative biotite content compared to the site specific rock types.

Laxemar rock types generally have a higher biotite content than Forsmark rocks and so can be expected to have a proportionately larger CEC. Fortunately, for the purposes of scaling sorption data for Laxemar rock to Forsmark site specific conditions, there are a large number of measurements of Fe content of rock from the two sites. These data take the form of whole rock geochemical analyses and are documented in the site investigation reports although are summarised in /Sidborn et al. 2010/. Assuming that the CEC of the rock samples is dominated by the biotite content of the rocks and that the measured Fe content is proportional to the biotite concentration, the CEC transfer factor can be estimated as:

$$f_{cec} = \frac{CEC_0}{CEC_{ref}} \approx \frac{[\text{Biotite }\%]_0}{[\text{Biotite }\%]_{ref}} \approx \frac{\text{Fe}_0}{\text{Fe}_{ref}} \qquad (5\text{-}8)$$

In a similar fashion to previous transfer factor definitions, the subscript zero specifies the CEC, biotite, or Fe content of the site specific rock and the subscript labelled *ref* is the corresponding measure for the crushed rock used in sorption experiments. Since the site specific rock types from the Forsmark and Laxemar areas have been studied using identical methods, the relative variation of Fe content between the sites is deemed a good proxy for calculation of a CEC transfer factor using Equation 5-8. Since the Fe content is reported as percentage Fe_2O_3 by mass, it is necessary to use a Beta distribution to model the data since the percentage by definition cannot be less than 0% or exceed 100%. From the specified mean and standard deviation of Fe_2O_3 content given in /Sidborn et al. 2010/, the parameters of the Beta distribution can be estimated and stochastic simulations made to calculate f_{cec} using a Monte-Carlo method. The uncertainty distribution for the f_{cec} transfer factor calculated in this fashion is shown in Figure 5-2 along with a lognormal fit to the data histogram.

For radionuclides where only literature data sources were available, the measured CEC of the rock was used assuming a very approximate CEC value of 1.0±0.5 cmol/kg for the Forsmark site-specific rock. In cases where no CEC data were available, a subjective assessment based on reported biotite content was used instead. The average biotite content of the reference metagranite (SKB rock code 101057) rock type in Forsmark is roughly 5.4% /Sandström and Stephens 2009/. In most cases, if the biotite content of the rock used in the literature sources was approximately the same (i.e. differing by not more than about 50%) then the CEC transfer factor was neglected.

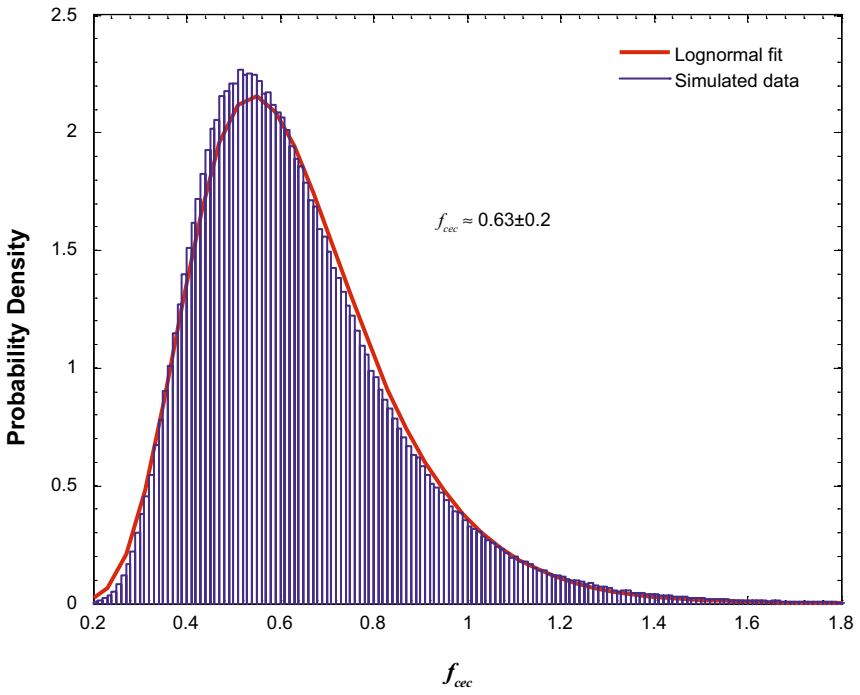

Figure 5-2. *Uncertainty distribution for the cation exchange capacity transfer factor, f_{cec} for the conversion of Laxemar R_d data (Ävrö granite, rock type 501044) to values appropriate for Forsmark rock (Forsmark metagranite, SKB rock code 101057) assuming CEC in approximate proportionality to measured Fe_2O_3 content. Although the Fe_2O_3 content of the rock (wt%) is modelled as a Beta distribution on the interval [0,1], the resulting uncertainty distribution for the ratio is well described by a lognormal distribution as indicated in the figure.*

Generally, the CEC is thought to have the largest impact on solutes that sorb by way of an ion-exchange mechanism and therefore the CEC transfer factor is only needed for a select few radionuclides. The radionuclides of Sr, Cs, and Ra are included in this group, although the apparent sensitivity of Ni sorption to ionic strength also suggests that a CEC correction is preferable even though its sorption mechanism may not necessarily be a strictly ion-exchange based process.

Although this is approximately consistent with the presumed sorption mechanism of these solutes, there are other radionuclides whose sorption is closely associated with the biotite content of the rock for various reasons. In particular, this affects the redox sensitive solutes U, Np, and Tc which are known to sorb strongly to biotite. In /Kienzler et al. 2009/, for example, the sorption of U, Np, and Tc was found to be strongly correlated with Fe content (being a proxy for biotite) as determined by combining data from α-autoradiography and SEM-EDX[1] studies for rock samples taken from the Äspö Hard Rock Laboratory (Äspö-HRL). Interestingly, no association was found between the Fe content and the sorption of Am and Pu which were sorbed heterogeneously on all exposed surfaces. It is noted, however, that the literature data are not unequivocal concerning the preferential sorption of Am and Pu and there are other investigations where Am and Pu have been found to sorb more strongly in association with biotite (e.g. /Anderson et al. 2007/). Interestingly, Pu sorption has been found to be strongly associated with the presence of Mn oxides on zeolitic tuff samples taken from Yucca mountain, although not in association with Fe oxides /Duff et al. 2001/.

Originally it was thought that the sorption of, for example, uranyl ion (UO_2^{2+}) was a cation exchange phenomenon rather than being related to reduction of U(VI) to the less mobile U(IV) form. This was predicated on the basis that U(VI) was observed to sorb strongly on biotite, although not on pyrite (e.g. /Beall et al. 1980/). More recently it has been suggested that the strong association of certain redox sensitive radionuclides with biotite might be related to reduction of oxidised forms by Fe(II), following surface complexation on frayed edges sites (FES) of micaceous minerals or on ferric oxy-hydroxide microprecipitates (e.g. /Cui and Eriksen 1996, Ilton et al. 2004, Lee et al. 2009a, b/). This process has also been shown to occur on non-biotite surfaces /Regenspurg et al. 2009/. There are also studies, e.g. /Singer et al. 2009/, that suggest the formation of UO_2 microprecipitates in association with mica minerals thereby blurring the distinction between sorption and surface precipitation. The situation is further complicated by the possibility that microbial activity can strongly influence these reactions (e.g. /Liu et al. 2009/). Although highly relevant for the mobility of redox sensitive radionuclides in surface environments and close to fracture surfaces in situ, the impact of microbially mediated reactions deep within the rock matrix is questionable on account of the large physical dimensions of microbes relative to that of the microporosity in the rock.

Correlation of sorptive properties with Fe or biotite content has also been reported for Se by /Jan et al. 2007, 2008/. Although Se is redox sensitive it is also interesting in that it theoretically should be speciated in a predominantly anionic form (i.e. aqueous phase speciation) in most situations. Under strongly reducing conditions the HSe^- specie is predominant, whereas under weakly reducing to oxidising conditions it exists primarily in an oxyanion form (SeO_3^{2-} or SeO_4^{2-}). In /Vandergraaf et al. 1982/ it is theorised that the association of Se with Fe containing pyroxenes (hornblende) is related to reaction with ferric oxyhydroxides to form ferroselenite precipitates. Other authors /Tachi et al. 1998/ suggest that the association of oxyanion species such as $HSeO_3^-$ is related to the point of zero charge (PZC) of ferric oxyhydroxides. In this mechanism, the PZC of ferric oxyhydroxides is close to the pH of the groundwater with the result that there is a non-negligible fraction of positively charged surface sites that can bind anions.

In many cases, the CEC of rock samples reported in literature sources were somewhat higher than the most likely CEC range of the Forsmark metagranite rock type. The use of a CEC transfer factor therefore was generally found to give a lower K_d range than assuming that the CEC has no effect. For this reason, in cases where there is a reasonable expectation that sorption might be related to biotite content, the CEC transfer factor has been cautiously applied. In cases where there is no strong evidence to suggest that sorption should be related to CEC, the transfer factor has not been used. The decision whether or not to use the transfer factor in recommending K_d ranges was however, handled on a case by case basis in a partially subjective manner.

[1] SEM-EDX (**S**canning **E**lectron **M**icroscope **E**nergy **D**ispersive **X**-ray spectroscopy).

Calculation of the groundwater chemistry transfer factor, f_{chem}

As discussed previously in Section 2.1.4, the primary variables pH and dissolved carbonate concentration (or pCO_2) are expected to have most influence on the sorption of surface complexing solutes. In this compilation, redox is considered separately and on a case by case basis. The predominant redox speciation is estimated by consideration of redox potentials predicted for projected in situ conditions at different times during the geochemical evolution of the repository environment. For radionuclides that sorb by way of an ion-exchange mechanism, on the other hand, the presence of competing cations is expected to have the greatest influence on sorptivity.

In many cases, pH and carbonate concentrations used in laboratory investigations are sufficiently different to those predicted for the repository environment that this needs to be considered as a factor when recommending K_d ranges for use in safety assessment calculations. In this context it is also important to consider possible differences in the specified groundwater composition prior to commencement of laboratory sorption measurements and at the conclusion of the experiment which might be many months apart. If there is uncertainty concerning the composition of contact solutions during sorption experiments, this uncertainty is unavoidably propagated into the ranges of sorption R_d values derived in the laboratory investigation.

There are a number of ways in which small differences in groundwater chemistry can have an impact upon K_d values. The most obvious are speciation effects whereby changes in, for example, pH or carbonate concentration change the relative abundance of various complexed forms of the radionuclide in solution. This can be viewed as an indirect competitive effect whereby dissolved ligands in the groundwater compete with surface reactive groups to bind the radionuclide. If there is a sufficient concentration of competing ligands in solution the concentration of the free radionuclide species may decrease to such an extent that sorption is reduced. For radionuclides that are less influenced by carbonate complexation, increased carbonate levels may decrease the sorptivity of groundwater solutes that compete directly for binding sites and thus enhance sorptivity of the radionuclide indirectly. On the other hand, dissolved ligands such as carbonate can also enhance sorption by way of forming ternary surface complexes with the dissolved radionuclide. The formation of ternary uranyl /Bargar et al. 1999/ and neptunyl /Arai et al. 2007/ carbonate complexes on hematite, for example, has been directly confirmed by spectroscopic measurements. Another way in which altered carbonate concentration can impact upon sorptivity is if carbonate species form independent surface complexes themselves in a competitive fashion with radionuclides (mainly relevant for oxyanions).

Given these different modes of action it is therefore difficult to predict, a priori, the effect of changed carbonate concentration unless very detailed knowledge of the identity of sorbing species is known since this can lead to both an increase or a decrease in sorptivity depending upon the particular reaction mechanisms involved. The presence of other solutes at elevated concentrations can also have an adverse impact on sorptivity due to competition for surface sites even if the competing solute sorbs less strongly. Direct competition for sorption sites with major groundwater cations is expected to be the principal mechanism affecting the sorption of ion-exchanging solutes.

Even if the sorption mechanism is such that only ligand competition in the aqueous phase needs to be considered (i.e. no direct competition for surface sites), it is difficult to predict the impact of altered speciation owing to the coupled nature of the reactions describing sorption and solution speciation. As an example, it is interesting to consider the case of Am sorption on site specific rocks from Forsmark and Laxemar in contact with fresh and saline groundwaters. The fresh groundwater type used in the laboratory investigations has a dissolved carbonate concentration roughly 12 times greater than the saline groundwater. In many models described in the literature, the sorption of Am is modelled assuming that free Am^{3+} ions bind to negatively charged surface hydroxyl sites according to a simple binary reaction template (e.g. /Wang and Anderko 2001/). Given that the speciation of Am can be dominated by carbonate complex forms in groundwater with elevated carbonate concentrations, this would suggest that the sorptivity of Am might be reduced in fresh water since one would expect relatively greater sequestration of Am in non-reactive carbonate forms. In fact, by comparing the speciation of Am in both groundwater types, one would naively expect the sorptivity of Am in fresh water to be reduced by at least three orders of magnitude due to direct competition by carbonate ligands. In the Forsmark and Laxemar site specific data for Am sorption, however, it is clear that the R_d values for saline conditions are about 30% less than those for fresh water (this appears to be a consistent result for both sites even given the uncertainty in contact water composition).

Even seemingly small changes in speciation resulting from the use of a different thermodynamic database in predictive modelling compared to that originally used for model fitting can have a relatively large impact on simulated groundwater compositions and predicted sorptivity. Although not strictly applicable to granite, it is useful to consider the surface complexation model for Am sorption on alumina described in /Wang and Anderko 2001/. Using this model it is predicted that the K_d should be about 70% greater in fresh water than for the saline water when using the NEA thermodynamic database /Hummel et al. 2002/. If, on the other hand, the SKB thermodynamic database /Duro et al. 2006/ is used, the predicted K_d is found to be roughly 30% less in fresh water than saline water. Although, this is a relatively small change it is important to acknowledge nonetheless that this is a qualitatively contrary result which has non-trivial implications if used as a basis for interpreting sorption experiment outcomes. The difference appears to be related to small numerical differences in the complexation constants for the various Am(III) species recognised by the NEA and SKB databases. It is therefore of some importance that internally consistent data sets are used if thermodynamic modelling is to be used to predict groundwater chemistry transfer factors for use in safety assessment modelling. This argument can also be extended to include the requirement that the groundwater compositions used in laboratory investigations are reliably quantified so that the resulting surface complexation model isn't parameterised with binding constants that are biased by inaccurate solution concentration data.

The relation between groundwater compositions used in the site descriptive modelling laboratory investigations and those predicted for the SR-Site temperate time domain /Salas et al. 2010/ are shown in Figure 5-3 (2,000 y) and Figure 5-4 (9,000 y). The pH was measured at the conclusion of the sorption experiments for a small number of control cases for the purpose of quality control. As can be seen from the data in Figure 5-3 and Figure 5-4, there was a non-negligible drift in pH observed during the sorption experiments carried out for the Forsmark and Laxemar site investigations which, in some cases was as much as 1.5 pH units. Although part of the variation might be related to small differences in operator technique or pH electrode calibration between the two institutions contracted to perform the measurements, the drift appears to be systematic, consistently positive (only one exception in the case of Saline water from Laxemar) and of sufficient magnitude to significantly confound mechanistic interpretation of the results.

In Figure 5-3 and Figure 5-4, the drift in pH has been interpreted as being related to a re-equilibration of the solution with a lower pCO_2 in the headspace of the sample vessels and glove box. This, however, is purely speculative and as noted previously in Section 5.1.1, there are alternative explanations for the pH drift that could potentially reproduce the observed behaviour without a net change in pCO_2. Moreover, it is not possible to make any quantitative estimates since the actual CO_2 partial pressure in the glove box is unknown and for much of the contact time (except during sampling) the groundwater rock suspensions were in sealed test tubes with limited head space.

Even in the absence of pH drift and associated CO_2 gas re-equilibration, the parameter space sampled in the site laboratory investigations is sufficiently dissimilar to the projected in situ conditions for SR-Site that there is some uncertainty concerning transferability of the R_d data to SR-Site groundwater conditions. In much of the data reported in the literature, it is not always clear if groundwater compositions are specified for starting solutions or for final compositions measured analytically at the conclusion of the experiments. The interpretation of results is therefore fraught with considerable uncertainty.

If reliable thermodynamic sorption models were available for the surface complexation of individual radionuclides it is possible, in principal, to calculate a theoretical response surface for the variation of K_d with changes in pH and dissolved carbonate and use this as the basis to calculate appropriate groundwater chemistry transfer factors. Although not used to estimate transfer factors in the sense that they are discussed here, /Turner and Pabalan 1999/ have proposed the use of thermodynamic sorption models in combination with statistics of measured (or modelled) groundwater compositional data to predict probability distributions of site specific K_d values. This is the essence of the concept referred to informally in the literature as the *smart* K_d approach (e.g. /Kulik 2002/). The idea is considered to have sufficient merit that a considerable amount of effort has been applied in recent years towards placing these ideas on a more robust footing /NEA 2005, Ochs et al. 2006a/.

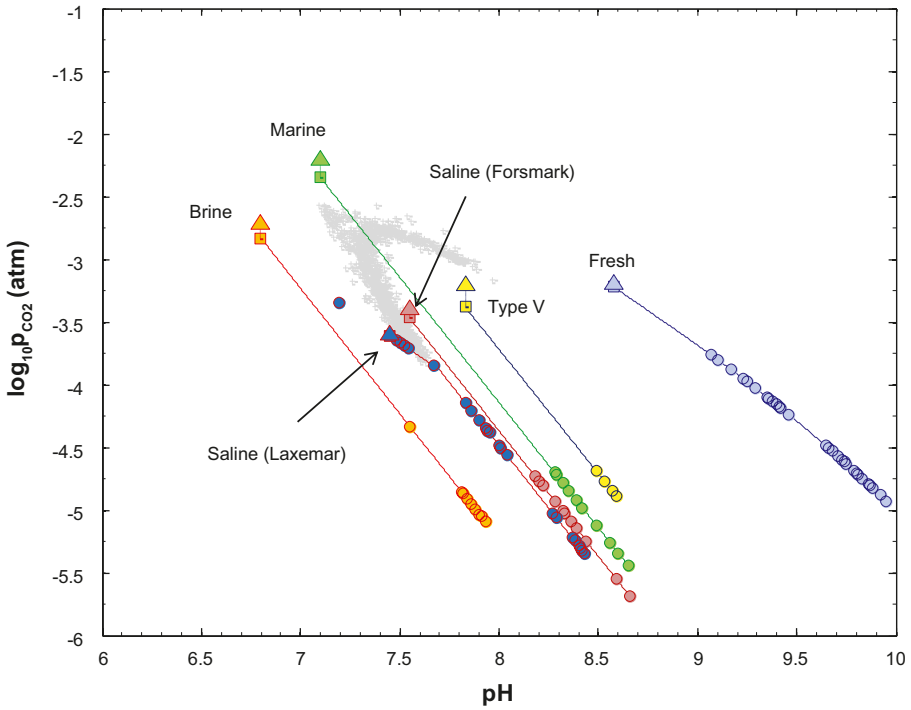

Figure 5-3. *Cross-plot of pCO_2 (log_{10}-units) vs. pH for characteristic groundwater types used in site descriptive modelling laboratory investigations (large triangular markers). The pH drift measured at the conclusion of the sorption experiments for a small number of control cases is indicated using small circular markers. The square marker shows the theoretical composition of the contact solutions after re-equilibration of specified solution compositions calculated using PHREEQC. The trajectory of the plotted values (solid lines) assumes degassing to a lower pCO_2 is responsible for the observed pH drift although other interpretations are possible. The small grey markers in the background show 1,000 randomly selected groundwater compositions projected for the SR-Site temperate time domain at 2,000 y.*

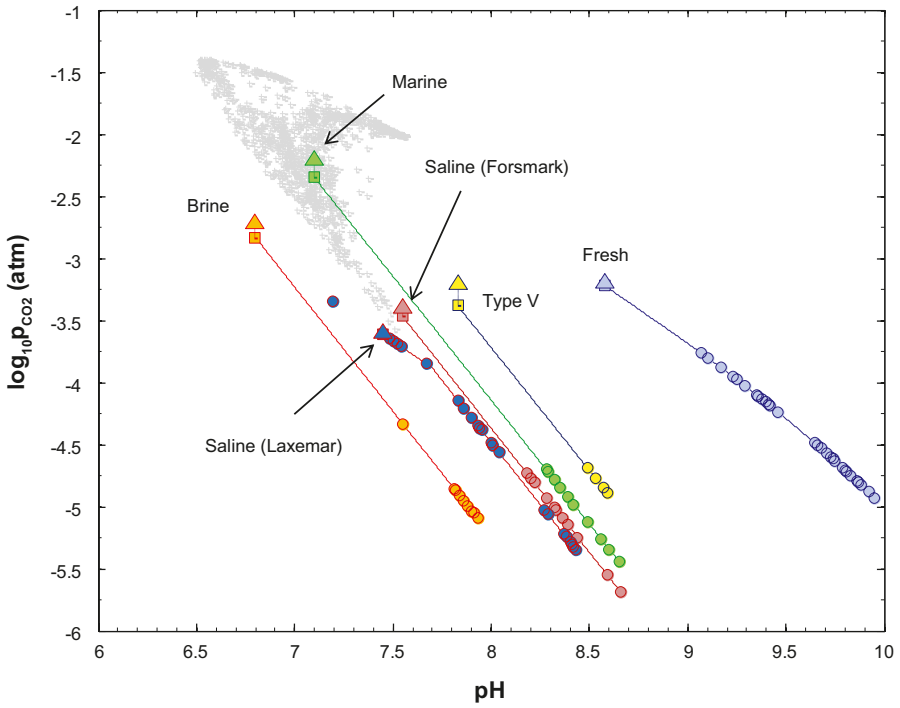

Figure 5-4. *Same as previous figure although compared against 1,000 randomly selected groundwater compositions projected for the SR-Site temperate time domain at 9,000 y.*

Thermodynamic modelling has been previously deployed with some success for the prediction of K_d values for site specific groundwater compositions in contact with bentonite /Bradbury and Baeyens 1997, 2005a, b/ and more recently for illite /Bradbury and Baeyens 2009a, b/. The method was also used by /Ochs and Talerico 2004, Ochs et al. 2006b/ to calculate K_d values appropriate for compacted bentonite buffer materials under site specific groundwater conditions for use in the SR-Can safety assessment /SKB 2006/. The same approach is also used in the current safety assessment SR-Site as documented in the Data report /SKB 2010b/.

This outcome can also be achieved if a sufficient number of sorption measurements are available for different groundwater parameter combinations that an empirical response surface based upon least squares regression can be estimated. This latter approach was used by /Vandergraaf et al. 1993/ to construct a far-field sorption database for crystalline rock. The quality of the calculated response surface, however, is only as good as the data used to constrain it and there is considerable opportunity for confounding factors and errors relating to the use of small data sets to influence the results. This, however, is also true of thermodynamic sorption models.

This should not be taken to indicate a diminishment of the detailed work carried out previously and described above. It is merely a restatement of the realities involved in attempting to characterise the sorptive properties of complex, heterogeneous rock matrices. Although the parametric models developed by /Vandergraaf et al. 1993/ were painstakingly assembled and methodologically robust, they still suffer from many of the same issues that plague the application of more sophisticated thermodynamic sorption models in safety assessment; i.e. the typically small number of rock samples represented in the underlying data sets and the minimal nature of the experimental designs mandated by the laboratory investigations to characterise the impact of key variables on many different radionuclides.

The fundamental lesson is that uncertainties implied by the variation of the key variables within parametric or thermodynamic models for projected in situ conditions most likely do not always reflect the true range of uncertainty. Probabilistic assessments based only on consideration of *visible (or known)* uncertainties therefore run the risk of considerably underestimating radiological risks associated with modelled scenarios. In the strategy for assessment of migration properties in bentonite /Ochs and Talerico 2004/, expert judgement is brought to bear on the problem by way of introducing additional uncertainty factors to expand the range of overall K_d uncertainty. Compacted bentonite, however, is a far more chemically homogeneous material than igneous bedrock with regard to sorption reactions.

A particular problem for the igneous rock types is that there are currently no thermodynamic models of acceptable accuracy that describe the sorption of solutes on the most active mineral phases that appear to dominate sorptivity. Moreover, as outlined previously with regard to the CEC transfer factor, it is not even clear in some cases which mineral phase dominates the sorptivity of the rock or whether significant errors are introduced by disregarding armouring[2] effects when assuming linear additivity of sorptive properties in complex mineral mixtures such as granite. Although there have been large advances in the past few years, surface complexation models for crystalline rock do not appear to be sufficiently robust at this time to predict groundwater chemistry transfer factors for use in safety assessment calculations.

If satisfactory empirical or thermodynamic models of sorption were available it would be possible to estimate a groundwater chemistry transfer factor by estimating a theoretical value for the K_d under the application conditions and comparing this with the theoretical K_d value for a reference groundwater. The chemistry transfer factor can then be defined as:

$$f_{chem} = \frac{K_{d(app)}}{K_{d(ref)}} \qquad (5\text{-}9)$$

Given that the selected contact groundwater compositions do not span the application groundwater compositions very well, and since the actual pH and carbonate concentrations in the laboratory experiments appear to be in some doubt, it does not seem appropriate at this time to use an empirical response surface for the calculation of f_{chem} for surface complexing radionuclides.

[2] Armouring – when the surface of one mineral is enclosed or occluded by another mineral in such a way that its surface reactivity or interfacial access to matrix porosity is less than that which would be predicted for the mineral given its crystal size and relative abundance in the rock.

Since there appears to be no acceptably reliable model (thermodynamic or empirical) that can account for uncertainty relating to groundwater composition in the case of the main surface complexing solutes studied in this compilation, the only option is to assume that all uncertainties relating to groundwater chemistry are internalised in the ranges of uncertainty of data sets used to recommend K_d ranges. For most surface complexing radionuclides this implies a pooling of data for all available groundwater compositions. If the application groundwater compositions are too different from those compositions for which measurement data are available, this represents a significant and presently unquantifiable uncertainty. Although the specific groundwater compositions used in experiments might potentially introduce such a bias, it is thought that the compositional variability of contact solutions is sufficiently large that the assumption is probably not unreasonable (given also that the small liquid volumes used in batch experiments do not constitute a large buffering capacity with regard to reactive processes and gas exchange).

For radionuclides that sorb by way of an ion-exchange mechanism, on the other hand, the pH and carbonate concentration are expected to play a subordinate role. In these cases, direct competitive effects with the major groundwater cations Ca^{2+}, Mg^{2+}, Na^{+}, K^{+} are expected to have a dominant impact on sorption. Although small changes in concentration might occur due to weathering reactions, these are likely to be minor relative to the large background concentration already existing in the groundwater types (particularly for the more saline groundwaters). A simple, single site cation exchange model has been developed previously for fine grained granite and diorite samples taken from the Äspö HRL /Byegård et al. 1998/ and in an earlier work for Finnsjön granite /Byegård et al. 1995/. The selectivity constants and other model parameters for these rock types are given in Table 5-5.

There are a number of uncertainties associated with the quantification of the selectivity coefficients in Table 5-5. For ion exchanging solutes one of the chief concerns is diffusive disequilibrium. Since pH drift and accompanying CO_2 re-equilibration are not expected to have a large impact on ion-exchange properties, data for the smallest size fraction and longest contact time would appear to be the most appropriate choice if the aim is to minimise possible bias due to diffusion. The particular data sets given in Table 5-5 are selected bearing this in mind. Data are given in the original references, however, for a number of different particle sizes and contact times. The larger selectivity coefficients estimated for Rb^{+} and Cs^{+} in association with Äspö fine-grained granite and diorite (i.e. relative to Finnsjön granite) could be related to diffusive disequilibrium given the different contact times used in the experiments.

Table 5-5. Selectivity coefficients (defined according to the Gaines-Thomas convention and relative to Ca^{2+}) and other parameters for the single site ion-exchange model derived for fine-grained granite and diorite from Äspö /Byegård et al. 1998/, and Finnsjön granite /Byegård et al. 1995/. Error estimates are given as 2σ values based upon the standard deviation of 2–4 replicate samples for the fine-grained granite and diorite samples. The calculation basis for error estimates are not specified in /Byegård et al. 1995/ for Finnsjön granit.

Rock type	Fine-grained granite	Diorite	Granite
Source location	Äspö	Äspö	Finnsjön
Pre-equilibration time	5 months	5 months	1 week
Contact time	14 days	14 days	8 days
CEC (cmol/kg)	6.8±1.0	9.1±0.6	0.44±0.06
Biotite content (%wt)	~1%	17%-25%	4%-6%
Size fraction	0.045 – 0.09 mm	0.045 – 0.09 mm	0.09 – 0.25 mm
Selectivity coefficients, K_c:			
Na^{+}	2±1	0.1±0.05	0.025±0.009
Mg^{2+}	n/a	n/a	11±2.2
K^{+}	n/a	n/a	66±4.7
Rb^{+}	(2±0.1)×10^{3}	(8±0.4)×10^{3}	730±210
Ca^{2+}	1	1	1
Sr^{2+}	4±1	2±0.4	1.8±0.3
Cs^{+}	(9±0.6)×10^{6}	(90±2)×10^{6}	(32±6.9)×10^{3}
Ba^{2+}	60±4	60±2	53±14

Another problem is the fact that biotite, being more fine grained than feldspar and other tectosilicate minerals has a tendency to be enriched in the smallest crushed size fractions. It is also possible that the biotite grains in the smaller size fractions are more damaged and have a greater proportion of frayed edge site than those in larger size fractions. This could be a potential source of bias for rocks with relatively high biotite contents if K_d values were to be abstracted directly for use in transport calculations. However, since we are only interested in calculating the relative change in K_d between different groundwater compositions to calculate f_{chem}, this should not have an impact on the results provided the difference in CEC is not so large that it significantly perturbs the contact water compositions.

Other possible issues concern:

- The accuracy with which solution compositions can be determined by analytical methods and the manner in which these uncertainties are propagated in mass balances used to quantify the exchange process.
- The potential for formation of precipitates such as barite and calcite as well as their solid solutions with Sr^{2+}. This could be partially ruled out in /Byegård et al. 1995, 1998/ by geochemical reasoning related to observations of cation desorption/dilution behaviour in response to rinsing with distilled water.
- The neglection of activity coefficients in the estimation procedure (both for the solution and solid phases).
- The mechanistic simplification implied by the assumption of a single-site cation exchange model.

Although there are a number of uncertainties associated with the quantification of selectivity coefficients in Table 5-5, it is thought that the data are sufficiently accurate that approximate chemistry transfer factors can be calculated for Cs^+, Sr^{2+}, and Ra^{2+} (assuming geochemical analogy between Ra^{2+} and Ba^{2+}) without introducing large errors. For the purpose of making estimates of f_{chem} in this data compilation, the selectivity coefficients for Äspö diorite were chosen as a basis for the calculations. A problem associated with this data set is that selectivities for Mg^{2+} and K^+ were not included. These missing reactions were accounted for by importing the corresponding selectivity coefficients measured for Finnsjön granite. Although this could be considered to be the use of internally inconsistent data sets, it is thought that Mg^{2+} and K^+ overall play a sufficiently minor role that the error introduced is relatively small.

The Forsmark saline groundwater was chosen as the reference groundwater since this has an ionic strength deemed to be closest to the projected groundwater composition under application conditions. Typically, there were also a larger number of sorption measurements performed on site specific materials and saline groundwater than for the other groundwater types which makes it an obvious choice (in terms of statistical suitability) for extrapolation of uncertainty distributions to other groundwater compositions. The only exception was for Sr where the fresh groundwater type was assumed as the reference. This was due to that the R_d measurements for saline groundwaters were sufficiently close to the detection limit that sorption could not be statistically quantified (see Appendix P).

The applicability of the resulting ion-exchange model and impact of various uncertainties has been tested in two ways:

- Comparing estimated K_d values extrapolated from saline groundwater with the measurement data for the other groundwater types not used in the extrapolation (only the reference groundwater data set are used in the extrapolation to application conditions). Comparison with the empirical data for the unused data sets therefore provides an independent quality control check on the applicability of the results. The comparison is made by plotting both the simulated data and empirical measurement data against ionic strength. If the simulated data line up in reasonable agreement along the qualitative ionic strength trend implied by the experimental data sets, then the model is deemed acceptable. This may be considered to be a consistency check on the epistemic uncertainty of the proposed model.
- Random perturbation of selectivity coefficients, K_c assuming independent and lognormally distributed uncertainty distributions calculated on the basis of the error estimates given in Table 5-5. Since the analytical methods used are expected to give rise to normally-distributed errors, the selectivity constants being defined as ratios of these variables are consequently expected to be lognormally distributed. Comparison of f_{chem} distributions calculated using the central values and stochastically perturbed values gives an indication of the aleatory uncertainty of the proposed model (i.e. insofar that the error estimates given for the selectivity coefficients are approximately order of magnitude correct).

Further details of the data qualification procedure can be found in the individual appendices dealing with the derivation of K_d values for Sr, Cs, and Ra sorption. A typical result of the calculations is shown in Figure 5-5 for Ra sorption where f_{chem} is plotted against ionic strength (logarithmic axes) for various groundwater compositions projected for the temperate case at different times.

In the case of Ni (which does exhibit a mild ionic strength dependency), it is not possible to use an ion exchange model to extrapolate to application conditions since there are no selectivity coefficients available for Ni sorption. Furthermore, it is not clear whether the sorption of Ni can be adequately described by a simple ion-exchange model or whether it should be modelled as a surface complexation reaction featuring roughly equally balanced outer-sphere and inner-sphere contributions. From the spectroscopic studies reported in the literature /Scheidegger et al. 1996, Elzinga and Sparks 1999/, it would appear that the latter mechanism is more likely. It is also not clear whether the trend is a true ionic strength dependency, or whether it is related to hydrolysis of the Ni^{2+} cation where pH is a latent variable correlated with ionic strength. In this particular case, a simplified empirical regression of R_d values as a function of ionic strength has been used to estimate K_d values for application conditions. Full details concerning this particular case can be found in Appendix M.

In general, the average shift in the central K_d estimate obtained by convolution of the individual probability density functions describing $K_d^{\wp}$ and f_{chem} is small relative to the level of overall uncertainty in the uncorrected data sets. Counterintuitively, the solutes that are most strongly influenced by ionic strength on account of their weak sorptivity exhibit a smaller shift than more strongly sorbing solutes that are less affected by ionic strength. This due to the larger underlying data uncertainty in the case of the more weakly sorbing solutes which tends to drown out the systematic trends that can be quantitatively related to evolving groundwater salinity. This should not be taken to mean that ionic strength is less important for the weakly sorbing solutes, but rather that the effect is more difficult to quantify for weakly sorbing solutes relative to the more strongly sorbing solutes.

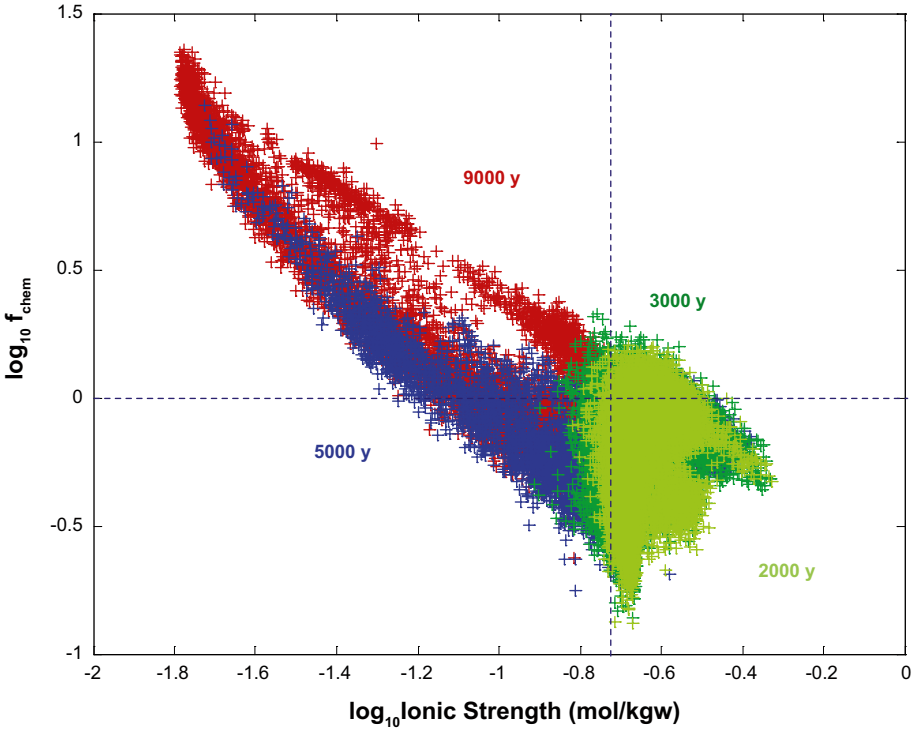

Figure 5-5. *Typical groundwater chemistry transfer factors, f_{chem} calculated for Ra sorption and application groundwater conditions in the temperate case study. The plotted data represent 10,000 randomly selected groundwater compositions calculated individually for each case using PHREEQC and the assumed ion exchange model. Data are given for 2,000 y (lime green markers), 3,000 y (dark green), 5,000 y (blue), 9,000 y (red). The plotted data, although partially obscuring each other gives an idea of the system-wide, relative variation of f_{chem} at different times implying a trend towards increased K_d values over time owing to decreasing groundwater salinity.*

It must also be remembered that since the changes in groundwater composition are not resolved on the level of individual migration paths, extrapolation to the groundwater situations existing at different times must consider the statistical distribution of spatially variable groundwater compositions throughout the entire repository volume which, in itself, introduces additional statistical dispersion in the calculation of K_d uncertainty ranges. It is therefore important when discussing the impact of evolving groundwater chemistry to distinguish between the true impact of ionic strength on the sorption process as it actually occurs from the impact that is statistically quantifiable for modelling purposes. Local changes in groundwater salinity are therefore likely to have a much more profound impact on sorptivity than has been quantified in the K_d recommendation. Since the K_d data are recommended for relatively saline conditions, this also means that the strength of sorption will be pessimistically underestimated during the bulk of repository evolution.

5.1.2 Possible biases in the quantification of radionuclide retention

The principal biases and uncertainties which might affect the magnitude of the appropriate K_d value for use in calculations have been outlined in previous sections. These biases concern both the extrapolation of data from laboratory investigations to application conditions in situ as well as the correct identification of sorptive retention processes in the laboratory. Here, the term *bias* is used to describe the various epistemic uncertainties (i.e. relating to a lack of knowledge) concerning the sorption processes as they are quantified and extrapolated from one reference condition to another. The most important characteristics of these biases are summarised in the following Sections.

Measurement of sorption

As outlined previously, laboratory sorption measurements are typically carried out on crushed rock samples for different contact times and groundwater compositions. The use of crushed materials is dictated by the need to minimise diffusive disequilibrium effects so that sorption measurements can be made in a realistic time frame. In most cases, the apparent partitioning ratio, R_d is then estimated by way of a radiometric mass balance relating the initial and final activity of the contacting solution with the amount of solute sorbed. Usually the amount sorbed is not measured directly, so the accuracy with which the initial and final solution activity can be quantified is of great importance for the overall accuracy of the R_d estimate.

If the activity variance of the initial blank solutions (i.e. reference solutions without added geological material) is sufficiently large relative to the final activity of the solution with geological materials added, then it might not be possible to quantify the existence of sorption in a statistical sense. Variations in the activity of the blank arise owing to issues of instrumental measurement precision as well as sorption of solutes on vessels or test-tube walls. This is a particular problem for strongly sorbing solutes which often necessitates the use of acidified blank solutions. Similarly, if the strength of sorption is sufficiently high that the remaining solute in the contact solution is at or below the limit of detection, then it may not be possible to quantify an upper limit to the R_d value. In a practical sense, this means that it is often difficult to reliably quantify the R_d of solutes much lower than about 10^{-4} m^3/kg or larger than ~1 m^3/kg.

As a direct consequence, it may not be possible to identify a lower limit for the sorption of certain solutes that sorb only weakly. In some cases this results in the assignment of non-sorbing status for solutes where sorption cannot be effectively quantified. For very strongly sorbing solutes, on the other hand, the inability to adequately establish an upper limit for sorptivity frequently results in the truncation of K_d ranges at lower levels than what might be physically motivated. Although the truncated upper limit of a high K_d data range is not in itself a problem, stochastic simulations will be biased towards lower values than what might be realistic thereby unnecessarily inflating risk estimates.

Other issues that compromise the soundness of sorption measurements include; 1) the possible bias introduced by incorrectly characterising precipitation or co-precipitation processes as ion-exchange or surface complexation sorptive processes, and 2) the formation of pseudo-colloids and eigencolloids during experiments if not correctly accounted for in data evaluation. If colloids are incorrectly identified as belonging to the solid phase (i.e. after ultra-filtration or centrifugation) sorption will be overestimated. If, on the other hand, colloids are identified as being part of the dissolved concentration in the aqueous phase, sorption will be underestimated.

Correct identification of redox species during laboratory experiments is a particular issue for the redox sensitive solutes. It is generally difficult to determine whether redox potentials are sufficiently low to maintain a reducing form for those solutes that are redox sensitive. For the radionuclides of interest in safety assessment this may lead to an underestimate of sorptivity if the redox potential is not sufficiently low to guarantee predominance of the (usually more strongly sorbing) reduced form. This is handled on a case by case basis and is documented in the appendices to this report.

Extrapolation of data to site-specific conditions

The crushing of rock materials results in the creation of new mineral surfaces that are not representative of the undisturbed in situ rock. This may include both freshly cleaved mineral surfaces as well as surfaces belonging to previously unconnected pore spaces in the rock matrix. Sorption might also occur preferentially in association with one, or more mineral phases which may not comprise more than a few percent of the total mineralogical composition of the rock. These minerals also typically dominate the cation exchange capacity (CEC) of the rock. The cation exchange capacities of rocks used in laboratory investigations are also not necessarily representative of the particular site specific rock types of importance. Sorption data derived from laboratory investigations are corrected for both surface area effects and CEC to more accurately represent in situ sorption properties of the intact rock matrix under application conditions.

As outlined in previous sections, the surface area of rock is typically assessed using the BET method. This gives an approximate estimate of the total surface area which can then be used to approximately relate the sorptive properties of different rock types and crushed size fractions, although does not give any information concerning the surface area of minerals that actually dominate sorption. As a consequence, mechanical transfer factors used to correct for differences in surface area between crushed and in situ rock may result in lower K_d estimates than what might be physically motivated. Further corrections made using CEC transfer factors assume that these corrections can be applied independently and in a multiplicative fashion thereby disregarding any correlation between these two variables. Since some correlation between sorptive surface area and CEC is considered likely, this may also lead to K_d estimates that, while defensible for safety assessment purposes, may be over-pessimistic with regard to physical realism.

Issues of statistical sample size (number)

It is probable that there is some degree of bias in the estimated uncertainty distributions for data obtained from literature sources since these are generally based on much smaller sample sets representing a restricted range of varied experimental parameters as compared to the site specific data sets. To account for the sample size biasing effect of the typically small data sets reported in the literature sources, the uncertainty of the mechanical and CEC transfer factors are fully propagated in the calculations to give an expanded uncertainty interval in the final data range. This was achieved using a re-sampling technique based on aggregation of the underlying uncertainty distributions for individual data points (assuming a Gaussian mixture model for uncertainty aggregation).

Since a large amount of variation was already apparent in the site specific data sets this technique was not deemed necessary in those cases and only the central best estimates for the mechanical and CEC transfer factor was used (i.e. for Sr, Cs, Ra, Ni, Am/Eu, U(VI), Np(VI)). This was considered justified since the propagation of the correction factor uncertainties might otherwise give over-inflated K_d data ranges.

Time dependent behaviour

A particular bias that has not been considered in the data assessment, concerns the interpretation of time dependent behaviour in laboratory measurements. The Forsmark and Laxemar site investigation data consisted of R_d values measured for different crushed size fractions and a geometric time schedule for contact times ranging from 1–180 days. However, since the time dependent behaviour in the raw data sets for site data appears to be a minor component of the overall variability/uncertainty, the data sets are considered in their entirety without any filtering with regard to particle size or contact time.

Generally it was found that attempts to fit the data to simplified models of time dependent behaviour (i.e. modelling of diffusive disequilibrium) gave rise to non-cautious K_d ranges owing to the uncertainty of other model parameters required to make the fit. A pronounced pH drift of up to 1.5 pH units was also documented in control samples at the conclusion of the sorption experiments which confers additional doubt on the assumption of diffusive disequilibrium being the sole mechanism for the observed time dependent behaviour in a number of cases.

5.2 Sorption data for specific radionuclides of interest

This section contains a brief overview of the main features of each radionuclide, or analogue group, designated as being of importance in the SR-Site safety assessment. This includes a basic description of the chemical reactive characteristics of each nuclide as well as a brief overview of data sources and principal uncertainties. More detailed information for each nuclide or analogue group may be found in the Appendices to this report.

As a basis for discussing the geochemical characteristics of each element, speciation calculations have been made for two representative groundwater compositions. The first is a highly saline groundwater with an ionic strength of roughly 1 M. The other is a fresh (i.e. non-saline) groundwater of ionic strength 6.4×10^{-3} M with the same composition as the fresh groundwater end-member used in the laboratory sorption studies carried out during the site investigations (see Table 3-5). The calculations were made for pH varied in the interval 7–9 with redox conditions determined by the same redox pairs as used in SR-Site hydrochemistry simulations /Salas et al. 2010/.

5.2.1 Americium (Am) and other trivalent actinides and lanthanides

Owing to the strong analogue chemistry of the trivalent actinides and lanthanides (as discussed in Section 3.2.1), sorption data for the pooled set of Am(III) and Eu(III) measurement data obtained from the site investigations are considered to be suitable for the selection of K_d values to represent the group as a whole. For the purposes of SR-Site, this group includes the nuclides of Ac, Am, Cm, Eu, Ho, Pu, Sm.

For the trivalent actinides and lanthanides, carbonate complexation in the aqueous phase is expected to exert a relatively strong competitive effect for binding of the free solute (e.g. Am^{3+}). Based on speciation calculations made using PHREEQC and the SKB-TDB /Duro et al. 2006/, the mono-carbonate complex $AmCO_3^+$ is expected to be the predominant aqueous specie for most groundwater compositions likely to be encountered. The relative importance of hydroxo- and carbonato-complexes, however, varies as a function of pH and total carbonate concentration which needs to be taken into consideration when discussing the speciation of Am(III). Different thermodynamic databases also appear to give different predictions on the relative importance of chloride complexation. The SKB-TDB, for example, predicts a relatively minor role for $AmCl^{2+}$ although with greater predominance for pH lower than 7. Use of the NEA thermodynamic database (NEA-TDB) /Hummel et al. 2002/, on the other hand, predicts a relatively stronger impact of chloride complexation owing to a difference in the equilibrium constants assigned for this reaction. All of the major aqueous complexes are cationic.

Sorption of elements belonging to this group is thought to be governed by an inner sphere surface complexation mechanism and it is consequently assumed that ionic strength effects can be neglected. If sorption occurs by binary surface complexation of the free metal ion with surface hydroxyl ligands, increased carbonate concentration is expected to decrease the K_d owing to competitive effects by aqueous phase complexation. It is interesting to note that although ternary carbonato- and hydroxo-carbonato surface complexes of Eu(III) have been inferred from spectroscopic measurements on phyllosilicates /Stumpf et al. 2002, Marques Fernandes et al. 2008, Fernandes et al. 2010/, there are no recognized analogous aqueous phase reactions for the formation of hydroxo-carbonato complexes in the above-mentioned thermodynamic databases that would strongly imply the possibility of this behaviour.

The site investigation data for Forsmark and Laxemar suggest a slightly reduced K_d value for fresh water relative to saline groundwater possibly owing to the effect of carbonate complexation. The effect, however, is weak relative to the overall data variability/uncertainty and cannot be accurately related to solution composition owing to undocumented drift in contact solution properties during the

course of the experiments. For this reason, data for the Am(III)/Eu(III) analogue system are pooled over all contact solutions and assumed to represent an overall uncertainty distribution arising due to groundwater compositional uncertainty. A more detailed account of the derivation of recommended K_d values for Am(III) and its analogues may be found in Appendix D.

A best estimate K_d value of 1.48×10^{-2} m³/kg is recommended for both Forsmark and Laxemar for all groundwater compositions. The uncertainty distribution is assumed to be lognormally distributed ($\log_{10} K_d = -1.83\pm0.72$). For stochastic simulations, it is recommended that the uncertainty distribution be sampled in log space between the 2.5% (5.74×10^{-4} m³/kg) and 97.5% percentiles (3.83×10^{-1} m³/kg).

5.2.2 Cadmium (Cd)

The principal radioisotope of Cd is the ^{113m}Cd fission product. This isotope has a relatively short half-life of 14.1 years and decays to the stable ^{113}In isotope. Owing to its relatively short half-life and because its decay product is a stable isotope, ^{113m}Cd is not expected to contribute significantly to far field dose rates under normal geosphere transport scenarios and is only likely to be important for accidental intrusion cases where geosphere transport is bypassed.

Cd is not considered to be redox sensitive and the Cd(II) valence is the only relevant redox state for normal groundwater conditions. In fresh groundwater the Cd^{2+} ion is expected to be the dominant species for dissolved cadmium in the pH range 7–8, although generally shifting towards a predominance of the carbonate complex, $CdCO_{3(aq)}$ at pH greater than 8. Chloride complexation, however, is relatively important for this element and the complexes $CdCl_2$, $CdCl^+$, $CdCl_3^-$ are expected to be dominant in groundwater of more saline character. Under strongly reducing conditions, the sulphide complexes $Cd(HS)_2$, $CdHS^+$, $Cd(HS)_3^-$, $Cd(HS)_4^{2-}$ are expected to be important. The SKB-TDB only considers the selenite and selenate complexes of Cd (i.e. $CdSeO_3$, $CdSeO_4$, $Cd(SeO_3)_2^{2-}$) on account of the fact that ^{113}Cd is not typically considered to be an important nuclide in far field transport calculations and because these species may be of more relevance for Se speciation within a spent fuel canister. The MinteqA2 database as distributed with PHREEQC was therefore used in speciation calculations to form the basis for the above discussion on the relative importance of chloride and carbonate complexation in groundwater. As noted above, the speciation of Cd in the geosphere is considered less relevant on account of its short half-life and this discussion is therefore mostly of interest with regard to the assessment of geochemical analogue behaviour.

Very little data appears to exist concerning the sorption of Cd on granitic rock types although there is a substantially larger amount of data existing for sorption on single minerals such as goethite, alumina, and silica. Although Cd shares certain geochemical similarities to Ni, this analogy is not very good owing to the considerably larger ionic radius and weaker hydrolysis of Cd^{2+}. Measurement data reported by e.g. /Prelot et al. 2002/ exhibit a sensitivity to ionic strength which suggests a predominantly ion-exchange, or outer-sphere surface complexation-based, sorption mechanism. In the absence of reliable data for Cd, and owing to its lesser importance for geosphere transport, it is recommended that sorption data for Ni is used for this nuclide.

5.2.3 Carbon-14 (^{14}C)

Under normal granitic groundwater conditions, bicarbonate ion (HCO_3^-) is expected to be the dominant dissolved species for the ^{14}C fission product (half life 5,730 y). The transport of the bicarbonate ion is difficult to model in the repository environment owing to isotope exchange with calcite minerals which are ubiquitous in the advective pore space. This process is likely to give a non-negligible retardation of ^{14}C transport. The adsorption of bicarbonate ion is postulated to occur by way of a surface complexation mechanism on both calcite /Van Cappellen et al. 1993/ as well as non-calcite minerals such as ferrihydrite /Appelo et al. 2002/ and goethite /Villalobos and Leckie 2001/. In laboratory investigations involving complex rock matrices such as granite, however, it is very difficult to distinguish true adsorption owing to the generally very weak interaction of bicarbonate and the possibility of bias due to carbonate mineral precipitation and exchange with inactive CO_2 in the headspace of reaction vessels.

Sorption of bicarbonate has been measured by /Allard et al. 1981/ on crushed granitic rock and deemed to be, for all practical purposes, non-sorbing ($K_d = 0$ m³/kg). In a later study, /Pinnioja et al. 1984/

measured sorption on thin sections of Rapakivi granite and tonalite, also finding sorption to be negligible. Parallel experiments using monolithic pieces of the above rock types identified weak sorption associated with dark minerals (as ascertained by autoradiography). The authors speculate, however, that the observed sorption in this case may be an artefact of carbonate mineral surface precipitation.

In the absence of unambiguous evidence indicating sorption of bicarbonate on granitic material, a K_d of 0 m^3/kg is therefore recommended for SR-Site transport calculations.

5.2.4 Cesium (Cs)

Radioisotopes of cesium are all fission products. The three isotopes of Cs in spent nuclear fuel have respective half-lives of 2.065 y (^{134}Cs), 2.3×10^6 y (^{135}Cs), and 30.17 y (^{137}Cs) /Audi et al. 2003/. The principal radioisotope of interest in SR-Site is ^{135}Cs on account of its long half-life.

Cs is not considered to be redox sensitive and the Cs(I) valence is the only relevant redox state for normal groundwater conditions. The Cs^+ ion is expected to be the dominant species for dissolved cesium under all foreseeable groundwater compositions, although with an increasing importance of the chloride complex, CsCl in increasingly saline groundwater. Cs is highly soluble and there are no solubility limiting minerals formed at the concentration levels likely to be encountered in SR-Site.

Cs(I) is expected to sorb by an ion-exchange mechanism and is known to sorb preferentially on phyllosilicate minerals such as biotite and its alteration product chlorite. Cs^+ is a relatively large cation with an ionic radius of 1.67 Å. This means that it has weak ion-dipole interactions with water and consequently, is weakly hydrated with a small hydrated radius. It can approach charged sites more closely and thus associate more strongly than other competing ions that have a larger sphere of hydration. This also implies that it competes strongly against other cations in groundwater for electrostatic ion-exchange sites. This is particularly prominent in interlayer regions of biotite where steric effects reduce access for competing cations.

The sorption of Cs(I) is highly non-linear owing to sorption on both frayed edge sites (FES) and phyllosilicate interlayers. Since the FES are much less abundant than the interlayer binding sites, the non-linearity of the sorption isotherm extends to very low concentrations. This non-linearity is frequently described using the Freundlich isotherm owing to its applicability over wide concentration ranges. The natural background level of the non-radioactive isotope ^{133}Cs is positively correlated with ionic strength and varies between about 0.1 mg/l and 10 mg/l in Forsmark and Laxemar groundwater (see Appendix A). It is the background concentration of the naturally occurring isotope that sets the appropriate concentration level for assessment of sorption since this is expected to far exceed the concentrations of transported Cs radioisotopes. If Cs concentrations are sufficiently high, there is a theoretical possibility of sorption irreversibility in phyllosilicate minerals with hydratable interlayers. This is due to collapse of the layers when hydrated interlayer cations are displaced by weakly hydrated Cs^+. Biotite, however, owing to its non-hydratable interlayer structure is not expected to behave in this manner.

Although phyllosilicate minerals exhibit strong selectivity for Cs^+, high concentrations of competing ion-exchanging solutes (Ca^{2+}, Mg^{2+}, Na^+, K^+) reduce the sorptivity of Cs(I). This gives rise to a strong anti-correlation of sorptivity with increasing ionic strength. In this compilation, the effect of ionic strength has been quantified by introducing a chemistry transfer factor to account for ion-exchange competition. The chemistry transfer factor was calculated using statistics of groundwater compositional variability together with a simplified ion-exchange model (see Section 5.1.1). The correction implied by the chemistry transfer factor is small relative to the overall uncertainty of the K_d estimate for Cs(I) sorption and amounts to (on average) no more than a factor of about two shift of the best estimate K_d value for the range of salinities encountered during the temperate time domain relative to the least favourable groundwater composition at 3,000 y.

The temporal variability of the salinity field surrounding the repository, however, is not uniform and the application of the chemistry transfer factor mostly results in a broadening of the uncertainty distribution. This is particularly true at later times where there is a larger range of salinities resulting from the diversity of hydrodynamic resistances characterising recharge flowpaths. Flowpaths transecting the repository that have low hydrodynamic resistance (small F-factors) can be expected to undergo greater temporal changes in salinity than flowpaths featuring high hydrodynamic resistance (large F-factors), where salinity levels may not change significantly. Since the temporal changes in groundwater chemistry

are not spatially resolved to individual radionuclide release locations, however, the overall distribution of groundwater compositions must be considered as part of an overall uncertainty associated with the use of a conditional K_d value to represent the average properties of flowpaths within the geosphere. A more detailed account of the derivation of recommended K_d values for Cs(I) may be found in Appendix E.

Since temporally variable K_d values cannot be modelled effectively in the current generation of safety assessment codes, K_d values are recommended for the most saline conditions expected during the repository groundwater evolution. A best estimate K_d value of 3.49×10^{-4} m^3/kg is therefore recommended for the Forsmark site for the most saline groundwater conditions expected at 3,000 y. The uncertainty distribution is assumed to be lognormally distributed ($\log_{10} K_d = -3.46\pm0.51$). For stochastic simulations, it is recommended that the uncertainty distribution be sampled in log space between the 2.5% (3.46×10^{-5} m^3/kg) and 97.5% percentiles (3.52×10^{-3} m^3/kg).

The higher CEC of Laxemar site-specific rock types results in the recommended K_d range being shifted upwards by roughly 0.3 log units for calculations involving the Laxemar site. This corresponds to an approximate doubling of the K_d value under the assumption of linear proportionality with CEC.

5.2.5 Chlorine (Cl)

The main species of the ^{36}Cl fission product (half-life 3.01×10^5 y) is expected to be chloride ion, Cl^-. For the purposes of safety assessment, the chloride ion, Cl^- can be reasonably assumed to be non-sorbing. A K_d value of 0 m^3/kg is therefore recommended for this species.

5.2.6 Lead (Pb)

Radioisotopes of lead arise in the decay chains of ^{238}U, ^{235}U, and ^{232}Th. The main radioisotope of interest for geosphere transport, however, is the ^{210}Pb daughter product of the ^{238}U decay chain. Although the other radioisotopes of Pb (^{214}Pb, ^{211}Pb, and ^{212}Pb) are significant gamma emitters in decay chain dose calculations, their geochemical properties are less important in transport calculations owing to their exceptionally short half-lives. Even the ^{210}Pb isotope has a relatively short half-life of 22.2 years meaning that its sorptivity is of only limited relevance for geosphere transport calculations. It is considered to be an important radionuclide, however, owing to its contribution to the far-field dose rate as a daughter nuclide in the ^{238}U decay chain.

Pb is not considered to be redox sensitive and the Pb(II) valence is the only relevant redox state for normal groundwater conditions. Similarly to Cd(II), the speciation of Pb(II) is strongly influenced by chloride complexation and the complexes $PbCl^+$, $PbCl_2$, $PbCl_3^-$, $PbCl_4^{2-}$ are expected to be dominant in saline groundwater. In fresh groundwater the carbonato-complexes ($PbCO_3$, $Pb(CO_3)_2^{2-}$, $PbHCO_3^+$) and, to a lesser extent, the hydroxo-complexes ($PbOH^+$, $PbOH_2$) tend to dominate. Under strongly reducing conditions, the sulphide complexes $Pb(HS)_2$ and $Pb(HS)_3^-$ may be important although to a lesser extent than for Cd sorption. The SKB-TDB only considers the selenite complex $PbSeO_3$ on account of the fact that ^{210}Pb has not previously been considered to be important in transport calculations, although the specie may be of relevance for Se speciation inside a spent fuel canister. The MinteqA2 database as distributed with PHREEQC was therefore used in speciation calculations to form the basis for the above discussion.

There is very little data for Pb sorption on granitic rock owing to its lesser status as a safety critical nuclide. The measurement data reported by /Papelis 2001/, however, have been used to give a very rough estimate for Pb(II) sorption that is probably sufficient for the purposes of SR-Site. Since the sorption of Pb(II) is expected to be dominated by an inner-sphere surface complexation mechanism for the pH and ionic strength ranges of interest in groundwater, the estimate is assumed to be approximately applicable for all groundwater compositions likely to be encountered. Owing to the limited data set used to form the K_d recommendation, this is probably not a robust assumption. Also, given its relatively short half-life, it is likely that ^{210}Pb produced by decay of transported ^{226}Ra in the near surface environment dominates the flux of ^{210}Pb to the biosphere. Since the hydrochemistry of the near surface environment is much more variable than the repository environment, the K_d recommendation is therefore uncertain. The transport of ^{210}Pb in the near surface is also more likely to be affected by pseudocolloid transport.

A best estimate K_d value of 2.52×10^{-2} m^3/kg is recommended for both Forsmark and Laxemar for all groundwater compositions. The uncertainty distribution is assumed to be lognormally distributed ($\log_{10} K_d = -1.60\pm0.56$). For stochastic simulations, it is recommended that the uncertainty distribution be sampled in log space between the 2.5% (2.05×10^{-3} m^3/kg) and 97.5% percentiles (3.10×10^{-1} m^3/kg). Due to the uncertainties outlined above, a case could be made for the use of the geochemical analogue Ni(II) as a sensitivity case study in place of the data ranges given for Pb(II). It is likely, however, that the use of the Ni(II) analogue is over-cautious since Ni sorption appears to be more strongly influenced by ionic strength. As also noted previously in Section 3.2.2, Pb^{2+} has a much larger first hydrolysis constant than Ni^{2+} indicating relatively stronger inner-sphere sorption. A more detailed account of the derivation of recommended K_d values for Pb(II) may be found in Appendix F.

5.2.7 Molybdenum (Mo)

The radioisotope ^{93}Mo is an activation product of ^{92}Mo found in the fuel rod alloy cladding and has a half-life of roughly 4,000 years. The molybdate oxyanion, MoO_4^{2-} is the only Mo species expected to exist at normal groundwater pH levels, although protonated forms can exist at low pH. For the purposes of safety assessment, the MoO_4^{2-} ion can be reasonably assumed to be non-sorbing. A K_d value of 0 m^3/kg is therefore recommended for this species.

5.2.8 Neptunium (Np)

The main Np radioisotope of interest in SR-Site is ^{237}Np which is mainly produced by decay of ^{241}Am (a daughter of ^{241}Pu decay). The ^{237}Np radioisotope has a half-life of 2.144×10^6 years. Neptunium is redox sensitive and can exist in a number of oxidation states from Np(III) to Np(VII) although only the Np(IV) and Np(V) redox states are relevant for normal groundwater compositions and Eh ranges. In the tetravalent state, $Np(OH)_4$ is the predominant specie in the pH interval 7–9, although $Np(OH)_3CO_3^-$ and $Np(OH)_3^+$ play a minor role. In the pentavalent state, either the NpO_2^+ specie (referred to as *neptunyl*) or $NpO_2CO_3^-$ may be dominant depending on pH and carbonate concentration with $NpO_2(CO_3)_2^{3-}$ typically in third place.

Quantification of Np sorption is complicated by its redox sensitivity and the fact that redox speciation in the tetravalent or pentavalent forms is rarely confirmed rigorously. Sorption investigations are usually performed under oxidising conditions at roughly atmospheric intensity or mildly reducing conditions. Reducing conditions are usually achieved in batch experiments closed to the atmosphere where the reducing intensity is determined by the balance between release of ferrous, Fe(II) ions from the rock and the rate of oxidation by residual oxygen in the headspace of the glove box. The oxidised pentavalent form is significantly more mobile than the reduced tetravalent form on account of its higher solubility and weak sorptivity. Np sorption is thought to occur primarily by way of an inner sphere surface complexation mechanism and therefore is relatively insensitive to groundwater salinity although sensitive to pH and carbonate concentration.

Sorption of Np on rocks was quantified during the Forsmark and Laxemar site investigations using site specific materials and different groundwater compositions /Byegård et al. 2008, Selnert et al. 2009/. Although the experiments were performed in a nitrogen glove box atmosphere, the apparently weak sorption of Np is indicative of Np(V) redox speciation although redox potential measurements were not made to confirm the redox status of the contact solutions. Sorption of Np under both oxidising and reducing conditions are reported by /Huitti et al. 1996/ for Rapakivi granite using a natural groundwater sample of marine type. Redox potentials measured during the anaerobic experiments varied from about +70 mV to –70 mV with the lower redox potentials corresponding to longer contact times. Although it is difficult to infer redox behaviour from measured electrode potentials, the transition from predominantly Np(IV) to Np(V) speciation occurs at a relatively high redox potential (roughly +100 mV) for the ranges of groundwater compositions used in the experiments.

Through-diffusion experiments involving Np(IV) are reported by /Yamaguchi et al. 2002/ for a 5 mm thick granite coupon in a 1.0 M $NaHCO_3$ solution (pH 8.8–9.0) under strongly reducing conditions achieved through the addition of sodium dithionite, $Na_2S_2O_4$. From interpretation of breakthrough data, a K_d value of $\sim6\times10^{-5}$ m^3/kg was obtained. These experiments, however, were carried out with a carbonate concentration at least three orders of magnitude higher than that expected for SR-Site and therefore competition by dissolved carbonate is expected to have considerably reduced the

sorptivity of Np(IV). At such high carbonate concentrations, the $Np(CO_3)_4^{4-}$ and $Np(CO_3)_5^{6-}$ species should dominate Np(IV) speciation. These complexed forms are not considered to contribute significantly towards Np(IV) speciation under normal groundwater conditions and therefore the sorption data are most likely not representative. Through-diffusion data for NpO_2^+ from an earlier study performed under oxidising conditions are also described in /Yamaguchi et al. 2002/ for a possibly more representative groundwater type. The K_d was calculated to be on the order of 4×10^{-6} m^3/kg which is somewhat lower than that estimated on the basis of the site investigation data and only just higher than the free storage capacity of the rock matrix porosity.

From autoradiographic studies, Np(V) is known to sorb preferentially in association with biotite /Kienzler et al. 2009/ in granitic rocks. It is possible that this is also accompanied by heterogeneous reduction to the tetravalent form in the microenvironment of biotite mineral grains. This complicates the interpretation of experimental data, however, since one could argue that this represents the sorption (possibly surface precipitation) of Np(IV) rather than Np(V). Operationally, however, it is assumed that sorption of Np(V) has been quantified and the unclear mechanism of Np(V) immobilisation on biotite is neglected. Np(V) has also been shown to form ternary surface complexes with carbonate /Arai et al. 2007/. This complicates predictions of the influence of dissolved carbonate since increased carbonate can both promote sorption of ternary complexes and reduce sorption by way of indirect competitive effects related to aqueous phase complexation.

Np sorption is thought to occur primarily by way of an inner sphere surface complexation mechanism and therefore is relatively insensitive to groundwater salinity although sensitive to pH and carbonate concentration. Since it is not currently possible to relate measured sorptivity to groundwater pH and carbonate concentration in a reliable fashion, the empirical data ranges for different groundwater compositions (redox considered separately) were pooled and the resulting distribution of values assumed to represent an overall uncertainty arising due to groundwater compositional variability and uncertainty. A more detailed account of the derivation of recommended K_d values for both Np(IV) and Np(VI) may be found in Appendix G.

Under oxidising conditions, a best estimate K_d value of 4.13×10^{-4} m^3/kg is recommended for Np(V) sorption at Forsmark for all groundwater compositions. The uncertainty distribution is assumed to be lognormally distributed ($\log_{10} K_d = -3.38\pm0.74$). For stochastic simulations, it is recommended that the uncertainty distribution be sampled in log space between the 2.5% (1.48×10^{-5} m^3/kg) and 97.5% percentiles (1.15×10^{-2} m^3/kg).

Since sorption of Np appears to be related to biotite content, the higher CEC of Laxemar rock types suggests that a correction needs to be made for transport calculations involving the Laxemar site. The higher CEC of Laxemar site-specific rock types results in the recommended K_d range being shifted upwards by roughly 0.3 log units. This corresponds to an approximate doubling of the K_d value under the assumption of linear proportionality with CEC.

Owing to the very small number of measurements reported for reducing conditions and underlying quantification uncertainties, the Np(IV) sorption data are not considered to be sufficiently well-qualified for extrapolation to SR-Site conditions. Recommended ranges of sorptivity for the Np(IV) redox form are therefore made using Pu(IV) as a geochemical analogue since these data were considered to be more reliable. It is noted, however, that the recommended K_d ranges based on the Pu(IV) analogy are still in reasonable agreement with the actual Np(IV) data although these were not used in the final recommendation.

Under reducing conditions, a best estimate K_d value of 5.29×10^{-2} m^3/kg is recommended for Np(IV) sorption at Forsmark for all groundwater compositions. The uncertainty distribution is assumed to be lognormally distributed ($\log_{10} K_d = -1.28\pm0.65$). For stochastic simulations, it is recommended that the uncertainty distribution be sampled in log space between the 2.5% (2.84×10^{-3} m^3/kg) and 97.5% percentiles (9.84×10^{-1} m^3/kg).

Based on the groundwater hydrochemistry simulations described in /Salas et al. 2010/, the predicted redox potential is thought to be sufficiently low that Np(IV) speciation can be generally assumed for geosphere transport calculations in SR-Site. It is noted, however, that towards the end of the temperate time domain (~9,000 y), the increasing carbonate concentration of the groundwater suggests that Np might be close to the Np(IV)/Np(V) transition zone if the $Fe^{2+}/Fe(OH)_3$ pair is deemed to control redox conditions.

5.2.9 Nickel (Ni)

The radioisotopes of nickel (^{59}Ni and ^{63}Ni) are activation products resulting from irradiation of the metallic cladding of fuel elements. The ^{59}Ni isotope has a half-life of 1.01×10^5 years and decays to form stable ^{59}Co. The ^{63}Ni isotope has a half-life of 100 years and decays to form stable ^{63}Cu. The ^{59}Ni isotope is consequently considered a nuclide of importance for geosphere transport calculations, whereas the ^{63}Ni isotope is considered less important.

Ni is not considered to be redox sensitive and the Ni(II) valence is the only relevant redox state for normal groundwater conditions. In fresh groundwater the Ni^{2+} ion is expected to be the dominant specie for dissolved nickel in the pH range 7–8, although generally shifting towards a predominance of the carbonate complex, $NiCO_3$ at pH greater than 8. Chloride complexation is important for this element and the $NiCl^+$ complex is frequently dominant in groundwater of more saline character. Under strongly reducing conditions, the $NiHS^+$ sulphide complex may also play an important role.

Ni sorption exhibits a weak sensitivity to ionic strength which might indicate an ion-exchange sorption mechanism, although a mixed inner and outer-sphere surface complexation mechanism is also possible. The magnitude of the first hydrolysis constant of the Ni^{2+} cation, on the other hand, suggests an inner sphere sorption mechanism is likely. In the literature, surface complexation modelling approaches have been frequently used to fit experimental data (e.g. /Bradbury and Baeyens 2005b, Olin et al. 2006/). It therefore cannot be entirely ruled out that the apparent ionic sensitivity of Ni(II) sorption might be related to hydrolysis effects since the contact groundwaters used in laboratory experiments typically also exhibit pH levels approximately correlated with ionic strength. We have chosen to interpret the empirical trend (operationally) as an ionic strength sensitivity, although it is noted that the systematic trend is also compatible with a hydrolysis-based rationalisation with regard to the SR-Site groundwater compositions as well as the contact groundwater end-members used in laboratory experiments.

Ni sorption was quantified during the Forsmark and Laxemar site investigations using site specific materials and several representative groundwater compositions /Byegård et al. 2008, Selnert et al. 2009/. Data are also reported by /Kulmala and Hakanen 1993/ for Olkiluoto tonalite and Rapakivi granite in contact with native samples of saline and fresh groundwater, respectively. The site investigation data were used to derive K_d values for SR-Site, while the Finnish data were used in a supporting role as a consistency check on the recommended data.

In this compilation, the effect of ionic strength has been quantified by introducing a chemistry transfer factor. The chemistry transfer factor was calculated using statistics of groundwater compositional variability together with a least squares regression model based on the laboratory data obtained during the site investigations. The data regression suggests that decreasing the ionic strength by an order of magnitude results in a roughly 2.5 times proportional increase in the K_d value. The use of a regression model also implies that if the sorptive variability is actually related to pH rather than ionic strength, the approximate correlation of pH and ionic strength nevertheless captures the correct empirical trend.

The correction implied by the chemistry transfer factor is small relative to the overall uncertainty of the K_d estimate for Ni(II) sorption and amounts to (on average) no more than a factor of about 1.4 shift of the best estimate K_d value for the range of salinities encountered during the temperate phase relative to the least favourable groundwater composition at 3,000 y. Here, it should be noted that the same caveats for the estimated impact of temporal variability of groundwater composition apply as discussed previously for Cs(I) sorption. A more detailed account of the derivation of recommended K_d values for Ni(II) may be found in Appendix H.

Since temporally variable K_d values cannot be modelled effectively in the current generation of safety assessment codes, K_d values are recommended for the most saline conditions expected during the repository groundwater evolution. A best estimate K_d value of 1.10×10^{-3} m^3/kg is therefore recommended for the Forsmark site for the most saline groundwater conditions expected at 3,000 y. The uncertainty distribution is assumed to be lognormally distributed ($\log_{10} K_d = -2.96\pm0.65$). For stochastic simulations, it is recommended that the uncertainty distribution be sampled in log space between the 2.5% (5.97×10^{-5} m^3/kg) and 97.5% percentiles (2.04×10^{-2} m^3/kg).

Although it has not been demonstrated that Ni(II) sorbs preferentially on biotite, the sensitivity to salinity conditions suggests that scaling of the K_d value with respect to CEC is not an unreasonable assumption. The higher CEC of Laxemar site-specific rock types results in the recommended K_d range being shifted upwards by roughly 0.3 log units for calculations involving the Laxemar site. This corresponds to an approximate doubling of the K_d value under the assumption of linear proportionality with CEC.

5.2.10 Niobium (Nb)

The radioisotopes of niobium (^{94}Nb and ^{93m}Nb) are activation products resulting from irradiation of the metallic cladding of fuel elements. The ^{94}Nb isotope has a half-life of 2.03×10^{4} years and decays to form stable ^{94}Mo. The metastable ^{93m}Nb isotope has a half-life of 16.1 years and undergoes gamma decay to form stable ^{93}Nb. The ^{94}Nb isotope is consequently considered a nuclide of importance for geosphere transport calculations, whereas the ^{93m}Nb isotope is considered of only minor importance.

Nb is not considered to be redox sensitive and the Nb(V) valence is the only relevant redox state for normal groundwater conditions. At circumneutral pH in both fresh and saline groundwater, the NbO_3^- oxyanion and $Nb(OH)_5$ hydroxo-complex are present in roughly equal proportion, although the balance shifts slightly to a greater predominance of NbO_3^- at higher pH. Although an additional $Nb(OH)_4^-$ hydroxo-complex exists at very low concentration there are no other recognised species of this element in the thermodynamic databases in common use.

Nb sorption data are reported by /Kulmala and Hakanen 1993/ for Olkiluoto tonalite and Rapakivi granite in contact with native groundwater samples of saline and fresh character, respectively. Very little difference in sorptivity is noted between the different groundwater compositions that could be reasonably related to ionic strength. Based on the hydrolysis reaction of Nb, however, it is thought that Nb should sorb principally by way of an inner sphere sorption mechanism. The empirical data ranges for different groundwater compositions were therefore pooled and the resulting distribution of values assumed to represent an overall uncertainty arising due to groundwater compositional variability and uncertainty. A more detailed account of the derivation of recommended K_d values for Nb(V) may be found in Appendix I.

A best estimate K_d value of 1.98×10^{-2} m^3/kg is recommended for both Forsmark and Laxemar for all groundwater compositions. The uncertainty distribution is assumed to be lognormally distributed ($\log_{10} K_d = -1.70\pm0.64$). For stochastic simulations, it is recommended that the uncertainty distribution be sampled in log space between the 2.5% (1.11×10^{-3} m^3/kg) and 97.5% percentiles (3.53×10^{-1} m^3/kg).

5.2.11 Palladium (Pd)

The main palladium radioisotope of interest in SR-Site is ^{107}Pd and is a fission product. It has a relatively long half-life of 6.5×10^{6} years and undergoes β-decay to form stable ^{107}Ag. Pd is not considered to be redox sensitive and the Pd(II) valence is the only relevant redox state for normal groundwater conditions. At circumneutral to alkaline pH in fresh groundwater, the $Pd(OH)_2$ hydroxo-complex is predominant. The $Pd(OH)_3^-$ and $PdOH^+$ complexes are also present, although at much lower concentration. Under saline conditions, the $PdCl_4^{2-}$ and, to a lesser extent, $PdCl_3^-$ chloride complexes dominate at pH 7 and below, although the balance shifts to a predominance of $Pd(OH)_2$ and $Pd(OH)_3^-$ above pH 8.

Pd sorption is poorly covered in the literature and only one study by /Tachi et al. 1999/ was found for granite in contact with water of varying ionic strength (simple NaCl solution) and pH. Based on the hydrolysis reaction of Pd^{2+} it is thought that Pd should sorb principally by way of an inner sphere sorption mechanism. Sorption of Pd was not observed to be influenced by ionic strength in this study which is as expected for the postulated sorption mechanism. The empirical data ranges for different groundwater compositions were therefore pooled and the resulting distribution of values assumed to represent an overall uncertainty arising due to groundwater compositional variability and uncertainty. Owing to the small number of data points and the non-representative contact solution composition, these data are considered uncertain although sufficiently well-qualified for the purposes of SR-Site. A more detailed account of the derivation of recommended K_d values for Pd(II) may be found in Appendix J.

A best estimate K_d value of 5.20×10^{-2} m^3/kg is recommended for both Forsmark and Laxemar for all groundwater compositions. The uncertainty distribution is assumed to be lognormally distributed ($\log_{10} K_d = -1.28\pm0.83$). For stochastic simulations, it is recommended that the uncertainty distribution be sampled in log space between the 2.5% (1.22×10^{-3} m^3/kg) and 97.5% percentiles (2.21 m^3/kg).

5.2.12 Plutonium (Pu)

The radioisotopes of plutonium are abundant in spent nuclear fuel and are present in the thorium ($4n$), neptunium ($4n+1$), and actinium ($4n+3$) decay series. They generally form only as by-products of neutron capture reactions and therefore do not occur in nature to any great extent with the exception of primordial ^{244}Pu which occurs in trace quantities. The isotopes of Pu in spent nuclear fuel and their half-lives are; ^{238}Pu (87.7 years), ^{239}Pu (2.41×10^4 years), ^{240}Pu (6.56×10^3 years), ^{241}Pu (14.4 years), and ^{242}Pu (3.75×10^5 years). The ^{240}Pu, ^{242}Pu, and ^{239}Pu radioisotopes are considered important nuclides for geosphere transport calculations in SR-Site, while ^{241}Pu and ^{238}Pu are considered of only minor importance.

Plutonium is redox sensitive and can exist as Pu(III), Pu(IV), Pu(V), and Pu(VI). Pu has relatively complex redox chemistry since it is possible for several redox states to persist simultaneously (see Appendix K). The different concentrations of carbonate present in fresh and saline groundwaters have a considerable impact on the species distribution of Pu in its various redox states. A brief overview of the main Pu species present in saline and fresh groundwater is given in Table 5-6.

Relatively detailed data sets for Pu sorption are reported by /Huitti et al. 1996/ and /Kulmala et al. 1998/ for various Finnish rock types in contact with native groundwater samples representative of the sites from where the rock bore core samples were obtained. Similarly to the other actinides, quantification of Pu sorption is complicated by its redox sensitivity and the fact that redox speciation is usually not confirmed rigorously by spectroscopy or wet analytical methods. This is mainly because such methods usually require much higher concentrations than are relevant for the characterisation of sorption in environmental systems. In the case of Pu, however, the situation is particularly complex since any pre-concentration or other treatment of the solution for analysis will also necessarily influence the relative concentrations of the different redox states. The propensity of Pu to undergo redox disproportionatation reactions is also of great relevance since the relative fractions of different redox states in solution may not be the same as that of sorbed Pu.

It is argued in Appendix K, by comparing first hydrolysis constants of Pu, that one would expect the sorbed fraction to be predominantly in the Pu(IV) state even when other redox forms are present in the aqueous phase. Similar reasoning for Pu(IV) redox speciation in the immobile phase is made by /Choppin et al. 1997, Choppin 2003/ based on consideration of the strong hydrolysis of Pu(IV) and low solubility product of $Pu(OH)_4$. This observation, however, also begs the question as to whether sorption of Pu is quantifiable at all given that it may not strictly be possible to describe it as a truly adsorptive process. Moreover, the exceptionally strong hydrolysis of Pu(IV) is also what drives the formation of polymeric eigencolloids which, depending on the phase separation technique used, might result in over- or under-estimation of sorptivity in laboratory experiments where redox transformations are likely to occur.

Since there is no way of determining exactly what the distribution of redox species is under experimental reducing conditions, it can only be assumed that the anoxic experimental conditions correspond to either Pu(III) or Pu(IV) predominance or possibly a mixed Pu(III,IV) redox state. For oxidising conditions, on the other hand, it is implicitly assumed that Pu(V) or Pu(VI) or a mixed Pu(V,VI) redox state exists. This is acknowledged as being simplistic, however, in that there is a *triple point* near ambient environmental conditions (~pH 8, ~Eh +600 mV) where equimolar concentrations of Pu(IV), Pu(V) and Pu(VI) is at least thermodynamically possible.

Table 5-6. Principal aqueous complexed forms in order of importance for various Pu redox states for saline (5×10^{-4} M HCO_3) and fresh (4×10^{-3} M HCO_3) groundwater compositions (pH 8). Only species comprising at least 5% of the total concentration are shown and are listed in order of importance.

	Saline	Fresh
Pu(III)	$PuOH^{2+}$, $PuCO_3^+$, Pu^{3+}	$Pu(CO_3)_2^-$,$PuCO_3^+$, $Pu(CO_3)_3^{3-}$
Pu(IV)	$Pu(OH)_4$	$Pu(OH)_4$
Pu(V)	PuO_2^+, $PuO_2CO_3^-$	$PuO_2CO_3^-$, PuO_2^+
Pu(VI)	PuO_2CO_3, $PuO_2(OH)_2$, PuO_2OH^+, $PuO_2(CO_3)_3^{2-}$	$PuO_2(CO_3)_2^{2-}$, PuO_2CO_3, $PuO_2(CO_3)_3^{4-}$

As for the other redox sensitive elements, sorption investigations are usually performed under oxidising conditions at roughly atmospheric intensity or under mildly reducing conditions. Reducing conditions are usually achieved in batch experiments closed to the atmosphere where the reducing intensity is determined by the balance between the reducing capacity of the contacting solution itself together with the release of ferrous, Fe(II) ions from the rock and the rate of oxidation by residual oxygen in the headspace of the glove box. In one of the abovementioned studies /Huitti et al. 1996/, Tc was used to verify reducing conditions indirectly in a complementary set of experiments. The use of Tc as a redox tracer is useful since it is easier to infer its redox state from the magnitude of its sorptivity. Since oxidation of essentially insoluble Tc(IV) to the highly soluble Tc(VII) occurs at a lower Eh than for the transition from Pu(III,IV) to Pu(V,VI) dominated redox speciation, this could be taken as indicative of sufficiently reducing conditions to observe sorption of reduced Pu species.

Through-diffusion experiments involving Pu(IV) are reported by /Yamaguchi and Nakayama 1998/ for 5 mm thick granite coupons in 0.1 M $NaHCO_3$ solution (pH 9.3) under mildly reducing conditions. From interpretation of breakthrough data, a K_d value of ~10^{-4} m^3/kg was obtained. In a separate study by /Yamaguchi et al. 2002/, through-diffusion of Pu was studied using the same method although under much more strongly reducing conditions achieved by addition of sodium dithionite. In this case, a K_d value of ~5×10^{-4} m^3/kg was obtained. In both studies, predominance of the Pu(IV) redox state was confirmed by a wet analytical method. These experiments, however, were carried out with a carbonate concentration at least two orders of magnitude higher than that expected for SR-Site conditions and are mostly of interest for studying the effective diffusivity of Pu(IV)-carbonate complexes rather than quantifying sorption under realistic groundwater conditions.

Unlike the redox sensitive actinides Np and U, autoradiographic studies described by /Kienzler et al. 2009/ show no strong evidence for preferential sorption of Pu on Fe-containing minerals (such as biotite) in granite. It is noted, however, that Pu was already in a tetravalent state in this study prior to sorption and therefore may represent a different sorption mechanism to that of Np(V) and U(VI). It should be noted, however, that the literature is not unequivocal regarding preferential sorption on biotite and there are other studies that have noted such behaviour /e.g. Anderson et al. 2007/. Although it is not clear in this case whether sorptivity should be correlated with biotite content or not, the relatively high CEC of the Finnish rock types suggests that neglection of the CEC transfer factor might be non-cautious. The data recommendation therefore assumes correlation of sorptivity with CEC as for the other redox sensitive actinides.

The data given by /Huitti et al. 1996/ and /Kulmala et al. 1998/ for oxidising conditions are used as a basis for the K_d recommendation for Pu(V,VI), while the data for reducing conditions are assumed to be approximately representative of Pu(IV) sorption. For the Pu(III) redox state, geochemical analogy with Am(III) is assumed. It is noted that the relative magnitude of the recommended data ranges are in qualitative agreement with the expectation that sorption of Pu(IV) should be stronger than Pu(III) by comparison of first hydrolysis constants. Pu sorption is thought to occur primarily by way of an inner sphere surface complexation mechanism and therefore is relatively insensitive to groundwater salinity although sensitive to pH and carbonate concentration. Since it is not currently possible to relate measured sorptivity to groundwater pH and carbonate concentration in a reliable fashion, the empirical data ranges for different groundwater compositions (redox considered separately) were pooled and the resulting distribution of values assumed to represent an overall uncertainty arising due to groundwater compositional variability and uncertainty. A more detailed account of the derivation of recommended K_d values for the various oxidation states of Pu may be found in Appendix K.

Under oxidising conditions, a best estimate K_d value of 9.14×10^{-3} m^3/kg is recommended for Pu(V,VI) sorption at Forsmark for all groundwater compositions. The uncertainty distribution is assumed to be lognormally distributed ($\log_{10} K_d = -2.04\pm0.60$). For stochastic simulations, it is recommended that the uncertainty distribution be sampled in log space between the 2.5% (6.19×10^{-4} m^3/kg) and 97.5% percentiles (1.35×10^{-1} m^3/kg).

For the Pu(III) redox state, a best estimate K_d value of 1.48×10^{-2} m^3/kg is recommended for Forsmark for all groundwater compositions. The uncertainty distribution is assumed to be lognormally distributed ($\log_{10} K_d = -1.83\pm0.72$). For stochastic simulations, it is recommended that the uncertainty distribution be sampled in log space between the 2.5% (5.74×10^{-4} m^3/kg) and 97.5% percentiles (3.83×10^{-1} m^3/kg).

A best estimate K_d value of 5.29×10^{-2} m^3/kg is recommended for Pu(IV) sorption at Forsmark for all groundwater compositions. The uncertainty distribution is assumed to be lognormally distributed ($\log_{10} K_d = -1.28\pm0.65$). For stochastic simulations, it is recommended that the uncertainty distribution be sampled in log space between the 2.5% (2.84×10^{-3} m^3/kg) and 97.5% percentiles (9.84×10^{-1} m^3/kg).

If it is assumed that the K_d for Pu sorption can be reasonably correlated with biotite content, the higher CEC of Laxemar rock types suggests that a correction needs to be made for transport calculations involving the Laxemar site. The higher CEC of Laxemar site-specific rock types results in the recommended K_d range being shifted upwards by roughly 0.3 units in log space. This corresponds to an approximate doubling of the K_d value under the assumption of linear proportionality with CEC.

Based on the groundwater hydrochemistry simulations described in /Salas et al. 2010/, it is found that the predicted redox potential should be sufficiently low that Pu(III) speciation can always be assumed for geosphere transport calculations in SR-Site. Given that the redox speciation of sorbed Pu might not correspond to that calculated for the aqueous phase, it could be argued that Pu(IV) might be a more likely candidate for the predominant redox state under repository conditions. Since Pu(III) is assigned a lower recommended K_d range, however, the assumption of Pu(III) redox speciation appears to be a cautious choice for geosphere transport calculations.

5.2.13 Protactinium (Pa)

Radioisotopes of protactinium arise in the decay chains of ^{238}U, ^{235}U, and ^{237}Np. The main radioisotope of interest for geosphere transport, however, is the ^{231}Pa daughter product of the ^{235}U decay chain (daughter of ^{239}Pu) which has a half-life of 3,300 years. Although Pa can nominally exist in both tetravalent and pentavalent form, only the pentavalent, Pa(V) redox state is considered relevant for normal groundwater conditions. Pa is therefore considered to be largely redox insensitive. In both fresh and saline groundwater, the electrically neutral PaO_2OH complex dominates Pa(V) speciation although PaO_2^+ may also be present at much lower concentration. Other aqueous complexes of Pa(V) are known, although they are thought to be present at such low concentrations as to be negligible.

Relatively detailed data sets are reported by /Kulmala et al. 1996/ and /Huitti et al. 1996/ for sorption of Pa on Finnish rock types in contact with native groundwater samples of varying composition (fresh and saline) for both oxidising and weakly reducing conditions. No substantive difference in sorptivity was noted between experiments made under oxic or anoxic conditions or for different groundwater compositions. Based on the hydrolysis reaction of Pa(V), it is thought that Pa(V) should sorb principally by way of an inner sphere sorption mechanism and should therefore be insensitive to ionic strength effects. The empirical data ranges for different groundwater compositions were therefore pooled and the resulting distribution of values assumed to represent an overall uncertainty arising due to groundwater compositional variability and uncertainty. A more detailed account of the derivation of recommended K_d values for Pa(V) may be found in Appendix L.

A best estimate K_d value of 5.92×10^{-2} m^3/kg is recommended for both Forsmark and Laxemar for all groundwater compositions. The uncertainty distribution is assumed to be lognormally distributed ($\log_{10} K_d = -1.23\pm0.48$). For stochastic simulations, it is recommended that the uncertainty distribution be sampled in log space between the 2.5% (6.76×10^{-3} m^3/kg) and 97.5% percentiles (5.18×10^{-1} m^3/kg).

5.2.14 Radium (Ra)

Radium isotopes are decay chain members for a number of actinides (^{238}U, ^{235}U, and ^{232}Th). The four principal isotopes of radium and their half-lives are ^{223}Ra (11.43 d), ^{224}Ra (3.66 d), ^{225}Ra (14.9 d), and ^{226}Ra (1,600 y). Since the first three isotopes have very short half-lives their sorptive properties are typically not considered important in geosphere transport calculations although they are important activity sources in their respective decay chains. Only the ^{226}Ra radioisotope is considered important for geosphere transport calculations in SR-Site.

Ra is not considered to be redox sensitive and the Ra(II) valence is the only relevant redox state for normal groundwater conditions. In typical saline groundwater, the Ra^{2+} cation is predominant although the chloride complex $RaCl^+$ may comprise up to 20% of the total Ra(II) concentration. In fresh water, the sulphate complex $RaSO_4$ may account for up to roughly 5% of the total Ra(II) concentration

whereas chloride complexation is negligible. Carbonate complexation and hydrolysis appears to play only a very minor role in the aqueous phase speciation of Ra(II) and may be generally neglected.

Ra is expected to sorb by way of an ion-exchange mechanism and its sorption therefore exhibits sensitivity to ionic strength. Measured activities of naturally occurring Ra(II) in groundwater are frequently correlated with its geochemical analogue, Ba(II) which is often cited as evidence of a solid solution solubility control involving the barite ($BaSO_4$) end-member. This behaviour, however, is also consistent with ion-exchange equilibria and it is difficult to draw specific conclusions purely on the basis of correlations between groundwater constituents.

Groundwater concentrations of Ba at both Forsmark and Laxemar are approximately saturated, or slightly oversaturated with respect to barite in pure phase form. Barite mineralisation in fracture coatings, however, appears to be rare at both sites and thus far has only been identified as small inclusions in galena (PbS) crystals /Sandström et al. 2008/. Naturally occurring Ra in groundwater is positively correlated with both Ba and other major cations (most particularly Ca) although the correlation is weak for Ba. This is discussed in more detail in Appendix A. The natural background concentration of Ra determines the relevant concentration range for Ra sorption since that transported from the repository is not expected to exceed the natural background level. Consideration of radiobarite solid solution is important for interpreting laboratory studies of sorption since groundwater compositions frequently exceed barite solubility limits. This can cast doubt on the magnitude of measured sorption if a solid solution of radiobarite is likely to form spontaneously.

Ra sorption was quantified during the Forsmark and Laxemar site investigations using site specific materials and several representative groundwater compositions /Byegård et al. 2008, Selnert et al. 2009/. Data are also reported by /Huitti et al. 1996/ and /Kulmala and Hakanen 1995/ for various granitic rock types from Finland in contact with native samples of saline and fresh groundwater. The site investigation data were used to derive K_d values for SR-Site, while the Finnish data were used in a supporting role as a consistency check on the recommended data. The groundwater compositions used in obtaining the experimental data were also screened for barite solubility as a means of quality control.

In this compilation, the effect of ionic strength has been quantified by introducing a chemistry transfer factor to account for ion-exchange competition. The chemistry transfer factor was calculated using statistics of groundwater compositional variability together with a simplified ion-exchange model (see Section 5.1.1). Since ion-exchange selectivity constants were not available for Ra^{2+} a geochemical analogy with Ba^{2+} was invoked. The correction implied by the chemistry transfer factor is small relative to the overall uncertainty of the K_d estimate for Ra(II) sorption and amounts to (on average) no more than a factor of about 2.4 shift of the best estimate K_d value for the range of salinities encountered during the temperate phase relative to the least favourable groundwater composition at 3,000 y. Here, it should be noted that the same caveats for the estimated impact of temporal variability of groundwater composition apply as discussed previously for Cs(I) sorption. A more detailed account of the derivation of recommended K_d values for Ra(II) may be found in Appendix M.

Since temporally variable K_d values cannot be modelled effectively in the current generation of safety assessment codes, K_d values are recommended for the most saline conditions expected during the repository groundwater evolution. A best estimate K_d value of 2.42×10^{-4} m^3/kg is therefore recommended for the Forsmark site for the most saline groundwater conditions expected at 3,000 y. The uncertainty distribution is assumed to be lognormally distributed ($\log_{10} K_d = -3.62\pm0.41$). For stochastic simulations, it is recommended that the uncertainty distribution be sampled in log space between the 2.5% (3.87×10^{-5} m^3/kg) and 97.5% percentiles (1.51×10^{-3} m^3/kg). It is noted that the absolute activities and relative activity ratios of naturally occurring ^{226}Ra and ^{222}Rn in groundwater at the Forsmark site are approximately consistent with the magnitude of sorption implied by the K_d range recommended for use in SR-Site (see Section 6.5).

The higher CEC of Laxemar site-specific rock types results in the recommended K_d range being shifted upwards by roughly 0.3 log units for calculations involving the Laxemar site. This corresponds to an approximate doubling of the K_d value under the assumption of linear proportionality with CEC.

5.2.15 Selenium (Se)

The ^{79}Se fission product is the principal radioisotope of Se of interest in SR-Site. The half-life of ^{79}Se has been subject to considerable uncertainty owing to its specific mode of beta decay, low activity, and difficulty in obtaining a sufficiently uncontaminated sample that an accurate measurement can be made. Different numerical values of the half-life of ^{79}Se have been used in some historic safety assessments. The current value used in SR-Site geosphere transport calculations is estimated at 3.77×10^5 years based on measurements reported by /Bienvenu et al. 2007/.

Se is redox sensitive and can exist in Se(–II), Se(0), Se(IV), and Se(VI) redox states. In the –II redox state it exists primarily as the HSe^- anion. In the tetravalent and hexavalent redox state, Se is predominantly speciated in oxyanion form as $HSeO_3^-$ and SeO_4^{2-}, respectively. Se(IV), and Se(VI) can act as a complexing ligand for a number of major groundwater cations and even other nuclides. Their concentrations, however, are usually much lower than the primary species described above. The elemental form of Se(0) is not expected to exist as an aqueous species although has been found to precipitate from solution in association with pyrite, FeS_2 /Breynaert et al. 2010/. This could potentially occur by way of a surface promoted reduction of sorbed Se(IV) or Se(VI).

Se is expected to sorb relatively weakly since anions only bind to positively charged sorption sites. This means that sorption will occur selectively on minerals that have a point of net zero proton charge close to the groundwater pH. For the ranges of groundwater compositions likely in SR-Site this would indicate a preference for sorption in association with ferric oxy-hydroxides and hematite microprecipitates in the rock matrix as demonstrated by /Jan et al. 2007, 2008/. Although groundwater composition is not expected to influence the distribution of complexed Se forms, competition for positive binding sites by dissolved carbonate theoretically may reduce sorptivity. Elevated pH levels also imply reduced sorptivity on account of lower abundance of positively charged surface sites above the point of zero charge.

It is difficult to predict the redox speciation of Se since multiple redox states frequently exist in thermodynamic disequilibrium /Beauwens et al. 2005/ and sorption studies may therefore represent mixed redox states even in very carefully controlled experiments. It could be argued that under sufficiently strong reducing conditions, hematite microprecipitates in the rock matrix could undergo reductive dissolution and release sorbed Se. Under such conditions, however, one might equally well expect solubility controlled transport of Se owing to precipitation of low solubility Se(-II) minerals (FeSe or $FeSe_2$) or possibly elemental Se(0).

Data for Se sorption on granite are reported by /Ticknor et al. 1996/ and /Papelis 2001/. Based on extrapolation from these data sets, a best estimate K_d value of 2.95×10^{-4} m³/kg is recommended for both the Forsmark and Laxemar sites for all groundwater compositions. The uncertainty distribution is assumed to be lognormally distributed ($\log_{10} K_d = -3.53\pm0.55$). For stochastic simulations, it is recommended that the uncertainty distribution be sampled in log space between the 2.5% (2.5×10^{-5} m³/kg) and 97.5% percentiles (3.48×10^{-3} m³/kg).

Although Se sorption could be reasonably assumed to be related to the biotite content of the rock (being the main source of Fe(II)), the data are considered sufficiently uncertain that this is neglected in the K_d recommendation. Owing to the large data uncertainties a case could also be made for the assumption of non-sorbing status for Se by appealing to arguments of caution as is customary for the other oxyanions. It is recommended that the impact of this uncertainty be therefore tested as a sensitivity case study if deemed necessary. A more detailed account of the derivation of recommended K_d values for the various redox states of Se may be found in Appendix N.

5.2.16 Silver (Ag)

The principal radioisotope of Ag is the ^{108m}Ag fission product which has a half-life of 418 years. Owing to its short half-life this nuclide is not expected to contribute significantly to far field dose rates under normal geosphere transport scenarios and is only likely to be important for accidental intrusion cases where geosphere transport is bypassed.

Ag is not considered to be redox sensitive and the Ag(I) valence is the only relevant redox state for normal groundwater conditions. Ag(I) is strongly complexed by chloride in both fresh and saline groundwaters to form AgCl and $AgCl_2^-$ whereas the free Ag^+ cation typically comprises less than 10% of the total Ag(I) concentration.

Calculations made using the MinteqA2 database suggest that the sulphide complexes AgHS, $Ag(HS)S_4^{2-}$ and $Ag(HS)_2^-$ may be important under strongly reducing conditions. Calculations made using this database also predict a prominent role for Ag_2Se under strongly reducing conditions. The SKB-TDB does not consider these additional species and the chloride complexed forms are therefore predicted to dominate for most groundwater compositions if this database is used in calculations.

Since ^{108m}Ag is not normally considered to be a safety critical nuclide there are no data sets available for Ag sorption on granitic rock types. For this reason a geochemical analogy with Cs(I) has been assumed in order to provide a recommended K_d range for this nuclide. The analogy is, however, not ideal owing to the greater importance of chloride complexes in the case of Ag(I) and the fact that sulphide complexes of Cs are not known to occur. The sorption of Ag(I) is thought to occur by way of an ion-exchange mechanism and its sorptivity is therefore sensitive to ionic strength effects. As noted previously in Section 3.2.2, the choice of Cs(I) as an analogue for Ag(I) is necessitated by a lack of data for any of the alternative geochemical analogues.

Since temporally variable K_d values cannot be modelled effectively in the current generation of safety assessment codes, K_d values are recommended for the most saline conditions expected during the repository groundwater evolution. A best estimate K_d value of 3.49×10^{-4} m^3/kg is therefore recommended for the Forsmark site for the most saline groundwater conditions expected at 3,000 y. The uncertainty distribution is assumed to be lognormally distributed ($\log_{10} K_d = -3.46\pm0.51$). For stochastic simulations, it is recommended that the uncertainty distribution be sampled in log space between the 2.5% (3.46×10^{-5} m^3/kg) and 97.5% percentiles (3.52×10^{-3} m^3/kg).

The higher CEC of Laxemar site-specific rock types results in the recommended K_d range being shifted upwards by roughly 0.3 log units for calculations involving the Laxemar site. This corresponds to an approximate doubling of the K_d value under the assumption of linear proportionality with CEC.

5.2.17 Strontium (Sr)

The principal radioisotope of Sr is the ^{90}Sr fission product which has a half-life of 28.7 years. Owing to its short half-life, its activity decays to trivial levels after about a thousand years. Strontium therefore has only minor significance for far-field transport calculations in SR-Site.

Sr is not considered to be redox sensitive and the Sr(II) valence is the only relevant redox state for normal groundwater conditions. In saline groundwater, the Sr^{2+} cation is predominant with the sulphate complex $SrSO_4$ being the next most important specie although typically comprising on the order of 1% of the total Sr(II) concentration. In fresh water, Sr^{2+} is also dominant with the carbonate complex $SrCO_3$ or $SrHCO_3^+$ accounting for about 3–5% of the total concentration depending on pH.

The sorption of Sr is relatively well studied on account of its importance for historical radiological incidents and geochemical similarity to Ca which is key to its radiological hazard. Sr(II) is expected to sorb by way of an ion-exchange mechanism and therefore exhibits sensitivity to ionic strength. Owing to its geochemical similarity to Ca, sorption of Sr is very weak. Sr(II) sorption was quantified during the Forsmark and Laxemar site investigations using site specific materials and several representative groundwater compositions /Byegård et al. 2008, Selnert et al. 2009/. The site investigation data were used to derive K_d values for SR-Site although for the more saline groundwater compositions, sorption was sufficiently weak as to be unquantifiable.

In this compilation, the effect of ionic strength has been quantified by introducing a chemistry transfer factor to account for ion-exchange competition. The chemistry transfer factor was calculated using statistics of groundwater compositional variability together with a simplified ion-exchange model (see Section 5.1.1). The correction implied by the chemistry transfer factor is small relative to the overall uncertainty of the K_d estimate for Sr(II) sorption and amounts to (on average) no more than a factor of about 1.14 shift of the best estimate K_d value for the range of salinities encountered during the temperate phase relative to the least favourable groundwater composition at 3,000 y. Here, it should be noted that the same caveats for the estimated impact of temporal variability of groundwater composition apply as discussed previously for Cs(I) sorption. A more detailed account of the derivation of recommended K_d values for Sr(II) may be found in Appendix P.

Since temporally variable K_d values cannot be modelled effectively in the current generation of safety assessment codes, K_d values are recommended for the most saline conditions expected during the repository groundwater evolution. A best estimate K_d value of 3.42×10^{-6} m^3/kg is therefore recommended for the Forsmark site for the most saline groundwater conditions expected at 3,000 y. The uncertainty distribution is assumed to be lognormally distributed ($\log_{10} K_d = -5.47\pm0.99$). For stochastic simulations, it is recommended that the uncertainty distribution be sampled in log space between the 2.5% (3.84×10^{-8} m^3/kg) and 97.5% percentiles (3.05×10^{-4} m^3/kg). It is noted that the storage capacity for Sr sorbed in the rock matrix is only slightly higher than that dissolved in the porewater itself meaning that uncertainty in the lower quantitative bound of the K_d distribution is largely irrelevant for geosphere transport calculations.

The higher CEC of Laxemar site-specific rock types results in the recommended K_d range being shifted upwards by roughly 0.3 log units for calculations involving the Laxemar site. This corresponds to an approximate doubling of the K_d value under the assumption of linear proportionality with CEC.

5.2.18 Technetium (Tc)

The principal radioisotope of Tc is ^{99}Tc which has a half-life of 2.11×10^5 years. Tc is redox sensitive and can exist as Tc(IV) or Tc(VII) in groundwater. In the tetravalent state, the $TcO(OH)_2$ complex is the predominant specie, although $TcO(OH)_3^-$ and Tc $(OH)_3CO_3^-$ play a minor role depending on pH and carbonate concentration. In the oxidised Tc(VII) state, the pertechnate oxyanion, TcO_4^- is the overwhelmingly dominant aqueous specie for all reasonable groundwater compositions.

Quantification of Tc sorption is complicated by its redox sensitivity although very weak sorption is usually considered evidence of the +VII (oxidised) redox state. For the purposes of safety assessment, the TcO_4^- ion can be reasonably assumed to be non-sorbing. A K_d value of 0 m^3/kg is therefore recommended for the Tc(VII) redox state. Under reducing conditions, Tc(IV) sorption is thought to occur primarily by way of an inner sphere surface complexation mechanism and therefore is considered to be relatively insensitive to groundwater salinity.

Data reported by /Huitti et al. 1996/ suggest very strong sorption of Tc(IV), although owing to the very small number of measurements and underlying quantification uncertainties, the data are not considered to be sufficiently well-qualified for extrapolation to SR-Site conditions. Recommended ranges of sorptivity for the Tc(IV) redox state are therefore made using Pu(IV) as a geochemical analogue since these data were considered to be more reliable. It is noted, however, that the recommended K_d ranges based on the Pu(IV) analogy are still in reasonable agreement with the actual Tc(IV) data although these were not used in the final recommendation. A more detailed account of the derivation of recommended K_d values for Tc(IV) may be found in Appendix Q.

Under reducing conditions, a best estimate K_d value of 5.29×10^{-2} m^3/kg is recommended for Tc(IV) sorption at Forsmark for all groundwater compositions. The uncertainty distribution is assumed to be lognormally distributed ($\log_{10} K_d = -1.28\pm0.65$). For stochastic simulations, it is recommended that the uncertainty distribution be sampled in log space between the 2.5% (2.84×10^{-3} m^3/kg) and 97.5% percentiles (9.84×10^{-1} m^3/kg).

Since sorption of Tc appears to be related to biotite content /Kienzler et al. 2009/, the higher CEC of Laxemar rock types suggests that a correction needs to be made for transport calculations involving the Laxemar site. The higher CEC of Laxemar site-specific rock types results in the recommended K_d range being shifted upwards by roughly 0.3 log units. This corresponds to an approximate doubling of the K_d value under the assumption of linear proportionality with CEC.

Based on the groundwater hydrochemistry simulations described in /Salas et al. 2010/, the predicted redox potential is thought to be sufficiently low that Tc(IV) speciation can be assumed for geosphere transport calculations in SR-Site. Towards the end of the temperate time domain (~9,000 y), however, the increasing carbonate concentration of the groundwater suggests that Tc might be close to the Tc(IV)/Tc(VII) transition zone if the $Fe^{2+}/Fe(OH)_3$ pair is deemed to control redox conditions.

5.2.19 Thorium (Th)

The radioisotopes of thorium are produced by the decay of long-lived actinides and their activities increase with time in spent nuclear fuel by in-growth (i.e. from decay of their actinide parents). The isotopes of thorium and their half-lives are ^{227}Th (18.68 days), ^{228}Th (1.9116 years), ^{229}Th (7.34×10^{3} years), ^{230}Th (7.538×10^{4} years), ^{231}Th (25.52 hours), and ^{234}Th (24.10 days). Only the ^{230}Th and ^{229}Th radioisotopes are considered important for geosphere transport calculations in SR-Site on account of their relatively long half-lives.

Th is not considered to be redox sensitive and the Th(IV) valence is the only relevant redox state for normal groundwater conditions. The speciation of Th in both fresh and saline groundwater is mostly dominated by the $Th(OH)_3CO_3^-$ hydroxo-carbonato complex although the $Th(OH)_4$ complex plays an increasingly important role at pH ≥ 8 in groundwater with low dissolved carbonate concentration. Thorium is generally considered to be largely immobile in natural systems; an assumption implicitly underlying its use in uranium disequilibrium studies.

Th is difficult to study experimentally owing to its strong hydrolysis and ability to form eigencolloids in aqueous solutions. Th(IV) sorption was studied in the site investigations although measurement problems meant that sorption proved impractical to quantify using the batch method employed. There are some older sorption studies in the literature although these do not appear to be sufficiently well-qualified to be used defensibly in SR-Site using the present methodology. Through-diffusion experiments are reported by /Park and Baik 2009/ on a granite coupon of unspecified thickness in a 0.1 M $NaHCO_3$ solution (pH 9.5). These experiments are appealing in that one would not expect colloidal Th(IV) material to be transported through the rock to any great extent. Based on the magnitude of apparent diffusivity reported, a K_d value of about 4×10^{-2} m^3/kg seems realistic. It should be noted, however, that the carbonate concentration used in these experiments is at least two orders of magnitude higher than the highest concentration expected during SR-Site and therefore the extrapolated K_d value may not be representative.

Interestingly, in that particular study the anionic tracer Cl^- was found to diffuse faster than tritiated water, which is the opposite of what one would expect in the presence of anion exclusion in confined pore spaces. This could be explained, however, if the coupon was sufficiently thin that macropores crossed the full width of the sample since diffusion would occur relatively unhindered in such pores while the storage capacity of the sample microporosity might be less accessible to anions. For the interpretation of the Th(IV) through-diffusion experiment this is relevant for two reasons; 1) for the assignment of an appropriate formation factor for diffusion given Th(IV) should be predominantly speciated as the $Th(OH)_3CO_3^-$ anion and, 2) because the initially fast transport through the macropores might underestimate the storage capacity of the rock over longer timescales since access to the microporosity is not hindered for the neutral $Th(OH)_4$ species.

Since the literature data for Th sorption are uncertain and possibly influenced by non adsorptive interactions, recommended K_d ranges for Th(IV) are made using Pu(IV) as a geochemical analogue since these data may be more reliable. There is no evidence to suggest that Th(IV) should sorb preferentially in association with biotite and therefore this has not been considered in the present recommendation. Th(IV) sorption is thought to occur primarily by way of an inner sphere surface complexation mechanism and therefore is relatively insensitive to groundwater salinity although sensitive to pH and carbonate concentration.

A best estimate K_d value of 5.29×10^{-2} m^3/kg is recommended for both Forsmark and Laxemar for all groundwater compositions. The uncertainty distribution is assumed to be lognormally distributed ($\log_{10} K_d = -1.28\pm0.65$). For stochastic simulations, it is recommended that the uncertainty distribution be sampled in log space between the 2.5% (2.84×10^{-3} m^3/kg) and 97.5% percentiles (9.84×10^{-1} m^3/kg). It should be noted that this range brackets the value estimated by interpretation of the through-diffusion experiments reported by /Park and Baik 2009/ and therefore appears to be defensible.

5.2.20 Tin (Sn)

The two principal radioisotopes of tin, ^{126}Sn and ^{121m}Sn are produced as fission products and have half-lives of 2.3×10^{5} years and 43.9 years, respectively. Consequently, only the ^{126}Sn radioisotope is of importance for geosphere transport calculations in SR-Site. Sn is redox sensitive and can exist

in a divalent, Sn(II) and tetravalent, Sn(IV) form. The Sn(IV) redox form, however, is dominant for all reasonable groundwater compositions and the Sn(II) redox state can usually be neglected. The hydroxo-complexes, $Sn(OH)_4$, $Sn(OH)_5^-$, and $Sn(OH)_6^{2-}$ are the dominant species in both fresh and saline groundwater. The $Sn(OH)_4$ specie tends to dominate at circumneutral pH, although $Sn(OH)_5^-$ and $Sn(OH)_6^{2-}$ take on greater prominence at pH 8 and above.

Sorption data for Sn(IV) are sparse in the literature on account of its relatively strong sorptivity and because it is not normally considered to be a safety critical nuclide. Some data are reported by /Ticknor et al. 1996/ and these have been used as a basis for the K_d recommendation in this data compilation. Sn(IV) is not expected to exhibit preferential sorption on biotite and therefore this has not been considered in the present recommendation. Sn(IV) sorption is thought to occur primarily by way of an inner sphere surface complexation mechanism and therefore is relatively insensitive to groundwater salinity although sensitive to pH. A more detailed account of the derivation of recommended K_d values for Sn(IV) may be found in Appendix O.

A best estimate K_d value of 1.59×10^{-1} m³/kg is recommended for both Forsmark and Laxemar for all groundwater compositions. The uncertainty distribution is assumed to be lognormally distributed ($\log_{10} K_d = -0.80\pm0.28$). For stochastic simulations, it is recommended that the uncertainty distribution be sampled in log space between the 2.5% (4.51×10^{-2} m³/kg) and 97.5% percentiles (5.58×10^{-1} m³/kg).

5.2.21 Tritium (^{3}H)

Tritium (^{3}H) with a half-life of 12.3 years is produced as both a fission product and as an activation product. Owing to its short half-life it decays to trivial levels after about a thousand years. Tritium therefore has very little significance for far-field transport calculations in SR-Site.

Although tritiated water molecules ($^3H^1HO$ and ^3H_2O) can disassociate and participate in protonation/deprotonation reactions with surface groups on mineral surfaces, the concentration of water molecules is so large in comparison that sorption is, for all practical purposes, non-existent in a safety assessment perspective. Tritium can therefore be reasonably assumed to be non-sorbing. A K_d value of 0 m³/kg is therefore recommended for this species.

5.2.22 Uranium (U)

The radioisotopes of uranium are the most abundant radionuclides in spent nuclear fuel as well as being ubiquitous in granitic rock as naturally occurring substances. The isotopes of uranium and their half-lives are; ^{232}U (68.9 years), ^{233}U (1.592×10^5 years), ^{234}U (2.455×10^5 years), ^{235}U (7.04×10^8 years), ^{236}U (2.342×10^7 years), ^{237}U (6.75 days), and ^{238}U (4.468×10^9 years). The ^{234}U, ^{235}U, and ^{238}U radioisotopes are present in both natural and enriched uranium as well as being initially present in spent fuel. The other U radioisotopes generally do not occur in nature. The ^{233}U, ^{234}U, ^{235}U, ^{236}U and ^{238}U radioisotopes are all considered important nuclides for geosphere transport calculations in SR-Site.

Uranium is one of the most well studied actinides partly because of its importance for nuclear waste safety and partly owing to its ubiquitous presence in environmental systems. Its particular redox chemistry also allows it to be used as a marker of geochemical alteration processes in uranium disequilibrium studies. Uranium is redox sensitive and can exist in a number of different oxidation states from +III to +VI, although only the +IV (*uranous*) and +VI (*uranyl*) states are usually considered sufficiently stable to occur in groundwater. U(V) also readily undergoes redox disproportionation to form U(IV) and U(VI) in groundwater which also makes it less relevant for safety assessment calculations. Although the U(V) state is ordinarily disregarded, speciation calculations made using the SKB-TDB suggest that a non-negligible fraction of U(V), on the order of a few percent, does appear to thermodynamically possible in under reducing conditions in SR-Site groundwaters at pH 7–8.

In the tetravalent state, $U(OH)_4$ is the overwhelmingly dominant specie in the pH interval 7–9 for all reasonable groundwater compositions. In the pentavalent state, only UO_2^+ is recognised in the SKB-TDB as the basis species for U(V). For the hexavalent state and in fresh groundwater, the carbonato-complex $UO_2(CO_3)_3^{4-}$ and, to a lesser extent, $UO_2(CO_3)_2^{2-}$ are dominant with UO_2CO_3 being of only minor significance. In saline groundwater, the $UO_2(CO_3)_2^{2-}$, and $UO_2(CO_3)_3^{4-}$ species are still predominant although $UO_2(OH)_3^-$, $UO_2(OH)_2$, UO_2CO_3, and UO_2OH^+ may also be important depending on the pH and carbonate concentration.

As for the other redox sensitive actinides, quantification of U sorption is complicated by its redox sensitivity and the fact that redox speciation in the tetravalent or hexavalent forms is rarely confirmed rigorously by spectroscopic or wet analytical methods. Sorption investigations are usually performed under oxidising conditions at roughly atmospheric intensity or mildly reducing conditions. Reducing conditions are usually achieved in batch experiments closed to the atmosphere where the reducing intensity is determined by the reducing capacity of the contact solution and the balance between release of ferrous, Fe(II) ions from the rock and the rate of oxidation by residual oxygen in the headspace of the glove box. This, however, is rarely sufficient to guarantee U(IV) redox speciation and the addition of a strong reducing agent such as sodium dithionite is usually required for this. Most of the studies in the open literature are for U(VI) since this is the most relevant redox state for terrestrial environmental conditions. The oxidised hexavalent form is significantly more mobile than the reduced tetravalent form on account of its higher solubility and weak sorptivity. U sorption is thought to occur primarily by way of an inner sphere surface complexation mechanism and therefore is relatively insensitive to groundwater salinity although sensitive to pH and carbonate concentration.

Sorption of U on rocks was quantified during the Forsmark and Laxemar site investigations using site specific materials and different groundwater compositions /Byegård et al. 2008, Selnert et al. 2009/. Even though the experiments were performed in a nitrogen glove box atmosphere, the apparently weak sorption of U is indicative of U(VI) redox speciation. Redox potential measurements, however, were not made to confirm the redox status of the contact solutions so this is speculative. Sorption of U under oxidising conditions are also reported by /Huitti et al. 1996/ for Rapakivi granite using a natural groundwater sample of marine type. Although there are some other sorption studies in the literature for U(IV), these do not appear to be sufficiently well-qualified to be used defensibly in SR-Site using the present methodology.

Through-diffusion experiments involving U(VI) are reported by /Yamaguchi and Nakayama 1998/ for 5 mm thick granite coupons in 0.1 M $NaHCO_3$ solution (pH 9.3) under oxidising conditions. From interpretation of breakthrough data, a K_d value of ~10^{-4} m^3/kg was obtained. These experiments, however, were carried out with a carbonate concentration at least two orders of magnitude higher than that expected for SR-Site conditions and are mostly of interest for studying the effective diffusivity of uranyl-carbonate complexes rather than sorption under realistic groundwater conditions.

From autoradiographic studies, U(VI) is known to sorb preferentially in association with biotite in granitic rocks /Kienzler et al. 2009/ and is possibly accompanied by heterogeneous reduction to the tetravalent form. As outlined previously for Np, this complicates the interpretation of experimental data since one could argue that this represents the sorption (possibly surface precipitation) of U(IV) rather than U(VI). Operationally, however, it is assumed that sorption of U(VI) has been quantified and the unclear mechanism of U(VI) immobilisation on biotite is neglected. U(VI) has also been shown to form ternary surface complexes with carbonate /Bargar et al. 1999/. This complicates predictions of the influence of dissolved carbonate since increased carbonate can both promote sorption of ternary complexes and reduce sorption by way of indirect competitive effects related to aqueous phase complexation.

The site specific data from Forsmark and Laxemar together with the data set from /Huitti et al. 1996/ have been used to make K_d recommendations in SR-Site for U(VI). Since it is not currently possible to relate measured sorptivity to groundwater pH and carbonate concentration in a reliable fashion, the empirical data ranges for different groundwater compositions (redox considered separately) were pooled and the resulting distribution of values assumed to represent an overall uncertainty arising due to groundwater compositional variability and uncertainty. A more detailed account of the derivation of recommended K_d values for U(VI) may be found in Appendix R.

Under oxidising conditions, a best estimate K_d value of 1.06×10^{-4} m^3/kg is recommended for U(VI) sorption at Forsmark for all groundwater compositions. The uncertainty distribution is assumed to be lognormally distributed ($\log_{10} K_d = -3.97\pm0.66$). For stochastic simulations, it is recommended that the uncertainty distribution be sampled in log space between the 2.5% (5.53×10^{-6} m^3/kg) and 97.5% percentiles (2.05×10^{-3} m^3/kg).

Since sorption of U appears to be related to biotite content, the higher CEC of Laxemar rock types suggests that a correction needs to be made for transport calculations involving the Laxemar site. The higher CEC of Laxemar site-specific rock types results in the recommended K_d range being shifted upwards by roughly 0.3 units in log space. This corresponds to an approximate doubling of the K_d value under the assumption of linear proportionality with CEC.

Owing to the lack of data for reducing conditions recommended K_d ranges for U(IV) are made using Pu(IV) as a geochemical analogue. Under reducing conditions, a best estimate K_d value of 5.29×10^{-2} m^3/kg is recommended for U(IV) sorption at Forsmark for all groundwater compositions. The uncertainty distribution is assumed to be lognormally distributed ($\log_{10} K_d = -1.28\pm0.65$). For stochastic simulations, it is recommended that the uncertainty distribution be sampled in log space between the 2.5% (2.84×10^{-3} m^3/kg) and 97.5% percentiles (9.84×10^{-1} m^3/kg).

Based on the groundwater hydrochemistry simulations described in /Salas et al. 2010/, it is found that the predicted redox potential is not sufficiently low that U(IV) speciation can always be assumed for geosphere transport calculations in SR-Site. Towards the end of the temperate time domain (~9,000 y), the increasing carbonate concentration of the groundwater suggests that U is most likely in a hexavalent state if the $Fe^{2+}/Fe(OH)_3$ pair is deemed to be controlling redox conditions. Even at early times while carbonate concentrations are still relatively low, hexavalent redox speciation cannot be ruled out. Interestingly, redox speciation as U(IV) is not necessarily a less pessimistic scenario since it constitutes a more concentrated secondary source of the ^{226}Ra daughter (mostly from the decay of ^{234}U). Owing to these uncertainties, it is therefore recommended that case studies considering both redox states (separately) are propagated in SR-Site geosphere transport calculations.

5.2.23 Zirconium (Zr)

The principal radioisotope of Zr is the ^{93}Zr activation product which has a half-life of 1.53×10^6 years. Zr is not considered to be redox sensitive and the Zr(IV) valence is the only relevant redox state for normal groundwater conditions. The $Zr(OH)_4$ hydroxo-complex is the overwhelmingly dominant species for all groundwater compositions likely to be encountered in SR-Site.

Sorption data for Zr(IV) are sparse in the literature on account of its relatively strong sorptivity and since it is not normally considered to be a safety critical nuclide. The data reported by /Kulmala and Hakanen 1993/ have been used as a basis for the K_d recommendation in this compilation. Zr(IV) is not expected to exhibit preferential sorption on biotite and therefore this has not been considered in the present recommendation. A more detailed account of the derivation of recommended K_d values for Zr(IV) may be found in Appendix S.

A best estimate K_d value of 2.13×10^{-2} m^3/kg is recommended for both Forsmark and Laxemar for all groundwater compositions. The uncertainty distribution is assumed to be lognormally distributed ($\log_{10} K_d = -1.67\pm0.35$). For stochastic simulations, it is recommended that the uncertainty distribution be sampled in log space between the 2.5% (4.48×10^{-3} m^3/kg) and 97.5% percentiles (1.02×10^{-1} m^3/kg).

6 Summary of recommended data for use in SR-Site

Based on the data extrapolation and qualification procedures described in Chapter 5, K_d data have been estimated for application conditions in SR-Site. The data are based on the use of Forsmark metagranite (SKB rock code 101057) as a reference rock type and consider the impact of all known sources of uncertainty that can be reasonably quantified. For the impact of temporally variable groundwater compositions, K_d values have been chosen cautiously (wherever feasible to do so) to reflect the least favourable conditions for transport retardation.

For calculations involving the Laxemar site, the data have been rescaled taking into consideration only the difference in cation exchange capacity (CEC) of site specific rock at the Laxemar site relative to the Forsmark site. Transfer factors for surface area and groundwater compositional effects are assumed to be identical for both sites owing to broad similarities in hydrochemical and microstructural features of each site. Based on the relative Fe-content of the dominant Forsmark and Laxemar rock types (used as a proxy for CEC), this implies that the arithmetic data ranges are simply increased by a factor of 1.6 to give the appropriate data range for Laxemar. This correction is also only made for those radionuclides where sorption is deemed to be related to the CEC of the rock.

Data for surface complexing radionuclides may be assumed to be applicable for all projected groundwater compositions as the specified uncertainty distributions implicitly include uncertainty arising due to groundwater compositional variation (as far as this can be reasonably assessed). The dominant redox species for those radionuclides that are known to exhibit redox sensitivity are established on the basis of speciation simulations made using PHREEQC in conjunction with the SKB-TDB thermodynamic database /Duro et al. 2006/. Specific details are discussed in the appendices to this report on a case by case basis for each radionuclide. Owing to uncertainty concerning the actual redox status of uranium under projected repository conditions, it is recommended that both the tetravalent, U(IV) and hexavalent, U(VI) cases are propagated within the safety assessment calculations as separate case studies.

For radionuclides that sorb by an ion-exchange or predominantly outer-sphere surface complexation mechanism, ionic strength is expected to have a relatively strong theoretical impact on sorptivity. Increased ionic strength typically results in a decrease of K_d for these solutes owing to sorption competition with other groundwater constituents. Cautiously scaled K_d values for these solutes are therefore given for the most saline conditions expected during repository evolution. The scaling factors for Cs, Sr, and Ra are derived from simulations made using PHREEQC and a single-site model of ion exchange in combination with projected statistics of ionic strength conditions in the repository volume. This is discussed on a case by case basis in the report appendices for each element concerned.

In the case of Ni, a statistical regression model is used which relates variations in apparent sorptivity with ionic strength. As noted previously in Section 5.2.9, an apparent sensitivity to ionic strength does not necessarily imply a strictly ion-exchange sorption mechanism and a mixed inner- and outer-sphere surface complexation mechanism is also possible as are other explanatory mechanisms. Where apparent sorption sensitivity to ionic strength is observed, the additional assumption of a CEC dependency generally gives lower extrapolated K_d values than neglect of CEC effects and therefore this may be considered a cautious assumption. This is also true for solutes which, although not sensitive to ionic strength, are suspected to sorb preferentially in association with CEC determining minerals such as biotite.

Periodic episodes of deep saline upconing or cryogenic brine formation associated with high flow conditions are not expected to occur for any significant length of time and therefore have been neglected in the recommendation of K_d values for SR-Site. Although ionic strength is known to have a strong impact on the sorption of ion-exchanging solutes, the overall range of data uncertainty is sufficiently large that the ionic strength correction factors are relatively small.

It must also be remembered that since the changes in groundwater composition are not resolved on the level of individual migration paths, extrapolation to the groundwater situations existing at different times must consider the statistical distribution of spatially variable groundwater compositions throughout the entire repository volume which, in itself, introduces additional statistical dispersion in the calculation of K_d uncertainty ranges. Since the K_d data are recommended for relatively saline conditions, this means that the strength of sorption will be pessimistically underestimated during the bulk of repository evolution.

Given the uncertainty of the underlying data set for lead and its possible contribution to far-field dose rates, it is also recommended that K_d values for Ni(II) are used as an analogue for Pb(II) sorption in sensitivity case studies. This might be considered an over-pessimistic assumption, however, given that Pb(II) is expected to sorb much more strongly than Ni(II) as predicted by comparison of first hydrolysis reaction constants (see Section 3.2.2).

The data are given in the form of lognormal distributions which implicitly include the combined impact of uncertainty as well as spatial and temporal variability. The median of the log-transformed K_d uncertainty distribution may be taken to be the best estimate value for central case deterministic calculations. Although flow path averaging effects would normally prescribe the use of the arithmetic mean K_d value, the use of the median is deemed a more cautious choice given that uncertainty (rather than variability) is expected to make the dominant contribution to the statistical dispersion of the recommended K_d data ranges.

6.1 Recommended K_d data for Forsmark

Sorption data recommended for use in SR-Site simulations of the Forsmark site are summarised in Table 6-1. The K_d data are given in the form of lognormal distributions characterised by a mean (μ) and standard deviation (σ). For stochastic simulations, it is suggested that the lognormal distributions are sampled uniformly between the upper and lower limits defined by the 2.5% and 97.5% percentiles specified as the lower and upper K_d limits in the table. The best estimate K_d value for use in deterministic calculations is given as the median of the K_d distribution.

Table 6-1. Recommended sorption partitioning coefficient, K_d values for use in SR-Site simulations of the Forsmark site. The predominant species for redox sensitive elements are highlighted in bold text. Values are given for the best estimate (median), parameters for the lognormal distribution (μ and σ), as well as lower and upper limits corresponding to the 2.5% and 97.5% percentiles, respectively.

Radionuclide (Redox State)	Best estimate K_d (m^3/kg)	$\log_{10}K_d - \mu$	$\log_{10}K_d - \sigma$	Lower K_d limit (m^3/kg)	Upper K_d limit (m^3/kg)
Ac(III)	$1.48\cdot10^{-2}$	–1.83	0.72	$5.74\cdot10^{-4}$	$3.83\cdot10^{-1}$
Ag(I)	$3.49\cdot10^{-4}$	–3.46	0.51	$3.46\cdot10^{-5}$	$3.52\cdot10^{-3}$
Am(III)	$1.48\cdot10^{-2}$	–1.83	0.72	$5.74\cdot10^{-4}$	$3.83\cdot10^{-1}$
C, HCO_3^-	0.0	–	–	0.0	0.0
C, CH_4	0.0	–	–	0.0	0.0
C, $-CO_2H$	0.0	–	–	0.0	0.0
Cd(II)	$1.10\cdot10^{-3}$	–2.96	0.65	$5.97\cdot10^{-5}$	$2.04\cdot10^{-2}$
Cl(-I)	0.0	–	–	0.0	0.0
Cm(III)	$1.48\cdot10^{-2}$	–1.83	0.72	$5.74\cdot10^{-4}$	$3.83\cdot10^{-1}$
Cs(I)	$3.49\cdot10^{-4}$	–3.46	0.51	$3.46\cdot10^{-5}$	$3.52\cdot10^{-3}$
Eu(III)	$1.48\cdot10^{-2}$	–1.83	0.72	$5.74\cdot10^{-4}$	$3.83\cdot10^{-1}$
H(I)	0.0	–	–	0.0	0.0
Ho(III)	$1.48\cdot10^{-2}$	–1.83	0.72	$5.74\cdot10^{-4}$	$3.83\cdot10^{-1}$
I(-I)	0.0	–	–	0.0	0.0
Mo(VI)	0.0	–	–	0.0	0.0
Nb(V)	$1.98\cdot10^{-2}$	–1.70	0.64	$1.11\cdot10^{-3}$	$3.53\cdot10^{-1}$
Ni(II)	$1.10\cdot10^{-3}$	–2.96	0.65	$5.97\cdot10^{-5}$	$2.04\cdot10^{-2}$
Np(IV)	$5.29\cdot10^{-2}$	–1.28	0.65	$2.84\cdot10^{-3}$	$9.84\cdot10^{-1}$
Np(V)	$4.13\cdot10^{-4}$	–3.38	0.74	$1.48\cdot10^{-5}$	$1.15\cdot10^{-2}$
Pa(IV)	$5.92\cdot10^{-2}$	–1.23	0.48	$6.76\cdot10^{-3}$	$5.18\cdot10^{-1}$
Pa(V)	$5.92\cdot10^{-2}$	–1.23	0.48	$6.76\cdot10^{-3}$	$5.18\cdot10^{-1}$
Pb(II)	$2.52\cdot10^{-2}$	–1.60	0.56	$2.05\cdot10^{-3}$	$3.10\cdot10^{-1}$
Pd(II)	$5.20\cdot10^{-2}$	–1.28	0.83	$1.22\cdot10^{-3}$	2.21
Pu(III)	$1.48\cdot10^{-2}$	–1.83	0.72	$5.74\cdot10^{-4}$	$3.83\cdot10^{-1}$
Pu(IV)	$5.29\cdot10^{-2}$	–1.28	0.65	$2.84\cdot10^{-3}$	$9.84\cdot10^{-1}$
Pu(V)	$9.14\cdot10^{-3}$	–2.04	0.60	$6.19\cdot10^{-4}$	$1.35\cdot10^{-1}$
Pu(VI)	$9.14\cdot10^{-3}$	–2.04	0.60	$6.19\cdot10^{-4}$	$1.35\cdot10^{-1}$

Radionuclide (Redox State)	Best estimate K_d (m^3/kg)	$\log_{10}K_d - \mu$	$\log_{10}K_d - \sigma$	Lower K_d limit (m^3/kg)	Upper K_d limit (m^3/kg)
Ra(II)	$2.42 \cdot 10^{-4}$	–3.62	0.41	$3.87 \cdot 10^{-5}$	$1.51 \cdot 10^{-3}$
S(-II)	0.0	–	–	0.0	0.0
Se(-II)	$2.95 \cdot 10^{-4}$	–3.53	0.55	$2.50 \cdot 10^{-5}$	$3.48 \cdot 10^{-3}$
Se(IV)	$2.95 \cdot 10^{-4}$	–3.53	0.55	$2.50 \cdot 10^{-5}$	$3.48 \cdot 10^{-3}$
Se(VI)	$2.95 \cdot 10^{-4}$	–3.53	0.55	$2.50 \cdot 10^{-5}$	$3.48 \cdot 10^{-3}$
Sm(III)	$1.48 \cdot 10^{-2}$	–1.83	0.72	$5.74 \cdot 10^{-4}$	$3.83 \cdot 10^{-1}$
Sn(IV)	$1.59 \cdot 10^{-1}$	–0.80	0.28	$4.51 \cdot 10^{-2}$	$5.58 \cdot 10^{-1}$
Sr(II)	$3.42 \cdot 10^{-6}$	–5.47	0.99	$3.84 \cdot 10^{-8}$	$3.05 \cdot 10^{-4}$
Tc(IV)	$5.29 \cdot 10^{-2}$	–1.28	0.65	$2.84 \cdot 10^{-3}$	$9.84 \cdot 10^{-1}$
Tc(VII)	0.0	–	–	0.0	0.0
Th(IV)	$5.29 \cdot 10^{-2}$	–1.28	0.65	$2.84 \cdot 10^{-3}$	$9.84 \cdot 10^{-1}$
U(IV)	$5.29 \cdot 10^{-2}$	–1.28	0.65	$2.84 \cdot 10^{-3}$	$9.84 \cdot 10^{-1}$
U(VI)	$1.06 \cdot 10^{-4}$	–3.97	0.66	$5.53 \cdot 10^{-6}$	$2.05 \cdot 10^{-3}$
Zr(IV)	$2.13 \cdot 10^{-2}$	–1.67	0.35	$4.48 \cdot 10^{-3}$	$1.02 \cdot 10^{-1}$

6.2 Recommended K_d data for Laxemar

Sorption data recommended for use in SR-Site simulations of the Laxemar site are summarised in Table 6-2 and are given in the same format as Table 6-1. The data are adjusted to reflect the higher CEC of the Laxemar site-specific rock types relative to Forsmark. Corrections are only made for those elements where sorption is deemed to be related to CEC (or biotite content) and where such data has been documented in the underlying data sets upon which the recommendations are made. This encompasses the solutes that are deemed to exhibit sorptive sensitivity to ionic strength; Ag, Cd, Cs, Ni, Ra, and Sr. Corrections are also made for Np, Pu, Tc, and U on account of their redox sensitivity and observations of preferential sorption in association with biotite as documented in the literature.

Table 6-2. Recommended sorption partitioning coefficient, K_d values for use in SR-Site for the Laxemar site. The predominant species for redox sensitive elements are highlighted in bold text. Values are given for the best estimate (median), parameters for the lognormal distribution (μ and σ), as well as lower and upper limits corresponding to the 2.5% and 97.5% percentiles, respectively.

Radionuclide (Redox State)	Best estimate K_d (m^3/kg)	$\log_{10}K_d - \mu$	$\log_{10}K_d - \sigma$	Lower K_d limit (m^3/kg)	Upper K_d limit (m^3/kg)
Ac(III)	$1.48 \cdot 10^{-2}$	–1.83	0.72	$5.74 \cdot 10^{-4}$	$3.83 \cdot 10^{-1}$
Ag(I)	$6.54 \cdot 10^{-4}$	–3.18	0.51	$6.49 \cdot 10^{-5}$	$6.60 \cdot 10^{-3}$
Am(III)	$1.48 \cdot 10^{-2}$	–1.83	0.72	$5.74 \cdot 10^{-4}$	$3.83 \cdot 10^{-1}$
C, HCO_3^-	0.0	–	–	0.0	0.0
C, CH_4	0.0	–	–	0.0	0.0
C, $-CO_2H$	0.0	–	–	0.0	0.0
Cd(II)	$2.07 \cdot 10^{-3}$	–2.68	0.65	$1.12 \cdot 10^{-4}$	$3.83 \cdot 10^{-2}$
Cl(-I)	0.0	–	–	0.0	0.0
Cm(III)	$1.48 \cdot 10^{-2}$	–1.83	0.72	$5.74 \cdot 10^{-4}$	$3.83 \cdot 10^{-1}$
Cs(I)	$6.54 \cdot 10^{-4}$	–3.18	0.51	$6.49 \cdot 10^{-5}$	$6.60 \cdot 10^{-3}$
Eu(III)	$1.48 \cdot 10^{-2}$	–1.83	0.72	$5.74 \cdot 10^{-4}$	$3.83 \cdot 10^{-1}$
H(I)	0.0	–	–	0.0	0.0
Ho(III)	$1.48 \cdot 10^{-2}$	–1.83	0.72	$5.74 \cdot 10^{-4}$	$3.83 \cdot 10^{-1}$
I(-I)	0.0	–	–	0.0	0.0
Mo(VI)	0.0	–	–	0.0	0.0
Nb(V)	$1.98 \cdot 10^{-2}$	–1.70	0.64	$1.11 \cdot 10^{-3}$	$3.53 \cdot 10^{-1}$
Ni(II)	$2.07 \cdot 10^{-3}$	–2.68	0.65	$1.12 \cdot 10^{-4}$	$3.83 \cdot 10^{-2}$
Np(IV)	$9.92 \cdot 10^{-2}$	–1.00	0.65	$5.33 \cdot 10^{-3}$	1.85
Np(V)	$7.75 \cdot 10^{-4}$	–3.11	0.74	$2.78 \cdot 10^{-5}$	$2.16 \cdot 10^{-2}$
Pa(IV)	$5.92 \cdot 10^{-2}$	–1.23	0.48	$6.76 \cdot 10^{-3}$	$5.18 \cdot 10^{-1}$

Radionuclide (Redox State)	Best estimate K_d (m^3/kg)	$\log_{10}K_d - \mu$	$\log_{10}K_d - \sigma$	Lower K_d limit (m^3/kg)	Upper K_d limit (m^3/kg)
Pa(V)	$5.92 \cdot 10^{-2}$	–1.23	0.48	$6.76 \cdot 10^{-3}$	$5.18 \cdot 10^{-1}$
Pb(II)	$2.52 \cdot 10^{-2}$	–1.60	0.56	$2.05 \cdot 10^{-3}$	$3.10 \cdot 10^{-1}$
Pd(II)	$5.20 \cdot 10^{-2}$	–1.28	0.83	$1.22 \cdot 10^{-3}$	2.21
Pu(III)	$2.78 \cdot 10^{-2}$	–1.56	0.72	$1.08 \cdot 10^{-3}$	$7.19 \cdot 10^{-1}$
Pu(IV)	$9.92 \cdot 10^{-2}$	–1.00	0.65	$5.33 \cdot 10^{-3}$	1.85
Pu(V)	$1.71 \cdot 10^{-2}$	–1.77	0.60	$1.16 \cdot 10^{-3}$	$2.53 \cdot 10^{-1}$
Pu(VI)	$1.71 \cdot 10^{-2}$	–1.77	0.60	$1.16 \cdot 10^{-3}$	$2.53 \cdot 10^{-1}$
Ra(II)	$4.53 \cdot 10^{-4}$	–3.34	0.41	$7.26 \cdot 10^{-5}$	$2.83 \cdot 10^{-3}$
S(-II)	0.0	–	–	0.0	0.0
Se(-II)	$2.95 \cdot 10^{-4}$	–3.53	0.55	$2.50 \cdot 10^{-5}$	$3.48 \cdot 10^{-3}$
Se(IV)	$2.95 \cdot 10^{-4}$	–3.53	0.55	$2.50 \cdot 10^{-5}$	$3.48 \cdot 10^{-3}$
Se(VI)	$2.95 \cdot 10^{-4}$	–3.53	0.55	$2.50 \cdot 10^{-5}$	$3.48 \cdot 10^{-3}$
Sm(III)	$1.48 \cdot 10^{-2}$	–1.83	0.72	$5.74 \cdot 10^{-4}$	$3.83 \cdot 10^{-1}$
Sn(IV)	$1.59 \cdot 10^{-1}$	–0.80	0.28	$4.51 \cdot 10^{-2}$	$5.58 \cdot 10^{-1}$
Sr(II)	$6.42 \cdot 10^{-6}$	–5.19	0.99	$7.21 \cdot 10^{-8}$	$5.71 \cdot 10^{-4}$
Tc(IV)	$9.92 \cdot 10^{-2}$	–1.00	0.65	$5.33 \cdot 10^{-3}$	1.85
Tc(VII)	0.0	–	–	0.0	0.0
Th(IV)	$5.29 \cdot 10^{-2}$	–1.28	0.65	$2.84 \cdot 10^{-3}$	$9.84 \cdot 10^{-1}$
U(IV)	$9.92 \cdot 10^{-2}$	–1.00	0.65	$5.33 \cdot 10^{-3}$	1.85
U(VI)	$2.00 \cdot 10^{-4}$	–3.70	0.66	$1.04 \cdot 10^{-5}$	$3.84 \cdot 10^{-3}$
Zr(IV)	$2.13 \cdot 10^{-2}$	–1.67	0.35	$4.48 \cdot 10^{-3}$	$1.02 \cdot 10^{-1}$

6.3 Comparison with the previous data compilation

A selection of the recommended data are shown in Figure 6-1 as box and whisker plots together with data previously used in SR-Can /SKB 2006/ for comparative purposes. Similar plots depicting the recommended data for trivalent actinides and lanthanides are given in Figure 6-2 (noting that the trivalent actinides and lanthanides are assumed to have identical sorption properties in the present data compilation).

In the box and whisker plots of the SR-Site data, the coloured portion of the box plot represents the 25%–75% interquartile range with the median given as the horizontal dividing line. Whiskers of the box plot represent the 2-sided 95% confidence interval of the data range. The whiskers for the SR-Can data are based on the notional upper and lower limits of the data as defined in /Crawford et al. 2006/ and do not necessarily correspond to a 95% confidence interval. For solutes not reported with a 25%–75% interquartile range in SR-Can, an approximate estimate of half the overall data range is assumed.

In most cases the SR-Site recommended K_d data ranges are somewhat less than those used previously in SR-Can with the exception of Sn(IV) and Pd(II) which are given higher ranges than that previously recommended. Recommended data ranges for these elements in SR-Can were taken directly from the corresponding recommendation in SR-97 /Carbol and Engkvist 1997/.

In /Carbol and Engkvist 1997/, Pd(II) is assumed to have similar sorptivity to Ni(II) and is therefore parameterised with a lower K_d range. The recommendation in SR-Site, on the other hand, is based on actual measurements with Pd(II) as reported by /Tachi et al. 1999/. The significantly higher first hydrolysis constant for Pd(II) relative to Ni(II) suggests that the previously used analogy, although cautious is less good and substantially stronger sorption is predicted in line with the literature data used in the present compilation.

Ra(II) is assigned a significantly lower K_d value in this compilation than in the previous SR-Can compilation. The previous recommendation, however, may have been biased by the use of data for groundwater compositions prone to radiobarite co-precipitation (as pointed out by /Stenhouse et al. 2008/). The current recommendation is predominantly based on the detailed data obtained from site specific rocks from Forsmark and Laxemar which are considered to be well qualified data sets and have been screened for the possibility of radiobarite co-precipitation.

Sn(IV) was previously given a low K_d range in /Carbol and Engkvist 1997/ owing to uncertainty concerning the redox state of this element as Sn(II,IV) and a concern that anionic chloride complexes may dominate its speciation in groundwater. In the current compilation, the reduced tetravalent form is considered to be most likely and chloride complexation is not expected to be important. The SR-Site recommendation is based on data reported by /Ticknor and McMurray 1996/ and is thought to be reasonable given that Sn(IV) has the highest first hydrolysis constant of all tetravalent solutes considered in this compilation which is indicative of relatively strong sorption.

Lead, Pb(II) has not been considered in previous data compilations and it therefore appears for the first time in SR-Site. As noted previously, the literature data set which underlies the K_d recommendation for Pb(II) is thought to be possibly less reliable and the use of the Ni(II) analogue is therefore proposed for sensitivity case studies even though this may be over-pessimistic.

Other elements and redox states are given approximately similar or lower K_d ranges for SR-Site based on the new data extrapolation procedures adopted in this report. In many cases, the uncertainty range is expanded in SR-Site relative to that used in previous recommendations. In some instances this is due to a substantially larger database of values. In other cases this is due to a more formal propagation of error estimates in the extrapolation procedure although this applies mostly to solutes where the literature data are considered to be associated with significant uncertainties due to low sample numbers.

A particular uncertainty in the SR-Site data compilation concerns the assumption of Pu(IV) as an analogue for the sorption of other tetravalent radionuclides. In previous compilations, Th(IV) has been used as an analogue owing to its insensitivity to redox conditions. The older literature data from which Th(IV) K_d recommendations were previously made in SR-Can, although reasonable, are considered by the present author to be less reliable on account of their high-end range and the possibility that undocumented surface precipitation or eigencolloid formation may have biased the

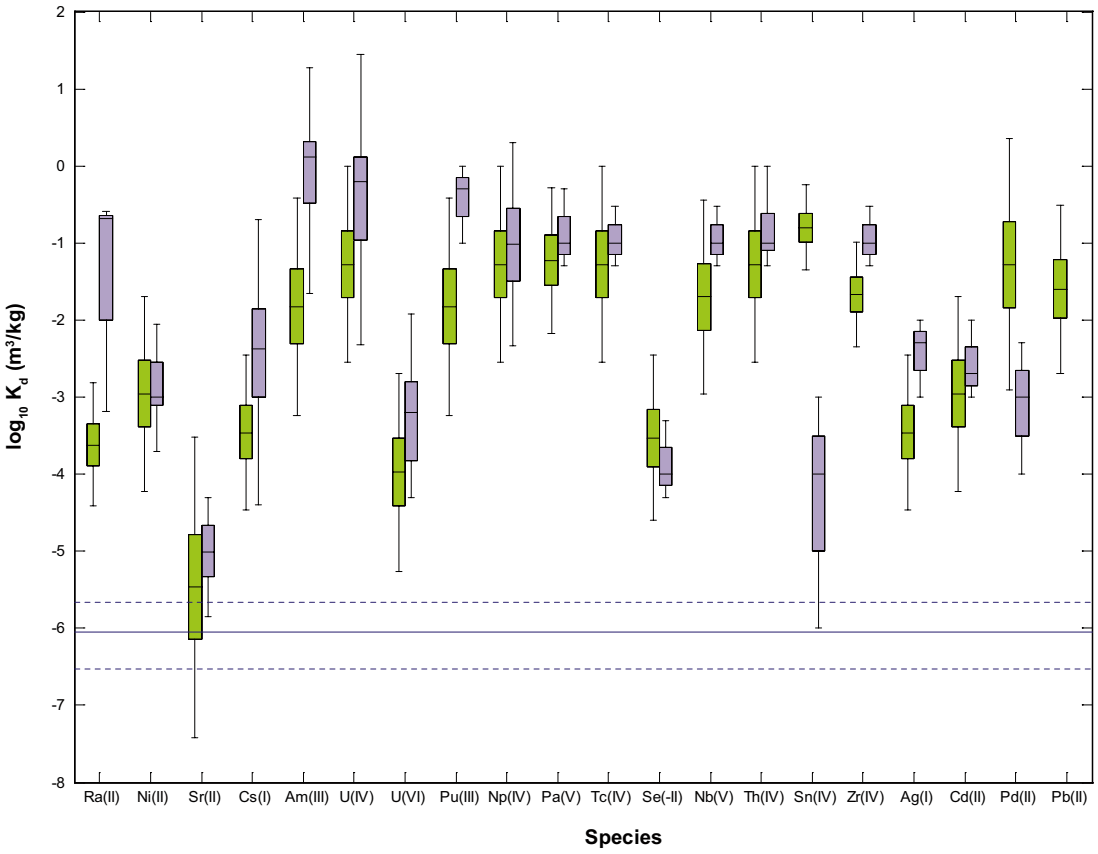

Figure 6-1. *Recommended K_d ranges (log_{10}-scale) for SR-Site calculations concerning the Forsmark site (green box and whisker plots). Data previously recommended for use in SR-Can are shown for comparative purposes (purple box and whisker plots). A lower effective bound on relevant K_d values is provided by the storage porosity of the rock matrix which is shown as the horizontal unbroken reference line along with the 2-sided 95% confidence interval of the estimate (broken lines).*

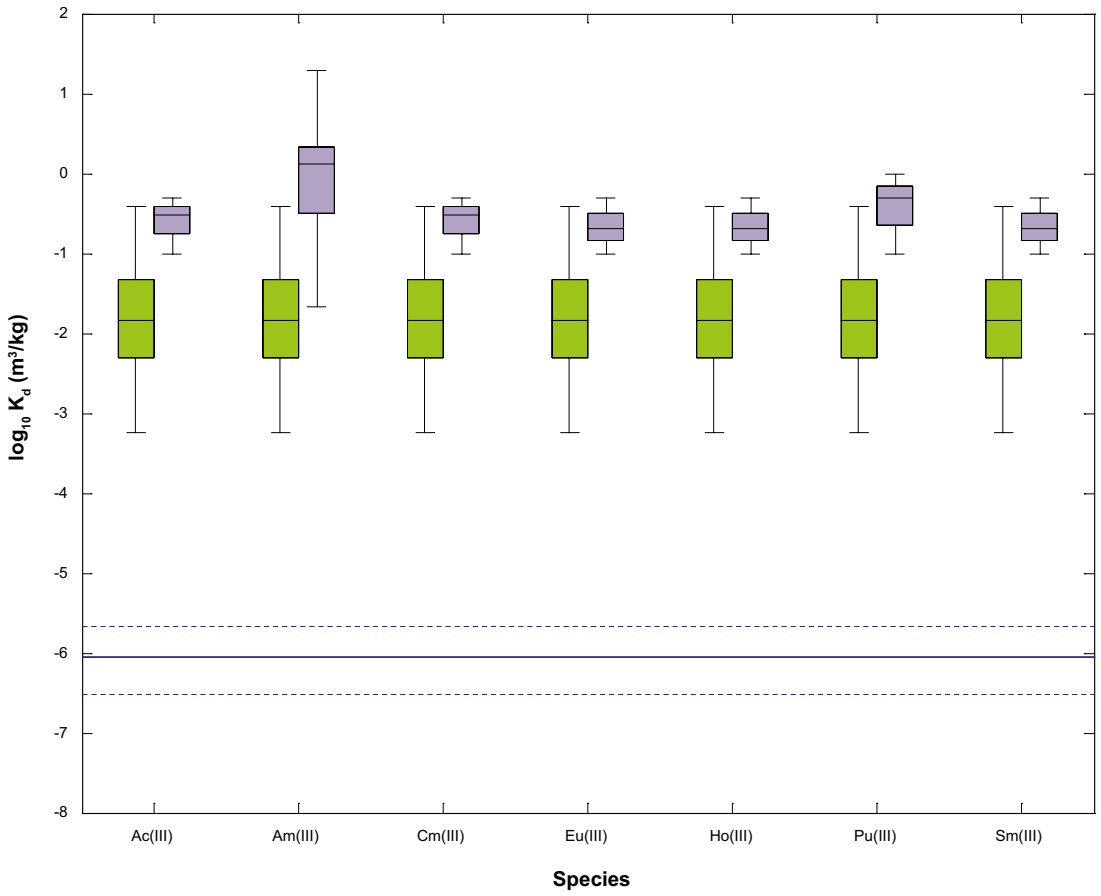

Figure 6-2. *Recommended K_d ranges (log_{10}-scale) for SR-Site calculations concerning the Forsmark site (green box and whisker plots). Data previously recommended for use in SR-Can are shown for comparative purposes (purple box and whisker plots). A lower effective bound on relevant K_d values is provided by the storage porosity of the rock matrix which is shown as the horizontal unbroken reference line along with the 2-sided 95% confidence interval of the estimate (broken lines).*

results. This is considered particularly likely for the tetravalent radionuclides on account of their strong hydrolysis. Furthermore, relevant BET surface area data and other experimental conditions were not recorded in the older references which renders difficult, any extrapolation to in situ conditions according to the quantification procedures adopted in this report.

The data reported by /Huitti et al. 1996/ and /Kulmala et al. 1998/ for Pu sorption under reducing conditions are considered to be qualified data sources on account of their detailed documentation of experimental procedures and conditions. Although multiple redox states of Pu can theoretically be present at the measured redox potentials documented in the references, it is thought that the measured sorptivity can be assumed to be approximately representative of Pu(IV) sorption.

The reasoning for this follows the discussion concerning redox states in Section 2.1.4 where it is postulated that any difference in sorptivity of two co-existing redox states would necessarily result in a readjustment of the redox species distribution between the aqueous and surface sorbed phases thus favouring the predominance of the more strongly sorbing redox state (assuming thermodynamic reversibility).

On the basis of the LFER methodology outlined in Section 3.2.1, sorption of the Pu(IV) redox state should be favoured over Pu(III) owing to its stronger hydrolysis. In any case, the LFER principle suggests that the K_d for Pu(IV) should be at least as high as that for Pu(III) and by analogy, the other trivalent lanthanides and actinides. Given that the tetravalent radionuclides are assigned K_d values that are only slightly higher than the corresponding values for Am(III)/Eu(III), this seems to be consistent with the data. It is therefore the opinion of the present author that the literature data for Pu sorption under reducing conditions, although not ideal, appear to constitute the most reliable source of sorption data for the tetravalent radionuclides of importance.

6.4 Comparison with data from the LTDE-SD project

As part of the geoscientific programme carried out at the Äspö Hard Rock Laboratory (HRL), a series of tracer experiments were performed with the aim of characterising diffusive uptake of various sorbing and non-sorbing radionuclides to the rock matrix under more realistic conditions than the experiments involving crushed materials typically used in laboratory investigations of sorption. The LTDE-SD (Long Term Diffusion Experiment – Sorption and Diffusion) experiment was therefore conceived to study the coupled processes of sorption and matrix diffusion while minimising confounding advective and hydrodynamic dispersion effects.

The in situ experiment consisted of a tracer test involving diffusive uptake to a confined rock stub at the so-called *niche section* in the Äspö HRL at an elevation of approximately –410 m (relative to sea level) /Nilsson et al. 2010, Widestrand et al. 2010a/. In addition to the in situ tracer test, independent laboratory studies were undertaken using core samples taken from the tracer test site as well as core samples obtained from the Forsmark and Laxemar site investigation areas /Widestrand et al. 2010b/. The laboratory investigations consisted of in-diffusion experiments performed on monolithic bore core samples as well as sorption measurements on crushed materials using the same methods employed previously in the site investigations. The results of the evaluation of the in-diffusion experiments documented by /Widestrand et al. 2010b/ are used here to compare with the data recommended for use in SR-Site.

Although this compilation deals exclusively with sorption data, it is important to recognise that K_d data are used in conjunction with effective diffusivity data when applied in safety assessment calculations. As outlined in Section 2.3.1, it is the material properties group, N_{MPG} defined in Equation 2-44 that can be shown to uniquely determine the residence time distribution of a transported radionuclide for the model of solute retardation used in SR-Site. More specifically, the retarded travel time for a given recovery fraction of a released solute pulse is proportional to the square of this number (equal to the product of effective diffusivity and volumetric storage capacity, D_eK). The case of a rock matrix with reduced sorptivity and increased effective diffusivity should therefore be indistinguishable from the case of increased sorptivity and decreased effective diffusivity, provided the magnitude of the D_eK product (or N_{MPG}) is preserved. This is a logical consequence of the solution given by /Neretnieks 1980/ as well as the analogous problem in heat conduction described by /Carslaw and Jaeger 1959/. In a practical sense, and provided the effective penetration depth associated with radionuclide transport is less than the maximum matrix depth assumed in modelling, any discrepancy between the true material properties (as described by D_e and K_d) and the values used in modelling is immaterial as long as D_eK (or N_{MPG}) is the same in both cases.

Although the depth dependent profiles of tracer concentrations in the rock matrix are significantly influenced by the individual values of effective diffusivity and K_d, it is only the lumped parameter group that describes the changes in concentration in the aqueous phase and consequently, the overall rate of diffusive uptake to the rock matrix. For this reason, when making comparisons between tracer tests and data recommended for use in safety assessment calculations, it is more appropriate to compare differences in the D_eK product rather than the absolute values of D_e and K_d in isolation.

In /Widestrand et al. 2010b/, estimates are made of D_e and K_d by least squares fitting of a diffusive uptake model to the time dependent aqueous phase concentration curve where one of the parameters is held constant at a value determined by independent measurement. In general, the procedure of fitting one or the other parameter gives results that are not exactly the same as the values obtained by independent testing. The data evaluations do, however, confirm that the D_eK product is the same in both cases.

Figure 6-3 shows a cross plot of D_eK values calculated using the recommended data for SR-Site with corresponding values estimated for the in-diffusion experiments described in /Widestrand et al. 2010b/. The SR-Site recommended value for the storage porosity, θ_m of the rock matrix under in situ stress conditions at Forsmark and Laxemar is given as 1.8×10^{-3} (0.18%) while the recommended effective diffusivity is given as a lognormal distribution with the following characteristics /SKB 2010b/:

$\log_{10} D_e \approx -13.7\pm0.25$ (cations)

$\log_{10} D_e \approx -14.2\pm0.25$ (anions)

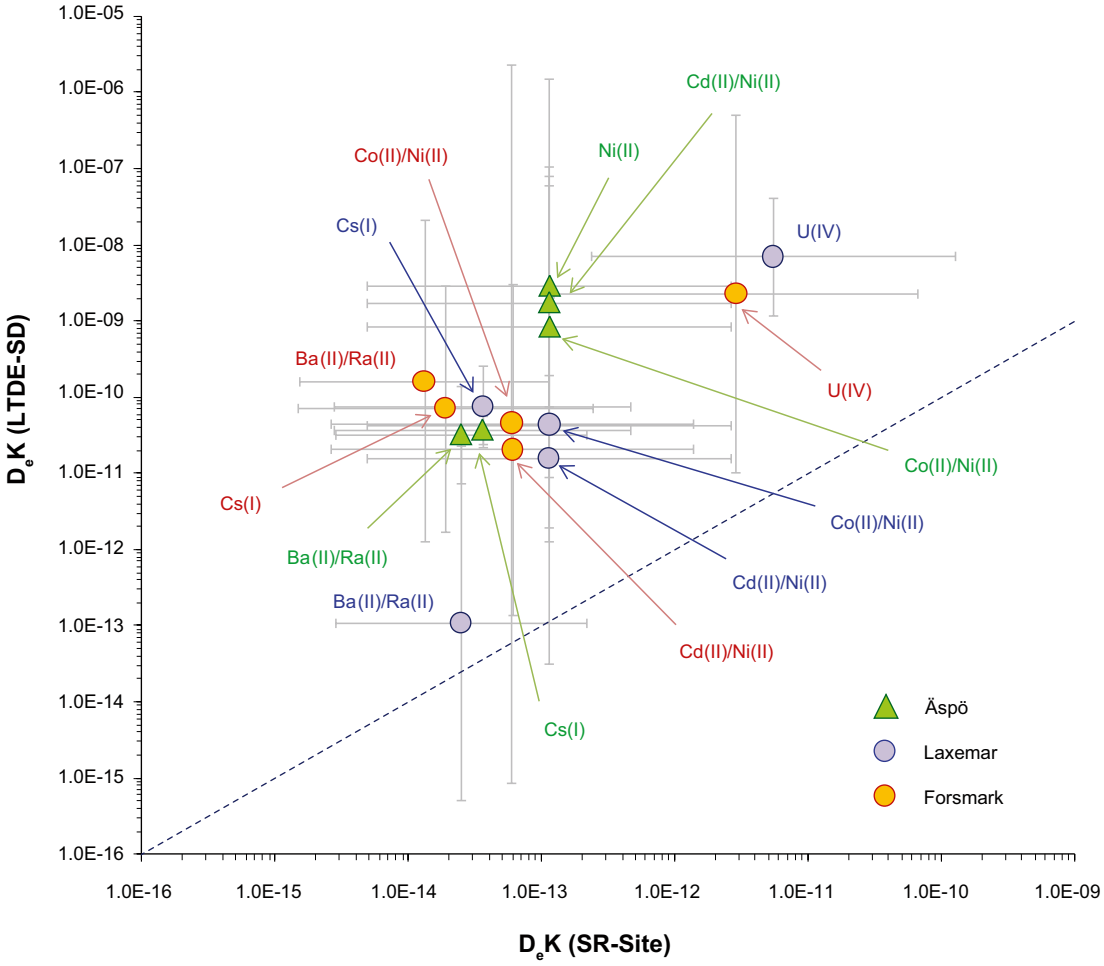

Figure 6-3. *Cross plot of the effective diffusivity and volumetric storage capacity product, D_eK (m^2/s) estimated using SR-Site recommended values and independent data obtained in the LTDE-SD experiment for monolithic samples of Äspö, Laxemar, and Forsmark site specific rocks /Widestrand et al. 2010b/. Markers indicate median values and error bars represent 2σ uncertainty limits. For plotting the horizontal ordinate, geochemical analogy with Ni(II) is assumed for both Co(II) and Cd(II), while Ra(II) is used as an analogue for Ba(II). The sloping broken line indicates the equivalence trend line for reference purposes.*

Since the recommended effective diffusivity range is assumed to be dominated by uncertainty rather than spatial variability, the best estimate D_e is taken to be the median value (i.e. 2×10^{-14} m^2/s for cations, 6.3×10^{-15} m^2/s for anions). In all cases, cationic status was assumed for diffusing solutes on the basis of their predicted speciation (see Table 3-2) for the contact water compositions specified in /Widestrand et al. 2010b/. On account of the relatively high uranium K_d values reported, U(IV) speciation is assumed. It is acknowledged, however, that this is a poorly supported assumption and the actual redox state is uncertain. In the comparison with SR-Site recommended data, Äspö rock (Ävrö granodiorite) is assumed to have roughly the same material properties as the Laxemar rock types.

By and large, the SR-Site recommended data give D_eK values lower than that estimated for the LTDE-SD experiment involving intact core samples, although the associated uncertainty ranges are large for both. With the possible exception of the Ba(II) tracer uptake on the Laxemar rock, the SR-Site recommended data would appear to cautiously under-predict radionuclide travel times by about 2–3 orders of magnitude, all other things being equal. The close correspondence between the LTDE-SD data estimates obtained for Ni(II), Co(II), and Cd(II) tracers also lend some support to the geochemical analogies invoked in the SR-Site data compilation (at least for the groundwater composition used in LTDE-SD). On the basis of these results it could therefore be argued that the data recommended for use in SR-Site are cautious relative to independently obtained estimates under more realistic mass transfer conditions.

6.5 Partial validation using natural tracer data

During the site investigations at Forsmark and Laxemar, activities of dissolved ^{222}Rn and ^{226}Ra were measured in the investigation boreholes. In addition to this, a large number of measurements were also made to characterise abundances of natural U-series nuclides sorbed or otherwise immobilised on fracture coatings /Sandström et al. 2008/. Together with the known uranium content of the rock as compiled by /Sandström and Stephens 2009/ for the Forsmark site, it is possible to estimate the relative rate of production of ^{226}Ra within the rock matrix and in fracture coatings provided secular equilibrium of the U-series decay chain can be assumed deep within the rock matrix. Based on this information it is possible to conclude that the overwhelming proportion of ^{226}Ra found in Forsmark groundwater originates from decay processes in the rock matrix and it is not produced in any significant quantity in the fracture filling minerals themselves.

Since most of the ^{226}Ra appears to originate in the rock matrix it is useful to compare ^{222}Rn and ^{226}Ra simultaneously since their absolute and relative activities encode a significant amount of information concerning the geochemical behaviour of the rock matrix and its interaction with groundwater. For this purpose, stochastic simulations were made using a modified version of the transport model described by /Neretnieks 2002/ and uncertainty distributions estimated for all parameters and variables that are known to influence the transport of naturally occurring ^{222}Rn and ^{226}Ra in situ. For variables that were poorly constrained (i.e. decay recoil capture efficiency, transport aperture, fracture coating thickness, instantaneous retardation in fracture coatings), broad log-uniform distributions were assumed covering the entire range of expected variation (see Appendix B for details).

The results of these simulations are shown in Figure 6-4 where the data are presented as a probability density for an ensemble of 10^5 realisations. The probability density is represented as a smoothed 2D histogram with 100 equally spaced bins along the principle axes of the figure. The expected ^{222}Rn and ^{226}Ra activities based on best estimate values of model parameters are indicated by red circular markers for different radium K_d case studies (with and without additional transport retardation in fracture coatings). The red curve shows the locus of expected variation for the best estimate ^{222}Rn and ^{226}Ra activities in response to altered K_d for radium. Measurement data from Forsmark boreholes are plotted as blue circular markers with shading proportional to the background Ca^{2+} concentration. Error bars are not shown on account their size being typically smaller than the plot markers used to represent the data on a log-log scale. The relative errors of the measurements are, however, roughly 4–6% based on radiometric counting statistics.

As noted in Appendix B, ^{226}Ra activity exhibits a strong correlation with Ca^{2+} concentration which is possibly indicative of reduced ion-exchange sorption in more saline groundwaters. It is noted that the measurement data plotted in the lower left-hand quadrant of Figure 6-4 correspond to shallow sampling locations with low Ca^{2+} concentrations. The prediction of greater sorptivity for samples exhibiting simultaneously low ^{222}Rn and ^{226}Ra activities is therefore qualitatively consistent with the measurement data as plotted in the figure.

As can be seen from Figure 6-4, the probability distribution of expected ^{222}Rn and ^{226}Ra activities agrees relatively well with the measurement data when the SR-Site recommended K_d distribution for radium is used in the simulations. In a probabilistic sense, the expected activity ranges for both ^{222}Rn and ^{226}Ra appear to be neither overestimated nor underestimated by a significant margin when considering all other sources of uncertainty. On the basis of this analysis, and assuming that the uncertainties of other governing variables are reasonably assessed, we therefore conclude that the SR-Site recommended K_d data for radium are both reasonable and defensible for use in safety assessment calculations.

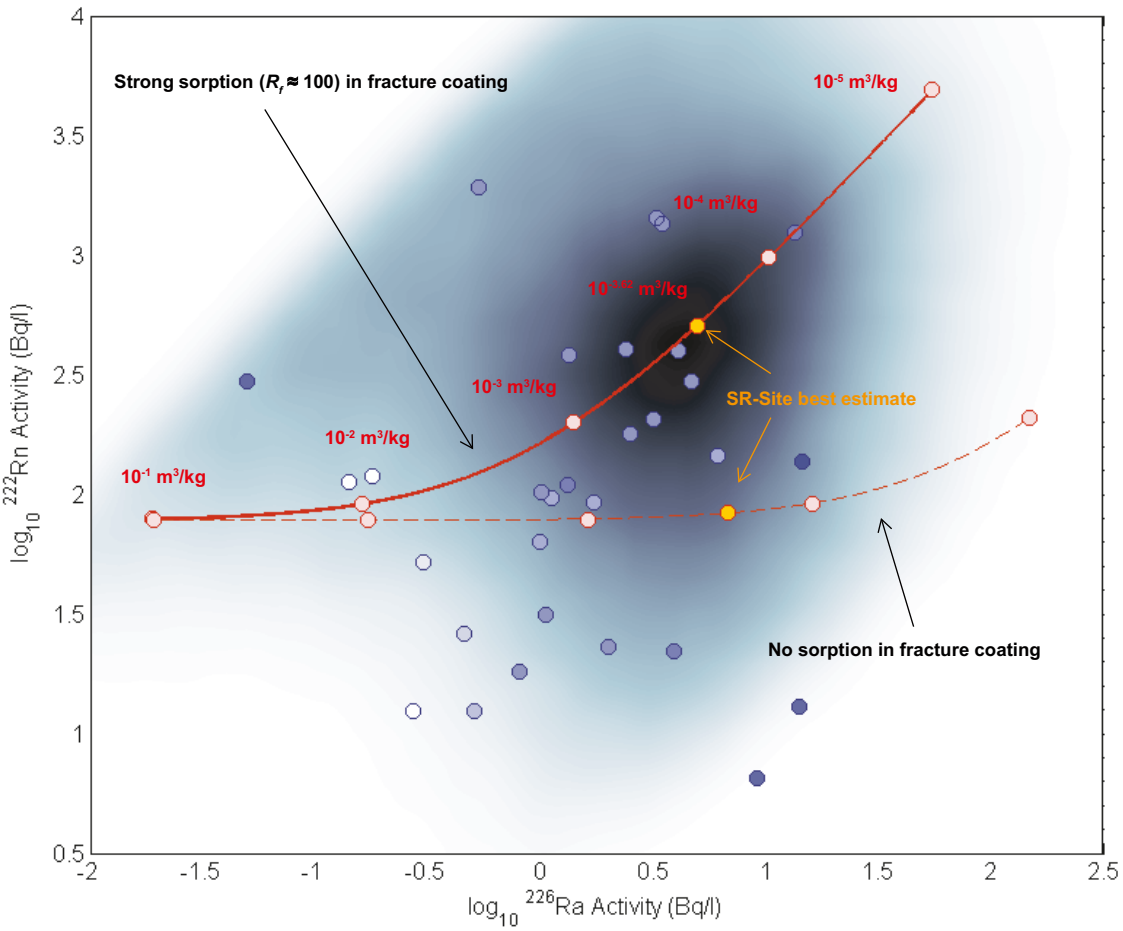

Figure 6-4. *Expected activity distributions of ^{222}Rn and ^{226}Ra activities plotted together with measurement data from Forsmark boreholes. The simulation data are presented as a probability density with darker shading indicating the most likely activity ranges (10^5 realisations) in the simulation ensemble. The red curve designates the locus of best estimate activities for the specified K_d values (red markers). The SR-Site best estimate is indicated in yellow shading. The measurement data points (blue circular markers) are shaded according to background Ca^{2+} concentration with lighter shading indicating lower concentration.*

7 References

SKB's (Svensk Kärnbränslehantering AB) publications can be found at www.skb.se/publications.

Ahrland S, Chatt J, Davies N R, 1958. The relative affinities of ligand atoms for acceptor molecules and ions. Quarterly Reviews, Chemical Society, 12, pp 265–276.

Akiba K, Hashimoto H, Kanno T, 1989. Distribution coefficient of cesium and cation exchange capacity of minerals and rocks. Journal of Nuclear Science and Technology, 26, pp 1130–1135.

Alexander W, Smith P, McKinley I, 2003. Modelling radionuclide transport in the geological environment: a case study from the field of radioactive waste disposal. In: Scott E M (ed). Modelling radioactivity in the environment. Amsterdam: Elsevier. (Radioactivity in the Environment 4), pp 109–146.

Alkhamis K A, Wurster D E, 2002. Prediction of adsorption from multicomponent solutions by activated carbon using single-solute parameters. Part II – Proposed equation. AAPS PharmSciTech, 3, pp 53–60.

Allard B, Rydberg J, Kipatsi H, Torstenfelt B, 1979. Disposal of radioactive waste in granitic bedrock. In: Fried S (ed). Radioactive waste in geologic storage: based on a symposium sponsored by the Division of nuclear chemistry and technology at the 176th meeting of the American chemical society, Miami Beach, Florida, 11–15 September 1978. Washington, DC: American Chemical Society. (ACS Symposium Series 100), pp 47–73.

Allard B, Torstenfelt B, Andersson K, 1981. Sorption studies of $H^{14}CO_3$ on some geologic media and concrete. In: Scientific basis for nuclear waste management: proceedings of the International symposium on the scientific basis for nuclear waste management held in Boston, Massachusetts, 17–20 November 1980. New York: Plenum Press. (Scientific Basis for Nuclear Waste Management 3), pp 465–472.

Allard B, Karlsson M, Tullborg E-L, Larson S Å, 1983. Ion exchange capacities and surface areas of some major components and fracture filling materials of igneous rocks. SKBF/KBS TR 83-64, Svensk Kärnbränslehantering AB.

Allard B, Ittner T, Torstenfelt B, 1985. Migration of trace elements into water-exposed natural fissure surfaces of granitic rock. Chemical Geology, 49, pp 31–42.

Anderson E B, Rogozin Y M, Smirnova E A, Bryzgalova R V, Andreeva N R, Malimonova S I, Shabalev S I, Fujiwara A, Tochiyama O, 2007. Sorption-barrier properties of granitoids and andesite-basaltic metavolcanites with respect to Am(III) and Pu(IV): 1. Absorption of Am and Pu from groundwater on monolithic samples of granitoids and andesite-basaltic metavolcanites. Radiochemistry, 49, pp 305–312.

André M, Malmström M E, Neretnieks I, 2008a. Determination of sorption properties of intact rock samples: New methods based on electromigration. Journal of Contaminant Hydrology, 103, pp 71–81.

André M, Neretnieks I, Malmström M E, 2008b. Measuring sorption coefficients and BET surface areas on intact drillcore and crushed granite samples. Radiochimica Acta, 96, pp 673–677.

André M, Malmström M E, Neretnieks I, 2009. Specific surface area determinations on intact drillcores and evaluation of extrapolation methods for rock matrix surfaces. Journal of Contaminant Hydrology, 110, pp 1–8.

Andrews J N, Hussain N, Batchelor A S, Kwakwa K, 1986. ^{222}Rn solution by the circulating fluids in a "hot dry rock" geothermal reservoir. Applied Geochemistry, 1, pp 647–657.

Andrews J N, Ford D J, Hussain N, Trivedi D, Youngman M J, 1989. Natural radioelement solution by circulating groundwaters in the Stripa granite. Geochimica et Cosmochimica Acta, 53, pp 1791–1802.

Appel J, 1973. Freundlich's adsorption isotherm. Surface Science, 39, pp 237–244.

Appelo C A J, Postma D, 1999. A consistent model for surface complexation on birnessite (–MnO2) and its application to a column experiment. Geochimica et Cosmochimica Acta, 63, pp 3039–3048.

Appelo C A J, Postma D, 2005. Geochemistry, groundwater and pollution. 2nd ed. Leiden: Balkema.

Appelo C A J, Van Der Weiden M J J, Tournassat C, Charlet L, 2002. Surface complexation of ferrous iron and carbonate on ferrihydrite and the mobilization of arsenic. Environmental Science & Technology, 36, pp 3096–3103.

Arai Y, Moran P B, Honeyman B D, Davis J A, 2007. In situ spectroscopic evidence for neptunium(V)-carbonate inner-sphere and outer-sphere ternary surface complexes on hematite surfaces. Environmental Science & Technology, 41, pp 3940–3944.

Audi G, Bersillon O, Blachot J, Wapstra A H, 2003. The evaluation of nuclear and decay properties. Nuclear Physics A, 729, pp 3–128.

Baeyens B, Bradbury M H, 2004. Cation exchange capacity measurements on illite using the sodium and cesium isotope dilution technique: effects of the index cation, electrolyte concentration and competition: modeling. Clays and Clay Minerals, 52, pp 421–431.

Bargar J R, Reitmeyer R, Davis J A, 1999. Spectroscopic confirmation of uranium(VI)-carbonato adsorption complexes on hematite. Environmental Science & Technology, 33, pp 2481–2484.

Baston G M N, Berry J A, Brownsword M, Heath T G, Tweed C J, Williams S J, 1995. Sorption of plutonium and americium on repository, backfill and geological materials relevant to the JNFL low-level radioactive waste repository at Rokkasho-Mura. In: Murakami T, Ewing R C (eds). Scientific basis for nuclear waste management XVIII: symposium held in Kyoto, Japan, 23–27 October 1994. Pittsburgh, PA: Materials Research Society. (Materials Research Society Symposium Proceedings 353), pp 957–964.

Baston G M N, Berry J A, Brownsword T G, Heathe T G, Ilet D J, McCrohan R, Tweed C J, Yui M, 1999. The sorption of polonium, actinium and protactinium onto geological materials. In: Wronkiewicz D J, Lee J H (eds). Scientific basis for nuclear waste management XXII: symposium held in Boston, Massachusetts, 30 November – 4 December 1998. Warrendale, PA: Materials Research Society. (Materials Research Society Symposium Proceedings 556), pp 1107–1114.

Beall G W, O'Kelley G D, Allard B, 1980. An autoradiographic study of actinide sorption on climax stock granite. ORNL-5617, Oak Ridge National Laboratory, U.S. Department of Energy.

Beauwens T, De Cannière P, Moors H, Wang L, Maes N, 2005. Studying the migration behaviour of selenate in Boom Clay by electromigration. Engineering Geology, 77, pp 285–293.

Berglund S, Selroos J-O, 2003. Transport properties site descriptive model. Guidelines for evaluation and modelling. SKB R-03-09, Svensk Kärnbränslehantering AB.

Berry J A, Hobley J, Lane S A, Littleboy A K, Nash M J, Oliver P, Smith-Briggs J L, Williams S J, 1989. Solubility and sorption of protactinium in the near-field and far-field environments of a radioactive waste repository. Analyst, 114, pp 339–347.

Bienvenu P, Cassette P, Andreoletti G, Bé M-M, Comte J, Lépy M-C, 2007. A new determination of ^{79}Se half-life. Applied Radiation and Isotopes, 65, pp 355–364.

Bolzan J A, Arvía A J, 1962. Hydrolytic equilibria of metallic ions – I: The hydrolysis of Co(II) ion in $NaClO_4$ solution. Electrochimica Acta, 7, pp 589–599.

Borkovec M, 1997. Origin of 1-pK and 2-pK models for ionizable water-solid interfaces. Langmuir, 13, pp 2608–2613.

Bostick B C, Vairavamurthy M A, Karthikeyan K G, Chorover J, 2002. Cesium Adsorption on Clay Minerals: an EXAFS spectroscopic investigation. Environmental Science & Technology, 36, pp 2670–2676.

Bowden J W, Posner A M, Quirk J P, 1977. Ionic adsorption on variable charge mineral surfaces. Theoretical charge development and titration curves. Australian Journal of Soil Research, 15, pp 121–136.

Bradbury M H, Baeyens B, 1997. A mechanistic description of Ni and Zn sorption on Na-montmorillonite Part II: modelling. Journal of Contaminant Hydrology, 27, pp 223–248.

Bradbury M H, Baeyens B, 1998. N_2-BET surface area measurements on crushed and intact minerals and rocks: A proposal for estimating sorption transfer factors. Nuclear Technology, 122, pp 250–253.

Bradbury M H, Baeyens B, 2005a. Experimental measurements and modeling of sorption competition on montmorillonite. Geochimica et Cosmochimica Acta, 69, pp 4187–4197.

Bradbury M H, Baeyens B, 2005b. Modelling the sorption of Mn(II), Co(II), Ni(II), Zn(II), Cd(II), Eu(III), Am(III), Sn(IV), Th(IV), Np(V) and U(VI) on montmorillonite: Linear free energy relationships and estimates of surface binding constants for some selected heavy metals and actinides. Geochimica et Cosmochimica Acta, 69, pp 875–892.

Bradbury M H, Baeyens B, 2009a. Sorption modelling on illite Part I: Titration measurements and the sorption of Ni, Co, Eu and Sn. Geochimica et Cosmochimica Acta, 73, pp 990–1003.

Bradbury M H, Baeyens B, 2009b. Sorption modelling on illite. Part II: Actinide sorption and linear free energy relationships. Geochimica et Cosmochimica Acta, 73, pp 1004–1013.

Brandt F, Bosbach D, Krawczyk-Bärsch E, Arnold T, Bernhard G, 2003. Chlorite dissolution in the acid pH-range: a combined microscopic and macroscopic approach. Geochimica et Cosmochimica Acta, 67, pp 1451–1461.

Brendler V, Vahle A, Arnold T, Bernhard G, Fanghanel T, 2003. RES^{3}T-Rossendorf expert system for surface and sorption thermodynamics. Journal of Contaminant Hydrology, 61, pp 281–291.

Breynaert E, Scheinost A C, Dom D, Rossberg A, Vancluysen J, Gobechiya E, Kirschhock C E A, Maes A, 2010. Reduction of Se(IV) in Boom Clay: XAS solid phase speciation. Environmental Science & Technology, 44, pp 6649–6655.

Brunauer S, Emmet P, Teller E, 1938. Adsorption of gases in multimolecular layers. Journal of the American Chemical Society, 60, pp 309–319.

Bruno J, De Pablo J, Duro L, Figuerola E, 1995. Experimental study and modeling of the U(VI)-Fe(OH)3 surface precipitation/coprecipitation equilibria. Geochimica et Cosmochimica Acta, 59, pp 4113–4123.

Bruno J, Bosbach D, Kulik D, Navrotsky A, 2007. Chemical thermodynamics of solid solutions of interest in nuclear waste management: a state-of-the-art report. Paris: Nuclear Energy Agency, Organisation for Economic Co-operation and Development. (Chemical Thermodynamics Vol. 10)

Byegård J, Skarnemark G, Skålberg M, 1995. The use of some ion-exchange sorbing tracer cations in in-situ experiments in high saline groundwaters. In: Murakami T, Ewing R C (eds). Scientific basis for nuclear waste management XVIII: symposium held in Kyoto, Japan, 23–27 October 1994. Pittsburgh, PA: Materials Research Society. (Materials Research Society Symposium Proceedings 353), pp 1077–1084.

Byegård J, Johansson H, Skålberg M, Tullborg E-L, 1998. The interaction of sorbing and non-sorbing tracers with different Äspö rock types. Sorption and diffusion experiments in the laboratory scale. SKB TR-98-18, Svensk Kärnbränslehantering AB.

Byegård J, Selnert E, Tullborg E-L, 2008. Bedrock transport properties. Data evaluation and retardation model. Site descriptive modelling, SDM-Site Forsmark. SKB R-08-98, Svensk Kärnbränslehantering AB.

Carbol P, Engkvist I, 1997. Compilation of radionuclide sorption coefficients for performance assessment. SKB R-97-13, Svensk Kärnbränslehantering AB.

Carslaw H S, Jaeger J C, 1959. Conduction of heat in solids. 2nd ed. Oxford: Clarendon.

Černík M, Borkovec M, Westall J C, 1996. Affinity distribution description of competitive ion binding to heterogeneous materials. Langmuir, 12, pp 6127–6137.

Choppin G R, 2003. Actinide speciation in the environment. Radiochimica Acta, 91, pp 645–650.

Choppin G R, Bond A H, Hromadka P M, 1997. Redox speciation of plutonium. Journal of Radioanalytical and Nuclear Chemistry, 219, pp 203–210.

Crawford J, 2006. Modelling in support of bedrock transport property assessment. Preliminary site description. Laxemar subarea – version 1.2. SKB R-06-28, Svensk Kärnbränslehantering AB.

Crawford J, 2008. Bedrock transport properties Forsmark. Site descriptive modelling, SDM-Site Forsmark. SKB R-08-48, Svensk Kärnbränslehantering AB.

Crawford J, Sidborn M, 2009. Bedrock transport properties Laxemar. Site descriptive modelling, SDM-Site Laxemar. SKB R-08-94, Svensk Kärnbränslehantering AB.

Crawford J, Neretnieks I, Malmström M, 2006. Data and uncertainty assessment for radionuclide Kd partitioning coefficients in granitic rock for use in SR-Can calculations. SKB R-06-75, Svensk Kärnbränslehantering AB.

Cronstrand P, 2005. Assessment of uncertainty intervals for sorption coefficients. SFR-1 uppföljning av SAFE. SKB R-05-75, Svensk Kärnbränslehantering AB.

Cui D, Eriksen T E, 1996. Reduction of pertechnetate in solution by heterogeneous electron transfer from Fe(II)-containing geological material. Environmental Science & Technology, 30, pp 2263–2269.

Curti E, 1999. Coprecipitation of radionuclides with calcite: estimation of partition coefficients based on a review of laboratory investigations and geochemical data. Applied Geochemistry, 14, pp 433–445.

Davis J A, Leckie J O, 1978. Surface ionization and complexation at the oxide/water interface II. Surface properties of amorphous iron oxyhydroxide and adsorption of metal ions. Journal of Colloid and Interface Science, 67, pp 90–107.

Davis J A, James R O, Leckie J O, 1978. Surface ionization and complexation at the oxide/water interface: I. Computation of electrical double layer properties in simple electrolytes. Journal of Colloid and Interface Science, 63, pp 480–499.

Davis J A, Coston J A, Kent D B, Fuller C C, 1998. Application of the surface complexation concept to complex mineral assemblages. Environmental Science & Technology, 32, pp 2820–2828.

Duff M C, 2001. Speciation and transformations of sorbed Pu on geologic materials: wet chemical and spectroscopic observations. In: Kudo A (ed). Plutonium in the environment: edited proceedings of the Second Invited International Symposium, Osaka, Japan, 9–12 November 1999. Amsterdam: Elsevier. (Radioactivity in the Environment 1), pp 139–157.

Duff M C, Hunter D B, Triay I R, Bertsch P M, Reed D T, Sutton S R, Shea-McCarthy G, Kitten J, Eng P, Chipera S J, Vaniman D T, 1999. Mineral associations and average oxidation states of sorbed Pu on tuff. Environmental Science & Technology, 33, pp 2163–2169.

Duff M C, Hunter D B, Triay I R, Bertsch P M, Kitten J, Vaniman D T, 2001. Comparison of two micro-analytical methods for detecting the spatial distribution of sorbed Pu on geologic materials. Journal of Contaminant Hydrology, 47, pp 211–218.

Duro L, Grivé M, Cera E, Domènech C, Bruno J, 2006. Update of a thermodynamic database for radionuclides to assist solubility limits calculation for performance assessment. SKB TR-06-17, Svensk Kärnbränslehantering AB.

Dyer J A, Trivedi P, Scrivner N C, Sparks D L, 2004. Surface complexation modeling of zinc sorption onto ferrihydrite. Journal of Colloid and Interface Science, 270, pp 56–65.

Dzombak D A, Morel F M M, 1990. Surface complexation modeling: hydrous ferric oxide. New York: Wiley.

Eisenman G, 1962. Cation selective glass electrodes and their mode of operation. Biophysical Journal, 2, pp 259–323.

Elert M, Gylling B, Lindgren M, 2004. Assessment model validity document FARF31. SKB R-04-51, Svensk Kärnbränlsehantering AB.

Elzinga E J, Sparks D L, 1999. Nickel sorption mechanisms in a pyrophyllite-montmorillonite mixture. Journal of Colloid and Interface Science, 213, pp 506–512.

Essén S A, Johnsson A, Bylund D, Pedersen K, Lundström U S, 2007. Siderophore production by Pseudomonas stutzeri under anaerobic conditions. Applied and Environmental Microbiology, 73, pp 5857–5864.

Farley K J, Dzombak D A, Morel F M M, 1985. A surface precipitation model for the sorption of cations on metal oxides. Journal of Colloid and Interface Science, 106, pp 226–242.

Fawcett W R, 2006. The effects of ion size on double layer properties: theory and monte carlo simulations. Interface Science and Technology, 11, pp 112–132.

Fernandes M M, Stumpf T, Baeyens B, Walther C, Bradbury M H, 2010. Spectroscopic Identification of Ternary Cm−Carbonate Surface Complexes. Environmental Science & Technology, 44, pp 921–927.

Gascoyne M, Schwarcz H P, 1986. Radionuclide migration over recent geologic time in a granitic pluton. Chemical Geology: Isotope Geoscience section, 59, pp 75–85.

Gascoyne M, Miller N H, Neymark L A, 2002. Uranium-series disequilibrium in tuffs from Yucca Mountain, Nevada, as evidence of pore-fluid flow over the last million years. Applied Geochemistry, 17, pp 781–792.

Glynn P D, Voss C I, 1999. Geochemical characterization of Simpevarp ground waters near the Äspö Hard Rock Laboratory. SKI Report 96:29, Statens kärnkraftinspektion (Swedish Nuclear Power Inspectorate).

Goldberg S, Criscenti L J, Turner D R, Davis J A, Cantrell K J, 2007. Adsorption desorption processes in subsurface reactive transport modeling. Vadose Zone Journal, 6, pp 407–435.

Grandia F, Merino J, Bruno J, 2008. Assessment of the radium-barium co-precipitation and its potential influence on the solubility of Ra in the near-field. SKB TR-08-07, Svensk Kärnbränslehantering AB.

Grenthe I, Stumm W, Laaksoharju M, Nilsson A C, Wikberg P, 1992. Redox potentials and redox reactions in deep groundwater systems. Chemical Geology, 98, pp 131–150.

Grenthe I, Plyasunov A V, Spahiu K, 1997. Estimations of medium effects on thermodynamic data. In: Grenthe I, Puigdomenech I (eds). Modelling in aquatic chemistry. Paris: OECD Nuclear Energy Agency, pp 325–426.

Hachiya K, Sasaki M, Ikeda T, Mikami N, Yasunaga T, 1984. Static and kinetic studies of adsorption-desorption of metal ions on a γ-alumina surface. 2. Kinetic study by means of pressure-jump technique. The Journal of Physical Chemistry, 88, pp 27–31.

Haworth A, 1990. A review of the modelling of sorption from aqueous solution. Advances in Colloid and Interface Science, 32, pp 43–78.

Hayes K F, Leckie J O, 1987. Mechanism of lead ion adsorption at the goethite-water interface. In: Davis J A, Hayes K F (eds). Geochemical processes at mineral surfaces. Washington, D.C.: American Chemical Society. (ACS Symposium Series 323), pp 114–141.

Hiemstra T, Van Riemsdijk W H, 1996. A Surface Structural Approach to Ion Adsorption: The Charge Distribution (CD) Model. Journal of Colloid and Interface Science, 179, pp 488–508.

Hiemstra T, De Wit J C M, Van Riemsdijk W H, 1989a. Multisite proton adsorption modeling at the solid/solution interface of (hydr)oxides: A new approach: II. Application to various important (hydr)oxides. Journal of Colloid and Interface Science, 133, pp 105–117.

Hiemstra T, Van Riemsdijk W H, Bolt G H, 1989b. Multisite proton adsorption modeling at the solid/solution interface of (hydr)oxides: A new approach: I. Model description and evaluation of intrinsic reaction constants. Journal of Colloid and Interface Science, 133, pp 91–104.

Hiemstra T, Venema P, Van Riemsdijk W H V, 1996. Intrinsic proton affinity of reactive surface groups of metal (hydr)oxides: The bond valence principle. Journal of Colloid and Interface Science, 184, pp 680–692.

Holzbecher E, 2000. "Predicted retardations of concentration fronts using a mass-balance approach" by Ronald K. Stoesell. Ground Water, 38, pp 808–809.

Huitti T, Hakanen M, Lindberg A, 1996. Sorption of cesium, radium, protactinium, uranium, neptunium, and plutonium on rapakivi granite. Posiva 96-23, Posiva Oy, Finland.

Huitti T, Hakanen M, Lindberg A, 1998. Sorption of cesium on Olkiluoto mica gneiss, granodiorite and granite. Posiva 98-11, Posiva Oy, Finland.

Hummel W, Berner U, Curti E, Pearson F J, Thoenen T, 2002. Nagra/PSI Chemical Thermodynamic Data Base 01/01. Radiochimica Acta, 90, pp 805–813.

Ilton E S, Haiduc A, Moses C O, Heald S M, Elbert D C, Veblen D R, 2004. Heterogeneous reduction of uranyl by micas: Crystal chemical and solution controls. Geochimica et Cosmochimica Acta, 68, pp 2417–2435.

Ittner T, Torstenfelt B, Allard B, 1988. Migration of the fission products strontium, technetium, iodine, cesium and the actinides neptunium, plutonium, americium in granitic rock. SKB TR 88-02, Svensk Kärnbränslehantering AB.

IUPAC, 1997. Compendium of chemical terminology: IUPAC recommendations. 2nd ed. Oxford: Blackwell Science.

Jan Y-L, Wang T-H, Li M-H, Tsai S-C, Wei Y-Y, Hsu C-N, Teng S-P, 2007. Evaluating adsorption ability of granite to radioselenium by chemical sequential extraction. Journal of Radioanalytical and Nuclear Chemistry, 273, pp 299–306.

Jan Y-L, Wang T-H, Li M-H, Tsai S-C, Wei Y-Y, Teng S-P, 2008. Adsorption of Se species on crushed granite: A direct linkage with its internal iron-related minerals. Applied Radiation and Isotopes, 66, pp 14–23.

Jenne E A (ed), 1998. Adsorption of metals by geomedia: variables, mechanisms, and model applications. London: Academic Press.

Johnsson A, Arlinger J, Pedersen K, Ödegaard-Jensen A, Abinsson Y, 2006. Solid-aqueous phase partitioning of radionuclides by complexing compounds excreted by subsurface bacteria. Geomicrobiology Journal, 23, pp 621–630.

Katz L E, Hayes K F, 1995. Surface complexation modeling: II. Strategy for modeling polymer and precipitation reactions at high surface coverage. Journal of Colloid and Interface Science, 170, pp 491–501.

Kienzler B, Vejmelka P, Römer J, Schild D, 2009. Actinide migration in fractures of granite host rock: laboratory and in-situ investigations. Nuclear Technology, 165, pp 223–240.

Kim Y, Kirkpatrick R J, 1997. ^{23}Na and ^{133}Cs NMR study of cation adsorption on mineral surfaces: Local environments, dynamics, and effects of mixed cations. Geochimica et Cosmochimica Acta, 61, pp 5199–5208.

Kinniburgh D G, 1986. General purpose adsorption isotherms. Environmental Science & Technology, 20, pp 895–904.

Kulik D A, 2002. Sorption modelling by Gibbs energy minimisation: towards a uniform thermodynamic database for surface complexes of radionuclides. Radiochimica Acta, 90, pp 815–832.

Kulik D A, 2006. Classic adsorption isotherms incorporated in modern surface complexation models: implications for sorption of actinides. Radiochimica Acta, 94, pp 765–778.

Kulmala S, Hakanen M, 1993. The solubility of Zr, Nb and Ni in groundwater and concrete water, and sorption on crushed rock and cement. Report YJT-93-21, Nuclear Waste Commission of Finnish Power Companies.

Kulmala S, Hakanen M, 1995. Sorption of alkaline-earth elements Sr, Ba and Ra from groundwater on rocks from TVO investigation areas. Report YJT-95-03, Nuclear Waste Commission of Finnish Power Companies.

Kulmala S, Hakanen M, Lindberg A, 1996. Sorption of protactinium on rocks in groundwaters from Posiva investigation sites. Posiva 96-18, Posiva Oy, Finland.

Kulmala S, Hakanen M, Lindberg A, 1998. Sorption of plutonium on rocks in groundwaters from Posiva investigation sites. Posiva 98-12, Posiva Oy, Finland.

Kurosawa S, James S C, Yui M, Ibaraki M, 2006. Model analysis of the colloid and radionuclide retardation experiment at the Grimsel Test Site. Journal of Colloid and Interface Science, 298, pp 467–475.

Laaksoharju M, Smellie J, Tullborg E-L, Gimeno M, Hallbeck L, Molinero J, Waber N, 2008. Bedrock hydrogeochemistry Forsmark. Site descriptive modelling, SDM-Site Forsmark. SKB R-08-47, Svensk Kärnbränslehantering AB.

Laaksoharju M, Smellie J, Tullborg E-L, Wallin B, Drake H, Gascoyne M, Gimeno M, Gurban I, Hallbeck L, Molinero J, Nilsson A-C, Waber N, 2009. Bedrock hydrogeochemistry Laxemar. Site descriptive modelling, SDM-Site Laxemar. SKB R-08-93, Svensk Kärnbränslehantering AB.

Langmuir D, 1997. Aqueous environmental geochemistry. Upper Saddle River, NJ: Prentice Hall.

Langmuir I, 1918. The adsorption of gases on plane surfaces of glass, mica and platinum. Journal of the American Chemical Society, 40, pp 1361–1403.

Latimer, 1926. The energy of solution of gaseous ions in relation to the effect of a charge upon the dielectric. Journal of the American Chemical Society, 48, pp 1234–1239.

Lee S Y, Baik M H, Lee Y B, 2009a. Adsorption of uranyl ions and microscale distribution on Fe-bearing mica. Applied Clay Science, 44, pp 259–264.

Lee S Y, Baik M H, Lee Y J, Lee Y B, 2009b. Adsorption of U(VI) ions on biotite from aqueous solutions. Applied Clay Science, 46(3), pp 255–259.

Liu C, Zachara J M, Zhong L, Heald S M, Wang Z, Jeon B-H, Fredrickson J K, 2009. Microbial Reduction of Intragrain U(VI) in Contaminated Sediment. Environmental Science & Technology, 43, pp 4928–4933.

Lützenkirchen J, 1999. The constant capacitance model and variable ionic strength: an evaluation of possible applications and applicability. Journal of Colloid and Interface Science, 217, pp 8–18.

Lützenkirchen J (ed), 2006. Surface complexation modelling. Amsterdam: Academic Press. (Interface Science and Technology 11)

Madsen L, 2006. Calcite: surface charge. In: Encyclopedia of surface and colloid science. 2nd ed. London: Taylor & Francis, pp 1084–1096.

Malmström M, Banwart S, Lewenhagen J, Duro L, Bruno J, 1996. The dissolution of biotite and chlorite at 25°C in the near-neutral pH region. Journal of Contaminant Hydrology, 21, pp 201–213.

Marques Fernandes M, Baeyens B, Bradbury M H, 2008. The influence of carbonate complexation on lanthanide/actinide sorption on montmorillonite. Radiochimica Acta, 96, pp 691–697.

McKinley I G, Scholtis A, 1993. A comparison of radionuclide sorption databases used in recent performance assessments. Journal of Contaminant Hydrology, 13, pp 347–363.

McKinley J P, Jenne E A, 1991. Experimental investigation and review of the "solids concentration" effect in adsorption studies. Environmental Science & Technology, 25, pp 2082–2087.

McKinley J P, Zachara J M, Heald S M, Dohnalkova A, Newville M G, Sutton S R, 2004. Microscale distribution of cesium sorbed to biotite and muscovite. Environmental Science & Technology, 38, pp 1017–1023.

Miller W, Alexander W R, Chapman N, McKinley I, Smellie J (eds), 2000. Geological disposal of radioactive wastes and natural analogues: lessons from nature and archaeology. Oxford: Pergamon.

NEA, 2001a. Confidence in models of radionuclide transport for site-specific assessment: workshop proceedings, Carlsbad, New Mexico, USA, 14–17 June 1999. Paris: Nuclear Energy Agency, Organisation for Economic Co-operation and Development.

NEA, 2001b. Using thermodynamic sorption models for guiding radioelement distribution coefficient (Kd) investigations: a status report. Paris: Nuclear Energy Agency, Organisation for Economic Co-operation and Development.

NEA, 2005. NEA Sorption Project, phase II: interpretation and prediction of radionuclide sorption onto substrates relevant for radioactive waste disposal using thermodynamic sorption models. Paris: Nuclear Energy Agency, Organisation for Economic Co-operation and Development.

Neretnieks I, 1980. Diffusion in the rock matrix: An important factor in radionuclide retardation. Journal of Geophysical Research, 85, pp 4397–4379.

Neretnieks I, 2002. Using ^{222}Rn to assess the fracture apertures in fractured rocks. In: Findikakis A. N. (ed). Proceedings of International Groundwater Symposium. Symposium held in Berkeley, California, 25–28 March, 2002, pp 1–9.

Neretnieks I, Rasmuson A, 1984. An approach to modeling radionuclide migration in a medium with strongly varying velocity and block sizes along a flowpath. Water Resources Research, 20, pp 1823–1836.

Nilsson K, Byegård J, Selnert E, Widestrand H, 2010. Äspö Hard Rock Laboratory. Long term sorption diffusion experiment (LTDE-SD). Results from rock sample analyses and modelling. SKB R-10-68, Svensk Kärnbränslehantering AB.

NIST, 2010. NIST/SEMATECH e-Handbook of Statistical Methods. [Online]. Available at: http://www.itl.nist.gov/div898/handbook/. [16 December 2010].

Noe D C, Veblen D R, 1999. HRTEM analysis of dislocation cores and stacking faults in naturally deformed biotite crystals. American Mineralogist, 84, pp 1925–1931.

Ochs M, Talerico C, 2004. SR-Can. Data and uncertainty asessment. Migration parameters for the bentonite buffer in the KBS-3 concept. SKB TR-04-18, Svensk Kärnbränslehantering AB.

Ochs M, Davis J A, Olin M, Payne T E, Tweed C J, Askarieh M M, Altmann S, 2006a. Use of thermodynamic sorption models to derive radionuclide Kd values for performance assessment: selected results and recommendations of the NEA sorption project. Radiochimica Acta, 94, pp 779–785.

Ochs M, Talerico C, Sellin P, Hedin A, 2006b. Derivation of consistent sorption and diffusion parameters and their uncertainties for compacted MX-80 bentonite. Physics and Chemistry of the Earth, Parts A/B/C, 31, pp 600–609.

Olin M, Puukko E, Puhakka E, Lehikoinen J, Lindberg A, Hakanen M, 2006. Sorption of nickel on biotite. VTT-R-08046-06, Technical Research Centre of Finland (VTT).

Painter S, Mancillas J, 2009. MARFA version 3.2.2 user's manual: migration analysis of radionuclides in the far field. SKB R-09-56, Svensk Kärnbränslehantering AB.

Papelis C, 2001. Cation and anion sorption on granite from the Project Shoal Test Area, near Fallon, Nevada, USA. Advances in Environmental Research, 5, pp 151–166.

Park C-K, Baik M-H, 2009. Diffusion of some chemical species through a granite considering their geochemical properties. Korean Journal of Chemical Engineering, 26, pp 1279–1285.

Parkhurst D L, Appelo C A J, 1999. User's guide to PHREEQC (version 2): a computer program for speciation, batch-reaction, one-dimensional transport, and inverse geochemical calculations. Water-Resources Investigations Report 99-4259, U.S. Geological Survey, Denver, Colorado.

Pauling L, 1929. The principles determining the structure of complex ionic crystals. Journal of the American Chemical Society, 51, pp 1010–1026.

Pinnioja S, Jaakkola T, Kämäräinen E-L, Koskinen A, Lindberg A, 1984. Sorption of carbon, cobalt, nickel, strontium, iodine, cesium, americium, and neptunium in rocks and minerals. Report YJT-84-19, Nuclear Waste Commission of Finnish Power Companies.

Poinssot C, Baeyens B, Bradbury M H, 1999. Experimental and modelling studies of caesium sorption on illite. Geochimica et Cosmochimica Acta, 63, pp 3217–3227.

Prelot B, Janusz W, Thomas F, Villieras F, Charmas R, Piasecki W, Rudzinski W, 2002. Adsorption of cadmium ions at the electrolyte/silica interface: I. Experimental study of surface properties. Applied Surface Science, 196, pp 322–330.

Przylibski T A, 2000. Estimating the radon emanation coefficient from crystalline rocks into groundwater. Applied Radiation and Isotopes, 53, pp 473–479.

Puigdomenech I, Rard J A, Plyasunov A V, Grenthe I, 1999. TDB-4. Temperature corrections to thermodynamic data and enthalpy calculations. Le Seine-St. Germain: OECD Nuclear Energy Agency.

Rasilainen K, Suksi J, Ruskeeniemi T, Pitkanen P, Poteri A, 2003. Release of uranium from rock matrix--a record of glacial meltwater intrusions? Journal of Contaminant Hydrology, 61, pp 235–246.

Regenspurg S, Schild D, Schäfer T, Huber F, Malmström M E, 2009. Removal of uranium(VI) from the aqueous phase by iron(II) minerals in presence of bicarbonate. Applied Geochemistry, 24, pp 1617–1625.

Righetto L, Azimonti G, Missana T, Bidoglio G, 1995. The triple layer model revised. Colloids and Surfaces A: Physicochemical and Engineering Aspects, 95, pp 141–157.

Rosenqvist J, 2002. Surface chemistry of Al and Si (hydr)oxides, with emphasis on nano-sized gibbsite (α-$Al(OH)_3$). Ph.D. thesis. Umeå University, Sweden.

Rusch U, Borkovec M, Daicic J, van Riemsdijk W H, 1997. Interpretation of competitive adsorption isotherms in terms of affinity distributions. Journal of Colloid and Interface Science, 191, pp 247–255.

Sahai N, 2000. Estimating sorption enthalpies and affinity sequences of monovalent electrolyte ions on xide surfaces in aqueous solutions. Geochimica et Cosmochimica Acta, 64, pp 3629–3641.

Salas J, Gimeno M J, Auqué L F, Molinero J, Gómez J, Juárez I, 2010. SR-Site – hydrogeochemical evolution of the Forsmark site. SKB TR-10-58, Svensk Kärnbränslehantering AB.

Sandström B, Stephens M B, 2009. Mineralogy, geochemistry, porosity and redox properties of rocks from Forsmark. Compilation of data fom the regional model volume for SR-Site. SKB R-09-51, Svensk Kärnbränslehantering AB.

Sandström B, Tullborg E-L, Smellie J, MacKenzie A, Suksi J, 2008. Fracture mineralogy of the Forsmark site. SDM-Site Forsmark. SKB R-08-102, Svensk Kärnbränslehantering AB.

Scheidegger A M, Fendorf M, Sparks D L, 1996. Mechanisms of nickel sorption on pyrophyllite: macroscopic and microscopic approaches. Soil Science Society of America Journal, 60, pp 1763–1772.

Schindler P W, Fürst B, Dick R, Wolf P U, 1976. Ligand properties of surface silanol groups. I. surface complex formation with Fe^{3+}, Cu^{2+}, Cd^{2+}, and Pb^{2+}. Journal of Colloid and Interface Science, 55, pp 469–475.

Selnert E, Byegård J, Widestrand H, Carlsten S, Döse C, Tullborg E-L, 2009. Bedrock transport properties. Data evaluation and retardation model. Site descriptive modelling, SDM-Site Laxemar. SKB R-08-100, Svensk Kärnbränslehantering AB.

Seo Y S, Jeong G C, Kim J S, Ichikawa Y, 2002. Microscopic observation and contact stress analysis of granite under compression. Engineering Geology, 63, pp 259–275.

Shibutani T, Suyama T, Shibata M, 1999. Sorption database for radionuclides on bentonite and rocks (in Japanese with English abstract). JNC Technical Report TN8410 99-050, Japan Nuclear Cycle Development Institute.

Sidborn M, Sandström B, Tullborg E-L, Delos A, Molinero J, Hallbeck L, Pedersen K, 2010. SR-Site: Oxygen ingress in the rock at Forsmark during a glacial cycle. SKB TR-10-57, Svensk Kärnbränslehantering AB. /slutgiltig titel?/

Singer D M, Maher K, Brown Jr. G E, 2009. Uranyl–chlorite sorption/desorption: evaluation of different U(VI) sequestration processes. Geochimica et Cosmochimica Acta, 73, pp 5989–6007.

SKB, 2004. RETROCK Project. Treatment of geosphere retention phenomena in safety assessments. Scientific basis of retention processes and their implementation in safety assessment models (WP2). Work package 2 report of the RETROCK concerted action. SKB R-04-48, Svensk Kärbränslehantering AB.

SKB, 2006. Long-term safety for KBS-3 repositories at Forsmark and Laxemar – a first evaluation. Main report of the SR-Can project. SKB TR-06-09, Svensk Kärnbränslehantering AB.

SKB, 2010a. Climate and climate-related issues for the safety assessment SR-Site. SKB TR-10-49, Svensk Kärnbränslehantering AB.

SKB, 2010b. Data report for the safety assessment SR-Site. SKB TR-10-52, Svensk Kärnbränslehantering AB.

SKB, 2010c. Geosphere process report for the safety assessment SR-Site. SKB TR-10-48, Svensk Kärnbränslehantering AB.

SKB, 2010d. Radionuclide transport report for the safety assessment SR-Site. SKB TR-10-50, Svensk Kärnbränslehantering AB.

SKB, 2011. Long-term safety for the final repository for spent nuclear fuel at Forsmark. Main report of the SR-Site project. SKB TR-11-01, Svensk Kärnbränslehantering AB.

Skopp J, 2009. Derivation of the Freundlich adsorption isotherm from kinetics. Journal of Chemical Education, 86, p 1341.

Sparks D L, 2003. Environmental soil chemistry. 2nd ed. San Diego, CA: Academic Press.

Sposito G, 1998. On Points of Zero Charge. Environmental Science & Technology, 32, pp 2815–2819.

Stenhouse M, Jégou C, Brown P, Meinrath G, Nitsche H, Ekberg C, 2008. Review of SR-Can: Evaluation of SKB's handling of spent fuel performance, radionuclide chemistry and geosphere transport parameters. External review contribution in support of SKI's and SSI's review of SR-Can. SKI Report 2008:17, Statens kärnkraftinspektion (Swedish Nuclear Power Inspectorate).

Stipp S L S, 1999. Toward a conceptual model of the calcite surface: hydration, hydrolysis, and surface potential. Geochimica et Cosmochimica Acta, 63, pp 3121–3131.

Stipp S L S, Konnerup-Madsen J, Franzreb K, Kulik A, Mathieu H J, 1998. Spontaneous movement of ions through calcite at standard temperature and pressure. Nature, 396, pp 356–359.

Stumm W, Hohl H, Dalang F, 1976. Interaction of metal ions with hydrous oxide surfaces. Croatica Chemica Acta, 48, pp 491–504.

Stumm W, Morgan J, 1996. Aquatic chemistry: chemical equilibria and rates in natural waters. 3rd ed. New York: Wiley.

Stumpf T, Bauer A, Coppin F, Fanghänel T, Kim J-I, 2002. Inner-sphere, outer-sphere and ternary surface complexes: a TRLFS study of the sorption process of Eu(III) onto smectite and kaolinite. Radiochimica Acta, 90, pp 345–349.

Suksi J, Rasilainen K, Casanova J, Ruskeeniemi T, Blomqvist R, Smellie J A T, 2001. U-series disequilibria in a groundwater flow route as an indicator of uranium migration processes. Journal of Contaminant Hydrology, 47, pp 187–196.

Sverjensky D A, 2003. Standard states for the activities of mineral surface sites and species. Geochimica et Cosmochimica Acta, 67, pp 17–28.

Tachi Y, Shibutani T, Sato H, Yui M, 1998. Sorption and diffusion behavior of selenium in tuff. Journal of Contaminant Hydrology, 35, pp 77–89.

Tachi Y, Shibutani T, Sato H, Shibata M, 1999. Sorption and diffusion behaviour of Palladium in bentonite, granodiorite and tuff. JNC Technical Report TN8400, Japan Nuclear Cycle Development Institute.

Teppen B J, Miller D M, 2006. Hydration energy determines isovalent cation exchange selectivity by clay minerals. Soil Science Society of America Journal, 70, pp 31–40.

Ticknor K V, McMurray J, 1996. A study of selenium and tin sorption on granite and goethite. Radiochmica Acta, 73, pp 149–156.

Ticknor K V, Vandergraaf T T, McMurry J, Boisvenue L, Wilkin D, 1996. Parametric studies of factors affecting Se and Sn sorption. AECL TR-723, COG-95-554, Atomic Energy of Canada Limited.

Tsai S-C, Wang T-H, Li M-H, Wei Y-Y, Teng S-P, 2009. Cesium adsorption and distribution onto crushed granite under different physicochemical conditions. Journal of Hazardous Materials, 161, pp 854–861.

Turner D R, Pabalan R T, 1999. Abstraction of mechanistic sorption model results for performance assessment calculations at Yucca Mountain, Nevada. Waste Management, 19, pp 375–388.

Um W, Papelis C, 2003. Metal ion sorption and desorption on zeolitized tuffs from the nevada test site. Environmental Science & Technology, 38, pp 496–502.

Van Cappellen P, Charlet L, Stumm W, Wersin P, 1993. A surface complexation model of the carbonate mineral-aqueous solution interface. Geochimica et Cosmochimica Acta, 57, pp 3505–3518.

van Hal R E G, Eijkel J C T, Bergveld P, 1996. A general model to describe the electrostatic potential at electrolyte oxide interfaces. Advances in Colloid and Interface Science, 69, pp 31–62.

Vandergraaf T T, Abry D R M, Davis C E, 1982. The use of autoradiography in determining the distribution of radionuclides sorbed on thin sections of plutonic rocks from the Canadian Shield. Chemical Geology, 36, pp 139–154.

Vandergraaf T T, Ticknor K V, Melnyk T W, 1993. The selection of a sorption data base for the geosphere model in the Canadian Nuclear Fuel Waste Management Program. Journal of Contaminant Hydrology, 13, pp 327–345.

Venema P, Hiemstra T, Weidler P G, van Riemsdijk W H, 1998. Intrinsic Proton affinity of reactive surface groups of metal (hydr)oxides: application to iron (hydr)oxides. Journal of Colloid and Interface Science, 198, pp 282–295.

Villalobos M, Leckie J O, 2001. Surface complexation modeling and FTIR study of carbonate adsorption to goethite. Journal of Colloid and Interface Science, 235, pp 15–32.

Vinson D S, Vengosh A, Hirschfeld D, Dwyer G S, 2009. Relationships between radium and radon occurrence and hydrochemistry in fresh groundwater from fractured crystalline rocks, North Carolina (USA). Chemical Geology, 260, pp 159–171.

Wang P, Anderko A, 2001. Thermodynamic Modeling of the Adsorption of Radionuclides on Selected Minerals. I: Cations. Industrial and Engineering Chemistry Research, 40, pp 4428–4443.

Wehrli B, Ibric S, Stumm W, 1990. Adsorption kinetics of vanadyl (IV) and chromium (III) to aluminum oxide: Evidence for a two-step mechanism. Colloids and Surfaces, 51, pp 77–88.

White A F, Brantley S L, 2003. The effect of time on the weathering of silicate minerals: why do weathering rates differ in the laboratory and field? Chemical Geology, 202, pp 479–506.

Widestrand H, Byegård J, Kronberg M, Nilsson K, Höglund S, Gustafsson E, 2010a. Äspö Hard Rock Laboratory. Long Term Sorption Diffusion Experiment (LTDE-SD). Performance of main in-situ experiment and results from water phase measurements. SKB R-10-67, Svensk Kärnbränslehantering AB.

Widestrand H, Byegård J, Selnert E, Skålberg M, Höglund S, Gustafsson E, 2010b. Long Term Sorption Diffusion Experiment (LTDE-SD). Supporting laboratory program - Sorption diffusion experiments and rock material characterisation. With supplement of adsorption studies on intact rock samples from the Forsmark and Laxemar site investigations. SKB R-10-66, Svensk Kärnbränslehantering AB.

Wold S, 2009. Sorption of prioritized elements on montmorillonite colloids and their potential to transport radionuclides. SKB TR-10-20, Svensk Kärnbränlsehantering AB.

Wu C-H, Kuo C-Y, Lin C-F, Lo S-L, 2002. Modeling competitive adsorption of molybdate, sulfate, selenate, and selenite using a Freundlich-type multi-component isotherm. Chemosphere, 47, pp 283–292.

Xu S, Harsh J B, 1990. Monovalent cation selectivity quantitatively modeled according to hard/soft acid/base theory. Soil Science Society of America Journal, 54, pp 357–363.

Yamaguchi T, Nakayama S, 1998. Diffusivity of U, Pu and Am carbonate complexes in a granite from Inada, Ibaraki, Japan studied by through diffusion. Journal of Contaminant Hydrology, 35, pp 55–65.

Yamaguchi T, Nakayama S, Okamoto H, 2002. Effective diffusivity of neptunium and plutonium in granite from Inada, Ibaraki, Japan under anaerobic conditions. Radiochimica Acta, 90, pp 863–868.

Zachara J M, Smith S C, Liu C, McKinley J P, Serne R J, Gassman P L, 2002. Sorption of Cs^+ to micaceous subsurface sediments from the Hanford site, USA. Geochimica et Cosmochimica Acta, 66, pp 193–211.

Zazzi Å, 2009. Chlorite: Geochemical properties, dissolution kinetics and Ni(II) sorption. Ph.D. thesis. Royal Institute of Technology (KTH), Stockholm, Sweden.

Zhu C, 2002. Estimation of surface precipitation constants for sorption of divalent metals onto hydrous ferric oxide and calcite. Chemical Geology, 188, pp 23–32.

Zhu C, 2004. Coprecipitation in the barite isostructural family: 1. Binary mixing properties. Geochimica et Cosmochimica Acta, 68, pp 3327–3337.

Appendix A

Estimation of groundwater trace constituent concentrations for ion-exchange modelling

In the hydrochemical simulations used to establish groundwater compositions for SR-Site, only the major constituents are considered. The major cations are Ca^{2+}, Na^{+}, Mg^{2+}, K^{+}, and Fe^{2+}/Fe^{3+} while the major anions are Cl^{-}, HCO_3^{-}, PO_4^{2-}, and HS^{-}/SO_4^{2-}. In order to calculate groundwater chemistry correction factors for the ion-exchanging solutes, however, it is also necessary to know the background concentrations of the minor groundwater constituents (including naturally occurring isotopes) that might compete for electrostatic binding sites with transported radionuclides. Specifically, we are interested in estimating the concentrations of Rb^{+}, Cs^{+}, Sr^{2+}, Ba^{2+}, and Ra^{2+} in order to include these in the ion-exchange calculations.

Although these data are not available for the projections of groundwater chemistry in SR-Site, there is a considerable database of groundwater analyses that was compiled during the site investigations for Forsmark /Laaksoharju et al. 2008/ and Laxemar /Laaksoharju et al. 2009/. If it is assumed that future states follow the same systematic trends as reflected in the present day chemical compositions, this information can be used to estimate the most likely concentration ranges for the minor solutes. In order to do this, however, it is necessary to identify the best correlating variables that describe these variations. Generally it was found that a power law correlation with Ca concentration as the independent variable was the best predictor of trace component concentration in the cases of Sr, Cs, and Rb (see Figure A-1 to Figure A-3). The correlation with Ca was found to be particularly good for Sr. While this could be a consequence of groundwater dilution (as indicated in Figure A-1) it is also consistent with ion-exchange competition or Sr solid solution formation with calcite.

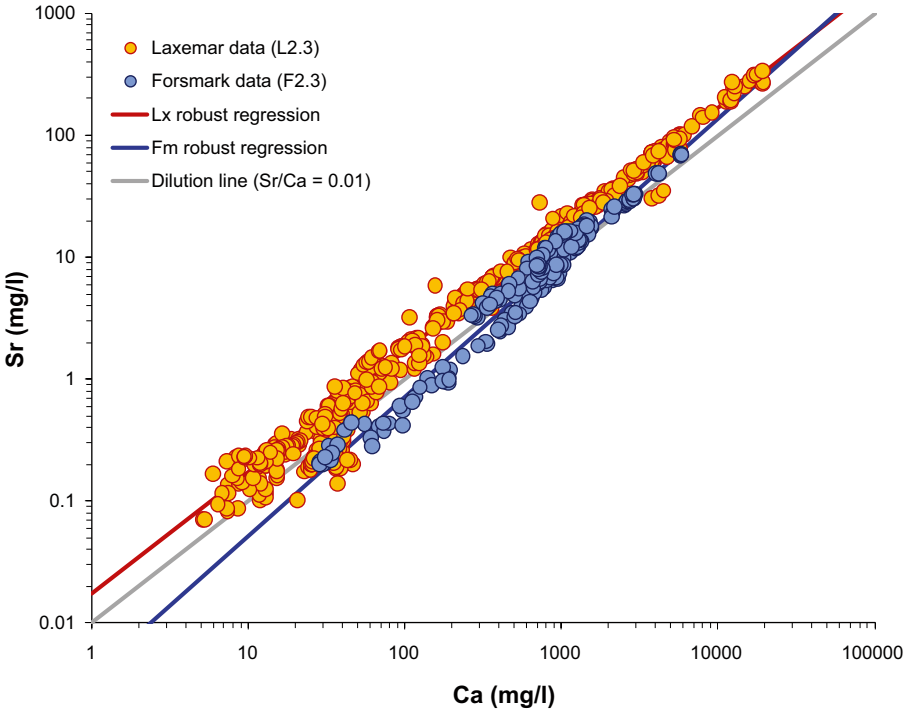

Figure A-1. *Cross plot of measured Sr (mg/l) concentrations in groundwater versus Ca (mg/l) where data are taken from the Forsmark and Laxemar site investigation database. A least squares regression curve is shown for each site assuming a power law correlation with Ca as well as a theoretical dilution line assuming Sr concentration equal to 1% of the Ca concentration.*

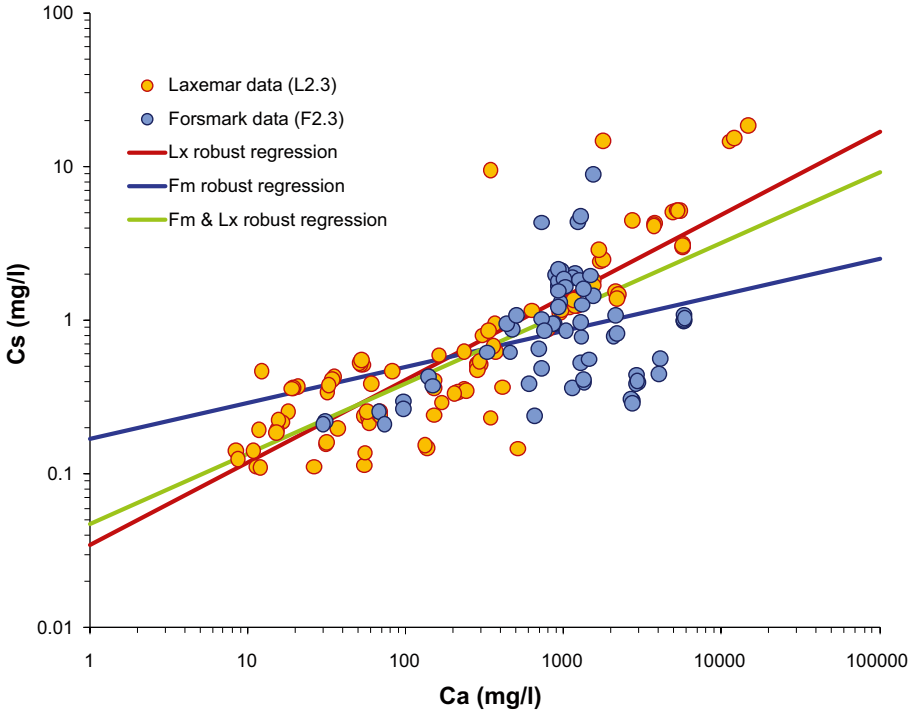

Figure A-2. *Cross plot of measured Cs (mg/l) concentrations in groundwater versus Ca (mg/l) where data are taken from the Forsmark and Laxemar site investigation database. Power-law regression curves are shown for each site considered separately as well as a curve for data pooled from both sites.*

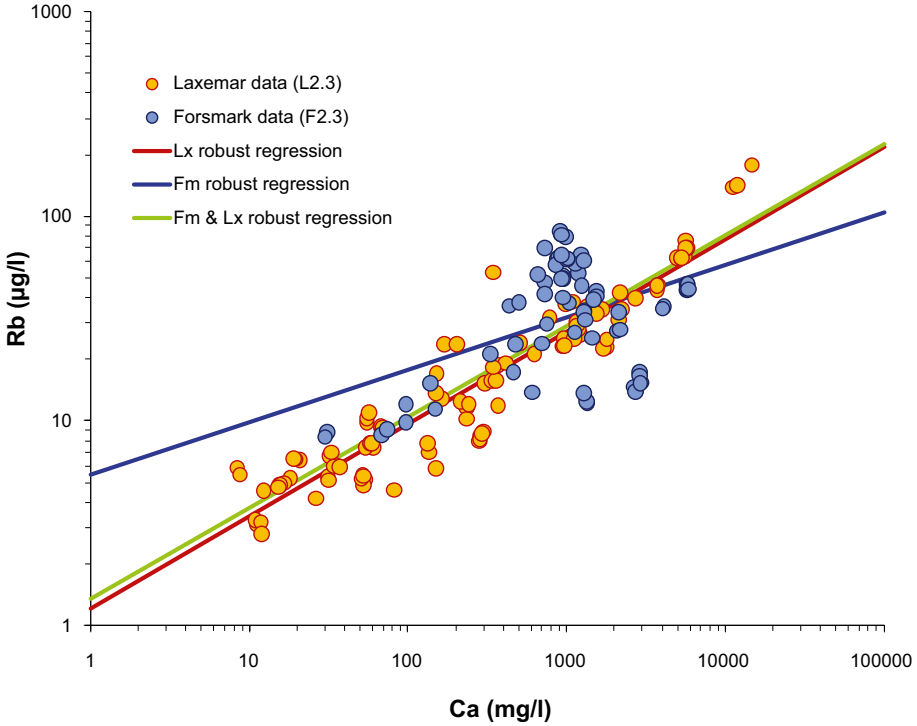

Figure A-3. *Cross plot of measured Rb (µg/l) concentrations in groundwater versus Ca (mg/l) where data are taken from the Forsmark and Laxemar site investigation database. Power-law regression curves are shown for each site considered separately as well as a curve for data pooled from both sites.*

Barium and radium were given special consideration since they may be mutually correlated by way of barite equilibrium/radiobarite co-precipitation in the groundwater. As can be readily seen from Figure A-4, the Ba and SO_4 content of the Forsmark and Laxemar groundwater do not appear to be correlated, although the compositions are relatively close to the theoretical locus of values obtained when barite is assumed to be the solubility controlling solid for Ba. In most cases, the concentrations of Ba and SO_4 appear to be slightly oversaturated, although this could be related to the presence of complexed sulphate species ($CaSO_4$ in particular) which are not accounted for in the theoretical solubility calculation. In the more saline groundwaters represented at Forsmark and Laxemar, the total SO_4 concentration can be as much as 2–3 times the free concentration owing to the presence of complexed sulphate species. The apparent oversaturation is therefore consistent with the behaviour of saline groundwater. Although the data suggest near equilibrium conditions with respect to barite solubility, Ba was also found to correlate relatively well with the Ca content of the groundwater as shown in Figure A-5.

Radium and barium were found to be only very weakly correlated, although the scatter is somewhat larger for the Laxemar data set. Since a greater proportion of the variation could be explained by correlation with Ca concentration, this was used a basis for estimating background concentrations of this element.

In the ion-exchange calculations used to estimate chemistry correction factors, the site specific correlations with Ca concentration were used to estimate the background concentrations of Sr, Cs, Rb, Ba, and Ra assuming that the established correlations are approximately valid for future groundwater states. The unknown concentrations were estimated stochastically using a power law correlation defined in the following form:

$$\log_{10}[M^{z+}] = a + b \cdot \log_{10}[Ca^{2+}] + \sigma R_n(0,1) \qquad \text{(A-1)}$$

Where a and b are the regression parameters obtained by robust linear least squares optimisation and s is the residual component of random variation that could not be related to the total Ca concentration. The $R_n(0,1)$ term represents a random normal deviate with mean of zero and variance of unity. The site-specific regression parameters are summarised in Table A-1.

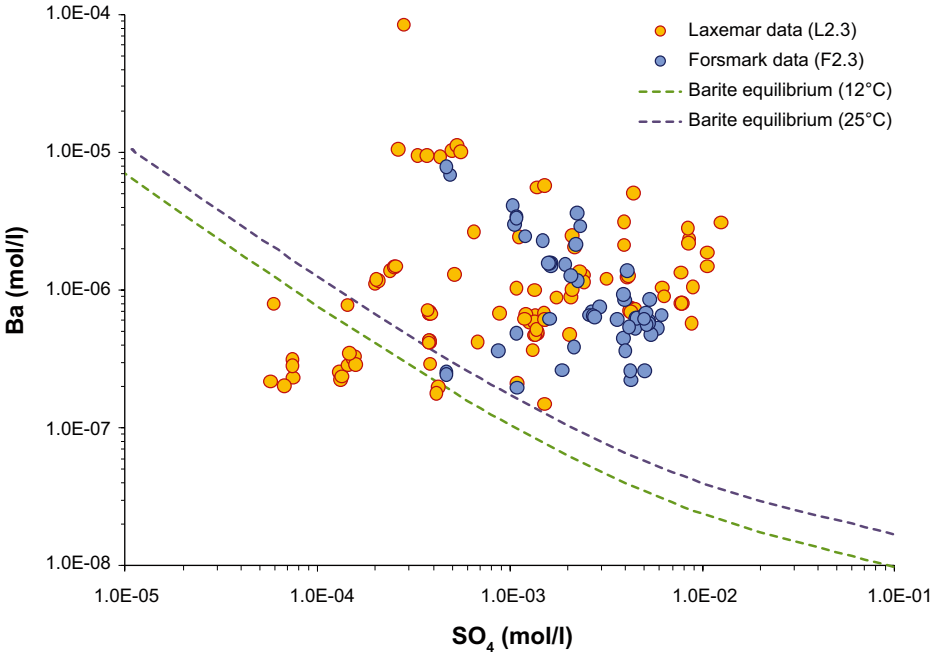

Figure A-4. *Cross plot of measured total Ba (mol/l) concentrations in groundwater versus total sulphate, SO_4 (mol/l) where data are taken from the Forsmark and Laxemar site investigation database. Curves are also drawn showing the locus of concentrations describing theoretical barite equilibrium at 12°C and 25°C, respectively (calculated using PHREEQC).*

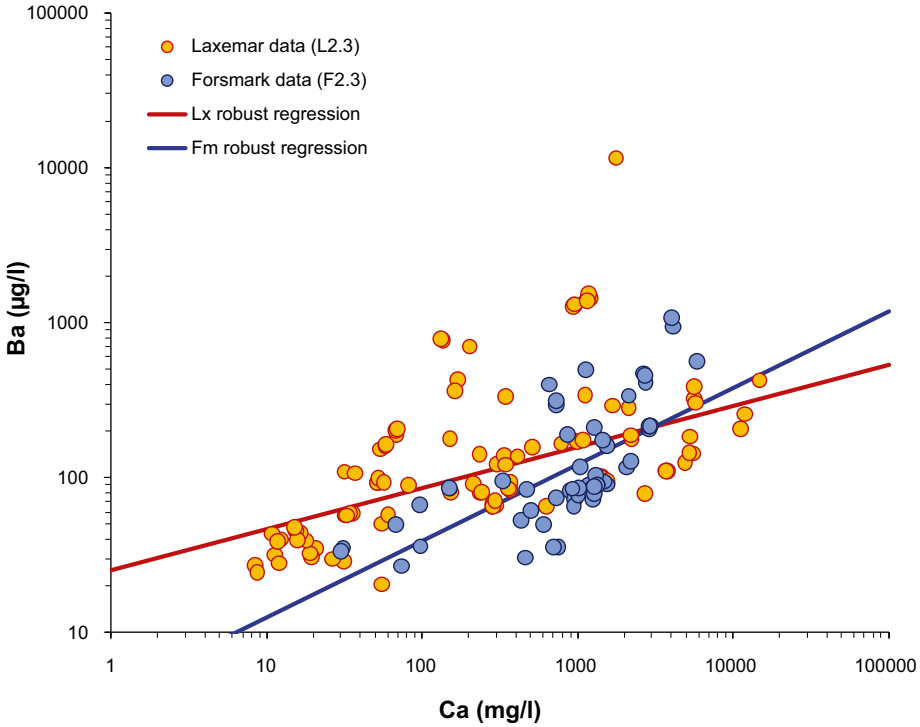

Figure A-5. *Cross plot of measured Ba (µg/l) concentrations in groundwater versus Ca (mg/l) where data are taken from the Forsmark (Fm) and Laxemar (Lx) site investigation database. Power-law regression curves are shown for each site considered separately.*

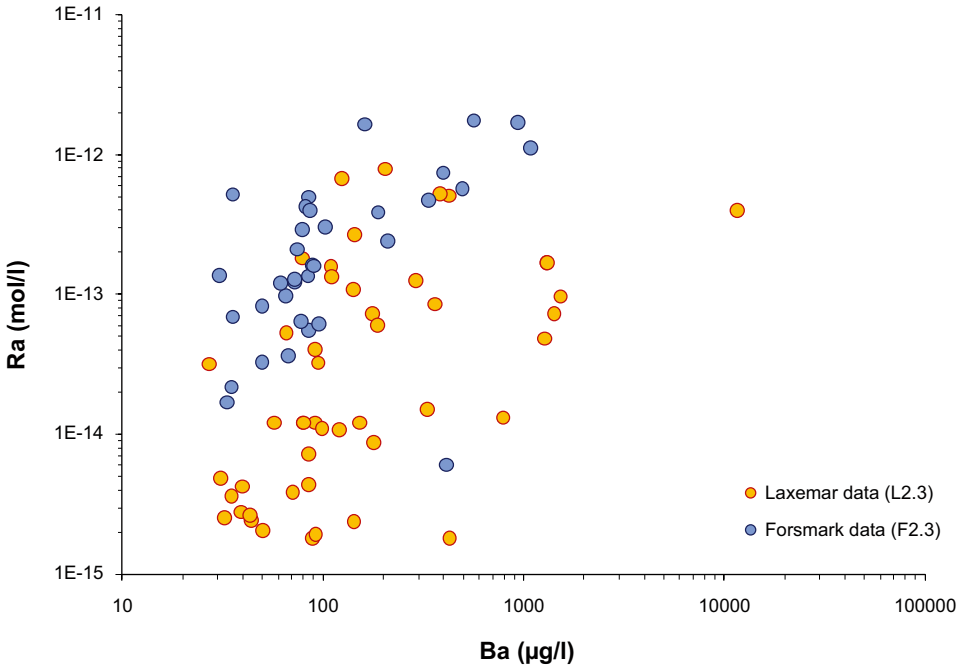

Figure A-6. *Cross plot of measured Ra (mol/l) concentrations in groundwater versus Ba (µg/l) where data are taken from the Forsmark and Laxemar site investigation database. No regression curves are drawn on account of the weak correlation between these solutes.*

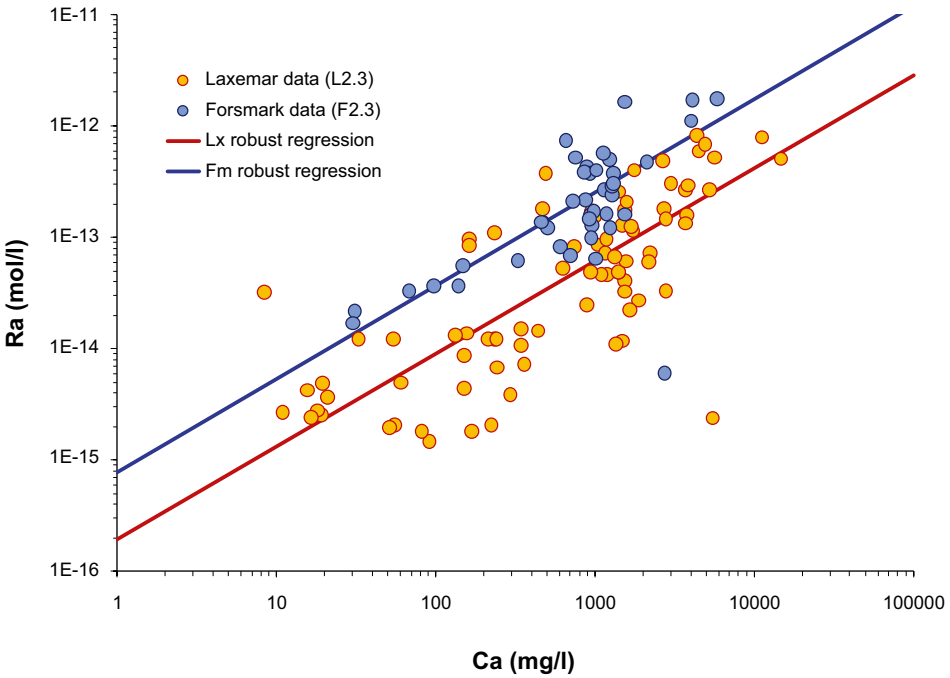

Figure A-7. *Cross plot of measured Ra (mol/l) concentrations in groundwater versus Ca (mg/l) where data are taken from the Forsmark (Fm) and Laxemar (Lx) site investigation database. Power-law regression curves are shown for each site considered separately.*

Table A-1. Correlations between concentrations of minor groundwater constituents and Ca (mg/l) as defined by Equation A-1. These are needed to establish relevant background concentrations for ion-exchange calculations which are then used to define groundwater chemistry correction factors for Sr, Cs, Rb, and Ra sorption in SR-Site.

Element	Site	a	b	σ
Sr (mg/l)	Fm	–2.426	1.143	0.1098
	Lx	–1.764	0.990	0.06742
Cs (mg/l)	Fm	–3.771	0.2337	0.3478
	Lx	–4.463	0.5373	0.2286
Rb (mg/l)	Fm	–2.264	0.2561	0.2846
	Lx	–2.917	0.4513	0.1322
Ba (mg/l)	Fm	–2.399	0.4946	0.3008
	Lx	–1.602	0.2658	0.3116
Ra (mol/l)	Fm	–15.12	0.8397	0.2844
	Lx	–15.71	0.8343	0.4818

The impact of stochastic uncertainty regarding the actual background concentrations of these minor constituents was addressed by complementary simulations in which the concentrations were set at constant levels equal to the expected average for the prevailing Ca concentrations projected in the SR-Site hydrochemical simulations. It was found that the variation of the chemistry correction factor was dominated by the statistics of the major groundwater constituents and the additional uncertainty introduced by the assumed correlations for minor constituents had negligible effect.

Appendix B

Corroboration of recommended K_d values for radium using natural tracer data

Given sufficient time in a suitably isolated geological system, a steady-state condition will eventually be reached whereby daughter radionuclides of the naturally occurring long-lived isotopes ^{238}U, ^{235}U, and ^{232}Th will be present at activity levels that are identical for each daughter nuclide in the decay chain. This process is referred to as *secular equilibrium*. Given that U is relatively soluble under oxidising or mildly reducing conditions and Th is largely immobile under both oxidising and reducing conditions, the activity ratios of various U and Th daughters encode qualitative information about alteration processes that may have occurred in the distant past. Since uranium is a relatively abundant trace element in granitic rocks, study of the isotopic disequilibrium between its daughter nuclides in the host rock and fracture coatings is useful for determining the geochronology and hydrochemical history of sites such as Forsmark and Laxemar (see e.g. /Gascoyne and Schwarcz 1986, Suksi et al. 2001, Gascoyne et al. 2002, Rasilainen et al. 2003/).

In practice, however, it is often difficult to draw robust quantitative conclusions for most U and Th daughter nuclides owing to uncertainties concerning the reconstruction of boundary conditions and the duration and timing of hydrochemical gradients imposed on the system at different times. Relative radium and radon activities in groundwater, on the other hand, (and on account of their short half-lives) can provide very useful information concerning matrix diffusion and sorption processes over timescales that are more manageable than those of the U and Th isotopes typically considered in uranium disequilibrium studies.

In some previous works, measured activities of ^{222}Rn in groundwater have been used to speculate on transport apertures of flow-bearing fractures in granitic rocks /Andrews et al. 1986, 1989, Neretnieks 2002/. In this appendix, the model described in /Neretnieks 2002/ is extended in a stochastic analysis to make predictions of expected background activities of ^{226}Ra and ^{222}Rn in groundwater for the purpose of corroborating the K_d ranges recommended for use in SR-Site for Ra(II) sorption.

Provided flow and transport has occurred for sufficient time that steady-state conditions can be assumed, the aqueous phase concentration of ^{226}Ra (denoted with subscript A) in the fracture relative to the equilibrium concentration in the rock matrix is given by as:

$$\frac{c_A}{c_{A(eq)}} = \frac{b_A + \dfrac{p_A}{c_{A(eq)}}}{b_A + R_{fA}\lambda_A} \cdot \left(1 - \exp\left(-\left(b_A + R_{fA}\lambda_A\right)t_w\right)\right) \qquad \text{(B-1)}$$

Here, b_A is a matrix flux term, p_A is the rate of ^{226}Ra production in fracture coatings lining the advective flowspace, and λ_A is the decay constant of ^{226}Ra. R_{fA} is a retardation factor accounting for fast equilibrium sorption on the fracture coatings. The variable t_w is the advective travel time from the point of origin of infiltrating meteoric water to the groundwater sampling location. This is also equal to the flowpath length divided by the flow velocity in the advective system. The definitions of the variables and parameters used in the equations developed in this section can be found in Table B-1.

Provided t_w for the particular flowpath is sufficiently large, an equilibrium fracture concentration will be reached whereby the exponential term in Equation B-1 can be neglected, giving:

$$\frac{c_{A(\infty)}}{c_{A(eq)}} \approx \frac{b_A + \dfrac{p_A}{c_{A(eq)}}}{b_A + R_{fA}\lambda_A} \qquad \text{(B-2)}$$

Table B-1. Definitions of variables and parameters used in Equations B-1–B-6.

Variable	Description
$c_{A(eq)} = \dfrac{q_A^0}{R_{pA} N_{av} \lambda_A}$ $\begin{cases} q_A^0 = q_0 \dfrac{\eta_p}{\theta_m} \\ q_0 = \dfrac{\left(10^3 \cdot m_{238U}\right)}{M_w} \rho_r N_A \lambda_{238U} \end{cases}$	Equilibrium concentration of ^{226}Ra deep within the rock matrix under steady-state conditions. The parameter q_A^0 is the rate of production of ^{226}Ra within the matrix pore-water assuming secular equilibrium with ^{238}U. N_{av} is Avogadro's number, $6.022 \cdot 10^{23}$.
$c_{B(eq)} = \dfrac{q_A^0}{N_{av} \lambda_B}$	Equilibrium concentration of ^{222}Rn deep within the rock matrix under steady-state conditions assuming secular equilibrium with respect to ^{226}Ra.
$b_A = \dfrac{2}{\delta_t} \theta_m \sqrt{\lambda_A D_{pA} R_{pA}}$ $D_{pA} \approx D_e / \theta_m$	Rock matrix flux term for ^{226}Ra
$b_B = \dfrac{2}{\delta_t} \theta_m \sqrt{\lambda_B D_{pB}}$ $D_{pB} \approx D_e / \theta_m$	Rock matrix flux term for ^{222}Rn
$R_{pA} = 1 + K_{dA}^m \rho_r \dfrac{(1-\theta_m)}{\theta_m}$	Rock matrix retardation factor for ^{226}Ra
$R_{fA} = 1 + \left(\theta_s + K_{dA}^s \rho_s\right) \dfrac{\delta_s}{\delta_t}$ $\dfrac{\delta_s}{\delta_t} = \dfrac{\beta}{(1-\beta)}$	Fracture coating retardation factor for ^{226}Ra. The parameter *b* is the fraction of the advective flowspace occupied by the fracture coating and is equal to the ratio of fracture coating thickness, δ_s and transport aperture, δ_t.
$R_{fB} = 1 + \theta_s \dfrac{\delta_s}{\delta_t} \approx 1$	Fracture coating retardation factor for ^{222}Rn
$p_A = A_{Th230} \dfrac{\rho_s \eta_f (1-\theta_s)}{N_{av}} \cdot \dfrac{\delta_s}{\delta_t}$	Rate of production of ^{226}Ra in the fracture coatings from decay of ^{230}Th.

If production of ^{222}Ra (the daughter nuclide of ^{226}Ra) in the fracture coatings is constant, the equation governing the equilibrium concentration of this nuclide (denoted with subscript *B*) in the fracture is similar to that given in Equation B-1 although using ^{222}Rn-specific parameters:

$$\frac{c_B}{c_{B(eq)}} = \frac{b_B + \dfrac{p_B}{c_{B(eq)}}}{b_B + R_{fB}\lambda_B} \cdot \left(1 - \exp\left(-\left(b_B + R_{fB}\lambda_B\right) t_w\right)\right) \tag{B-3}$$

In most cases of relevance for granitic groundwater systems, the matrix flux term b_B is smaller than the decay term $R_{fB}\lambda_B$ and thus the equilibrium fracture concentration of ^{222}Rn has a strong inverse relationship with transport aperture. The concentration of ^{222}Rn measured in boreholes therefore

allows us to speculate on the likely ranges of transport apertures in situ, provided all other parameters comprising Equation B-3 are well-constrained by independent data.

We consider here the situation whereby ^{226}Ra released from the rock matrix also sorbs on the fracture coatings lining the advective pore space. In this situation, the rate of production of ^{222}Rn is not strictly constant, but also depends on t_w. Assuming that the recoil capture efficiency of surface sorbed ^{226}Ra is close to 100%, the production rate of ^{222}Rn in the fracture coating is given by:

$$p_B = R_{fA}\lambda_A {}^{C}{}_{A(\infty)} \left(1-\exp(-(b_A+R_{fA}\lambda_A)t_w)\right) \quad \text{(B-4)}$$

The steady-state mass balance for ^{222}Rn then can be written as:

$$\frac{\partial c_B}{\partial t_w} = b_B c_{B(eq)} - \left(b_B + R_{fb}\lambda_B\right)c_B + R_{fA}\lambda_A c_{A(\infty)}\left(1-\exp\left(-\left(b_A + R_{fA}\lambda_A\right)t_w\right)\right) \quad \text{(B-5)}$$

It should be noted that the expression *steady-state* here refers strictly to the time rate of concentration change at any specific location along a flowpath. Although the differential equation is written in terms of an advective travel time, this is in simply a proxy for the ratio between flowpath length and advective velocity. Equation B-5 cannot be solved analytically since the variables of concentration and advective travel time are not separable and therefore a numerical integration is required. For sufficiently large t_w, Equation B-5 can be shown to converge to the fracture concentration equilibrium limit:

$$\frac{c_{B(\infty)}}{c_{B(eq)}} \approx \frac{b_B + \dfrac{R_{fA}\lambda_A c_{A(\infty)}}{c_{B(eq)}}}{b_B + R_{fb}\lambda_B} \quad \text{(B-6)}$$

In order to use Equation B-2 and B-6 to make predictions of ^{226}Ra and ^{222}Rn in situ concentrations in situ, it is necessary to define numerical values for the various parameters comprising the mass balance equations. Since many of these parameters are associated with significant uncertainties, we use a stochastic analysis whereby assumed uncertainty distributions are used. Certain parameters are sufficiently well known that constant values can be approximately assigned without introducing significant errors. These parameter values are given in Table B-2. Model parameters associated with significant uncertainties are given in Table B-3.

Using the central best estimates of the uncertainty distributions defined in Table B-3 (i.e. median values of the specified uncertainty distributions), a preliminary simulation was made using Matlab to obtain the steady state concentrations of ^{226}Ra and ^{222}Rn as a function of advective travel time. Although the analytical solution for ^{226}Ra could be obtained directly from Equation B-1, it was necessary to integrate Equation B-5 using a suitable numerical solver to obtain the corresponding curve for ^{222}Rn. The results of this analysis are shown in Figure B-1 and Figure B-2 and indicate that equilibrium activities in the fracture water are typically reached for advective travel times in excess of a few tens of years.

Table B-2. Data constants used in stochastic simulations.

Constant	Value	Description
λ_{238U}	4.92×10^{-18} s^{-1}	Decay constant for ^{238}U ($t_{½}$ = 4.468×10^{9} years)
λ_A	1.37×10^{-11} s^{-1}	Decay constant for ^{226}Ra ($t_{½}$ = 1,602 years)
λ_B	2.10×10^{-6} s^{-1}	Decay constant for ^{222}Rn ($t_{½}$ = 3.823 days)
θ_m	0.18%	Matrix porosity recommended for use in SR-Site /SKB 2010b/
θ_s	10%	Assumed fracture coating porosity (negligible effect of uncertainty)
ρ_r	2,656 kg/m^3	Assumed density of rock matrix (negligible effect of uncertainty)
ρ_s	2,700 kg/m^3	Assumed density of fracture coating (negligible effect of uncertainty)

Table B-3. Uncertainty distributions used in stochastic simulations.

Variable	Distribution	Model parameters	Description/Reference
η_p ($\approx \eta_f$)	Log-uniform	min–max range = 0.01–0.1	Recoil capture efficiency factor Approximate range based on discussions in /Neretnieks 2002/
D_e	Lognormal	$\log_{10} D_e \begin{cases} \mu_{10} = -13.7 \\ \sigma_{10} = 0.2 \end{cases}$	Effective diffusivity (m^2/s) recommended for use in SR-Site /SKB 2010b/
$A_{230\mathrm{Th}}$	Lognormal	$\log_{10} A_{230\mathrm{Th}} \begin{cases} \mu_{10} = 2.34 \\ \sigma_{10} = 0.62 \end{cases}$	^{230}Th activity (Bq/kg) in fracture coating /Sandström et al. 2008/
$m_{238\mathrm{U}}$	Lognormal	$\log_{10} m_{238\mathrm{U}} \begin{cases} \mu_{10} = -5.39 \\ \sigma_{10} = 0.17 \end{cases}$	^{238}U content of rock matrix (ppm) /Sandström and Stephens 2009/
β	Log-uniform	min–max range = 0.1–0.9	Fracture coating fractional occupancy (assumed range)
δ_t	Log-uniform	min–max range = 1×10^{-5}–5×10^{-3}	Fracture transport aperture (m) (assumed range)
R_{fA}	Log-uniform	min–max range = 1–10^4	Fracture retardation factor (assumed range)
K^A_{dm}	Lognormal	$\log_{10} K^m_{dA} \begin{cases} \mu_{10} = -3.62 \\ \sigma_{10} = 0.41 \end{cases}$	Rock matrix K_d (m^3/kg) for Ra sorption recommended for use in SR-Site

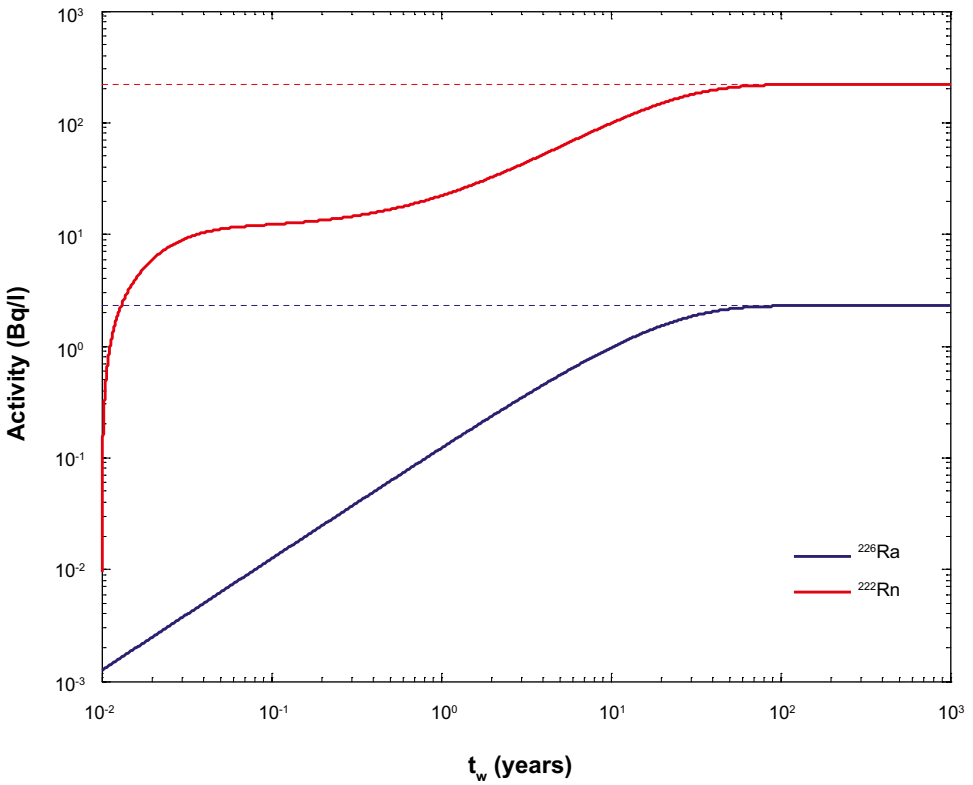

Figure B-1. *Predicted steady-state activity of ^{226}Ra and ^{222}Rn in groundwater as a function of advective residence time (i.e. from the point of origin of infiltrating meteoric water to the groundwater sampling location). A limiting equilibrium condition is reached for residence times greater than a few tens of years as indicated by the horizontal broken reference lines.*

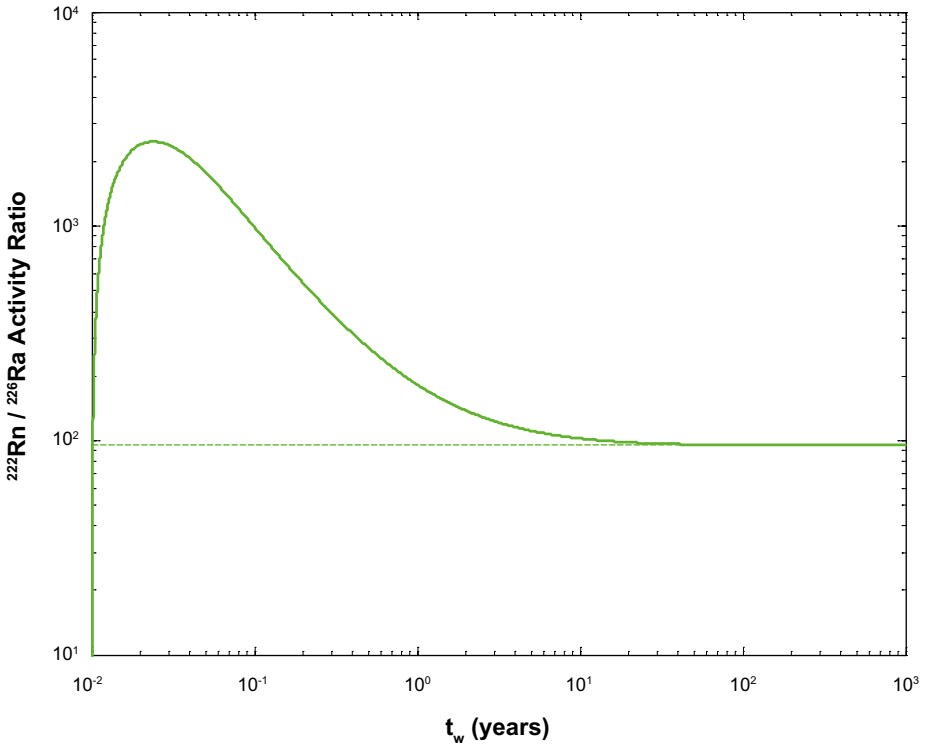

Figure B-2. *Predicted steady-state activity ratio of ^{222}Rn/^{226}Ra in groundwater as a function of advective residence time (i.e. from the point of origin of infiltrating meteoric water to the groundwater sampling location). A limiting equilibrium condition is reached for residence times greater than a few tens of years as indicated by the horizontal broken reference line.*

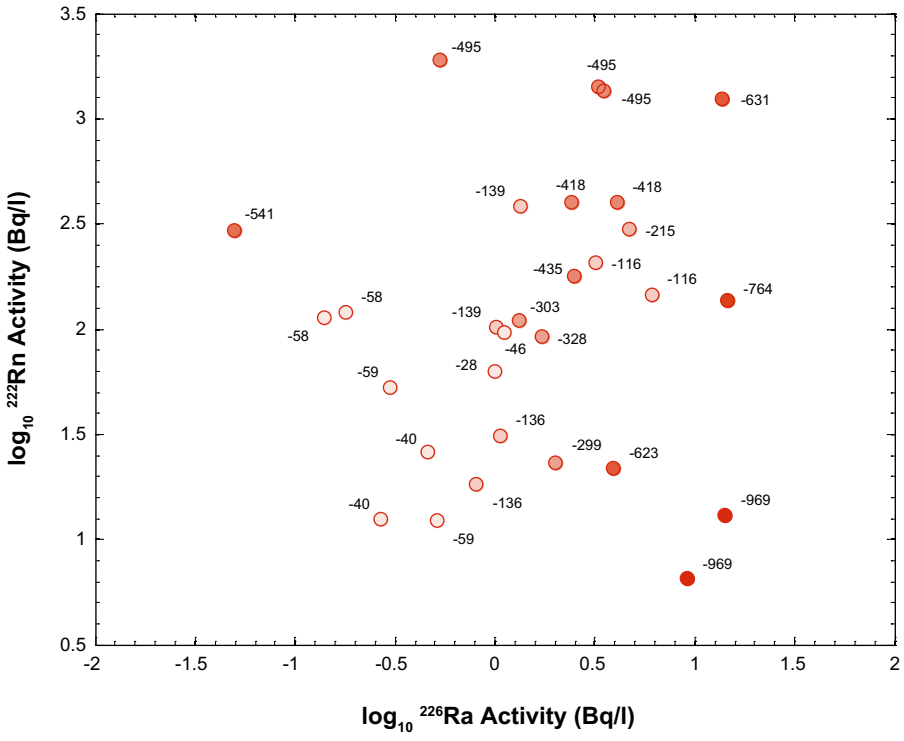

Figure B-3. *Cross-plot of measured activities (Bq/l) of ^{222}Rn and ^{226}Ra in groundwater at the Forsmark site. Markers are coloured according to sampling elevation (masl) with shading darkening towards lower (i.e. deeper) elevations. The actual sampling elevation is annotated in the figure for each data point.*

Typical activities of ^{226}Ra and ^{222}Rn in Forsmark groundwater

There are a number of ^{226}Ra and ^{222}Rn measurements that were made in borehole sections during the Forsmark site investigation /Laaksoharju et al. 2008/. These data are presented in Figure B-3 and Figure B-4 as cross-plots of ^{222}Rn versus ^{226}Ra activity. Error bars are not shown on account their size being typically smaller than the plot markers used to represent the data on a log-log scale. The relative errors of the measurements are, however, roughly 4–6% based on radiometric counting statistics.

Generally, the lower Ca^{2+} concentrations correspond to shallower sampling depths as expected for the site. This is more apparent if the Ca^{2+} concentration data are plotted directly against sampling elevation as in Figure B-5. A plot of the ^{222}Rn/^{226}Ra activity ratio is shown in Figure B-6 and shows very little correlation with depth. It is not known whether the waters sampled in these borehole sections are representative of sufficiently long advective travel times that equilibrium conditions can be assumed. It is interesting to note, however, that the largest ^{222}Rn/^{226}Ra activity ratios are found in two relatively deep borehole sections (KFM02A at –495 m and KFM08A at –541 m). Coupled with the low ^{226}Ra concentrations measured in these borehole sections, it appears likely that these represent borehole sections featuring unusually strong sorption within fracture coatings.

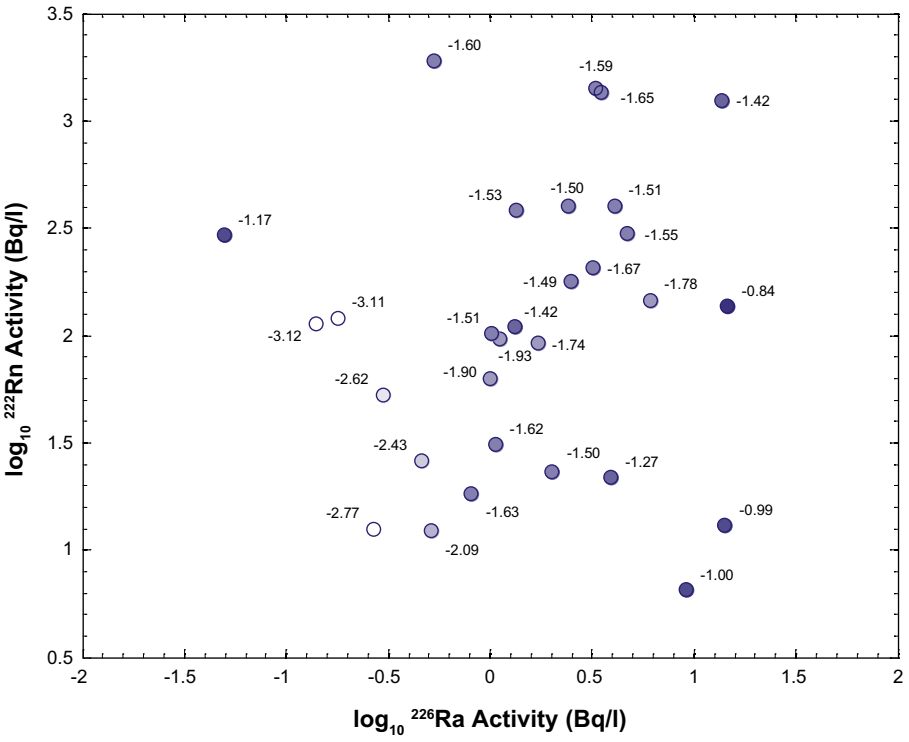

Figure B-4. *Cross-plot of measured activities of ^{222}Rn and ^{226}Ra in groundwater at the Forsmark site. Markers are coloured according to total Ca^{2+} concentration with shading darkening towards higher Ca^{2+} concentrations in the groundwater. The actual log_{10}-transformed Ca^{2+} concentration (mol/l) is annotated in the figure for each data point.*

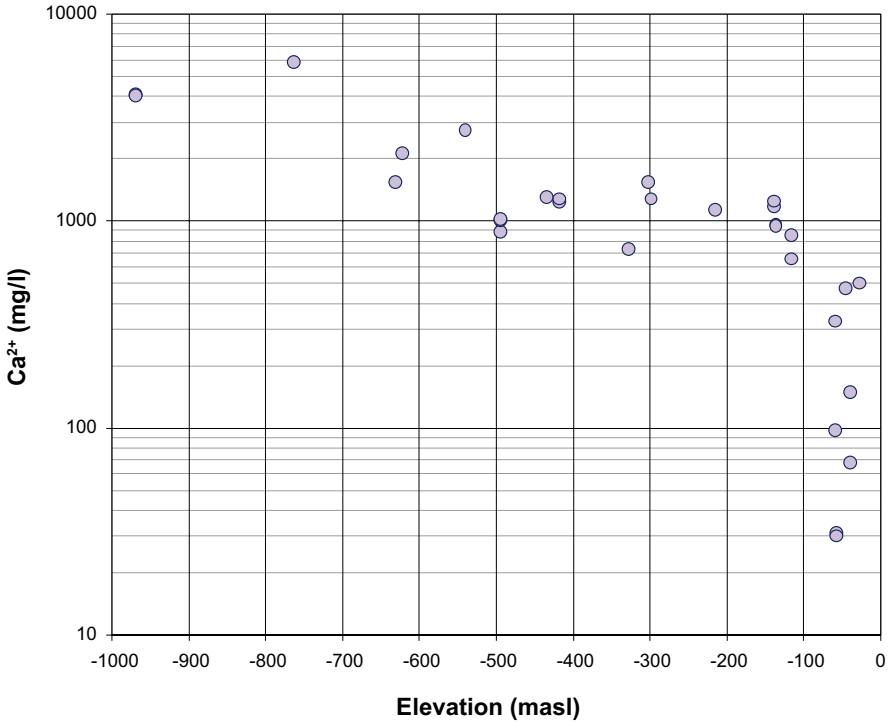

Figure B-5. *Total dissolved Ca^{2+} concentration in sampled borehole sections at Forsmark plotted against sampling elevation (masl).*

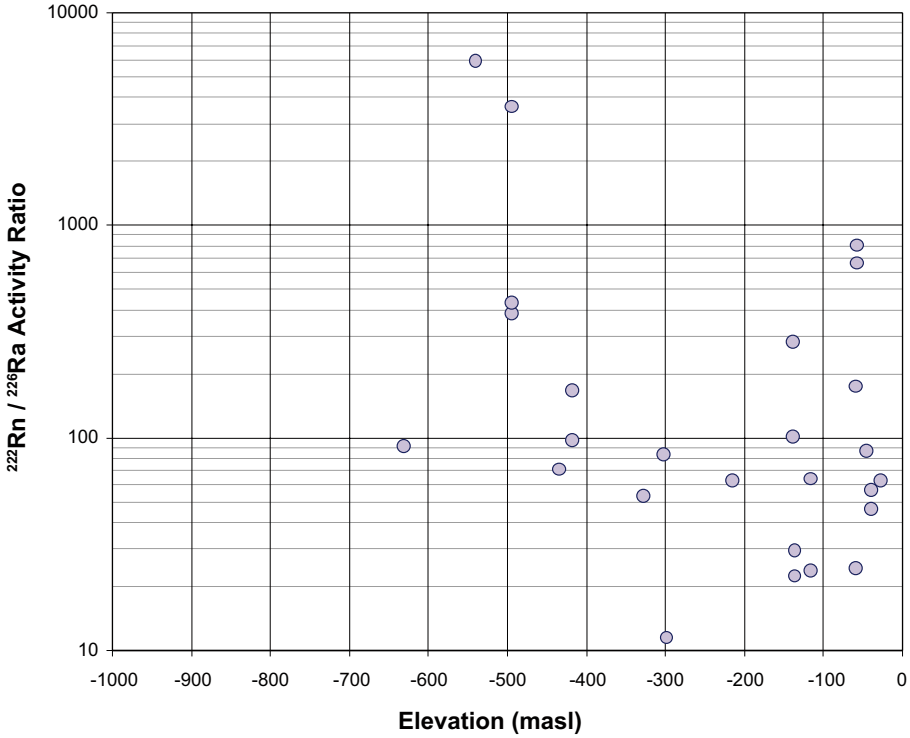

Figure B-6. *$^{222}Rn/^{226}Ra$ activity ratio in sampled borehole sections at Forsmark plotted against sampling elevation (masl).*

Expected equilibrium activities of ^{226}Ra and ^{222}Rn in Forsmark groundwater

The aqueous equilibrium activity of ^{222}Rn and ^{226}Ra in fracture water for the central best estimate data are plotted in Figure B-7 (red circular marker) together with the measurement values from the Forsmark site (blue shaded circular markers). The matrix equilibrium activities of the nuclides ($c_{A(eq)}$ and $c_{B(eq)}$) are indicated by the vertical and horizontal broken reference lines. Many of the variables and parameters that influence the relative activities of these nuclides interact in a complex and non-linear fashion which makes data interpretation difficult. In order to understand these interactions, deterministic simulations were made whereby each of the most important (and least well constrained) variables were individually varied while all other variables and parameters were held constant at their best estimate values. This analysis allows us to understand the systematic effect of the different sources of uncertainty and how they might impact upon predicted in situ activities of ^{222}Rn and ^{226}Ra. The results are shown in Figure B-7 as coloured curves with arrows indicating the direction of increase for each of the variables indicated by text annotations in the figure.

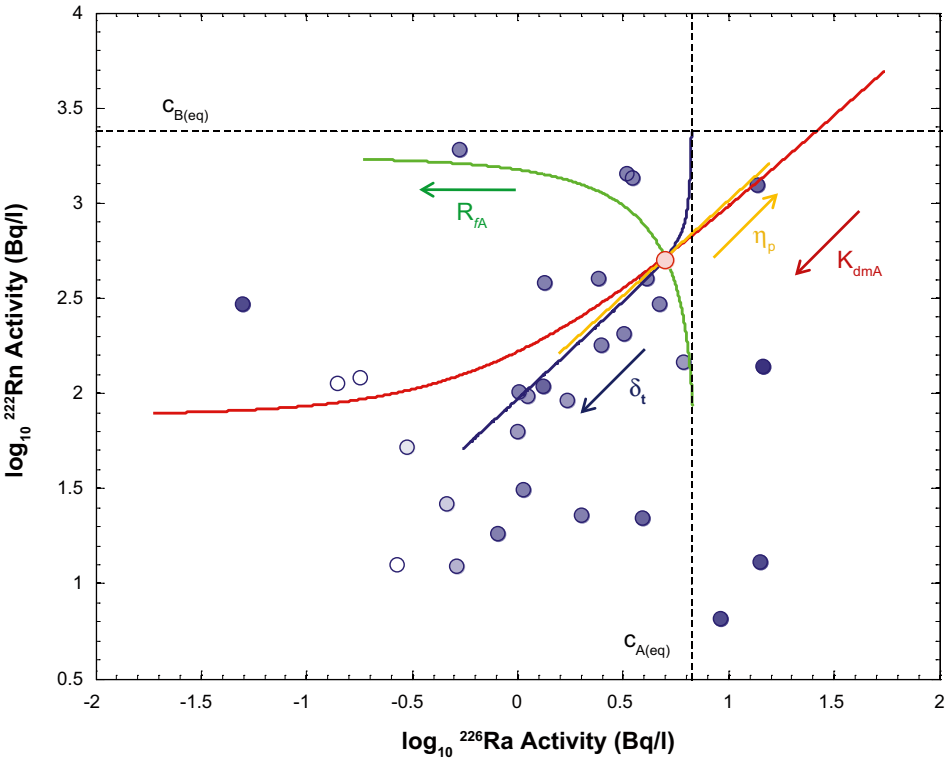

Figure B-7. *Simulated activity trends plotted together with measurement data from Forsmark boreholes. The red circular marker indicates the expected equilibrium ^{222}Rn and ^{226}Ra activity for the central best estimate parameters used previously to generate the curves in Figure B-1. The coloured trend lines indicate the impact of varying the indicated parameters individually while all other parameters are held constant (arrows showing the direction of relative increase). The vertical and horizontal broken lines indicate the rock matrix equilibrium activities of each nuclide. Measurement data points are shaded according to background Ca^{2+} as in Figure B-4.*

The main conclusions that can be drawn from the variation analysis are:

- η_p (recoil capture efficiency factor) affects the aqueous equilibrium activity of both nuclides in the rock matrix and therefore has a direct impact on the concentration driving force for out-diffusion from the rock matrix. Increasing η_p therefore results in a proportional increase in predicted ^{222}Rn and ^{226}Ra activity in fracture water all other things being equal. The orange coloured curve represents η_p varied in the range 0.01–0.1.
- K^A_{dm} (matrix sorptivity of Ra) influences the mobility of Ra in the rock matrix and thereby has a direct impact on the out-diffusion of ^{226}Ra to the fracture water. ^{222}Rn is produced both by decay of ^{226}Ra within the rock matrix and in the fracture itself. Increasing K^A_{dm} therefore decreases the amount of ^{222}Rn that can be produced by decay in the fracture, while production of ^{222}Rn within the rock matrix remains undiminished. This explains the non-linear form of the red coloured curve representing K^A_{dm} varied in the range 10^{-5}–10^{-1} m^3/kg.
- $R_{f\mathrm{A}}$ (equilibrium retardation factor sorbed Ra in the fracture coatings) influences the amount of Ra dissolved in the fracture water while facilitating a higher overall Ra loading in the fracture owing to the retardation of advective transport. Increasing $R_{f\mathrm{A}}$ gives increased production of ^{222}Rn owing to the proportionally larger amounts of ^{226}Ra accumulated in the fracture coatings under equilibrium conditions. There is a limit, however, to the amount of Ra that can be accumulated in the fracture coatings (owing to the finite amount of Ra that can be mobilised from the rock matrix) which gives a diminished impact on ^{222}Rn production beyond a certain level. This explains the non-linear form of the green curve representing $R_{f\mathrm{A}}$ varied in the range 1–10^4. In the absence of sorption on fracture coatings, the ^{226}Ra activity in the fracture approaches the limit given by the rock matrix equilibrium activity as indicated by the asymptotic behaviour near the vertical broken line representing $c_{A(eq)}$.
- δ_t (fracture transport aperture) has a strong impact on ^{222}Rn activity in the fracture water owing to the interplay between out-diffusion from the rock matrix and relatively fast decay. This explains the non-linear form of the dark blue curve representing δ_t varied in the range 10 µm–5 mm. For very low transport apertures, the activity in the fracture approaches the limit determined by the rock matrix equilibrium activity as indicated by the asymptotic behaviour near the horizontal broken line representing $c_{B(eq)}$.

In a recent paper /Vinson et al. 2009/ suggest that the measured ratio of ^{222}Rn/^{226}Ra in groundwater is proportional to the K_d value for Ra. This, however, is only strictly true deep within the rock matrix or in the limit of very low transport aperture with weak or no sorption on fracture coatings (or alternatively, very high matrix pore diffusivity as might be found in sedimentary rock). For realistic conditions at the Forsmark site, the ^{222}Rn/^{226}Ra ratio cannot be interpreted simply in this fashion.

Since the governing variables partially offset or reinforce each other and generally interact in an essentially non-linear fashion, it is very difficult to determine whether the independently measured activities of natural tracers at Forsmark are consistent with ranges of K_d recommended for use in SR-Site (i.e. for the purpose of modelling Ra transport from a repository for spent nuclear fuel). If such a comparison were possible, this would be very valuable for corroboration of recommended K_d data and a broad indication of the robustness of the extrapolation methods used in the present data compilation.

In order to address this question, stochastic simulations were made using the uncertainty distributions specified in Table B-3. As demonstrated by the deterministic simulations shown in Figure B-7, these variables are relatively poorly constrained considering the impact that they might have on expected ^{222}Rn and ^{226}Ra activities. As a first step in this analysis, variables were assigned values stochastically from their assumed uncertainty distributions with the exception of K^A_{dm} which was set at different constant levels ranging from 10^{-4} m^3/kg (weak sorption) to 10^{-1} m^3/kg (strong sorption). The intention of this was to gain an appreciation of the impact of radium matrix sorptivity while simultaneously considering all other known uncertainties. The results of these simulations are shown in Figure B-8 where the data are presented as a probability density for an ensemble of 10^5 realisations. The probability density is represented as a smoothed 2D histogram with 100 equally spaced bins along the principle axes of the figure.

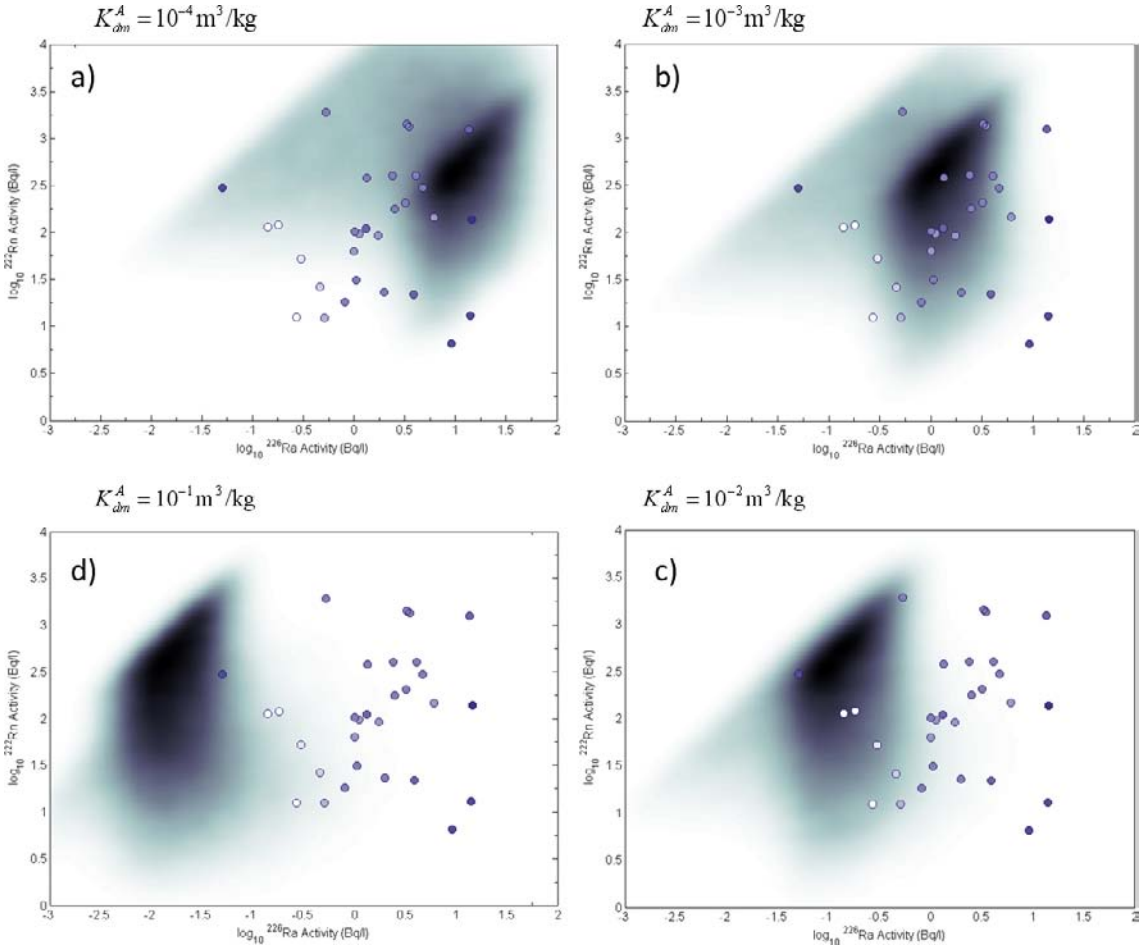

Figure B-8. *Expected activities of ^{222}Rn and ^{226}Ra activities plotted together with measurement data from Forsmark boreholes. The simulation data presented as probability densities with darker shading indicating most likely data ranges (10^5 realisations) in the simulation ensemble. The figures show clockwise from a) to d), the impact of increasingly strong sorption of Ra in the rock matrix. The measurement data points are shaded according to background Ca^{2+} concentration as in previous figures.*

In the second step, all variables were assigned values stochastically from their assumed uncertainty distributions including K^A_{dm} which was assigned directly from the lognormal distribution recommended for use in SR-Site. Figure B-9 shows the result of the ensemble simulations where all known sources of uncertainty are considered simultaneously. From Figure B-8, it is clear that the most appropriate value of K^A_{dm} giving best agreement with the measurement data lies somewhere between 10^{-3} and 10^{-4} m^3/kg. It is also interesting to note that the measurement data featuring with the lowest ^{222}Rn and ^{226}Ra activities (bottom left hand quadrant of the measurement data cluster) are also associated with the lowest background concentrations of Ca^{2+}. This appears consistent with the understanding of Ra(II) sorption which predicts greater ion-exchange sorptivity under increasingly dilute conditions.

As can be seen from Figure B-9, the probability distribution of predicted ^{222}Rn and ^{226}Ra activities agree relatively well with the measurement data when the SR-Site recommended K_d distribution for Ra(II) is used in the simulations. In a probabilistic sense, the expected activity ranges for both ^{222}Rn and ^{226}Ra appear to be neither overestimated nor underestimated by a significant margin. On the basis of this analysis, and assuming that the uncertainties of other governing variables are reasonably assessed, we therefore conclude that the recommended K_d data for Ra(II) are both reasonable and defensible for application in SR-Site.

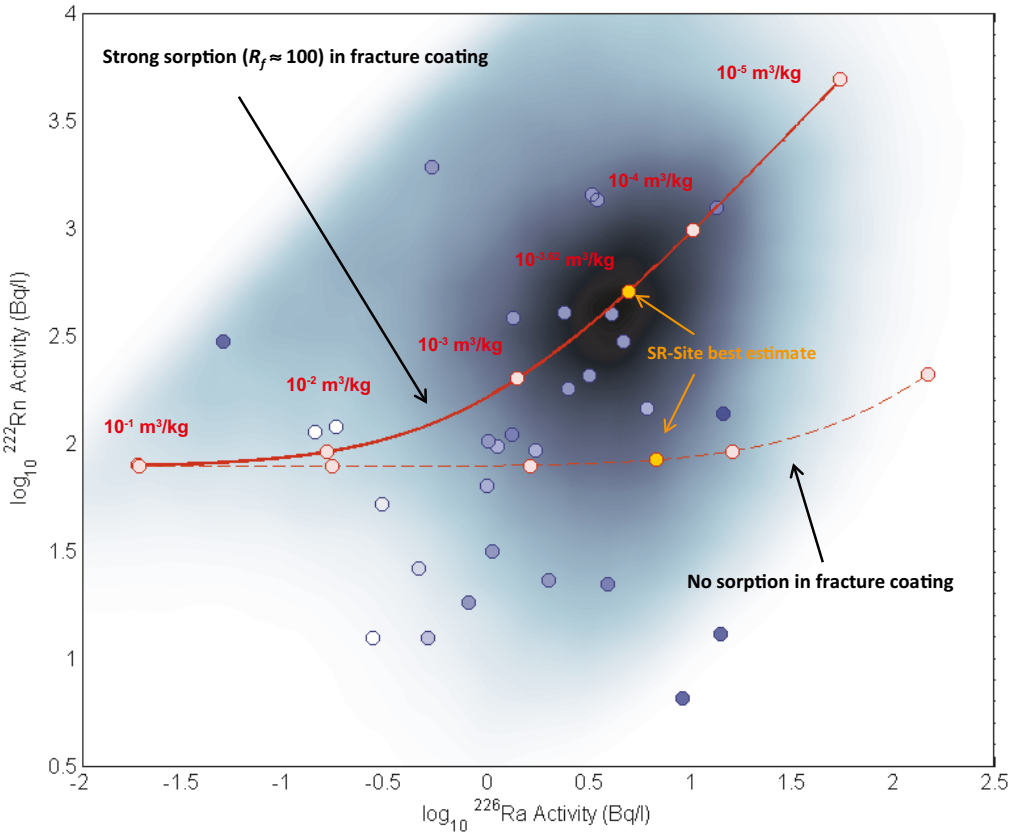

Figure B-9. *Expected activity distributions of ^{222}Rn and ^{226}Ra activities plotted together with measurement data from Forsmark boreholes. The simulation data are presented as a probability density with darker shading indicating the most likely activity ranges (10^5 realisations) in the simulation ensemble. The red curve designates the locus of best estimate activities for the specified K_d values (red markers). The SR-Site best estimate is indicated in yellow shading. The measurement data points (blue circular markers) are shaded according to background Ca^{2+} concentration as in previous figures.*

Owing to natural variability in the fracture system, it appears unlikely that narrower uncertainty estimates of transport aperture and fracture retardation are possible to achieve. On the other hand, the uncertainty distribution for the recoil capture efficiency factor, η_p could be improved significantly by measurement of radon out-diffusion from core samples of Forsmark site specific rocks. Although the theoretical estimates of η_p given by /Neretnieks 2002/ agree with values cited by /Glynn and Voss 1999/ for groundwaters near the Äspö HRL (η_p in the approximate range 0.1–10%), it is noted that measurements from other sites (e.g. /Przylibski 2000/) indicate that higher η_p values are sometimes possible. If η_p for the Forsmark site specific rock types has been underestimated, this would necessitate numerically larger K^A_{dm} values to accommodate the same fit with the measurement data. More accurate empirical data for Forsmark rock types therefore has the potential to result in possibly increased recommended K_d values for Ra.

Appendix C

Handling of literature data uncertainties

Since many of the literature data sets outlined in Table 3-6 are based upon relatively small sample sizes, it was deemed necessary to develop specialised procedures to aid in the estimation of realistic uncertainty bounds. As already noted in Section 3.2.4, this was achieved primarily through the use of statistical resampling methods. This appendix provides a step-by-step account of the specific procedures which have been used in these particular cases.

When data sets are comprised largely of replicate measurements representing a limited range of experimental conditions, a small spread of K_d values is typically obtained which may not give a true representation of the underlying data uncertainty. In many cases, the variance of the data set may even be less than the error of individual estimates arising due to measurement uncertainties. For this reason, the uncertainties of individual measurements have been formally propagated in the analysis together with the additional uncertainties associated with the transfer factors used to extrapolate the data to site-specific conditions.

In the Finnish literature data references /Kulmala and Hakanen 1993, 1995, Huitti et al. 1996, 1998, Kulmala et al. 1996, 1998/, R_d data are given without error estimates and in some cases are reported as "≥" relative to a specified value owing to issues relating to the upper limit of quantification. The associated sorption percentages (S%), however, are given together with specified error estimates based on radiometric counting statistics. The percentage sorbed is calculated by a radiometric mass balance based on the initial and the final activity of the sorbing solute. Unlike the method used in the site investigations (i.e. spiking with a radiolabeled stock solution), the radionuclide *spikes* in these cases were prepared by evaporating an acidified solution of known activity to dryness onto Teflon strips which were then placed with the rock-groundwater samples that had been pre-equilibrated for some time. At the conclusion of the experiments, the remaining activity of the Teflon strips was measured and the decay-compensated data used in a radiometric mass balance to estimate the percentage sorbed:

$$S(\%) = \frac{\frac{A_{tracer} - A_{teflon}}{V} - \frac{A_{sample}}{V_{sample}}}{\frac{A_{tracer} - A_{teflon}}{V}} \cdot 100\% \qquad \text{(C-1)}$$

Where,

A_{tracer} = activity of the original dried Teflon platelet,
A_{teflon} = remaining activity on the Teflon platelet (i.e. undissolved),
A_{sample} = activity of the sampled solution,
V = total volume of the contact solution,
V_{sample} = volume of the sampled solution.

The R_d data are estimated in terms of the percentage sorbed, S(%) which is also calculated using a mass balance:

$$R_d = \frac{S(\%)}{100 - S(\%)} \cdot \frac{V}{m} \qquad \text{(C-2)}$$

The term V/m in Equation C-2 is the liquid to solid ratio (LS) in units suitable for estimating R_d in the customary units of m^3/kg. In general, the uncertainty in percentage sorbed has a highly non-linear impact on the estimation of R_d. Since S(%) is confined to the interval 0%–100%, it is proper to assume a Beta distributed uncertainty range for a specified mean and standard deviation of this variable. An illustration of the non-linear relationship between R_d and S(%) is given in Figure C-1 under the assumption of Beta-distributed S(%).

As can be readily appreciated from Figure C-1, the closer one gets to 100% sorption, the larger the uncertainty of the estimated R_d value. This is a particular problem for strongly sorbing solutes when the data are presented in this manner, since the percentage sorbed is typically very close to 100% in the relevant pH range of interest thereby giving a large upper uncertainty bound for the R_d estimate.

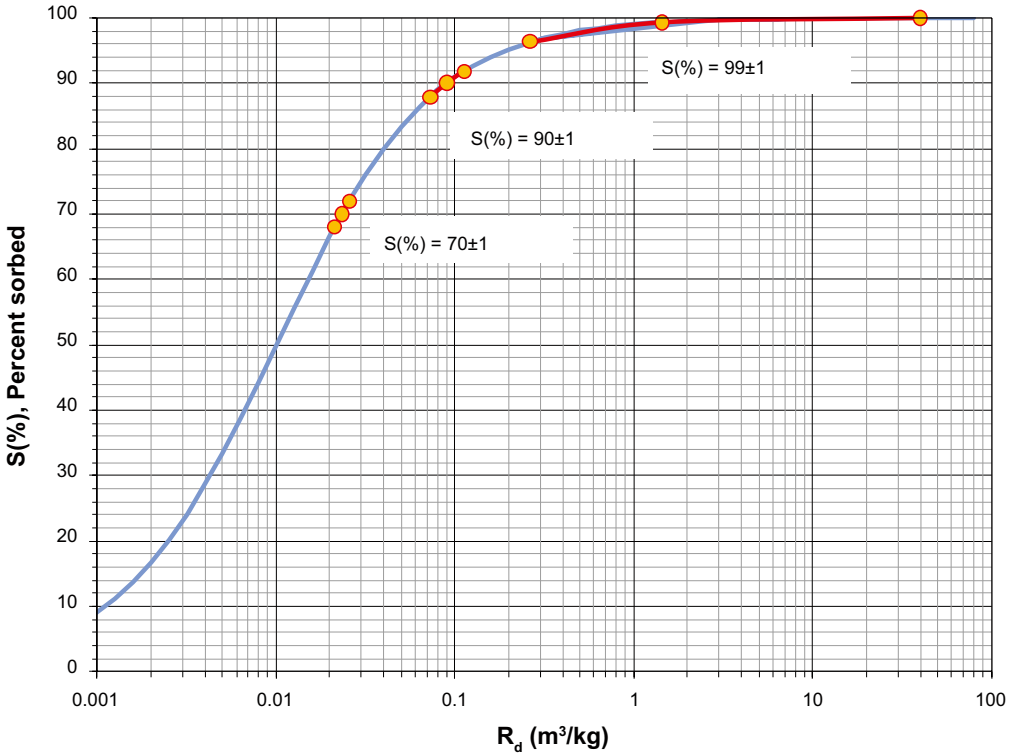

Figure C-1. *Illustration of the relationship between percentage sorbed, S(%) and R_d (m3/kg) for various cases of S(%) specified as a mean and standard deviation and for a liquid to solid ratio of 10 ml/g. R_d prediction spans are given as the median and 95% confidence interval.*

There is, of course, an upper limit to S(%) that will always fall short of 100%. This is given by the method detection limit (MDL) for the analytical method used to quantify activity (or concentration) in the sampled contact solution. In most of the cases examined in this compilation, the MDL is not known or at least not specified in the particular reference. Although the literature data used in this compilation are generally considered to be of relatively high quality, the form of the reported values and the typically small number of replicates is not always ideal for making safety assessment recommendations.

In order to obtain numerical ranges of R_d including uncertainty estimates suitable for application in safety assessment, a re-calculation procedure was adopted. This was based upon a Monte-Carlo approach whereby a large number of Beta-distributed random deviates were generated for each S(%) data point with specified uncertainty and then the corresponding R_d values were calculated with the aid of Equation C-2. In order to do this, the parameters of the Beta distribution, $B(\alpha, \beta)$ must be estimated. If S(%) is normalised to the interval S[0,1], the a and b parameters can be estimated using the following formulae /NIST 2010/:

$$\alpha = S\left(\frac{S(1-S)}{\sigma_S^2} - 1\right) \tag{C-3}$$

$$\beta = (1-S)\left(\frac{S(1-S)}{\sigma_S^2} - 1\right) \tag{C-4}$$

Figure C-2 shows a typical result obtained for two cases of a specified S(%) with a given uncertainty and an LS ratio of 10 ml/g which is common in the cited literature references. As can be seen from the Figure, the lower S(%) estimate of 90±1% gives a resulting R_d uncertainty distribution that is relatively narrow (–1.04±0.05) and well described by the lognormal distribution, whereas an S(%) estimate of 99±1% gives a broad (0.25±0.6), right skewed distribution that is not well modelled by the lognormal fit.

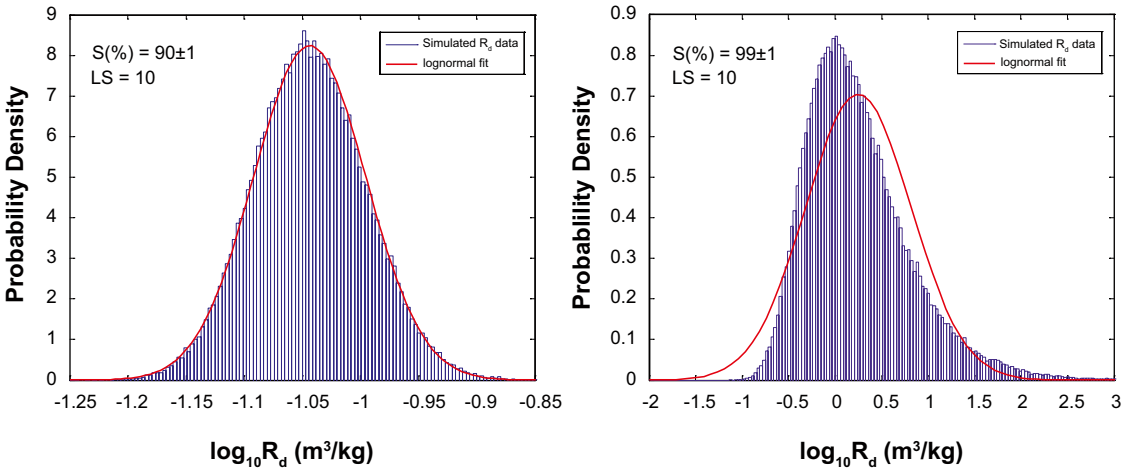

Figure C-2. *Typical results obtained in Monte-Carlo re-calculation of R_d values based on sorption percentages specified with a given uncertainty and an LS ratio of 10 ml/g.*

After re-calculation of the individual R_d values and their uncertainty ranges, the raw data are then individually extrapolated to in situ conditions using the mechanical and CEC transfer factors (f_m and f_{cec}). Since the transfer factors themselves are uncertain, the estimated errors of the transfer factors are propagated formally in the calculations using Gauss error propagation rules and assuming no correlation between f_m and f_{cec}. The transfer factor corrections and the error calculations are carried out on the log-transformed R_d values. Although some of the individual data points featuring high sorptivity may have uncertainty distributions featuring significant right-hand skew (in log-space), the assumption of log-normality is considered reasonable since the propagation of uncertainties and aggregation of data tends to give rise to lognormal behaviour by way of the central limit theorem.

In this compilation we have taken the view that the overall uncertainty of the ensemble of K_d estimates in a data set is best represented by assuming a convex combination of the underlying (assumed) log-normal uncertainties where equal weighting is given to each data point (i.e. a Gaussian mixture model for uncertainty aggregation in log space). This is achieved by random sampling of the individual K_d uncertainty distributions where the overall distribution is then obtained as the ensemble of resampled values. The best way to illustrate this is to demonstrate the procedure by way of an example. Table C-1 shows a particular data set taken from /Kulmala and Hakanen 1995/ which concerns sorption of Ra(II) on a porphyric granodiorite in contact with a natural sample of fresh groundwater. Although not atypical, this data set is interesting in that it exhibits a number of features that illustrate the consequences of the various assumptions made in the extrapolation to in situ conditions which are relevant to the estimation of overall uncertainty.

Table C-1. Example of a typical data set taken from a literature source (in this case sorption of Ra(II) on Kivetty porphyric granodiorite in contact with fresh groundwater /Kulmala and Hakanen 1995/). The raw data R_d values are first re-calculated by Monte-Carlo to obtain their associated uncertainties under the assumption of Beta-distributed S(%). The transfer factors, f_m and f_{cec} and their estimated errors (2σ) are based on the BET surface area and CEC of the literature data samples relative to the Forsmark metagranite reference rock type. Extrapolated K_d values and their uncertainties are obtained by Gauss error propagation in log space.

d (mm)	LS (ml/g)	S(%)	$\log_{10} R_d$ (m^3/kg)	$\log_{10} f_m$ (–)	$\log_{10} f_{cec}$ (–)	$\log_{10} K_d$ (m^3/kg)
< 0.1	5	98.3±1.0	–0.459±0.285	–2.10±0.23	–1.04±0.37	–3.59±0.52
< 0.1	10	99.2±0.1	0.097±0.055	–2.10±0.23	–1.04±0.37	–3.04±0.43
< 0.1	50	96.3±0.4	0.117±0.049	–2.10±0.23	–1.04±0.37	–3.02±0.43
< 0.1	100	94.8±0.7	0.265±0.062	–2.10±0.23	–1.04±0.37	–2.87±0.43
< 0.1	200	89.0±0.5	0.209±0.022	–2.10±0.23	–1.04±0.37	–2.93±0.43
< 2.0	10	93.5±0.2	–0.842±0.014	–1.06±0.23	–1.04±0.37	–2.93±0.43

Figure C-3 shows the re-calculated R_d data plotted in the form of probability density functions (PDF's) for each of the six data points given in Table C-1. Also shown is the ensemble cumulative distribution based on a resampling of the underlying uncertainty distributions and best estimate PDF based on the mean and standard deviation of the resampled values. For comparison a "naive" PDF is shown which is based simply on the mean and standard deviation of the six central estimate values without additional consideration of the individual measurement uncertainties. There are several features in this data set that are interesting to note. Firstly, the apparent outlier in the case of the first narrow peak on the left-hand side of the figure represents the data point for the size fraction given as < 2.0 mm in Table C-1. The smaller R_d in this case reflects the smaller accessible sorptive surface area equilibrated in the 21 day contact time used in the experiments. It is not possible to say from the reported data whether this is due to diffusive disequilibrium or strictly a surface area scaling effect related to particle size. In all likelihood the reduced R_d value represents a mix of these two confounding factors.

A further feature of note is the apparent increase in K_d with increasing LS ratio. Although the differences are for the most part relatively small, this is a typical behaviour in laboratory measurements referred to as the *solids concentration effect* /McKinley and Jenne 1991/. Different mechanisms have been proposed to explain this since theoretically for an ion exchange or surface complexation sorption mechanism, the R_d should be constant for a single binding site type, dilute radionuclide concentration, and a constant contact solution composition. In some cases, drift in solution composition or co-precipitation processes might be responsible for this effect. In the present case, these explanations seem unlikely since Ra(II), being an ion-exchanger, is not strongly influenced (at least not directly) by pH or carbonate, nor does it seem likely that ion-exchange reactions should lead to a significant drift in the major cation composition of the contact solution. Solid solutions involving radiobarite can also be reasonably ruled out by consideration of the contact solution compositions with regard to barite equilibrium. Although it is not possible to say with certainty what the true cause is, we prefer the explanation by /McKinley and Jenne 1991/ that explains the trend as a result of a number of different binding sites with different sorption affinities giving rise to Freundlich isotherm behaviour.

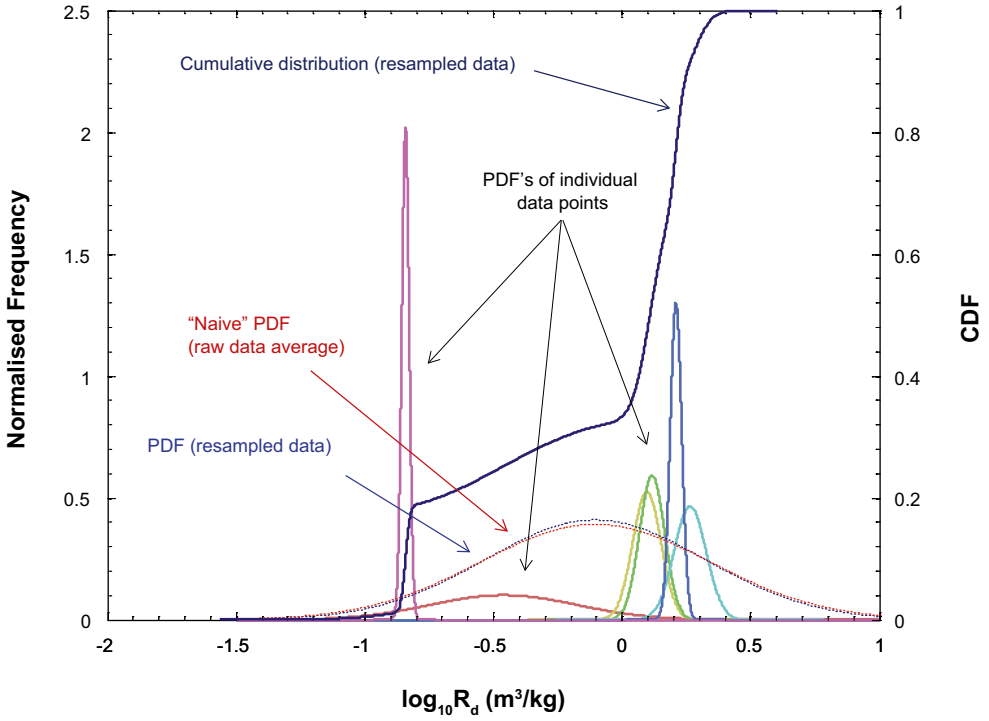

Figure C-3. *Estimated uncertainty distributions (PDF's) for the individual R_d values prior to extrapolation (based on the data in Table C-1) together with the resampled cumulative ensemble distribution (CDF). Also shown is the "naive" PDF (broken red curve) based on the mean and standard deviation of the central values only and the best estimate PDF (broken blue curve) for the R_d data where the underlying uncertainties are included in the calculation.*

A third feature of importance for the estimation of uncertainty is the very broad low peak, centred roughly at –0.46 in Figure C-3 (corresponding to the first data point in Table C-1). The importance of this data point becomes more obvious when the raw R_d values are extrapolated to site-specific conditions using f_m and f_{cec}. It should be noted that the CEC transfer factor, in particular, is very uncertain since the CEC of the site specific rock types is not known accurately and the CEC of the rock in the cited reference is assessed using a different analytical technique. Furthermore, the CEC of the larger particle size is also unknown and the value for the smaller size fraction must be used instead for this calculation. Figure C-4 shows the results of the extrapolation and resampling procedure.

Although the formal error propagation gives relatively wide uncertainty estimates for the individual K_d values extrapolated to site-specific conditions, the spread of the extrapolated central estimates is very small. As can be seen from Figure C-4, the extrapolated and resampled uncertainty distribution is somewhat broader than the "naive" extrapolated distribution. Moreover, the statistical dispersion in the naive PDF can be shown to be largely due to a single outlying data point (the low peak centred at –0.46 in Figure C-3). What is interesting about this particular peak is that it appears to be a "fluke" since all the other data values, including that for the larger size fraction, are very tightly clustered. Perhaps, however, the tight clustering of the other data points is the fluke and in the event that the outlier had not been measured, the uncertainty would then have been underestimated by a large margin. The impact of this single data point can be illustrated by removing the outlier and recalculating the extrapolation as shown in Figure C-5.

As can be seen in Figure C-5, removing the single outlying data point has a large impact on the statistical dispersion of the estimated uncertainty distribution. When the uncertainties associated with the individual measurement values and the transfer factors are propagated in the calculation, however, the resulting uncertainty distribution is much less sensitive to the existence or non-existence of individual data points. Although no individual data points are actually excluded in the data analysis for representative rock types presented in this compilation, this example does show the potential for underestimation of uncertainty ranges in small data sets if the underlying uncertainties are not handled properly in the data extrapolation procedure.

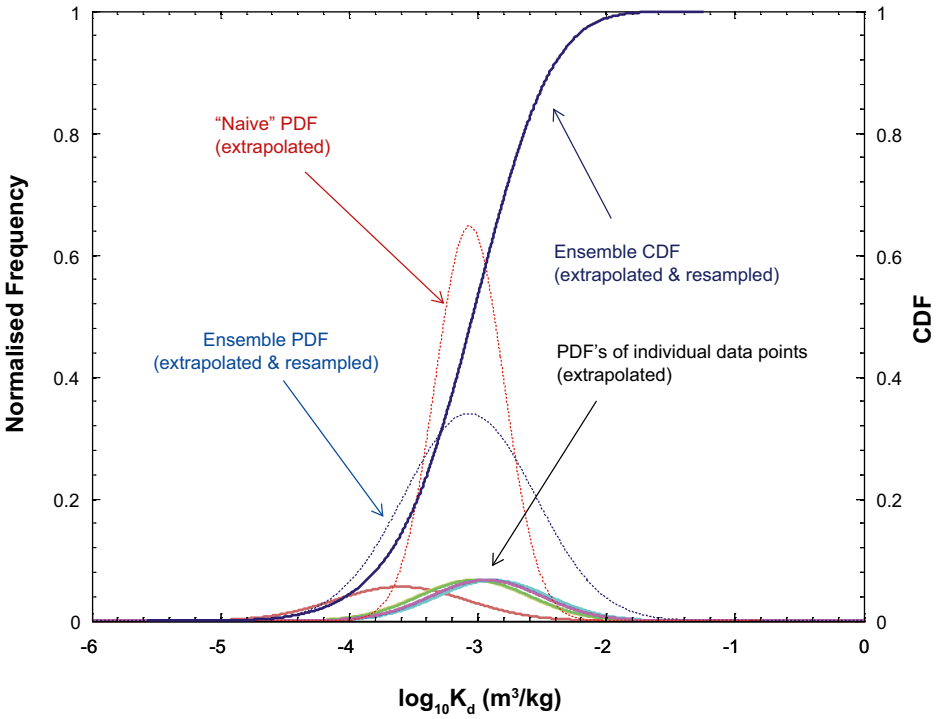

Figure C-4. *Estimated uncertainty distributions (PDF's) for the individual R_d values after extrapolation where the various uncertainties are formally propagated in the calculation (based on the data in Table C-1) together with the resampled cumulative ensemble distribution (CDF). Also shown is the "naive" PDF (broken red curve) based on the mean and standard deviation of the corrected central values (without consideration of the underlying measurement or transfer factor uncertainties) and the best estimate PDF (broken blue curve) which is based on the extrapolated and resampled data with all uncertainties included in the calculation.*

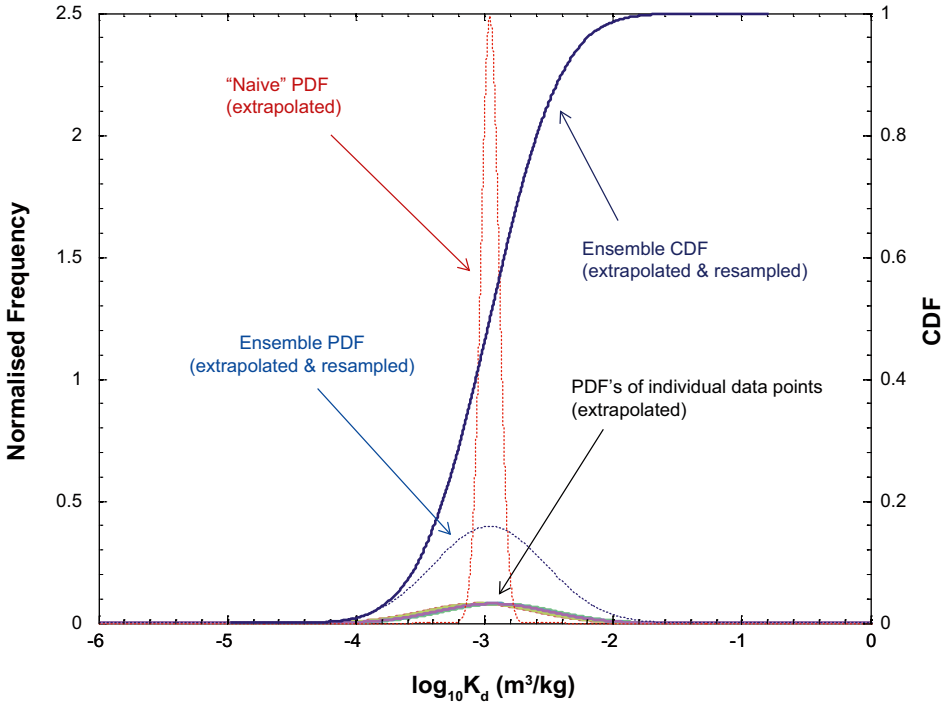

Figure C-5. *Estimated uncertainty distributions as described previously in Figure C-4, although with the outlier data point removed resulting in a much narrower uncertainty range for the naive PDF (broken red curve). Although the Ensemble CDF and PDF have slightly reduced uncertainty ranges, the change is relatively minor since the underlying measurement and extrapolation uncertainties dominate the overall uncertainty.*

It was deemed that full propagation of data uncertainties in this manner was not necessary for the site specific data on account of the much larger data sets available implying a much smaller probability of fluke measurements significantly influencing the results. Another reason is that the transfer factors for site specific materials are considered to be more accurate than those calculated for literature data since the materials have been characterised using largely identical methods. Consequently, the uncertainty of the extrapolation is a smaller component of the overall data uncertainty and could be reasonably neglected for the site investigation data. Also, since the physical interpretation of the transfer factors themselves is subject to additional conceptual uncertainty it was thought that formal propagation of errors might lead to physically unrealistic uncertainty ranges with the concomitant possibility of risk dilution in stochastic simulations. Given that the uncertainty ranges in most cases already cover 2–4 orders of magnitude prior to propagation of underlying uncertainties, this was considered a reasonable judgement.

In general, however, the increased uncertainty range obtained by full propagation of the underlying uncertainties only makes a minor contribution to the uncertainty ranges estimated for the site specific data. Figure C-6 shows the impact of neglecting underlying uncertainties for the calculation of the K_d uncertainty ranges for Ra(II) and Am(III) using the site specific data. In both cases, the increase in statistical dispersion is relatively small, although slightly larger for Ra(II) since this was a smaller data set than that for Am(III).

The data for Ra(II) consist of 75 data points representing different size fractions, contact times, and replicate measurements for the Forsmark saline reference groundwater. Ra(II) was one of the solutes where ion-exchange modelling could be used to estimate a chemistry transfer factor, f_{chem} to account for spatial variability and uncertainty in the application groundwater compositions. As well as the shift implied by the central value of f_{chem}, the uncertainty distribution of the transfer factor introduces additional dispersion in the K_d range recommended for application groundwater conditions (3,000 y in the temperate domain). It should be noted that the uncertainty range for Ra(II) depicted in Figure C-6

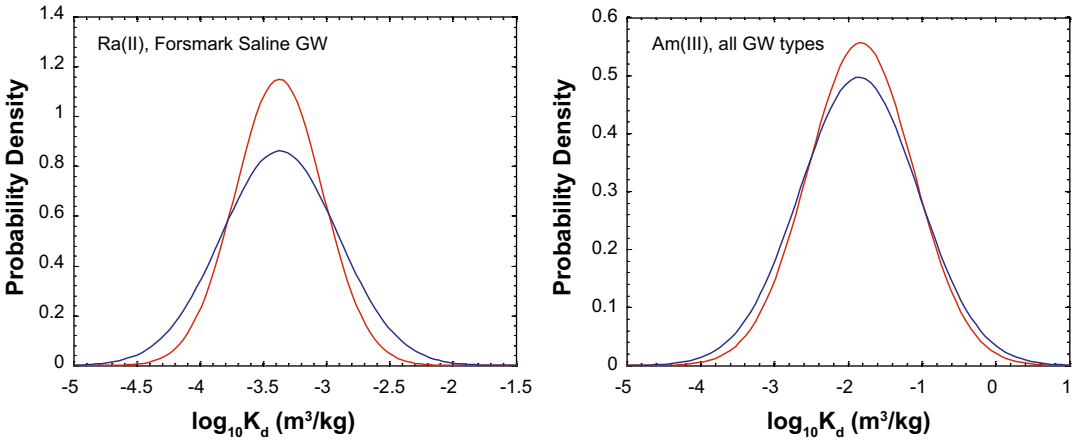

Figure C-6. *Estimated uncertainty distributions for Ra(II) and Am(III) based on site specific data. The red curve shows the uncertainty distribution calculated without formal propagation of underlying measurement and transfer factor uncertainties. The blue curve shows the uncertainty distribution calculated with full propagation of uncertainties.*

is prior to convolution with the f_{chem} transfer factor which results in a slightly expanded range for the uncertainty estimate. The data for Am(III), on the other hand, consists of 2,063 data points representing different size fractions, contact times, and replicate measurements for all groundwater compositions pooled together as an ensemble. In this case, the increase in statistical dispersion obtained by formally propagating the underlying uncertainties is negligible.

Appendix D

K_d data derivation sheet for trivalent actinides and lanthanides

Overview and evaluation of site investigation data

Site specific sorption data were obtained for Am(III) and Eu(III) during the site investigations at Forsmark /Byegård et al. 2008/ and Laxemar /Selnert et al. 2009/. These data are summarised in the bedrock transport properties site descriptive model /Crawford 2008/ and are the basis for K_d values recommended for use in SR-Site. Owing to the close geochemical analogy amongst the various trivalent actinides and lanthanides, the experimental R_d data for both Am(III) and Eu(III) were pooled and are assumed to be applicable to all solutes falling into this category. In most cases there is a time dependency in the experimental data with a clear trend towards higher R_d values at increasing times. The data also exhibit a relatively clear surface area dependency whereby smaller crushed particle sizes are associated with larger sorptivities than larger particle size fractions. A typical time series for Am(III) sorption on Forsmark metagranite (SKB rock code 101057) is shown in Figure D-1.

Since the R_d value is quantified by way of a radiometric mass balance, any discrepancy in the activity estimated for the blank sample (a triplicate measurement) relative to that of the rock-containing sample has a direct impact on the estimated magnitude of sorption. This might be the reason for the slight dip in R_d at a contact time of 92 days as can be seen for all three size fractions in Figure D-1.

If the apparent time dependency were to be interpreted as a diffusive disequilibrium process, the lack of tendency to plateau to a constant value would normally suggest that none of the particle size fractions have reached diffusive equilibrium for the range of contact times investigated. The relatively even vertical spacing of the data sets in log-log space, however, is not fully consistent with a simplified model of particle diffusion where sorption also occurs on external surfaces of the crushed particles. Since smaller crushed size fractions are expected to have a greater proportion of external surface area relative to that of their internal microporosity, the slope of the diffusive uptake curve would be expected to be steeper for larger particle size fractions. This is because smaller particle sizes, having a larger proportion of external surface area, are proportionally less affected by diffusive disequilibrium involving internally accessible surfaces.

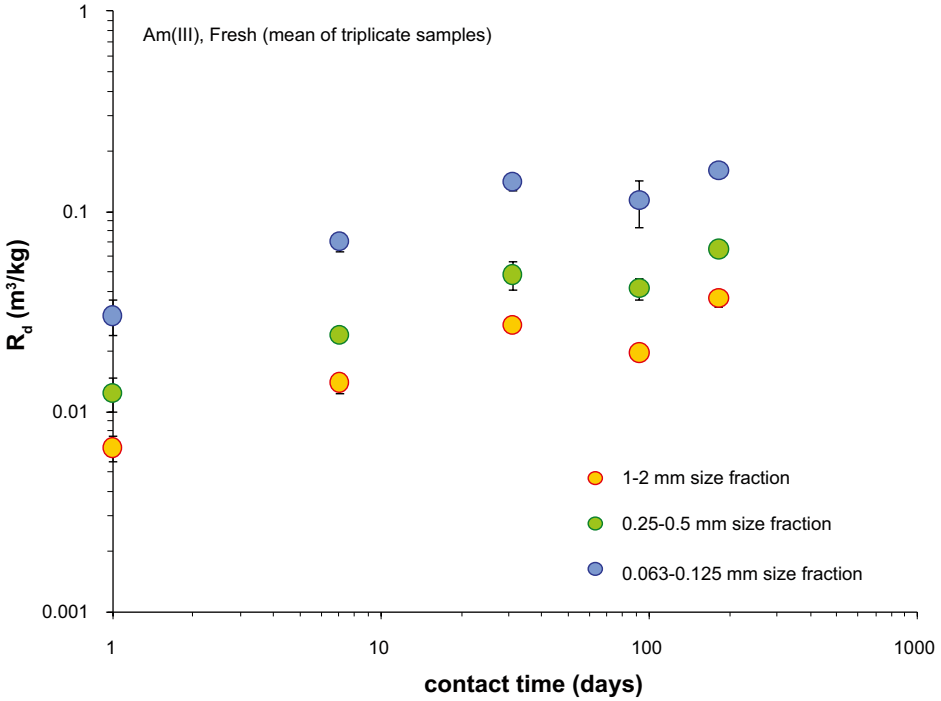

Figure D-1. *Typical time series for Am(III) sorption R_d (m^3/kg) measured in the Forsmark site investigation laboratory studies. There is a clear sorption dependency on both particle size and time. The slight dip in R_d at the second last sampling time relates to the radiometric mass balance method used to quantify sorption using blank samples (see text for explanation).*

The relative slopes of the time series curves for different size fractions are also difficult to reconcile with a bimodal diffusion process where sorption occurs primarily in association with an accessory mineral such as biotite. If this were the case, there would not be such a large effect of surface area since the average biotite content of the rock should be roughly the same in all size fractions (even allowing for minor differences in biotite enrichment in different grain sizes). It is also noted that owing to the large hydrated radius of trivalent actinides and lanthanides, inter-lamellar diffusion into individual biotite grains does not seem a particularly plausible scenario and any association with biotite would therefore be mostly restricted to frayed edge sites (FES).

In /Kienzler et al. 2009/ sorptive uptake of Am was studied on core sample monoliths obtained from the Äspö Hard Rock Laboratory (HRL). In the resulting analysis of autoradiograph data combined with SEM-EDX mapping of iron content, it was found that Am sorbed inhomogenously on all mineral surfaces with no correlation with regard to Fe content (Fe being a proxy marker for biotite and hornblende content of granitic rocks). In much earlier autoradiographic studies by /Allard et al. 1985/, as well as /Ittner et al. 1988/ and /Beall et al. 1980/ sorption was observed to occur on all exposed surfaces although more strongly on biotite. In /Anderson et al. 2007/, on the other hand, autoradiographs of Am sorption on monolithic samples of Siberian granitoids gave indications of diffusive uptake of Am into biotite crystals. No specific details of this are given in the reference and the author of the present report interprets this to mean diffusion into cleavage microcracks rather than true interlayer diffusion. Although some of the literature appears to suggest (although not unequivocally) sorptive association with biotite, there is essentially no direct spectroscopic evidence for replacement of interlayer K^+ ions in biotite with Am^{3+} or any of its analogue elements used in experiments.

An attempt was made to model the data using a single rate diffusion model with sorption on external and internal particle surfaces. In the model there are a number of uncertain parameters that need to be estimated. Apart from the K_d value for sorption, other parameters that need to be assessed include the effective diffusivity of the crushed rock particles and the specific sorptive surface area of the rock separated into contributions from an internal and external surface area component. The surface area of the crushed rock could be estimated from BET surface area measurements carried out on duplicate samples of two different size fractions (0.063–0.125 mm and 2–4 mm). Linear regression of the BET surfaces areas allows an estimate of the contributions by internal and external surfaces to be approximately characterised (see, for example, /André et al. 2008b/). Since the particle size fractions used in the sorption experiments were sometimes different from the particle sizes used in the BET measurements, the regression equation was used to interpolate the appropriate surface area for the calculation. The effective diffusivity of crushed particles is unknown although for the purposes of making these calculations an uncertainty distribution was assumed based on a lognormal distribution with subjectively assessed 95% confidence bounds corresponding to 10^{-12}–10^{-15} m^2/s. This is slightly larger than the uncertainty interval considered appropriate for intact rock samples, although reflects the fact that individual particles could feature smaller or larger diffusivities than monolithic samples owing to the upscaling effect of larger sample sizes.

The results of this analysis are shown in Figure D-2 where K_d is treated as a fitting parameter while sorptive surface area and effective diffusivity are assigned from their associated uncertainty distributions in a stochastic fashion. The stochastic nature of the simulation allows uncertainties in the underlying parameter set to be propagated forward in the assessment of a probabilistic range of likely K_d values for the rock.

Apart from the fact that the modelled uptake curves do not match the measurement data very well, an interesting outcome of the simulations is that the resulting best estimate K_d distribution has a larger range of uncertainty than the original empirical R_d data set to which the model is fitted. This is largely due to the propagated effect of uncertain effective diffusivity and internal/external surface area which inflates the uncertainty of the K_d estimate considerably. When diffusive disequilibrium is considered there is the possibility that the measured R_d value is less than the true K_d value for the rock as indicated by the blue coloured bars on the right hand side of the figure. When only surface area effects are considered, however, the measured R_d value generally over-predicts the K_d value owing to the increased external surface area of crushed rock relative to the surface area of its internal porosity.

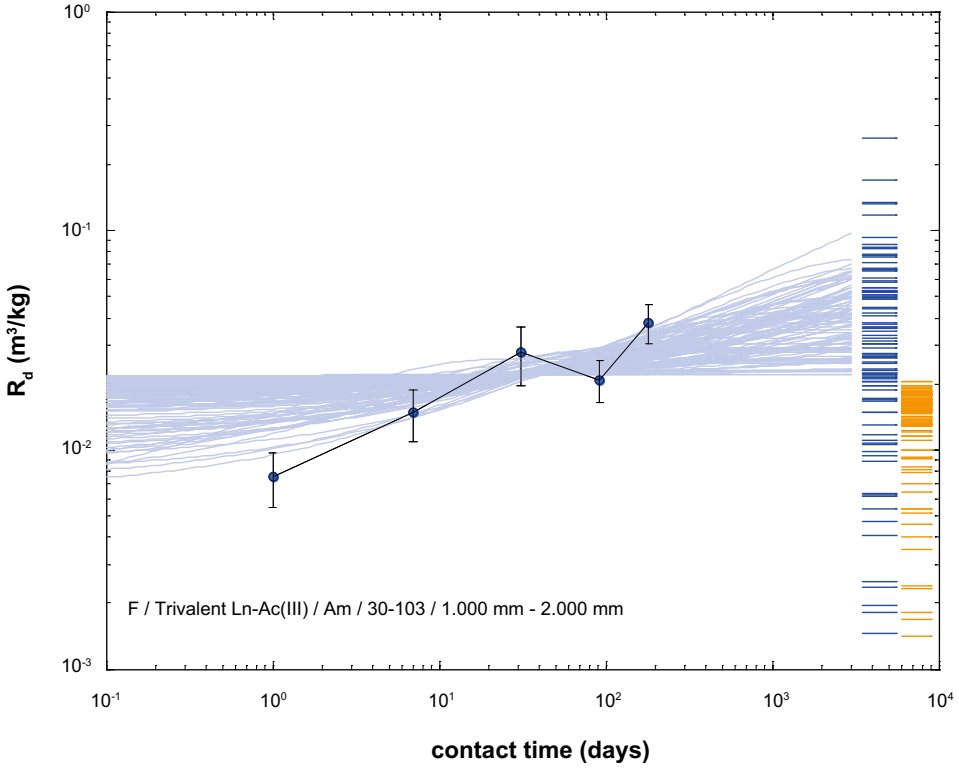

Figure D-2. *Monte-Carlo simulation results assuming a single rate diffusion model with effective diffusivities and sorptive surfaces areas assigned stochastically from their associated uncertainty distributions. The swarm of light blue curves underlying the experimental data points (dark blue markers) represent curves for 1,000 realisations where K_d is the fitting parameter. The blue coloured bars on the right-hand side are a plot of 100 randomly selected best fit K_d values taken from the simulations, while the orange coloured bars are the corresponding best fit K_d values where diffusion is neglected and only surface area effects are modelled.*

As already discussed in Chapter 5, a pH drift of as much as 1.5 pH units was observed in a number of control samples over the course of the 180 day sorption experiments. For solutes that sorb by way of a surface complexation mechanism, this can have a considerable impact upon results since the K_d value can easily be altered by an order of magnitude or more in response to such a pH change. In attempting to interpret the data we therefore are faced with the possibility that the time dependency observed in the data set is related to some process other than simple diffusive disequilibrium (chemical kinetics are not considered on account of the very long equilibration time).

The crushed rock samples had been pre-equilibrated with synthetic groundwater for a period of 89 days (with 10 water changes during the first 36 days) prior to spiking with the radionuclide tracer. The long pre-equilibration time would possibly disqualify proton exchange since such processes would be expected to reach equilibrium much more quickly. Chemical weathering reactions involving the rock samples is a distinct possibility since the crushing procedure exposes new mineral surfaces that might react slowly and release cations. If the glove box in which the samples were stored was not sufficiently oxygen free, then the slow release of Fe(II) from biotite combined with the possible formation of ferric oxyhydroxide microprecipitates could have a strong impact on the magnitude of the observed sorption owing to the strong sorption typically associated with such minerals. Increases of BET surface area by as much as a factor of three, for example, have been measured by e.g. /Huitti et al. 1996/ on crushed granite equilibrated with groundwater for 3 weeks. This could be related to weathering or precipitation of secondary minerals and the increase of surface area would also imply a positive pH drift owing to proton exchange reactions involving the newly created surfaces (all other things being equal).

Scoping calculations were made using PHREEQC and the surface complexation model for Am described in /Baston et al. 1995/ as reported in the RES^{3}T database[1] /Brendler et al. 2003/. The surface complexation reaction is based upon a ternary reaction involving Am^{3+} and two carbonate molecules with a strong surface site of ferrihydrite therefore also implying a strong dependency on carbonate concentration. For the very low radionuclide concentrations used in the experiments, precipitation of about a microgram of ferrihydrite (or 0.3 mg/l) appears to be sufficient to boost the apparent K_d value by roughly the same amount observed in the laboratory experiments. This, however, is equivalent to 350–400 times the initial total concentration of Fe specified for the groundwater used in the experiment and therefore this particular explanation may not be realistic.

Although the release of Fe^{2+} and its subsequent oxidation can lead to the formation of ferric oxy-hydroxides, this process should not have a significant net effect on pH owing to pH-buffering related to the precipitation process. The source of the pH increase therefore could instead be related to the release of other cations or the re-equilibration of solution carbonate concentrations to a lower carbon dioxide partial pressure (pCO_2) in the glove box. Either of these processes could give rise to the observed change in pH and influence the sorption of Am.

If the time dependency originates in a diffusive disequilibrium process, then data for the largest size fraction and longest contact time would be the most appropriate to use in making K_d recommendations since this would minimise the impact of both surface area effects and diffusive disequilibrium. If, on the other hand, drift in pH and pCO_2 or the formation of secondary minerals is the source of the time dependency, a good argument can be made for the selection of data for smallest size fraction and shortest contact time.

Since it is unclear which process or combination of processes gives rise to the time dependency of the measured R_d values, a decision was taken to consider the data set in its entirety and not to filter out values on the basis of particle size or contact time. Although the trend in individual data series is generally towards greater R_d values with increasing time, the trend of the aggregate data set is relatively small and tends to be overshadowed by differences arising due to the surface area of different size fractions. The choice to make corrections for the increased surface area of the crushed size fractions while neglecting time dependent effects of unclear origin therefore appears to be cautious for the purposes of safety assessment calculations.

Selection of representative data for site specific conditions

The procedure for derivation of K_d values relevant for application within SR-Site consisted of the following steps:

1. The R_d data for each groundwater type, taken separately, was pooled without any additional filtering by rock type, contact time, or particle size.
2. A normalising surface area transfer factor (f_A) was first used to convert the raw R_d data for different particle size fractions to R_d^0 values corresponding to the reference crushed rock size fraction (2–4 mm) using Equation 5-6.
3. A mechanical damage transfer factor (f_m) was then used to account for the difference in surface area between the reference size fraction of crushed rock and that of monolithic samples deemed to be approximately representative of the in situ rock. This transfer factor was calculated using Equation 5-7 and allows K_d^0 to be calculated. The transfer factor was applied assuming the geometric mean value as the central value. Only the central value of the f_m distribution was propagated in the subsequent calculations. Sample-specific f_m values were calculated individually for the same borehole sampling intervals as the samples used in the sorption experiments.

[1] RES^{3}T (Rossendorf Expert System for Surface and Sorption Thermodynamics), http://www.fzd.de/db/RES3T.login (accessed 2010-04-01)

The cation exchange capacity (CEC) transfer factor, f_{cec} was neglected on the basis that Am is not thought to sorb preferentially in association with bitotite (e.g. /Kienzler et al. 2009/). Since there are no thermodynamic or empirical models of acceptable accuracy which could be used to describe Am sorption on granitic rock, all uncertainty relating to variable or uncertain groundwater composition is assumed to be internalised in the aggregate data set combining K_d data for all groundwater compositions. Estimated K_d^0 data corrected for surface area and mechanical damage effects are plotted in Figure D-3 assuming Forsmark metagranite (SKB rock code 101057) as a representative rock type for the Forsmark site.

Recommended K_d data for SR-Site application conditions

If it is assumed that the principal uncertainties relating to variable groundwater composition are internalised in the individual data sets shown in Figure D-3, a recommended range for application in SR-Site can be defined by aggregating these into a global data set. The relevant K_d range for application in SR-Site is given in Figure D-4.

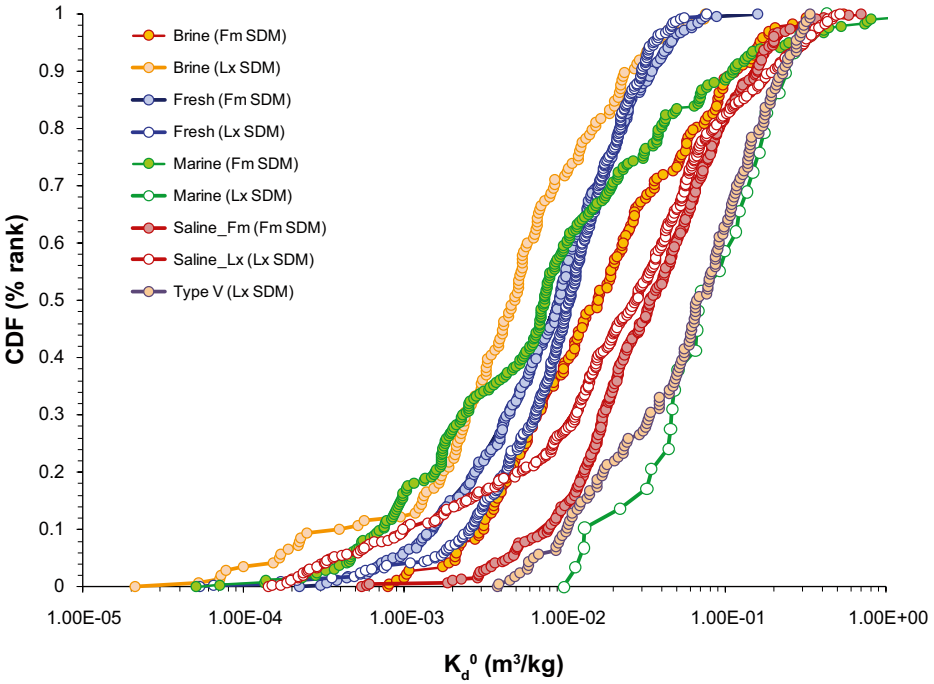

Figure D-3. *Corrected K_d^0 (m^3/kg) values calculated for Am(III)/Eu(III) sorption based on raw R_d data for site-specific rock types and groundwater compositions as reported in the Forsmark (Fm SDM) and Laxemar (Lx SDM) site investigations. Only surface area and mechanical damage transfer factors (f_A and f_m) have been considered in the estimation procedure. The raw data are corrected to give values deemed appropriate for Forsmark metagranite (SKB rock code 101057) under in situ conditions and are presented as an empirical cumulative distribution function (CDF).*

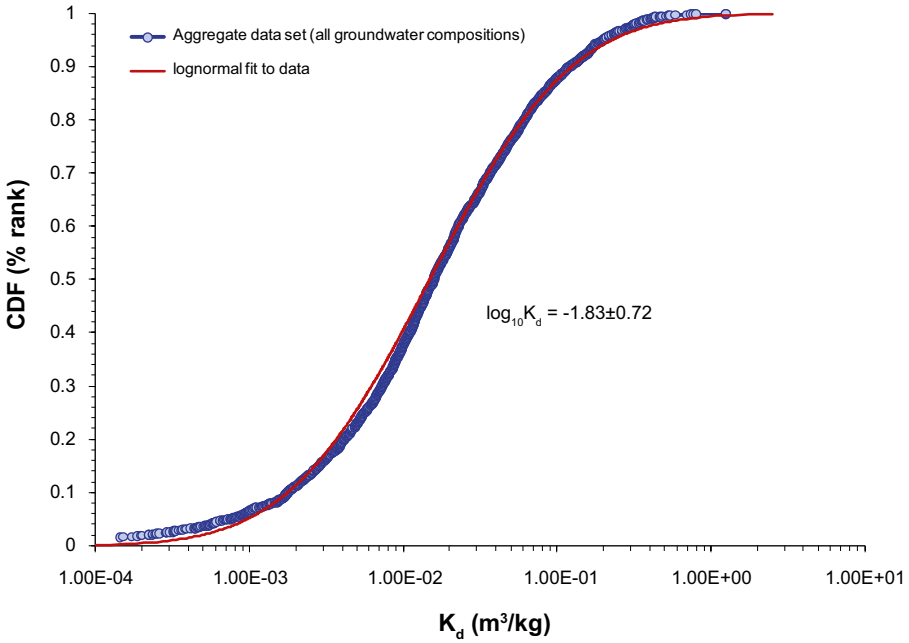

Figure D-4. *Recommended K_d (m^3/kg) data for Am(III) sorption for use in SR-Site calculations for Forsmark. The data range is considered to be applicable to all groundwater compositions and assumes Forsmark metagranite (SKB rock code 101057) as a representative rock type. The parameters of the lognormal distribution fit to the data are indicated in the figure.*

Appendix E

K_d data derivation sheet for cesium (Cs)

Overview and evaluation of site investigation data

Site specific sorption data were obtained for Cs(I) during the site investigations at Forsmark /Byegård et al. 2008/ and Laxemar /Selnert et al. 2009/. These data are summarised in the bedrock transport properties site descriptive model /Crawford 2008/ and are the basis for K_d values recommended for use in SR-Site. In most cases (although there are some exceptions) there is a time dependency in the experimental data with a clear trend towards higher R_d values at increasing times. The data also exhibit a relatively clear surface area dependency whereby smaller crushed particle sizes are associated with higher sorptivities than larger size fractions. A typical time series for Cs(I) sorption on Forsmark metagranite (SKB rock code 101057) is shown in Figure E-1.

It is interesting to note the inflection in the slope of the temporal trend at 92 days as shown in Figure E-1. This is at the same location as the dip noticed in the corresponding data set for Am(III) shown in Figure D-1. As discussed previously in the case of Am(III) sorption, if the apparent time dependency were to be interpreted as a diffusive disequilibrium process, the lack of tendency to plateau to a constant value would normally suggest that none of the particle size fractions have reached diffusive equilibrium for the range of contact times investigated. The relatively even vertical spacing of the data sets in log-log space, however, is not fully consistent with a simplified model of particle diffusion where sorption also occurs on external surfaces of the crushed particles.

As described previously for Am(III) sorption on site-specific materials, the relative slopes of the time series curves for different size fractions seems difficult to reconcile with a bimodal model of diffusive uptake since smaller surface area effects would be expected. In this case, however, Cs^+ is expected to displace interlayer K^+ ions in biotite. If access to individual biotite grains or grain clusters in the larger size fractions is hindered by way of a lower connected porosity this could potentially account for some of the observed difference if the diffusive uptake into biotite interlayers is considered to be rate limiting.

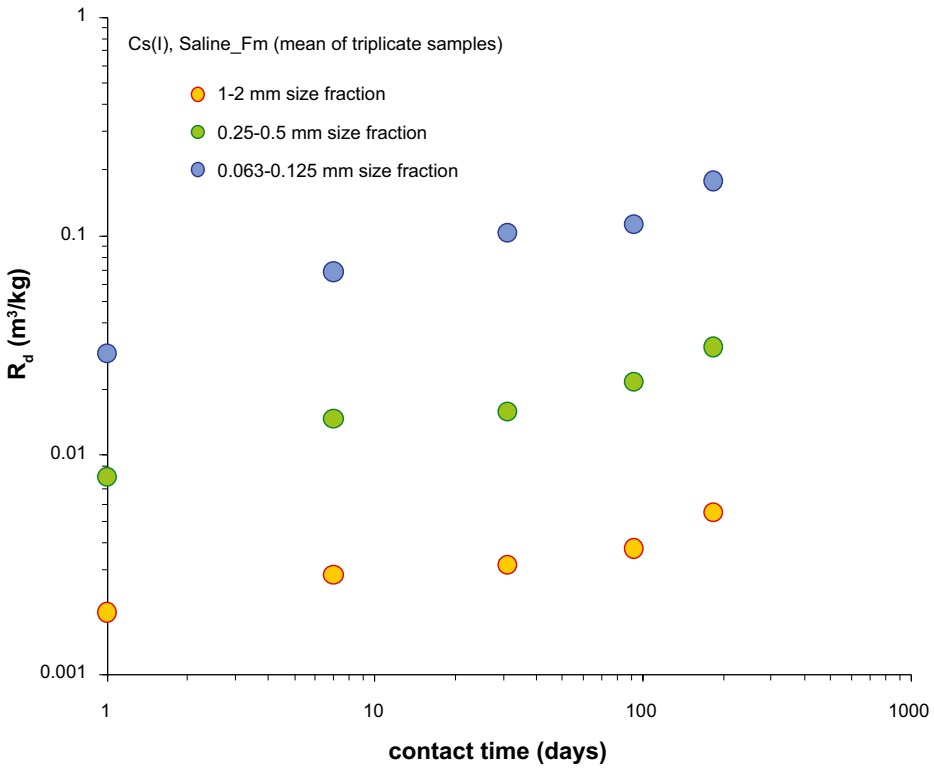

Figure E-1. *Typical time series for Cs(I) sorption R_d (m^3/kg) measured in the Forsmark site investigation studies. There is a clear sorption dependency on both particle size and time.*

Although sequestration of Cs(I) on the frayed edge sites and internal surfaces of biotite grains is well described in the literature and confirmed by direct spectroscopic evidence (e.g. /Bostick et al. 2002, Zachara et al. 2002, McKinley et al. 2004/), it is not possible to fit a simple diffusion and sorption model to account for diffusive disequilibrium without introducing additional uncertainties. As indicated previously for Am(III) sorption this gives rise to overall ranges of data uncertainty that are larger than the span of the raw data and therefore might not be cautious for application in safety assessment calculations. For this reason, the data for Cs(I) sorption have been treated by considering the data set in its entirety and not filtering values on the basis of crushed size fraction or contact time. As noted previously for Am(III), although the trend in individual data series is generally towards greater R_d values with increasing time, the trend of the aggregate data set is small relative to the overall data variability.

Selection of representative data for site specific conditions

The procedure for derivation of Cs(I) K_d values relevant for application within SR-Site consisted of the following steps:

1. The R_d data for each groundwater type, taken separately, was pooled without any additional filtering by rock type, contact time, or particle size.
2. A normalising surface area transfer factor (f_A) was first used to convert the raw R_d data for different particle size fractions to R_d^0 values corresponding to the reference crushed rock size fraction (2–4 mm) using Equation 5-6.
3. A mechanical damage transfer factor (f_m) was then used to account for the difference in surface area between the reference size fraction of crushed rock and that of monolithic samples deemed to be approximately representative of the in situ rock. This transfer factor was calculated using Equation 5-7 and applied assuming the geometric mean as the central value. Only the central value of the f_m distribution was propagated in the subsequent calculations. Sample-specific f_m values were calculated individually for the same borehole sampling intervals as the samples used in the sorption experiments.
4. A cation exchange capacity (CEC) transfer factor, f_{cec} was used to account for differences between the CEC of site specific rock at Forsmark and the rock used in the laboratory experiments which includes samples taken from Laxemar with different CEC. The transfer factor was calculated using Equation 5-8 and applied assuming the geometric mean as the central value. The same transfer factor was for all samples used in the sorption experiments since CEC estimates were not available on sample by sample basis. Only the central value of the f_{cec} distribution was propagated in the subsequent calculations.
5. A groundwater chemistry transfer factor, f_{chem} was used to account for differences in the major ion composition of the groundwater used in experiments and those projected for application conditions. A distribution of f_{chem} values was estimated using the ion-exchange model described in Section 5.1.1 and applied by stochastically combining estimated values of f_{chem} with randomly selected values from the K_d^0 probability distribution estimated for Forsmark saline groundwater (this Monte-Carlo sampling procedure is equivalent to convolution of the individual probability density functions).

Estimated K_d^0 data corrected for surface area normalisation, mechanical damage, and CEC effects using Equation 5-2 are plotted in Figure E-2 assuming Forsmark metagranite (SKB rock code 101057) as a representative rock type for the Forsmark site.

The theoretical K_d was calculated using PHREEQC and the SKB-TDB /Duro et al. 2006/ for 10,000 randomly selected groundwater compositions taken from the SR-Site temperate domain simulations /Salas et al. 2010/. The ion-exchange model described in Section 5.1.1 was used assuming selectivity coefficients for Äspö diorite as a basis for calculations. Comparison of K_d values calculated in this manner with the corresponding theoretical result for the Forsmark saline reference water allows the groundwater chemistry transfer factor, f_{chem} to be calculated in straight-forward fashion for the projected application conditions using Equation 5-9. Since the data are normalised in the calculation, f_{chem} is relatively insensitive to the uncertain CEC of the simulated rock-water system for a single site ion-exchange model provided the differences are not so great that significantly perturbed groundwater compositions would result.

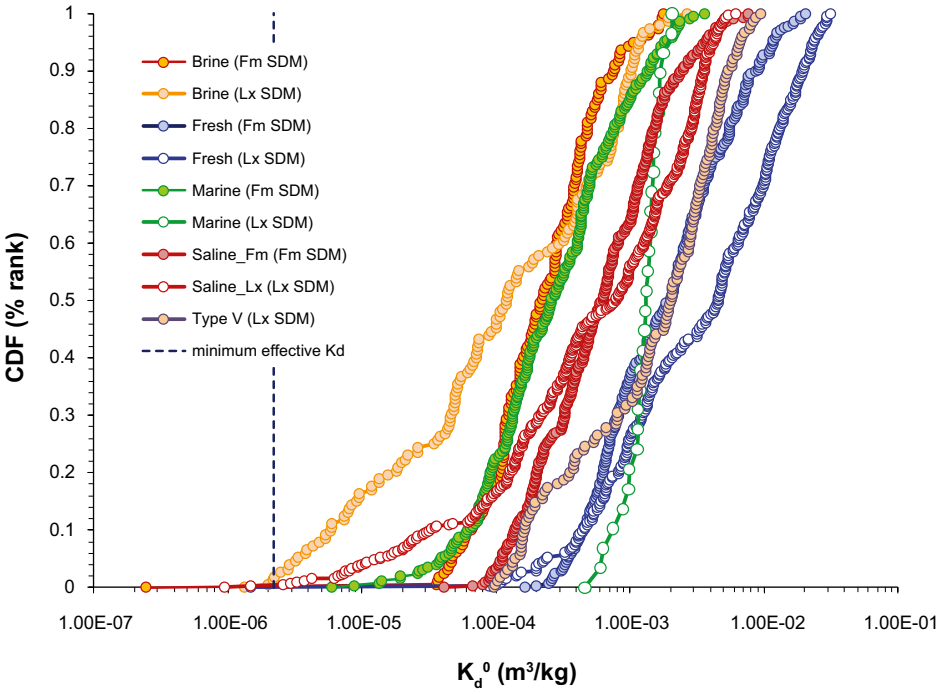

Figure E-2. *K_d^0 (m^3/kg) values calculated for Cs(I) sorption based on raw R_d data for site-specific rock types and groundwater compositions as reported in the Forsmark (Fm SDM) and Laxemar (Lx SDM) site investigations. Surface area normalisation, mechanical damage, and CEC transfer factors (f_A, f_m, and f_{cec}) have been considered in the estimation procedure. The raw data are corrected to give values deemed appropriate for Forsmark metagranite (SKB rock code 101057) under in situ conditions and are presented as an empirical cumulative distribution function. A minimum effective K_d reference line is plotted in the figure indicating the upper 95% confidence limit for the matrix storage capacity of the rock based on water saturation porosity.*

In the SR-Site groundwater simulations, only the major ions are specified. For the purpose of simulating ion-exchange processes involving trace components not included in these simulations, the concentrations of these constituents need to be estimated. This was achieved by constructing correlations between groundwater components using the hydrochemical data available from the site investigations /Laaksoharju et al. 2008, 2009/ as a basis and using these correlations to estimate the likely concentrations of tracer components under application conditions. It was generally the case that Ca concentration was the best predictor of the trace components Cs, Sr, Rb, and Ba. Full details concerning how these correlations were established and implemented can be found in Appendix A.

Simulation results for the central case selectivity coefficients are given in Figure E-3 and indicate a slightly decreased K_d at early times relative to the reference groundwater. At longer times, however, the progressive freshening of the groundwater due to intrusion of a meteoric component gives elevated K_d values relative to the reference groundwater.

Additional simulations were carried out to quantify the impact of uncertainty in the selectivity coefficients using the 2σ error estimates specified in Table 5-5 as a calculation basis and assuming lognormally distributed uncertainties. Since changing the selectivity coefficient influences the theoretical K_d value for both the randomly sampled SR-Site groundwater and for the reference groundwater, it was necessary to perform paired simulations. For the 10,000 randomly sampled groundwater compositions, an additional 10,000 simulations were required to establish the reference state for each perturbed set of selectivity coefficients. The results of this analysis are shown in Figure E-4 and indicate a relatively small impact of aleatory uncertainty.

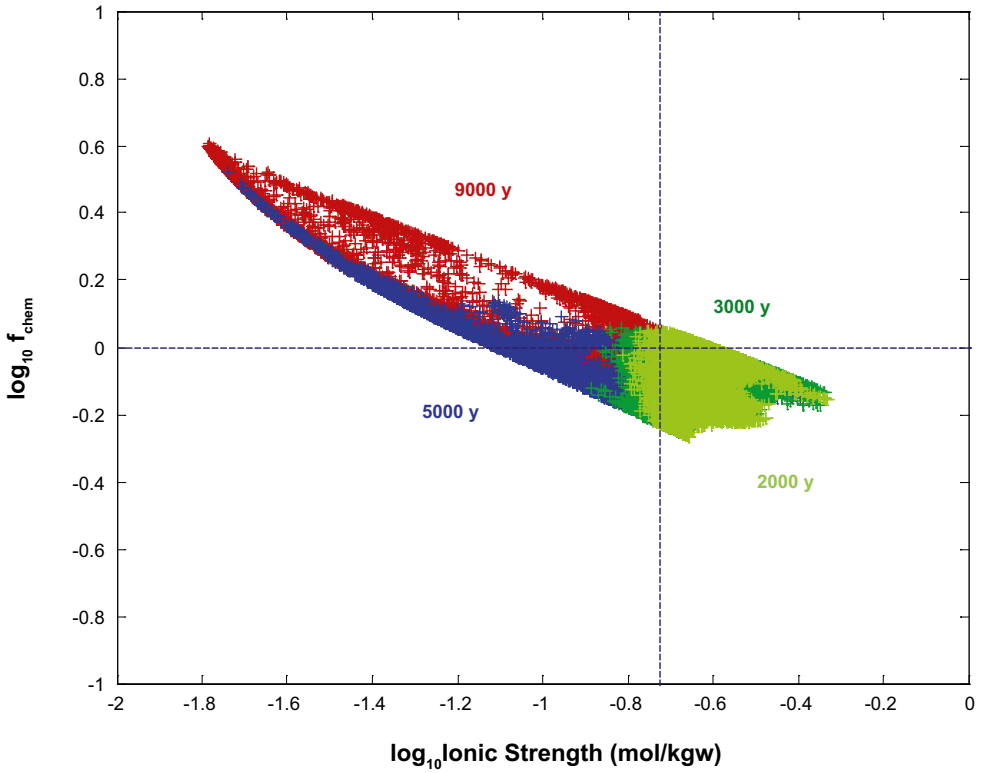

Figure E-3. *Chemistry transfer factors, f_{chem} calculated for Cs(I) sorption at application groundwater conditions in the SR-Site temperate case. The plotted data represent 10,000 randomly selected groundwater compositions calculated individually using PHREEQC and the assumed ion exchange model (central case selectivity coefficients). Data are given for 2,000 y (lime green markers), 3,000 y (dark green), 5,000 y (blue), 9,000 y (red). The cross-hairs in the figure represent the relative location of the reference saline groundwater for Forsmark.*

Using the calculated f_{chem} distribution, it is possible to estimate K_d values appropriate for application groundwater compositions by convolution of the individual probability density functions or by using an equivalent stochastic method. The latter method, being simpler to implement numerically, was chosen and used to estimate the K_d values presented in this compilation. The stochastic method was based upon random sampling (10^5 samples) of the individual probability density functions and multiplication of the individually sampled values using Equation 5-3. The resulting distributions of K_d values are plotted in Figure E-5 to Figure E-8 for different times during the temperate calculation cases and include the additional impact of stochastically perturbed selectivity coefficients as described above.

Although only the K_d^0 data set for the reference Forsmark saline groundwater was used to extrapolate to application conditions, the plotted results of the calculations indicate a generally very good agreement with the K_d^0 values for groundwaters that were not used in the calculations. The assumption of the simplified, single-site ion-exchange model and selectivity coefficients derived for the Äspö diorite rock therefore appears to give an acceptably low level of uncertainty with regard to Cs(I) sorption for the purposes of SR-Site safety assessment calculations.

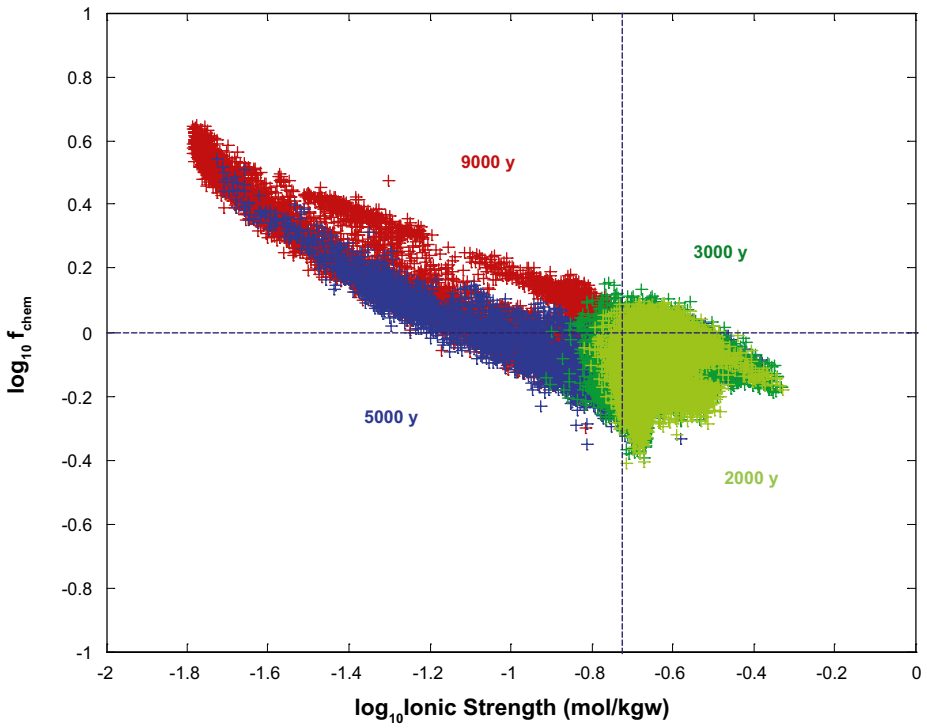

Figure E-4. *Chemistry transfer factors, f_{chem} calculated for Cs(I) sorption at application groundwater conditions in the SR-Site temperate case. The plotted data represent 10,000 randomly selected groundwater compositions calculated individually using PHREEQC and the assumed ion exchange model. The plotted data include the additional effect of random perturbation of selectivity coefficients conforming to their error estimates. Data are given for 2,000 y (lime green markers), 3,000 y (dark green), 5,000 y (blue), 9,000 y (red). The cross-hairs in the figure represent the relative location of the reference groundwater.*

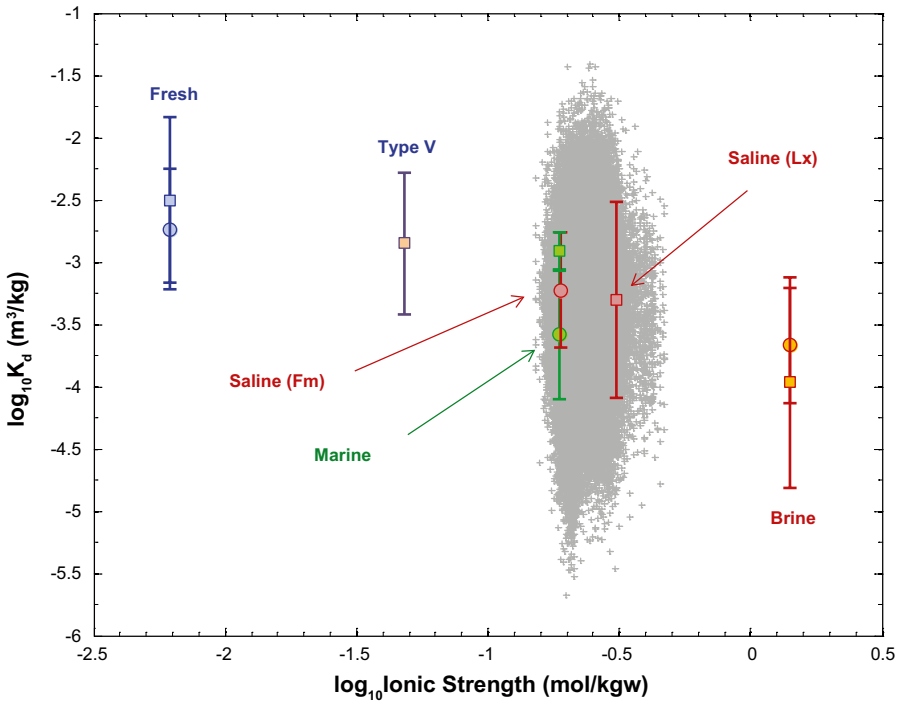

Figure E-5. *Cross-plot of K_d (m^3/kg) values for Cs(I) versus ionic strength (mol/kgw) on logarithmic axes. The recommended data are for SR-Site application conditions at 2,000 y in the temperate case and are plotted as the swarm of grey markers. K_d^0 data are plotted as geometric means with 1σ standard errors for the different groundwater compositions used in the site investigation.*

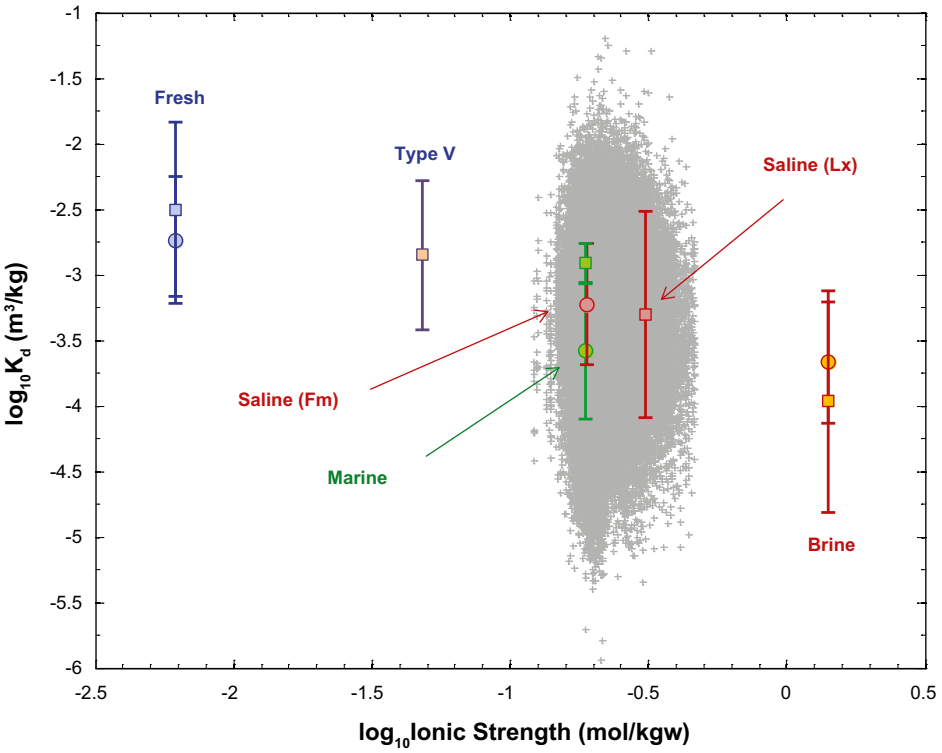

Figure E-6. *Cross-plot of K_d (m^3/kg) values for Cs(I) versus ionic strength (mol/kgw) on logarithmic axes. The recommended data are for SR-Site application conditions at 3,000 y in the temperate case and are plotted as the swarm of grey markers. K_d^0 data are plotted as geometric means with 1σ standard errors for the different groundwater compositions used in the site investigation.*

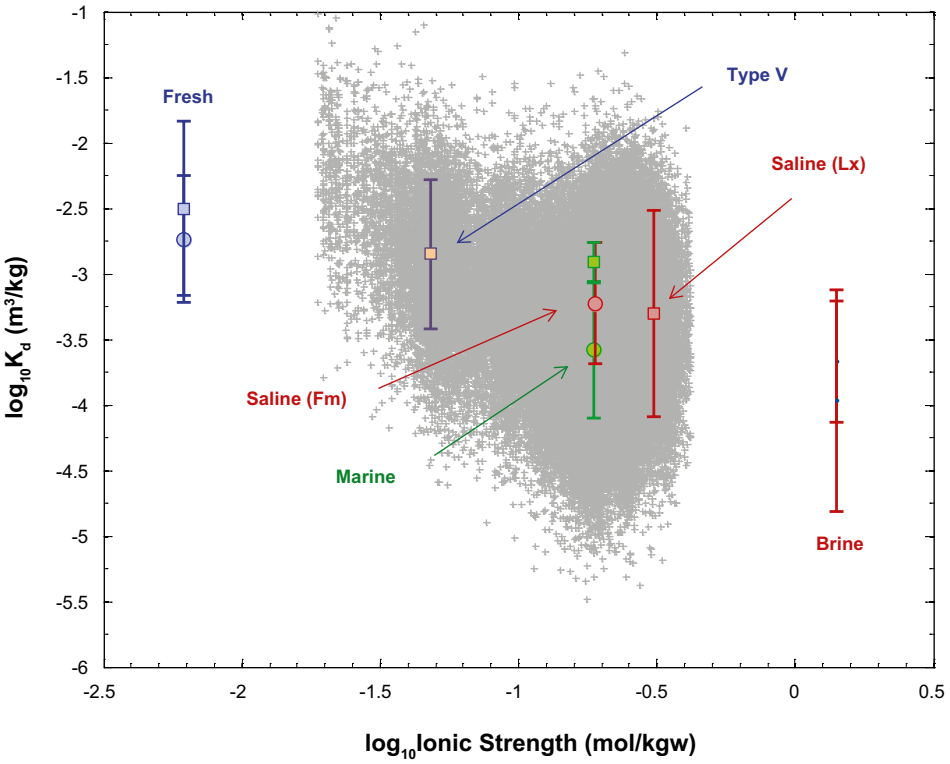

Figure E-7. *Cross-plot of K_d (m^3/kg) values for Cs(I) versus ionic strength (mol/kgw) on logarithmic axes. The recommended data are for SR-Site application conditions at 5,000 y in the temperate case and are plotted as the swarm of grey markers. K_d^0 data are plotted as geometric means with 1σ standard errors for the different groundwater compositions used in the site investigation.*

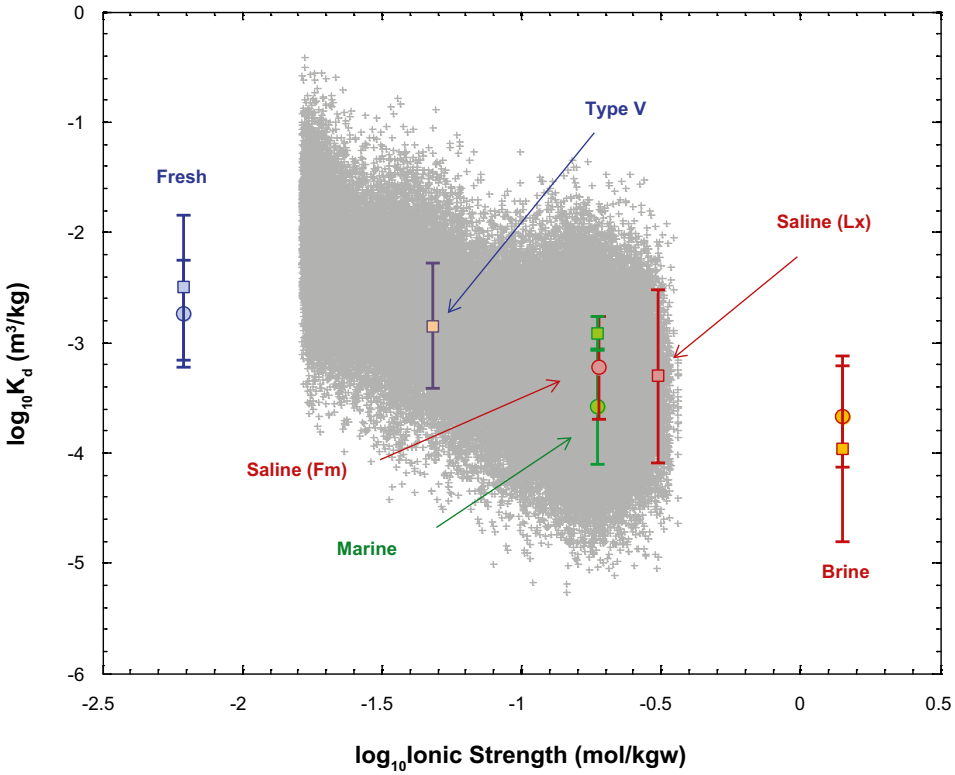

Figure E-8. *Cross-plot of K_d (m^3/kg) values for Cs(I) versus ionic strength (mol/kgw) on logarithmic axes. The recommended data are for SR-Site application conditions at 9,000 y in the temperate case and are plotted as the swarm of grey markers. K_d^0 data are plotted as geometric means with 1σ standard errors for the different groundwater compositions used in the site investigation.*

Recommended K_d data for SR-Site application conditions

Based on the ion-exchange simulations described in the previous section, the following K_d ranges are recommended for use at different times in the hydrogeochemical evolution of the repository environment:

$\log_{10} K_d \approx -3.44 \pm 0.51$ (t = 2,000 y) (E-1)

$\log_{10} K_d \approx -3.46 \pm 0.51$ (t = 3,000 y) (E-2)

$\log_{10} K_d \approx -3.38 \pm 0.51$ (t = 5,000 y) (E-3)

$\log_{10} K_d \approx -3.10 \pm 0.62$ (t = 9,000 y) (E-4)

As can be seen from the recommended data, the changing salinity of the repository environment has only a weak impact on the K_d uncertainty distribution, with a tendency to towards slightly higher sorptivities with time. Since it is not possible to consider temporally variable K_d values in safety assessment calculations, the time period giving the lowest K_d value is recommended to be used for calculations. This corresponds to the groundwater conditions existing at 3,000 y. Generally the numerically calculated K_d uncertainties were found to be lognormally distributed with the exception of 9,000 y where the fitted lognormal distribution doesn't fully capture the positive skew of the data set (see Figure E-9).

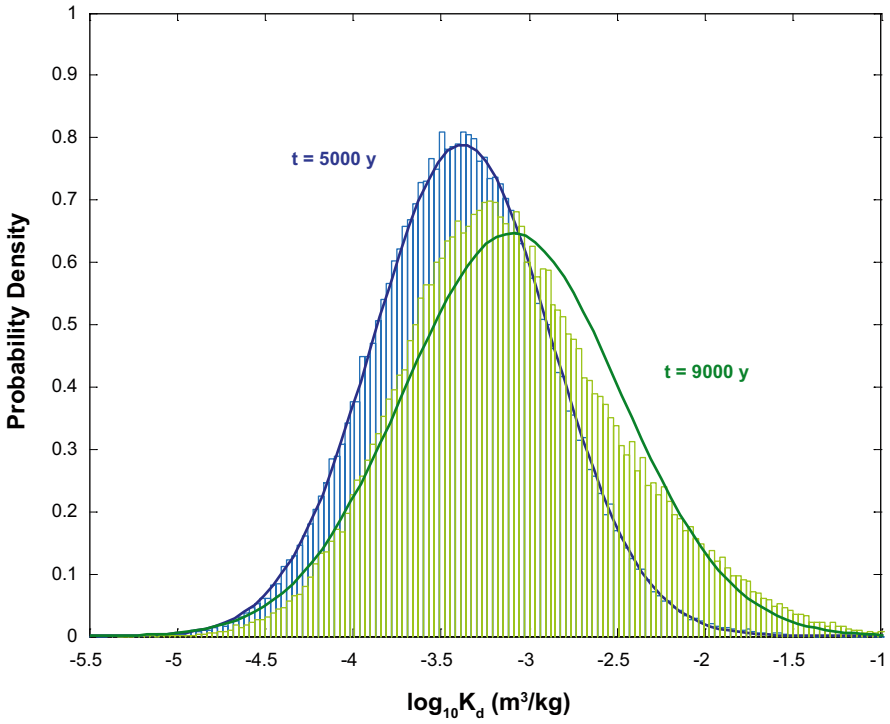

Figure E-9. *Comparison of K_d (m^3/kg) distributions predicted for Cs(I) at 5,000 y and 9,000 y. The data are plotted in histogram form with a fitted lognormal distribution in each case. The data set for 9,000 y exhibits a slight positive skew relative to the lognormal fit.*

Appendix F

K_d data derivation sheet for lead (Pb)

Overview and evaluation of available literature data

The sorption of Pb on granitic rock is poorly covered in the literature and only one study /Papelis 2001/ has been found where sorption has been characterised using relevant materials and water compositions. In the reported experiments, pH dependent sorption edges were measured on finely crushed Shoal granite (≤ 0.075 mm) in contact with water of variable ionic strength (0.01, 0.1, and 1.0 M $NaNO_3$) and for a range of Pb(II) concentrations (10^{-7}, 10^{-5}, 10^{-4} M). The liquid to solid ratio used in the experiments was 100 ml/g. In addition, the sorption was measured for three different synthetic groundwaters reflecting groundwater compositions of three different wells at the site.

The actual composition of the groundwaters is not well documented in the reference although the HC-4 groundwater type is described as being composed of approximately equal concentrations of calcium and sodium cations (~65 mg/l) and roughly equal concentrations of chloride, sulphate, and bicarbonate anions (~100 mg/l). Although Freundlich isotherm parameters were derived for the Pb(II) sorption, the concentrations used were several orders of magnitude higher than what is expected for transport of Pb(II) in the repository environment. For this reason, only the K_d values estimated for a Pb(II) concentration of 10^{-7} M are used in this report.

The pH of the synthetic waters was adjusted by adding small amounts of 1 M HNO_3 or 0.1 M NaOH prior to the commencement of the experiments. Although the pH at the conclusion of the experiments was not measured, it is reasonable to expect only a small drift in pH on account of the relatively high liquid to solid ratio used in the experiments.

Additional experiments were also carried out on a high ionic strength (0.63 M) synthetic groundwater, H-2 (presented only as a pH adsorption edge graphic in the reference). These experiments indicated that there was essentially no quantifiable ionic strength dependency for the sorption of Pb at pH ³ 6 for the comparison between HC-4 and H-2. Other experimental, sorption edge data for ionic strengths of 0.1 M and 1.0 M ($NaNO_3$ background electrolyte) are not presented as numerical tables in the reference although they are given instead in graphical form. These results appear to exhibit no quantifiable difference in sorptivity for the range of ionic strengths investigated. This was interpreted by /Papelis 2001/ as an indication of strong binding by way of inner sphere surface complexation.

Selection of representative data for site specific conditions

The R_d data corresponding to groundwater HC-4 were chosen as being the most relevant data set for extrapolation to site specific conditions at Forsmark. The BET surface area of the crushed rock was determined by /Papelis 2001/ to be approximately 0.79 m^2/g. Since only one particle size was used in the experiments, it was only necessary to use a single correction factor to extrapolate the data to Forsmark rock under in situ conditions. Assuming the measured BET surface area for monolithic samples of Forsmark metagranite (SKB rock code 101057) reported by /André et al. 2009/, the mechanical damage transfer factor, f_m was estimated to be:

$$\log_{10} f_m \approx -1.70 \pm 0.23 \qquad \text{(F-1)}$$

Since no error estimate is given for the BET surface area of the crushed rock, the error estimate for f_m is estimated assuming only the standard error (2σ) of the Forsmark metagranite surface area. This will tend to underestimate the true uncertainty of f_m. No CEC data or any proxy information that could be used to infer CEC is given in the reference and therefore f_{cec} is neglected.

Table F-1. Summary of Pb(II) numerical sorption data reported by /Papelis 2001/ for crushed granite samples taken from the Project Shoal underground test area (Nevada, USA).

water type Ionic strength (M) initial pH	$NaNO_3$ 0.01 R_d (m^3/kg)	HS-1 (Na-HCO_3) 0.0058 R_d (m^3/kg)	HC-4 (Na-Ca-Cl-SO_4-HCO_3) 0.01 R_d (m^3/kg)
4	1.78×10^{-2}	4.08×10^{-2}	n/a
5	4.53×10^{-2}	4.49×10^{-2}	n/a
6	3.56×10^{-1}	1.33	0.733
7	2.4	~100	1.9
8	~100	~100	4.9
9	~100	~100	n/a

Recommended K_d data for SR-Site application conditions

Assuming the average and standard deviation of the three R_d values for HC-4 groundwater given in Table F-1 allows a very approximate lognormally distributed range of uncertainty to be estimated for Pb(II) sorption which should be reasonably justifiable for the SR-Site application groundwater conditions. Since the sample size is very small, the 2σ standard error estimate was propagated in the calculations. The recommended K_d (m^3/kg) range estimated in this manner is:

$$\log_{10} K_d \approx -1.6 \pm 0.6 \qquad \text{(F-2)}$$

Since the sorption of Pb(II) is expected to be dominated by an inner-sphere complexation mechanism in the pH and ionic strength range of interest, this value is assumed for all application groundwater compositions. Although there is a weak geochemical analogy between Pb and Ni, it is not clear whether using recommended K_d data for Ni would be an over-pessimistic assumption owing to a possibly greater sensitivity of sorption to ionic strength in the case of Ni. Unfortunately, there appear to be no studies documented in the literature where the comparative sorption of Pb and any of its analogue solutes have been measured simultaneously under relevant pH and ionic strength conditions. It is noted, however, that a non-trivial ionic strength dependency was observed for Pb sorption on zeolitised tuff from Nevada /Um and Papelis 2003/ which suggests that under certain conditions, outer-sphere complexation/ion-exchange behaviour might occur. If Pb is deemed to be important radionuclide for safety calculations, a case could be made by appealing to arguments of caution for adopting recommended K_d data for Ni(II) as an alternative to the uncertain range estimated for Pb(II) in Equation F-2.

Appendix G

K_d data derivation sheet for neptunium (Np)

Overview of site investigation data

Site specific sorption data were obtained for Np during the site investigations at Forsmark /Byegård et al. 2008/ and Laxemar /Selnert et al. 2009/. These data are summarised in the bedrock transport properties site descriptive model /Crawford 2008/ and are the basis for K_d values recommended for use in SR-Site under oxidising to mildly reducing conditions.

Although sorption experiments were carried out in an inert glove box atmosphere, the intensity of the sorption and the fact that no particular effort was made to maintain reducing conditions suggests that Np was most likely present in the pentavalent redox state, Np(V). Given that there were only a relatively small number of measurements available from the site investigations and because of the sensitivity of Np(V) sorption to possibly drifting pH and redox conditions, no attempt was made to interpret the data with regard to time dependent behaviour. The Forsmark site data are based on rock samples taken from two borehole sections while the Laxemar site data are based on rock samples taken from a single borehole section.

Overview of available literature data

The most detailed set of sorption data for relevant rock types and groundwater compositions in the open literature is documented by /Huitti et al. 1996/. In this study, sorption was measured on crushed rock samples from three borehole sections representing three different alteration types of Rapakivi granite (Hästholmen, Finland). The sorption experiments were carried out under both oxic and anoxic conditions using a natural groundwater sample (LPVA2) with an ionic strength of about 0.17 M and liquid to solid ratio of 10 ml/g. The groundwater was dominated by NaCl with a composition close to that of the Marine groundwater type used in the Forsmark and Laxemar laboratory investigations. Owing to the large iron content of the groundwater (~6 mg/l), the groundwater samples used in the oxic experiments were equilibrated with the ambient atmosphere for a period of a week and filtered (0.22 µm Millipore filter) prior to use. For experiments carried out under anoxic conditions, the sampled groundwater was preserved in nitrogen atmosphere to prevent oxidation of the Fe(II) content of the water (~5 mg/l).

Sorption experiments were carried out on three samples of granite described as fresh, weathered, and altered. Generally it was found that the sorption of Np did not scale linearly with BET surface area and R_d values estimated for the weathered and altered samples were somewhat less than what would be otherwise predicted on the basis of their larger surface areas. Material properties of the rock samples are given in Table G-1.

Table G-1. Material properties of rock types investigated by /Huitti et al. 1996/. Means and standard deviations given for three replicate samples.

Sample	YT5-1	YT5-2	YT5-3
Type	Fresh	Weathered	Altered
A_{BET} (m^2/g)	0.31±0.01	3.51±1.94	1.0±0.12
CEC (cmol/kg)	1.01±0.28	3.7±0.17	1.7±0.17
Biotite (vol%)	3.8%	4.2%	1.4%
Hornblende (vol%)	5.2%	–	–
Chlorite (vol%)	1.2%	12.4%	2.6%
Fe oxides, amorphous (mg/g)	1.2–1.5	0.89–0.99	1.2–1.5
Fe oxides, crystalline (mg/g)	0.14–0.19	2.8–3.2	2.1–2.2

The R_d data compiled in /Huitti et al. 1996/ are estimated in terms of the percentage sorbed, S(%) which is calculated with the aid of a radiometric mass balance. Owing to underlying uncertainty in the data and the small number of samples, the methods outlined in Appendix C were used to estimate expanded ranges of uncertainty. There are 12 numerical data points for each of the three alteration types of Rapakivi granite that were used in the experiments under oxic conditions. These represent Np(V) spike concentrations in the range 10^{-13} M, 10^{-9} M, and 10^{-7} M (4 replicates for each concentration level and rock type). Since there were no large disparities in sorption strength between the different concentrations, no distinction was made between these data sub-sets in the subsequent analysis. The contact time was 40 days for the 10^{-9} M and 10^{-7} M spike concentrations and 28 days for the 10^{-13} M spike concentration level.

For the experiments performed under anoxic conditions, a contact time of 31 days and 77 days was used for two sets of three replicates for each rock type. Since the dissolution of Np activity on the Teflon platelets was typically incomplete under anoxic conditions, the spike concentration varied from sample to sample. The sorption was sufficiently strong under anoxic conditions that only the minimum R_d value could be reported. An example of some of the data reported in /Huitti et al. 1996/ is given in Table G-2.

As can be seen from Table G-2, the R_d estimates obtained under oxic conditions are likely to be relatively precise given the S(%) ranges reported. The degree of sorption under anoxic conditions, however, was so strong that it is nearly impossible to determine the R_d with any kind of accuracy.

Selection of representative data for site specific conditions

Np is somewhat unusual in that a mixture of site data and literature data have been considered in the recommendation of K_d ranges for use in SR-Site safety assessment calculations. Although the site specific data are primarily used to establish the recommended K_d data range, the Finnish data from /Huitti et al. 1996/ are used in a supporting role to provide a consistency check on the values derived from site specific materials studied in the Forsmark and Laxemar site investigations. The selection procedure and associated calculations are described separately since data handling procedures were different for the site investigation and literature data.

Table G-2. Results of sorption measurements on fresh Rapakivi granite under oxic and anoxic conditions. Final pH and Eh values were measured for the experiments performed under anoxic conditions.

Conc. (M)	contact time	S(%)	R_d (m3/kg)	final pH	final Eh (mV)
10^{-13}	28 days	64.4±1.2	0.019		
		56.8±1.3	0.014		
		55.3±1.4	0.013		
		57.9±1.3	0.014		
10^{-9}	28 days	64.1±3.6	0.019		
		62.6±3.8	0.018		
		69.1±3.4	0.024		
		63.2±1.4	0.018		
10^{-7}	28 days	60.7±1.0	0.016		
		56.5±1.0	0.014		
		61.1±0.9	0.017		
		61.1±0.9	0.016		
n/a	31 days	100±1	≥ 1.4	7.95	+54
		100±1	≥ 1.3	7.94	+62
		99±1	≥ 1.6	7.99	+68
n/a	77 days	98.1±1	≥ 1.1	7.80	–65
		100±1	≥ 1.1	7.76	–65
		100±1	≥ 1.2	7.66	–69

Site specific data from Forsmark and Laxemar

The procedure for derivation of K_d values for Np(V) sorption relevant for application within SR-Site consisted of the following steps:

1. The R_d data for each groundwater type, taken separately, was pooled without any additional filtering by rock type, contact time, or particle size.
2. A surface area transfer factor (f_A) was first used to normalise the raw R_d data for different particle size fractions to R_d^0 values corresponding to the reference crushed rock size fraction (2–4 mm) using Equation 5-6.
3. A mechanical damage transfer factor (f_m) was then used to account for the difference in surface area between the reference size fraction of crushed rock and that of monolithic samples deemed to be approximately representative of the in situ rock. This transfer factor was calculated using Equation 5-7 and applied assuming the geometric mean as the central value. Only the central value of the f_m distribution was propagated in the subsequent calculations. Sample-specific f_m values were calculated individually for the same borehole sampling intervals as the samples used in the sorption experiments.
4. A cation exchange capacity (CEC) transfer factor, f_{cec} was used to account for differences between the CEC of site specific rock at Forsmark and the rock used in the laboratory experiments which includes samples taken from Laxemar with different CEC. The transfer factor was calculated using Equation 5-8 and applied assuming the geometric mean as the central value. The same transfer factor was for all samples used in the sorption experiments since CEC estimates were not available on sample by sample basis. Only the central value of the f_{cec} distribution was propagated in the subsequent calculations.

Since Np(V) has been shown to sorb preferentially in association with biotite, the CEC transfer factor is considered relevant for this radionuclide even though Np(V) sorption is thought to occur primarily by way of a surface complexation mechanism. Estimated K_d^0 data corrected for surface area normalisation, mechanical damage, and CEC effects using Equation 5-2 are plotted in Figure G-1. Here, it is implicitly assumed that the measured R_d data correspond to the sorption of the Np(V) redox species.

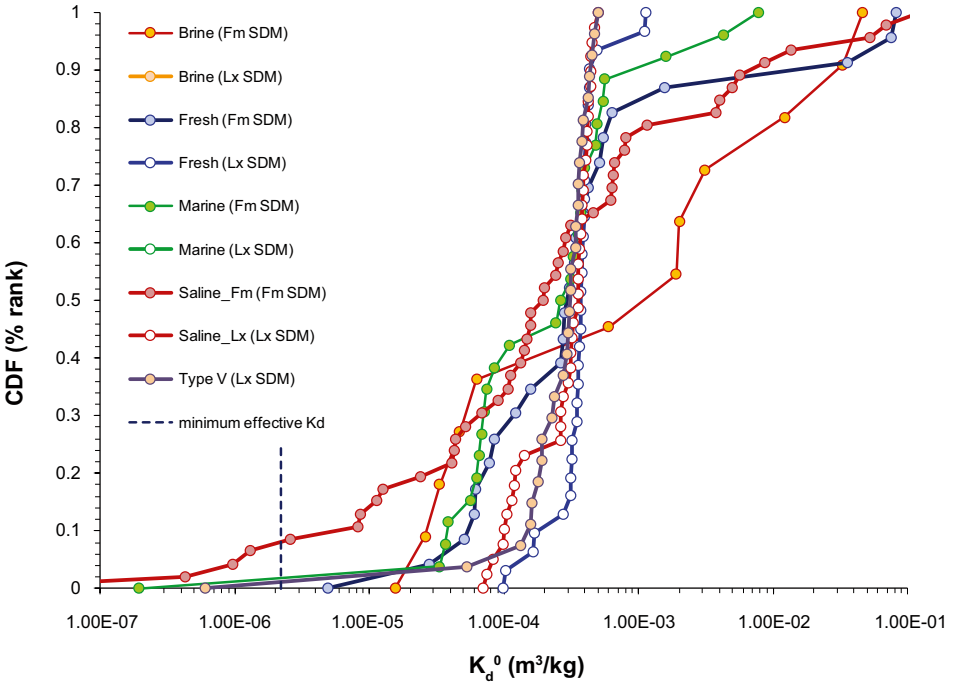

Figure G-1. *K_d^0 (m^3/kg) values calculated for Np(V) sorption based on raw R_d data for site-specific rock types and groundwater compositions as reported in the Forsmark (Fm SDM) and Laxemar (Lx SDM) site investigations. Surface area normalisation, mechanical damage, and CEC transfer factors (f_A, f_m, and f_{cec}) have been considered in the estimation procedure. The raw data are corrected to give values deemed appropriate for Forsmark metagranite (SKB rock code 101057) under in situ conditions and are presented as an empirical cumulative distribution function. A minimum effective K_d reference line is plotted in the figure indicating the upper 95% confidence limit for the matrix storage capacity of the rock based on water saturation porosity.*

Certain very low K_d^0 values (in some cases less than the minimum effective K_d reference line) arise due to random errors dominating the radiometric mass balance when sorption is close to the limit of quantification. Roughly 16% of the Forsmark saline data set consists of very low or negative values owing to random errors of this sort implying a censored lower limit for the data set.

Literature data for Rapakivi granite

From the sorption percentages and their uncertainties tabulated in the reference, the values of R_d and their associated error estimates were re-estimated using the Monte Carlo approach outlined in Appendix C. Based on the sorption percentage ranges, S(%) reported in Table G-2 for oxic conditions, it is expected that the uncertainty estimates of the re-calculated data can be reliably assumed to be lognormally distributed for oxic conditions. Since there are only a very limited number of data points, the individual R_d values and their uncertainties were then re-sampled assuming a convex combination of the underlying lognormal uncertainties. This is the main motivation for the recalculation of the literature R_d values to obtain the associated error estimates. The composite distribution of R_d values thus obtained is shown in Figure G-2.

As can be seen from the data plotted in Figure G-2, the re-sampled data indicate that there are only minor differences between the sorptivities measured for the different alteration types of Rapakivi granite. It should also be noted that the relatively small spread of the data is related to the small number of measurements and the narrow uncertainty spans of the estimated values. There are, however, relatively large differences between the BET surface areas and the CEC measured for these different rock types that do not translate into corresponding shifts in sorptivity. In this work a decision was taken to disregard the data for weathered and altered rock since the surface area and CEC transfer factors would thereby imply excessively low (i.e. over-pessimistic) K_d values for application conditions that may not be physically meaningful. Since there are many uncertainties in the quantitative extrapolation of K_d values for safety assessment, the selection of the most geologically similar material and rejection of data for substantially dissimilar materials is deemed by the author to be appropriate in this case given that the characteristics of Np sorption on granitic rock and its relation to surface area and CEC is not fully understood at this time.

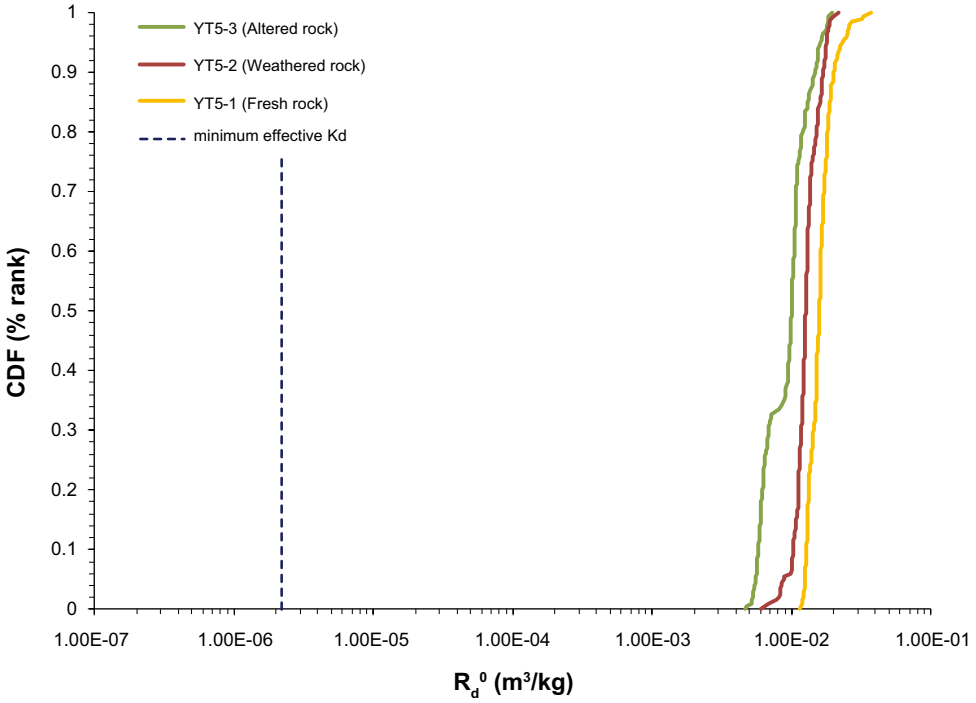

Figure G-2. *R_d^0 (m^3/kg) values calculated for Np(V) sorption based on literature R_d data and presented as an empirical cumulative distribution function for Rapakivi granite samples described as being fresh, weathered, and altered. The individual data points and their uncertainties have been re-estimated from tabulated sorption percentage data and then re-sampled to give the composite distribution plotted in the figure.*

The R_d data corresponding to the fresh Rapakivi granite were chosen as being the most relevant data set for extrapolation to site specific conditions at Forsmark. The BET surface area and CEC of the crushed rock is given in Table G-1. Since only one particle size was used in the experiments, it was only necessary to use a single correction factor to extrapolate the data to Forsmark rock under in situ conditions. Assuming the measured BET surface area for monolithic samples of Forsmark metagranite (SKB rock code 101057) reported by /André et al. 2009/, the mechanical damage transfer factor, f_m and its formal uncertainty was estimated to be:

$$\log_{10} f_m \approx -1.29 \pm 0.23 \qquad \text{(G-1)}$$

Estimation of the CEC transfer factor, f_{cec} is somewhat more difficult on account of both that the CEC of the Forsmark material is not known to an acceptable degree of precision and that different methods have been used to measure the CEC. In this case it was necessary to assume a CEC of 1.0±0.5 cmol/kg, for Forsmark metagranite which should be regarded as an order of magnitude estimate of the true CEC and its associated uncertainty. On the basis of this assumption, the CEC transfer factor is estimated to be:

$$\log_{10} f_{cec} \approx -0.1 \pm 0.43 \qquad \text{(G-2)}$$

Using the f_m and f_{cec} transfers factors, estimated K_d^0 values were calculated for the original 12 data points. On account of the limited number of data points, the individual K_d^0 values and their uncertainties were re-sampled assuming a convex combination of the underlying lognormal distributions, now including the additional uncertainties of the f_m and f_{cec} transfer factors. The resulting, translated and expanded uncertainty distribution for K_d^0 is shown in Figure G-3.

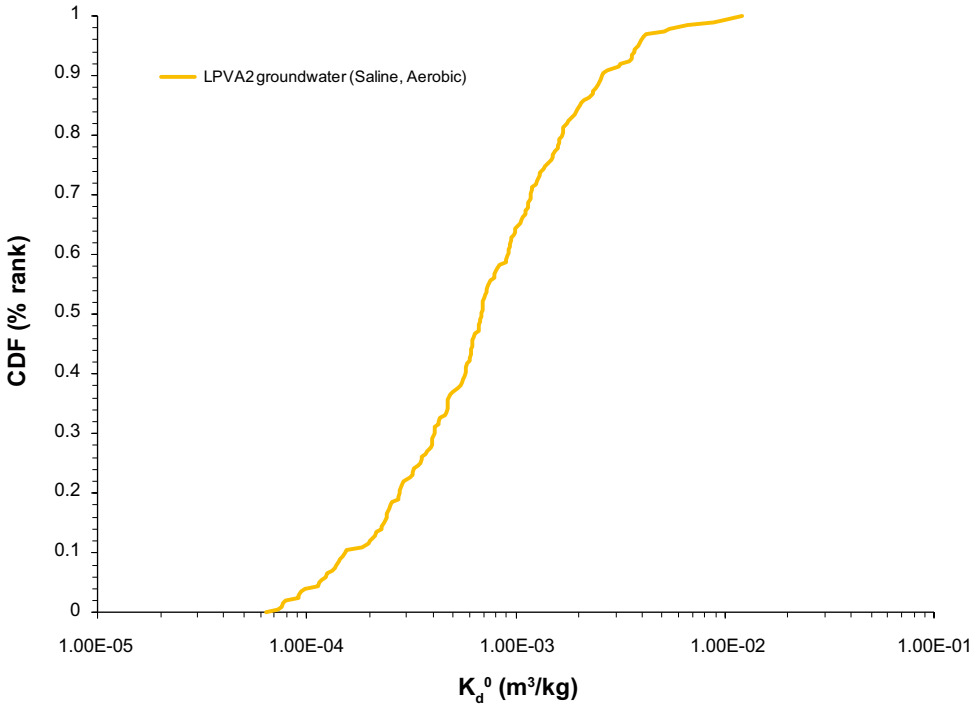

Figure G-3. *K_d^0 (m^3/kg) values calculated for Np(V) sorption based on literature R_d data. Surface area normalisation, mechanical damage, and CEC transfer factors (f_m, and f_{CEC}) have been considered in the estimation procedure. The raw data are corrected to give values deemed appropriate for Forsmark metagranite (SKB rock code 101057) under in situ conditions and are presented as an empirical cumulative distribution function.*

Recommended K_d data for SR-Site application conditions

The site investigation data and literature derived values (taken from Figure G-1 and Figure G-3) are shown side by side in Figure G-4. Although the K_d^0 values derived from site specific and literature data show reasonable agreement, they have been processed in different ways and it is possible that this could introduce unnecessary bias if the different data sets were to be combined numerically. Bearing this in mind, and the fact that a relatively good data set was already available for the site specific materials, the data from /Huitti et al. 1996/ have not been used in the final K_d recommendation and should instead be considered as a consistency check on the values derived independently from the site investigation data.

If it is assumed that the principal uncertainties relating to variable groundwater composition are internalised in the individual data sets shown previously in Figure G-1, a recommended range for application in SR-Site can be defined by aggregating these into a global data set. The relevant K_d range for application in SR-Site is given in Figure G-5.

Assessment of predominant redox state under application groundwater conditions

To ascertain the principal redox state of Np under application groundwater conditions, the speciation of Np was calculated for 20,000 randomly sampled groundwater compositions taken from the SR-Site temperate domain simulations /Salas et al. 2010/. The calculations were made for the prevailing groundwater chemistry at time 2,000 y, 3,000 y, 5,000 y, and 9,000 y using PHREEQC and the SKB-TDB /Duro et al. 2006/. Since it is not certain which redox couple can be assumed to dominate the groundwater redox conditions in the SR-Site temperate case groundwater simulations, two different redox couples were assumed as individual case studies for groundwater redox control. These are:

a) The Fe^{2+} / $Fe(OH)_3$ redox pair using equilibrium constants consistent with the calibration model derived by /Grenthe et al. 1992/.

b) The SO_4^{2-}/FeS_{am} redox pair.

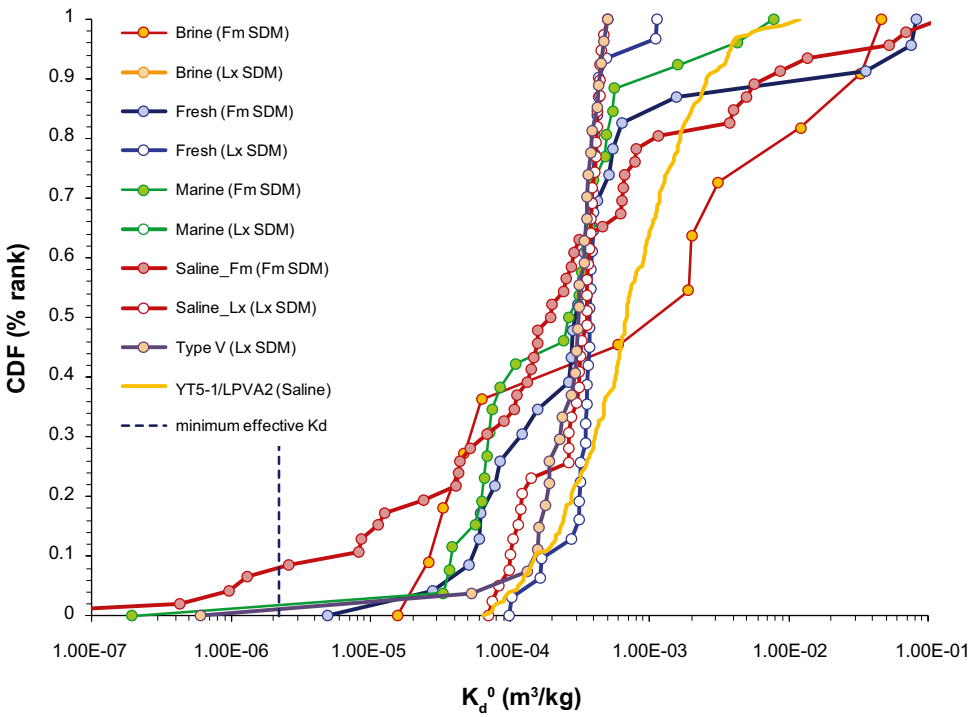

Figure G-4. *K_d^0 (m^3/kg) values calculated for Np(V) sorption corrected to give values deemed appropriate for Forsmark metagranite (SKB rock code 101057) under in situ conditions. This figure combines the data from the site investigations (Figure G-1) and literature data (Figure G-3) and indicates a relatively good agreement between the data sets of different origin.*

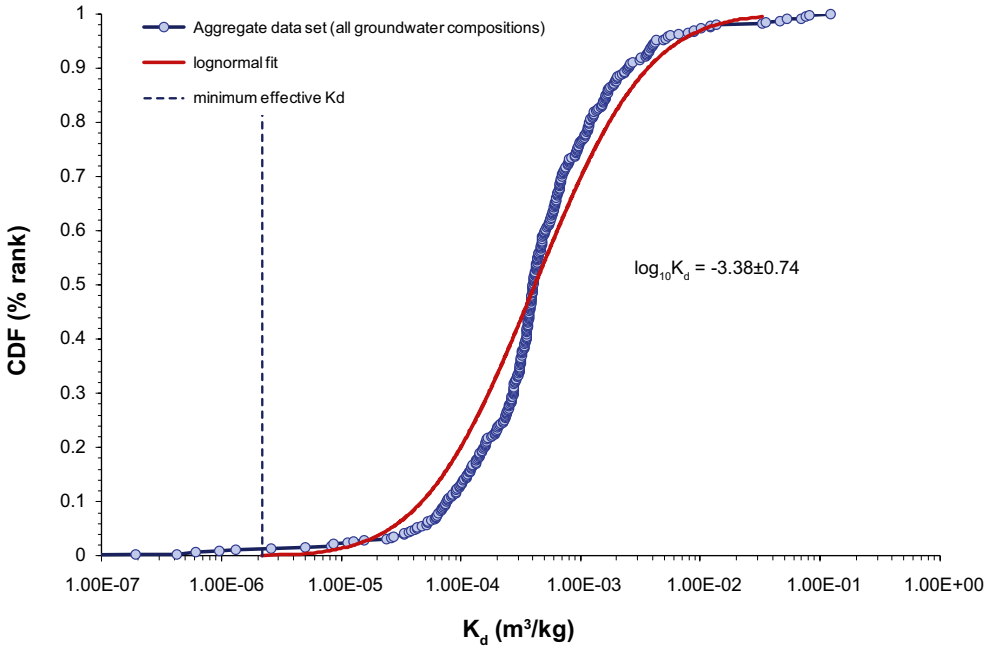

Figure G-5. *Recommended K_d (m^3/kg) values for Np(V) sorption for use in SR-Site calculations. The data range is considered to be applicable to all groundwater compositions and assumes Forsmark metagranite (SKB rock code 101057) as a representative rock type. The parameters of the lognormal distribution fit to the data are indicated in the figure.*

In addition to calculating the actual speciation of Np in the application groundwater, sweep calculations were made for a range of hypothetical redox potentials to ascertain the location of the redox transition point where the Np(IV) and Np(V) species are present in roughly equal concentrations. For numerical reasons this was done only for the convex hull of data points describing the envelope of pH and total carbonate concentrations in the application groundwater. From these data, a plane of best fit can then be calculated for the transition point which can be shown to be valid for all groundwater compositions within the convex hull. This provides a visual means of ascertaining how close the system is to the point of Np(IV)/Np(V) redox transition. The redox parameter space calculated in this fashion is plotted in Figure G-6 for the groundwater compositions existing at 2,000 y in the temperate case groundwater simulations.

Although the location of the plane of best fit roughly demarcates the regions of predominance of the oxidising and reducing forms of Np, it does not show the full extent of the region where non-negligible fractions of both redox species can co-exist. The redox sweep data are therefore plotted in Figure G-7 where the fraction of the reduced Np(IV) form is given as a function of redox potential.

There is a general tendency for the redox potential to decrease over time in the SR-Site temperate case simulations due to the freshening of the groundwater with a meteoric component of higher carbonate content. The redox parameter space is plotted in Figure G-8 for the groundwater compositions existing at 9,000 y. These represent the highest redox potentials encountered in the temperate time period simulated for SR-Site. As can be seen from Figure G-8 and Figure G-9, conditions are sufficiently reducing at 9,000 y for Np(IV) to be the dominant redox species.

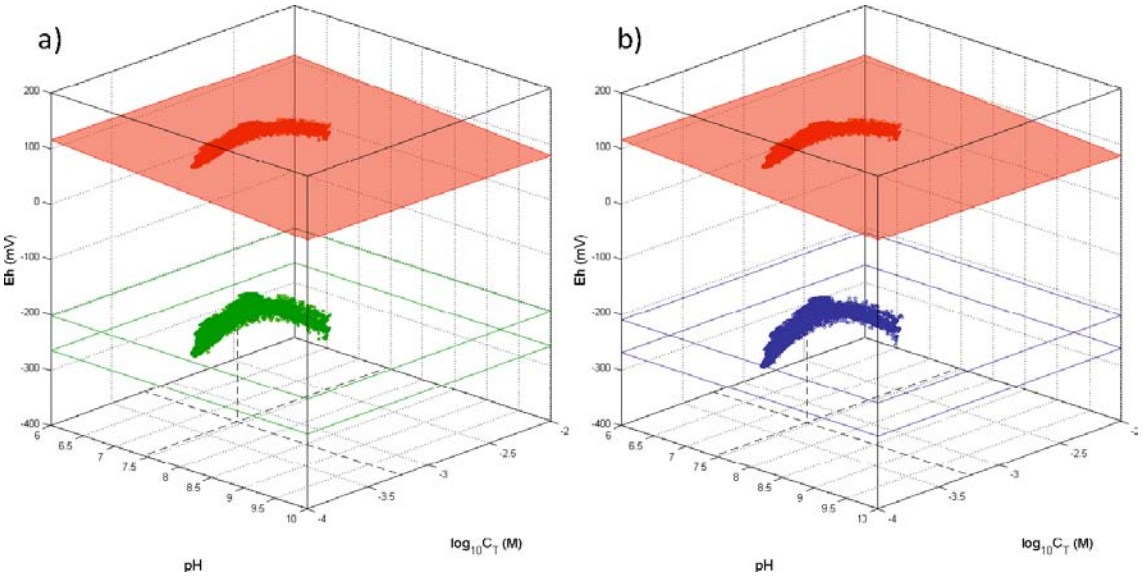

Figure G-6. *Redox parameter space for 20,000 randomly selected SR-Site temperate case groundwater compositions at 2,000 y for (a) $Fe^{2+}/Fe(OH)_3$ redox couple, and (b) SO_4^{2-}/FeS_{am} redox couple. The calculations indicate that all sampled groundwater compositions are sufficiently reducing for Np(IV) to be the dominant redox species (min and max Eh range indicated by green and blue coloured outline rectangles). The theoretical transition region where Np(IV) and Np(V) are present in equal concentration is indicated by the red plane (red markers are mapped to the plane at the same pH and carbonate coordinates as the actual groundwater compositions for reference purposes).*

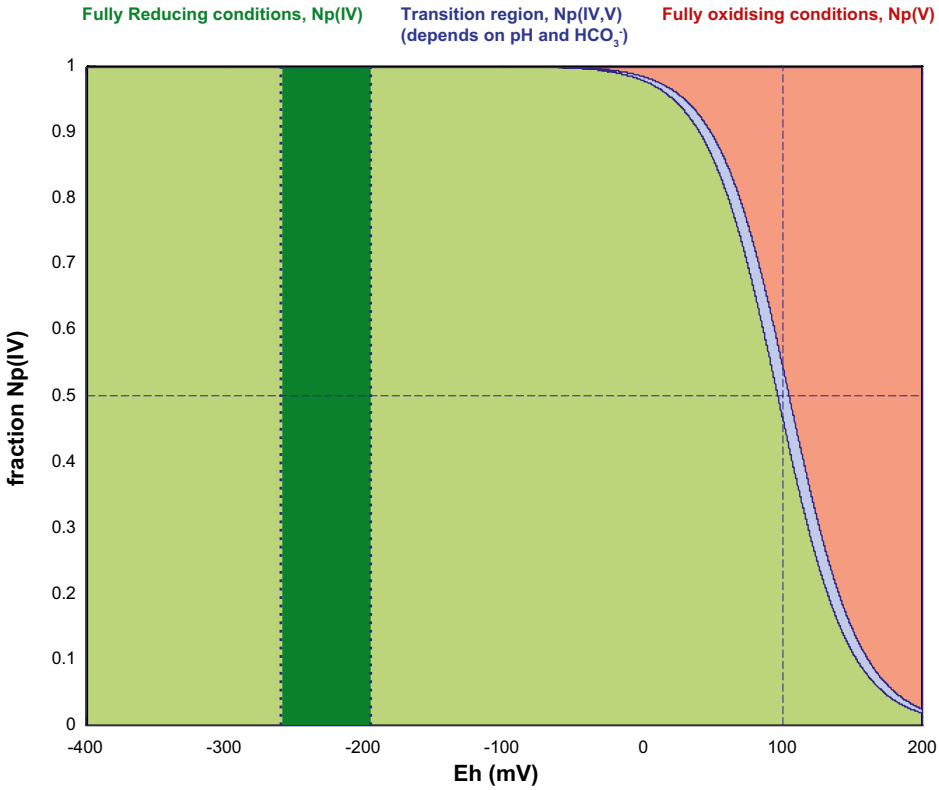

Figure G-7. *Theoretical redox transition zone for Np (blue shaded region) compared with redox conditions in SR-Site temperate case at 2,000 y (dark green shaded region) which encompasses the potential span of both the $Fe(OH)_3$ and FeS_{am} redox cases. The light green and red shaded areas represent fully reducing (100% Np(IV)) and fully oxidising (100% Np(V)) conditions, respectively. The cross-hairs in the figure approximately indicate the centroid of the transition point for the application groundwater pH and carbonate ranges illustrated previously in Figure G-6.*

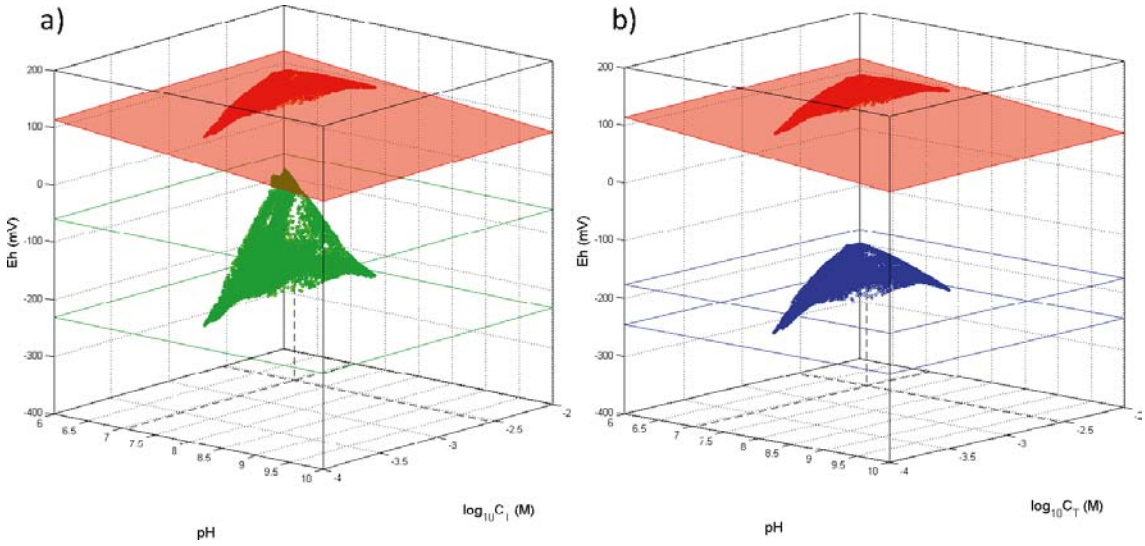

Figure G-8. *Redox parameter space for 20,000 randomly selected SR-Site temperate case groundwater compositions at 9,000 y for (a) $Fe^{2+}/Fe(OH)_3$ redox couple, and (b) SO_4^{2-}/FeS_{am} redox couple. The calculations indicate that all sampled groundwater compositions are sufficiently reducing for Np(IV) to be the dominant redox species (min and max Eh range indicated by coloured rectangles). The theoretical transition region where Np(IV) and Np(V) are present in equal concentration is indicated by the red plane (red markers are mapped to the plane at the same pH and carbonate coordinates as the actual groundwater compositions for reference purposes).*

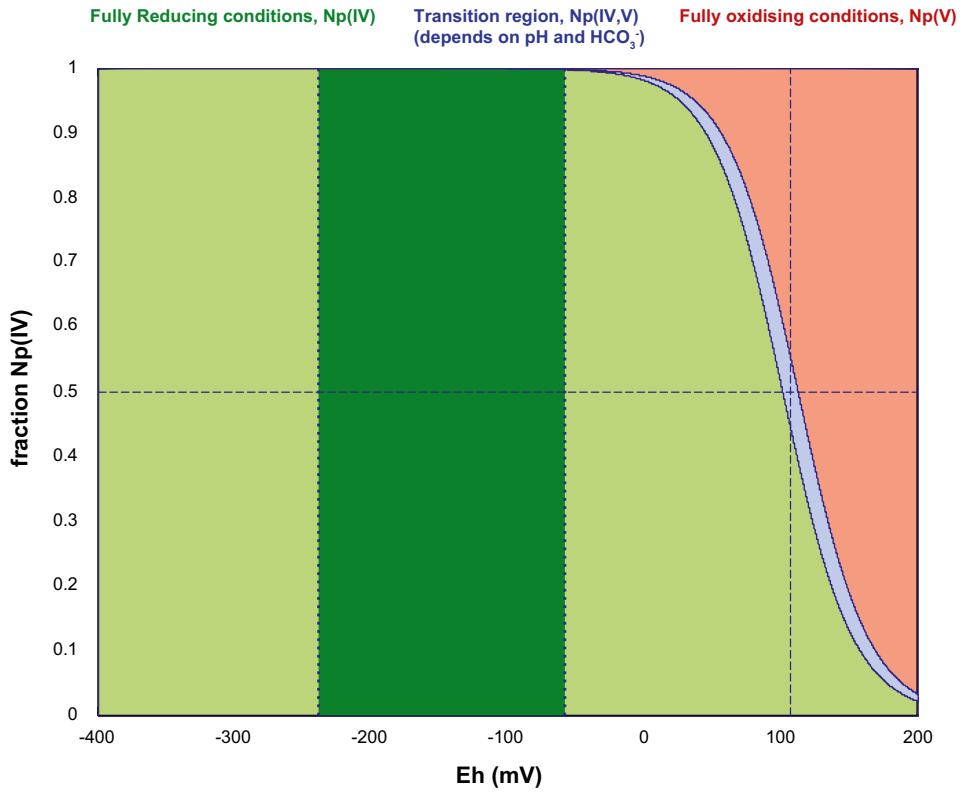

Figure G-9. *Theoretical redox transition zone for Np (blue shaded region) compared with redox conditions in SR-Site temperate case at 9,000 y (dark green shaded region) which encompasses the potential span of both $Fe(OH)_3$ and FeS_{am} redox cases. The light green and red shaded areas represent fully reducing (100% Np(IV)) and fully oxidising (100% Np(V)) conditions, respectively. The cross-hairs in the figure approximately indicate the centroid of the transition point for the application groundwater pH and carbonate ranges illustrated previously in Figure G-8.*

Appendix H

K_d data derivation sheet for nickel (Ni)

Overview of site investigation data

Site specific sorption data were obtained for Ni(II) during the site investigations at Forsmark /Byegård et al. 2008/ and Laxemar /Selnert et al. 2009/. These data are summarised in the bedrock transport properties site descriptive model /Crawford 2008/ and are the basis for K_d values recommended for use in SR-Site. In most cases (although there are some exceptions) there is a time dependency in the experimental data with a clear trend towards higher R_d values at increasing times. The data also exhibit a relatively clear surface area dependency whereby smaller crushed particle sizes are associated with higher sorptivities than larger size fractions. A typical time series for Ni(II) sorption on Forsmark metagranite (SKB rock code 101057) is shown in Figure H-1.

The Forsmark site data are based on rock samples taken from three borehole sections while the Laxemar site data are based on rock samples taken from a single borehole section. For the same reasons discussed previously in relation to Cs(I) sorption, no attempt has been made to model the time dependency of the data. The data for Ni(II) sorption therefore have been treated by considering the raw data set in its entirety without filtering on the basis of crushed size fraction or contact time.

Overview of available literature data

The most detailed set of sorption data for relevant rock types and groundwater compositions in the open literature is documented by /Kulmala and Hakanen 1993/. In this study, sorption was measured on two crushed rock samples taken from different sites. These were a tonalite (Olkiluoto) crushed to a particle size specified as less than 3 mm, and a Rapakivi granite (Hästholmen) crushed to a particle size specified as less than 2 mm. The sorption experiments were carried out under oxic conditions using natural groundwater samples native to each site. The Olkiluoto groundwater (TVO-GW) was fresh in character with an ionic strength of 0.017 M. The Hästholmen groundwater (IVO-GW)

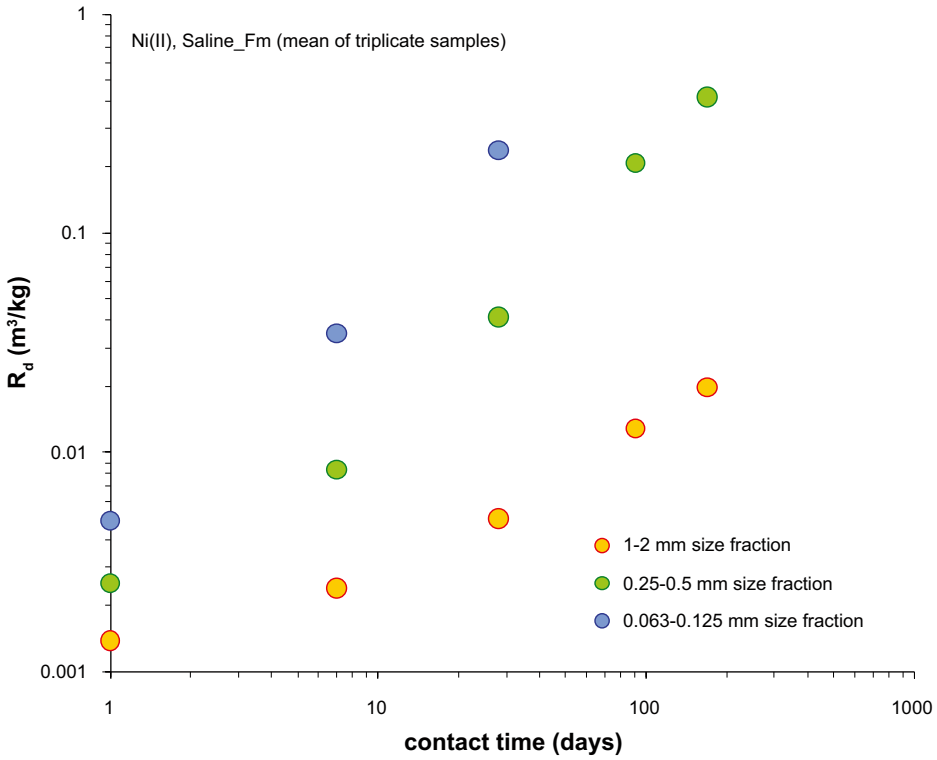

Figure H-1. *Typical time series for Ni(II) sorption R_d (m^3/kg) measured in the Forsmark site investigation studies. There is a clear sorption dependency on both particle size and time.*

was more saline with an ionic strength of 0.21 M. R_d values and sorption percentages, S(%) were estimated for contact times ranging from 7 days to 6 months for a Ni spike concentrations in the range of 3×10^{-8} –1.3×10^{-7} M. The R_d data compiled in /Kulmala and Hakanen 1993/ are given without error estimates although the sorption percentages are specified with uncertainties. In all there were 84 measurements of R_d for each rock type corresponding to different spike concentrations and contact times.

Selection of representative data for site specific conditions

For Ni(II) sorption, a mixture of site data and literature data have been considered in the recommendation of K_d ranges for use in SR-Site safety assessment calculations. Although the site specific data are primarily used to establish the recommended K_d data range, the Finnish data from /Kulmala and Hakanen 1993/ are used in a supporting role to provide a consistency check on the values derived from site specific materials studied in the Forsmark and Laxemar site investigations. The selection procedure and associated calculations are described separately since data handling procedures were different for the site investigation and literature data.

Site specific data from Forsmark and Laxemar

Since the sorption of Ni(II) appears to exhibit an ionic strength dependency, the procedure for derivation of K_d values relevant for application within SR-Site consisted of the same steps as described previously for Cs(I). The main difference in this case is that no suitable ion-exchange or surface complexation model is available to describe the ionic strength dependency of Ni(II) sorption. Estimated K_d^0 data corrected for surface area normalisation, mechanical damage, and CEC effects are plotted in Figure H-2 assuming Forsmark metagranite (SKB rock code 101057) as a representative rock type for the Forsmark site. Although the uncertainty ranges for the individual data sets are large, there is a clear tendency towards greater sorptivity under low ionic strength conditions relative to that obtained for the more saline groundwater types.

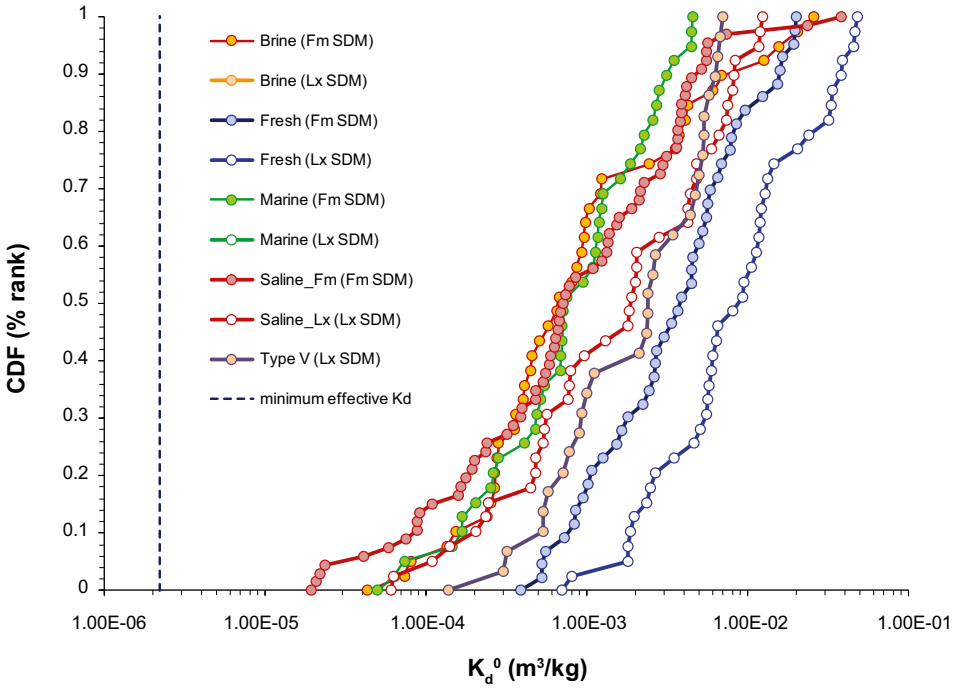

Figure H-2. *K_d^0 (m^3/kg) values calculated for Ni(II) sorption based on raw R_d data for site-specific rock types and groundwater compositions as reported in the Forsmark (Fm SDM) and Laxemar (Lx SDM) site investigations. Surface area normalisation, mechanical damage, and CEC transfer factors (f_A, f_m, and f_{cec}) have been considered in the estimation procedure. The raw data are corrected to give values deemed appropriate for Forsmark metagranite (SKB rock code 101057) under in situ conditions and are presented as an empirical cumulative distribution function. A minimum effective K_d reference line is plotted in the figure indicating the upper 95% confidence limit for the matrix storage capacity of the rock based on water saturation porosity.*

Literature data for Tonalite and Rapakivi granite

Using the procedures outlined in Appendix C, the R_d values and their error estimates were re-calculated from the S(%) values given in /Kulmala and Hakanen 1993/. The individual R_d values and their uncertainties were then re-sampled assuming a convex combination of the underlying uncertainty distributions. The composite distribution of R_d values thus obtained is shown in Figure H-3.

Although the data plotted in Figure H-3 have not been corrected for differences in BET surfaces area or CEC, the data appear to exhibit an ionic strength dependency with the fresh groundwater sample giving higher R_d values relative to the saline groundwater. No BET surface area or CEC measurement data are given in /Kulmala and Hakanen 1993/, although BET data are given in other reports /Huitti et al. 1996, 1998/ for the same materials crushed to the same grain size. Assuming the measured BET surface area for monolithic samples of Forsmark metagranite (SKB rock code 101057) reported by /André et al. 2009/, the mechanical damage transfer factor, f_m and its formal uncertainty (2σ) was estimated to be:

$\log_{10} f_m \approx -1.23 \pm 0.26$ (Olkilutoto tonalite) (H-1)

$\log_{10} f_m \approx -1.29 \pm 0.23$ (Hästholmen, Rapakivi granite) (H-2)

The CEC is unknown for these rock types although the biotite content has been estimated to 6.6% by volume for Olkiluoto tonalite /Huitti et al. 1998/ and 3.8% for Rapakivi granite from Hästholmen /Huitti et al. 1996/. Given that the biotite content of Forsmark metagranite is roughly 5.4% by volume /Sandström and Stephens 2009/, this allows the estimation of a very approximate CEC transfer factor:

$\log_{10} f_{cec} \approx -0.087$ (Olkilutoto tonalite) (H-3)

$\log_{10} f_{cec} \approx 0.15$ (Hästholmen, Rapakivi granite) (H-4)

Using the f_m and f_{cec} transfer factors, estimated K_d^0 values were calculated for the original data points. Owing to the large uncertainties associated with the transfer factors, the individual K_d^0 values and their uncertainties were re-sampled assuming a convex combination of the underlying lognormal distributions, now including the additional uncertainty of the f_m transfer factor. Since it was not possible to estimate a formal uncertainty for the CEC transfer factor, the additional uncertainty arising due to this transfer factor was neglected. The resulting, translated and expanded uncertainty distribution for K_d^0 is shown in Figure H-4.

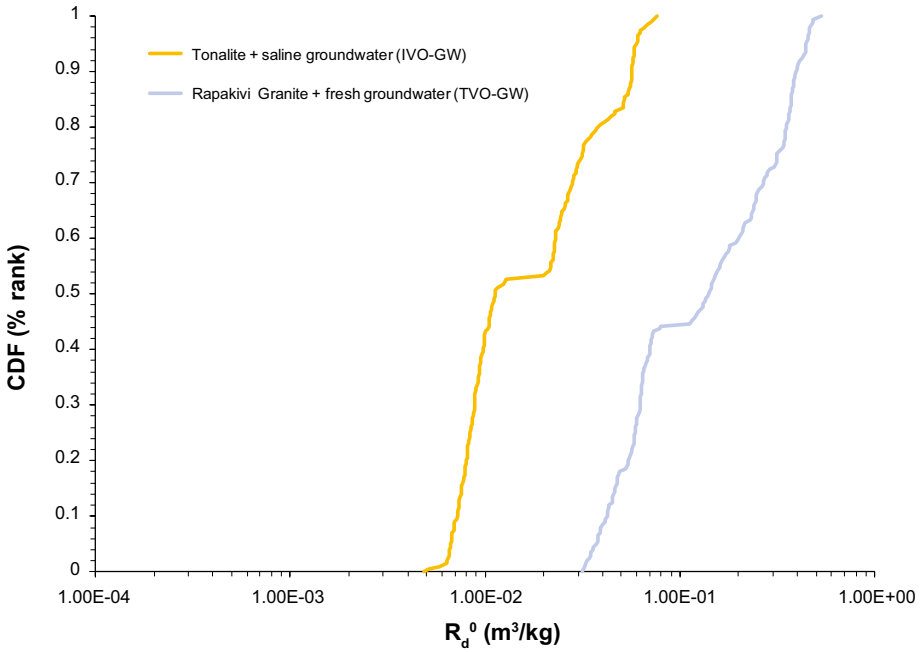

Figure H-3. *R_d^0 (m^3/kg) values calculated for Ni(II) sorption based on literature R_d data and presented as an empirical cumulative distribution function for Olkiluoto tonalite (TVO-GW) and Rapakivi granite samples (IVO-GW). The individual data points and their uncertainties have been re-calculated from tabulated sorption percentage data and then re-sampled to give the composite distribution plotted in the figure.*

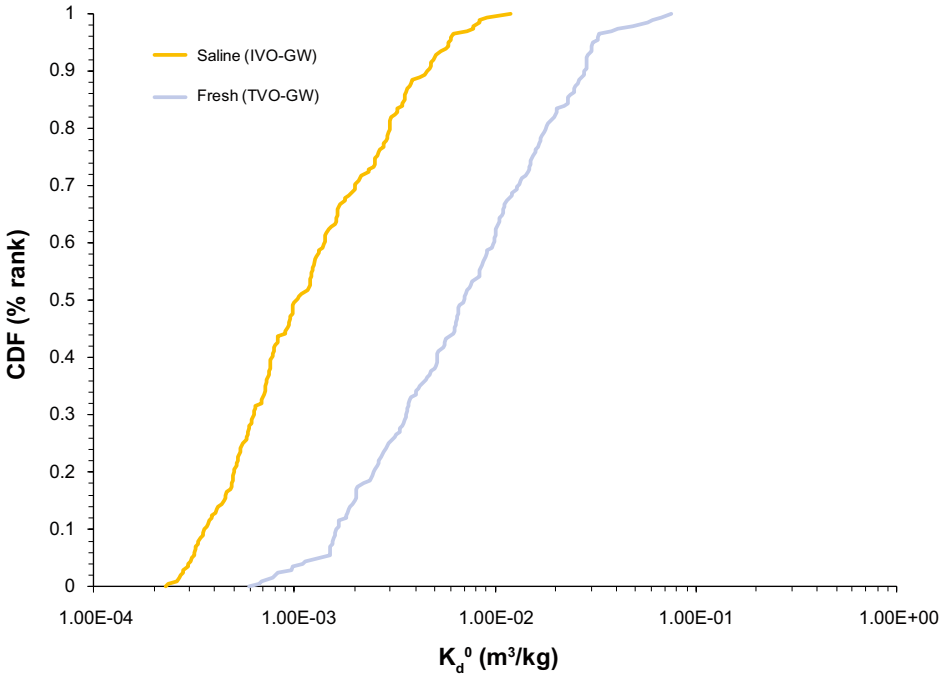

Figure H-4. *K_d^0 (m^3/kg) values calculated for Ni(II) sorption based on literature R_d data. Surface area normalisation, mechanical damage, and CEC transfer factors (f_m, and f_{CEC}) have been considered in the estimation procedure. The raw data are corrected to give values deemed appropriate for Forsmark metagranite (SKB rock code 101057) under in situ conditions and are presented as an empirical cumulative distribution function.*

Recommended K_d data for SR-Site application conditions

The site investigation data and literature derived values (taken from Figure H-2 and Figure H-4) are shown side by side in Figure H-5. Although the K_d^0 values derived from site specific and literature data show reasonable agreement, they have been processed in different ways and it is possible that this could introduce unnecessary bias if the different data sets were to be combined numerically. Bearing this in mind, and the fact that a relatively good data set was already available for the site specific materials, the data from /Kulmala and Hakanen 1993/ have not been used in the final K_d recommendation and should instead be considered as a consistency check on the values derived independently from the site investigation data.

Since an appropriate ion-exchange or surface complexation model is not available to provide chemistry transfer factors for application groundwater conditions, a stochastic approach based upon linear regression of the individual data sets was employed. The method was based on random sampling (10^5 samples) of the ionic strength distribution of the application groundwater to obtain the independent variable. The regression equation was then used directly to estimate the expected change in K_d resulting from variable ionic strength plus a random error for the unexplained variation. The resulting K_d values are plotted in Figure H-6 to Figure H-9 for the SR-Site calculation cases corresponding to the temperate time domain.

Although the spread of the simulated data (grey markers) in the cross-plots appears large, it should be noted that this represents the entire extrapolated data set whereas the individual groundwater types are plotted with 1σ error bars. Generally the data indicate that the random error component is larger than the systematic trend due to ionic strength variation.

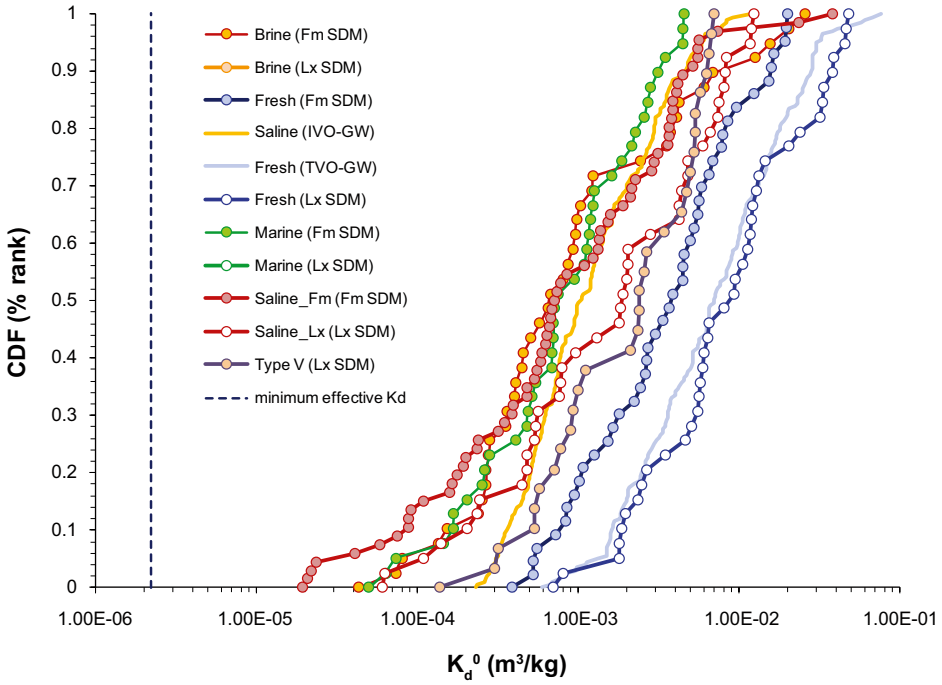

Figure H-5. *K_d^0 (m^3/kg) values calculated for Ni(II) sorption corrected to give values deemed appropriate for Forsmark metagranite (SKB rock code 101057) under in situ conditions. This figure combines the data from the site investigations (Figure H-2) and literature data (Figure H-4) and indicates a relatively good agreement between the data sets of different origin.*

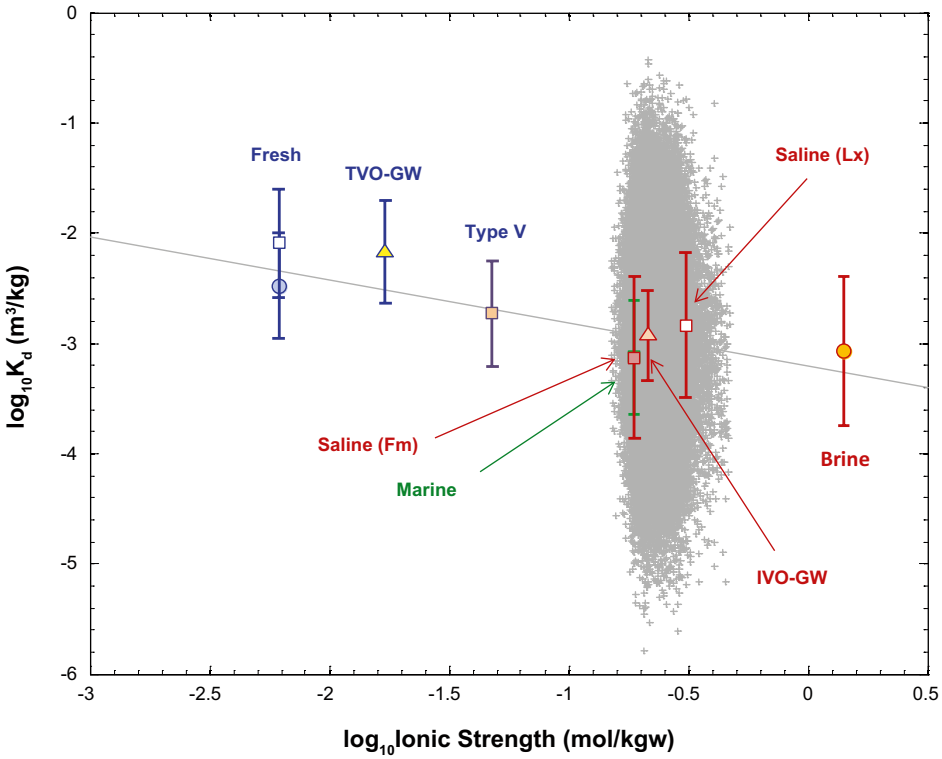

Figure H-6. *Cross-plot of K_d (m^3/kg) values for Ni(II) versus ionic strength (mol/kgw) on logarithmic axes. The recommended data are for SR-Site application conditions at 2,000 y in the temperate case and are plotted as the swarm of grey markers. K_d^0 data are plotted as geometric means with 1σ standard errors for the different groundwater compositions used in the site investigation.*

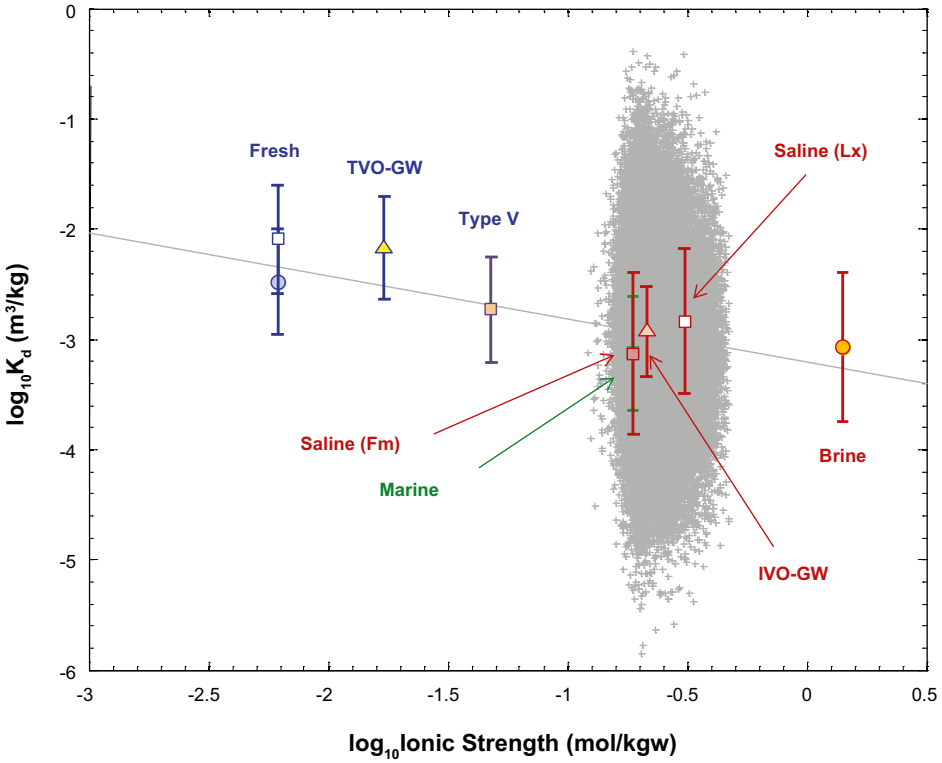

Figure H-7. *Cross-plot of K_d (m^3/kg) values for Ni(II) versus ionic strength (mol/kgw) on logarithmic axes. The recommended data are for SR-Site application conditions at 3,000 y in the temperate case and are plotted as the swarm of grey markers. K_d^0 data are plotted as geometric means with 1σ standard errors for the different groundwater compositions used in the site investigation.*

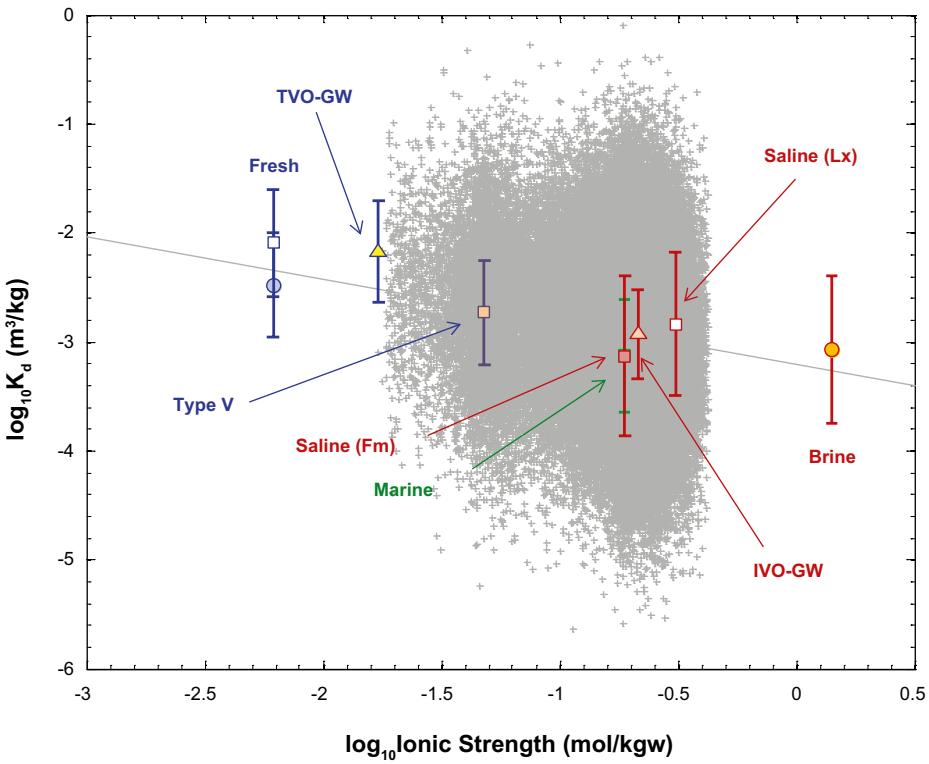

Figure H-8. *Cross-plot of K_d (m^3/kg) values for Ni(II) versus ionic strength (mol/kgw) on logarithmic axes. The recommended data are for SR-Site application conditions at 5,000 y in the temperate case and are plotted as the swarm of grey markers. K_d^0 data are plotted as geometric means with 1σ standard errors for the different groundwater compositions used in the site investigation.*

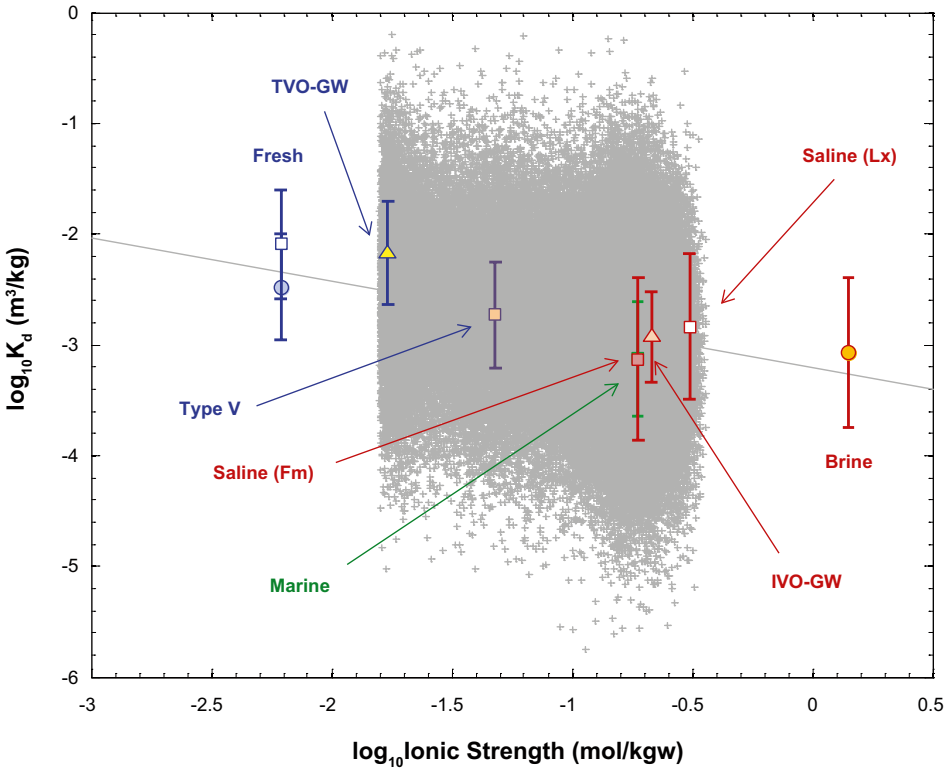

Figure H-9. *Cross-plot of K_d (m^3/kg) values for Ni(II) versus ionic strength (mol/kgw) on logarithmic axes. The recommended data are for SR-Site application conditions at 9,000 y in the temperate case and are plotted as the swarm of grey markers. K_d^0 data are plotted as geometric means with 1σ standard errors for the different groundwater compositions used in the site investigation.*

Based on the regression model calculations, the following K_d ranges for Ni(II) are recommended for use at different times in the hydrogeochemical evolution of the repository environment:

$\log_{10} K_d \approx -2.96 \pm 0.65$ (t = 2,000 y) (H-5)

$\log_{10} K_d \approx -2.96 \pm 0.65$ (t = 3,000 y) (H-6)

$\log_{10} K_d \approx -2.91 \pm 0.65$ (t = 5,000 y) (H-7)

$\log_{10} K_d \approx -2.82 \pm 0.65$ (t = 9,000 y) (H-8)

As can be seen from the recommended data, the changing salinity of the repository environment has only a weak impact on the K_d distribution, with a tendency to towards slightly higher sorptivities with time. Since it is not possible to consider temporally variable K_d values in safety assessment calculations, the time period giving the lowest K_d value is recommended to be used for calculations. This corresponds to the groundwater conditions existing at 3,000 y. Generally the numerically calculated K_d uncertainties were found to be lognormally distributed (see Figure H-10).

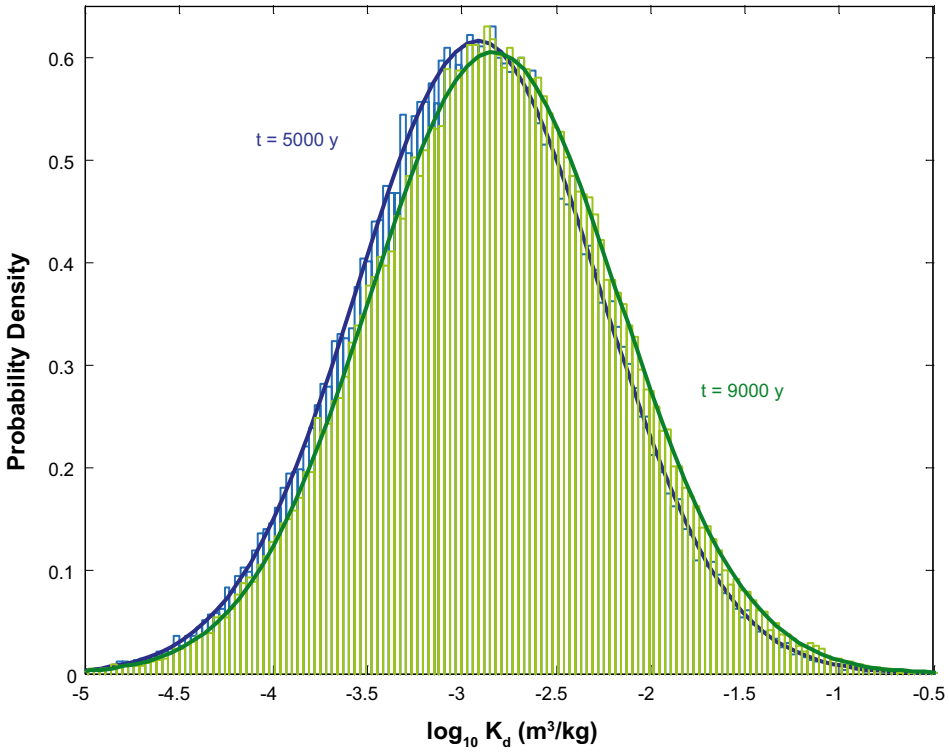

Figure H-10. *Comparison of K_d (m^3/kg) distributions predicted for Ni(II) at 5,000 y and 9,000 y. The data are plotted in histogram form with a fitted lognormal distribution in each case. Both data sets are well described by a lognormal distribution.*

Appendix I

K_d data derivation sheet for niobium (Nb)

Overview and evaluation of available literature data

The most detailed set of Nb sorption data for relevant rock types and groundwater compositions is documented by /Kulmala and Hakanen 1993/. In this study, sorption was measured on two crushed rock samples taken from different sites. These were a tonalite (Olkiluoto) crushed to a particle size specified as less than 3 mm, and a Rapakivi granite (Hästholmen) crushed to a particle size specified as less than 2 mm. The sorption experiments were carried out under oxic conditions using natural groundwater samples native to each site. The Olkiluoto groundwater (TVO-GW) was fresh in character with an ionic strength of 0.017 M. The Hästholmen groundwater (IVO-GW) was more saline with an ionic strength of 0.21 M. The R_d values and sorption percentages, S(%) were estimated for contact times ranging from 7 days to 6 months for Nb(V) spike concentrations in the range 2.8×10^{-11} –6.8×10^{-10} M. The R_d data compiled in /Kulmala and Hakanen 1993/ are given without error estimates although the sorption percentages are specified with uncertainties as noted previously for Ni(II). In all there were 72 R_d measurements for each rock type corresponding to different spike concentrations and contact times.

Selection of representative data for site specific conditions

The R_d values and their error estimates were re-calculated from the raw data in /Kulmala and Hakanen 1993/ using the procedure outlined in Appendix C. The individual R_d values and their uncertainties were then re-sampled assuming a convex combination of the underlying uncertainty distributions. The composite distribution of R_d values thus obtained is shown in Figure I-1.

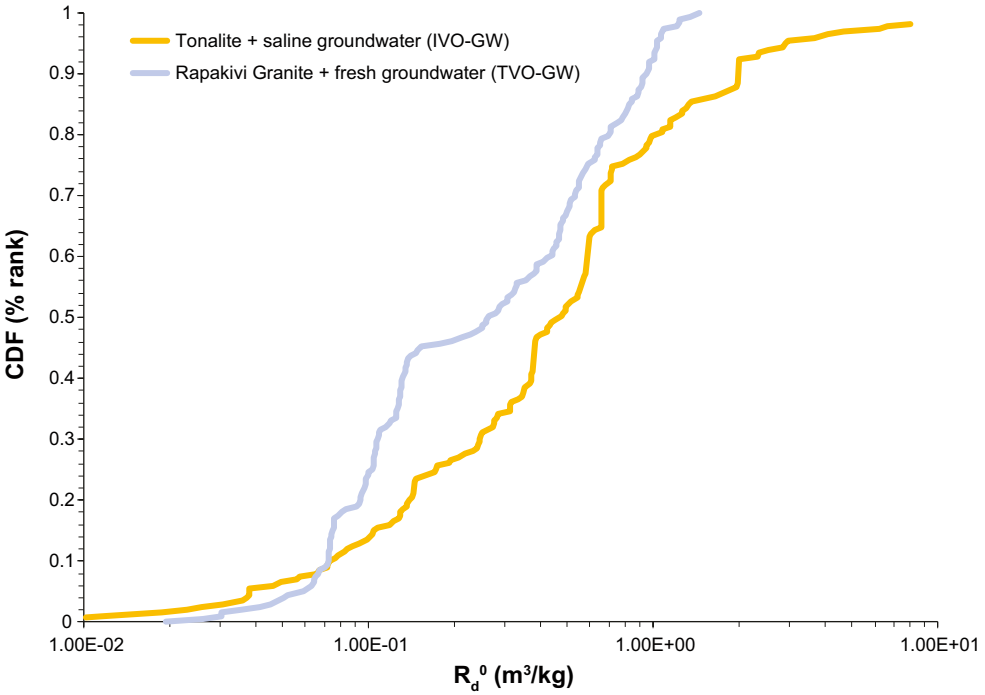

Figure I-1. *R_d^0 (m^3/kg) values calculated for Nb(V) sorption based on literature R_d data and presented as an empirical cumulative distribution function for Olkiluoto tonalite (TVO-GW) and Rapakivi granite samples (IVO-GW). The individual data points and their uncertainties have been re-estimated from tabulated sorption percentage data and then re-sampled to give the composite distribution plotted in the figure.*

No large differences are noted between the data sets for saline and fresh groundwater types which is in keeping with the postulated (inner-sphere) surface complexation sorption mechanism. No BET surface area or CEC measurement data are given in /Kulmala and Hakanen 1993/, although BET data are given in other reports /Huitti et al. 1996, 1998/ for the same materials crushed to the same grain size. Since the rock types are the same as discussed previously for Ni(II) sorption (Appendix H), the same mechanical damage and CEC transfer factors have been used:

$\log_{10} f_m \approx -1.23 \pm 0.26$ (Olkilutoto tonalite) (I-1)

$\log_{10} f_m \approx -1.29 \pm 0.23$ (Hästholmen, Rapakivi granite) (I-2)

And,

$\log_{10} f_{cec} \approx -0.087$ (Olkilutoto tonalite) (I-3)

$\log_{10} f_{cec} \approx 0.15$ (Hästholmen, Rapakivi granite) (I-4)

Using the f_m and f_{cec} transfer factors, estimated K_d^0 values were calculated for the original data points. Owing to the large uncertainties associated with the transfer factors, the individual K_d^0 values and their uncertainties were then re-sampled assuming a convex combination of the underlying lognormal distributions, now including the additional uncertainty of the f_m transfer factor. Since it was not possible to estimate a formal uncertainty for the CEC transfer factor, the additional uncertainty arising due to this transfer factor was neglected. The resulting, translated and expanded uncertainty distribution for K_d^0 is shown in Figure I-2.

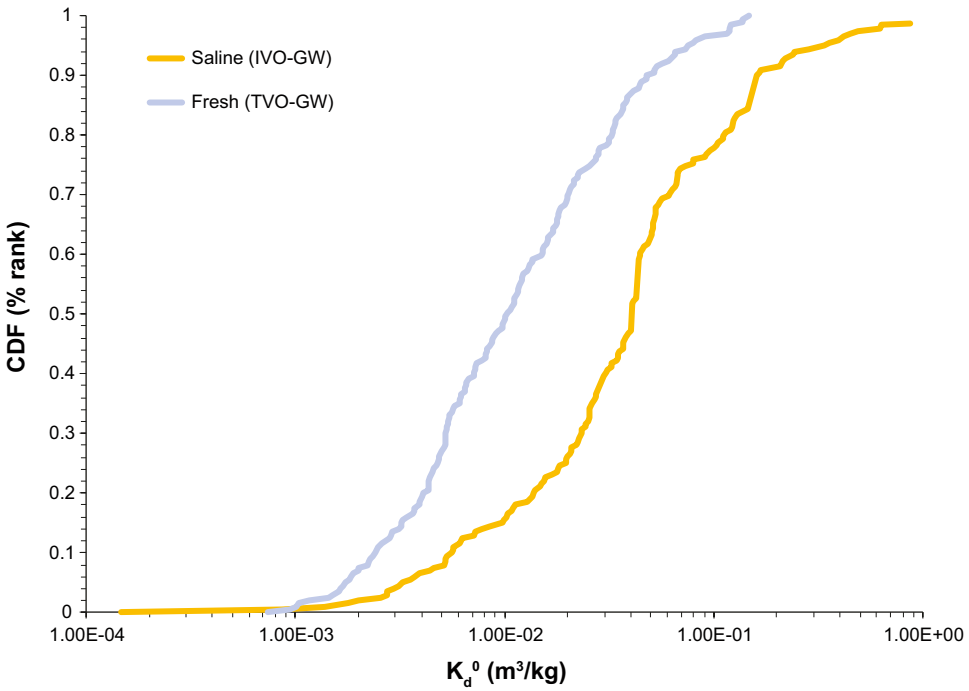

Figure I-2. *K_d^0 (m^3/kg) values calculated for Nb(V) sorption based on literature R_d data. Surface area normalisation, mechanical damage, and CEC transfer factors (f_m, and f_{cec}) have been considered in the estimation procedure. The raw data are corrected to give values deemed appropriate for Forsmark metagranite (SKB rock code 101057) under in situ conditions and are presented as an empirical cumulative distribution function.*

Recommended K_d data for SR-Site application conditions

If it is assumed that the principal uncertainties relating to variable groundwater composition are internalised in the individual data sets shown in Figure I-2, a recommended range for application in SR-Site can be defined by aggregating these into a global data set. The relevant K_d range for application in SR-Site is given in Figure I-3.

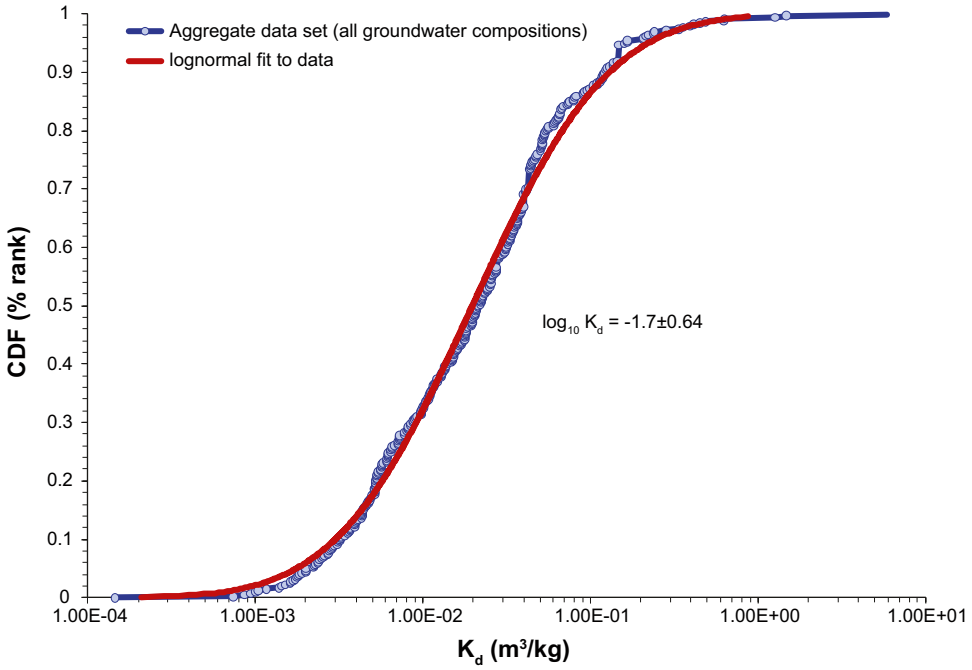

Figure I-3. *Recommended K_d (m^3/kg) values for Nb(V) sorption for use in SR-Site calculations. The data range is considered to be applicable to all groundwater compositions and assumes Forsmark metagranite (SKB rock code 101057) as a representative rock type. The parameters of the lognormal distribution fit to the data are indicated in the figure.*

Appendix J

K_d data derivation sheet for palladium (Pd)

Overview of available literature data

The sorption of Pd on granitic rock is poorly covered in the literature and only one study /Tachi et al. 1999/ has been found where sorption has been characterised using relevant materials and water compositions. This reference was not available in original form, being an internal technical report of the former Japan Nuclear Cycle Development Institute (JNC). Data values from this reference are reported, however, in the JNC Sorption database /Shibutani et al. 1999/. In the reported experiments, pH dependent sorption was measured on finely crushed granodiorite (≤ 0.355 mm) from Gunma, Japan. The contact solutions were simple NaCl dilutions of ionic strength 0.01 M and 0.1 M and the spike concentration was reported as 5×10^{-8} M. In the experiments, liquid to solid ratios of 50 ml/g and 500 ml/g were used and the contact time was 30 days.

Selection of representative data for site specific conditions

Since no major differences were apparent between individual R_d values reported for different ionic strengths and liquid to solid ratios, the data are taken as is and are plotted in Figure J-1 as an aggregate data set.

The BET surface area of the crushed granodiorite was reported as 0.7 m^2/g. Since only one particle size was used in the experiments, it was only necessary to use a single transfer factor to extrapolate the data to Forsmark rock under in situ conditions. The mechanical damage transfer factor, f_m was therefore estimated to be:

$$\log_{10} f_m \approx -1.65 \pm 0.23 \qquad \text{(J-1)}$$

Since no error estimate is given for the BET surface area of the crushed rock, the error estimate for f_m is estimated assuming only the standard error (2σ) of the Forsmark metagranite surface area. This will tend to underestimate the true uncertainty of f_m. No CEC data are given for the granodiorite used in the experiments, although the biotite content has been estimated to be roughly 4.32% by volume.

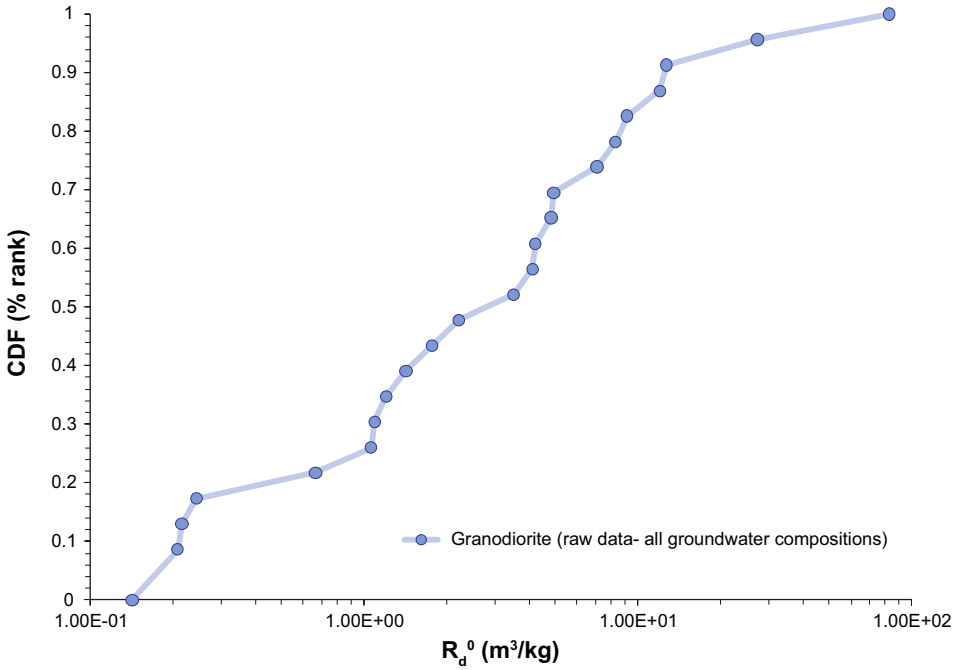

Figure J-1. *R_d^0 (m^3/kg) values calculated for Pd(II) sorption based on literature R_d data and presented as an empirical cumulative distribution function for Japanese granodiorite. Since there are no major differences between the data for different water compositions (0.01 M and 0.1 M) and liquid to solid ratios (50 ml/g and 500 ml/g), the data are given as an aggregate set.*

Since Forsmark metagranite has a biotite content of roughly 5.4% by volume /Sandström and Stephens 2009/, the CEC transfer factor, f_{cec} is estimated to be:

$$\log_{10} f_{cec} \approx 0.1 \qquad \text{(J-2)}$$

Since CEC transfer factors based upon estimated ranges of biotite content are particularly uncertain and because the factor calculated in Equation J-2 implies only a slightly increased sorptivity for the extrapolation to Forsmark site specific rock, this has been neglected in subsequent calculations.

Recommended K_d data for SR-Site application conditions

Estimated K_d^0 values were calculated for Forsmark metagranite using the mechanical damage transfer factor only (f_{cec} is neglected on grounds of caution). If it is assumed that the principal uncertainties relating to variable groundwater composition are internalised in the data, this data can be deemed suitable for SR-Site application conditions. The recommended K_d range for use in SR-Site transport calculations is given in Figure J-2.

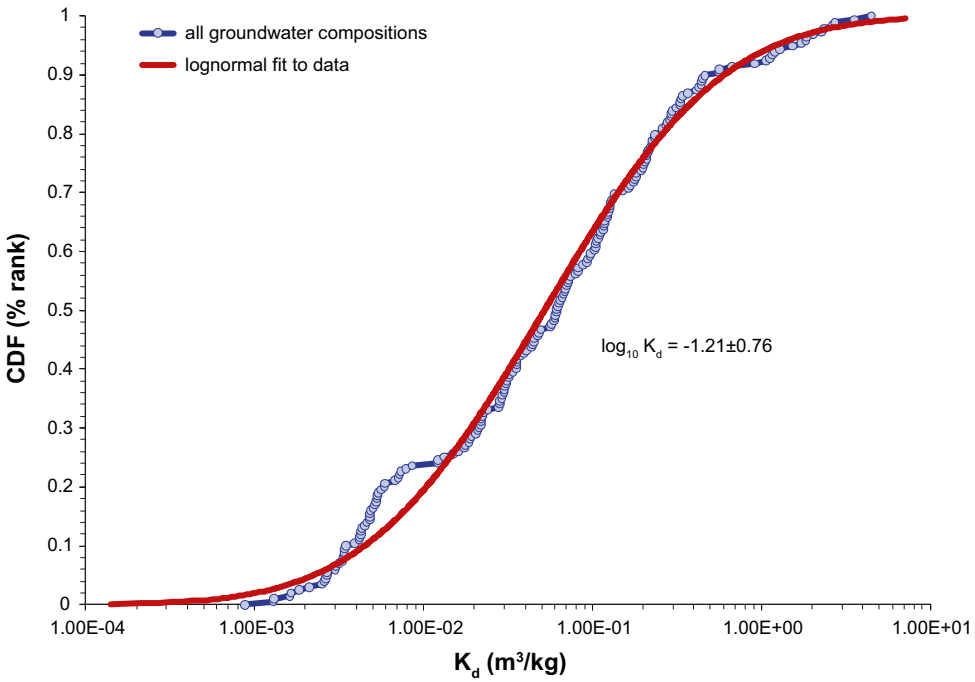

Figure J-2. *Recommended K_d (m^3/kg) values for Pd(II) sorption for use in SR-Site calculations. The data range is considered to be applicable to all groundwater compositions and assumes Forsmark metagranite (SKB rock code 101057) as a representative rock type. The parameters of the lognormal distribution fit to the data are indicated in the figure.*

Appendix K

K_d data derivation sheet for plutonium (Pu)

Overview of available literature data

The most detailed data sets for sorption of Pu on relevant rock types and groundwaters are documented by /Huitti et al. 1996/ and /Kulmala et al. 1998/. In these studies, sorption was measured on crushed rock taken from various sites in Finland. The sorption experiments were carried out under both oxic and anoxic conditions using natural groundwater samples native to the various sites and a liquid to solid ratio of 10 ml/g. For experiments carried out under anoxic conditions, the sampled groundwater was preserved in a nitrogen atmosphere to prevent oxidation of the Fe(II) content of the water. Spike concentrations of Pu were in the range 3.3×10^{-13}–5.7×10^{-10} M for oxic experiments and 1.9×10^{-12}–1.1×10^{-9} M for anoxic conditions. Material properties of the rock samples and groundwaters used by /Huitti et al. 1996/ and /Kulmala et al. 1998/ are given in Table K-1.

Table K-1. Material properties of Finnish rock types investigated by /Huitti et al. 1996/ and /Kulmala et al. 1998/. Means and standard deviations are given for three replicate samples where available.

Sample	**YT5-1**	**YT5-2**	**YT5-3**
Type	Fresh granite	Weathered granite	Altered granite
Source location	Hästholmen	Hästholmen	Hästholmen
Groundwater	LPVA2	LPVA2	LPVA2
Groundwater type	Saline	Saline	Saline
particle size (mm)	≤ 2.0	≤ 2.0	≤ 2.0
A_{BET} (m^2/g)	0.31±0.01	3.51±1.94	1.0±0.12
CEC (cmol/kg)	1.01±0.28	3.7±0.17	1.7±0.17
Biotite (vol%)	3.8%	4.2%	1.4%
Hornblende (vol%)	5.2%	–	–
Chlorite (vol%)	1.2%	12.4%	2.6%
Sample	**OL1**	**OL2A**	**OL2B**
Type	Mica gneiss	Granodiorite/tonalite	Granodiorite/granite
Source location	Olkiluoto	Olkiluoto	Olkiluoto
Groundwater	OLKR5	OLKR5	OLKR5
Groundwater type	Saline	Saline	Saline
particle size (mm)	≤ 2.0	≤ 2.0	≤ 2.0
A_{BET} (m^2/g)	0.95	0.22	0.36
CEC (cmol/kg)	1.5±0.4	2.1±0.4	1.8±0.4
Biotite (vol%)	32.4	6.6	0.2
Hornblende (vol%)	–	–	–
Chlorite (vol%)	–	6.4	0.2
	Ro1A	**Ro1B**	**Ro1C**
Type	Tonalite	Leukotonalite	Mica gneiss
Source location	Romuvaara	Romuvaara	Romuvaara
Groundwater	RoKR4	RoKR4	RoKR4
Groundwater type	Fresh	Fresh	Fresh
particle size (mm)	≤ 2.0	≤ 2.0	≤ 2.0
A_{BET} (m^2/g)	0.28	0.23	0.18
CEC (cmol/kg)	1.8±0.4	1.8±0.3	1.3±0.4
Biotite (vol%)	16.4	2.6	31.2
Hornblende (vol%)	–	–	–
Chlorite (vol%)	–	0.6	0.2
	Ki4A	**Ki4B**	
Type	Porphyritic granite	Porphyritic Granodiorite	
Source location	Kivetty	Kivetty	
Groundwater	KiKR4	KiKR4	
Groundwater type	Fresh	Fresh	
particle size (mm)	≤ 2.0	≤ 2.0	
A_{BET} (m^2/g)	0.21	0.22	
CEC (cmol/kg)	1.2±0.4	1.9±0.2	
Biotite (vol%)	5.4	12.0	
Hornblende (vol%)	4.0	4.4	
Chlorite (vol%)	–	–	

The data compiled by /Huitti et al. 1996/ and /Kulmala et al. 1998/ are estimated in terms of the percentage sorbed, S(%) calculated with the aid of a radiometric mass balance. The actual R_d data in the references are given without error estimates and in some cases reported as "≥" a specified value owing to detection limit issues. In order to obtain numerical ranges of K_d including uncertainty estimates, the procedures outlined in Appendix C were used. Since there are only a small number of R_d values for each rock type, re-sampling of the R_d values and their associated errors allows a more realistic range of data uncertainty to be estimated. The composite distribution of R_d values obtained for each rock type is shown in Figure K-1 for the experiments performed under oxic conditions and in Figure K-2 for anoxic conditions.

It is interesting to note the much larger R_d values estimated for the OL1, OL2A, and OL2B rock types from Olkiluoto in the data set for oxic conditions. When interpreting these data sets it is important to remember that the estimation of R_d using Equation C-2 is subject to severe restrictions when the sorption percentage approaches 100%. As can be seen from Figure C-1, an R_d of ~1 m^3/kg is approximately the upper limit of quantitative discrimination of the method for a liquid to solid ratio of 10. Even for R_d values in the range 0.1–1 m^3/kg, the upper tail of the formally calculated uncertainty distribution is inflated and possibly not physically meaningful. For this reason, any reported R_d values greater than 1 m^3/kg should be considered suspect for the given liquid to solid ratio. This, of course, does not mean that the R_d cannot physically be larger than 1 m^3/kg, but rather that such large R_d values are frequently not possible to quantify to an acceptable degree of accuracy.

The reason for the very high R_d values obtained for OL1, OL2A, and OL2B rock types, however, can be traced to the excessive precision with which the S(%) values for these rocks are tabulated in /Kulmala et al. 1998/. In the original data set, the sorption percentages are specified with five digit precision and without error estimates (the sorption percentages reported range from 99.982% to 99.997%). Although error estimates aren't given, the specified number of significant figures implies a standard error of no more than about 0.001%. Using these values gives very large R_d estimates with highly inflated upper tails of their uncertainty distributions. Since such large values appear to be an artefact of the estimation procedure using excessively precise S(%) values, these data sets are neglected from subsequent calculations for oxic conditions.

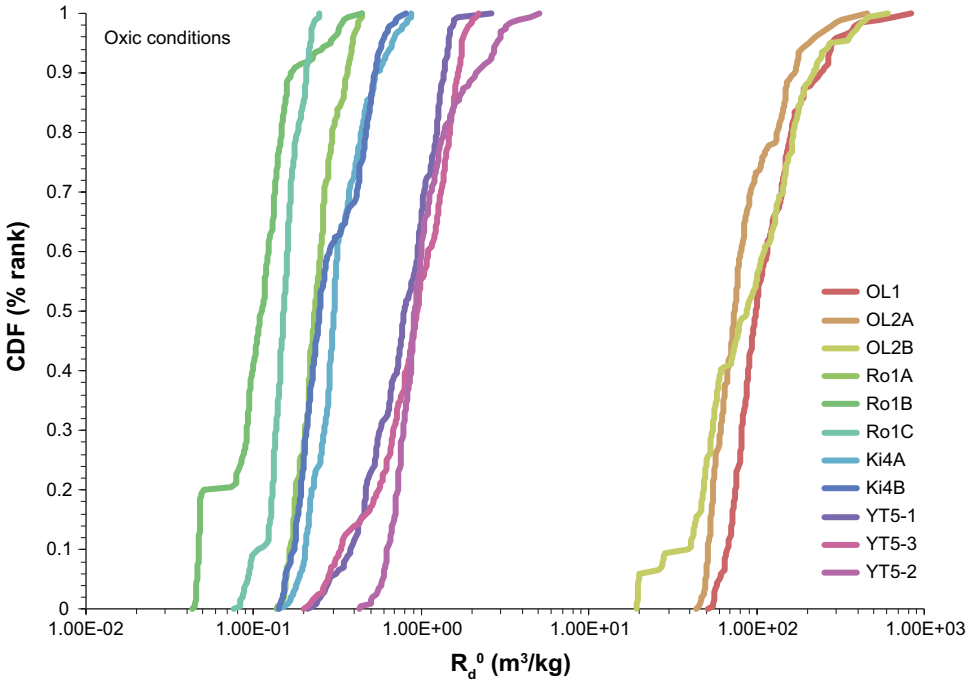

Figure K-1. *R_d^0 (m^3/kg) values calculated for Pu sorption under oxic conditions, based on literature R_d data and presented as an empirical cumulative distribution function for rocks taken from Finnish investigation sites. The individual data points and their uncertainties have been re-estimated from tabulated sorption percentage data and then re-sampled to give the composite distributions plotted in the figure.*

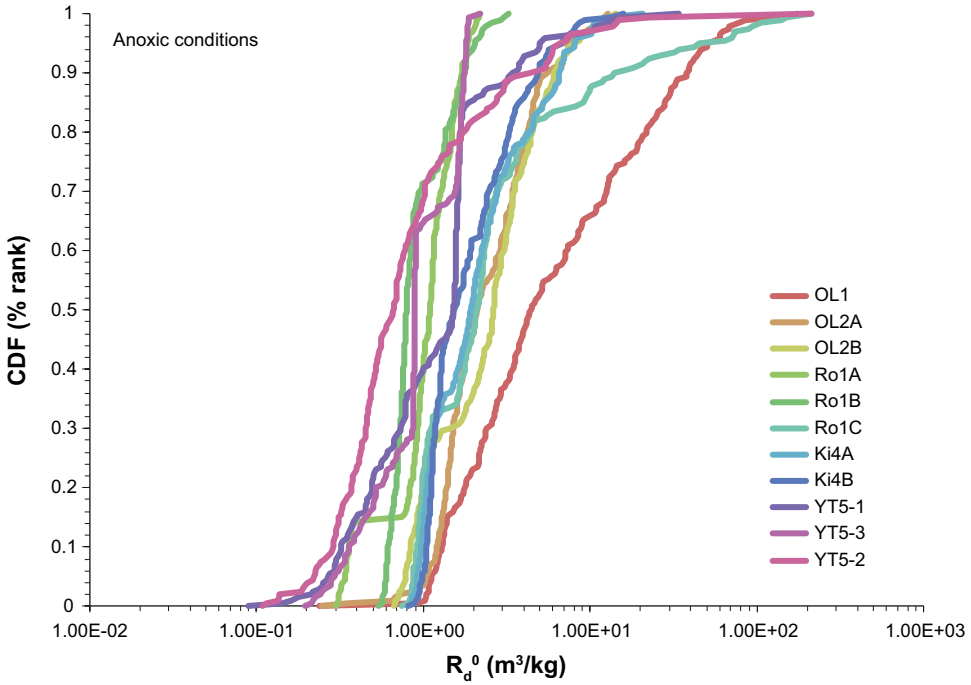

Figure K-2. *R_d^0 (m^3/kg) values calculated for Pu sorption under anoxic conditions, based on literature R_d data and presented as an empirical cumulative distribution function for rocks taken from Finnish investigation sites. The individual data points and their uncertainties have been re-estimated from tabulated sorption percentage data and then re-sampled to give the composite distributions plotted in the figure.*

Although the same argumentation could be used to remove the corresponding data for these rock types under anoxic conditions, the lower degree of precision with which the sorption percentages are reported and the fact that numerical error estimates are given (sorption percentages range from 99.0±0.1% to 99.9±0.1%) suggests that these data might be more reliable.

As noted previously for Np sorption (Appendix G), the marked differences in BET surface area and CEC reported for the fresh, weathered, and altered samples of Rapakivi granite do not appear to translate into corresponding shifts in sorptivity. The sorptivity of these three rock types as reported by /Huitti et al. 1996/ appears to be very similar. As previously, the data sets for the weathered and altered rock have been disregarded since the BET surface areas and CEC values would otherwise imply unrealistic transfer factors giving excessively low K_d estimates for application conditions.

Selection of representative data for site specific conditions

Based on the reported BET surface areas and CEC data, mechanical damage and CEC transfer factors have been estimated for each rock type. These transfer factors are summarised in Table K-2. Although Pu has not been conclusively shown to associate preferentially (or not) with biotite, CEC transfer factors have been assumed to be relevant for extrapolation to site specific conditions by appealing to arguments of caution. The CEC of all rock types studied by /Huitti et al. 1996, Kulmala et al. 1998/ are higher than for Forsmark specific rock types which implies a slight downward shift of recommended K_d values.

Since the BET surface areas of the crushed rock used in the experiments are supplied without error estimates, the uncertainty of f_m is dominated by the uncertainty of the surface area of the Forsmark site specific rock. Using the f_m and f_{cec} transfer factors, estimated K_d^0 values were calculated. Rock types OL1, OL2A, and OL2B have been discounted from the oxic data set for the reasons outlined previously. The weathered and altered Rapakivi granites, YT5-2 and YT5-3 have been excluded from both oxic and anoxic data sets on the basis that they may not extrapolate well to Forsmark site-specific rock types.

Table K-2. Mechanical damage and CEC transfer factors estimated for rock types reported by /Huitti et al. 1996, Kulmala et al. 1998/ assuming Forsmark metagranite (SKB rock code 101057) as the target rock type (A_{ref} = 0.018±0.005 m²/g, *CEC* = 1.0±0.5 cmol/kg) and propagation of 2σ error estimates in the uncertainty calculations.

Rock type	$\log_{10} f_m$	$\log_{10} f_{cec}$
OL1 (mica gneiss)	–1.78±0.23	–0.27±0.42
OL2A (granodiorite/tonalite)	–1.15±0.23	–0.44±0.40
OL2B (granodiorite/granite)	–1.36±0.23	–0.37±0.41
Ro1A (tonalite)	–1.25±0.23	–0.37±0.41
Ro1B (granite/leukotonalite)	–1.17±0.23	–0.38±0.39
Ro1C (mica gneiss)	–1.06±0.23	–0.20±0.44
Ki4A (porhyritic granite)	–1.13±0.23	–0.15±0.45
Ki4B (porhyritic granodiorite)	–1.15±0.23	–0.42±0.37
YT5-1 (granite)	–1.29±0.23	–0.10±0.43

Owing to the large uncertainties associated with the transfer factors, the individual K_d^0 values and their uncertainties were then re-sampled assuming a convex combination of the underlying lognormal distributions, now including the additional uncertainty of the f_m and f_{cec} transfer factors. The resulting, translated and expanded uncertainty distribution for K_d^0 is shown in Figure K-3 for oxic conditions and Figure K-4 for anoxic conditions.

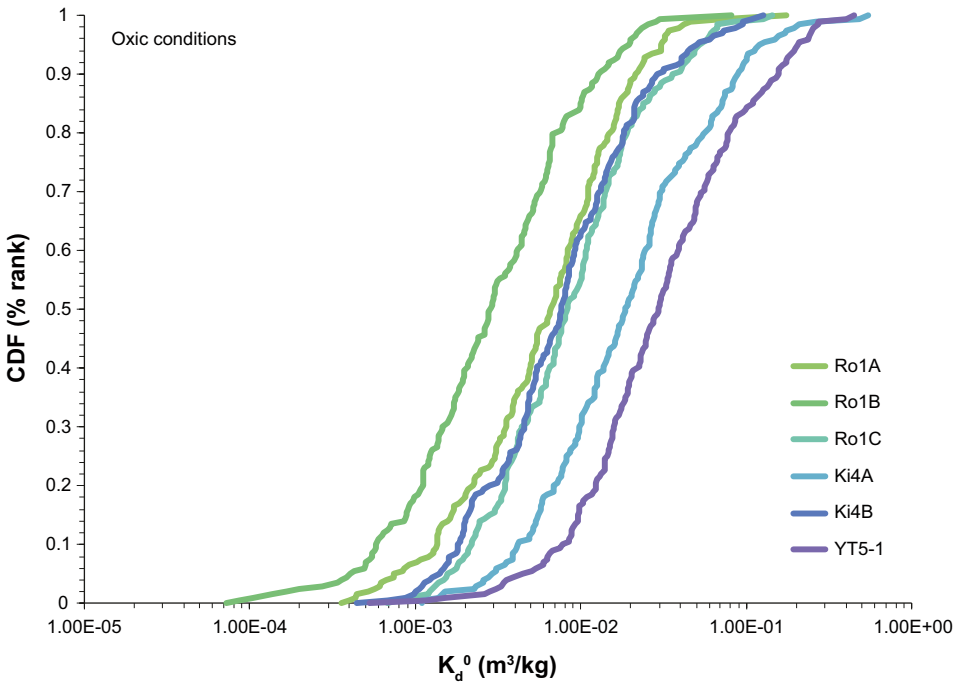

Figure K-3. *K_d^0 (m^3/kg) values calculated for Pu sorption under oxic conditions based on literature R_d data. Mechanical damage and CEC transfer factors (f_m, and f_{cec}) have been considered in the estimation procedure. The raw data are corrected to give values deemed appropriate for Forsmark metagranite (SKB rock code 101057) under in situ conditions, resampled and presented as an empirical cumulative distribution function.*

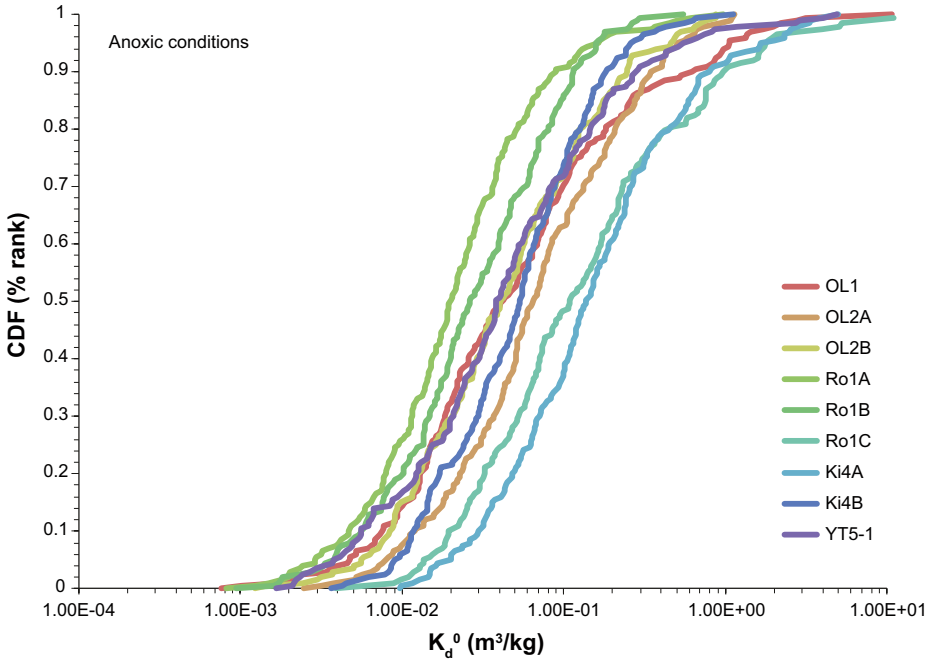

Figure K-4. *K_d^0 (m^3/kg) values calculated for Pu sorption under anoxic conditions based on literature R_d data. Mechanical damage and CEC transfer factors (f_m, and f_{cec}) have been considered in the estimation procedure. The raw data are corrected to give values deemed appropriate for Forsmark metagranite (SKB rock code 101057) under in situ conditions, resampled and presented as an empirical cumulative distribution function.*

Redox speciation of Pu under laboratory conditions

Pu is redox sensitive and can exist in as many as four different oxidation states in groundwater (i.e., +III, +IV, +V, +VI). Pu is a very special case amongst the radionuclides owing to its complex redox speciation and since it is possible for several different redox species to co-exist simultaneously. Indeed there are a number of so-called "triple points" where up to three different redox forms can be present in equimolar amounts at equilibrium for a given pH and Eh. Under certain conditions (typically close to the triple points), redox disproportionation reactions can occur which give rise to mixed redox states /Langmuir 1997/. Some examples of such reactions are:

$$\underset{(V)}{2PuO_2^+} + 4H^+ \rightleftharpoons \underset{(VI)}{PuO_2^{2+}} + \underset{(IV)}{Pu^{4+}} + 2H_2O \qquad \text{(K-1)}$$

$$\underset{(IV)}{3Pu^{4+}} + 2H_2O \rightleftharpoons \underset{(III)}{2Pu^{3+}} + \underset{(VI)}{PuO_2^{2+}} + 4H^+ \qquad \text{(K-2)}$$

In the laboratory investigations described by /Huitti et al. 1996/ and /Kulmala et al. 1998/, pH and Eh measurements were made on the contact solutions at the conclusion of the anoxic experiments. In summary, the following results were obtained:

- For the LPVA2 (Hästholmen) groundwater used by /Huitti et al. 1996/, the Eh was typically found to be in the range –42 mV to +1 mV with a pH ranging from 7.2 to 8.4 after a contact time of 73 days. The reducing capacity of the initial groundwater was reported as 0.7 mg/l ($KMnO_4$).
- For the OLKR5 (Olkiluoto) groundwater used by /Kulmala et al. 1998/, the Eh was typically found to be in the range –428 mV to –138 mV with a pH ranging from 7.9 to 8.6. The reducing capacity of the initial groundwater was reported as 80 mg/l ($KMnO_4$).
- For the RoKR4 (Romuvaara) groundwater used by /Kulmala et al. 1998/, the Eh was typically found to be in the range –358 mV to –144 mV with a pH ranging from 9.1 to 9.7. The reducing capacity of the initial groundwater was reported as 2.8 mg/l ($KMnO_4$).
- For the KiKR4 (Kivetty) groundwater used by /Kulmala et al. 1998/, the Eh was typically found to be in the range –361 mV to –235 mV with a pH ranging from 9.1 to 9.8. The reducing capacity of the initial groundwater was reported as 2.9 mg/l ($KMnO_4$).

Owing to the low concentration of redox species in the low ionic strength groundwaters RoKR4 and KiKR4, some of the samples were spiked with Tc(VII) as an internal standard to verify that sufficiently reducing conditions were obtained for sorption of reduced Tc(IV) to occur. This was motivated on account of the fact that electrode-based Eh measurements can be inaccurate for waters of low reducing capacity. The sorption of Tc was consistent with this process and the authors therefore concluded that the Eh in each of these cases was likely to be no more than about –150 mV to –50 mV. Although an internal standard was not employed in /Huitti et al. 1996/, the LPVA2 groundwater was pronounced reducing with regard to Tc(IV)/Tc(VII) redox speciation in parallel experiments investigating Tc sorption.

Using the initial groundwater compositions specified in the references, the redox speciation of Pu was calculated with the aid of PHREEQC and the SKB-TDB /Duro et al. 2006/ thermodynamic database for a span of Eh values ranging from –400 mV to +750 mV. The results of these calculations are shown in Figure K-5.

Assuming an ambient partial pressure of oxygen ranging between 10^{-6} and 0.21 atm, the experiments carried out under oxic conditions appear to be indicative of Pu(V) or Pu(VI) sorption (blue shaded regions in Figure K-5), although the overlap of the predominance regions of the pentavalent and hexavalent forms means that the sorption measurements most likely reflect a mixed redox state. For anoxic conditions the speciation of Pu appears to be dominated by the trivalent form for OLKR5, RoKR4, and KiKR4 groundwaters, and the tetravalent state dominates for LPVA2 groundwater. It

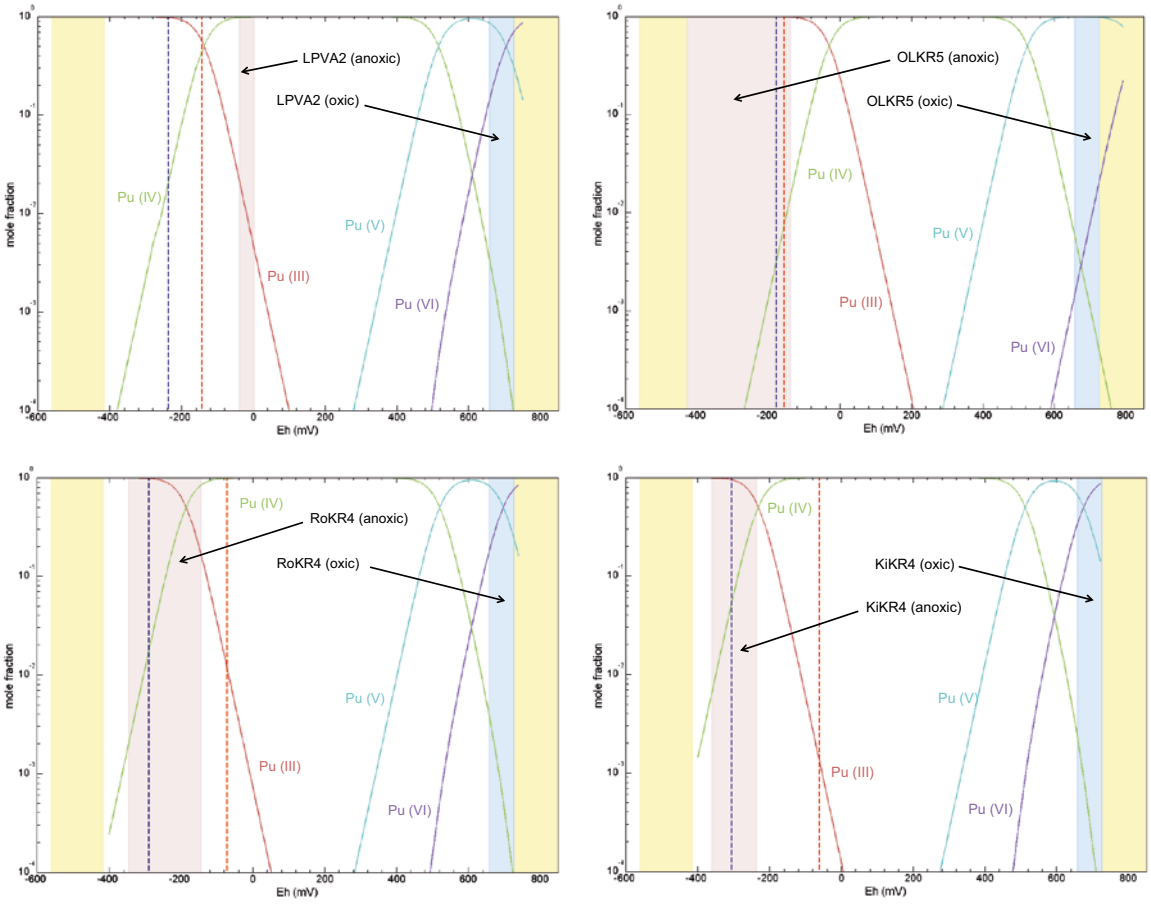

Figure K-5. *Pu redox speciation as a function of Eh (mV) for the different groundwaters used in laboratory experiments assuming fixed pH and carbonate concentration levels equal to specified starting values for each groundwater. Grey-red shading represents ranges of reported Eh values measured under anoxic conditions; blue shading represents approximate Eh ranges expected for ambient conditions; green shading represents upper and lower stability limits for water. The vertical broken lines represent the theoretical Eh calculated by PHREEQC for the specified groundwater compositions (blue) and assuming redox control by the* $Fe^{2+}/Fe(OH)_3$ *redox pair (red).*

should be noted, however, that the calculations are only very approximate in that they only consider the speciation in the aqueous phase and no consideration is given to the possibility of pH and carbonate compositional drift during the experiments. An additional uncertainty is the accuracy with which the Eh can be measured since the assumption of redox control by the $Fe^{2+}/Fe(OH)_3$ redox pair would, at least in some cases, suggest slightly different equilibrium Eh values (as shown in Figure K-5).

By comparing the thermodynamic constants for Pu^{3+} and Pu^{4+} hydrolysis in the SKB thermodynamic database, it appears likely that the tetravalent form might sorb more strongly than the trivalent form (inner-sphere surface complexes). This raises an intriguing possibility with regard to sorption in a system where a mixed redox state characterises the redox speciation in the groundwater: The stronger sorption of the tetravalent form would imply a depletion of Pu(IV) in the aqueous phase relative to Pu(III) concentration. If the Eh of the groundwater was controlled by another redox pair and the Pu is present at trace concentration levels (i.e. Pu does not significantly influence the Eh itself), the aqueous phase speciation might then adjust to re-establish the original proportion of Pu(III) and Pu(IV) as required by the controlling redox couple. Assuming all other things being equal this would logically lead to further sorption of Pu(IV) and depletion of the aqueous phase. Based on this reasoning, it could be argued that any mismatch between Pu(III) and Pu(IV) sorption strength would necessarily lead to the sorptive retention of Pu in the more strongly sorbing form, which in this case appears to be Pu(IV).

Although spectroscopic studies using XANES techniques have been used to distinguish the speciation of sorbed Pu on geological minerals (e.g. /Duff et al. 1999/), there appear to be no spectroscopic studies that would directly support the hypothesis outlined above. The situation is also complicated by the possibility that the mineral surfaces themselves might promote oxidation of Pu(III) to Pu(IV) as has been observed to occur in the case of Ce(III) and Ce(IV) sorption /Duff 2001/.

Recommended K_d data for SR-Site application conditions

If it is assumed that the principal uncertainties relating to groundwater composition are internalised in the individual data sets shown in Figure K-3 and Figure K-4 (noting that redox state as it relates to oxic and anoxic conditions is treated as a separate variable), a recommended range of K_d values for application conditions can be defined by aggregating the data sets together. The relevant K_d ranges for application in SR-Site are given in Figure K-6.

Under oxic conditions, it is not possible to distinguish between the pentavalent, Pu(V) and hexavalent, Pu(VI) states and therefore the K_d under these conditions is assumed to be representative of both redox forms. For anoxic conditions, the Eh values measured during the sorption experiments indicate a possible dominance of the trivalent form in the aqueous phase, although there is sufficient uncertainty that it is not really possible to say with certainty whether Pu(III) or Pu(IV) is the dominant redox form. Based on the hydrolysis constants for Pu(III) and Pu(IV), however, it is suspected that Pu might be sorbed mainly in the tetravalent state even if the Pu present in the aqueous phase is mostly trivalent. Owing to this uncertainty and since there is relatively good data already existing for the trivalent actinides and lanthanides, it is assumed that the laboratory measurement data obtained under anoxic conditions is approximately representative of Pu(IV) sorption.

It appears that the redox conditions prevailing at repository depth under application conditions (see next section) are sufficiently reducing for Pu(III) to be the predominant redox form. Since the laboratory measurements possibly represent mixed redox states, the K_d for Pu(III) is assumed by analogy to be the same as that derived for other trivalent actinides and lanthanides. The literature data based K_d value for Pu under anoxic conditions is assumed as an analogue for the tetravalent radionuclides Np(IV), Tc(IV), U(IV), Th(IV). Although this might not be entirely correct, the choice is cautious since the site specific data for Am(III)/Eu(III) suggest slightly lower K_d values for Pu(III) than those derived from the literature data for Pu under anoxic conditions.

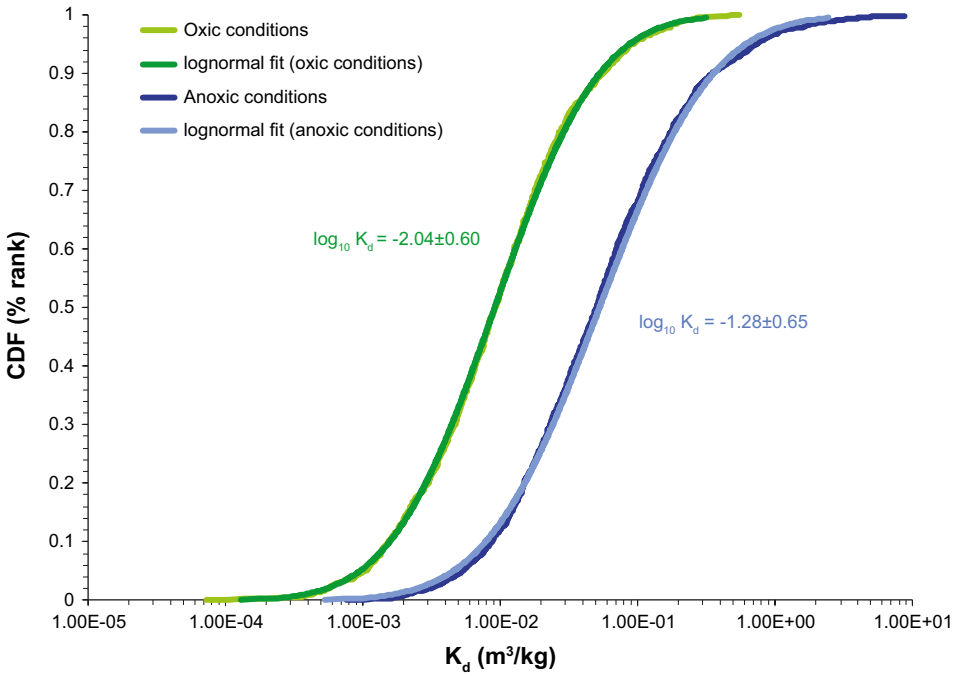

Figure K-6. *Recommended K_d (m^3/kg) values for Pu sorption for use in SR-Site calculations. The data range is considered to be applicable to all groundwater compositions and assumes Forsmark metagranite (SKB rock code 101057) as a representative rock type. The parameters of the lognormal distribution fit to the data are indicated in the figure.*

Assessment of predominant redox state under application groundwater conditions

In order to ascertain the principal redox state of Pu under application groundwater conditions, the speciation of Pu was calculated for 20,000 randomly sampled groundwater compositions taken from the SR-Site temperate domain simulations /Salas et al. 2010/. The calculations were made for the prevailing groundwater chemistry at time 2,000 y, 3,000 y, 5,000 y, and 9,000 y using PHREEQC and consider the same redox controlling processes as discussed previously for Np sorption (Appendix G).

In addition to calculating the actual speciation of Pu in the application groundwater, sweep calculations were made for a range of hypothetical redox potentials to ascertain the location of the transition point where Pu(III,IV) gives way to Pu(V,VI) dominated redox speciation. The transition point is taken to be where the sum of trivalent and tetravalent species is equal to the sum of pentavalent and hexavalent species. For numerical reasons this was done only for the convex hull of data points describing the envelope of pH and total carbonate concentrations in the application groundwater. From these data, a plane of best fit can then be calculated for the transition point which can be shown to be valid for all groundwater compositions within the convex hull. This provides a visual means of ascertaining how close the system is to the point of transition between predominantly reduced and predominantly oxidised speciation. The redox parameter space calculated in this fashion is plotted in Figure K-7 for the groundwater compositions existing at 2,000 y in the temperate case groundwater simulations.

Although the location of the plane of best fit roughly demarcates the regions of Pu(III,IV) and Pu(V,VI) predominance, it does not show the full extent of the region where multiple reducing and oxidising species can co-exist. The redox sweep data are therefore plotted in Figure K-8 where the fraction of reduced Pu (i.e. the sum of trivalent and tetravalent forms) is plotted as a function of redox potential.

There is a general tendency for the redox potential to decrease over time in the SR-Site temperate domain simulations due to the freshening of the groundwater with a meteoric component of higher carbonate content. The corresponding simulation results for groundwater compositions existing at 9,000 y are plotted in Figure K-9 and Figure K-10. It is noted that the groundwater redox potentials are sufficiently low for Pu(III) to be assumed as the dominant redox species for SR-Site transport simulations (cf. Figure K-5).

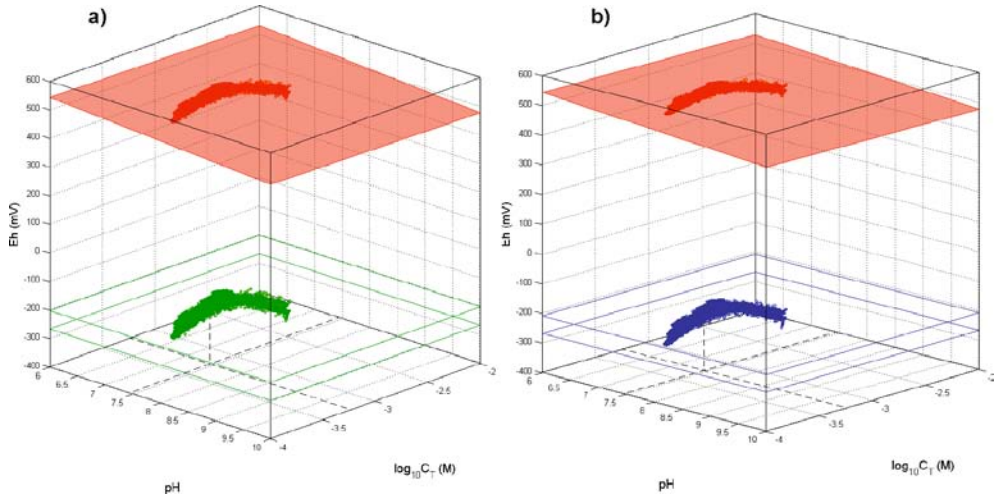

Figure K-7. *Redox parameter space for 20,000 randomly selected SR-Site temperate case groundwater compositions at 2,000 y for (a) $Fe^{2+}/Fe(OH)_3$ redox couple, and (b) SO_4^{-2}/FeS_{am} redox couple. The calculations indicate that all sampled groundwater compositions are sufficiently reducing for Pu(III) to be the dominant redox species (min and max Eh range indicated by green and blue coloured outline rectangles). The theoretical transition region separating reducing conditions (Pu(III,IV) predominance) and oxidising conditions (Pu(V,VI) predominance) is indicated by the red plane (red markers are mapped to the plane at the same pH and carbonate coordinates as the actual groundwater compositions for reference purposes).*

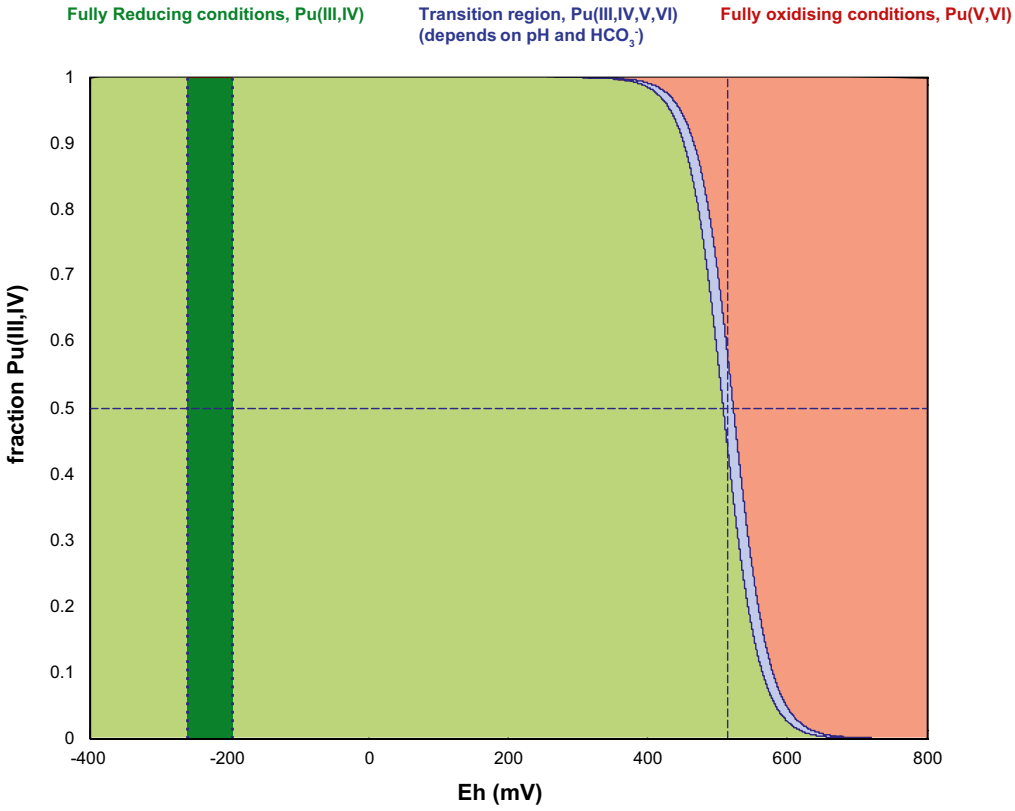

Figure K-8. *Theoretical redox transition zone for Pu (blue shaded region) compared with redox conditions in SR-Site temperate case at 2,000 y (dark green shaded region) which encompasses the potential span of both the $Fe(OH)_3$ and FeS_{am} redox cases. The light green and red shaded areas represent fully reducing (100% Pu(III,IV)) and fully oxidising (100% Pu(V,VI)) conditions, respectively. The cross-hairs in the figure approximately indicate the centroid of the transition point for the application groundwater pH and carbonate ranges illustrated previously in Figure K-7.*

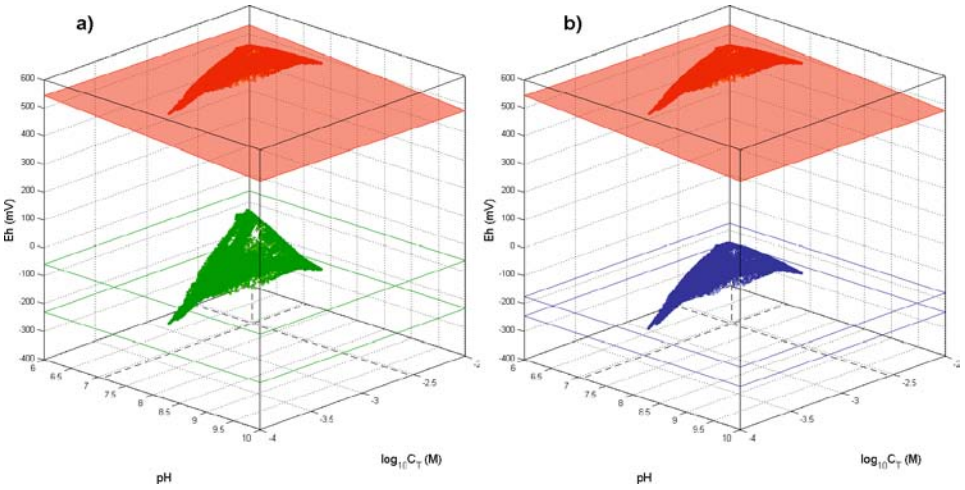

Figure K-9. *Redox parameter space for 20,000 randomly selected SR-Site temperate case groundwater compositions at 9,000 y for (a) $Fe^{2+}/Fe(OH)_3$ redox couple, and (b) SO_4^{-2}/FeS_{am} redox couple. The calculations indicate that all sampled groundwater compositions are sufficiently reducing for Pu(III) to be the dominant redox species (min and max Eh range indicated by green and blue coloured outline rectangles). The theoretical transition region separating reducing conditions (Pu(III,IV) predominance) and oxidising conditions (Pu(V,VI) predominance) is indicated by the red plane (red markers are mapped to the plane at the same pH and carbonate coordinates as the actual groundwater compositions for reference purposes).*

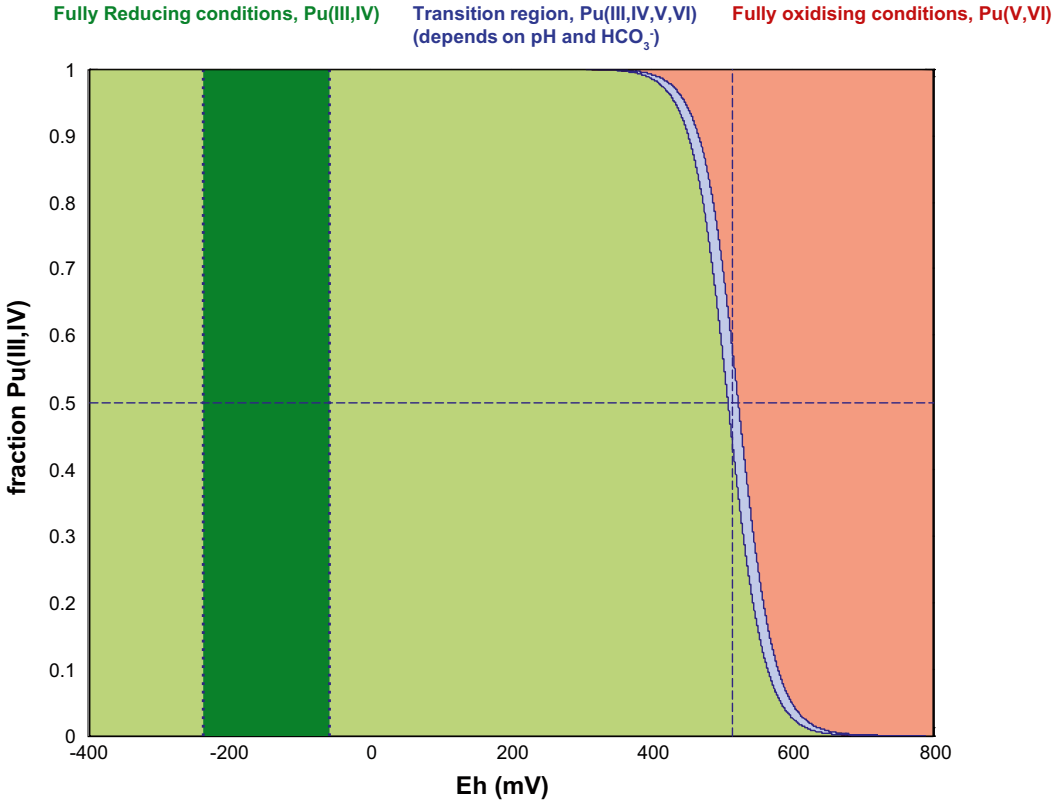

Figure K-10. *Theoretical redox transition zone for Pu (blue shaded region) compared with redox conditions in SR-Site temperate case at 2,000 y (dark green shaded region) which encompasses the potential span of both the $Fe(OH)_3$ and FeS_{am} redox cases. The light green and red shaded areas represent fully reducing (100% Pu(III,IV)) and fully oxidising (100% Pu(V,VI)) conditions, respectively. The cross-hairs in the figure approximately indicate the centroid of the transition point for the application groundwater pH and carbonate ranges illustrated previously in Figure K-9.*

Appendix L

K_d data derivation sheet for protactinium (Pa)

Overview of available literature data

The most detailed data sets for sorption of protactinium on relevant rock types and groundwaters are documented by /Kulmala et al. 1996/ and /Huitti et al. 1996/. In these studies, sorption was measured on crushed rock taken from various sites in Finland. The sorption experiments were carried out under both oxic and anoxic conditions using natural groundwater samples native to the various sites and a liquid to solid ratio of 10 ml/g. For experiments carried out under anoxic conditions, the sampled groundwater was preserved in a nitrogen atmosphere to prevent oxidation of the Fe(II) content of the water. Spike concentrations of Pa(V) were in the range 10^{-13}–10^{-10} M for both oxic and anoxic experiments. Material properties of the rock samples and groundwaters used are the same as those discussed previously for Pu sorption (Appendix K). There are other data sets in the open literature for Pa sorption, notably /Berry et al. 1989/ for sorption on Caledonian granite and /Baston et al. 1999/ for a Japanese granodiorite. These data were deemed of lesser quality owing to the lack of supporting data documentation and therefore have not been used.

The data compiled by /Kulmala et al. 1996/ and /Huitti et al. 1996/ are estimated in terms of the percentage sorbed, S(%) calculated with the aid of a radiometric mass balance. The actual R_d data in the references are given without error estimates and in some cases reported as "≥" a specified value owing to detection limit issues. In order to obtain numerical ranges of K_d including uncertainty estimates, the procedures outlined in Appendix C were used. Since there are only a small number of R_d values for each rock type, re-sampling of the R_d values and their associated errors allows a more realistic range of data uncertainty to be estimated. Since there were no major differences between the data ranges obtained under oxic and anoxic conditions, the data for both sets of experiments were pooled. The composite distribution of R_d values obtained for each rock type is shown in Figure L-1.

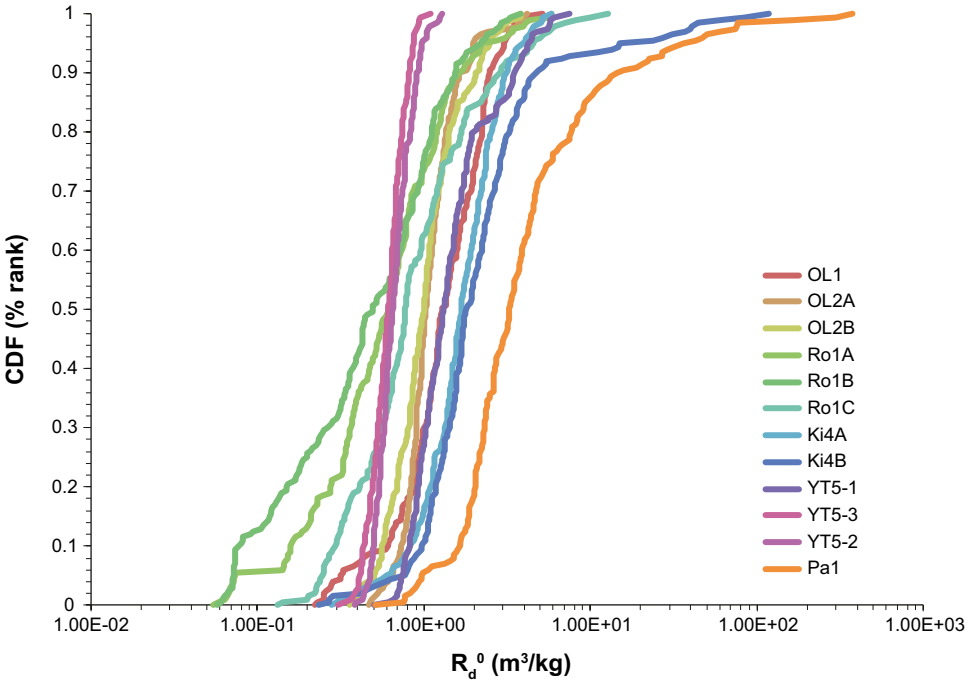

Figure L-1. *R_d^0 (m^3/kg) values calculated for Pa(V) sorption based on literature R_d data and presented as an empirical cumulative distribution function for rocks taken from Finnish investigation sites (data are pooled for oxic and anoxic conditions). The individual data points and their uncertainties have been re-estimated from tabulated sorption percentage data and then re-sampled to give the composite distributions plotted in the figure.*

As can be seen from Figure L-1, there is an additional rock type (Pa1) which was not previously documented in Appendix K. This is mica gneiss rock type taken from the Palmottu natural analogue study site and is known to also contain pyrite. This data set has been included here for reference purposes although has not been subsequently used for deriving site specific K_d values owing to that no BET surface area data were documented for these samples.

Selection of representative data for site specific conditions

Based on the reported BET surface area data, mechanical damage transfer factors were estimated for each rock type. These transfer factors are the same as those previously summarised in Table K-2. Redox speciation calculations using PHREEQC indicate that Pa(V) should be present under all conceivable field conditions and therefore the tendency for redox sensitive nuclides to sorb on biotite with accompanying redox transformation does not seem to apply in particular this case. Therefore, unlike the sorption of some of the other redox sensitive solutes, there appears to be no good reason to suspect that Pa should sorb preferentially on biotite and so a CEC transfer factor has not been used.

As noted previously, the uncertainty of the mechanical damage transfer factor, f_m is dominated by the uncertainty of the estimated surface area of the Forsmark site specific rock since the BET surface areas of the crushed rock used in the experiments are supplied without error estimates. Using the f_m transfer factors, estimated K_d^0 values were calculated for the original data points. For the same reasons outlined previously, the weathered and altered Rapakivi granites, YT5-2 and YT5-3 have been excluded on the basis that they do not extrapolate well to Forsmark site-specific rock types.

Owing to the large uncertainties associated with the mechanical damage transfer factor, the individual K_d^0 and their uncertainties were re-sampled assuming a convex combination of the underlying lognormal distributions including the additional uncertainty of the f_m transfer factor. The resulting, expanded uncertainty distribution for K_d^0 is shown in Figure L-2.

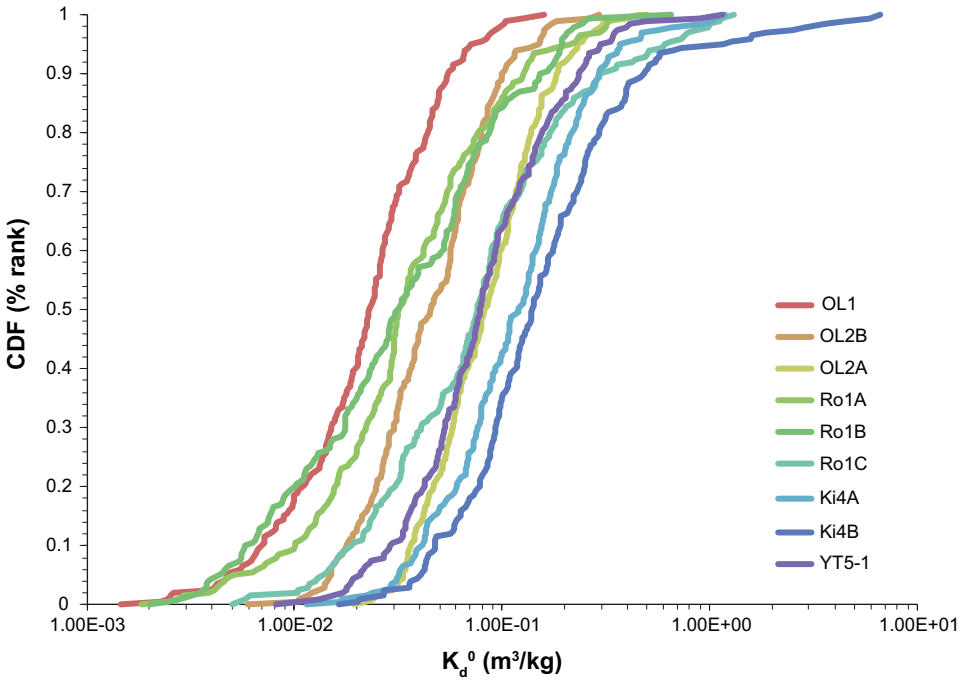

Figure L-2. *K_d^0 (m^3/kg) values calculated for Pa sorption based on literature R_d data (data are pooled for oxic and anoxic conditions). Only the mechanical damage transfer factor, f_m has been considered in the estimation procedure. The raw data are corrected to give values deemed appropriate for Forsmark metagranite (SKB rock code 101057) under in situ conditions, resampled and presented as an empirical cumulative distribution function.*

Recommended K_d data for SR-Site application conditions

If it is assumed that the principal uncertainties relating to groundwater composition are internalised in the individual data sets shown in Figure L-2, a recommended range of K_d values for application conditions can be defined by aggregating the data sets together. The relevant K_d range for application in SR-Site are given in Figure L-3. Since redox speciation calculations indicate that Pa(V) should be present under all projected groundwater compositions, Pa is not considered to be redox sensitive.

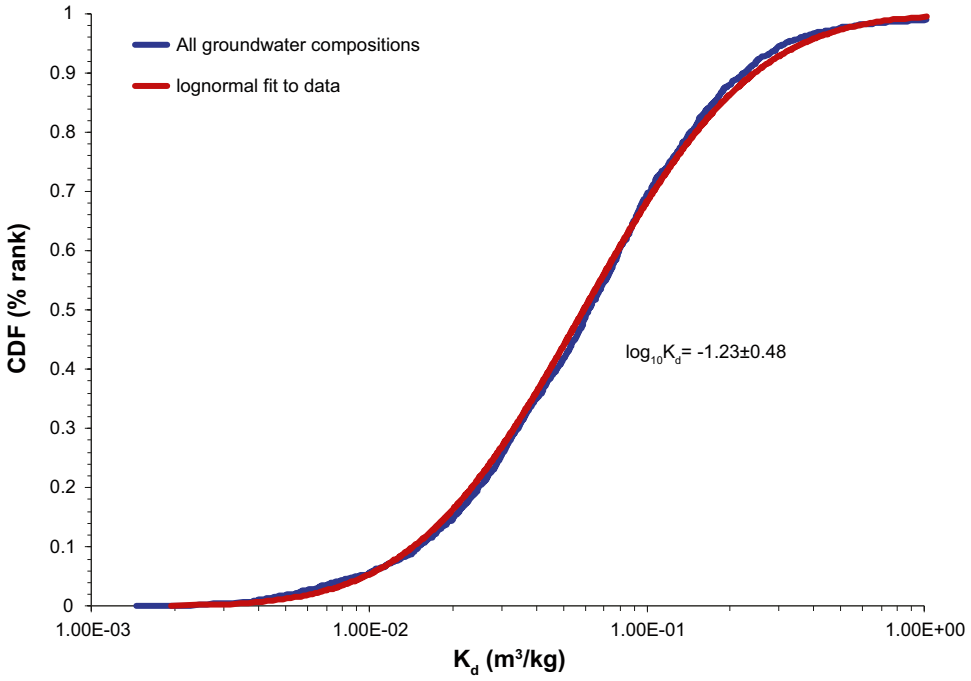

Figure L-3. *Recommended K_d (m^3/kg) values for Pa(V) sorption for use in SR-Site calculations. The data range is considered to be applicable to all groundwater compositions and assumes Forsmark metagranite (SKB rock code 101057) as a representative rock type. The parameters of the lognormal distribution fit to the data are indicated in the figure.*

Appendix M

K_d data derivation sheet for radium (Ra)

Overview and evaluation of site investigation data

Site specific sorption data were obtained for Ra(II) during the site investigations at Forsmark /Byegård et al. 2008/ and Laxemar /Selnert et al. 2009/. These data are summarised in the bedrock transport properties site descriptive model /Crawford 2008/ and are the basis for K_d values recommended for use in SR-Site. In most cases (although there are some exceptions) there is a time dependency in the experimental data with a clear trend towards higher R_d values at increasing times. The data also exhibit a relatively clear surface area dependency whereby smaller crushed particle sizes are associated with higher sorptivities than larger size fractions. A typical time series for Ra(II) sorption on Forsmark metagranite (SKB rock code 101057) is shown in Figure M-1.

As was noted for a number of other solutes studied in the site investigation work, there is an inflection in the slope of the temporal trend at 91 days as shown in Figure M-1. It is possible that this is related to an inaccurately estimated blank solution activity error since it appears in all three size-fraction data series. The existence of similar deviations in the data recorded for several solutes suggests the error might be possibly due to either operator error involving weighing of samples or some inaccuracy in calibration of the radiometric counting device used to measure activity on that particular day.

The Forsmark data are based on samples taken from two borehole sections while the Laxemar data are based on a single borehole section. For the same reasons outlined previously for Cs(I), no attempt has been made to model the time dependency of the data. The data for Ra(II) have therefore been treated by considering the data set in its entirety without filtering of values on the basis of crushed size fraction or contact time.

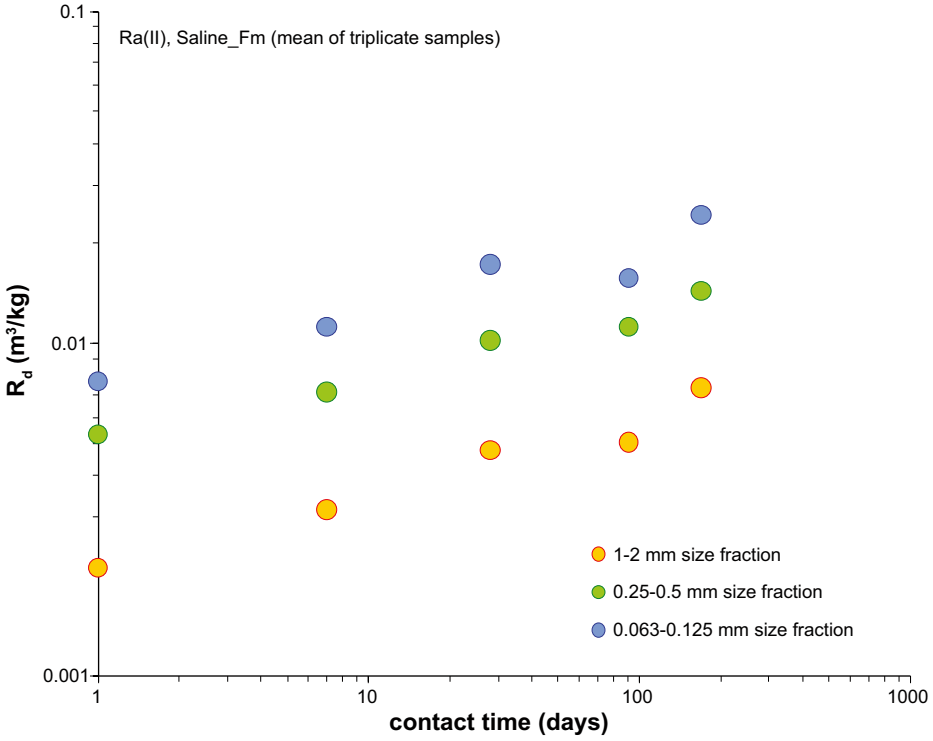

Figure M-1. *Typical time series for Ra(II) sorption R_d (m^3/kg) measured in the Forsmark site investigation studies. There is a clear sorption dependency on both particle size and time.*

Overview of available literature data

The most detailed data sets for sorption of Ra(II) on relevant rock types and groundwaters are documented by /Kulmala and Hakanen 1995/ and /Huitti et al. 1996/. In these studies, sorption was measured on crushed rock taken from various sites in Finland. The sorption experiments described by /Kulmala and Hakanen 1995/ were carried out using natural groundwater samples for a liquid to solid ratio varying between 10–100 ml/g and a contact time of roughly 20 days. The spike concentration of Ra(II) was 2.7×10^{-10} M. The sorption experiments described by /Huitti et al. 1996/ also use natural groundwater samples, a liquid to solid ratio of 10 ml/g, a contact time of 21 days, and a Ra(II) spike concentration of £ 10^{-7} M. In the study by /Kulmala and Hakanen 1995/, the liquid to solid ratio was varied to simulate the effect of a variable spike concentration. In /Huitti et al. 1996/, on the other hand, the analogue solute Ba(II) was added at a concentration ranging between 10^{-7} M and 10^{-3} M to simulate the effect of variable concentration. A summary of the material properties of the rock samples and groundwaters used by /Kulmala and Hakanen 1995/ and /Huitti et al. 1996/ are given in Table M-1.

Table M-1. Material properties of Finnish rock types investigated by /Kulmala and Hakanen 1995/ and /Huitti et al. 1996/. Means and standard deviations are given for multiple replicate samples where available.

Sample	**YT5-1**	**YT5-2**	**YT5-3**
Type	Fresh granite	Weathered granite	Altered granite
Source location	Hästholmen	Hästholmen	Hästholmen
Groundwater	LPVA2	LPVA2	LPVA2
Groundwater type	Saline	Saline	Saline
particle size (mm)	≤ 2.0	≤ 2.0	≤ 2.0
A_{BET} (m^2/g)	0.31±0.01	3.51±1.94	1.0±0.12
CEC (cmol/kg)	1.01±0.28	3.7±0.17	1.7±0.17
Biotite (vol%)	3.8%	4.2%	1.4%
Hornblende (vol%)	5.2%	–	–
Chlorite (vol%)	1.2%	12.4%	2.6%
Sample	**OL-KR5a**	**RO-KR3a**	**KI-KR1a**
Type	Mica gneiss	Gneiss	Porphyric granodiorite
Source location	Olkiluoto	Romuvaara	Kivetty
Groundwater	OLKR5	OLKR5	OLKR5
Groundwater type	Saline	Saline	Saline
particle size (mm)	≤ 0.1	≤ 0.1	≤ 0.1
	≤ 2.0	≤ 2.0	≤ 2.0
A_{BET} (m^2/g)	2.97±0.02	1.73±0.02	1.98±0.01
	0.79±0.01	0.17±0.01	0.18±0.01
CEC (cmol/kg)	10.2±0.4	17.8±0.1	7.7±0.5
Biotite (vol%)	20.9±2	17.4±0.3	11.4±2.8
Hornblende (vol%)	–	10.9±4.9	5.2±1.3
Chlorite (vol%)	–	≤ 0.2	≤ 0.2
	OL-KR5b	**RO-KR3b**	**KI-KR1b**
Type	Tonalite	Leukotonalite	Mica gneiss
Source location	Romuvaara	Romuvaara	Romuvaara
Groundwater	KiKR4	KiKR4	KiKR4
Groundwater type	Fresh	Fresh	Fresh
particle size (mm)	≤ 0.1	≤ 0.1	≤ 0.1
	≤ 2.0	≤ 2.0	≤ 2.0
A_{BET} (m^2/g)	2.97±0.02	1.73±0.02	1.98±0.01
	0.79±0.01	0.17±0.01	0.18±0.01
CEC (cmol/kg)	10.2±0.4	17.8±0.1	7.7±0.5
Biotite (vol%)	20.9±2	17.4±0.3	11.4±2.8
Hornblende (vol%)	–	10.9±4.9	5.2±1.3
Chlorite (vol%)	–	≤ 0.2	≤ 0.2

The data presented in both literature references are estimated in terms of the percentage sorbed, S(%) calculated with the aid of a radiometric mass balance. The actual R_d data in the references are given without error estimates and in some cases reported as "≥" a specified value owing to detection limit issues. In order to obtain numerical ranges of K_d including uncertainty estimates, the procedures outlined in Appendix C were used. Since there are only a small number of R_d values for each rock type, re-sampling of the R_d values and their associated errors allows a more realistic range of data uncertainty to be estimated. Only the data where additional Ba(II) has not been added are used in this report owing to the risk of barite precipitation which has a high potential to bias the results. The composite distribution of R_d values obtained for the different rock type and groundwater combinations are shown in Figure M-2.

Selection of representative data for site specific conditions

For Ra(II), a mixture of site data and literature data have been considered in the recommendation of K_d ranges for use in SR-Site safety assessment calculations. As described previously for Ni(II) sorption, the site investigation data are used mainly to establish the recommended K_d data while the Finnish literature data are used in a supporting role to provide a consistency check on the values derived from the site specific materials. The selection procedure and associated calculations are described separately since data handling procedures were different for the site investigation and literature data.

One particular confounding factor regarding radium sorption is the possibility of barite precipitation accompanied by radiobarite solid solution formation. For this reason, only data sets where the groundwater composition was not likely to result in barite oversaturation were propagated further in the analysis. In order to ascertain the effect of barite precipitation, PHREEQC calculations were made using the specified groundwater compositions from the site investigation and literature data. Radiobarite solid solution equilibrium was modelled assuming ideal mixing behaviour which is not an unreasonable assumption considering the similar ionic radii of Ra (1.73 Å) and Ba (1.61 Å) and similarity in crystal lattices of $RaSO_4$ and $BaSO_4$ (e.g. /Zhu 2004/).

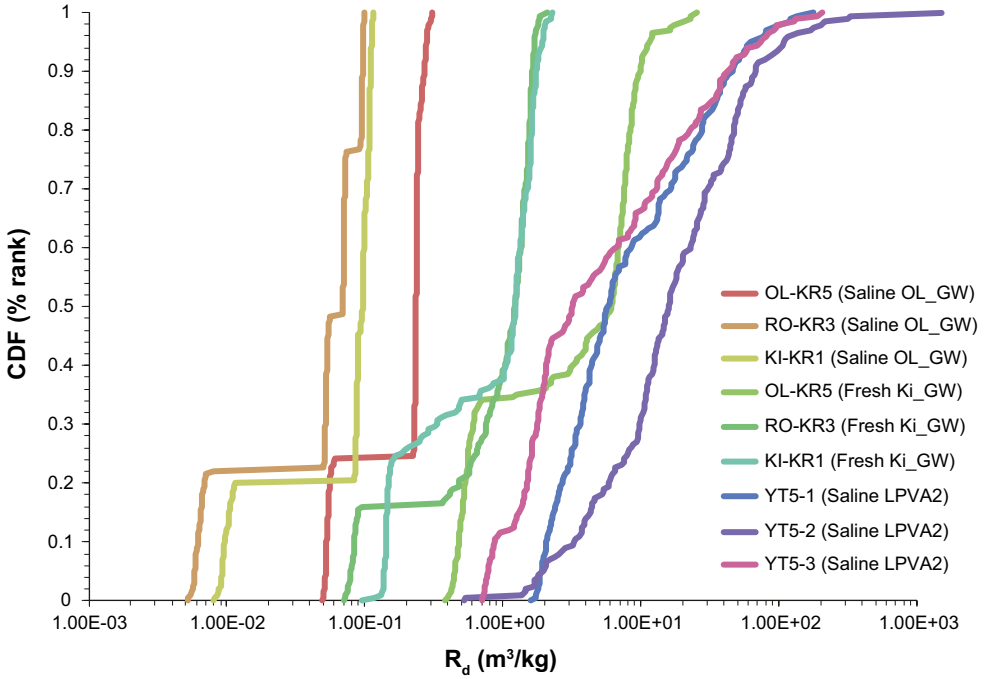

Figure M-2. *R_d^0 (m^3/kg) values calculated for Ra sorption based on literature R_d data and presented as an empirical cumulative distribution function for rocks taken from Finnish investigation sites. The individual data points and their uncertainties have been re-estimated from tabulated sorption percentage data and then re-sampled to give the composite distributions plotted in the figure.*

Although linear sorption using the K_d approach cannot be modelled directly in PHREEQC, it is possible to simulate linear sorption partitioning by defining a hypothetical surface complexation reaction with a large excess of surface sites and an appropriately scaled equilibrium constant. The apparent R_d value where radiobarite retention is erroneously lumped with sorption can then be compared to the R_d value for the purely sorptive retention process. The results of this analysis are shown in Figure M-3.

As can be seen from Figure M-3, the Fresh, Marine, and Type V groundwater types from the site investigations and the LPVA2 groundwater from /Huitti et al. 1996/ were found to have a significant potential for bias due to barite precipitation. None of the other groundwater types had sufficiently high barium and sulphate concentrations to result in barite precipitation.

Site specific data from Forsmark and Laxemar

Since the sorption of Ra(II) appears to exhibit an ionic strength dependency, the procedure for derivation of K_d values relevant for application within SR-Site consisted of the same steps as described previously for Cs(I). Estimated K_d^0 data corrected for surface area normalisation, mechanical damage, and CEC effects using Equation 5-2 are plotted in Figure M-4 assuming Forsmark metagranite (SKB rock code 101057) as a representative rock type for the Forsmark site. Although the uncertainty ranges for the individual data sets are large, there is a clear tendency towards greater sorptivity under low ionic strength conditions relative to that obtained for the more saline groundwater types.

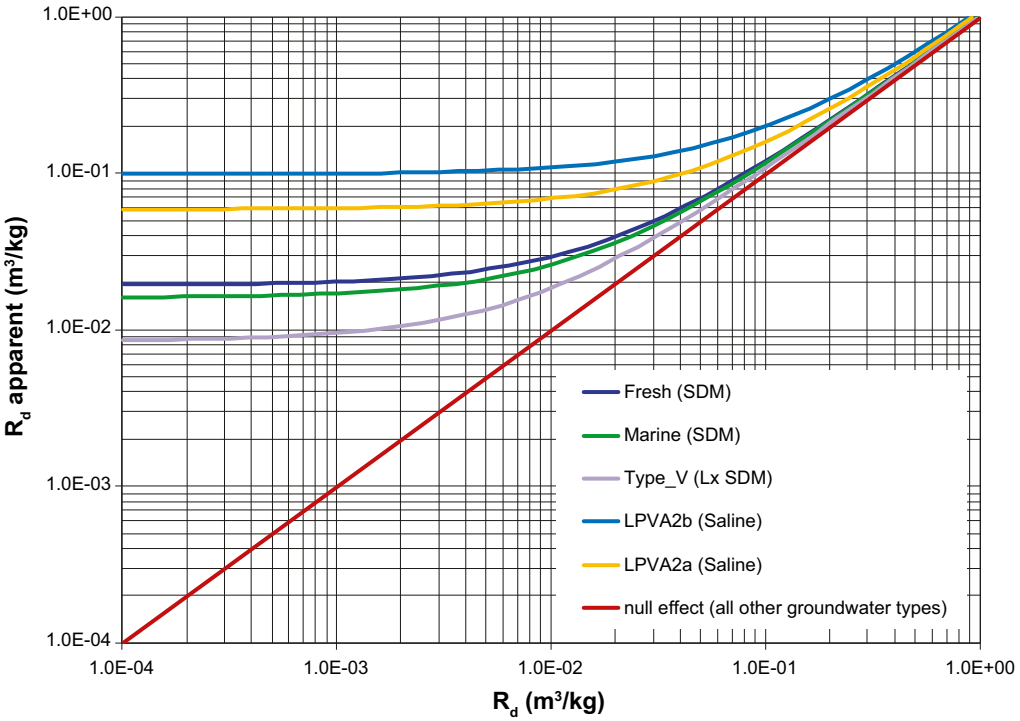

Figure M-3. *Theoretical impact of barite precipitation and accompanying radiobarite solid solution formation on measured R_d values calculated using PHREEQC for the specified groundwater compositions. The vertical axis shows the "apparent" R_d obtained where the solid solution effect is lumped together with sorption, while the horizontal axis shows the "true" R_d value for sorption (ion-exchange) only.*

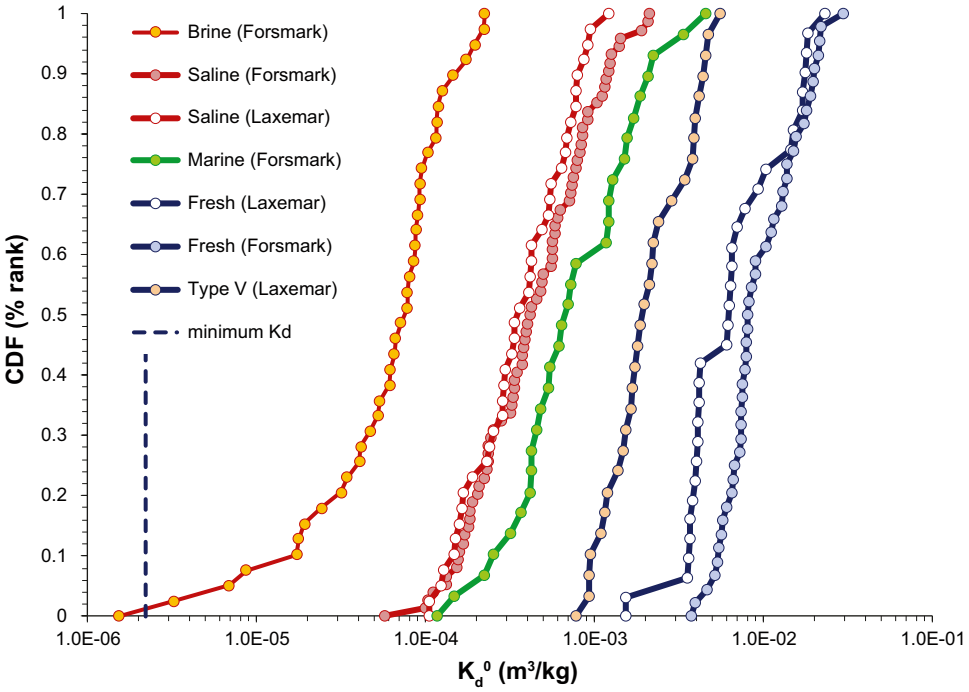

Figure M-4. *K_d^0 (m^3/kg) values calculated for Ra(II) sorption based on raw R_d data for site specific rock types and groundwater compositions as reported in the Forsmark (Fm SDM) and Laxemar (Lx SDM) site investigations. Surface area normalisation, mechanical damage, and CEC transfer factors (f_A, f_m, and f_{cec}) have been considered in the estimation procedure. The raw data are corrected to give values deemed appropriate for Forsmark metagranite (SKB rock code 101057) under in situ conditions and are presented as an empirical cumulative distribution function. A minimum K_d reference line is plotted in the figure indicating the upper 95% confidence limit for the matrix storage capacity of the rock based on water saturation porosity.*

Literature data for Finnish rock types

Based on the reported BET surface areas and CEC data, mechanical damage and CEC transfer factors were estimated for each rock type (summarised in Table M-2). These transfer factors were then used to estimate re-scaled values for the individual data points in the raw data set. Owing to the low number of replicate samples the K_d^0 values and their uncertainties were re-sampled assuming a convex combination of the underlying lognormal distributions, now also including the additional uncertainty of the f_m and f_{cec} transfer factors. The data for the different rock types were pooled and the resulting rescaled and expanded uncertainty distributions for the three different groundwater types are shown in Figure M-5.

Corrections for groundwater chemistry in SR-Site

The theoretical K_d was calculated using PHREEQC and the SKB thermodynamic database for 10,000 randomly selected groundwater compositions taken from the SR-Site temperate domain simulations /Salas et al. 2010/. The exchange model described in Section 5.1.1 was used assuming selectivity coefficients for Äspö diorite as a basis for calculations. Comparison of K_d values calculated in this manner with the corresponding theoretical result for the Forsmark saline reference water allows the groundwater chemistry transfer factor, f_{chem} to be calculated in straight-forward fashion for the projected application conditions. Background concentrations of the components (Cs, Sr, Rb, and Ba) in the groundwater were estimated using correlations derived from the site investigation hydrochemistry data. Full details concerning how these correlations were established and implemented can be found in Appendix A.

Simulation results for f_{chem} are given in Figure M-6 and indicate a slightly decreased K_d at early times relative to the reference groundwater. At longer times, however, the progressive freshening of the groundwater due to intrusion of a meteoric component gives elevated K_d values relative to the reference groundwater.

Table M-2. Mechanical damage and CEC transfer factors estimated for rock types used by /Kulmala and Hakanen 1995/ and /Huitti et al. 1996/ assuming Forsmark metagranite (SKB rock code 101057) as the target rock type (A_{ref} = 0.018±0.005 m²/g, *CEC* = 1.0±0.5 cmol/kg) and propagation of 2 s error estimates in the uncertainty calculations.

Rock type	Size fraction	$\log_{10} f_m$	$\log_{10} f_{cec}$
OL-KR5	< 0.1 mm	–2.28±0.23	–1.16±0.36
	< 2 mm	–1.70±0.23	–1.16±0.36
RO-KR3	< 0.1 mm	–2.04±0.23	–1.40±0.36
	< 2 mm	–1.03±0.23	–1.40±0.36
KI-KR1	< 0.1 mm	–2.10±0.23	–1.04±0.37
	< 2 mm	–1.06±0.23	–1.04±0.37
YT5-1	< 2 mm	–1.29±0.23	–0.10±0.43

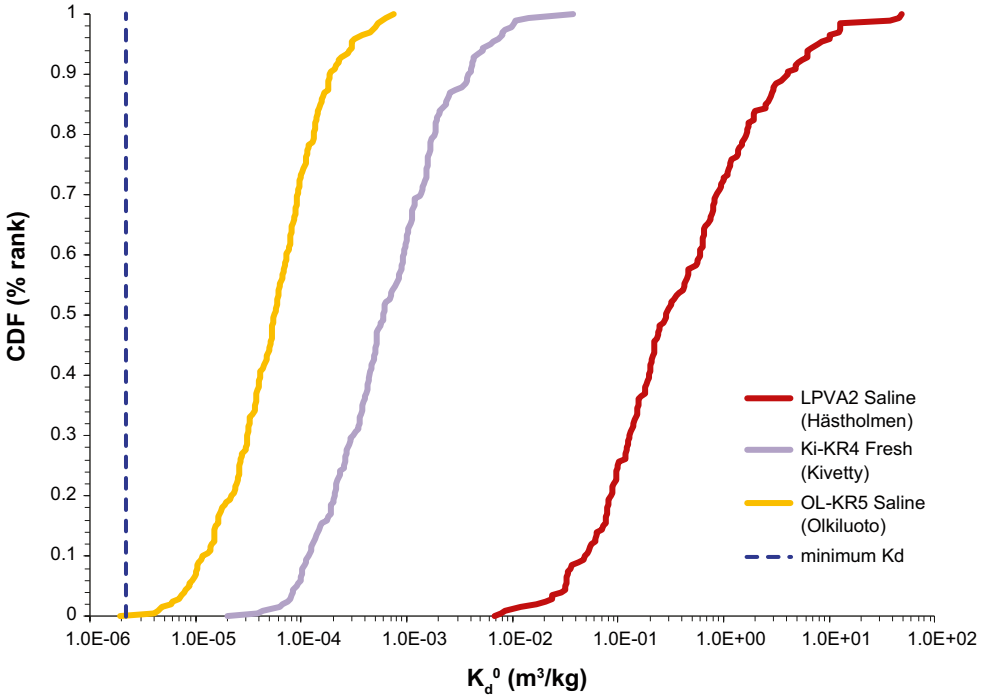

Figure M-5. *K_d^0 (m³/kg) values calculated for Ra(II) sorption based on literature R_d data. Mechanical damage and CEC transfer factors (f_m, and f_{cec}) have been considered in the estimation procedure. The raw data are corrected to give values deemed appropriate for Forsmark metagranite (SKB rock code 101057) under in situ conditions and are presented as an empirical cumulative distribution function. A minimum K_d reference line is plotted in the figure indicating the upper 95% confidence limit for the matrix storage capacity of the rock based on water saturation porosity.*

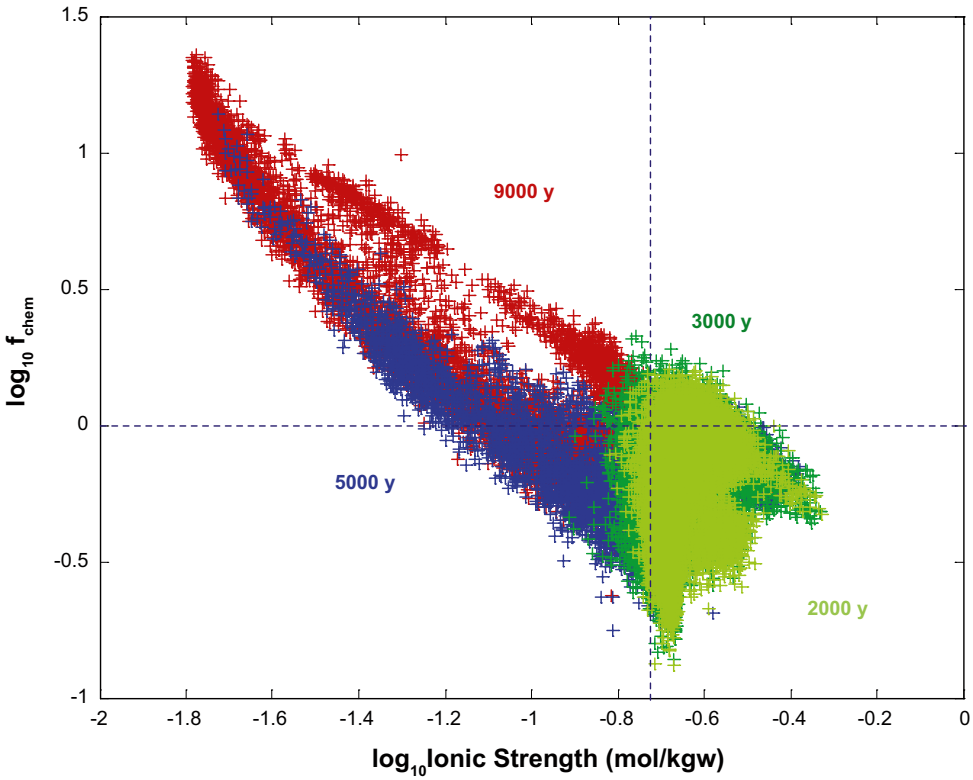

Figure M-6. *Chemistry transfer factors, f_{chem} calculated for Ra(II) sorption at application groundwater conditions in the SR-Site temperate case. The plotted data represent 10,000 randomly selected groundwater compositions calculated individually using PHREEQC and the assumed ion exchange model. Data are given for 2,000 y (lime green markers), 3,000 y (dark green), 5,000 y (blue), 9,000 y (red). The cross-hairs in the figure represent the relative location of the reference groundwater (Forsmark saline).*

Using the calculated f_{chem} distribution, it is possible to estimate K_d values appropriate for application groundwater compositions by convolution of the individual probability density functions or by using an equivalent stochastic method. The latter method being simpler to implement numerically was chosen and used to estimate the K_d values presented in this compilation. The stochastic method was based upon random sampling (10^5 samples) of the individual probability density functions and multiplication of the individually sampled values. The resulting distributions of K_d values are plotted in Figure M-7 to Figure M-10 for different times during the temperate domain calculation cases.

Recommended K_d data for SR-Site application conditions

Based on the ion-exchange simulations described in the previous section, the following K_d ranges are recommended for use at different times in the hydrogeochemical evolution of the repository environment:

$\log_{10} K_d \approx -3.59 \pm 0.41$ (t = 2,000 y) (M-1)

$\log_{10} K_d \approx -3.62 \pm 0.41$ (t = 3,000 y) (M-2)

$\log_{10} K_d \approx -3.53 \pm 0.40$ (t = 5,000 y) (M-3)

$\log_{10} K_d \approx -3.25 \pm 0.54$ (t = 9,000 y) (M-4)

As can be seen from the recommended data, the changing salinity profile of the repository environment has only a weak impact on the K_d uncertainty distribution, with a tendency to towards slightly higher sorptivities with time. Since it is not possible to consider temporally variable K_d values in safety assessment calculations, the time period giving the lowest K_d value is recommended to be used for calculations. This corresponds to the groundwater conditions existing at 3,000 y. Generally the numerically calculated K_d uncertainties were found to be lognormally distributed with the exception of 9,000 y where the fitted lognormal distribution doesn't fully capture the positive skew of the data set. The K_d uncertainty distributions are plotted in Figure M-11 as cumulative distribution functions (CDF).

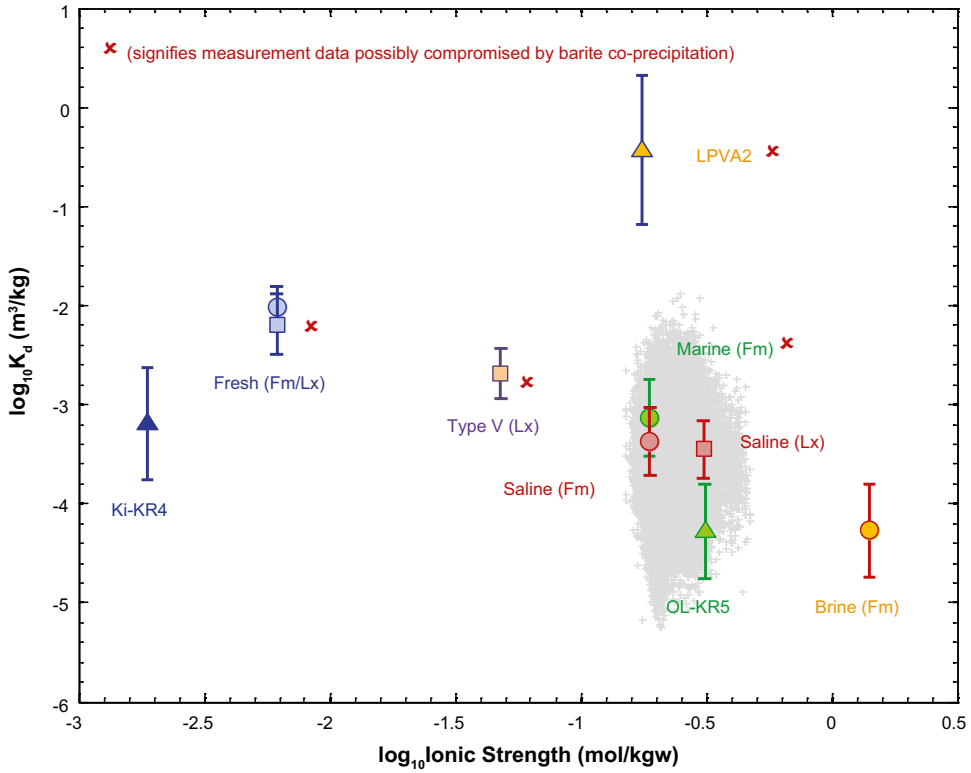

Figure M-7. *Cross-plot of K_d (m^3/kg) values for Ra(II) versus ionic strength (mol/kgw) on logarithmic axes. The recommended data are for SR-Site application conditions at 2,000 y in the temperate case and are plotted as the swarm of grey markers. K_d^0 data are plotted as geometric means with 1σ standard errors for the different groundwater compositions used in the site investigation.*

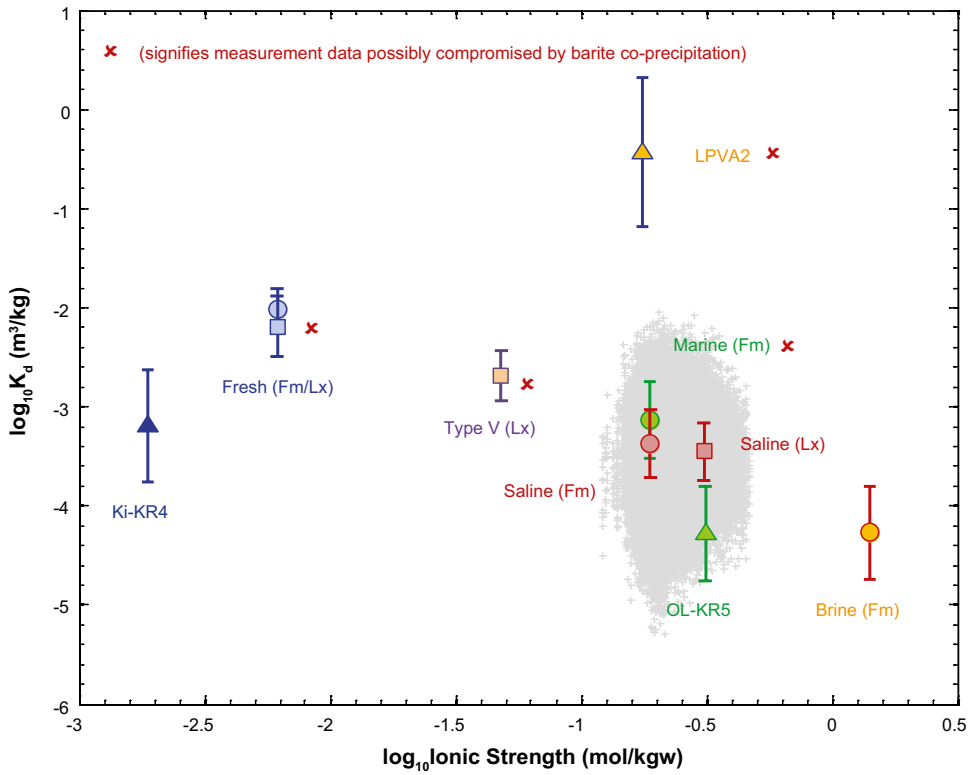

Figure M-8. *Cross-plot of K_d (m^3/kg) values for Ra(II) versus ionic strength (mol/kgw) on logarithmic axes. The recommended data are for SR-Site application conditions at 3,000 y in the temperate case and are plotted as the swarm of grey markers. K_d^0 data are plotted as geometric means with 1σ standard errors for the different groundwater compositions used in the site investigation.*

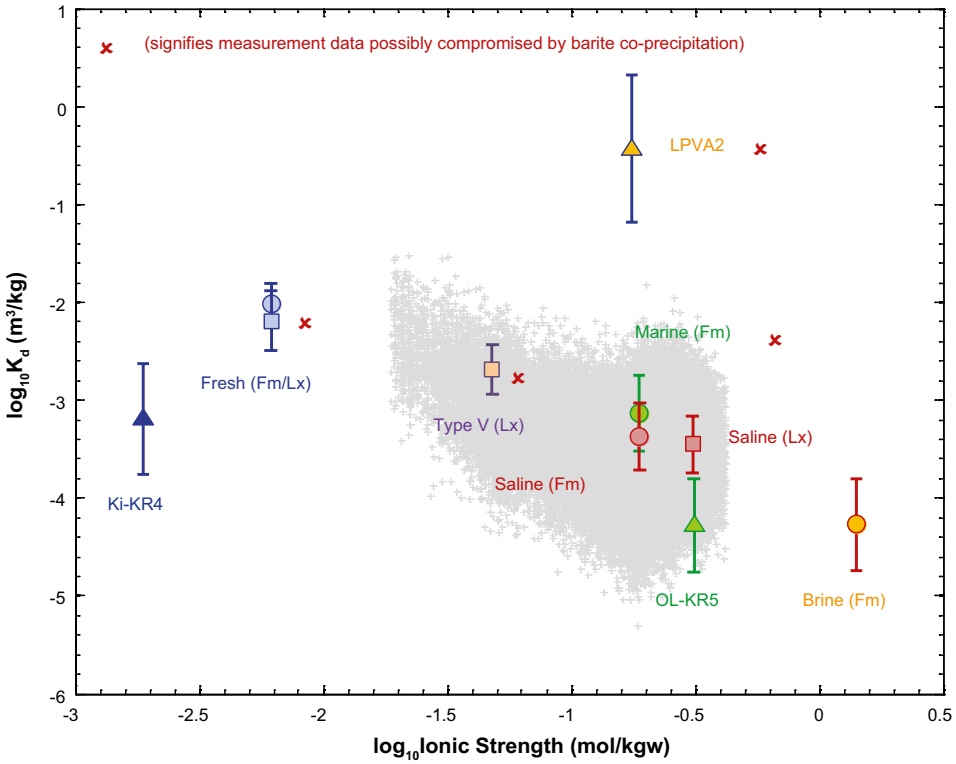

Figure M-9. *Cross-plot of K_d (m^3/kg) values for Ra(II) versus ionic strength (mol/kgw) on logarithmic axes. The recommended data are for SR-Site application conditions at 5,000 y in the temperate case and are plotted as the swarm of grey markers. K_d^0 data are plotted as geometric means with 1σ standard errors for the different groundwater compositions used in the site investigation.*

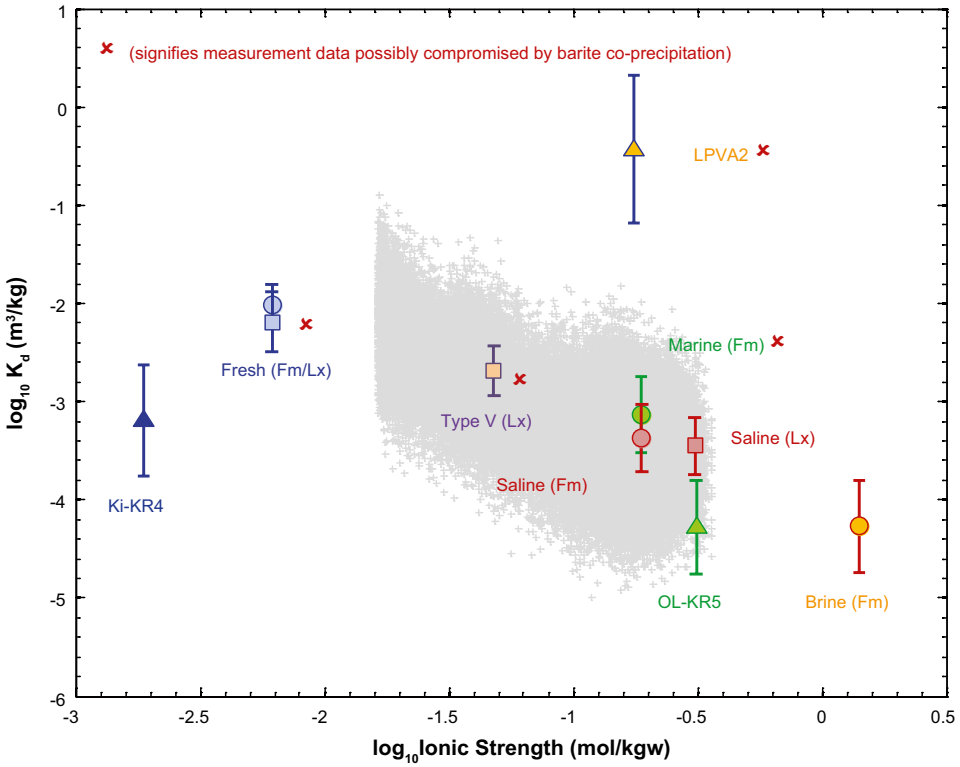

Figure M-10. *Cross-plot of K_d (m^3/kg) values for Ra(II) versus ionic strength (mol/kgw) on logarithmic axes. The recommended data are for SR-Site application conditions at 9,000 y in the temperate case and are plotted as the swarm of grey markers. K_d^0 data are plotted as geometric means with 1σ standard errors for the different groundwater compositions used in the site investigation.*

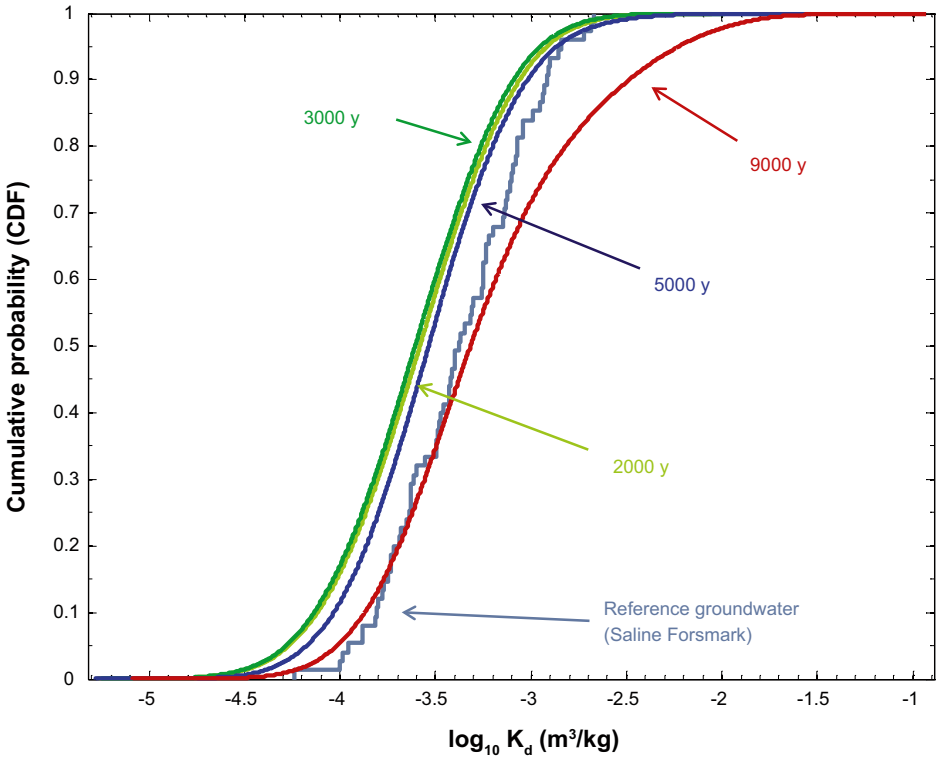

Figure M-11. *Uncertainty of recommended K_d (m^3/kg) values for Ra(II) sorption plotted as a cumulative probability distribution (CDF). The smooth curves represent the K_d values corrected for groundwater chemistry at different times during the temperate period. The jagged curve shows the original K_d^0 distribution estimated for the reference groundwater (Forsmark saline).*

Appendix N

K_d data derivation sheet for selenium (Se)

Overview and evaluation of available literature data

The sorption of Se on granitic rock is poorly covered in the literature and there are only a small number of studies where data are given for relevant rock types and groundwater compositions. Some data are given by /Ticknor et al. 1996/ for Se sorption on granite using several different spike concentrations of Se, different ionic strengths, pH levels, and fulvic acid concentrations. Data are also reported by /Papelis 2001/ where pH dependent sorption edges were measured on granite in contact with variable ionic strength synthetic groundwater and for different spike concentrations of Se. The raw measurement data from both references are given in Figure N-1.

In the study by /Ticknor et al. 1996/ sorption experiments were carried out under oxic conditions using a synthetic groundwater. The rock samples were crushed and sieved to give a particle size range of 0.106–0.180 mm. Half of the measurements were made using synthetic water samples conditioned by 28 days of pre-equilibration with the granite rock type being studied (Lac du Bonnet, Manitoba), while half were made using non-conditioned groundwater. The three groundwaters used in the experiments were non-saline to saline in character with ionic strengths of roughly 0.003 M, 0.025M, and 0.23 M, respectively. The pH was also adjusted to give initial pH values ranging from 7.0 to 9.0. The pH of the different contact solutions was measured at the conclusion of the experiments and found to be in the range 7.6–9.3. Different amounts of fulvic acid (specified as dissolved organic carbon, DOC) were added to the contact solutions ranging from 0 mg/l to 10 mg/l DOC.

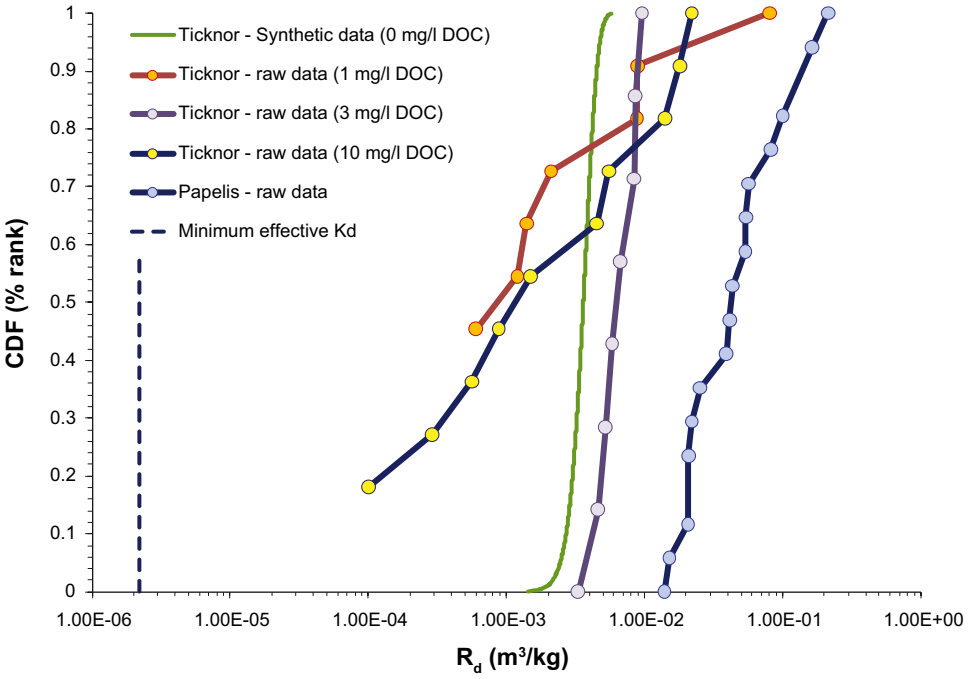

Figure N-1. *R_d (m^3/kg) values calculated for Se sorption based on literature data and presented as an empirical cumulative distribution function for granite in contact with synthetic groundwater representing different ionic strengths and different initial pH levels. Separate curves are given for different amounts of fulvic acid used in the experiments. The truncated shape of the empirical distribution for 1 mg/l and 3 mg/l DOC implies sorptivity below the detection limit and the data points are therefore excluded from the figure. An estimated normal distribution (labelled "synthetic data") is shown for the baseline case of no fulvic acid since only a single value with an error estimate is given by /Ticknor et al. 1996/ in this instance.*

R_d values were estimated for a contact time of 28 days for a Se spike concentration ranging from 10^{-8} to10^{-4} M and a liquid to solid ratio of 40 ml/g. The R_d data are given without error estimates. A total of 32 measurements were reported corresponding to different combinations of the experimental design parameters including a small number of replicates. A baseline estimate of sorption ($R_d \approx (3.6\pm0.7) \times 10^{-3}$ m^3/kg) in the absence of fulvic acid and for a spike concentration of roughly 10^{-8} M is also given in the reference although how many measurements the estimate is based is not specified.

The data from /Papelis 2001/ consist of pH dependent sorption edges measured for finely crushed Shoal granite (≤ 0.075 mm) in contact with water of variable ionic strength (0.01–1.0 M $NaNO_3$) and for Se concentrations in the range 10^{-6}–10^{-5} M. The liquid to solid ratio used in the experiments was 100 ml/g. Sorption experiments were also performed for a synthetic groundwater roughly matching the composition in a sampled borehole at the site. The ionic strength of the synthetic groundwater was roughly 0.01 M. The contact water compositions used by /Papelis 2001/ are the same as described previously for Pb(II) sorption (see Appendix F).

Selection of representative data for site specific conditions

The measurement of Se sorption is complicated by the fact that it is redox sensitive and can exist in Se(–II), Se(IV), and Se(VI) redox states. In the –II redox state it exists primarily as the HSe^- anion. In the +IV and +VI redox state, Se is predominantly speciated in oxyanion form ($SeO_3^{2-}$and SeO_4^{2-}, respectively). All three redox states are expected to exhibit relatively weak sorption since they can only bind to positively charged sorption sites.

As already outlined in Section 3.2.2, oxyanions should only sorb appreciably to minerals that have a pH point of zero proton charge near the prevailing pH of the groundwater where non-negligible proportions of positively charged binding sites might exist. The sorption of Se(IV,VI) has been previously shown by /Jan et al. 2007, 2008/ to be associated with the leachable Fe fraction of granite as assessed by sequential extraction. The easily leached Fe fraction in granite is most likely to take the form of hematite microprecipitates associated with biotite. In this compilation it is assumed that all three redox states exhibit similar sorptivity although /Jan et al. 2008/ find some evidence that Se(VI) is possibly less sorptive than Se(IV). Under the oxic conditions of the sorption experiments it is thought that predominance of the Se(IV) or Se(VI) redox state is most likely although it is not possible to distinguish which.

The baseline (no fulvic acid) R_d value and its error estimate reported by /Ticknor et al. 1996/ are assumed as a basis for calculations in this compilation since they appear to be the least ambiguous with regard to the varied experimental parameters. The BET surface area of the crushed granite was reported as 0.18±0.01 m^2/g. Since only one particle size was used in the experiments, it was only necessary to use a single transfer factor to extrapolate the data to Forsmark rock under in situ conditions. The mechanical damage transfer factor, f_m was therefore estimated to be:

$$\log_{10} f_m \approx -1.06\pm0.23 \qquad \text{(N-1)}$$

The crushed granite used by /Papelis 2001/ was reported to have a BET surface area of 0.79 m^2/g. Since no error estimate was given for the BET surface area, it is not possible to make an estimate of the uncertainty in this case. The mechanical damage transfer factor, f_m was therefore estimated to be:

$$\log_{10} f_m \approx -1.64 \qquad \text{(N-2)}$$

No CEC data are given for the granite used in either of the experiments. The iron content, however, has been estimated to be roughly 2.17% by volume (as Fe_2O_3) for the granite studied by /Ticknor et al. 1996/ and 1.91% (as FeO) for the granite described by /Papelis 2001/. Since Forsmark metagranite has an iron content of roughly 2.7% by volume (as Fe_2O_3) /Sandström and Stephens 2009/, the CEC transfer factor, f_{cec} can assumed to be approximately unity given that the true CEC can only be guessed very approximately. It is also noted that the relative Fe content of the different rock types would imply a slight upwards adjustment of the scaled K_d value for Forsmark metagranite in any case. The neglection of CEC in this case therefore appears to be a cautious assumption.

Recommended K_d data for SR-Site application conditions

Estimated K_d^0 values were calculated for Forsmark metagranite using the mechanical damage transfer factor only (f_{cec} is neglected). If it is furthermore assumed that the principal uncertainties relating to variable groundwater composition are internalised in the data, this data can be deemed suitable for SR-Site application conditions. The recommended K_d range for use in SR-Site transport calculations is given in Figure N-2 and is based on the baseline R_d estimate given by /Ticknor et al. 1996/. Extrapolated K_d data derived from the raw data given by /Papelis 2001/ are also shown in the figure for comparative purposes.

In the opinion of the present author, the sorption of Se is not sufficiently well quantified that an unequivocal recommendation can be given. Given that there are large uncertainties in the extrapolated data, a good argument could be made for expanding the error bounds of the recommended uncertainty distribution. To this end, three different cases are presented in Figure N-2 corresponding to 2σ, 4σ, and 8σ estimates of the initial measurement error specified by /Ticknor et al. 1996/ for the baseline R_d measurements. All three cases have the same median value (best estimate) although tails of varying size.

Although the 8σ distribution covers a larger uncertainty interval, it appears to be a less appropriate choice since there is a risk that K_d might be overestimated in stochastic simulations (i.e. in the upper tail of the uncertainty distribution). The 2σ distribution, on the other hand, is likely to be underestimated on account of the small underlying data set. The 4σ estimate appears to be a more cautious choice since it does not give values significantly higher than the extrapolated empirical data set from /Papelis 2001/ while at the same time giving a adequate range of uncertainty that is more likely to be representative. In spite of this recommendation, the data are highly uncertain and a case could also be made for the neglection of Se sorption on the grounds of caution. The impact of this uncertainty could, however, be tested as a sensitivity case study in safety assessment calculations if deemed necessary.

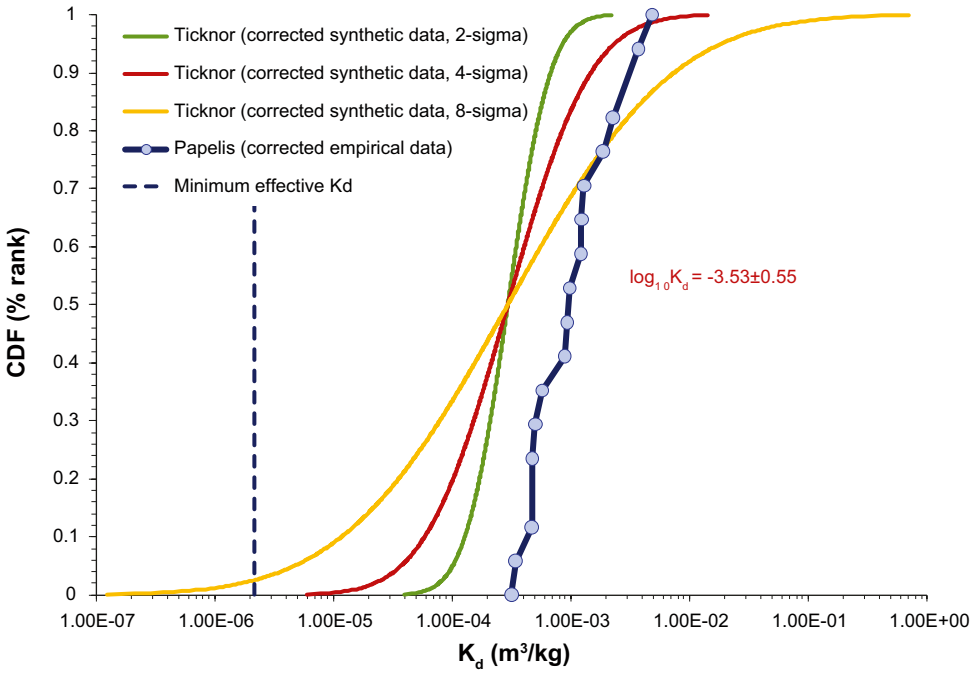

Figure N-2. *Recommended K_d (m^3/kg) values for Se sorption for use in SR-Site calculations. The data range is considered to be applicable to all groundwater compositions and assumes Forsmark metagranite (SKB rock code 101057) as a representative rock type. The parameters of the recommended lognormal distribution are indicated in the figure (4σ error estimate) and are based upon the data given by /Ticknor et al. 1996/. For comparative purposes, curves corresponding to the 2σ and 8σ cases are also drawn as well as a corrected empirical distribution for the data given by /Papelis 2001/.*

Appendix O

K_d data derivation sheet for Tin (Sn)

Overview and evaluation of available literature data

The sorption of Sn on granitic rock is poorly covered in the literature and there appears to only one study by /Ticknor et al. 1996/ where data are given for relevant rock types and groundwater compositions. One other study by the same authors is acknowledged /Ticknor and McMurray 1996/, although the data appear to be of common origin.

In the study by /Ticknor et al. 1996/ sorption experiments were carried out under oxic conditions using a synthetic groundwater. The rock samples were crushed and sieved to give particle size range of 0.106–0.180 mm. Half of the measurements were made using synthetic water samples conditioned by 28 days of pre-equilibration with the granite rock type being studied (Lac du Bonnet, Manitoba), while half were made using non-conditioned groundwater. The groundwaters used in the experiments were non-saline to saline in character with an ionic strength ranging from 0.003 M to 0.23 M, respectively. The pH was also adjusted to give initial pH values of 7.0, 8.0, and 9.0 in the contact solutions. The pH of the different contact solutions was measured at the conclusion of the experiments and found to be in the range 7.6–9.3.

R_d values were estimated for a contact time of 28 days for a Sn(IV) spike concentration of roughly 10^{-8} M and a liquid to solid ratio of 40. The R_d data are given without error estimates. A total of 32 measurements were reported for different ionic strengths and initial pH values, as well as two different dissolved concentrations of fulvic acid (1 mg/l and 10 mg/l). A baseline estimate of sorption ($R_d \approx -3.8 \pm 1.0$ m^3/kg) in the absence of fulvic acid is also given in the reference although it is not specified how many measurements the estimate is based on.

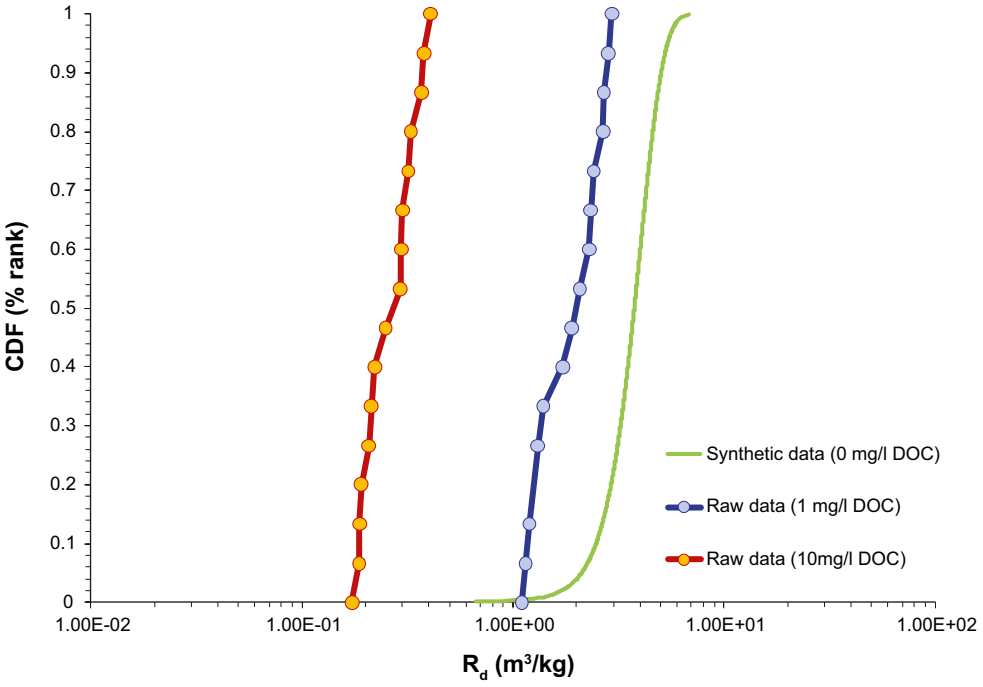

Figure O-1. *R_d (m^3/kg) values calculated for Sn(IV) sorption based on literature data and presented as an empirical cumulative distribution function for Granite in contact with synthetic groundwater representing two different ionic strengths (Fresh and Saline) and three different initial pH levels (pH 7–9). Separate curves are given for different amounts of fulvic acid used in the experiments. An estimated normal distribution (labelled "synthetic data") is shown for the baseline case of no fulvic acid since only a single value with an error estimate is given by /Ticknor et al. 1996/ in this instance.*

Since sorption in the presence of fulvic acid is not strictly relevant for sorption of Sn(IV) in the repository environment, only the measurements carried out at the lower concentration level of fulvic acid (1 mg/L DOC) have been considered thereby giving 16 measurements upon which to base the recommendation for SR-Site. The author of this compilation considers the value derived for sorption in the absence of fulvic acid, not sufficiently qualified to be used for this recommendation except as a comparative estimate.

Although the inclusion of even low concentrations of fulvic acid is not ideal for the purposes of data selection for SR-Site, in the absence of other reliable sources of sorption data it is thought that the use of these data is defensible nonetheless since the presence of organic complexing agents is expected to decrease the R_d value by way of competitive binding effects in solution.

Although /Ticknor et al. 1996/ developed a fitted parametric surface to the experimental design reflected in the experimental parameters, the author of the present compilation does not consider the underlying data set to be sufficiently well established statistically to be used in making K_d recommendations for SR-Site. Since very little difference was noted between the R_d values reported for different ionic strengths and pH values, the data set have therefore been considered as an aggregate set. The effect of groundwater compositional uncertainty is thereby implicitly contained in the uncertainty range derived for the recommended K_d in the aggregate set.

Selection of representative data for site specific conditions

The R_d values reported by /Ticknor et al. 1996/ for 1 mg/l DOC (fulvic acid) are assumed as a basis for calculations in this compilation for the reasons outlined in the previous section. The BET surface area of the crushed granite was reported as 0.18±0.01 m^2/g. Since only one particle size was used in the experiments, it was only necessary to use a single transfer factor to extrapolate the data to Forsmark rock under in situ conditions. The mechanical damage transfer factor, f_m was therefore estimated to be:

$$\log_{10} f_m \approx -1.06 \pm 0.23 \qquad \text{(O-1)}$$

No CEC data are given for the granite used in the experiments, although the iron content (given as Fe_2O_3) has been estimated to be roughly 2.17% by volume. Since Forsmark metagranite has an iron content of roughly 2.7% by volume (Fe_2O_3) /Sandström and Stephens 2009/, the CEC transfer factor, f_{cec} is assumed to be approximately unity given that the CEC can only be guessed very approximately. Although there is no evidence to suggest for or against preferential sorption of Sn(IV) with biotite, its general insensitivity to the expected range of groundwater redox conditions would suggest that CEC effects can possibly be neglected in any case. Since no error estimates were specified for the original raw data, only the error estimate of the mechanical damage transfer factor was propagated through the calculations to give the recommended distribution for SR-Site. The overall uncertainty is therefore possibly underestimated.

Recommended K_d data for SR-Site application conditions

Estimated K_d^0 values were calculated for Forsmark metagranite using the mechanical damage transfer factor only (f_{cec} is neglected). If it is furthermore assumed that the principal uncertainties relating to variable groundwater composition are internalised in the data, this data can be deemed suitable for SR-Site application conditions. The recommended K_d range for use in SR-Site transport calculations is given in Figure O-2. The synthetic data shown previously in Figure O-1 was also corrected for mechanical damage effects and is shown for comparative purposes in Figure O-2. In this case, the original error estimate was doubled (i.e. assuming a 2σ error) and reinterpreted as a lognormal uncertainty distribution.

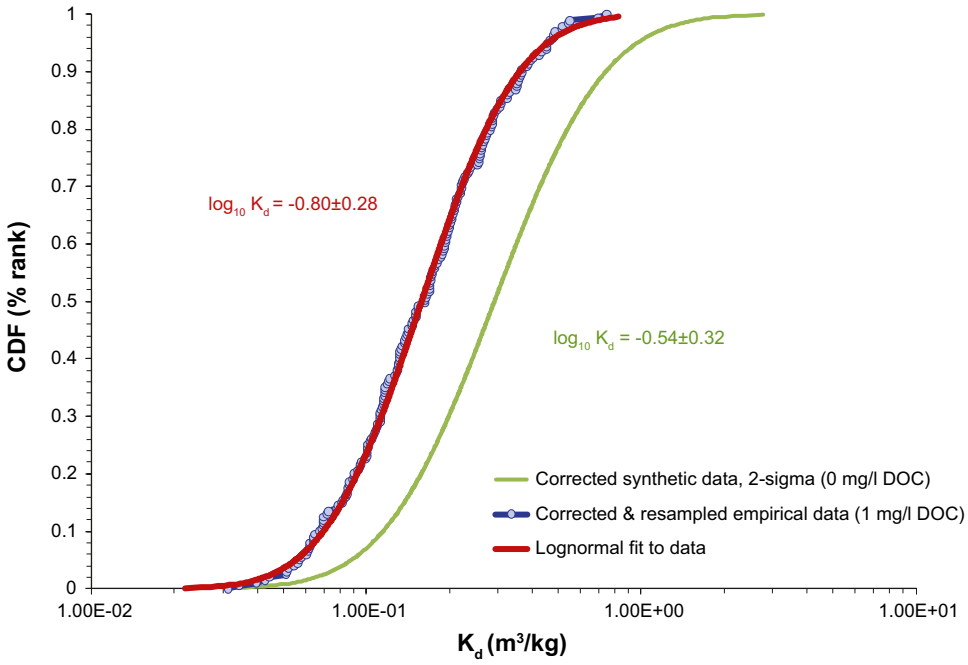

Figure O-2. *Recommended K_d (m^3/kg) values for Sn(IV) sorption for use in SR-Site calculations. The data range is considered to be applicable to all groundwater compositions and assumes Forsmark metagranite (SKB rock code 101057) as a representative rock type. The parameters of the lognormal distribution fit to the data are indicated in the figure. For comparative purposes, a corrected distribution is also shown for the synthetic data estimate (assuming a 2σ error estimate and reinterpreted as a lognormal distribution).*

Appendix P

K_d data derivation sheet for strontium (Sr)

Overview and evaluation of site investigation data

Site specific sorption data were obtained for Sr(II) during the site investigations at Forsmark /Byegård et al. 2008/ and Laxemar /Selnert et al. 2009/. These data are summarised in the bedrock transport properties site descriptive model /Crawford 2008/ and are the basis for K_d values recommended for use in SR-Site. In most cases there is a time dependency in the experimental data with a clear trend towards higher R_d values at later times. The data also exhibit a relatively clear surface area dependency whereby smaller crushed particle sizes are associated with higher sorptivities than larger size fractions. A typical time series for Sr(II) sorption on Forsmark metagranite (SKB rock code 101057) is shown in Figure P-1.

For the same reasons as outlined previously, no attempt has been made to model the time dependency of the data. The data have therefore been treated by considering the data set in its entirety without filtering of values on the basis of crushed size fraction or contact time. Sr(II) is particularly problematic since its sorption is very weak and in some cases not possible to quantify. It is not uncommon for the apparent partitioning coefficient, R_d to be negative owing to random errors in the measurement of concentration where the amount sorbed is less than the standard error of the measurement itself. In such cases it is not generally possible to quantify whether sorption has, in fact, occurred.

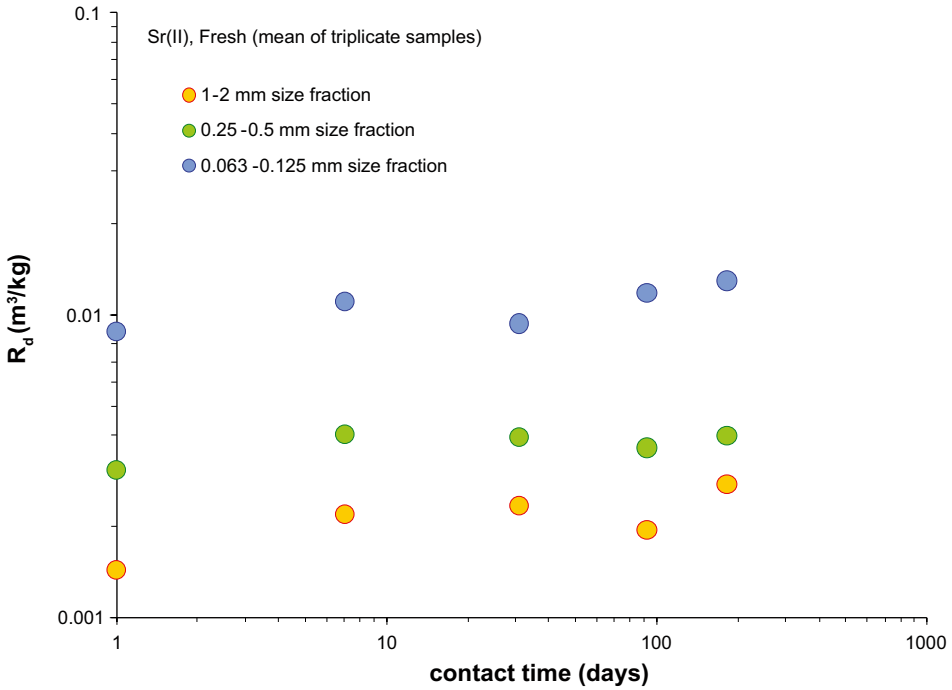

Figure P-1. *Typical time series for Sr(II) sorption R_d (m^3/kg) measured in the Forsmark site investigation studies. There is a clear sorption dependency on both particle size and time.*

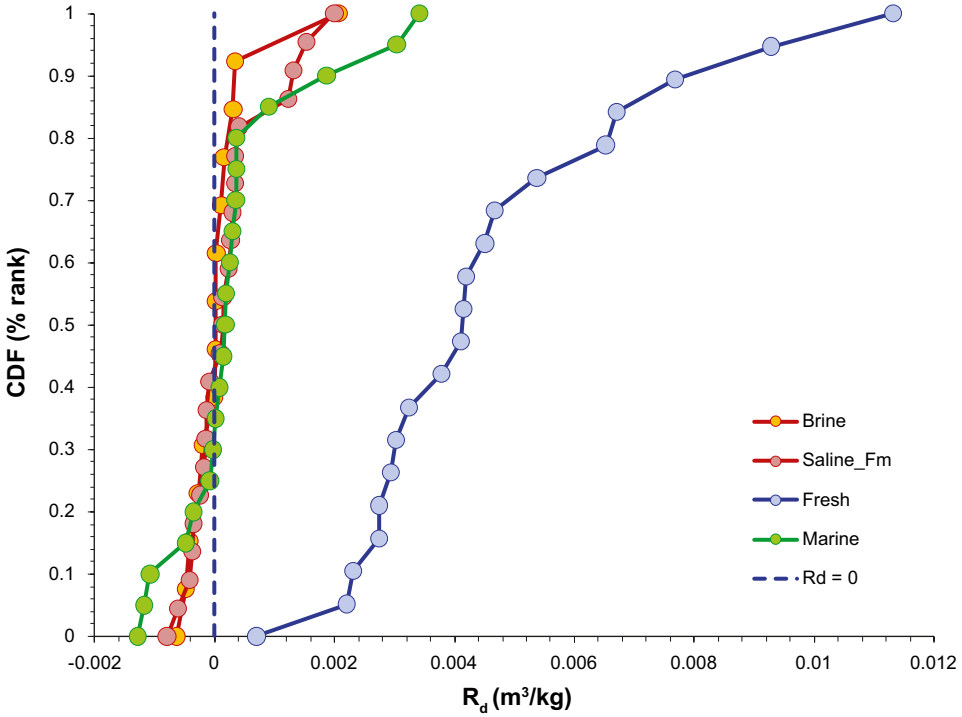

Figure P-2. *Comparison of R_d (m^3/kg) values estimated for Sr(II) sorption based upon Forsmark site investigation data. The plotted series correspond to the 1–2 mm size fraction and longest contact time (~180 days). Only the Fresh groundwater data set contains a sufficient proportion of non-negative values that the estimated R_d value can be considered to be statistically quantifiable. Sorption is sufficiently weak for saline, brine and marine groundwaters as to be effectively unquantifiable (i.e. approximately equal numbers of positive and negative R_d values reflecting random errors in the activities measured for blank samples).*

Selection of representative data for site specific conditions

The procedure for derivation of Sr(II) K_d values relevant for application in SR-Site is the same as that outlined previously for Cs(I) and the other ion-exchanging solutes and is not discussed further here. Estimated K_d^0 data corrected for surface area, mechanical damage, and CEC effects using Equation 5-2 are plotted in Figure P-3 assuming Forsmark metagranite (SKB rock code 101057) as a representative rock type for the Forsmark site. Although the uncertainty ranges for the individual data sets are large, there is a clear tendency towards greater sorptivity under low ionic strength conditions relative to that obtained for the more saline groundwater types. Some of the R_d values for the data sets corresponding to saline, marine, and brine groundwater types are sufficiently low that the extrapolated K_d values are significantly lower than the minimum effective K_d value corresponding to storage of freely dissolved solute in the rock matrix porosity.

Similarly to the other ion-exchanging solutes studied in the site investigations, chemistry transfer factors were estimated for the groundwater compositions expected under SR-Site conditions. In order to do this, the theoretical K_d was calculated using PHREEQC and the SKB-TDB /Duro et al. 2006/ for 10,000 randomly selected groundwater compositions taken from the SR-Site temperate domain simulations /Salas et al. 2010/. The exchange model described in Section 5.1.1 was used assuming selectivity coefficients for Äspö diorite as a basis for calculations. Comparison of K_d values calculated in this manner with the corresponding theoretical result for the Forsmark saline reference water allows the groundwater chemistry transfer factor, f_{chem} to be calculated in straight-forward fashion for the projected application conditions using Equation 5-9. Since the data are normalised in the calculation, the final value of f_{chem} is relatively insensitive to the CEC of the simulated rock-water system provided the differences are not so great that very different groundwater compositions result.

In the SR-Site groundwater simulations, only the major ions are specified. For the purpose of simulating ion-exchange processes involving trace components not included in these simulations, the concentrations of these constituents need to be estimated in some way. Background concentrations of the components

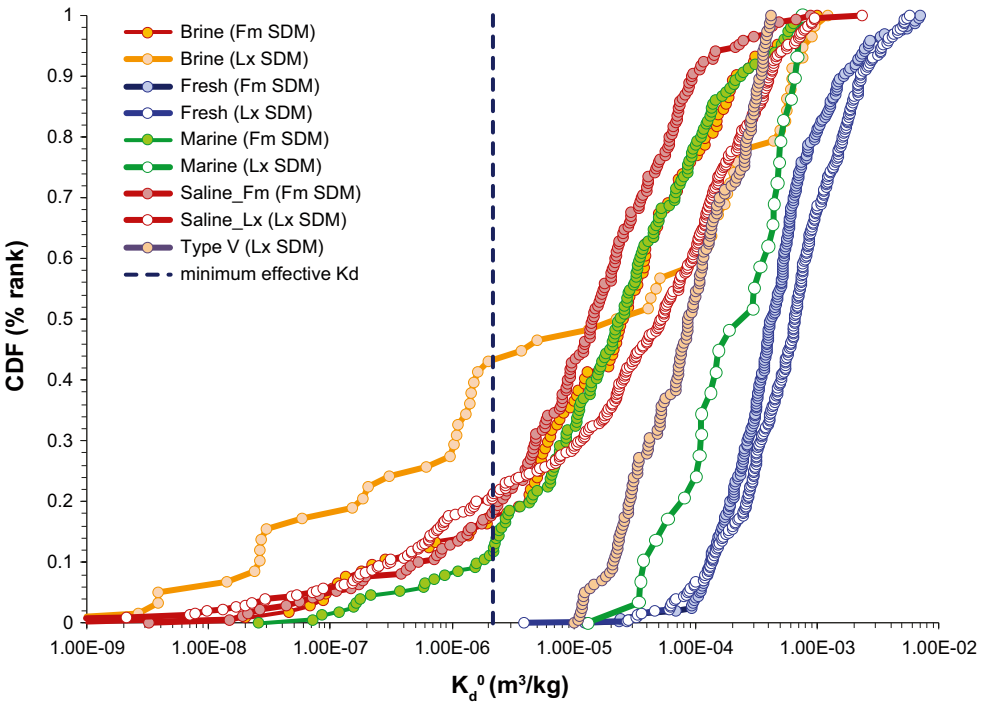

Figure P-3. *K_d^0 (m^3/kg) values calculated for Sr(II) sorption based on raw R_d data for site-specific rock types and groundwater compositions as reported in the Forsmark (Fm SDM) and Laxemar (Lx SDM) site investigations. Surface area normalisation, mechanical damage, and CEC transfer factors (f_A, f_m, and f_{cec}) have been considered in the estimation procedure. The raw data are corrected to give values deemed appropriate for Forsmark metagranite (SKB rock code 101057) under in situ conditions and are presented as an empirical cumulative distribution function. A minimum effective K_d reference line is plotted in the figure indicating the upper 95% confidence limit for the matrix storage capacity of the rock based on water saturation porosity*

(Cs, Sr, Rb, and Ba) in the groundwater were estimated using correlations derived from the site investigation hydrochemistry data. Full details concerning how these correlations were established and implemented can be found in Appendix A.

Simulation results for the central case selectivity coefficients are given in Figure P-4 and indicate a slightly decreased K_d at early times relative to the reference groundwater. At longer times, however, the progressive freshening of the groundwater due to intrusion of a meteoric component gives elevated K_d values relative to the reference groundwater. In this case, the reference groundwater was taken to be fresh water on account of the very uncertain R_d estimates obtained for the more saline groundwater compositions. As can be seen from Figure P-4, the groundwater compositions during the SR-Site temperate period are somewhat more saline than the reference groundwater thereby implying a reduction of up to 2 orders of magnitude for the central best estimate K_d value.

Additional simulations were carried out to quantify the impact of uncertainty in the selectivity coefficients using the 2σ error estimates specified in Table 5-5 and assuming lognormally distributed uncertainties. The results of this analysis are shown in Figure P-5 and indicate a relatively small impact of aleatory uncertainty.

Using the calculated f_{chem} distribution, it is possible to estimate K_d values appropriate for application groundwater compositions by convolution of the individual probability density functions or by using an equivalent stochastic method. The latter method being simpler to implement numerically was chosen and used to estimate the K_d values presented in this compilation. The stochastic method was based upon random sampling (10^5 samples) of the individual probability density functions and multiplication of the individually sampled values using Equation 5-3. The resulting distributions of K_d values are plotted in Figure P-6 to Figure P-9 for different times during the temperate calculation cases and include the additional impact of stochastically perturbed selectivity coefficients as described above.

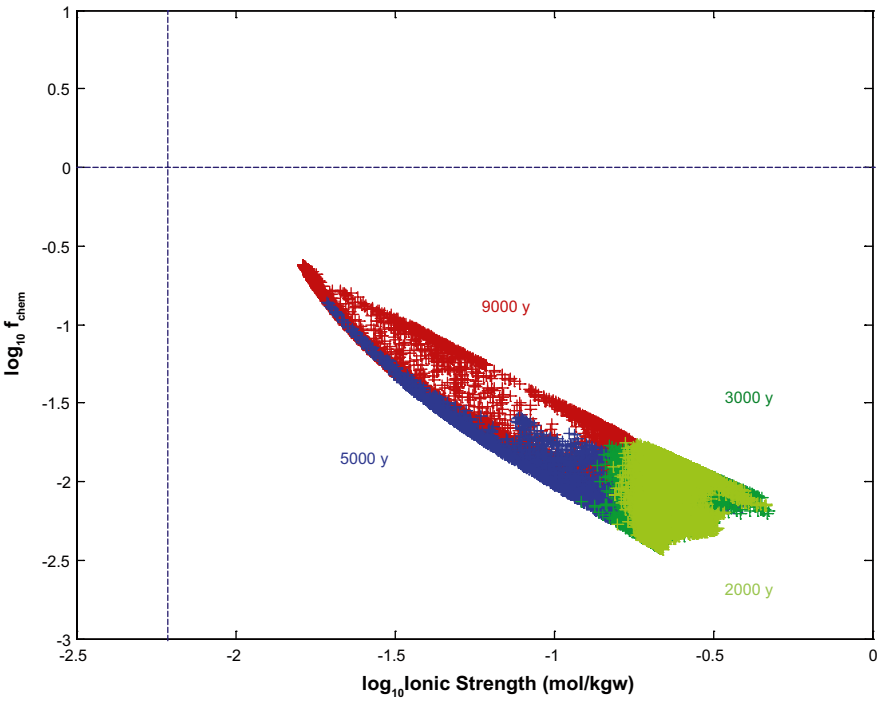

Figure P-4. *Chemistry transfer factors, f_{chem} calculated for Sr(II) sorption at application groundwater conditions in the SR-Site temperate case. The plotted data represent 10,000 randomly selected groundwater compositions calculated individually using PHREEQC and the assumed ion exchange model (central case selectivity coefficients). Data are given for 2,000 y (lime green markers), 3,000 y (dark green), 5,000 y (blue), 9,000 y (red). The cross-hairs in the figure represent the relative location of the reference groundwater (fresh).*

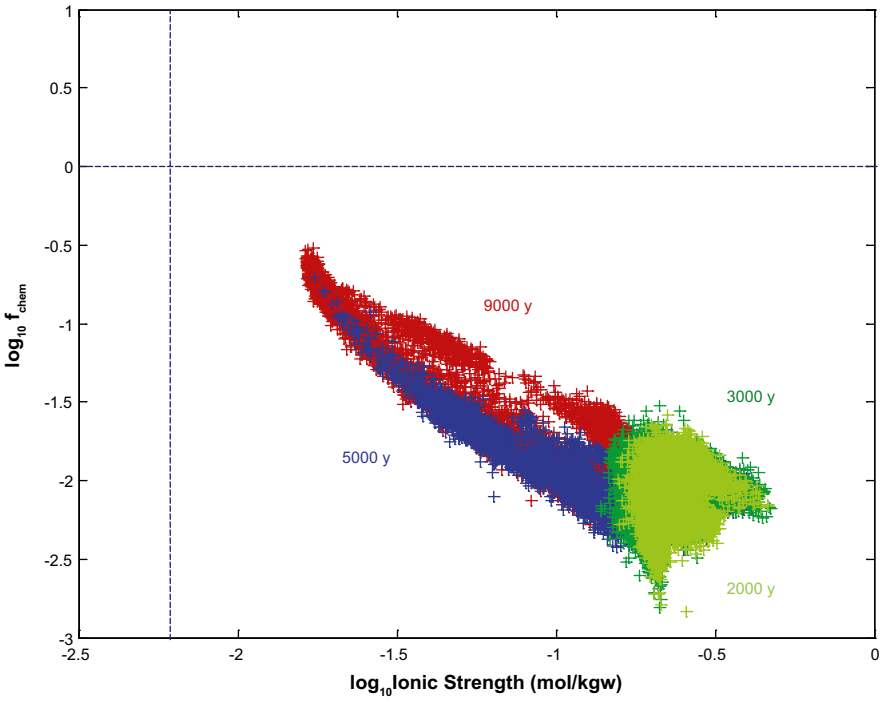

Figure P-5. *Chemistry transfer factors, f_{chem} calculated for Sr(II) sorption at application groundwater conditions in the SR-Site temperate case. The plotted data represent 10,000 randomly selected groundwater compositions calculated individually using PHREEQC and the assumed ion exchange model (central case selectivity coefficients). The plotted data include the additional effect of random perturbation of selectivity coefficients conforming to their error estimates. Data are given for 2,000 y (lime green markers), 3,000 y (dark green), 5,000 y (blue), 9,000 y (red). The cross-hairs in the figure represent the relative location of the reference groundwater (fresh).*

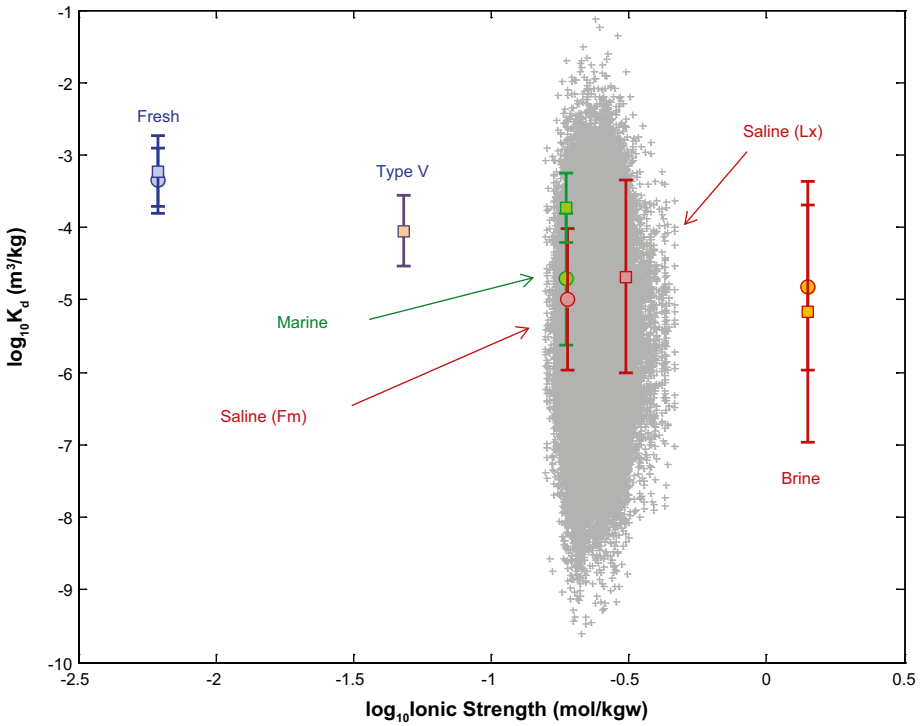

Figure P-6. *Cross-plot of K_d (m^3/kg) values for Sr(II) versus ionic strength (mol/kgw) on logarithmic axes. The recommended data are for SR-Site application conditions at 2,000 y in the temperate case and are plotted as the swarm of grey markers. K_d^0 data are plotted as geometric means with 1σ standard errors for the different groundwater compositions used in the site investigation.*

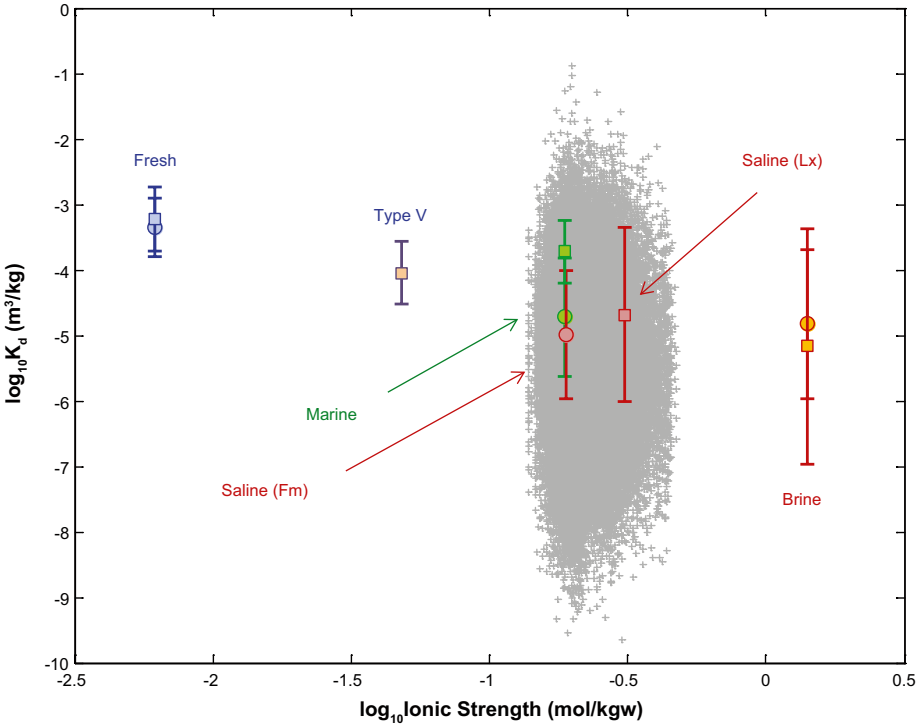

Figure P-7. *Cross-plot of K_d (m^3/kg) values for Sr(II) versus ionic strength (mol/kgw) on logarithmic axes. The recommended data are for SR-Site application conditions at 3,000 y in the temperate case and are plotted as the swarm of grey markers. K_d^0 data are plotted as geometric means with 1σ standard errors for the different groundwater compositions used in the site investigation.*

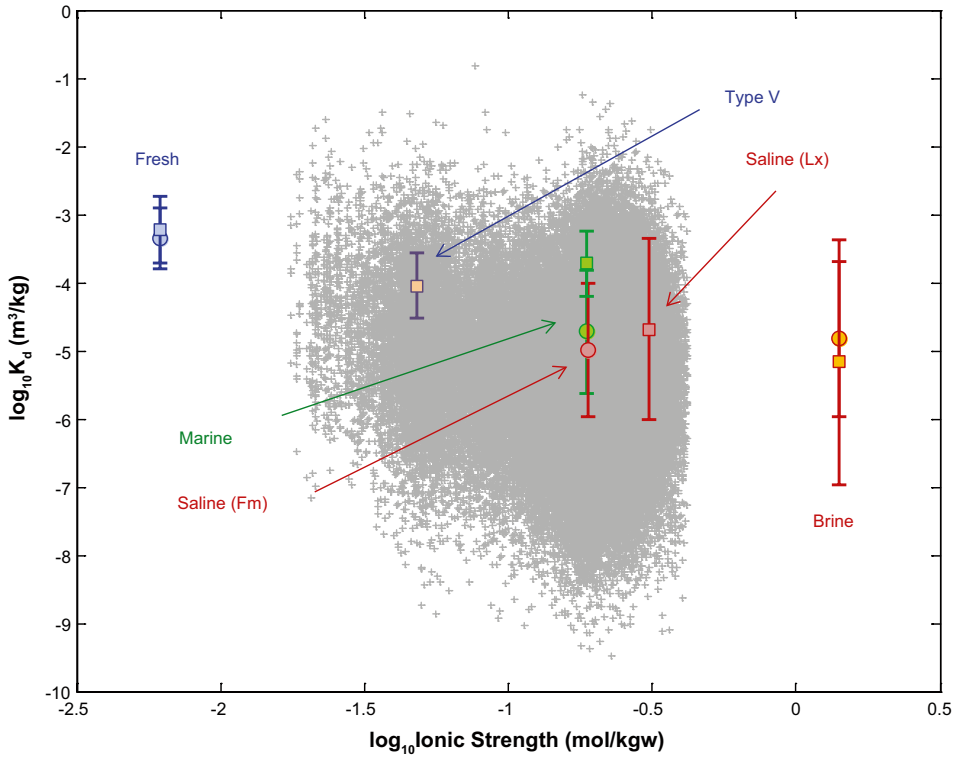

Figure P-8. *Cross-plot of K_d (m^3/kg) values for Sr(II) versus ionic strength (mol/kgw) on logarithmic axes. The recommended data are for SR-Site application conditions at 5,000 y in the temperate case and are plotted as the swarm of grey markers. K_d^0 data are plotted as geometric means with 1σ standard errors for the different groundwater compositions used in the site investigation.*

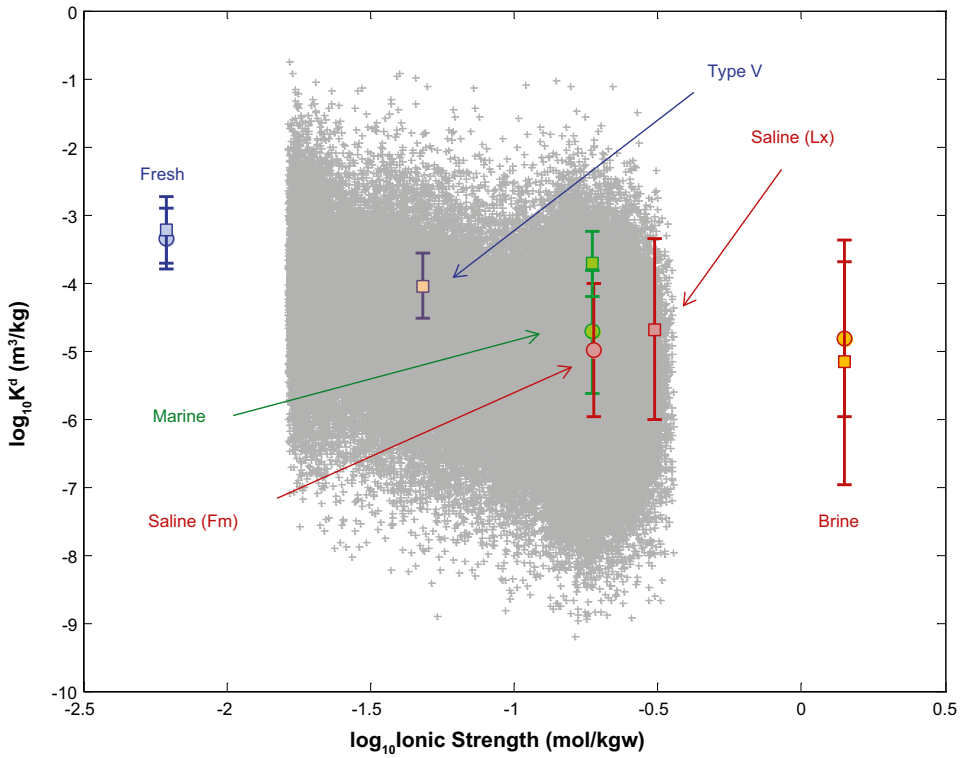

Figure P-9. *Cross-plot of K_d (m^3/kg) values for Sr(II) versus ionic strength (mol/kgw) on logarithmic axes. The recommended data are for SR-Site application conditions at 9,000 y in the temperate case and are plotted as the swarm of grey markers. K_d^0 data are plotted as geometric means with 1σ standard errors for the different groundwater compositions used in the site investigation.*

Although only the K_d^0 data set for the fresh reference groundwater was used to extrapolate to application conditions, the plotted results of the calculations indicate a fair qualitative agreement with the K_d^0 values for groundwaters that were not used in the calculations. It is acknowledged, however, that there is significant spread in the data that makes it difficult to properly ascertain the accuracy of the predictions. The assumption of the simplified, single-site ion-exchange model and selectivity coefficients derived for the Äspö diorite rock, however, appears to give an acceptably low level of epistemic uncertainty with regard to Sr(II) sorption for the purposes of SR-Site safety assessment calculations involving Forsmark site specific conditions.

Recommended K_d data for SR-Site application conditions

Based on the ion-exchange simulations described in the previous section, the following K_d ranges are recommended for use at different times in the hydrogeochemical evolution of the repository environment:

$\log_{10} K_d \approx -5.44 \pm 0.99$ (t = 2,000 y) (P-1)

$\log_{10} K_d \approx -5.47 \pm 1.0$ (t = 3,000 y) (P-2)

$\log_{10} K_d \approx -5.38 \pm 0.99$ (t = 5,000 y) (P-3)

$\log_{10} K_d \approx -5.11 \pm 1.05$ (t = 9,000 y) (P-4)

As can be seen from the recommended data, the changing salinity of the repository environment has only a weak impact on the K_d distribution, with a tendency to towards slightly higher sorptivities with time. Since it is not possible to consider temporally variable K_d values in safety assessment calculations, the time period giving the lowest K_d value is recommended to be used for calculations. This corresponds to the groundwater conditions existing at 3,000 y. The numerically calculated K_d uncertainty distributions were found to be conform relatively well to a lognormal distribution. Unlike Cs(I) and Ra(II), the predicted uncertainty distribution for K_d at 9,000 y was not found to be significantly skewed due to the broadly skewed distribution of ionic strengths prevailing in the groundwater at this time (cf. Figure P-5). This is thought to be due to the uncertainty of the underlying reference data set (i.e. K_d^0 for fresh water) which seems to dominate the statistical dispersion of the extrapolated data.

K_d data derivation sheet for technetium (Tc)

Overview and evaluation of available literature data

The most detailed set of Tc sorption data for relevant rock types and groundwater compositions in the open literature is documented by /Huitti et al. 1996/. In this study, sorption was measured on crushed rock samples from three borehole sections representing three different alteration types of Rapakivi granite (Hästholmen, Finland). The sorption experiments were carried out under anoxic conditions using a natural groundwater sample (LPVA2) with an ionic strength of about 0.17 M and a liquid to solid ratio of 10 ml/g. The groundwater was dominated by NaCl with a composition close to that of the Marine groundwater type used in the Forsmark and Laxemar laboratory investigations. The spike concentration of Tc was 10^{-8} M. The range of redox potentials measured during the experiments together with the known pH and carbonate concentration of the contact solutions suggest speciation in the tetravalent, Tc(IV) form. This is consistent with the magnitude of sorption measured during the experiments, since the oxidised heptavalent, Tc(VII) form is only very weakly sorbed (for all practical purposes, it may be considered non-sorbing).

Sorption experiments were carried out on three samples of granite described as fresh, weathered, and altered. As noted previously for other solutes, it was generally found that the sorption of Tc did not scale linearly with BET surface area and R_d values estimated for the weathered and altered samples were somewhat less than what would be otherwise predicted on the basis of their increased surface area. The rock samples were the same as described previously for Np sorption (Appendix G, Table G-1).

The data for Tc are estimated in terms of the percentage sorbed, S(%) calculated with the aid of a radiometric mass balance. The actual R_d data in the references are given without error estimates and in some cases reported as "≥" a specified value owing to detection limit issues. In order to obtain numerical ranges of K_d including uncertainty estimates, the procedures outlined in Appendix C were used. Since there are only a small number of R_d values for each rock type, re-sampling of the R_d values and their associated errors allows a more realistic range of data uncertainty to be estimated. The composite distribution of R_d values obtained for each rock type is shown in Figure Q-1.

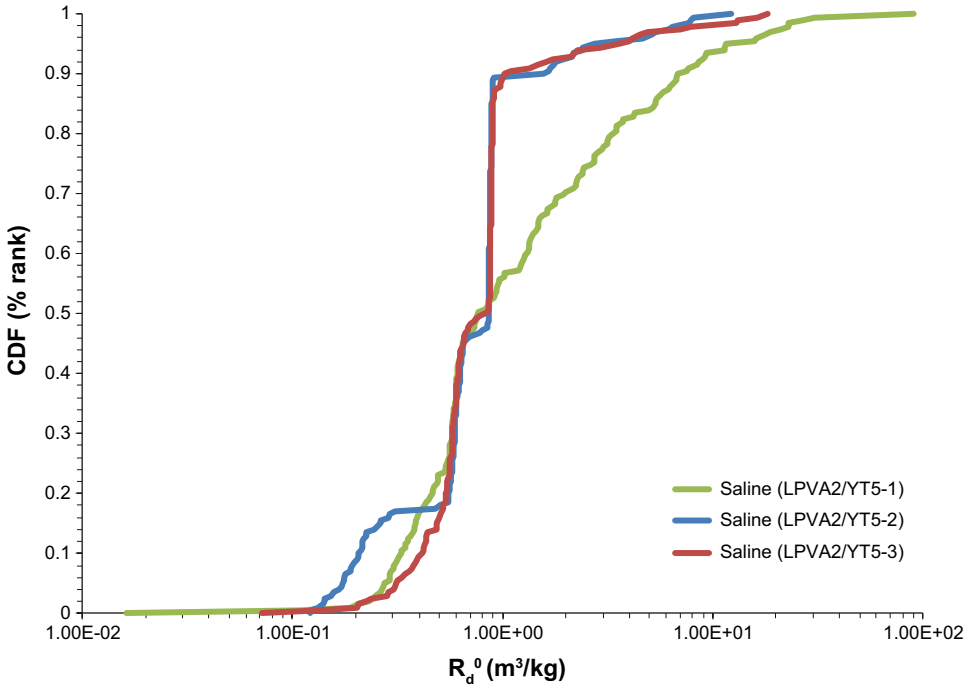

Figure Q-1. *R_d^0 (m^3/kg) values calculated for Tc(IV) sorption under anoxic conditions, based on literature R_d data and presented as an empirical cumulative distribution function for rocks taken from Finnish investigation sites. The individual data points and their uncertainties have been re-estimated from tabulated sorption percentage data and then re-sampled to give the composite distributions plotted in the figure.*

Selection of representative data for site specific conditions

As can be seen from Figure Q-1, the re-sampled data indicate that there are only minor differences between the sorptivities measured for the different alteration types of Rapakivi granite. In general, the sorptivity was very strong (in most cases S ≈ 99±1%) and thereby close to the limit of quantification. This gives rise to relatively large tailing in the uncertainty distribution given the small number of measurements (6 measurements). This weakly bounded upper limit on the magnitude of sorption in this case could be a potential source of bias.

As noted previously for the rock samples used in this particular study, the relatively large differences between the BET surface areas and CEC measured for these different materials do not translate into correspondingly large shifts in sorptivity. For the same reasons as outlined previously (Appendix G), only the data for the unaltered rock type YT-1 have been propagated further in the analysis.

As noted previously for the rock samples used in this particular study (Appendix G), the differences in BET surface area and CEC reported for the fresh, weathered, and altered samples of Rapakivi granite do not appear to translate into correspondingly large shifts in sorptivity. The sorptivity of these three rock types as reported by /Huitti et al. 1996/ appears to be very similar. As previously, the data sets for the weathered and altered rock have been disregarded since the BET surface areas and CEC values would otherwise imply unrealistic transfer factors giving excessively low K_d estimates for application conditions. Only the data for the unaltered rock type YT-1 have therefore been propagated further in the analysis.

Since the same materials were used for Np sorption measurements, the same f_m and f_{cec} transfer factors were used as described previously in Appendix G. Using the f_m and f_{cec} transfers factors, estimated K_d^0 values were calculated for the original 6 data points. On account of the limited number of data points, the individual K_d^0 values and their uncertainties were then re-sampled assuming a convex combination of the underlying lognormal distributions, now including the additional uncertainties of the f_m and f_{cec} transfer factors. The resulting translated and expanded uncertainty distribution for K_d^0 is shown in Figure Q-2.

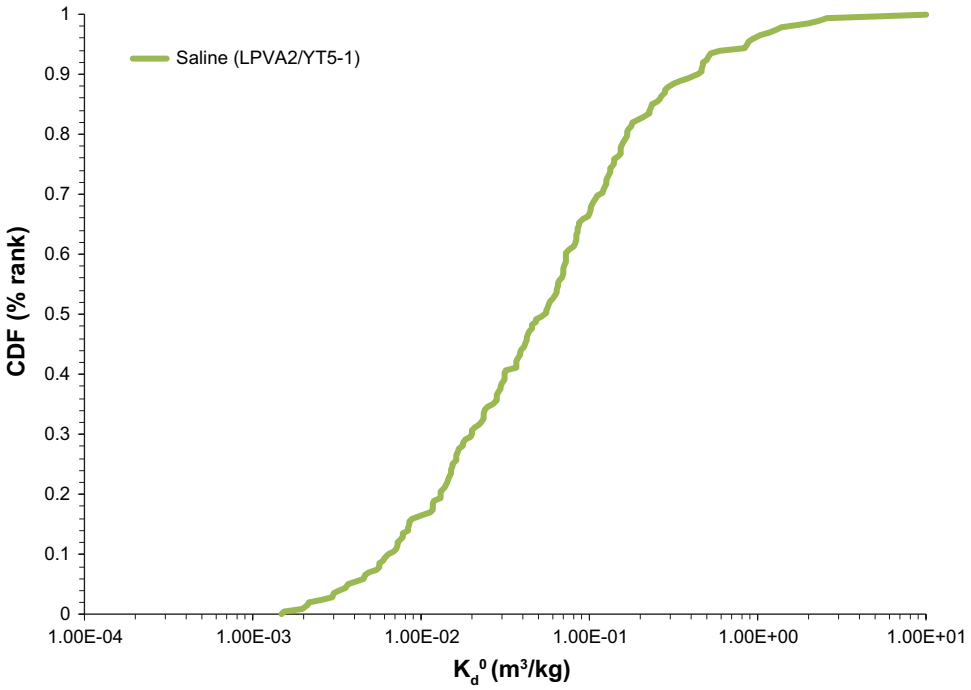

Figure Q-2. *K_d^0 (m³/kg) values calculated for Tc(IV) sorption based on literature R_d data. Surface area normalisation, mechanical damage, and CEC transfer factors (f_m, and f_{cec}) have been considered in the estimation procedure. The raw data are corrected to give values deemed appropriate for Forsmark metagranite (SKB rock code 101057) under in situ conditions and are presented as an empirical cumulative distribution function.*

Recommended K_d data for SR-Site application conditions

Since there is only one relevant data set for Tc(IV) sorption, a lognormal fit was made to the re-sampled uncertainty distribution shown in Figure Q-2 assuming that the principal uncertainties relating to variable groundwater composition are internalised in the data set (see Figure R-5). Owing to the very strong sorption measured in these experiments and the potential for bias in estimating the uncertainty distribution, the recommendation for SR-Site is to use the uncertainty distribution proposed for Pu(IV) instead since this is based upon a substantially larger data set. Interestingly, the proposed distribution for Pu(IV) is almost identical to that estimated for Tc(IV). This agreement does not necessarily mean that the data are accurate since the Pu data are also characterised by strong sorption ($S \geq 99 \pm 0.1\%$) and could be affected by the same inherent quantification biases. In the case of Pu, however, the reported error of the sorption percentage, S% was a factor 10 lower than that reported for Tc. This means that the variance of the aggregate data set has a larger influence on the estimated uncertainty for Pu sorption than the error of the individual measurements as in the case of Tc.

Assessment of predominant redox state under application groundwater conditions

In order to ascertain the principal redox state of Tc under application groundwater conditions, the speciation of Tc was calculated for 20,000 randomly sampled groundwater compositions taken from the SR-Site temperate domain simulations /Salas et al. 2010/. The calculations were made for the prevailing groundwater chemistry at time 2,000 y, 3,000 y, 5,000 y, and 9,000 y using PHREEQC and the SKB-TDB /Duro et al. 2006/. Since it is not certain which redox couple can be assumed to dominate the groundwater redox conditions in the SR-Site temperate case groundwater simulations, two different redox couples have been assumed as individual case studies for groundwater redox control.

In addition to calculating the actual speciation of Tc in the application groundwater, sweep calculations were made for a range of hypothetical redox potentials to ascertain the location of the redox transition point where the Tc(IV) and Tc(VII) species are present in roughly equal concentrations. For numerical reasons this was done only for the convex hull of data points describing the envelope of pH and total carbonate concentrations in the application groundwater. From these data, a plane of

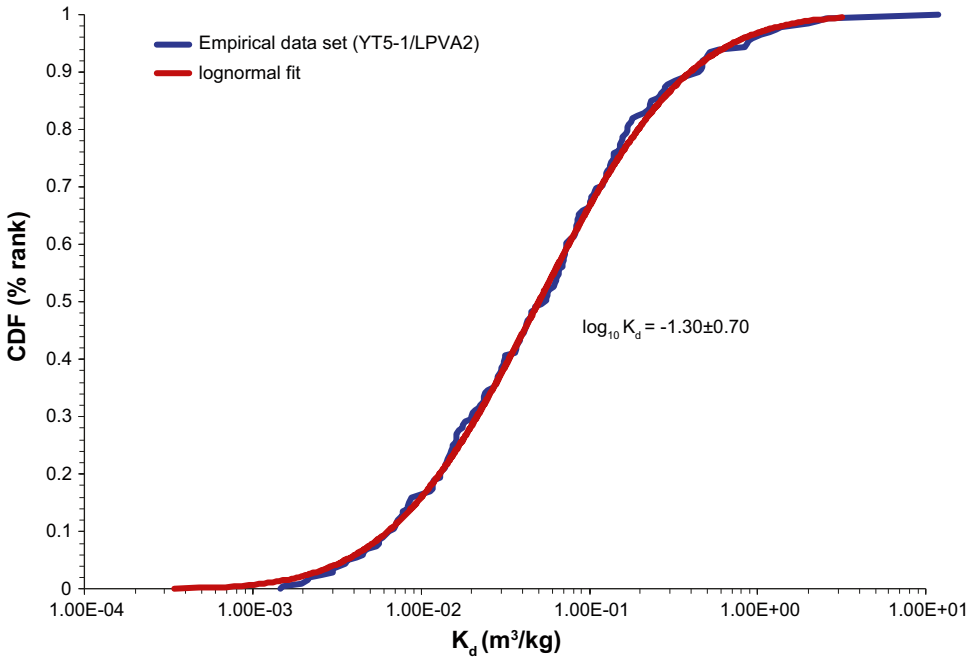

Figure Q-3. *Recommended K_d (m^3/kg) values for Tc(IV) sorption for use in SR-Site calculations. The data range is considered to be applicable to all groundwater compositions and assumes Forsmark metagranite (SKB rock code 101057) as a representative rock type. The parameters of the lognormal distribution fit to the data are indicated in the figure.*

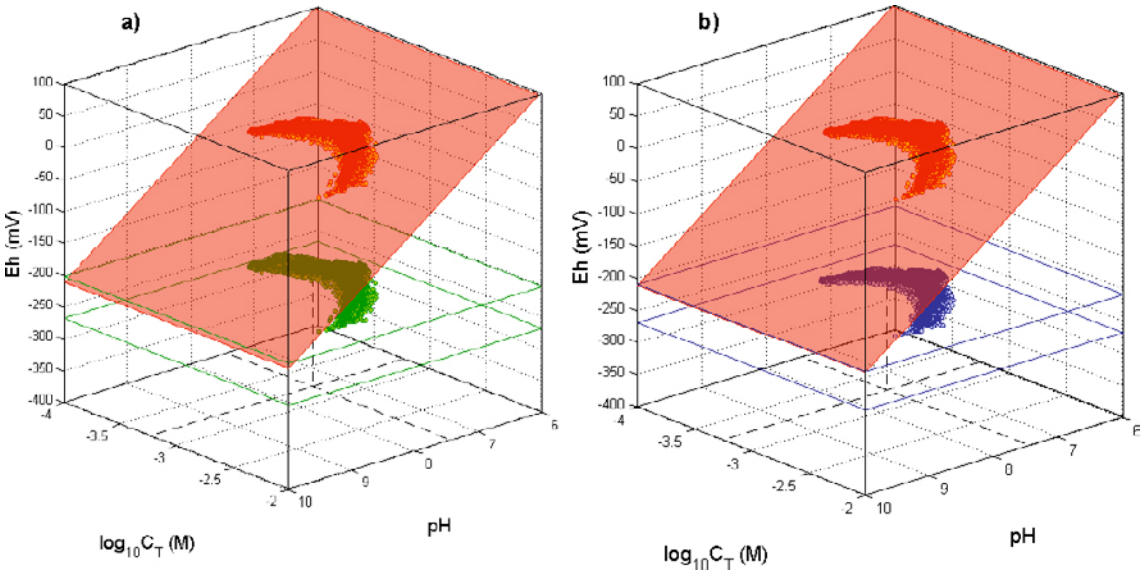

Figure Q-4. *Redox parameter space for 20,000 randomly selected SR-Site temperate case groundwater compositions at 2,000 y for (a) $Fe^{2+}/Fe(OH)_3$ redox couple, and (b) SO_4^{-2}/FeS_{am} redox couple. The calculations indicate that sampled groundwater compositions are sufficiently reducing for Tc(IV) to be the dominant redox species (min and max Eh range indicated by green and blue coloured outline rectangles). The theoretical transition region where Tc(IV) and Tc(VII) are present in equal concentration is indicated by the red plane.*

best fit can then be calculated for the transition point which can be shown to be valid for all groundwater compositions within the convex hull. This provides a visual means of ascertaining how close the system is to the point of Tc(IV)/Tc(VII) redox transition. The redox parameter space calculated in this fashion is plotted in Figure Q-4 for the groundwater compositions existing at 2,000 y in the temperate domain simulations.

Although the location of the plane of best fit roughly demarcates the regions of predominance of the oxidising and reducing forms of Tc, it does not show the full extent of the region where non-negligible fractions of both redox species can co-exist. The redox sweep data are therefore plotted in Figure Q-5 where the fraction of the reduced Tc(IV) form is given as a function of redox potential.

There is a general tendency for the redox potential to decrease over time in the SR-Site temperate case simulations due to the freshening of the groundwater with a meteoric component of higher carbonate content. The redox parameter space is plotted in Figure Q-6 for the groundwater compositions existing at 9,000 y. These represent the highest redox potentials encountered in the temperate time period simulated for SR-Site. As can be seen from Figure Q-4 to Figure Q-7, the redox potential projected for SR-Site groundwater conditions is sufficiently low that fully reducing conditions are generally assured. It is therefore recommended that redox speciation in the form of Tc(IV) is assumed for transport modelling purposes in SR-Site.

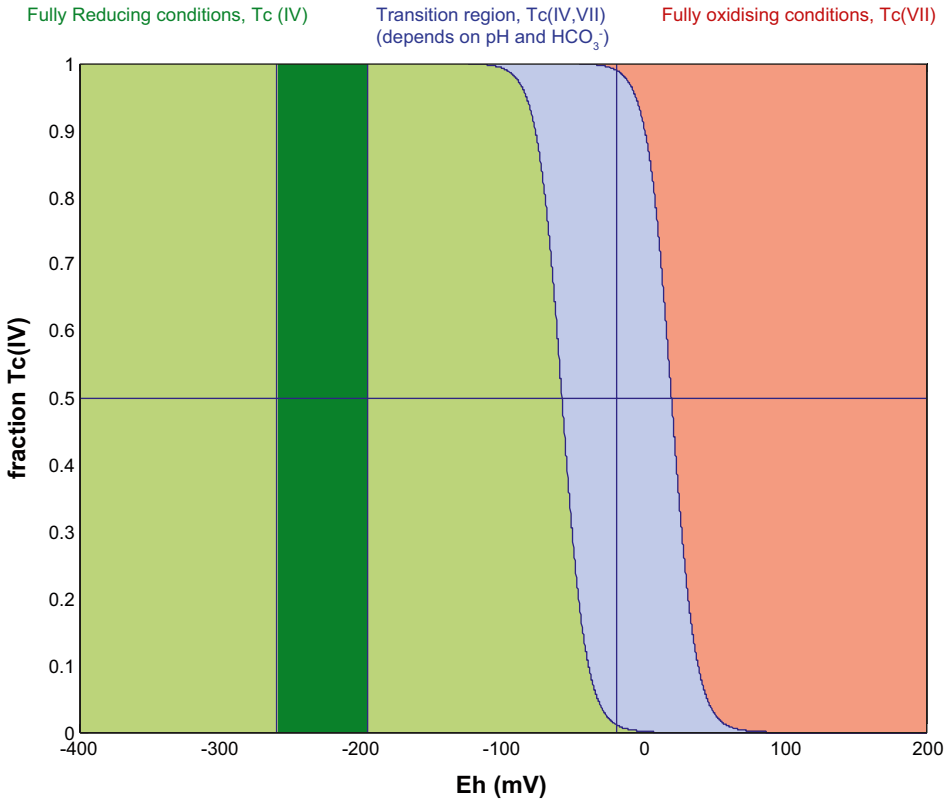

Figure Q-5. *Theoretical redox transition zone for Tc (blue shaded region) compared with redox conditions in SR-Site temperate case at 2,000 y (dark green and dark red shaded region with boundaries marked vertical broken lines) which encompasses the potential span of both the $Fe(OH)_3$ and FeS_{am} redox cases. The light green and red shaded areas represent fully reducing (100% Tc(IV)) and fully oxidising (100% Tc(VII)) conditions, respectively. The cross-hairs in the figure approximately indicate the centroid of the transition point for the application groundwater pH and carbonate ranges illustrated previously in Figure Q-4.*

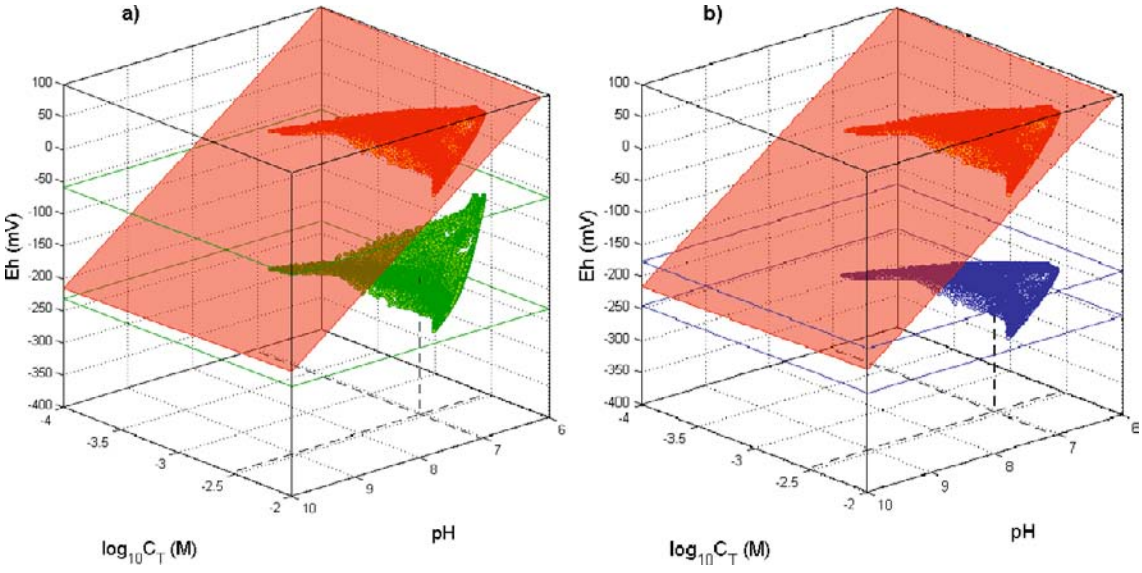

Figure Q-6. *Redox parameter space for 20,000 randomly selected SR-Site temperate case groundwater compositions at 9,000 y for (a) $Fe^{2+}/Fe(OH)_3$ redox couple, and (b) SO_4^{-2}/FeS_{am} redox couple. The calculations indicate that sampled groundwater compositions are sufficiently reducing for Tc(IV) to be the dominant redox species (min and max Eh range indicated by green and blue coloured outline rectangles). The theoretical transition region where Tc(IV) and Tc(VII) are present in equal concentration is indicated by the red plane.*

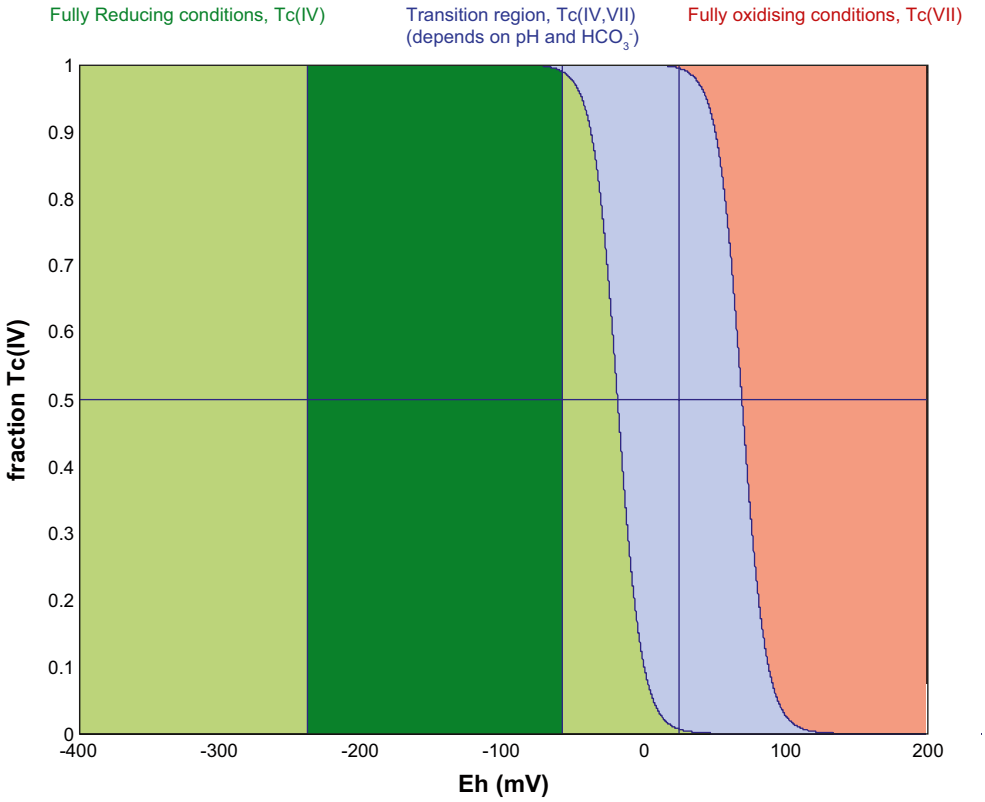

Figure Q-7. *Theoretical redox transition zone for Tc (blue shaded region) compared with redox conditions in SR-Site temperate case at 9,000 y (dark green shaded region) which encompasses the potential span of both $Fe(OH)_3$ and FeS_{am} redox cases. The light green and red shaded areas represent fully reducing (100% Tc(IV)) and fully oxidising (100% Tc(VII)) conditions, respectively. The cross-hairs in the figure approximately indicate the centroid of the transition point for the application groundwater pH and carbonate ranges illustrated previously in Figure Q-6.*

Appendix R

K_d data derivation sheet for uranium (U)

Overview and evaluation of site investigation data

Site specific sorption data were obtained for U during the site investigations at Forsmark /Byegård et al. 2008/ and Laxemar /Selnert et al. 2009/. These data are summarised in the bedrock transport properties site descriptive model reports /Crawford 2008, Crawford and Sidborn 2009/ and are the basis for K_d values recommended for use in SR-Site under oxidising to mildly reducing conditions.

Although sorption experiments were carried out in an inert glove box atmosphere, the intensity of the sorption and the fact that no particular effort was made to artificially maintain reducing conditions suggests that U was most likely present in the hexavalent redox state, U(VI). Given that there were only a relatively small number of measurements available from the site investigations and because of the sensitivity of U(VI) sorption to possibly drifting pH and redox conditions, no attempt was made to interpret the data with regard to time dependent behaviour. The Forsmark site data are based on rock samples taken from two borehole sections while the Laxemar site data are based on rock samples taken from a single borehole section.

Overview and evaluation of available literature data

The most detailed set of U sorption data for relevant rock types and groundwater compositions in the open literature is documented by /Huitti et al. 1996/. In this study, sorption was measured on crushed rock samples from three borehole sections representing three different alteration types of Rapakivi granite (Hästholmen, Finland). The sorption experiments were carried out under both oxic and anoxic conditions using a natural groundwater sample (LPVA2) with an ionic strength of about 0.17 M and liquid to solid ratio of 10 ml/g. The groundwater was dominated by NaCl with a composition close to that of the Marine groundwater type used in the Forsmark and Laxemar laboratory investigations. Owing to the large iron content of the groundwater (~6 mg/l), the groundwater samples used in the oxic experiments were equilibrated with the ambient atmosphere for a period of a week and filtered (0.22 μm Millipore filter) prior to use. No experiments were made for U sorption under reducing conditions. On account of the oxic experimental conditions and the generally weak sorption measured, the most likely redox form is assumed to be U(VI). Spike concentrations of U were in the range 10^{-5}–10^{-8} M.

Sorption experiments were carried out on three samples of granite described as fresh, weathered, and altered. As noted previously for other solutes, it was generally found that the sorption of U did not scale linearly with BET surface area and R_d values estimated for the weathered and altered samples were somewhat less than what would be otherwise predicted on the basis of their increased surface area. The rock samples were the same as described previously for Np sorption (Appendix G, Table G-1).

The data for U are estimated in terms of the percentage sorbed, S(%) which is calculated with the aid of a radiometric mass balance. The actual R_d data in the references are given without error estimates and in some cases reported as "≥" a specified value owing to detection limit issues. In order to obtain numerical ranges of K_d including uncertainty estimates, the procedures outlined in Appendix C were used. Since there are only a small number of R_d values for each rock type, re-sampling of the R_d values and their associated errors allows a more realistic range of data uncertainty to be estimated. The composite distribution of R_d values obtained for each rock type is shown in Figure R-1.

Selection of representative data for site specific conditions

U is unusual in that a mixture of site data and literature data have been considered in the recommendation of K_d ranges for use in SR-Site. The selection process and associated calculations are described separately, however, since data handling procedures were different for the site investigation and literature data.

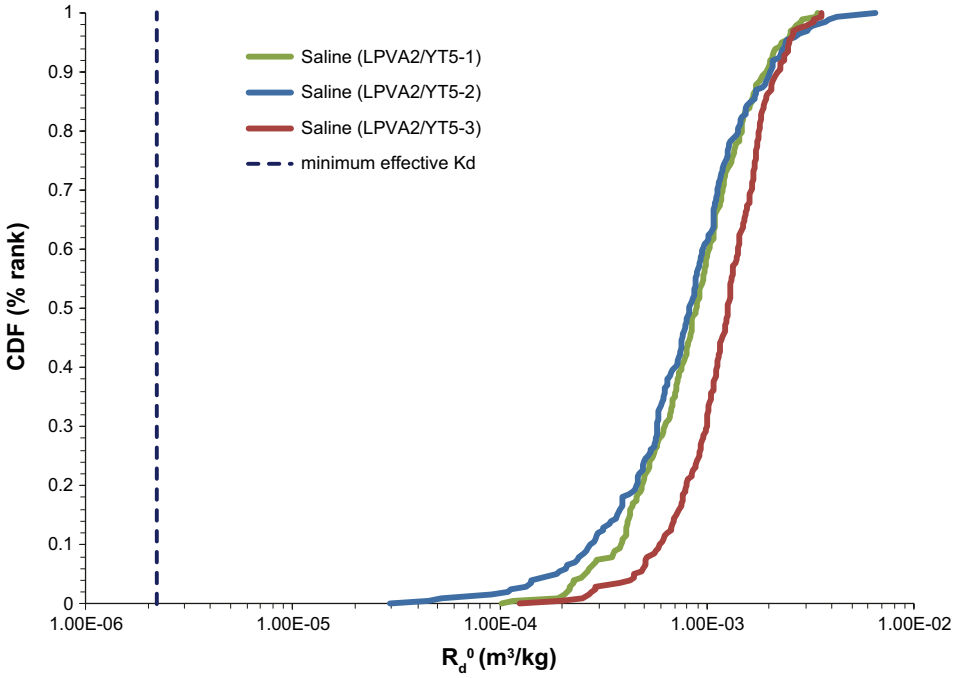

Figure R-1. *R_d^0 (m^3/kg) values calculated for U(VI) sorption under oxic conditions, based on literature R_d data and presented as an empirical cumulative distribution function for rocks taken from Finnish investigation sites. The individual data points and their uncertainties have been re-estimated from tabulated sorption percentage data and then re-sampled to give the composite distributions plotted in the figure.*

Site specific data from Forsmark and Laxemar

The procedure for derivation of U(VI) Kd values for application in SR-Site is similar to that used for Np (Appendix G). Since U(VI) has been shown to sorb preferentially in association with biotite, the CEC transfer factor is considered relevant for this nuclide even though U(VI) sorption is thought to occur primarily by way of a surface complexation mechanism. Although it cannot be guaranteed that the sorption of U(VI) on biotite is not simultaneously accompanied by heterogeneous reduction of the sorbed species to the strongly sorbed U(IV) form, the data are still considered to be broadly representative of U(VI) sorption for the purposes of data selection. Estimated K_d^0 data corrected for surface area, mechanical damage, and CEC effects are plotted in Figure R-2. Here, it is implicitly assumed that the measured R_d data correspond to U(VI) sorption.

Literature data for Rapakivi granite

As can be seen from Figure R-1, the re-sampled data indicate that there are only minor differences between the sorptivities measured for the different alteration types of Rapakivi granite. The relatively small spread of the data is related to the small number of measurements and the narrow uncertainty spans of the estimated values. As noted previously for the rock samples used in this particular study, the relatively large differences between the BET surface areas and CEC measured for these different materials do not translate into correspondingly large shifts in sorptivity. For the same reasons as outlined previously (Appendix G), only the data for the unaltered rock type YT-1 have been propagated further in the analysis.

Since the same materials were used for Np sorption measurements, the same f_m and f_{cec} transfer factors were used as described previously in Appendix G. Using the f_m and f_{cec} transfers factors, estimated K_d^0 values were calculated for the original 12 data points. On account of the limited number of data points, the individual K_d^0 values and their uncertainties were then re-sampled assuming a convex combination of the underlying lognormal distributions, now including the additional uncertainties of the f_m and f_{cec} transfer factors. The resulting expanded uncertainty distribution for K_d^0 is shown in Figure R-3. Although not plotted in the Figure it can also be noted that the BET surface areas and CEC of the altered materials imply sufficiently large correction factors that a large portion of the extrapolated K_d uncertainty distributions would be less than the minimum effective K_d value for aqueous storage in the matrix porosity (indicated by the vertical broken line in Figure R-3).

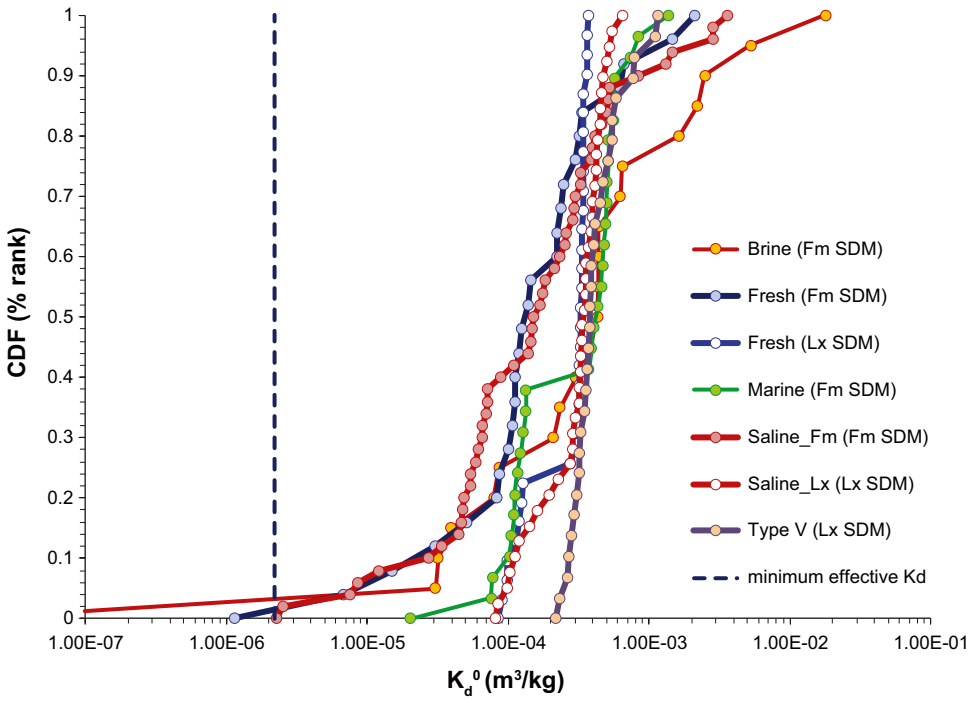

Figure R-2. *K_d^0 (m^3/kg) values calculated for U(VI) sorption based on raw R_d data for site-specific rock types and groundwater compositions as reported in the Forsmark (Fm SDM) and Laxemar (Lx SDM) site investigations. Surface area normalisation, mechanical damage, and CEC transfer factors (f_A, f_m, and f_{CEC}) have been considered in the estimation procedure. The raw data are corrected to give values deemed appropriate for Forsmark metagranite (SKB rock code 101057) under in situ conditions and are presented as an empirical cumulative distribution function. A minimum effective K_d reference line is plotted in the figure indicating the upper 95% confidence limit for the matrix storage capacity of the rock based on water saturation porosity.*

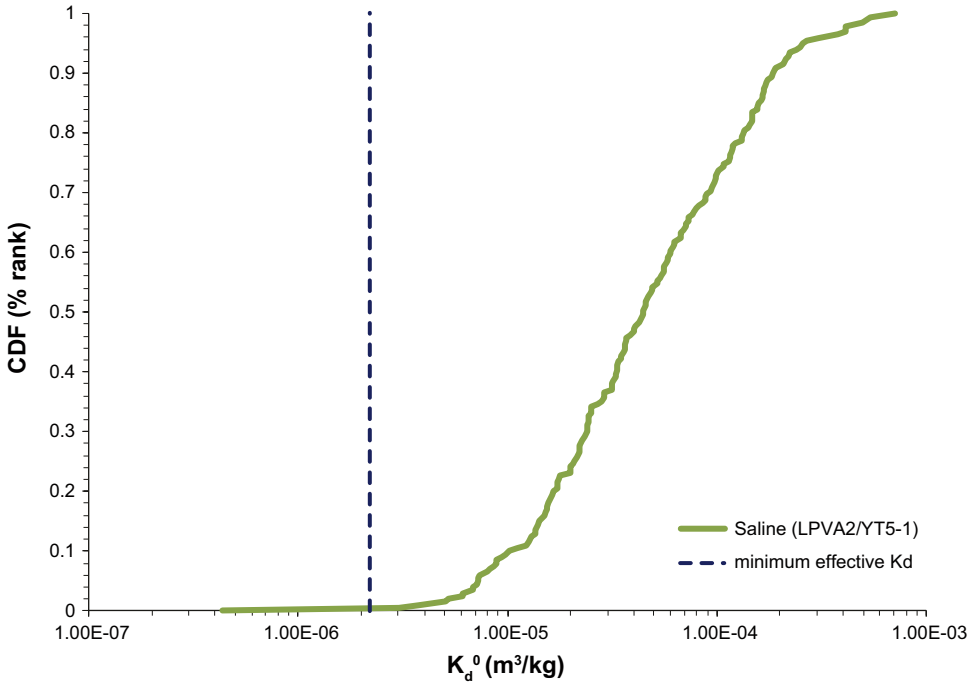

Figure R-3. *K_d^0 (m^3/kg) values calculated for U(VI) sorption based on literature R_d data. Mechanical damage and CEC transfer factors (f_m, and f_{CEC}) have been considered in the estimation procedure. The raw data are corrected to give values deemed appropriate for Forsmark metagranite (SKB rock code 101057) under in situ conditions and are presented as an empirical cumulative distribution function.*

Recommended K_d data for SR-Site application conditions

The site investigation data and literature derived values (taken from Figure R-2 and Figure R-3) are shown side by side in Figure R-4. Although the K_d^0 values derived from site specific and literature data show reasonable agreement, they have been processed in different ways and it is possible that this could introduce unnecessary bias if the different data sets are combined numerically. Unlike Np(V), however, the estimated uncertainty distribution for K_d based on the literature data is at the lower end of the range for the composite data set. For this reason, the data sets have been combined in this particular case even though this could conceivably introduce bias. This is justified in the current compilation by appealing to arguments of caution.

If it is assumed that the principal uncertainties relating to variable groundwater composition are internalised in the individual data sets shown previously in Figure R-4, a recommended range for application in SR-Site can be defined by aggregating these into a global data set. The relevant K_d range for application in SR-Site is given in Figure R-5.

Assessment of predominant redox state under application groundwater conditions

In order to ascertain the principal redox state of U under application groundwater conditions, the speciation of U was calculated for 20,000 randomly sampled groundwater compositions taken from the SR-Site temperate domain simulations /Salas et al. 2010/. The calculations were made for the prevailing groundwater chemistry at time 2,000 y, 3,000 y, 5,000 y, and 9,000 y using PHREEQC and the SKB-TDB /Duro et al. 2006/.

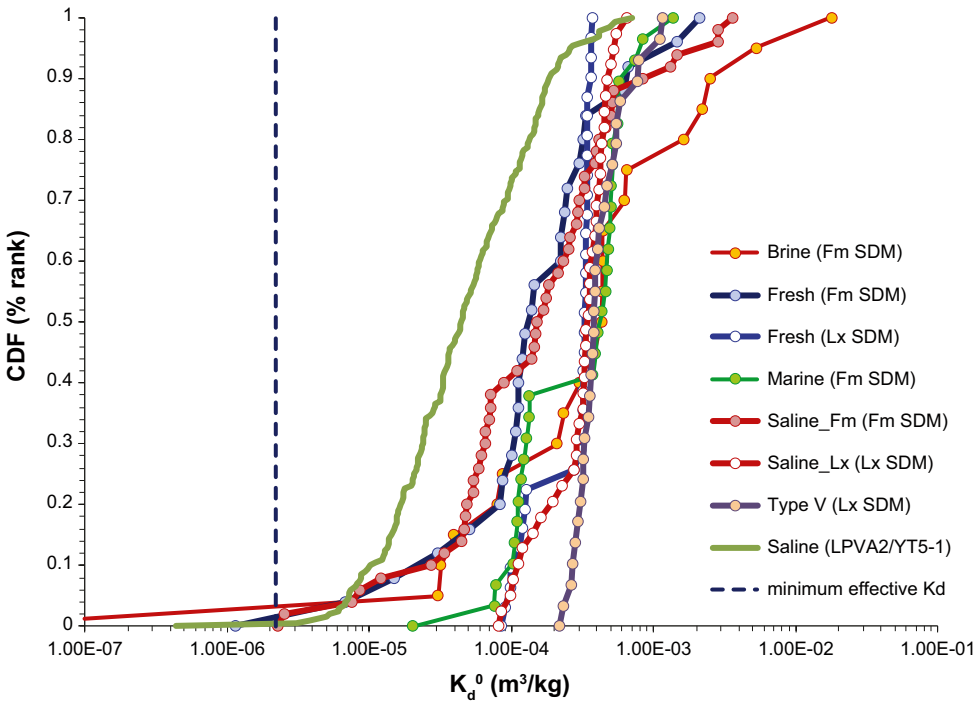

Figure R-4. *K_d^0 (m^3/kg) values calculated for U(VI) sorption corrected to give values deemed appropriate for Forsmark metagranite (SKB rock code 101057) under in situ conditions. This figure combines the data from the site investigations (Figure R-2) and literature data (Figure R-3) and indicates a relatively good agreement between the data sets of different origin.*

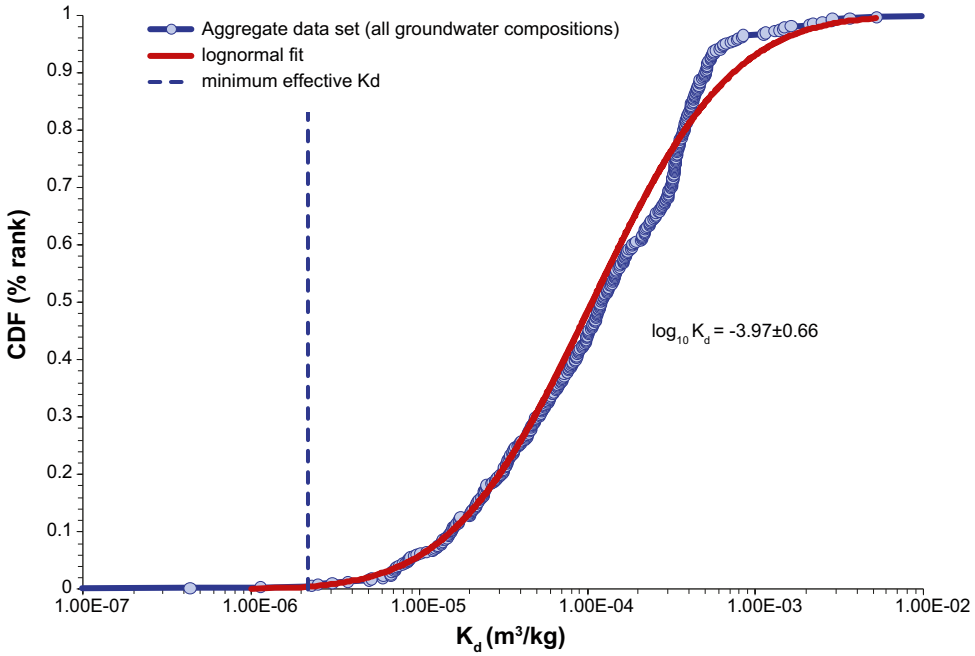

Figure R-5. *Recommended K_d (m^3/kg) values for Np(V) sorption for use in SR-Site calculations. The data range is considered to be applicable to all groundwater compositions and assumes Forsmark metagranite (SKB rock code 101057) as a representative rock type. The parameters of the lognormal distribution fit to the data are indicated in the figure.*

In addition to calculating the actual speciation of U in the application groundwater, sweep calculations were made for a range of hypothetical redox potentials to ascertain the location of the redox transition point where the U(IV) and U(VI) species are present in roughly equal concentrations. For numerical reasons this was done only for the convex hull of data points describing the envelope of pH and total carbonate concentrations in the application groundwater. From these data, a plane of best fit can then be calculated for the transition point which can be shown to be valid for all groundwater compositions within the convex hull. This provides a visual means of ascertaining how close the system is to the point of U(IV)/U(VI) redox transition. The redox parameter space calculated in this fashion is plotted in Figure R-6 for the groundwater compositions existing at 2,000 y in the temperate case groundwater simulations.

Although the location of the plane of best fit roughly demarcates the regions of predominance of the oxidising and reducing forms of U, it does not show the full extent of the region where non-negligible fractions of both redox species can co-exist. The redox sweep data are therefore plotted in Figure R-7 where the fraction of the reduced U(IV) form is given as a function of redox potential.

There is a general tendency for the redox potential to decrease over time in the SR-Site temperate domain simulations due to the freshening of the groundwater with a meteoric component of higher carbonate content. The redox parameter space is plotted in Figure R-8 for the groundwater compositions existing at 9,000 y. These represent the highest redox potentials encountered in the temperate time period simulated for SR-Site.

As can be seen from Figure R-6 to Figure R-9, the redox potential projected for SR-Site groundwater conditions is generally not sufficiently low to always guarantee fully reducing conditions. This assumes, of course, that the concentration (dissolved and immobile) of U is sufficiently low that it does not have a strong impact on the redox chemistry of the groundwater. Within the near-field repository environment there could be a substantial amount of mineralised uranium (i.e. in the form of UO_2 or other solubility limiting phase). In these locations the mobility of uranium might therefore be self-limiting owing to the redox buffering effect of the uranium mineralisation itself.

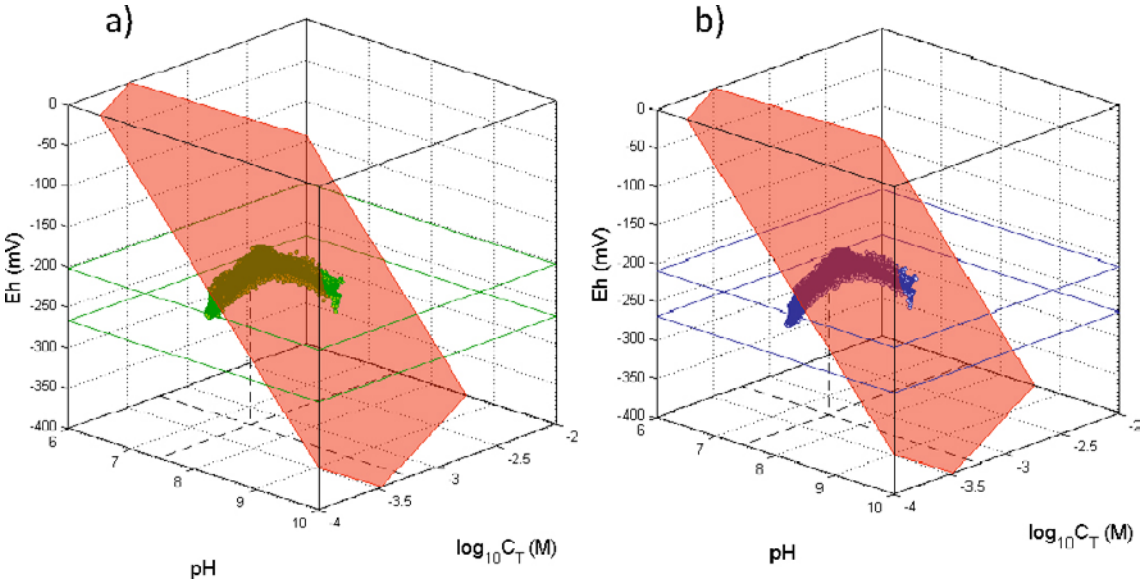

Figure R-6. *Redox parameter space for 20,000 randomly selected SR-Site temperate case groundwater compositions at 2,000 y for (a) $Fe^{2+}/Fe(OH)_3$ redox couple, and (b) SO_4^{-2}/FeS_{am} redox couple. The calculations indicate that sampled groundwater compositions cannot be guaranteed to be sufficiently reducing for U(IV) to be the dominant redox species (min and max Eh range indicated by coloured rectangles). The theoretical transition region where U(IV) and U(VI) are present in equal concentration is indicated by the red plane.*

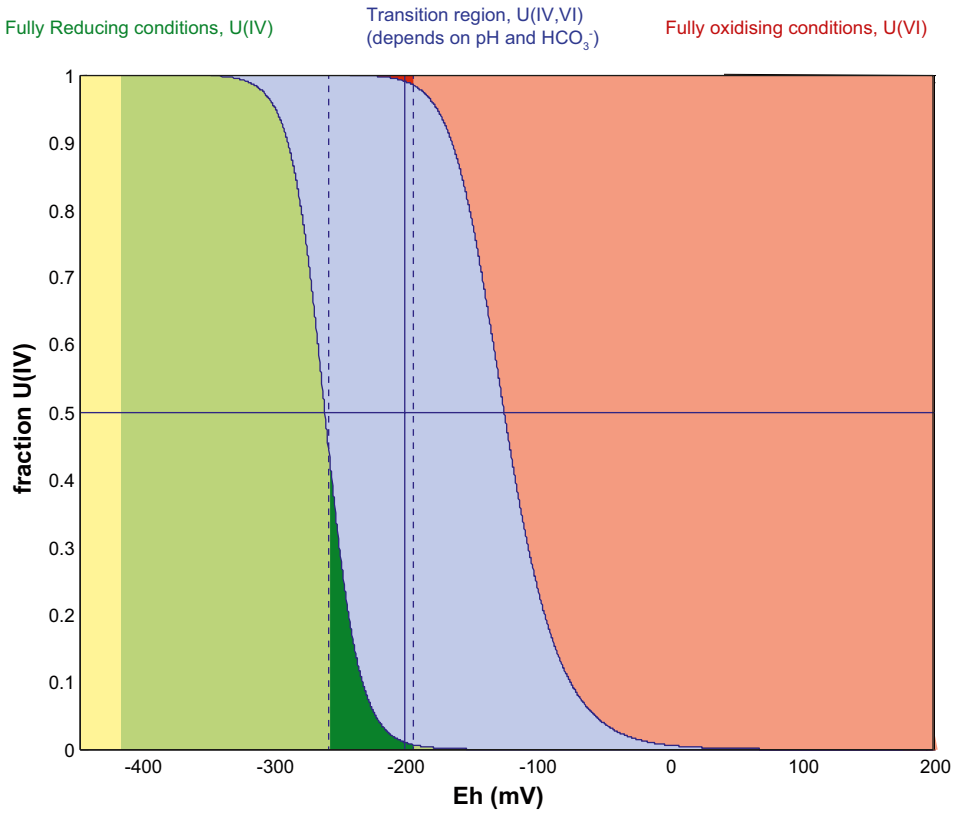

Figure R-7. *Theoretical redox transition zone for U (blue shaded region) compared with redox conditions in SR-Site temperate case at 2,000 y (dark green and dark red shaded region with boundaries marked vertical broken lines) which encompasses the potential span of both the $Fe(OH)_3$ and FeS_{am} redox cases. The light green and red shaded areas represent fully reducing (100% U(IV)) and fully oxidising (100% U(VI)) conditions, respectively. The cross-hairs in the figure approximately indicate the centroid of the transition point for the application groundwater pH and carbonate ranges illustrated previously in Figure R-6. The yellow shaded region on the left-hand side indicates the stability limit for water.*

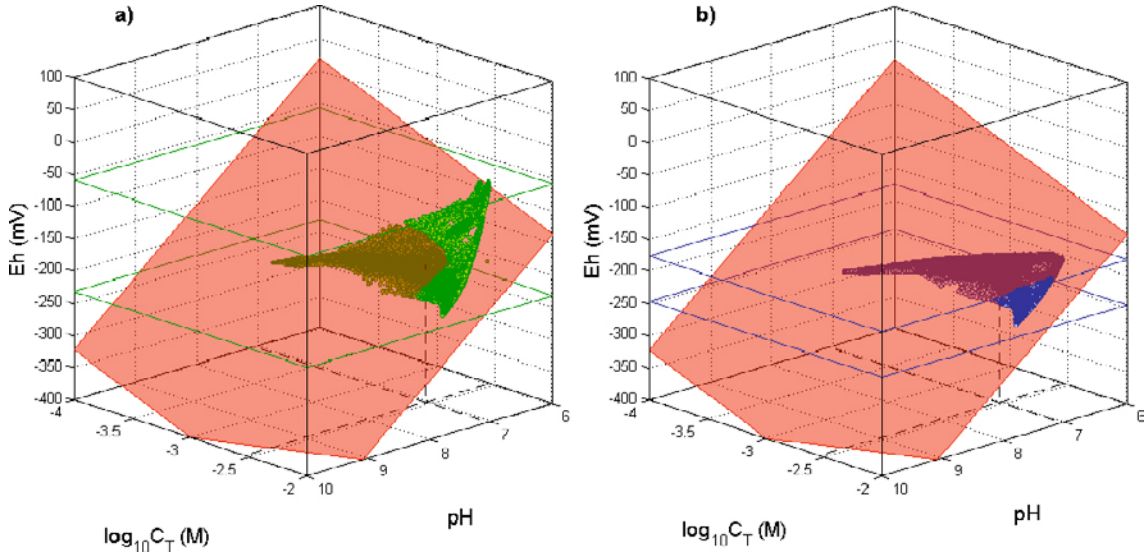

Figure R-8. *Redox parameter space for 20,000 randomly selected SR-Site temperate case groundwater compositions at 9,000 y for (a) $Fe^{2+}/Fe(OH)_3$ redox couple, and (b) SO_4^{-2}/FeS_{am} redox couple. The calculations indicate that sampled groundwater compositions cannot be guaranteed sufficiently reducing for U(IV) to be the dominant redox species (min and max Eh range indicated by coloured rectangles). The theoretical transition region where U(IV) and U(VI) are present in equal concentration is indicated by the red plane.*

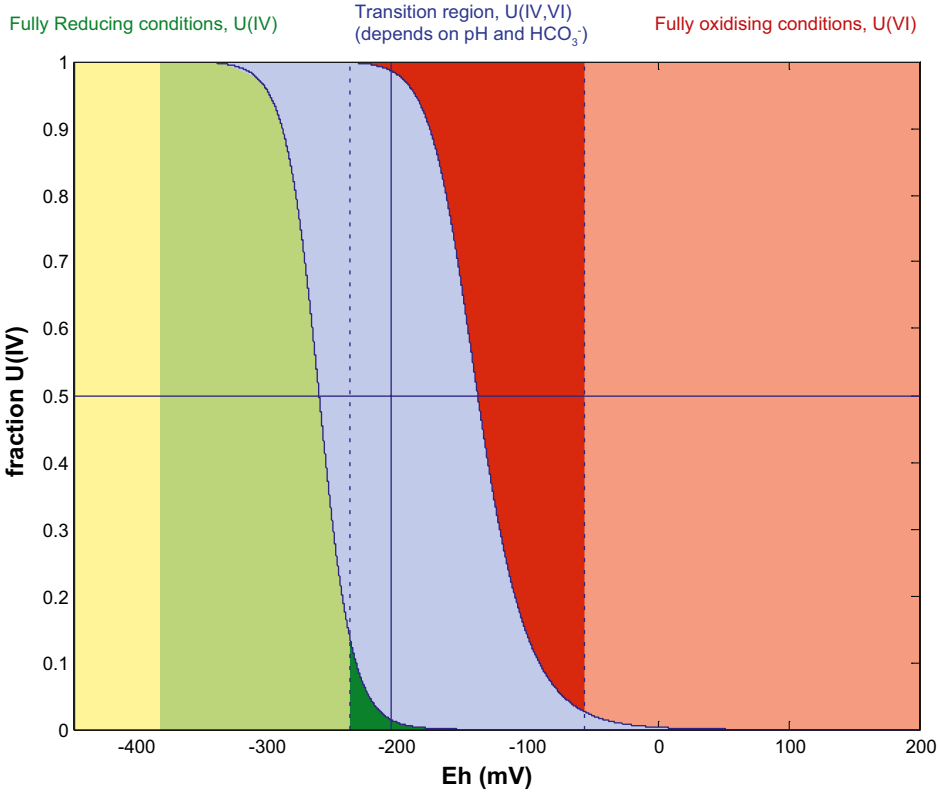

Figure R-9. *Theoretical redox transition zone for U (blue shaded region) compared with redox conditions in SR-Site temperate case at 9,000 y (dark green and dark red shaded region) which encompasses the potential span of both $Fe(OH)_3$ and FeS_{am} redox cases. The green and red shaded areas represent fully reducing (100% U(IV)) and fully oxidising (100% U(VI)) conditions, respectively. The cross-hairs in the figure approximately indicate the centroid of the transition point for the application groundwater pH and carbonate ranges illustrated previously in Figure R-8.*

In the far-field, however, where U is not expected to be present in sufficiently high concentration to buffer redox conditions, the statistics of groundwater composition imply a strong spatial variability in redox state. In some locations, conditions might allow U(IV) to be the dominant redox state, although in other locations U(VI) might dominate. In most cases, however, a mixed composition of U(IV) and U(VI) can probably be expected. Since ^{226}Ra is a prominent daughter nuclide in the ^{238}U decay chain, redox speciation in the less mobile tetravalent form would constitute a more concentrated secondary source of ^{226}Ra. The assumption of the least sorbing redox state for U therefore cannot be taken to be the most pessimistic choice in safety assessment calculations. It is therefore recommended that both redox states are propagated to SR-Site as separate case studies in order to ascertain the consequences of this uncertainty.

Appendix S

K_d data derivation sheet for zirconium (Zr)

Overview and evaluation of available literature data

The sorption of Zr(IV) on granitic rock is poorly covered in the literature and only one study /Kulmala and Hakanen 1993/ has been found where sorption has been characterised in sufficient detail to be deemed qualified. An earlier study by /Allard et al. 1979/ is acknowledged although, on account of the small number of measurements and because no BET surface areas were reported, the results are considered less useful for extrapolation using the methodology outlined in this report.

It is noted that although BET surface area data were not actually recorded by /Kulmala and Hakanen 1993/, data are available in a later reference for crushed samples of the same rock type taken from the same site. In the study by /Kulmala and Hakanen 1993/, sorption was measured on a single size fraction of tonalite (Olkiluoto, Finland) crushed to a particle size specified as less than 3 mm. The BET data reported in /Huitti et al. 1998/ for similar materials are, however, for a size fraction specified as less than 2 mm. In the absence of more accurate data, the BET surface area of the slightly coarser material was assumed to be roughly the same as the crushed rock samples used by /Kulmala and Hakanen 1993/.

The sorption experiments were carried out under oxic conditions using a natural groundwater sample native to the site. The Olkiluoto groundwater (TVO-GW) was fresh in character with an ionic strength of 0.017 M. R_d values and sorption percentages were estimated for contact times ranging from 7 days to 6 months for Zr(IV) spike concentrations in the range 1.7×10^{-9}–1.5×10^{-7} M and a liquid to solid ratio of 10. The R_d data are given without error estimates. The sorption percentages, however, are specified with uncertainty estimates. A total of 72 measurements were reported for different contact times, spike concentrations, and separation procedures (i.e. centrifugation with and without additional ultrafiltration). Owing to the broadly similar R_d values reported for the different experimental conditions, the data set was considered in its entirety without any filtering.

Selection of representative data for site specific conditions

Using the procedures outlined in Appendix C, the R_d values and their error estimates were recalculated from the raw data in /Kulmala and Hakanen 1993/. The individual R_d values and their uncertainties were then re-sampled assuming a convex combination of the underlying uncertainty distributions. The composite distribution of R_d values thus obtained is shown in Figure S-1.

The BET surface area of the crushed tonalite was reported as 0.28±0.04 m^2/g. The mechanical damage transfer factor, f_m was therefore estimated to be:

$$\log_{10} f_m \approx -1.23\pm0.26 \qquad \text{(S-1)}$$

No CEC data are given for the tonalite used in the experiments, although the biotite content has been estimated to be roughly 6.6% by volume by /Huitti et al. 1998/. Since Forsmark metagranite has a biotite content of roughly 5.4% by volume /Sandström and Stephens 2009/, the CEC transfer factor, f_{cec} is assumed to be approximately unity given that the CEC can only be guessed very approximately. Although there is no evidence to suggest for, or against preferential sorption of Zr(IV) in association with biotite, its general insensitivity to groundwater redox conditions would suggest that CEC effects can possibly be neglected in any case.

Recommended K_d data for SR-Site application conditions

Estimated K_d^0 values were calculated for Forsmark metagranite using the mechanical damage transfer factor only (f_{cec} is neglected). If it is furthermore assumed that the principal uncertainties relating to variable groundwater composition are internalised in the data, this data can be deemed suitable for SR-Site application conditions. The recommended K_d range for use in SR-Site transport calculations is given in Figure S-2.

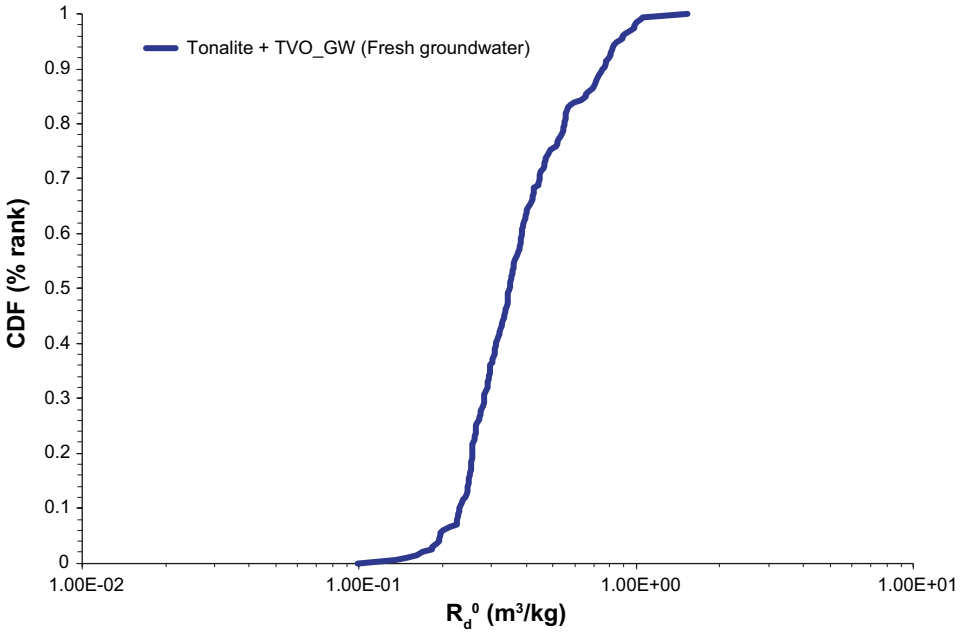

Figure S-1. *R_d (m^3/kg) values calculated for Zr(IV) sorption based on literature R_d data and presented as an empirical cumulative distribution function for tonalite (Olkiluoto, Finland) in contact with a groundwater characterised as fresh.*

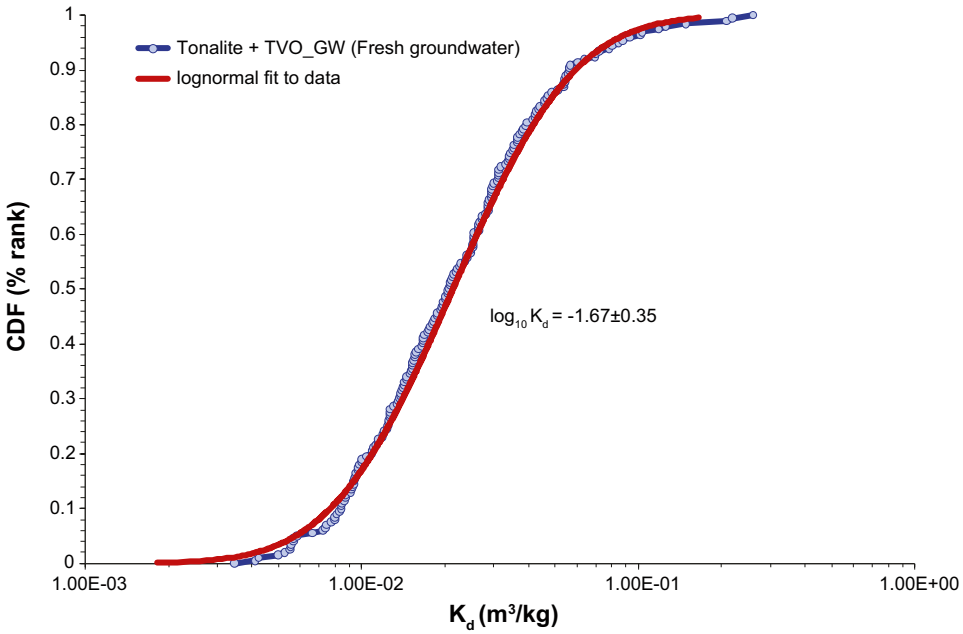

Figure S-2. *Recommended K_d (m^3/kg) values for Zr(IV) sorption for use in SR-Site calculations. The data range is considered to be applicable to all groundwater compositions and assumes Forsmark metagranite (SKB rock code 101057) as a representative rock type. The parameters of the lognormal distribution fit to the data are indicated in the figure.*